

## 01.01 New Structures

### 01.01.01

#### 4-amino-5-hydroxymethyl-2-methylpyrimidine Phosphate Synthase is a Novel Member of the Radical SAM Superfamily.

Steve Ealick, Yue Li, Abhishek Chatterjee, Tadhg P. Begley, Dept. of Chemistry and Chemical Biology, Cornell Univ., Ithaca, NY 14853.

Thiamin (vitamin B1) is essential in all living organisms. Thiamin pyrophosphate is the active form of vitamin B1 and plays a key role in carbohydrate metabolism and in branched-chain amino acid biosynthesis. Vitamin B1 was the first vitamin to be discovered, but the last to have its biosynthesis unraveled. In prokaryotes, the thiazole and pyrimidine moieties are biosynthesized separately and then coupled to form thiamin monophosphate. A final phosphorylation generates thiamin pyrophosphate. The biosynthesis of the thiamin thiazole has been extensively studied; however, until recently little was known about the biosynthesis of the thiamin pyrimidine. In eukaryotes, the thiazole and pyrimidine moieties are also biosynthesized separately, but the enzymes required are completely different from the ones of the prokaryotic pathway. The details of the eukaryotic pathway are just beginning to emerge.

In prokaryotes, 4-amino-5-hydroxymethyl-2-methylpyrimidine phosphate (HMP-P) synthase catalyzes the conversion of aminoimidazole ribonucleotide (AIR), an intermediate on the purine biosynthetic pathway, to HMP-P in what has been called the most complex unresolved rearrangement in primary metabolism. We have studied HMP-P synthase for over a decade but only recently have determined its three-dimensional structure and reconstituted its activity *in vitro*. The structure of HMP-P synthase suggested that it is a previously unrecognized member of the radical SAM superfamily. Additional biochemical studies demonstrated that HMP-P synthase requires an Fe-S cluster, that SAM is a cosubstrate and that the reaction products are HMP-P and 5'-deoxyadenosine. Interestingly, HMP-P synthase is more structurally similar to a group of adenosylcobalamin-dependent enzymes than to the known radical SAM enzymes. These new structural and biochemical results will be described, and the implications for catalytic mechanism will be discussed.

### 01.01.02

#### Capturing Hammerhead Ribozyme Structures in Action by Altering the Rate of Catalysis.

Young-In Chi<sup>1</sup>, Monika Martick<sup>2</sup>, Rosalind Kim<sup>3</sup>, William G. Scott<sup>2</sup>, Sung-Hou Kim<sup>3</sup>, <sup>1</sup>Center for Structural Biology, Dept. of Molecular and Cellular Biochemistry, Univ. of Kentucky, Lexington, KY 40536, <sup>2</sup>Center for the Molecular Biology of RNA, Sinsheimer Lab, Univ. of California, Santa Cruz, CA, 95064, <sup>3</sup>Dept. of Chemistry, Univ. of California, Berkeley, CA.

We have obtained active pre-catalytic (enzyme-substrate complex) and post-catalytic (enzyme-product complex) crystal structures of a full-length hammerhead ribozyme that cleaves in the crystal. Using the natural satellite tobacco ringspot virus (sTRSV) hammerhead RNA sequence, the self-cleavage reaction was modulated by substituting the general base of the ribozyme, G12, with A12, a purine variant with a much lower pK<sub>a</sub> that does not significantly perturb the ribozyme's atomic structure. The active but slowly cleaving ribozyme thus permits isolation of enzyme-substrate and enzyme-product complexes without modifying the nucleophile or leaving group of the cleavage reaction, nor any other aspect of the substrate. The pre-dissociation enzyme-product complex structure reveals RNA and metal ion interactions potentially relevant to



transition-state stabilization that are absent in pre-catalytic structures. In addition, our structures reveals distinctive tertiary contacts from the parasite *Schistosoma mansoni* (Sma) full-length hammerhead ribozyme (1), and a subsequent analysis of the limited sequence and structural conservation within the tertiary contact region of two classes of full-length hammerhead revealed how two conformational switches activate the hammerhead ribozyme for catalysis and regulate the nuclease-ligase internal equilibrium that is critical within the rolling circle replicative cycle of RNA viroids and satellite virus RNAs.

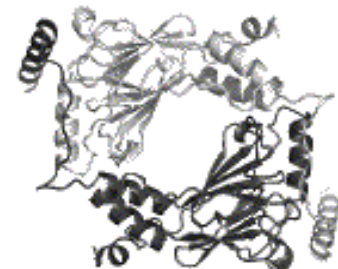
1. Martick, M., and Scott, W. G. (2006) *Cell* 126, 309-320.

### 01.01.03

#### Activation of the Interferon Regulatory Factors: Crystal Structure of Dimeric IRF-5.

William E. Royer, Weijun Chen, Suvana S. Lam, Hema Srinath, Celia A. Schiffer, Kai Lin, Dept. of Biochemistry and Mol. Pharm., Univ. of Massachusetts Med. School, Worcester, MA 01605.

Members of the Interferon Regulatory Factor (IRF) family of proteins play important roles in development of the immune system, host defense, inflammation and apoptosis. Activation of these proteins in the cytoplasm is triggered by phosphorylation of Ser/Thr residues in a C-terminal autoinhibitory region. Phosphorylation stimulates dimerization, transport into the nucleus and assembly with the coactivator CBP/p300 to activate transcription of type I interferons and other target genes. We present here the 2.0Å resolution crystal structure of a dimeric form of the IRF-5 transactivation domain (residues 215-477) in which Ser 440 has been mutated to the phosphomimetic Asp. The structure reveals a striking mechanism of dimerization in which the C-terminal autoinhibitory domain attains a highly extended conformation permitting extensive contacts to a second subunit. Based on comparison with crystal structures of IRF-3, these results provide a structural basis for the coupling between dimerization and CBP binding in IRF family members, in which the C-terminal autoinhibitory domain plays a dual role. In the unphosphorylated form, the C-terminal autoinhibitory domain binds to and masks the hydrophobic CBP/p300 binding surface. Phosphorylation stimulates the unfolding of the C-terminal autoinhibitory domain which then forms extensive contacts with a second IRF-5 subunit, leaving a hydrophobic surface free for binding CBP/p300.



### 01.01.04

#### Structure and Mechanism of a Metal Sensing Regulatory RNA.

A. Ramesh, C.A. Wakeman, C.E. Dann III, W.C. Winkler, Dept. of Biochemistry, The Univ. of Texas Southwestern Medical Center, Dallas, TX, 75390, USA.

Metals, while essential for various cellular functions, can be cytotoxic in excess amounts. Therefore metal concentrations are tightly regulated in cells. Metal homeostasis mechanisms have been described so far, with proteins playing the key role. Recently, it has been suggested that RNA based, protein-free systems could be involved in metal homeostasis. Riboswitches are metabolite sensing mRNA elements that control gene expression. Metabolite binding is often accompanied by conformational rearrangements in the riboswitch. This then affects gene expression through transcription attenuation, initiation of translation or by affecting mRNA stability. In this study

we have identified and characterized the M-box RNA, a 5' UTR RNA element or riboswitch that can directly respond to magnesium ions in the cell, and in turn regulate the expression of downstream genes. In *Bacillus subtilis* these are genes encoding magnesium transport proteins. Our experiments show that gene-regulation by the M-box RNA occurs through transcription attenuation. The M-box RNA functions as a genetic 'off' switch, turning off genes in the presence of higher concentrations of magnesium. Using X-ray crystallography we have solved a 2.6 Å structure of the M-box RNA in its magnesium bound state. The structure comprises three closely packed helices brought together by tertiary interactions to form a metal binding core. There are six magnesium ions in this core region. In the magnesium bound state Watson-Crick base pairing along with A-minor motifs and other tertiary contacts help sequester nucleotides from the anti-terminator region. This allows the formation of a terminator stem which is required for transcription attenuation.

### 01.01.05

**Structure Determination of a Substrate-Channeled Proline Catabolic Enzyme Using Deviant Crystals.** Jack Tanner, Univ. of Missouri, Columbia, MO.

Metabolism is built of complex networks of enzymes that form links by sharing substrate and product molecules. Some of these shared molecules are not freely diffusing, but instead are channeled from one enzyme to another. In general, the mechanisms by which reactive molecules are passed between enzyme active sites are poorly understood. Here, I will describe the first structure of the bifunctional substrate-channeling enzyme Proline utilization A (PutA). This enzyme catalyzes the two step oxidation of proline to glutamate via spatially separated proline dehydrogenase and pyrroline-5-carboxylate dehydrogenase domains. I will discuss some of the details of structure determination in addition to describing the structure and its implications.

Three crystal forms were used to determine the structure: apparent hexagonal, apparent tetragonal and monoclinic. The hexagonal and tetragonal forms exhibited intensity statistics indicative of crystal pathologies. Experimental phases obtained from the hexagonal form led to a partial model, but refinement stalled, necessitating a search for other crystal forms. The structure was eventually refined to high resolution using the monoclinic form, which was obtained after cleaving the histidine tag. The structure of this 1000-residue protein reveals a unique system of internal cavities and tunnels that we suggest is used for substrate channeling.

### 01.01.06

**Structural Mimicry and Ribosome Manipulation by a Viral RNA.** J.S. Kieft, D.A. Costantino, A. Keel, J.S. Pflugsten, Dept. of Biochemistry and Molecular Genetics, Univ. of Colorado Denver School of Medicine, Aurora, CO 80010.

Single-stranded RNA viruses are some of the simplest infectious pathogens known, in some cases encoding only four genes and in most cases encoding less than ten. Yet, they include viruses of medical and economic concern, including hepatitis C virus, hepatitis A virus, foot-and mouth disease virus, and poliovirus, among many others. These viruses all encode and require specific RNA structures that interact with and manipulate the host cell, yet in most cases the structural basis for their role in infection remains unknown. This lack of structural data is due in part to the fact that RNA crystallography has lagged behind protein crystallography, but new methods, techniques, and interest are allowing us to start closing that gap. In this presentation, I will present a brief overview of new methods that

are helping to make RNA structure determination available to the larger community.

I will also present new structures of viral internal ribosome entry site (IRES) RNAs that reveal how these virally encoding RNAs "hijack" the host cell's protein making machinery and use it to make viral proteins in a mechanism that is very different from the canonical pathway. These structures, when combined with cryo-EM reconstructions of RNA-ribosome complexes and biophysical analysis of the folded RNAs, show how the viral RNA uses a combination of stable structures, dynamic structures, local molecular mimicry, and global positional mimicry to manipulate the host cell and drive translation from the viral RNA. Because IRES RNAs are found in a variety of pathogenic viruses (including all of those mentioned above), understanding the structural basis for this mechanism may inform future therapeutic design.

## 01.02 Engage Your Brain

### 01.02.01

**Data Collection – Not Enough to Press the Button.** Z. Dauter, Macromolecular Crystallography Laboratory, NCI, Argonne Natl. Lab., Argonne, IL 60439, USA.

The progress in crystallographic methodology, including data collection techniques, observed within last decade, has made all steps of protein structure solution much easier and quicker. Macromolecular crystallography became a routine tool in structural biology and, as a result, its practitioners are on average less experienced and tend to rely on highly automated procedures provided by the currently available software. However, data collection is the last truly experimental stage of the crystal structure solution, and suboptimal data quality will make all subsequent, computational, steps more difficult. In spite of high level of automation, measurement of diffraction data is not a mere technicality. Various excellent data collection and processing programs provide suggestions based on vast experience of their authors, but the available options are not always properly used to optimize the data collection strategy. Moreover, protein crystals display a very wide range of properties, and no unique strategy can satisfy all particular requirements. It is therefore usually not enough to rely on the intelligence programmed in the software, but it may be good to interpret each case individually, applying human intelligence directly.

### 01.02.02

**Likelihood, Parameter Estimation, and Decision Making in Macromolecular Crystallography.** C.W. Carter, Jr., Dept of Biochem. Biophys., CB 7260, UNC Chapel Hill, Chapel Hill, NC.

Likelihood appears at first to be a strange concept. Computing the probability that a hypothesis assigns to experimental data seems to invert how we usually think of probabilities. However, models have consequences, and the different probabilities given to the observations by competing hypotheses provide an optimal basis for deciding between them. Likelihood is closely linked to Bayes's Theorem, which made an appearance in macromolecular crystallography via French and Wilson, who showed its value in improved estimates for intensities of weak reflections. Seminal papers by Bricogne developed a robust treatment of the underlying Bayesian probabilistic foundations of reciprocal and real-space parameter estimation (Bricogne, 1997). Although the fundamental level of these papers makes them somewhat difficult to assimilate, the persistent reader is repaid handsomely for the effort. Many subsequent contributions extended applications to problems of both

phase and coordinate refinement. Computer programs implementing likelihood relationships have become increasingly widespread, leading to substantial qualitative and quantitative improvements. Examples abound, however, showing that these programs do not substitute for continuing to use your brain. Supported by NIGMS.

Sivia, D.S. (1996). *Data Analysis: A Bayesian Tutorial*, Clarendon Press, Oxford, UK. Bricogne, G. (1997). *Bayesian Statistical Viewpoint on Structure Determination: Basic Concepts and Examples*. *Methods in Enzymology* 276, 361-423.

### 01.02.03

**It All Happens at Once – Magnitude Estimation of Uncertainty Components.** Dominika Borek<sup>1</sup>, Marcin Cymborowski<sup>2</sup>, Wlodek Minor<sup>2</sup>, Zbyszek Otwinowski<sup>1</sup>, <sup>1</sup>Dept. of Biochemistry, UT Southwestern, Dallas, TX, <sup>2</sup>Dept. of Molecular Physiology and Biological Physics, Univ. of Virginia, Charlottesville, VA.

With high quality macromolecular crystal, automated software can generate a refined structure in hours. However, the process of designing strategies when the experiment does not lead to an expected solution is not automated, mostly due to difficulties in the abstraction of complex interactions between experimental factors and how they impact phasing procedures.

The crystallographic experiment and computational procedures following it can be considered in terms of signal-to-error (S/E) ratio, where the error is a sum of random noise, irreproducible experimental effects and inadequate or incomplete modeling of signal. Difficulties in solving structures indicate that either S/E ratio is unfavorable or sources of error have not been properly estimated or identified for a particular case. S/E ratio may be improved either in the subsequent experiments if the source of error is identified and removed or by reexamining the existing diffraction data to identify unrecognized sources of uncertainty, estimate their magnitude and correct the phasing signal for their impact.

We developed a hierarchical, iterative procedure to address the issue of experiments with complex error characteristics. The iterative approach applied in this process allows for the optimal identification and estimates many sources of uncertainty, including radiation-induced non-isomorphism, anomalous signal, non-isomorphism due to differences between crystals *etc.*

The details of the procedure and examples showing its great impact on solving a group of cases taken from the authors' practice will be presented.

### 01.02.04

**Phasing in Spite of Complications, and Sometimes Thanks to the Complications.** Gerard Bricogne, Global Phasing Ltd, Cambridge CB3 0AX, UK.

### 01.02.05

**Juggling with Space Groups: Structure of a Fragment of the *Streptococcus mutans* Adhesin Antigen I/II.** Champion Deiganayagam.

### 01.02.06

**Macromolecular Crystal Structures Involving Non-Merohedral Twinning and/or Non-crystallographic Translation.** Kanagalaghatta Rajashankar, NE-CAT, Advanced Photon Source, ANL, 9700 South Cass Ave., Argonne, IL 60439.

Merohedral twinning is a frequent occurrence in macromolecular crystallography. Today's advanced software systems provide us with

very powerful tools to diagnose and treat many of the merohedrally twinned data sets. On the other hand, non-merohedral twinning is not as frequent as merohedral twinning, though it does occur much more often than one would think. Often such data sets get discarded. Some of the data sets with inherent non-crystallographic translation also face similar fate because of the difficulties involved in obtaining anything useful out of them. However, there exist possibilities to rescue at least some of these data sets using a bit of human intelligence and available software. Couple of case studies will be presented during the meeting.

This work is supported by NE-CAT and National Center for Research Resources (RR-15301).

## 01.03 Difficult Structures

### 01.03.01

**X-ray Structure of the Zinc Transporter YiiP.** M. Lu, D. Fu, Dept. of Biology, Brookhaven National Lab, Upton, NY 11973, USA.

YiiP is an integral membrane transporter protein that catalyzes zinc/proton exchange across the inner membrane of *Escherichia coli*. Mammalian homologs of YiiP play critical roles in zinc homeostasis and cell signalling. Here we report the structure determination of YiiP in complex with zinc at 3.8 Å-resolution. Multiple isomorphous replacement and anomalous scattering method was employed to calculate the electron density map at 4.0 Å-resolution, which was further improved by cross-crystal averaging, B-factor sharpening and phase extension to 3.8 Å-resolution. This allowed us to build an atomic model of YiiP and to refine the structural model to 3.8-Å resolution with an  $R_{\text{free}}$  of 32.9%. The structure suggests that the functional unit of YiiP is a homodimer, which is held together in a parallel orientation through four Zn<sup>2+</sup> ions at the interface of cytoplasmic domains, whereas the two transmembrane domains swing out to yield a Y-shaped structure. In each protomer, the cytoplasmic domain adopts a metallochaperone-like protein fold, while each transmembrane domain features a bundle of six transmembrane helices and a tetrahedral Zn<sup>2+</sup>-binding-site located in a cavity that is open to both the membrane outer leaflet and the periplasm. Structural interpretations of existing biochemical data have provided a framework to understand the molecular mechanisms underlying Zn<sup>2+</sup> selectivity and Zn<sup>2+</sup>-for-H<sup>+</sup> exchange during zinc transport.

We thank staff at National Synchrotron Light Source for help with data collection. This research is supported by National Institutes of Health and U.S. Dept. of Energy.

### 01.03.02

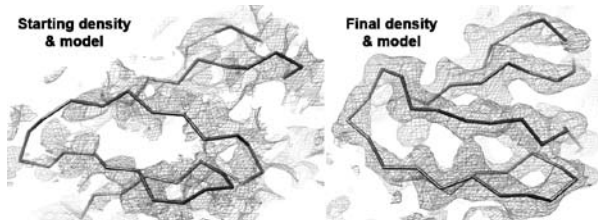
**Crystal Structure of the Maltose Transporter.** Jue Chen, Michael L. Oldham, Dheeraj Khare, Florante A. Quioco, Amy L. Davidson, Biological Sciences, Purdue Univ., West Lafayette, IN.

The maltose uptake system of *E. coli* is a well-characterized member of the ATP-binding cassette transporter superfamily. Here we present the 2.8 Å crystal structure of the maltose transporter in complex with the binding protein, maltose, and ATP. This structure, stabilized by a mutation that prevents ATP hydrolysis, captures an outward-facing conformation of the transmembrane subunits with a closed, ATP-binding cassette dimer. Maltose is occluded within a transmembrane cavity, approximately halfway into the lipid bilayer. The binding protein docks onto the entrance of the cavity in an open conformation and serves as a cap to ensure unidirectional translocation of the sugar molecule. These results provide direct evidence for a concerted mechanism of transport, in which solute is transferred from the binding protein to the transmembrane subunits when the cassette dimer closes to hydrolyze ATP.

**01.03.03**

**A Virus Structure Determined at 3.8Å With Less Than One Third of the Data Reveals Evolution in Action.** Jeffrey A. Speir, Derek J. Taylor, Fiona M. Pringle, L. Andrew Ball, John E. Johnson, The Scripps Research Inst., La Jolla, CA 92037, Univ. of Alabama, Birmingham, AL 35294, USA.

Tetraplexes have 400Å diameter particles composed of 240 identical coat proteins (~70kDa) that undergo pH dependent dynamics and autocatalytic cleavage after capsid assembly, making them model systems for the study of maturation hydrolysis in viruses. Providence Virus (PrV) is the first tetraplex identified in a cell culture system, and a single frozen crystal of authentic PrV in spacegroup C2 allowed collection of a 29% complete x-ray data set to 3.8Å resolution. The C-centering defines the positions, only a single degree of rotational freedom, and 30-fold NCS for the two particles in the unit cell. Despite the poor resolution, limited data, and a low identity phasing model, the self rotation function gave a strong signal and initial phases refined with 30-fold averaging produced a partially interpretable map. Multiple rounds of model fitting, refinement and averaging eventually produced an excellent map allowing side chain placement in all four subunits in the viral asymmetric unit. The extended N- and C-termini in PrV have swapped roles relative to those of NwV, the only other structure determined from this family. The helical NwV C-termini support a flat contact surface necessary to form the T=4 particle. In PrV, this role is now taken by ordered N-termini with a different fold. Additionally, one PrV C-terminus extends across a 2-fold axis to form an anti-parallel helix dimer with the 2-fold related subunit, which binds a small section of duplex RNA. Thus, different polypeptides perform both new and conserved functions and establish an interesting evolutionary relationship between these capsid structures.

**01.03.04**

**Hybrid LRR Technique and Crystal Structures of the Toll-like Receptor Complexes.** Jie-Oh Lee, Dept. of Chemistry, KAIST, 373-1 Kusong-dong, Yusong-gu, Daejeon Korea.

Toll-like Receptors (TLRs) are central to vertebrate innate immune responses. To facilitate soluble expression and crystallization of human TLRs with bound ligands, we have developed a novel technique that we term the “Hybrid LRR Technique”. The hagfish VLR proteins were chosen as the fusion partners and connected to human TLRs at the conserved “LxxLxLxxN” regions. The hybrid LRR technique neither interrupts function of TLR nor causes substantial structural changes. TLR4 and MD-2 form a heterodimer that recognizes LPS from Gram negative bacteria. TLR2 in association with TLR1 or TLR6 responds to microbial lipoproteins and lipopeptides. The crystal structures reveal that TLR1, 2 and 4 are atypical members of the LRR family and are composed of N-terminal, central and C-terminal domains. The β sheet of the central domain shows unusually small radii and large twist angles. MD-2 binds to the concave surface of the N-terminal and central domains of TLR4. The interaction with Eritoran, a candidate anti-sepsis drug, is mediated by a hydrophobic internal pocket in MD-2. Binding of the tri-acylated lipopeptide, Pam<sub>3</sub>CSK<sub>4</sub>, induced the formation of an “m” shaped heterodimer of the TLR1 and TLR2 ectodomains

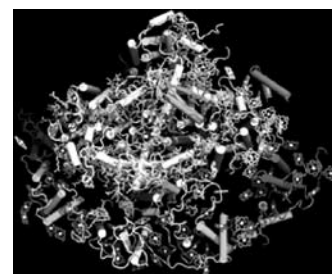
whereas binding of the di-acylated lipopeptide, Pam<sub>2</sub>CSK<sub>4</sub> did not. The three lipid chains of Pam<sub>3</sub>CSK<sub>4</sub> mediate the heterodimerization of the receptor; the two ester-bound lipid chains are inserted into a pocket in TLR2, while the amide-bound lipid chain is inserted into a hydrophobic channel in TLR1. An extensive hydrogen bonding network, as well as hydrophobic interactions, between TLR1 and TLR2 further stabilize the heterodimer. We propose that formation of the TLR dimer brings the intracellular TIR domains close to each other to promote dimerization and initiate signaling.

**01.03.05**

**A Plant Photosystem I Design in the Light of Evolution.** Alexey Amunts, Omri Drory, Nathan Nelson, Biochemistry Dept., Faculty of Life Sciences, Tel Aviv Univ., Israel.

A plant Photosystem I (PSI) is a large membrane super-complex of protein and non-protein components that catalyzes the first step of oxygenic photosynthesis. Functionally, PSI captures sunlight through highly sophisticated pigment network and uses the energy to perform the light-driven transmembrane electron transfer. Structurally, the super-complex consists of the reaction center complex (RC), which provides the core of PSI, where the bulk of the light capturing and the charge separation reaction take place and the light harvesting complex (LHCI), which serves as an additional antenna system that maximizes light harvesting by collecting solar radiation and transmitting the energy to the core complex. PSI performs a photochemical activity with the unprecedented quantum yield of close to 1.0, being the most efficient light capturing and energy conversion device in nature.

The X-ray crystal structure of the intact PSI was solved at 3.4 Å resolution<sup>[1]</sup>. The remarkable feature of PSI structure is the unprecedented extremely high content of non-protein components – approximately one third of the total mass of about 650 KDa consists of different co-factors. The current structure reveals intriguing insights regarding unique interactions between the RC and the LHCI complexes and provides a structural basis for understanding how PSI interacts with LHCI under high light intensity conditions. In addition, putative docking sites of the soluble electron carriers are described for the first time at almost atomic accuracy.



The final model of 17 protein subunits, 168 chlorophylls, 3 Fe<sub>4</sub>-S<sub>4</sub> clusters and 5 carotenoids, provides the most complete available picture of a plant PSI.

[1] Amunts, A., Drory, O. & Nelson, N. (2007) *Nature*, 447, 58-63.

**01.03.06**

**Structure Determination of S<sub>MK</sub> Riboswitch via Micro-crystallography.** Changrui Lu, Kanagalaghatta Rajashankar, Fran Ding, Tina Henkin, Ailong Ke, Cornell Univ., Ithaca, NY.

Riboswitches are 5'-untranslated regions of bacterial messenger RNAs that directly regulate the expression of proteins involved in the synthesis of certain metabolites, which accounts for a total of 2-3% of genetic regulation in bacteria. Riboswitches control transcription and translation by folding into highly organized tertiary structures in the presence of ligand. Here we present a 2.2Å resolution crystal structure of the S<sub>MK</sub> riboswitch from *metK* genes in lactic acid bacteria bound to SAM.

The high resolution needle crystals are generally 10-20 microns wide and over 500 microns in lengths. Accurate data collection requires strong microbeams of 20 microns or less with through-beam camera for correct centering during rotation. Due to fast radiation decay, crystals need to be mounted parallel to the rotational axis, allowing multiple datasets to be collected and scaled together along the crystal. Experimental phases were obtained by SAD dataset from heavy metal soaked crystals. Final structure is solved by a combination of SAD phasing and molecular replacement with ideal helix-loop structures.

The S<sub>MK</sub> RNA folds into an “inverse Y” shaped structure consisting of helix-loop structures brought together around the ligand binding site at a three-way junction. Fourteen phylogenetically conserved nucleotides are responsible for the formation of a SAM-binding pocket and specific recognition of SAM against closely related molecules such as SAH. Such specificity is achieved through a combination of unique base triples and electro static interactions. Binding of SAM stabilizes the three-way junction, resulting in the sequestration of SD sequence into a double-helix, thus preventing the translation initiation of the downstream message by the ribosome.

### 01.03.07

**Structure of the  $\beta$ 1 Adrenergic Receptor: Progress in Obtaining Recombinant G Protein Coupled Receptor Structures.** Gebhard F X Schertler, MRC Laboratory of Molecular Biology, Hills Rd., Cambridge CB2 0QH, UK.

G protein coupled receptors (GPCRs) are remarkably versatile signaling molecules. There has been significant progress in understanding the pharmacology, cell biology and physiology of this large family of membrane proteins over past two decades. Yet we still know very little about the structural basis of GPCR-mediated signal transduction. I will discuss recent progress in efforts to obtain high-resolution crystal structures of recombinant stabilised rhodopsin and beta adrenergic receptors. Stabilisation of the expressed receptors is essential for success in crystallisation and data collection. The development of micro crystallography techniques has played an important role in this effort, allowing the collection of diffraction data from crystals that are too small and heterogeneous to analyse using conventional synchrotron radiation sources. Mammalian membrane proteins are invariably more unstable than bacterial membrane proteins after detergent solubilisation and purification, which makes them far more difficult to crystallise. We have developed a generic methodology based upon alanine scanning mutagenesis and a selection strategy to improve the thermostability of any membrane protein. This was used to stabilise the  $\beta$ 1 adrenergic receptor. The thermostabilised mutant  $\beta$ AR-m23 contained 6 mutations and was more stable than the wild type protein by 21°C. This allowed the purification and crystallisation of the protein in small detergents, that normally causes the receptor to denature and aggregate. The structure clearly shows the ligand in the receptor binding pocket and will be compared with the recently determined structures of the  $\beta$ 2 $\alpha$ 2 adrenergic receptor and the rhodopsin structure. Similarities and differences between rhodopsin and catecholamin receptors will be highlighted. The implications of the new GPCR structure templates for modelling other GPCRs will be discussed. Further progress in this area will provide new mechanistic insights into GPCR signal transduction and enhance rational structure-based drug discovery for this large family of pharmacological targets.

Maria J. Serrano-Vega, Francesca Magnani, Yoko Shibata & Christopher G. Tate\* (2008) *Conformational thermostabilisation of the  $\beta$ -adrenergic receptor in a detergent-resistant form.* Proc Natl Acad Sci USA **105**, 877-882. Tony Warne, Maria J. Serrano-Vega, Jillian G. Baker#, Rouslan Moukhametianov, Patricia C. Edwards, Richard Henderson, Andrew G.W. Leslie, Christopher G. Tate\*, Gebhard F.X. Schertler\* (2008) *Structure of  $\beta$ 1 adrenergic G protein-coupled receptor.* Manuscript in preparation. \*MRC Laboratory of Molecular Biology, Cambridge, UK. #School of Medicine, Inst. of Cell Signalling, Nottingham UK.

## 01.04 Structural Enzymology

### 01.04.01

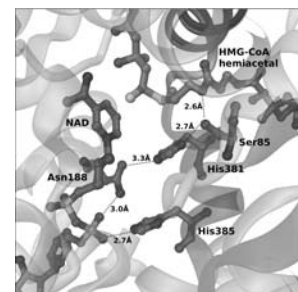
**Insights into Blue-light Photoreceptors - How to BLUF.** Ilme Schlichting, Max Planck Inst. for Medical Research, Dept. of Biomolecular Mechanisms, 69120 Heidelberg, Germany.

BLUF (sensor of Blue Light Using FAD) domain containing proteins control diverse cellular processes such as gene expression, nucleotide metabolism and motility, by relaying blue light signals to distinct output units. Despite its crucial and widespread functions, the mechanism of BLUF signal transduction has remained elusive. Recent insight into the structure, the structural changes induced by light, and the interaction with output domains will be presented.

### 01.04.02

**CoA as Catalyst: A Detailed Study of Hydride Transfer in HMG-CoA Reductase.** C. Nicklaus Steussy<sup>1\*</sup>, Chandra J. Duncan<sup>1</sup>, Tim Schmidt<sup>1</sup>, Louise V. Wrensford<sup>2</sup>, John W. Burgner<sup>1,2</sup>, Victor W. Rodwell<sup>3</sup>, Cynthia V. Stauffacher<sup>4</sup>. <sup>1</sup>Dept. of Biological Sciences, Purdue Univ., West Lafayette, IN, <sup>2</sup>Dept. of Chemistry, Albany State Univ., Albany GA, <sup>3</sup>Dept. of Biochemistry, Purdue Univ., West Lafayette, IN, <sup>4</sup>Dept. of Biological Sciences, Purdue Cancer Center, Purdue Univ., West Lafayette, IN.

HMG-CoA reductase catalyzes the four-electron reduction of HMG-CoA to free CoA and mevalonate. The mevalonate ultimately is converted to isopentenyl-diphosphate, the fundamental building block of cholesterol, steroid based hormones and membrane transfer signals. In bacteria this pathway contributes to the virulence of *Staphylococcal* and *Streptococcal* pathogens. To better understand the nature of this reaction, our laboratory has undertaken a comprehensive structural study of the mechanism of HMG-CoA reductase in bacteria utilizing the enzyme from *Pseudomonas mevalonii*. We have soaked crystals of *P. mevalonii* HMG-CoA reductase with multiple combinations of ligands, slow substrates, products, and inhibitors, resulting in over 70 high resolution data sets that explore the reaction space of the enzyme. We have found that the CoA ligand makes a novel contribution to the catalytic mechanism as the conformation of its pantothenic backbone changes during the reaction sequence. The binding of NAD(H) and its reduction of HMG-CoA to the hemiacetal intermediate is associated with the formation of a hydrogen bonding network connecting the CoA to the nucleotide. This network positions histidine 381 in its catalytic position, and stabilizes the C-terminal 50 residues of the enzyme to form the ‘flap domain’ over the active site. This presentation traces these events of the first hydride transfer through a series of high resolution x-ray crystal structures.



### 01.04.03

**Structures of Cytochrome *c* Oxidase Reveal a Conformational Change upon Reduction and a Steroid Binding Site, Both Impacting the K Proton Path.** S. Ferguson-Miller, L. Qin, D.A. Mills, C. Hiser, R.M. Garavito, BMB Dept., Mich. St. Univ., E. Lansing, MI.

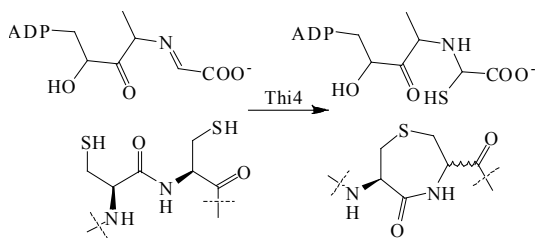
A major question regarding the mechanism of energy transduction by cytochrome *c* oxidase (CcO) is whether the coupling of electron and proton transfer involves significant conformational change. We

have solved the structures of un-reduced, reduced and re-oxidized forms of *R. sphaeroides* CcO at 2.0 - 2.2 Å. The reduced form shows little change in overall structure except in the vicinity of heme  $a_3$  where the entire porphyrin ring and the hydroxyl-farnesyl tail are shifted and rotated 1-3 Å. The distance between the OH group of the farnesyl tail and the OH group of Y288, normally 2.6 Å, increases to 4.0 Å, opening the top of the K proton channel. The  $\text{Cu}_B$  - heme  $a_3$  metal-metal distance is also greater, and density attributed to OH/ $\text{H}_2\text{O}$  in the unreduced structure is gone. These changes are reversed in the re-oxidized crystal structure. No such change has been reported in the bovine CcO. The region below heme  $a_3$  is also impacted by the heme movement, showing 1-2 Å shifts in helix VIII containing critical residues in the K path. Another structure of *RsCcO*, crystallized in the presence of the bile salt deoxycholate, reveals a high occupancy binding site in the region of the K-channel, with the carboxyl group positioned at its entrance. Reduction leads to loss of the deoxycholate binding. Bile acids are strong inhibitors of the bovine CcO and a binding site is found in the same location as for *RsCcO*. In contrast, *RsCcO* is activated by these steroids, especially a low-activity mutant form where the carboxyl group at the K-path entrance is removed. The results suggest that redox state-induced conformational change, and a conserved steroid binding site, could both regulate proton uptake in the K path. (NIH GM26916; MSU REF03-016)

#### 01.04.04

**Structure Based Enzymology of the Formation of Several Intermediates from the Thiamin Biosynthetic Enzyme Thi4 in *Saccharomyces cerevisiae*.** Christopher T. Jurgenson, Abhishek Chatterjee, Amrita Hazra, Frank C. Schroeder, Ying Han, Tadhg P. Begley, Steven E. Ealick, Dept. of Chemistry and Chemical Biology, Cornell Univ., Ithaca NY.

Thiazole synthase (Thi4) from yeast catabolizes NAD to form an adenylated thiazole carboxylate (ADT) product required for thiamin biosynthesis. The previously reported structure of Thi4 was used to identify active site residues for mutational analysis. Mutations were required to generate a construct which did not have endogenously bound ADT, since ADT could not be removed from the native enzyme without denaturation. Two active site mutants, C205S and H200N, retained activity but had no bound ligand. The structures of ADP-ribose, ADP-ribulose and an advanced intermediate were characterized from these Thi4 mutants. The sulfur transfer step has been shown to come from an internal cysteine residue by ESI-MS and electron density maps. The mechanism of sulfur transfer generates a lanthionine residue, which is an unprecedented posttranslational modification to be used in a biosynthetic pathway. The final step in thiazole biosynthesis involves the aromatization of a thiazole carboxylate tautomer in bacteria through the mechanism of the newly annotated aromatase TenI. A catalytic histidine acts as a base to remove a hydrogen atom from the C2 position of the tautomer and place it on C6 to aromatize the thiazole ring. Structural comparisons between TenI and Thi4 show that active site histidine residue in TenI



corresponds to the same structural position as the His200 - the same residue that, when mutated to

asparagine, results in a mutant incapable of forming the thiazole ring.

#### 01.04.05

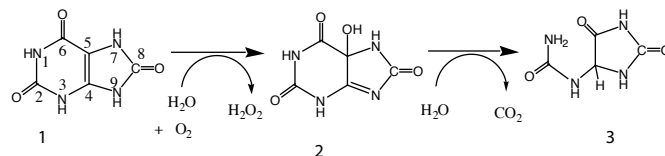
**An Interlocked Dimer of the Protelomerase TelK Distorts DNA Structure for the Formation of Hairpin Telomeres.** Tom Ellenberger.

#### 01.04.06

**Insight Into the Mechanism of the Cofactor-Less Urate Oxidase: X-Ray Structures with Molecular Oxygen and With the Dehydrourate Intermediate.** Nathalie Colloc'h\*, Laure Gabison#, Guillaume Marassio\*, Jacques H. Abraini\*, Mohamed Chiadmi#, Thierry Prangé#, \*CI-NAPS, UMR 6232, Univ. de Caen, CNRS, Centre Cyceron, Caen, France, #UMR 8015, Univ. de Paris V, CNRS, Faculté de Pharmacie, Paris, France.

Urate oxidase (UOX) catalytic mechanism is intriguing, since this enzyme catalyzes in presence of molecular oxygen the hydroxylation of uric acid (1) to 5-hydroxyisourate (5-HIU) (2), with no cofactor or metal ion. 5-HIU is further enzymatically transformed to S-allantoin (3).

To unravel this cofactor-less mechanism, different X-ray structures have been solved. The X-ray structure of UOX with a competitive inhibitor under pure oxygen pressure (10 to 40 bars) has shown that the location of the molecular oxygen advocates for a hydroperoxyisourate intermediate. The X-ray structure of UOX with its natural substrate, uric acid, in presence of cyanide which inhibits the reaction, shows that the substrate is modified by the enzyme to give the dianion N3-N7. In this structure, the observed intermediate is likely to be dehydrourate, which is the intermediate following the primary hydroperoxyisourate intermediate. The different X-ray

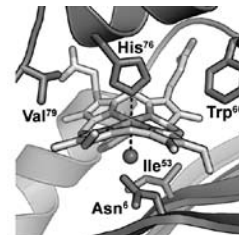


structures of UOX with a uric acid like inhibitor evidence a water molecule which is likely to be the activated water molecule that abstracts a proton from the urate monoanion. This water molecule will later hydroxylates the dehydrourate intermediate to yield the final product, 5-HIU. A second water molecule hydrogen-bonded to the substrate is also implicated in the reprotonation of the dehydrourate intermediate, leading to 5-HIU.

#### 01.04.07

**Ruffling of Metalloporphyrins Bound to the Heme Degrading Enzymes IsdG and IsdI.** M.E.P. Murphy\*, W.C. Lee\*, G. Ukpabi\*, M.L. Reniere#, Eric P. Skaar#, \*Univ. of British Columbia, Vancouver, BC, Canada V6T 1Z3, #Vanderbilt Univ. Medical Center, Nashville, TN, 37232.

IsdG and IsdI are two paralogous enzymes from *Staphylococcus aureus* that reductively degrade hemin. Structures determined of the apo-proteins revealed that these enzymes are distinct from the well-known heme oxygenase family. The crystal structures of an inactive N7A variant of IsdG in complex with Fe<sup>3+</sup>-protoporphyrin IX (IsdG-hemin) and of IsdI in complex with cobalt protoporphyrin IX (IsdI-CoPPIX) were solved to 1.8 Å or better resolution. These structures show that the metalloporphyrins are buried into similar deep clefts and the propionic acids form salt bridges to two Arg residues. His<sup>77</sup> (IsdG) or His<sup>76</sup> (IsdI), a critical residue required for activity, is coordinated to the Fe<sup>3+</sup> or Co<sup>3+</sup> atoms, respectively. The bound



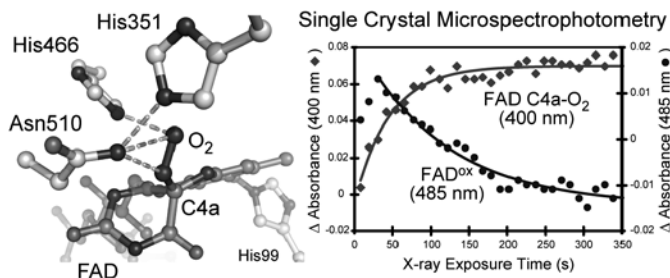
porphyrin rings form extensive steric interactions in the binding cleft such that the porphyrin rings are highly distorted from planar. This distortion can be described as ruffled and places the  $\beta$ - and  $\delta$ -*meso* carbons proximal to the distal oxygen-binding site. In the IsdG-hemin structure,  $\text{Fe}^{3+}$  is pentacoordinate and the distal side is occluded by the side chain of Ile<sup>55</sup>. However, in the structure of IsdI-CoPPiX, the distal side of the CoPPiX accommodates a chloride ion in a cavity formed through a conformational change in Ile<sup>55</sup> (see figure). The chloride ion participates in a hydrogen bond to the side chain amide of Asn<sup>6</sup>. These structures suggest a reaction mechanism in which a reactive peroxide intermediate proceeds with nucleophilic oxidation at the  $\beta$ - or  $\delta$ -*meso* carbon of the hemin.

This work is supported by a CIHR Operating Grant MOP-49597 (MEPM) and by a USPHS grant AI69233 from the NIAID. Data were collected at SSRL on beamlines 9-2 and 7-1.

#### 01.04.08

**Observation of a Flavin-C4a-Oxygen Intermediate by Crystallographic, Spectroscopic, and Computational Methods.** A.M. Orville<sup>1</sup>, R. Prabhakar<sup>2</sup>, G.T. Lountos<sup>3</sup>, S. Finnegan<sup>4</sup>, G. Gadda<sup>4</sup>, Biology Dept., Brookhaven National Laboratory<sup>1</sup>, Upton, NY 11973, Dept. of Chemistry, Univ. of Miami<sup>2</sup>, Coral Gables, FL 33146, Macromolecular Crystallography Laboratory, Center for Cancer Research, National Cancer Inst. at Frederick<sup>3</sup>, Frederick, MD 21702, Dept. of Chemistry, Georgia State Univ.<sup>4</sup>, Atlanta, GA 30302.

Flavoproteins are ubiquitous and fundamentally important to all aerobic organisms because the flavin isoalloxazine ring system often reacts with  $\text{O}_2$ . Indeed, flavin C4a-OOH or C4a-OH intermediates have been proposed in many flavoenzyme reaction mechanisms, but have only rarely been detected by transient kinetic methods because of their reactivity and instability. The electron density maps for the 1.86 Å resolution crystal structure of choline oxidase reveal a flavin C4a- $\text{O}_2$  adduct. Single-crystal microspectrophotometry shows that the adduct forms rapidly *in situ* at 100 K via synchrotron x-ray photoreduction of the FAD, and reaction with  $\text{O}_2$  from within the



aerobic crystal matrix. Two atomic models fit the electron density equally well for the unique isoalloxazine ring system: either a C4a-OO(H) or a C4a-O(H) FAD adduct. Density functional theory calculations (B3LYP/6-31G(d,p)) were used to determine the electronic structure for both flavin adducts, and to estimate the relative contributions of the active site hydrogen bonding that stabilizes the observed structure. We conclude that the choline oxidase active site structure promotes and stabilizes the C4a- $\text{O}_2$  adduct, and that the photoreduction and cryogenic conditions fail to establish the correct proton inventory required to complete the reduction of oxygen to hydrogen peroxide.

## 01.05 Computational Crystallography Nuts and Bolts

### 01.05.01

**Macromolecular Crystal Diffraction Data Collection: Opinions About Best Practices.** J.W. Pflugrath, Rigaku Americas, Corp., 9009 New Trails Dr., The Woodlands, TX 77381 USA.

While the minimum requirements for a diffraction data set are completeness in the unique Miller indexes to a given resolution, many other factors play a role in achieving good statistics and good redundancy required for optimal phasing and crystal structure refinement. Many aspects of optimizing the diffraction data collection experiment with 2D detectors are dealt with, including choice of crystal, exposure time, rotation width per image, axes to scan, scan setting angles, multiple scans, rotation ranges, potential collisions, multiple detector positions, spot overlap, and tolerance for completeness. In this talk we will delve more into the computational aspects of modern best practices used by the algorithms in the d\*TREK suite. d\*TREK is flexible, customizable, device-independent software and toolkit which collects and processes single crystal X-ray diffraction images from two-dimensional position sensitive detectors such as IP and CCD detectors. In the end, we learn that careful experimental technique pays off more than clever computational algorithms.

### 01.05.02

**Introduction to Experimental Phasing of Macromolecules.** George M. Sheldrick, Lehrstuhl für Strukturchemie, Georg-August-Universität, D37077 Göttingen, Germany.

These days, experimental phasing usually means SAD (single wavelength anomalous diffraction) or MAD (multiple wavelength anomalous diffraction). Although for crystals that only diffract to low resolution it is still worth the extra effort of collecting MAD data, more structures are now determined using SAD, exploiting the anomalous scattering of native sulfur or metals, iodide or bromide ions from a soak, or selenium from a MAD experiment that was thwarted by radiation damage. In this introduction the principles of SAD and MAD phasing will be illustrated with the help of the programs SHELXC/D/E,<sup>1</sup> however most of the comments would apply to other programs too. In many cases these programs are accessed via a graphical user interface (GUI) or wizard designed to guide less experienced users. First the extent of the anomalous signal is assessed and used to guide the location of the 'heavy' atoms by integrated Patterson and dual-space direct methods. These atoms provide reference phases that enable starting protein phases to be estimated. The native protein phases are then improved by density modification, designed to make the density look more like that of a real macromolecule. The resulting maps can be improved further by incorporating the phase information from (partial) tracing of peptide chains and by applying NCS (non-crystallographic symmetry). For crystals that diffract to 2Å or better, it may be possible to obtain a further improvement by extrapolating the phase information to the data that were not actually measured (the *free lunch algorithm*).

1. Sheldrick GM. *Acta Cryst.* (2008). D64, 112-122.

### 01.05.03

**Tools for Easy and Difficult Problems: Automation of Structure Determination.** T.C. Terwilliger, Los Alamos National Laboratory, Los Alamos, NM 87545, E-mail: terwilliger@lanl.gov.

Why automate macromolecular X-ray crystal structure determination?

How do you automate something so complicated as this? This talk will try to address these two questions. Some reasons to automate structure determination are (1) it makes straightforward cases accessible to a wider group of structural biologists, (2) it makes difficult cases more feasible for experts, (3) it can speed up the process, and (4) it can help reduce errors. Many of these advantages are related to the fact that if software is highly automated, then a user can afford to try many different possibilities and choose the most successful. Others come from the incorporation of systematic procedures for evaluation of map or model quality in automated approaches. To automate a process as complicated as macromolecular X-ray crystal structure determination you need (1) tools to carry out each individual step on the process, (2) seamless transfer of information between steps, (3) a way to decide what is good, and (4) a way to make decisions about what to do next. Examples from the SOLVE and PHENIX software packages, which are capable of highly automated macromolecular structure determination, will be used to illustrate how to automate structure determination and to speculate on the future of automation on macromolecular structure determination.

The PHENIX software is available at <http://www.phenix-online.org>.

#### 01.05.04

Paul Emsley. No abstract submitted.

#### 01.05.05

**Using Local Validation to Improve Your Structure and Streamline its Completion.** David C. Richardson, Jane S. Richardson, Duke Univ., Durham, NC.

Structure validation is becoming more than just a final checkout before deposition to ensure that global quality criteria meet community standards. The growing trend is toward proactive use of local validation outliers to diagnose and correct model problems throughout the refinement/rebuilding process. The most useful and powerful local criteria include:

- steric clashes (with explicit hydrogens) and hydrogen bonds
- difference maps and real-space correlations
- backbone dihedral-angle combinations
- sidechain rotamers for proteins and sugar pucker for nucleic acids
- solvent peak analysis
- bond angle outliers

Our MolProbity web server helps crystallographers find local violation clusters of multiple such criteria, and where possible tries to diagnose the underlying problem: for example, a residue showing a particular pattern of all-atom clashes and angle and dihedral outliers is likely to have had its sidechain fit backwards into ambiguous density and thus might be fixed by turning it around.

Strategies for combining currently available tools will be discussed, as well as prospects for further automation, and underlying issues such as the inherent trade-off between using extra information to improve structural accuracy versus keeping that information independent to better validate the accuracy.

#### 01.05.06

**Some Effects of Experimental Error on Substructure Determination.** Hongliang Xu, Charles M. Weeks, Hauptman-Woodward Med. Res. Inst. & Str. Biol. Dept., SUNY at Buffalo, 700 Ellicott St., Buffalo, NY 14203.

Protein structure determination has typically been a two-step process. One first locates the positions of heavy atoms using isomorphous or anomalous difference data and then completes the phasing of

the whole protein structure by using the heavy-atom substructure as a bootstrap. The dual-space-based *Shake-and-Bake* procedure is one of the most successful direct methods for finding heavy-atom positions.

When SIRAS or MAD data are available, it is a common practice to estimate the substructure structure factors by combining all the anomalous and dispersive differences in the form of  $F_A$  values. It is suggested by theory, and widely believed by protein crystallographers, that  $F_A$  amplitudes should be closer to the true substructure amplitudes than amplitudes based on peak anomalous difference data ( $PK_{ano}$ ) or dispersive difference data ( $IP_{iso}$ ) alone. We have investigated this belief using the computer program *SnB* and the MAD data for 19 known protein substructures. The results indicate that, depending on the program parameters that are used,  $F_A$  values yield the highest success rate for only 5-6 of these data sets, and in some cases fail to give solutions at all. On the other hand, by following a strategy of trying both the anomalous and the dispersive differences *separately and alternately*, solutions were found for all 19 substructures that we examined. The explanation appears to be that, by combining all the available information in one  $F_A$  estimate, the probability is higher that erroneous measurements made for one wavelength will contaminate the data and prevent solutions from occurring. The alternating strategy has been implemented in the computer program *BnP* that can be downloaded from [www.hwi.buffalo.edu/BnP/](http://www.hwi.buffalo.edu/BnP/).

This research was supported by NIH grant GM072023.

#### 01.05.07

**Incorporating Stereochemical Restraints in a Resolution Dependent Manner.** Dale E. Tronrud, Howard Hughes Medical Inst. and the Inst. of Molecular Biology, Univ. of Oregon, Eugene, OR 97401 USA.

Refinement programs of today include information from the diffraction pattern and a library of standard values for stereochemistry. If the molecule exhibits deviations from the standard values the program will attempt to find a compromise between the two sources of information. This is a problem because we would prefer that the model reflect the information in the diffraction data set, if that information is reliable. Deviations from ideal stereochemistry are interesting and should not be discouraged, if they are really present in the crystal.

I will propose a solution to this conflict in which the model will be restrained to the standard values only if the diffraction data does not have sufficient information to define the stereochemistry itself. This solution depends on the ability to express the stereochemical restraints in a fashion that allows them to be filtered in reciprocal space. Those aspects of the model that are poorly defined by the structure factors, specifically, can be restrained to the standard values, while other aspects that are well defined will not be distorted by geometric restraints.

In this method information present in the observed diffraction pattern that defines bond lengths and angles will never be overridden by the restraint library, and yet no difficult decisions need be made to accomplish this outcome. As the resolution of the data set becomes higher the standard values of the library naturally become less and less important.

## 01.06 Systematic Molecular Anatomy, Structural Phylogeny, & Evolution

### 01.06.01

**Building a Structural Phylogeny of the SCOR Binding Pocket.** Robert Huether, Vladimir Pletnev, Timothy C. Umland, Charles M. Weeks, Sanjay Connare, William Duax, Hauptman-Woodward Inst., 700 Ellicott St., Buffalo, NY 14203, SUNY Buffalo, Buffalo NY.

The short chain oxidoreductase (SCOR) enzyme superfamily is structurally, highly homologous. There are over 10,000 members that catalyze the oxidation or reduction of >300 substrates. Their sequences are however, very distant. Sequence identities of two proteins with the same substrate as low as 29%. This is one reason homologous sequence identity has failed to annotate unknown SCOR sequences with a known substrate. Using 17-crystal structures with bound molecules, we found nine key locations in the substrate binding loops that are generally responsible for substrate interaction. Evolutionarily, if two proteins are orthologous they retain critical information for folding, catalysis and substrate binding. Binding of substrates therefore should not have changed between given orthologs. For 8,777 SCOR proteins, the nine substrate-binding fingerprints were used to generate an all versus all identity matrix. A neighbor-joining tree was built that grouped the 8,777 SCOR proteins into substrate specific families where proteins that have the same nine residues groups closer together than those that did not. This technique removed that bias that is introduced because the sequence identity is so low in this superfamily. This analysis can identify the substrates of unknown SCOR proteins and mislabeled SCOR proteins. Additionally this technique can be expanded to other superfamilies. The work is supported by NIH Grant No. DK26546.

### 01.06.02

**Combining Protein Sequence and X-Ray Structure to Trace 3 Billion Years of Molecular Evolution.** W.L. Duax, R. Huether, V. Pletnev, S. Connare, Hauptman-Woodward Medical Research Inst., Buffalo, NY, SUNY, Buffalo, NY.

There are 10,500 members of one subgroup of the short chain oxidoreductase enzyme (SCOR) family in SWISS-Prot/TrEMBL. We have unequivocally identified 3 to 40 members of this SCOR subgroup in every species for which entire genomes have been sequenced. The divergence of evolution of the sequences, protein folding, cofactor preference and recognition, quaternary structure and substrate specificity of members of this SCOR subgroup provide precise details concerning the processes of gene mutation, gene duplication, amino acid insertions and deletions that has taken place in these proteins over the course of 3 billion years. The  $\beta$ -ketoacyl [acyl carrier protein] reductase ( $\beta$ -k-ACPR) enzymes, a 1200 member subset of the subgroup, are essential to fatty acid biosynthesis in bacteria and plants and an identifiable homolog has been characterized as a carbonyl reductase enzyme in mammals. We have discovered that (1) NADP<sup>+</sup> binding in  $\beta$ -k-ACPRs was originally contingent upon a Thr residue in the  $\beta_2\alpha_3$  turn, (2) some members of the family use NAD<sup>+</sup> as a reducing cofactor, (3) a specific dimer assembly is stabilized by the stacking of aromatic groups at the dimer interface and (4) a previously undetected conserved sequence at the C-terminus (GGMXM), stabilizes a quaternary structure required for activity. Our analysis indicates that the primordial members of the  $\beta$ -k-ACPR family probably arose in  $\alpha$ -proteobacteria and that the most ancient surviving members are characterized by the presence of multiple open reading frames (MORFs), an extreme codon bias in their DNA and an amino acid bias in their protein composition. This work is supported by NIH Grant No. DK26546.

### 01.06.03

**Statistical Evaluation of the Rodin-Ohno Hypothesis: Sense/Antisense Coding of Ancestral Class I and II Aminoacyl-tRNA Synthetases.** Gurkan Yardimci, Charles W. Carter, Jr., Dept. of Biochemistry and Biophysics, Univ. of North Carolina, Chapel Hill, NC.

Aminoacyl tRNA synthetases occur in two different classes - Class I and Class II - which share little sequence or structure homology. It is hypothesized that these two classes might have arisen on a single gene, one coded by one strand and the other coded by the complementary strand, as suggested by Rodin-Ohno<sup>1</sup>. Pham et al.,<sup>2</sup> support this hypothesis, reporting complementarity in 45% of middle bases of codons from an alignment of minimal catalytic domain coding sequences for Class I TrpRS and a Class II HisRS. Here, we introduce an automated procedure for obtaining sense/anti-sense alignments where one protein is in 3' to 5' direction and the other one is 5' to 3' direction. The alignments are used to assess the degree of complementarity of codon middle bases. We have tried different routines to identify and align appropriate segments from the MCDs of the two classes. These include dynamic programming, block alignments and anchoring with respect to conserved sequence motifs. Structural alignments obtained using Delaunay tetrahedralization (TETRADA<sup>3</sup>) are also incorporated to pinpoint conserved regions to be used in the alignments. We find 35% to 45% mean middle base identity among a small dataset of Class I and Class II enzymes by using different sense/anti-sense alignment methods as mentioned above. We are currently developing a comprehensive test of the null hypothesis, in order to assess the statistical significance of these values, as well as multivariate clustering methods to establish phylogenies. Supported by NIGMS 78227.

1. Rodin, S. N. & Ohno, S. *Orig. Life Evol. Biosph.* 25, 565-589 (1995).
2. Pham, Y. et al. 25, 851-862 (2007).
3. Roach, J. M., Sharma, S., Kapustina, M. & Carter, C. W., Jr. *PROTEINS: Struct. Funct. Bioinf.* 60, 66-81 (2005).

### 01.06.04

**Crystal Structure of an Ancient Protein: Evolution by Architectural Epistasis.** Eric A Ortlund<sup>1</sup>, Jamie T Bridgman<sup>2</sup>, Doug M Ormoff<sup>1</sup>, Jason Bischof<sup>1</sup>, Matthew R Redinbo<sup>1</sup> and Joe W Thornton<sup>2</sup>, <sup>1</sup>Dept. of Chemistry, Univ. of North Carolina, Chapel Hill, NC, 27599, <sup>2</sup>Center for Ecology and Evolutionary Biology, Univ. of Oregon, Eugene, OR, 97403.

The structural mechanisms by which proteins have evolved new functions are known only indirectly. As a result, most insights have been circumstantial, inferred from comparisons of extant protein structures or predictions based on homology models that use extant structures as backbones. We report x-ray crystal structures of a resurrected ancestral protein—the ~450 million-year-old precursor of vertebrate glucocorticoid (GR) and mineralocorticoid (MR) receptors. This common ancestor existed before the divergence of the aldosterone-insensitive GR of bony vertebrates from the aldosterone-sensitive GR of cartilaginous fishes. Using structural, phylogenetic, and functional analysis, we identify the specific set of historical mutations that recapitulate the evolution of GR's hormone specificity from an MR-like ancestor. These substitutions repositioned crucial residues to create new receptor-ligand and intraprotein contacts. Strong epistatic interactions occur because one substitution changes the conformational position of another site. "Permissive" mutations—substitutions of no immediate consequence, which stabilize specific elements of the protein and allow it to tolerate subsequent function-switching changes—played a major role in determining GR's evolutionary trajectory.

**01.06.05**

**Enzymological Characterization of the TrpRS Minimal Catalytic Domain.** Yen Pham, Charles W. Carter, Jr. Dept. of Biochemistry and Biophysics, Univ. of North Carolina, Chapel Hill, NC 27599.

Is the older the smaller and simpler in protein evolution? To address the question, we have been studying the catalytic properties of a 130-residue peptide derived from the active site of *B. stearrowthermophilus* Tryptophanyl-tRNA synthetase. Our design of this “minimal catalytic domain” for TrpRS - the smallest member of class I aaRS - will help clarify if such a small number of amino acids could have sufficed for catalysis in the primitive world<sup>1</sup>. We will describe an expression system with which most of the MCD remains soluble and active, allowing further characterization of its catalytic properties. Parameters for the amino acid activation activity detected from both renatured and soluble MCD in our preliminary experiments provide supporting evidence that a simpler form of aaRS functioned early in the evolution of translation. An ancestral gene with catalytic activities comparable to those of the TrpRS MCD might have coded for a short polypeptide chain that was only about 130 amino acid long, compared to the much larger contemporary aaRSs. The sense/antisense model proposed by Rodin and Ohno has addressed in a unique way the co-existence of structurally and mechanistically distinct class I and class II aaRS. Their hypothesis describes one gene whose both strands carry genetic information coding for the two aaRS classes. The fact that the CP1 connecting peptide is not required for catalytic activity provides important evidence that class I aaRS might have been consistent with coding opposite similar ancestral class II MCDs<sup>1</sup>. Supported by NIGMS 78227.

1. Pham, Y. et al. *Mol. Cell* 25, 851-862 (2007).

**01.06.06**

**The Structural Basis of Ribozyme-Catalyzed RNA Assembly.** Michael P. Robertson, William G. Scott, The Center for the Molecular Biology of RNA and Dept. of Chemistry and Biochemistry, Univ. of California Santa Cruz, Santa Cruz, CA, USA.

Life originated, according to the RNA World hypothesis, from self-replicating ribozymes that catalyzed ligation of RNA fragments. We have solved the 2.6 Å crystal structure of a ligase ribozyme that catalyzes regiospecific formation of a 5',3'-phosphodiester bond between the 5'-triphosphate and the 3'-hydroxyl termini of two RNA fragments. Invariant residues form tertiary contacts that stabilize a flexible stem of the ribozyme at the ligation site, where an essential magnesium ion coordinates three phosphates. The structure of the active site permits us to suggest how transition-state stabilization and a general base may catalyze the ligation reaction required for prebiotic RNA assembly.

## 01.07 How Structures are Used by Others

**01.07.01**

**What Do Other People Want from Your Crystal Structure?** Jane S. Richardson, David C. Richardson, Duke Univ., Durham, NC.

A macromolecular crystallographer usually has a fairly specific purpose in mind for doing a given structure, culminating in a publication and perhaps leading to further related structures in the future. However, once solved and deposited a structure has a very long lifetime of potential use by many other people for a variety of sometimes entirely unforeseen purposes. Even the “back side” of your structure is worth real care, both because fixing it might make

the density in the active site more interpretable, and also because it may turn out later to be the allosteric binding site for a key control factor in the functional pathway. We will discuss some of the relatively easy ways crystallographers can add more end-user value to their structures.

Probably the most important constituency for macromolecular structures is researchers working in the relevant parts of biology and biomedicine, including teachers and students whose better understanding is a very worthwhile outcome. It helps them if your PDB file includes information like the biological unit, site records, functionally related files, and the possible existence of mystery density in a binding site.

Computational biologists are major users of structures, both to study dynamics or binding or docking in your specific structure and also to build homology models or fit cryoEM density. They would prefer experimental structures to satisfy physics and include all atoms. However, there is probably no clear answer to the thorny problem of how best to treat poorly observed atoms.

Another future use of your structure is its improvement when methods for phasing, model completion, and refinement inevitably develop further, which of course means deposition of structure factors and documentation of methods.

The general conclusion is that in addition to the central objective of carefully testing your current research hypotheses on a model that best matches the best data you can feasibly collect, there are many users out there who are looking for a physically and chemically realistic molecular model and an easily accessible description of the things you saw in it.

**01.07.02**

**Statistical Analysis of Protein Structures: Electron Density, Conformational Analysis, and Protein-protein Interfaces.** Roland L. Dunbrack, Jr. Maxim Shapovalov, Qifang Xu, Guoli Wang, Daniel Ting, Michael I. Jordan, , Inst. for Cancer Research, Fox Chase Cancer Center, Philadelphia PA 19111, Roland.Dunbrack@fccc.edu.

The Protein Data Bank (PDB) provides a rich source of information when viewed as a whole. Statistical analysis of structural features from atom-atom contacts to biological and crystallographic interfaces have become a branch of modern bioinformatics and computational biology. We will present results of several studies that seek to improve our understanding of protein structure and our ability to predict structure from sequence, when an experimental structure is not yet available. First, electron densities have been used to verify coordinate positions and to understand the nature of side-chain rotamers and multi-conformational side chains. Second, we have used modern non-parametric statistical methods including kernel density estimates and the hierarchical Dirichlet process to produce smooth and differentiable probability density estimates for backbone-dependent rotamer libraries and neighbor-residue-dependent Ramachandran maps. Finally, we have examined structures of homologous proteins in different crystal forms to identify likely biologically relevant interfaces. All methods developed are or will be presented as tools available to the crystallographic community.

**01.07.03**

**Dramatic Changes of Protein Structure in Evolution.** Nick Grishin, Biochemistry, Univ. of Texas Southwestern Medical Center, HHMI, 5323 Harry Hines Blvd, Dallas, TX 75390 USA.

Most common molecular events in sequence evolution are point

mutations, insertions/deletions and non-homologous recombination. Effects of these events on protein spatial structure will be discussed, and a few examples of significant structural rearrangements that frequently lead to fold change in evolution will be shown.

#### 01.07.04

**Sampling Slow Conformational Switches in Proteins.** Donald Hamelberg, J. Andrew McCammon, Howard Hughes Medical Inst., Dept. of Chemistry and Biochemistry, Univ. of California at San Diego, La Jolla, CA.

Complex systems are often characterized by rough and complicated energy landscapes with high barriers, and the transitions over these barriers are infrequent. Even though they are rare, such transitions play a central role in conformational switching in biomolecules. However, many of these slow transitions cannot be simulated directly using traditional molecular dynamics (MD) because of nanosecond to sub-microsecond timescale limitations. We show that our MD approach can accelerate the conformational transitions and extend the time scale in all-atom simulations of biomolecules. We also show that this method allows for the thermodynamic and kinetic rate information to be recaptured.

#### 01.07.05

**Computational Prediction of Structures of Protein Complexes and Multi-domain Proteins.** Jeffrey J. Gray, Chemical and Biomolecular Engineering, Johns Hopkins Univ., Baltimore, MD.

We use crystal structures of single domains of proteins for computational prediction of the structures of protein-protein complexes (docking) and of multi-domain proteins (domain assembly). In this talk, I will discuss recent algorithmic innovations in our multi-scale, Monte-Carlo-plus-minimization algorithms. In one study, we have developed a method for docking ensembles of structures to capture the backbone flexibility inherent in binding, shedding light on theories of conformer selection and induced fit. In a second study, we have developed a new set of combinatorial Monte Carlo moves to predict the structure of domain-insert proteins (where one domain is sequentially inserted in the middle of a second domain) without disrupting structures of the individual domains, providing a means to study naturally occurring proteins as well as engineered constructs with complex function.

## 01.08 Practical Approaches to Improving the Formation and Diffraction Quality of Protein Crystals

#### 01.08.01

**Target Evaluation Coupled with Salvage Pathways to Increase Success Rates for Protein Production & Crystallization.** Ian A. Wilson, The Joint Center for Structural Genomics, The Scripps Research Institute, 10550 N. Torrey Pines Rd., La Jolla, CA 92037.

One of the most interesting outcomes from structural genomics projects has been the ability to assess the propensity of any given protein sequence to produce soluble protein and then to crystallize and, hence, enable prediction of the likelihood of successful structure determination. Based on experimental work at the JCSG, combined with analysis of a large learning set extracted from TargetDB (<http://targetdb.pdb.org>), which tracks target status for PSI as well as some other centers, predictions can be made of the likely outcome for

obtaining both protein and crystals that lead to structures for any particular target (Slabinski *et al.*, 2008). This information can be then be used to suggest how to change a target construct to improve structure success. The prediction software is available through a web server, XtalPred (<http://ffas.burnham.org/XtalPred-cgi/xtal.pl>). Once soluble protein is obtained, usually in small-scale expression at first, modifications can be made to the constructs or to the protein to improve the likelihood of crystallization through the use of salvage pathways. Multiple biophysical analyses combined with these multiple rescue strategies and crystallization robotics are now improving the success rates for individual targets.

Grant Sponsor: National Institute of General Medical Sciences, Protein Structure Initiative; Grant Number: U54 GM074898.

Slabinski, L., Jaroszewski, L., Rodrigues, A.P.C., Rychlewski, L., Wilson, I.A., Lesley, S.A., Godzik, A. (2007). The challenge of protein structure determination - lessons from structural genomics. *Protein Sci.* 16:2472-82.

#### 01.08.02

**The Importance of Nucleation and Seeding in Protein Crystallization; Case Studies using Microseed Matrix Seeding.** Allan D'Arcy, Frederic Villard, Novartis Inst. for Biomedical Research, Protease Platform, Basel, Switzerland.

The formation of nuclei in a crystallization experiment requires the interaction of protein molecules until a critical size of aggregate is created. It is not unusual when screening for crystallization conditions to find many clear drops even at high concentrations, in these cases the where nucleation has not occurred spontaneously, the introduction of seeds to form nucleation sites should have a significant effect.

In 2004 Ireton *et al.* introduced the concept of microseed matrix seeding, (Ireton, 2004). We have modified this procedure to enable automation. Using an Oryx robot (Douglas Instruments), the seed stocks are pipetted simultaneously with the protein and reservoir solutions into 96 well plates. Initial results have been very encouraging, hit rates are dramatically increased and improved crystal quality is also observed. In many cases crystals have been obtained in completely different conditions from those where the original seeds were obtained. We have tested >10 proteins and our results suggest that this method could have widespread applications in either obtaining initial hits or during the optimization procedure. Examples will be shown for both these cases and also some other interesting phenomena which we have observed.

Bergfors, T. (2003). "Seeds to crystals". *J Struct Biol.* 142, 66-76. Bertini, I., Calderone, V., Cosenza, M., Fragai, M., Lee, Y.M., Luchinat, C., Mangani, S., Terni, B. & Turano, P. (2005). Conformational variability of matrix metalloproteinases: beyond a single 3D structure. *Proc. Natl. Acad. Sci. USA*, 102, 5334-5339. u, M., Li, P., Li, M., Li, W., Yao, T., Wu, J., Gu, W., Cohen, R. & Shi, Y. (2002). Crystal Structure of a UBP-Family Deubiquitinating Enzyme in Isolation and in Complex with Ubiquitin Aldehyde. *Cell* 111, 1041-1054. Ireton, G.C. & Stoddard, B.L. (2004). Microseed matrix screening to improve crystals of yeast cytosine deaminase. *Acta Cryst.* D60, 601-605. Luft, J.R. & DeTitta, G.T. (1999). A method to produce microseed stock for use in the crystallization of biological macromolecules. *Acta Cryst.* D55, 988-993.

#### 01.08.03

**Order from Chaos - The Design and Interpretation of High-throughput Crystallization Screens to Guide Optimization.** E.H. Snell<sup>1,2</sup>, R. Nagel<sup>1</sup>, J.R. Luft<sup>1,2</sup>, A. Wojtaszczyk<sup>1,3</sup>, J. Wolfley<sup>1</sup>, M. Said<sup>1</sup>, M.E. Snell<sup>1</sup>, M.A. Parker<sup>4</sup>, G.T. DeTitta<sup>1,2</sup>, <sup>1</sup>Hauptman-Woodward Medical Research Inst., <sup>2</sup>Dept. of Structural Biology, SUNY at Buffalo, 700 Ellicott St., Buffalo, NY, <sup>3</sup>Canisius College, 2001 Main St., Buffalo NY, <sup>4</sup>Brown Univ., Providence, RI.

High-throughput crystallization screening tests many chemical conditions to locate an initial hit. Conditions are then optimized to produce crystals for diffraction. The Center for High Throughput

Structural Biology (CHTSB) provides a high-throughput crystallization screening service available to the outside community. 1536 different experiments are performed with about 400  $\mu$ L of macromolecule solution. Images are recorded automatically from each experiment over time. The interpretation of the resulting data can be challenging.

The 1536 CHTSB cocktail conditions are divided into two groups. The first, ~1000 conditions, are made up of an incomplete factorial sampling 36 salts, 8 buffers and 5 different PEGs. The remaining conditions are comprised of commercially available screens. Images from the crystallization experiments are sorted into several categories of outcomes. Images can be classified into multiple categories. For the incomplete factorial case, presenting these outcomes in chemical space readily identifies variables that are critical for the crystallization of a particular sample and clearly displays crystallization trends. The chemical space plot provides phase information on the sample that is especially relevant for crystallization. Equally important, it also provides information on the crystallization space that has not been sampled. The commercial screens supplement this information; the grid screens by fine sampling a small area to identify possible signatures of small chemical effects and the other screens providing a coarse sampling that identifies outlier conditions and relates previous results to the information obtained in the chemical space analysis. The combination of an incomplete factorial design, with a graphical representation of the results is powerful. It produces not only potential crystallization hits, but also an appropriate chemical direction for optimizing those hits.

This work is funded by the John R. Oishei foundation, the DOE, Erie County, NY, and through NIH U54 GM074899.

#### 01.08.04

**Screening for New Ligands; A Key to Higher Protein Crystallization Success Rate.** Masoud Vedadi, Abdellah Allali-Hassani, Guillermo Senisterra, Gregory A. Wasney, Patrick Finerty, Jr., Aled M. Edwards, Cheryl Arrowsmith, Structural Genomics Consortium, Univ. of Toronto, Toronto, Ont., Canada.

Identification of small molecules that bind to and stabilize proteins can promote their crystallization as well as provide valuable functional information. Identifying optimum buffer conditions which further stabilize aggregating or hard to concentrate proteins also often results in obtaining more soluble proteins that can be further concentrated and screened for crystallization conditions. Availability of a generic screening method which is not dependent on the activity of proteins, and can rapidly identify small molecules that interact with proteins, greatly facilitates analyzing the binding specificity of different members of any family of proteins. We have employed differential static light scattering (DSL) and differential scanning fluorimetry (DSF) to investigate the thermostability and ligand binding specificity of our protein targets. The presence of identified ligands in many cases (about 10%) resulted in crystallization of hard to crystallize proteins and improved crystal quality thus allowing structure determination. Screening proteins against customized libraries of compounds also generated chemical fingerprints for each protein, and provided the opportunity to compare the small molecule binding specificity of different members of each family.

#### 01.08.05

**Solubility Screen to Improve Crystallization Trials and a Two Step Approach to Uncoupling Crystal Condition Searches.**

Timothy C. Mueser\*, Aude Izaac\*, Raj Gosavi, Constance Schall, Univ. of Toledo, Dept. of Chemistry\* and Chemical Engineering, Toledo, OH 43606 USA.

Standard protocol for the crystallization of macromolecules typically involves testing an enormous number of chemical and physical parameters using sparse-matrix screens. Positive results are then required to define the next stages of experimentation. In the absence of positive results, few options are available. We presented a simple solubility screen for improving crystallization trials (Collins *et al.* (2004). *Acta Cryst.* D60, 1674–1678) derived from the ‘Ion Screen’, a systematic crystallization screen (Mueser *et al.* (2000). *Biochemistry*, 39, 15353–15364) that is the precursor to Hampton Research’s ‘PEG/Ion screen’ (Bob Cudney, personal communication). In the 2004 study, we obtained diffraction quality crystals of an archaeal nuclease where previous attempts without optimization failed to produce crystals. We proposed that improvement of solubility lowers the energy barrier to nucleation allowing crystal growth at a lower level of supersaturation. In our 2006 study, we investigated the utility of a solubility screen on ‘test’ proteins to determine if improvements are possible (Izaac *et al.* *Acta Cryst.* (2006). D62, 833–842). We also proposed a method to uncouple the constituents of crystallization screens. The salt and buffer components can be defined by a solubility screen and precipitating agents and additives can then be assessed using vapor-diffusion crystallization experiments. In our most recent study, we analyzed the effect of cryoprotectants on solubility (Gosavi *et al.* submitted, 2008) and note that enhancement of solubility by these additives is directly correlated to improvement in crystal growth.

#### 01.08.06

**Macromolecular Crystal Annealing: Updating Techniques and Understanding Variables.**

B. Leif Hanson\*, Unmesh Chinte<sup>^</sup>, Binal Shah<sup>^</sup>, Rajendrakumar Gosavi<sup>^</sup>, Constance Schall<sup>^</sup>, \*Dept. of Chemistry and A&S Instrumentation Center, <sup>^</sup>Dept. of Chemical and Environmental Engineering, Univ. of Toledo, Toledo OH.

Annealing a macromolecular crystal is understood to be the momentary raising of temperature of a crystal displaying unsatisfactory diffraction prior to returning it to cryogenic cooling for data measurement. Subsequent diffraction will be manifestly improved if the crystal annealing was successful. Although much is practiced under the rubric of annealing, our preferred protocol still calls for the removal of the unsatisfactory crystal from the pin, incubation of the crystal in cryoprotectant, then reflash-cooling the crystal. Although the 3 minute incubation period is somewhat arbitrary, this time allows the cryoprotectant solution to fully penetrate the crystal and reach equilibrium. The primary objection to *in situ* annealing techniques is the inability to control environmental variables, including ambient temperature, relative humidity and cryoprotectant diffusion gradients. Good cryocrystallographic practice is essential for successful annealing. Factors that can impinge on annealing are also those affecting flash-cooling including crystal size, the incubation protocol for the crystal in cryoprotectant, the concentration of cryoprotectant and the temperature of the cryogen. Discussion will focus on these parameters and will include specific examples and strategies that may facilitate successful annealing.

## 02.01 Fiber Diffraction and Friends

### 02.01.01

**Fiber Diffraction and Cryo-electron Microscopy Applied to Filamentous Viruses.** Gerald Stubbs, Amy Kendall, Wen Bian, Michele McDonald, Sarah Baumgarten, Timothy Bowles, Jian Shi, Phoebe Stewart. Center for Structural Biology, Vanderbilt Univ., Nashville, TN 37235.

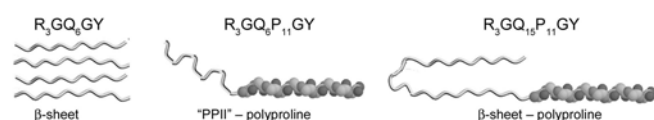
Fiber diffraction and cryo-electron microscopy are complementary and synergistic techniques in structural analyses of filamentous biological assemblies. Electron microscopy data contain both phases and amplitudes, whereas fiber diffraction data do not contain phases and often contain only overlapping amplitudes. However, fiber diffraction data often extend to considerably higher resolution than electron microscopy data. In the determination of helical symmetry, fiber diffraction can provide very accurate symmetries, but with inherent ambiguity. The ambiguity is less when moderately high resolution data are available, but in most cases can not be completely eliminated. Electron microscopy generally provides less accuracy, but is often sufficiently accurate to resolve the fiber diffraction ambiguities. Once helical symmetry has been determined, low to moderate resolution reconstructions from electron microscopic data can be used to resolve overlapping amplitudes and predict phases for fiber diffraction data, allowing more accurate reconstructions. In favorable cases, phases can be extended to higher resolution using fiber diffraction data. These principles have been applied to filamentous plant viruses including potexviruses and potyviruses.

Supported by grants NSF MCB-0235653 and MCB-0234001. Fiber diffraction data collected at BioCAT, supported by NIH RR-08630 and DOE W-31-109-ENG-38, and at SSRL, supported by DOE and NIH.

### 02.01.02

**Polyproline Changes Threshold Polyglutamine Length in Fibril Formation.** Gregory Damell<sup>1</sup>, Joseph Orgel<sup>2</sup>, Stephen Meredith<sup>1</sup>. <sup>1</sup>Dept. of Biochemistry, Univ. of Chicago, Chicago, IL, <sup>2</sup>Dept. of Biology, Illinois Inst. of Technology, Chicago, IL.

Polyglutamine (polyQ) aggregation into amyloid fibrils is associated with toxicity in several neurodegenerative diseases, including Huntington's Disease (HD). Fibril formation by huntingtin protein and clinical symptoms of HD occur when its polyQ domain expands beyond a critical threshold of  $\approx 40$  residues. In huntingtin, flanking polyproline (polyP) sequences C-terminal to this polyQ domain abrogate huntingtin amyloidogenesis<sup>1</sup>. We investigated the structural basis of this phenomenon using fiber x-ray diffraction, electron microscopy, film and solution circular dichroism, and size exclusion chromatography on a set of synthesized polyQ and polyQ-polyP peptides modeled after this N-terminal region. Our results show that polyQ peptides with  $\geq$  six Q's formed  $\beta$ -sheet amyloid, as shown by electron microscopy, film CD, and x-ray diffraction (4.8, 8-10 Å reflections). In contrast, the polyP segment of the polyQ-polyP peptides reduced  $\beta$ -sheet content of shorter polyQ peptides and altered the lateral packing of fibrils. The presence of the polyP domain increased the threshold for amyloid formation from six to fifteen Q residues, thus acting as an effective cis-inhibitor to aggregation. In conjunction with recent solid-state NMR data of polyQ fibrils<sup>2</sup> and our recent solution NMR data, we present a model to account for the polyQ-length-dependent disordering effect caused by the polyP



segments. Our findings suggest that polyP helps to solubilize polyQ segments by sterically preventing polyQ residues from packing into fibrils and by inducing non- $\beta$ -sheet conformations in the polyQ residues.

Bhattacharyya, A et al. J. Mol. Biol. 2006, 355 (3): 524-35. Shewmaker, F et al. PNAS USA. 2006, 103 (52): 19754-19759.

### 02.01.03

**Studies of Amyloid and Amyloid-Related Structures in Natural Fibres and Virus-Derived Peptide Sequences.** S.M. Tiggelaar, E. Mossou, M., Kasotakis, P. Callow, K.H. Gardner, R.C. Denny, E. Mitchell, A. Mitraki, V.T. Forsyth, Partnership for Structural Biology, Inst. Laue Langevin, 6 Rue Jules Horowitz, Grenoble, France.

We describe recent structural studies of amyloid type structures formed in two quite separate systems.

The first is a peptide system from the adenovirus fibre. This peptide, which in the normal viral context adopts a triple-beta spiral structure<sup>1</sup>, adopts an amyloid structure in the absence of suitable registration motifs<sup>2-4</sup>. Current work on this is focused on the use of neutron diffraction to obtain important information about the involvement of water in these cross-beta systems.

The second system is a naturally occurring fibre formed in the eggstalk of the insect *Chrysopa flavis*. Here high quality X-ray diffraction data has been obtained and is being used to model the cross-beta structure and in particular to investigate sequence-specific information that may be significant in intersheet interactions.

1. van Raaij MJ, Mitraki A, Lavigne G, Cusack S, *Nature* 401, 935-938 (1999).
2. Papanikolopoulou, K., Schoehn, Forge, G., Forsyth, V.T., Riek, C., Hernandez, J.-F., Ruigrok, R., Mitraki, A., *Journal of Biological Chemistry* 280: 2481-2490 (2005).
3. Retsos H, Papanikolopoulou K, Filipini C, Riek C, Gardner KH, Forsyth VT, Mitraki A, *Nanobiotechnology* 1(3), 219-226 (2005).
4. Papanikolopoulou K, Teixeira S, Belrhali H, Forsyth VT, Mitraki A, van Raaij M, *Journal of Molecular Biology*, 342, 1, pp 219-227 (2004).

### 02.01.04

**Iota-Carrageenan: A Paradigm of Cation Dependent Polymorphism, Pseudopolymorphism and Molecular Heterogeneity.** Rengaswami Chandrasekaran, Srinivas Janaswamy, Whistler Center for Carbohydrate Research, Purdue Univ., West Lafayette, IN 47907, janaswam@purdue.edu.

Carrageenans, sulfated polysaccharides extracted from marine algae, are used in food applications due to their ability to complex with other hydrocolloids. They hold promise in pharmaceutical industries as well due to their *anti*-coagulant, *anti*-therapeutic, *anti*-tumor and *anti*-HIV activities. Also, reports suggest that regular inclusion of carrageenan in the human diet reduces blood cholesterol and lipid levels. Their basic structure has a linear galactan backbone of  $\rightarrow 3$ - $\beta$ -D-galactopyranose-(1 $\rightarrow$ 4)- $\alpha$ -D-galactopyranose-(1 $\rightarrow$  or 3,6-anhydro analog along with variable amount of sulfation at hydroxyl positions, and fifteen carrageenans have been identified so far.

Within the family,  $\iota$ -carrageenan has been widely studied with regard to its gelation behavior. X-ray diffraction studies on hydrated  $\iota$ -carrageenan fibers have unveiled distinct packing arrangements with similar helical structures in the presence of mono and divalent cations. Detailed structure analyses of  $Na^+$  and  $Ca^{2+}$  forms have yielded accurate molecular details of secondary and tertiary interactions. In particular, the half-staggered double helix is stabilized by interchain O-6H...O-2 and O-2H...O-5 hydrogen bonds. The negatively charged sulfate groups are on the helix surface and actively promote stronger interhelix bridges via calcium than sodium

ions. Any change in the ester group orientations seems to alter the polymer shape and helix-helix bridges leading to the formation of new packing arrangements. Further, cations such as  $Zn^{2+}$  and  $Ni^{2+}$  are even capable of perturbing the helix integrity yielding a non-half-staggered double helix. The observation of several stable ensembles as well as polymer shapes unequivocally suggests that  $\iota$ -carrageenan has greater functional versatility than hitherto thought.

### 02.01.05

**Molecular Structure, Ligand Binding and Collagenolysis of the Native Type I Collagen Fibril.** Joseph Orgel, James San Antonio, Shawn Sweeney, Rong Wang, Shiamalee Perumal, Olga Antipova, Biological Chemical and Physical Science, Illinois Institute of Technology, 3101 S. Dearborn Ave., Chicago, IL 60083 USA.

We describe the molecular structure of the collagen fibril and how it affects collagen proteolysis or “collagenolysis”. The fibril forming collagens are major components of all mammalian connective tissues, providing the structural and organizational framework for skin, blood vessels, bone, tendon and other tissues. The triple-helix of the collagen molecule is resistant to most proteinases, and the matrix metalloproteinase’s (MMP) that do proteolyze collagen are affected by the architecture of collagen fibrils, which are notably more resistant to collagenolysis than lone collagen monomers. Until now, there has been no molecular explanation for this. Full or limited proteolysis of the collagen fibril is known to be a key process in normal growth, development, repair and cell differentiation, as well as in cancerous tumor progression and heart disease. Peptide fragments generated by collagenolysis, and the conformation of exposed sites on the fibril as a result of limited proteolysis, regulate these processes and that of cellular attachment, but it is not known how or why. Using computational and molecular visualization methods (see below), we found that the arrangement of collagen monomers in the fibril (its architecture) protects areas vulnerable to collagenolysis and strictly governs the process. This in turn affects the accessibility of a cell interaction site located near the cleavage region. Our observations suggest that the C-terminal telopeptide must be proteolyzed before collagenase can gain access to the cleavage-site. Collagenase then binds to the substrate’s “interaction domain”, which facilitates the triple-helix unwinding/dissociation function of the enzyme prior to collagenolysis. The complementary techniques used in this study include: fiber diffraction, single crystal crystallography, Atomic Force Microscopy (AFM), Electron Microscopy (EM) and molecular visualization / computational methods.

### 02.01.06

**Molecular Structure of the Native Type II Collagen Fibril.** Olga Antipova, Kalpana Ramakrishnan, Dengli Qiu, Rong Wang, Joseph Orgel, Biological Chemical and Physical Science, Illinois Institute of Technology, 3101 S. Dearborn Ave., Chicago, IL 60083 USA.

The fibrous collagens are amongst the most important structural proteins known to man. They are ubiquitous in animals and form the structural basis of various organ tissues as well as vasculature, skin, bones and cartilage. In addition to their biomechanical properties and functions, these fibrous supramolecular arrays contain numerous ligand binding sites for non-collagen molecules involved in fibrillogenesis and tissue digestion that occur at key life stages in all mammals, as well as in normal growth and repair. Understanding how collagen imparts strength to the fabric of connective tissues, as well as its role in orchestrating the (dynamic) organization of the extracellular matrix (ECM), requires knowledge of how collagen monomers are organized in the tissues native state. Some connective

tissues, such as those formed chiefly by type II and type I collagen exhibit strong evidence of being highly crystalline in their native state. Described here is progress towards determining the structure of type II collagen and understanding the role that it plays in forming the ECM. The complementary techniques used in this study include: fiber diffraction, single crystal crystallography, Atomic Force Microscopy (AFM), Electron Microscopy (EM) and molecular visualization / computational methods.

## 03.01 General Interest I

### 03.01.01

**Two Men and a Genome: A Poor Man’s Approach to Structural Genomics.** J.D. Ng, R.C. Hughes, M.L. Byrne, D. Marsic, Laboratory for Structural Biology, Univ. of Alabama in Huntsville, 301 Sparkman Dr., MSB 203C, Huntsville, AL 35899, USA.

A non-automated procedure has been developed to rapidly clone and express the proteins of targeted coding regions from the genome sequence of a novel anaerobic hyperthermophilic archaeon, *Thermococcus thio-reducens*. Selected open reading frames were identified and used for PCR (Polymerase Chain Reaction) amplification in 96 well configuration or used to guide whole gene synthesis. The amplified products were cloned into expression vectors without the use of restriction digest or ligation. Protein expression trials were performed on all clones, and those observed to show overexpression were used for large scale protein production. Protein crystallization trials were executed on purified proteins by high throughput screening methods exploring hundreds of crystallization conditions at a time. By incorporating proven strategies developed from large structural genomic centers with practical innovations, we have constructed a mini-pipeline in which a small group consisting of as few as two people can survey 1500 open reading frames for cloning, expression, crystallization and structure determination for less than \$200,000.

The development of a mini-pipeline structural genomics was supported in part by NSF STTR-05605 and NSF-EPSCoR (EPS-0447675). Crystallographic data was collected at APS on the SERCAT beamline. Hughes, R. and Ng, J.D. (2007). Can small laboratories do structural genomics? *Crystal Growth and Design* 7:2226-2238.

### 03.01.02

**Selenium Derivatization of Nucleic Acids for Phasing and Crystallization in Crystallography.** Zhen Huang, Jiansheng Jiang, Jia Sheng, Nicolas Carrasco, Dept. of Chemistry, Georgia State Univ., Atlanta, GA 30303, huang@gsu.edu.

X-ray crystallography is a powerful tool for structure determination of RNA structure, RNA-protein and DNA-protein complexes with high resolution. Derivatization with heavy atoms for phase determination, however, has largely slowed down structural determination of nucleic acids with novel folds. Recently we have developed a novel strategy to derivatize RNA and DNA by directly replacing oxygen with selenium [1-3]. We find that the Se-derivatized DNA structures have virtually identical structures to the corresponding native structures, while the conventional Br-derivatization caused severe perturbations on the local backbone and hydration [1]. Furthermore, we found that the Se-derivatization can facilitate crystallization and the diffraction quality is high. Our results suggest that the Se derivatization is a better alternative to the conventional Br derivatization. This Se derivatization strategy via the atom-specific substitution will significantly facilitate crystal structure studies of nucleic acids and their protein complexes.

This work is supported by NIH (GM069703) and NSF (MCB-0517092).

Jiang, Sheng, Carrasco, Huang\*, "Selenium Derivatization of Nucleic Acids for Crystallography", *Nucleic Acids Research*, 2007, 35, 477-485. Salon, Sheng, Jiang, Chen, Caton-Williams, Huang\*, "Oxygen Replacement with Selenium at the Thymidine 4-position for the Se-Base-Pairing and Crystal Structure Studies", *Journal of American Chemical Society*, 2007, 129, 4862-4863. Sheng, Jiang, Salon, and Huang\*, "Synthesis of a 2'-Se-Thymidine Phosphoramidite and Its Incorporation into Oligonucleotides for Crystal Structure Study", *Organic Letter*, 2007, 9, 749-752. Caton-Williams, Huang\*, "Synthesis and DNA Polymerase Incorporation of Colored 4-Selenothymidine Triphosphate with a Single Atom Substitution", *Angewandte Chemie Int. Ed.*, 2007, in press. Carrasco, Caton-Williams, Brandt, Wang, Huang\*, "Efficient Enzymatic Synthesis of Phosphoroselenoate RNA Using Adenosine 5'-( $\alpha$ -P-seleno)triphosphate", *Angewandte Chemie*, 2006, 45, 94-97.

### 03.01.03

**An Example of Successful Sulfur SAS Phasing using Medium-Resolution Data: Crystal Structure of *Archaeoglobus fulgidus* ORF 1382.** J.-Y. Zhu, Z.-Q. Fu, L. Chen, H. Xu, J. Chrzas, J. Rose, B.C. Wang, Southeast Collaboratory for Structural Genomics and SER-CAT, Dept. of Biochemistry and Molecular Biology, Univ. of Georgia, Athens, GA 30602.

Here we report the three-dimensional crystal structure of *Archaeoglobus fulgidus* ORF 1382 solved by sulfur SAS using two, 2.3 Å data sets collected on 22-ID, SER-CAT using 1.9 Å X-rays. The 95-residue AF1382 contains five sulfur atoms, with four from methionine residues. When the selenomet labeled protein failed to give well diffracting crystals two data sets were collected on native crystals for sulfur SAS phasing. The two 360° data sets were then merged to increase the anomalous scattering signal-to-noise level of the data since the individual data sets failed to give a structure. Using the merged data set SGXPro was able to solve the structure with 56 of the 95 residues being auto built from the initial RESOLVE electron density map. The final structure contains 85 residues and has an Rwork and Rfree of 23.9% and 28.0%, respectively. Our work not only shows the effectiveness and power of the sulfur SAS method, but also indicates that (1) we do not need to pursue high-resolution data to determine crystal structures with anomalous scattering signal from sulfur atoms; (2) redundancy plays a more important role.

### 03.01.04

**New Optics for Molecular Macromolecular Crystallography.** Kris F. Tesh<sup>1</sup>, Angela Criswell<sup>1</sup>, Licai Jiang<sup>2</sup>, Bret Simpson<sup>1</sup>, Boris Verman<sup>2</sup>, Cheng Yang<sup>1</sup>, Joseph D. Ferrara<sup>1</sup>, <sup>1</sup>Rigaku Americas Corp., 9009 New Trails Dr. The Woodlands, TX 77381, <sup>2</sup>Rigaku Innovative Technologies, 1900 Taylor Road, Auburn Hills, MI, 48326.

We have developed two new VariMax™ optics for macromolecular crystallography, one for screening very small samples and the other for easy switchover between Cr and Cu radiation.

It is well known that automated crystallization methods produce smaller crystals. In order to provide for better screening of initial hits for further optimization of crystallization conditions, better screening for subsequent data collection at synchrotrons or even rapid data collection at home, we have developed a very high flux optic, the VariMax-VHF [US Pat. No.: 7,245,699]. This new optic provides a beam of 100  $\mu$ m FWHM focused at the sample with up to 3.5 fold more flux at 100  $\mu$ m than conventional optics when coupled to a microfocus rotating anode source [US Pat. No. 6,823,042]. These enhanced properties of the beam provide for easier analysis of small crystals and faster screening of routine samples.

Additionally, now that SAD techniques have surpassed MAD as the primary method for structure solution, we have developed the VariMax-DW, [US Pat. No.: 6,014,423], a revolutionary dual-wavelength optic. This optic is designed to allow for easy switchover between chromium and copper radiation with only minor realignment of the optics path. It is accomplished by providing two sets of optical surfaces (one for each wavelength) and one slit to choose the desired wavelength. In this paper we will present results on the efficacy of both optics for macromolecular crystallography applications.

### 03.01.05

**Automating Crystallography (somewhat) from Start to Finish.** Joel Bard, Mark Johnson, Kristine Svenson, Erik Vogan, Kevin Parris, Lydia Mosyak, Will Somers, Structural Biology and Computational Chemistry, Wyeth Research, Cambridge, MA.

The use of macromolecular x-ray crystallography for drug design requires rapid generation of high quality co-structures of a large number of compounds bound to their receptors. A wide variety of opportunities to automate the repetitive tasks encountered at all phases of the structure determination process have recently become available. We have applied these tools to crystallization, data collection both at home and at the synchrotron, data processing, structure determination, and structure validation and deposition. In trying to find the most efficient ways to use valuable protein reagents, we have compared the results and costs of using a variety of crystallization robots for screening. We also describe our experiences with crystal mounting robots and remote synchrotron data collection. Finally, we describe scripts developed in house to ease the management of projects with many structures and to automate the initial steps of solving co-structures with small molecule ligands using PHENIX.

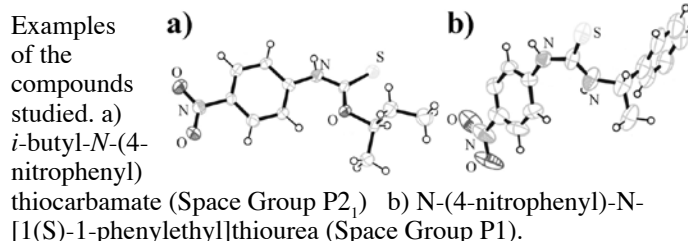
### 03.01.06

**Synthesis, Structures, Morphologies and Optical Properties of Some New Chiral Thiocarbamates and Thioureas.** Werner Kaminsky, Donald Responde, Dan Daranciang, Joey Gallegos, Dep. of Chemistry, Univ. of Washington, Seattle, WA, USA.

We set out to engineer chemically and structurally related small chiral molecules for studying non-linear optical properties satisfying four important issues,

- 1) high number of mobile electrons, which is key for potential nonlinear optical applications
- 2) selected hydrogen bonds which structures molecular packing and enhances crystal growth
- 3) high X-ray scattering capability
- 4) non-centro symmetric space group,

which are satisfied when reacting isothiocyanates (ITC) (R-phenyl-N=C=S, R=H, F, Cl, Br, I, NO<sub>2</sub>) with enantiopure 2-butanol or  $\alpha$ -methyl-benzyl-amine ( $\alpha$ -MBA). Aromatic rings of ITCs provide mobile electrons, sulfur satisfies condition 2 and 3, and the enantiopure reactants enforce aspect 4. The compounds were synthesized by heating ITC in dried 2-butanol at 90°C for one hour. ITC was reacted with  $\alpha$ -MBA following a procedure described in [1]. Crystals were grown from ethanol via slow evaporation. Morphologies were compared with those calculated from a modified Bravais-Friedel; Donnay-Harker model [2]. Structures were obtained with the Nonius FR590 Kappa CCD diffractometer. Refractive indices were measured utilizing the 3-height method. Optical property tensors of second harmonic generation, electro optic effect, and optical rotatory power were estimated with the DES model [3] and compared to experimental data.



[1] M. Avalos, R. Babiano, A. Cabanillas, P. Cintas, F. J. Higes, J. L. Jimenez, and J. C. Palacios. *J. Org. Chem.* 1996, 61, 3738-3748. [2] W. Kaminsky. *J. Appl. Cryst.* 2007, 40, 382-385. [3] W. Kaminsky, A.M. Glazer. *Z.Kristallogr.* 1997, 212, 283-296.

## 03.02 General Interest II

### 03.02.01

**In Pursuit of the Trouble-Free Photon: Low Maintenance, High Brilliance X-ray Sources for the Home Lab.** M. Benning<sup>1</sup>, A. Coetzee<sup>2</sup>, A. Storm<sup>2</sup>, B. Schierbeek<sup>2</sup>, <sup>1</sup>Bruker AXS Inc., Madison, WI 53711 USA, <sup>2</sup>Bruker AXS B.V., Delft, the Netherlands.

In recent years X-ray source technology has advanced rapidly. The combination of microfocus sources with multilayer optics has brought synchrotron-like performance to the home laboratory for crystallography applications. Developments in source technology and modern optics have greatly expanded user's options. Until recently, the choice of an X-ray source for the home laboratory had been a compromise between high brilliance and low maintenance. Conventional rotating anode generators had notoriously short filament life-times, resulting in more frequent down-time, often at critical times. Stationary sealed tube systems, although much more robust, yielded orders of magnitude less intensity and were not feasible alternatives for studying weakly diffracting samples.

Modern microfocusing sealed tube X-ray sources, such as Incoatec Microfocus Source ( $I\mu S^{\text{TM}}$ ), are low maintenance, high-brilliance sources which can significantly improve the capabilities of home laboratory instruments when combined with multilayer mirrors. High brilliance microfocus rotating anode sources, like the MICROSTAR ULTRA II, combine intensities exceeding that of second generation synchrotron beam lines with stability, reliability and ease of use.

This study reviews the types of sources available and compares their performance and maintenance requirements. The suitability of different source classes for various applications is also investigated.

### 03.02.02

**Translational and Rotational Calibration of Stationary Area Detectors.** J. Kaercher, M. Ruf, Bruker AXS Inc., Madison, WI.

The advent of fully automated low-cost single-crystal X-ray diffractometers with stationary area detectors necessitated the development of new methods for the instrument alignment and calibration. An area detector, like any three-dimensional object, possesses six positional degrees of freedom: three translational and three rotational. During integration of single-crystal diffraction data, these detector parameters are needed for the calculation of reflection positions on the diffraction images.

If the detector is stationary and cannot be moved to different offset angles or distances, strong correlations exist between the detector's positional degrees of freedom and other parameters of the hardware or of the sample. These correlations imply that physically meaningful values for all parameters are difficult to obtain from a combined least-squares refinement during integration.

The solution is to determine values for the six degrees of freedom of the detector from independent experiments that eliminate existing correlations as much as possible. Once they have been established, the detector parameters can then be constrained during integration of single-crystal diffraction data. The application of this method is not limited to stationary detectors but can be used for area detectors in general. The paper will present suitable experiments and explain their properties and analysis.

### 03.02.03

**Small X-ray Beams for Small Crystals: Pushing the Limits of Home-lab X-ray Sources.** J. Wiesmann<sup>1</sup>, J. Graf<sup>1</sup>, C. Michaelsen<sup>1</sup>, T. Schulz<sup>2</sup>, D. Stalke<sup>2</sup>, <sup>1</sup>Incoatec GmbH, D-21502 Geesthacht, Germany, <sup>2</sup>Inst. for Inorganic Chemistry, Univ. of Goettingen, D-37077 Goettingen, Germany.

The concept of using a microfocus X-ray source in combination with X-ray optics for diffraction experiments was first pioneered by U. Arndt in the early 90's. Since then, there have been numerous research activities for finding suitable combinations of high-brilliant microfocusing sealed tube X-ray sources and X-ray optics (e.g. capillaries, TR mirrors). A major breakthrough was the development of graded multilayer mirrors by H. Göbel.

Combining graded multilayer mirrors with a state-of-the-art high-brilliance microfocus sealed tube results in a new class of high-brilliant X-ray sources for the home lab. These sources are characterized by a high performance (high flux densities, high spatial resolution) and excellent beam stability together with a low power consumption and low maintenance. Third generation microfocusing sealed tube sources, such as  $I\mu S$  (Incoatec Microfocus Source), are now well established and give a performance beyond that of typical traditional X-ray sources used in single crystal diffraction, powder diffraction and small angle scattering applications - at power settings far below 1 kW.

We will present selected results from single crystal diffraction experiments with  $I\mu S$  for Mo- $K_{\alpha}$  radiation. The flux density obtained from this source is about 1.5 times the flux density of a 5 kW rotating anode plus graphite monochromator on a 100  $\mu\text{m}$  sample. In our experiments with very small crystals ( $\leq 50 \mu\text{m}$ ), we have achieved gain factors of up to 3. Our results show that this source-optics-combination for  $I\mu S$  is very well suited for the structure determination on small crystals, as well as on medium sized samples.

### 03.02.04

**Cluster Analysis in Crystallography.** C.J. Gilmore, G. Barr, W. Dong, A. Parkin, C.C. Wilson, WestCHEM, Dept. of Chemistry, Univ. of Glasgow, Glasgow G12 8QQ, Scotland, UK.

Cluster analysis is a widely used tool for partitioning data into groups or clusters according to their similarities. It is widely used in the data mining literature, but its use in crystallography is surprisingly limited. Presented here is a general overview of the method and its applications as used by the crystallography groups at Glasgow:

Classifying the results of high throughput screening experiments that search for polymorphs, salts and co-crystals using powder X-ray (and optionally Raman) data to analyse the results [1,2].

Unravelling the results of Cambridge Structural Database searches - making sense of 4,000 hits or more. [3,4].

Comparing whole crystal structures - putting the comparisons on a numerical footing [5].

Validating structures derived from powder data where the data quality is poor [6].

In all cases, the basic methodology is the same, but it is important to have the correct visualization tools, and this paper will discuss dendrograms, metric multidimensional scaling, parallel coordinate plots, silhouettes - in fact, many of the tools of modern data mining techniques - with applications to crystallography.

C.J. Gilmore, G. Barr, and J. Paisley, *J. Appl. Cryst.* (2004). 37, 231-242. G. Barr, W. Dong and C.J. Gilmore, *J. Appl. Cryst.* (2004). 37, 243-252. G. Barr, C.J. Gilmore, A. Parkin and C.C. Wilson, *J. Appl. Cryst.* (2005). 38, 833-841. A. Parkin, G. Barr, C.J. Gilmore and C.C. Wilson, *CrystEngComm.* (2006). 8, 257-264. A. Parkin, G. Barr, W.

Dong, C.J. Gilmore, D. Jayatilaka, J.J. McKinnon, M.A. Spackman and C.C. Wilson, *CrystEngComm* (2007), 9, 648-652. G. Barr, W. Dong, C.J. Gilmore, A. Kern, A. Parkin and C.C. Wilson, *Z. Krist.* (2007), 26, 209-214.

### 03.02.05

**Anomalous Dispersion for Dummies.** Carla Slebodnick, Dept. of Chemistry, Virginia Polytechnic Inst. and State Univ., Blacksburg, VA.

Friedel's Law no longer holds if anomalous scattering atoms are present in an acentric crystal. This is the take home message in any crystallography textbook. Exactly why this inequality happens, however, is rarely addressed at the non-expert level. This presentation aims to explain to the non-expert how anomalous dispersion contributes to the overall intensity of a reflection, as well as why anomalous scattering causes Friedel's law to fail for acentric structures. The structure factor equation will be used to analyze and summarize the 4 possible cases: 1) centric space group without anomalous dispersion, 2) centric space group with anomalous dispersion, 3) acentric space group without anomalous dispersion, and 4) acentric space group with anomalous dispersion.

## 04.01 Challenges in Industrial Crystallography

### 04.01.01

**Crystal Structure of Synthetic Hydrotungstite,  $O_2(OH)_2(H_2O)$ .** James A. Kaduk, Judith B. Sentman, INEOS Technologies, P.O. Box 3011 MC F-9, Naperville IL 60563 USA.

Hydrotungstite,  $WO_3(OH)_2(H_2O)$  or  $H_2WO_4(H_2O)$  (PDF 00-016-0166 and 00-018-1420) occurs as an alteration product in the oxidized zone of a hydrothermal tungsten ore deposit at the Calacalani mine in Bolivia, and thin films of hydrotungstite have been used as humidity sensors. It is reported to crystallize in  $P2/m$  with  $a = 7.379(5)$ ,  $b = 6.901(5)$ ,  $c = 3.748(5)$  Å, and  $\beta = 90.36(16)^\circ$ . The powder pattern of a greenish yellow precipitate from an inductively-coupled plasma (ICP) specimen preparation of a W-containing sample matched that of hydrotungstite well, but the unit cell and powder pattern were more complicated than had been reported. Application of lattice matching techniques to the reported unit cell yielded the chemically-plausible analogue "yellow molybdenic acid",  $MoO_3(H_2O)_2$ , which has the ICSD formula type AX5. A further search for Mo-containing compounds having this formula type yielded the mineral sidwellite,  $MoO_3(H_2O)_2$ , which crystallizes in  $P2_1/n$  with  $a = 10.487(1)$ ,  $b = 13.850(1)$ ,  $c = 10.617(1)$  Å, and  $\beta = 91.62(9)^\circ$ , and has been studied using neutron powder diffraction. The sidwellite cell is an  $8\times$  supercell of the reported hydrotungstite cell, and the sidwellite structure served as a good initial model for a Rietveld refinement of the hydrotungstite structure. The hydrogen positions were determined by a quantum chemical geometry optimization, which permitted analysis of the hydrogen bonding pattern. The structure consists of corner-sharing layers of tilted  $WO_6$  octahedra in the  $ac$  plane. Pointing into the interlayer region *trans* to each tungsten atom are a coordinated water molecule and a W=O group. The interlayer region is occupied by water molecules, which are hydrogen bonded to the layers. Hydrotungstite is properly formulated  $[WO_3(H_2O)](H_2O)$ . The structure of the mineral tungstite,  $WO_3(H_2O)$ , has been reported, but the topologies of the layers in sidwellite and tungstite differ. A combination of quantum calculations and Rietveld refinement was used to determine the best model for the topology of the hydrotungstite layer. The quantum calculations help establish the relative energies of hydrotungstite and tungstite.

### 04.01.02

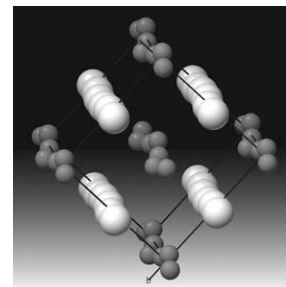
**Electron Crystallography in Petroleum Industrial Research.** Douglas L. Dorset, Advanced Characterization, ExxonMobil Research & Engineering Co., Inc., 1545 Rt. 22E, Annandale, NJ.

Circumventing limitations to powder diffraction studies of microcrystalline preparations imposed by reflection overlap, electron crystallography now plays an important role for quantitative structural characterization in the petroleum industry, as illustrated by a few examples: The study of new zeolitic frameworks began with improved unit cell and space group determinations based on non-overlapped reciprocal lattices constructed from tilted single microcrystals. Electron crystallography has made important contributions to the determination of new microporous structures, e. g., MCM-22, BEC, SSZ-48 and others. In other applications, graphitization processes, transforming vacuum residua to cokes, are easily studied by electron diffraction, giving insights into local and long range order. Polyolefin structures have been determined, most recently the chain packing of precisely branched atactic polyethylenes. Finally, the polydisperse linear chain assemblies of petroleum waxes in solid solutions and phase separated mixtures are uniquely elucidated by electron crystallography.

### 04.01.03

**Charge Flipping Approach to Inorganic Structures from Powder Data.** Scott T. Misture, Kazuo Inamori School of Engineering, Alfred Univ., Alfred, NY 14802.

Of course a range of problems are encountered in the academic laboratory, from bio-inspired materials to classic metals. Add to this variety the extensive use of in-situ analysis and one finds many new phases, some of which are stable under ambient conditions and others that are not. The talk will highlight several interesting examples where charge flipping was of great value in providing at least partial structures from very low-quality powder data. Although we undertake even some synchrotron studies, the samples of primary interest are often not well-ordered, or the high temperature study is particularly difficult, resulting in poor data. We show, however, that even poor data can be used successfully in structure solution. Combining charge flipping with rigid body simulated annealing has been very useful for structures with tricky light atom positions, and will also be discussed.

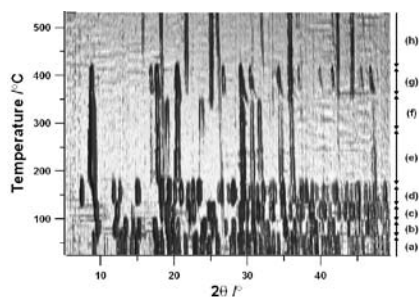


### 04.01.04

**2D-XRPD, a Powerful Tool for the Understanding of Various Defects in Sorel Cements.** Robert Dinnebie, Max-Planck Inst. for Solid State Research, Stuttgart, Germany, Kunihisa Sugimoto, Rigaku Corp., Tokyo, Japan, Thomas Schlecht, Ostfildern, Germany.

In 1867, the French physicist Stanislas Sorel found out that high quality cement is formed by mixing magnesium oxide with an aqueous solution of magnesium chloride. Many properties of this Sorel cement are superior to those of Portland cement (e.g. high fire resistance, low thermal conductivity, high resistance to abrasion etc). On the down side, magnesia cements shows a poor resistance to prolonged exposure to water. During the binding process, ternary magnesium oxychloride phases are formed, which are of key importance for the properties of the cement. A detailed knowledge of the ternary phase diagram  $MgO-MgCl_2-H_2O$  is therefore necessary to understand

the properties of these cements and to perform any type of qualitative or quantitative phase analysis. The use of inferior components and/or excess water leads to various problems like the occurrence of cracks in expanding or contracting floors, decoloring, crumbling floors etc. To investigate



2D-XRPD in dependence on temperature showing the decomposition of Bischofite

these phenomena, we recently determined the missing crystal structures of all binder phases from XRPD data and performed 2D-XRPD measurements in dependence on temperature and humidity<sup>1-4</sup>. This allowed us to perform full QPA by the Rietveld method in a routine fashion and to understand/avoid certain types of defects in these floors.

<sup>1</sup> K. Sugimoto, R.E. Dinnebier, T. Schlecht. (2006). *J. Appl. Cryst.* 39, 739-744.

<sup>2</sup> K. Sugimoto, R.E. Dinnebier, T. Schlecht. (2007). *Powder Diffraction* 22(1), 64-67.

<sup>3</sup> K. Sugimoto, R.E. Dinnebier, J.C. Hanson (2007). *Acta Cryst.* B63, 235-242.

<sup>4</sup> K. Sugimoto, R.E. Dinnebier, T. Schlecht, *Acta Cryst.* (2007). B63, 805-811.

#### 04.01.05

**Chemical Crystallography as a Routine Analytical Tool for Preparative Chemists.** Charles Campana, Michael Ruf, Joerg Kaercher, Bruker AXS Inc., 5465 E. Cheryl Pkwy, Madison, WI 53711.

The precise knowledge of the molecular geometry of molecular compounds is becoming increasingly important in nearly all fields of chemical and biological research. The three-dimensional atomic coordinates obtained from crystallographic studies are often used as a starting point for most molecular modeling, drug design and molecular orbital calculations. Indeed, many of the most significant advanced in structural chemistry would not have been possible without the results obtained from crystallographic analysis.

Historically, the determination of crystal structures was considered to be a costly and time-consuming process, carried out on expensive research instruments operated by trained x-ray crystallographic specialists. Although convenient and timely access to x-ray diffractometers is essential to chemists who are carrying out frontier research, for many industrial chemists, the routine use of x-ray crystallography has been limited because they are often required to send samples away to off-site service laboratories for analysis and then wait days (or months) for the results.

The introduction of a new generation of automatic, economical x-ray crystallography systems allows synthetic chemists to produce atomic resolution, 3-D structures in their own laboratories, quickly and easily, at the touch of a button. These new instruments take structure determination to the next level by automating all aspects of the structure determination: from sample mounting and alignment through data collection, structure solution and refinement, validation and report generation. For the first time, x-ray structure determination may be used by preparative chemists as a routine analytical tool.

#### 04.01.06

**Trials and Tribulations in Pursuit of Structure-Based Drug Design Targeted at MAPKAP Kinase-2.** Ravi Kurumbail, Nicole Caspers, Huey Sheng Shieh, William Stallings, Gennadiy Poda, Jennifer Pawlitz, Teena Stults, Richard Broadus, Suzanne Bolten, Robin Weinberg, Marvin Meyers, David Anderson, Robert Mourey,

Pfizer Global R&D, Groton and St. Louis Laboratories, Groton, CT.

MAPKAP Kinase-2 (MK-2) is a protein kinase that mediates one of the signaling cascades involved in the biosynthesis of the pro-inflammatory cytokine, tumor necrosis factor (TNF). It functions downstream of p38 kinase which has been a highly successful target for structure-based drug design. In contrast, structural biology studies of MK-2 have been a challenge for most. While well-formed crystals of MK-2 can be readily obtained under a variety of salt-based crystallization conditions, most of them suffered from limited diffraction resolution and lack of reproducibility in diffraction. A large initiative was undertaken in our laboratories to profile nearly 100 protein constructs in order to identify a suitable protein reagent for structural biology studies. Several of these were studied in crystallization experiments but we were unable to improve the diffraction resolution beyond 3.0 Å because of high solvent content (>70%). In spite of these challenges, we were successful in obtaining crystal structures of MK-2 complexed with AMP-PNP, staurosporine and a limited number of proprietary inhibitors. These structures have enabled us to dock real and virtual compounds to MK-2 and to engineer specificity over other kinases. Moreover, the crystal structures have played a significant role in optimization of binding affinity and to improve pharmacokinetic properties of lead compounds. The presentation will highlight some of our key learnings gleaned from the pursuit of this challenging structural biology target.

#### 04.01.07

**Overcoming Protein Expression, Purification and Crystallization Obstacles in Support of Structure-Based Drug Design in Industry.** Melissa Harris, D. Alessi, S. Archer, C. Banotai, W. Brown, J. Dyer, S. Foltin, S. Guru, J. Hagadorn, S. Holley, J. Knafels, A. McCarthy, L. McDowell, M. Melnik, R. Miller, W. Mueller, J. Ohren, D. Omecinsky, R. Sarver, C. Spessard, F. Sun, Y. Xhu, B. Finzel, Pfizer R&D, Ann Arbor, MI.

Structure-based drug design (SBDD) technology has come a long way since its early days in 1980s. While significant strides have been made over the last decade, there are still several technical hurdles that emerge repeatedly in our pursuit of developing a robust system for iterative SBDD. The first essential step is production of sufficient quantities of high quality, soluble protein suitable for crystallization. Intelligent, parallel construct design and experimentation in multiple expression systems has proven critical for success at this step of the process. Presence of appropriate tags helps to streamline protein purification and facilitate the production of homogenous protein that is indispensable for success in the subsequent crystallization. Identification and optimization of a co-crystallization or soaking protocol to rapidly produce diffraction quality co-crystals with multiple compounds continues to be a challenge for us even with the technological advances in crystallization robotics and imaging. Utilization of specialized screens and seeding techniques has proven essential for many difficult projects. Lastly, co-crystallization with small molecules that have poor aqueous solubility or weak binding affinity for the target can be daunting and we have taken advantage of biophysical methods such as Isothermal Denaturation or NMR for triaging compounds. The presentation will highlight how we approached these common technical obstacles in our pursuit of the structural biology studies of NMDA receptor NR1 and select antibacterial targets.

#### 04.01.08

**Crystallography as a Screening Tool: Challenges of Fragment Based Drug Discovery.** John Spurlino, Frank Lewandowski, Cindy Milligan, Carsten Schubert, Marta Abad, Richard Alexander, Johnson & Johnson PRD, LLC, Extton, PA.

Fragment Based Drug Discovery is a tool employed by industry to discover binding pockets for small fragments to utilize in developing novel compounds. The challenge of determining the large number of structures required for a fragment based discovery program necessitated the use of a number of unique paradigms to effectively drive chemistry. High throughput screening of crystallization conditions and optimization of multiple leads to provide several chances for the best crystal system for soaks increases the efficiency. Typically 1000 compounds are screened in sets of five, which requires at least 200 crystals to soak, freeze, mount, collect, process, refine and examine. Robotics and automation software help increase the throughput, but effective use of time requires the use of a screening paradigm at the first level.

## 06.01 Structure and Dynamics of Hydrogen Bonded Systems

### 06.01.01

**Neutron Diffraction Studies of Hydrogen Bonded Systems: An Overview.** Thomas F. Koetzle, IPNS, Argonne National Laboratory, Argonne, IL 60439.

Beginning with work carried out in the 1950's at the first generation of research reactors, including, e.g., pioneering studies at Oak Ridge on ice and at Harwell on KDP, neutron diffraction studies have played a central role in advancing our understanding of hydrogen bonding. In the 1960's and '70's, with the advent of high flux reactor sources, the range of materials investigated was extended, and work included systematic single-crystal studies of amino acids and sugars, as well as the first neutron structures of proteins. Structures of metal hydrides were studied and revealed unconventional hydrogen bonding involving hydrogen bound to metals. Beginning around 1980, studies at pulsed neutron sources have made increasingly important contributions.

Despite much progress, applications of single-crystal neutron diffraction continue to be extremely flux limited and are constrained by the requirement for mm-size crystals for many problems. These limitations are currently being addressed through the realization of powerful instruments at a new generation of neutron sources, including the TOPAZ and MaNDi single-crystal diffractometers under development at SNS.

Following an historical overview, this presentation will illustrate topics of current interest with results of recent single-crystal work, including studies at IPNS of andrographolide, an active diterpenoid natural product, and tetraacetyethane, a material that exhibits a temperature-dependent migration of the proton in its short, strong intramolecular O-H-O hydrogen bond.

Work supported by the U.S. Department of Energy, Office of Science, Office of Basic Energy Sciences, under contract DE-AC02-06CH11357.

### 06.01.02

**Complementary Single-crystal X-ray Diffraction and Neutron Powder-diffraction Studies of Hydrogen-bonded Small-molecule Systems at High Pressure.** D.R. Allan, Diamond Light Source, Harwell Science and Innovation Campus, Oxfordshire UK.

Molecular materials contain a rich spectrum of interaction types from the relatively weak van der Waals interaction, through the more moderate ionic bond and hydrogen bond, to the relatively strong covalent bond — and as these interactions depend strongly on intermolecular distance, high-pressure provides a powerful means of altering their relative hierarchy of strengths. A systematic

study of molecular systems at high pressure is rewarding, therefore, as competition between the various interaction types can cause phase transitions and also lead to the alteration of structure property relationships. Over the past few years, along with only a very small number of other groups world-wide, we have been conducting a systematic series of studies on the high-pressure crystal structures of a variety of molecular systems including: organic materials, such as simple functional compounds, pharmaceutical compounds, amino acids, peptides, and more recently proteins; along with inorganic materials, such as the oxoacids and their hydrates, and the hydroxide salts of selected alkali ( $\text{MOH}\cdot n\text{H}_2\text{O}$ , where  $M = \text{Li, K, Na and Cs}$ ). All of these systems have been studied, principally, with single-crystal x-ray diffraction techniques and as many of the compounds are liquids at ambient conditions, the crystals have often required to be grown within the diamond-anvil cell once the compound has been “frozen” on the application of pressure. Once the crystal structures have been solved with x-ray techniques we use complementary time-of-flight high-pressure neutron powder-diffraction methods to establish the full structures, including the accurate location of the hydrogen atoms. A number of examples from our most recent work will be discussed including our studies of the oxoacids sulphuric acid, phosphoric acid, nitric acid and a number of their hydrate phases.

### 06.01.03

**Solid-state NMR and the Strong Hydrogen Bond.** G.S. Harbison, J. Zhou, X. Zhao, Dept. of Chemistry, Univ. of Nebraska at Lincoln, Lincoln, NE 68588, USA.

NMR has been used to examine the potential surface and wavefunction for hydrogen atom displacement in strongly hydrogen-bonded systems. The measurement of dipolar couplings allows us to probe the root-mean cubed average distance between hydrogens and other NMR nuclei, such as  $^{14}\text{N}/^{15}\text{N}$  and  $^{17}\text{O}$ , while other interactions, such as the electric quadrupole interaction of the hydrogen-bond deuteron with the local electric field gradient, and the chemical shielding of the proton or deuteron, are also sensitive probes of the state of the hydrogen bond. The temperature-dependence of these interactions allows us to explore low-lying vibrationally excited states, which are particularly important in low-barrier systems. All of these interactions can be calculated using modern quantum chemical methods, with the caveat that careful attention has to be paid to the full vibrational wavefunction, including anharmonic cross-couplings that are neglected in conventional normal mode analysis. Finally, crystallographic perturbations can be introduced by the isotopes themselves, ranging from conventional equilibrium isotope effects, to genuine isotope-driven polymorphism. We will review our results on several such systems, including isotope partitioning in the sulfate salt of the Zundel cation ( $\text{H}_3\text{O}_2^+$ ), isotopomeric polymorphism in 4-methylpyridinium pentachlorophenolate, and the very short hydrogen bond in several enolized 2,4-dicarbonylic molecules.

### 06.01.04

**Quantum Wavepacket *ab initio* Molecular Dynamics: An Approach for Computing Dynamically Averaged Vibrational Properties Including Critical Nuclear Quantum Effects.** Srinivasan S. Iyengar, Dept. of Chemistry and Physics, Indiana Univ., Bloomington, IN 47408.

We have introduced a computational methodology to study vibrational spectroscopy in clusters inclusive of critical nuclear quantum effects. This approach is based on the recently developed quantum wavepacket *ab initio* molecular dynamics method that combines quantum wavepacket dynamics with *ab initio* molecular

dynamics. The computational efficiency of the dynamical procedure is drastically improved (by several orders of magnitude) through the utilization of wavelet-based techniques combined with time-dependent deterministic sampling to achieve stable, picosecond length, quantum-classical dynamics of electrons and nuclei in clusters. The dynamical information is employed to construct a novel cumulative flux/velocity correlation function, where the wavepacket flux from the quantized particle is combined with classical nuclear velocities to obtain vibrational properties such as vibrational density of states. Computational extensions along with demonstration of the procedure for a few example problems will be discussed. It is shown that the approach provides good agreement with experimental results. In addition, a general hierarchical procedure is also provided, based on electronic structure harmonic frequencies, classical *ab initio* molecular dynamics, computation of nuclear quantum-mechanical eigenstates, and employing quantum wavepacket *ab initio* dynamics to understand vibrational spectroscopy in hydrogen-bonded clusters that display large degrees of anharmonicities. If time permits, applications of the method to biological hydrogen tunneling problems will also be discussed.

[1] I. Sumner and S.S. Iyengar, "Quantum Wavepacket *ab Initio* Molecular Dynamics: An approach for computing dynamically averaged vibrational spectra including critical nuclear quantum effects". *J. Phys. Chem. A*, 111, 10313-10324 (2007).

[2] J. Jakowski, I. Sumner and S.S. Iyengar, "Computational Improvements to Quantum Wavepacket *Ab Initio* Molecular Dynamics using a potential-adapted, time-dependent deterministic sampling technique". *Journal of Chemical Theory and Computation* 2 1203-1219 (2006).

[3] S.S. Iyengar and J. Jakowski, "Quantum Wavepacket *Ab Initio* Molecular Dynamics: An approach to study quantum dynamics in large systems". *J. Chem. Phys.* 122 114105 (2005).

### 06.01.05

**Deep Inelastic Neutron Scattering Measurements of the Born-Oppenheimer Potential and Dynamics of Hydrogen Bonds.** George Reiter, Univ. of Houston, Houston, TX.

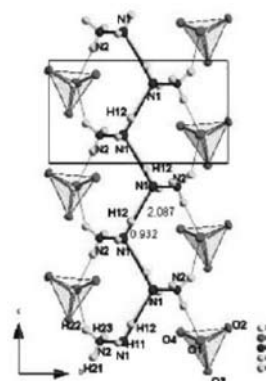
Deep Inelastic Neutron Scattering (DINS) is neutron scattering at energies for which the impulse approximation is accurate, corresponding to energy transfers on the order of 2-100 meV. In this limit, one can measure the momentum distribution of the protons in the hydrogen bond. The momentum distribution, determined by the localization of the proton in its surroundings, is a very detailed local probe of those surroundings. In the case of symmetric non-interacting bonds, the data provides a direct measurement of the Born-Oppenheimer potential surface. We will describe the first such measurement on the superprotonic conductor  $\text{RB}_3\text{H}(\text{SO}_4)_2$ . The measurements are sensitive to coherent motion of the protons, as in a double-well potential. This shows up as an oscillation in the momentum distribution, if the temperature is less than the tunnel splitting. We will describe several systems in which coherence appears, including hydrogen intercalated in Mn, KDP, water in nanotubes and water in the pores of xerogel.

### 06.01.06

**Single Crystal Neutron Diffraction and Inelastic Neutron Scattering Spectroscopy of Proton Conductor Lithium Hydrazinium Sulfate.** M.R. Hudson<sup>1</sup>, P.M.B. Piccoli<sup>2</sup>, A.J. Schultz<sup>2</sup>, B.S. Hudson<sup>1</sup>, <sup>1</sup>Syracuse Univ., Syracuse, NY, 13244, <sup>2</sup>IPNS, Argonne National Laboratory, Argonne, IL 60439.

Lithium hydrazinium sulfate ( $\text{LiN}_2\text{H}_5\text{SO}_4$ ) is a proton conductor containing an  $\text{NH}_2^-$  hydrogen bonded chain along the *c*-axis. In this material, the protonic conductivity of  $\text{LiN}_2\text{H}_5\text{SO}_4$  is highly anisotropic being very much higher along this axis than perpendicular to it. Single crystal neutron diffraction studies were carried out on  $\text{LiN}_2\text{H}_5\text{SO}_4$  in both the protonated and perdeuterated forms at 20 K and 298 K with both crystallizing in space group  $Pna2_1$ . The protonated  $\text{LiN}_2\text{H}_5\text{SO}_4$

has cell dimensions of  $a=9.907 \text{ \AA}$ ,  $b=8.917 \text{ \AA}$ ,  $c=5.12 \text{ \AA}$  at 20 K. These cell parameters increase as a function of temperature in the protonated form. INS spectra were also collected for  $\text{LiN}_2\text{H}_5\text{SO}_4$  using both the HRMECS spectrometer at IPNS and TOSCA at ISIS. INS spectra of oriented single crystals with the *c*-axis parallel and perpendicular to the incoming radiation will also be discussed. Periodic DFT calculations on the material were performed and the results compared to the INS spectra. Neutron diffraction is important in locating the hydrogen atoms leading to better assignment of the vibrational spectra.

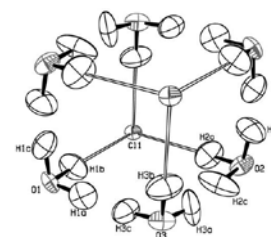


Work at ANL was supported by the U.S. DOE, Office of Basic Energy Sciences, under contract DE-AC02-06CH11357.

### 06.01.07

**Neutron Diffraction Structure of a Discrete Dichloride Hexahydrate Cube as a Tris(diisopropylamino)cyclopropenium Salt.** P.M. Piccoli,<sup>a</sup> A. Schultz,<sup>a</sup> O. Curnow,<sup>b</sup> J. Butchard,<sup>b</sup> D. Garrett,<sup>b</sup> R.G.A.R. Maclagan,<sup>b</sup> <sup>a</sup>IPNS, Argonne National Laboratory, Argonne IL, 60439 USA, <sup>b</sup>Dept. of Chemistry, Univ. of Canterbury, Christchurch 8140, New Zealand.

The nature of hydrogen bonding in solvated ion clusters is fundamental to the understanding of solvation phenomena, and is relevant to many scientific fields. While the structures of polar, monohalide hydrate clusters have been investigated experimentally and theoretically, relatively little is known about dihalide hydrates. The structure of an isolated dichloride hexahydrate cube was first determined by X-ray diffraction,<sup>1</sup> however at that time it was not possible to distinguish between two possible hydrogen bonding arrangements. Single crystal neutron diffraction at 20 K has since determined that the hydrogen positions along the  $\text{O}\cdots\text{O}$  edges of the cube are half-occupied, resulting in an average structure with molecular  $D_{3d}$  symmetry. Hydrogen atoms that lie along the  $\text{O}\cdots\text{Cl}$  edges of the cube are fully occupied. Structural comparisons to similar hexahydrate cubes will be drawn.



Work at ANL was supported by the U.S. DOE, Office of Science, Office of Basic Energy Sciences, under contract DE-AC02-06CH11357.

(1) Butchard, J. R.; Curnow, O. J.; Garrett, D. J.; Maclagan, R. G. A. R. *Angew. Chem. Int. Ed.* 2006, 45, 7550.

## 09.01 Understanding the Nano-scale Using Small Angle Scattering

### 09.01.01

**Dynamics and Thermodynamics at the Nanoscale.** Michael Mackay, Erin McGarrity, Phillip Duxbury, Amalie Frischknecht, Anish Tuteja, R. S. Krishnan, Jon Kiel, Jon Seppala, Erica Tseng., Chemical Engineering and Materials Science, Michigan State Univ., 2527 Engineering Bldg., East Lansing, MI 48824.

Here I discuss how nanoparticles influence the physical and transport properties of polymeric materials. Firstly, and most importantly, we find that small angle neutron scattering can be used to show when the two components produce stable blends. Nanoparticle – polymer miscibility is dictated by following the proper thermodynamic route and

a few simple heuristics we have developed. The most important is that the nanoparticle should be smaller than the polymer radius of gyration.

Only when stable mixtures are produced do unusual phenomena occur. The polymer melt's viscosity is found to decrease upon nanoparticle addition, a phenomenon we discovered, at odds with Einstein's century old prediction. Furthermore, X-ray photon correlation spectroscopy was used to show that the nanoparticles diffuse  $\sim 100$  times faster than predicted by the Stokes-Einstein relation. Other material properties such as: thermal degradation, electrical conductivity, tensile modulus, etc. are all found to be enhanced. Thus, it appears that provided a stable nanoparticle-polymer mixture is formed, then unusual and enhanced properties result.

However, even when stable blends are expected it is possible to promote phase separation near a solid substrate. This segregation can be controlled to make unique one, two and three-dimensional structures in thin polymer films as confirmed by a combination of neutron reflectivity and transmission electron microscopy measurements.

So, in summary, we are able to control polymer-nanoparticle miscibility in the bulk and in thin films to manufacture interesting and useful materials. All this would not be possible without scattering techniques to characterize the materials.

### 09.01.02

**New Insight into Hierarchical Structures of Carbon Black Dispersed in Polymer Matrices: A Combined Small-angle Scattering Study.** Tadanori Koga<sup>1,2</sup>, Takeji Hashimoto<sup>1,3,4</sup>, Mikihiro Takenaka<sup>1,3</sup>, Kazuya Aizawa<sup>5</sup>, Naoya Amino<sup>6</sup>, Masao Nakamura<sup>1,7</sup>, <sup>1</sup>Hashimoto, Polymer Phasing Project, ERATO, JST, Japan, <sup>2</sup>Chem. & Molecular Eng., Dept. of Matls Science & Eng., Stony Brook Univ., Stony Brook, NY, <sup>3</sup>Dept. of Polymer Chem., Kyoto Univ., Katsura, Kyoto, Japan, <sup>4</sup>Advanced Science Research Center, <sup>5</sup>Quantum Beam Science Directorate, Japan Atomic Energy Agency, Ibaraki, Japan, <sup>6</sup>Yokohama-rubber, Co., Kanagawa, Japan, <sup>7</sup>ZEON Co., Kanagawa, Japan.

Using a combined ultra-small-angle and small-angle scattering (CSAS) method of neutrons and x-rays, we investigated hierarchical structures of carbon black (CB) highly loaded in polyisoprene (PI) and poly(styrene-random-butadiene) copolymer (SBR) under mechanical field (defined respectively as CB/PI and CB/SBR) as well as in toluene under a sonic field (defined as CB/Toluene). In order to analyze each structure level comprising the hierarchical structures of CB from the CSAS profiles, we employed the unified Guinier/power-law approach proposed by Beaucage [Beaucage, G. *J. Appl. Cryst.* 1995, 28, 717]. Furthermore, in order to extract not only sizes but also shapes of the structure elements, we developed a modified approach, in which the Guinier scattering function utilized in the Beaucage approach was replaced by a form factor of the corresponding structure. Comparison of the scattering profiles from CB/PI and CB/SBR with CB/Toluene clarified that (i) the smallest structure elements of CB (that further form mass-fractal objects) in PI and SBR were not an unbreakable unit of the CB filler which resulted after sonification in toluene but were instead composed of the several unbreakable units bounded together by polymer chains (defined as "dispersible units") and (ii) sizes and shapes of the dispersible units depended on the polymer matrix: Its size was larger in PI than in SBR. (iii) Moreover, the enlarged size of the dispersible unit in PI was found to enlarge the upper cutoff length of the mass-fractal structure in PI, while the mass-fractal dimensions themselves remained unchanged between PI and SBR. Hence, the detailed characterizations of the hierarchical structures by using CSAS shed new light on the dispersion process of the filler compound in the polymer matrix.

### 09.01.03

**Composite Polymer – Nanoparticles Aggregates in Mixed Complex Systems Seen by Small Angle Neutron Scattering.** F. Boué<sup>1</sup>, J. Gummel<sup>1</sup>, F. Cousin<sup>1</sup>, C. Chevigny<sup>1</sup>, N. Jouault<sup>1</sup>, S. Lorrain<sup>1</sup>, S. Charles<sup>1</sup>, G. Bourget<sup>1</sup>, D. Gigmes<sup>2</sup>, J. Jestin<sup>1</sup>, <sup>1</sup>Laboratoire Léon Brillouin CNRS-CEA UMR Saclay, Gif-sur-Yvette France, <sup>2</sup>CROPS UMR, Normandie-Niemen Marseille Cedex 20 France.

We will discuss two examples of "large" (several tenth nanometers) aggregates obtained from mixtures of two species, and including the two species. These aggregates are well defined in size, and the precise origin remains to understand in detail, while their properties can be interesting. In both cases, the available range of density of neutron scattering length given by deuteration of one species makes possible a quite accurate description of their content.

The first type is observed when mixing a synthetic polyelectrolyte solution, Sodium Poly(Styrene Sulfonate), NaPSS, with a model globular protein solution, lysozyme, in a given region of the ( $C_{\text{prot}}$ ,  $C_{\text{polyel}}$ ) phase diagram. Mixtures of aqueous solvent with normal water and heavy water ( $D_2O$ ) can be made in such proportions that they have the same density of scattering length, so have a nul contrast either with the protein, or with the polyelectrolyte. Because NaPSS can be deuterated, the contrast with the other species can be reasonably high. Under such conditions, we have been able :

to show the existence of compact aggregates containing both polyelectrolyte chains and proteins. At low  $q$ , by fitting to the signal of a sphere, the front factor gives access to an effective contrast, and by comparing the lysozyme signal and the NaPSS scattering, we can titrate in situ the concentration of each species, hence the charge ratio.  $-/+_{\text{actual}}$  which we can compare to the introduced one  $-/+_{\text{intro}}$ .

- to localize labeled counterions in the complexes and show that their release through all solvent is an entropic contribution towards aggregate formation.

-to extrapolate the form factor of an individual chain inside the complexes, using normal and deuterated chains, and show that a particular overlapping threshold is the trigger of cluster formation.

The second type of aggregates is obtained when dispersing polymer grafted nanoparticles inside a matrix of the same polymer. No solvent is present, grafted polymers can be deuterated or not.

- although grafting increases compatibility between the matrix, and the nanoparticles, they appear to form clusters, with well defined characteristic separation distances.

- under stretching, the scattering of the system will be discussed to show that additional information can be gained by understanding how internal structure, global shape, and mutual arrangement of these mixed soft-hard clusters are deformed.

In both cases, such better description allows to imagine some applications for these structures.

### 09.01.04

**Nanoscale Structure and Dynamics of Self-assembling Soft Matter Probed by Synchrotron SAXS.** Theyencheri Narayanan<sup>1</sup>, Drazen Zanchi<sup>2</sup>, Anuj Shukla<sup>1</sup>, Thomas Weiss<sup>1</sup>, Michael Gradzielski<sup>3</sup>, <sup>1</sup>European Synchrotron Radiation Facility, Grenoble, France, <sup>2</sup>Laboratoire de Physique Theorique et Hautes Energies, Univ. Pierre et Marie Curie, Paris, France, <sup>3</sup>Stranski Laboratorium fur Physikalische und Theoretische Chemie, Technische Univ. Berlin, Berlin, Germany.

While scattering techniques are widely used to probe nanoscale structure and dynamics of self-assembled soft matter, applications to

dilute and low contrast systems are often restricted by the detection limit. Combining the high brightness of modern synchrotron sources with state-of-the-art detectors, this detection limit can be significantly lowered. The ability to detect weak structural features and probe the underlying dynamics by means of scattering techniques offers new possibilities which are not easily accessible to other methods. Probing the structural kinetics could in turn provide a comprehensive understanding of the underlying nanostructure. This will be demonstrated by means of two examples. In the first case, the self-assembly of model membranes (unilamellar vesicles) was investigated by time-resolved scattering experiments following the rapid mixing of anionic and cationic or zwitterionic micelles. In this case, subtle differences in the synergy of surfactant pairs lead to significant difference in the membrane properties which are more strikingly manifested in the dynamics of self-assembly. Optimizing these conditions is critical to obtain desired membrane properties especially in applications such as nano-reactors or templates. The second example, deals with the self-assembly of casein micelles with plant tannins. Casein micelles constitute the major protein component of milk which are hierarchically self-assembled complexes containing large quantity of calcium phosphate well above the solubility limit. The nanoscale organization of calcium phosphate within the protein matrix as such is a longstanding question. Many tanniferous plants use the tannin-induced protein aggregation as a protection mechanism against parasitic viruses or bacteria. Rather surprisingly, tannins make the casein micelle superstructure more compact without changing the global size but at the same time modify the nanoscale substructure completely. The route by which the tannins disintegrate the nanostructure within casein micelles in turn provides a possibility to systematically elucidate the underlying nanostructure.

#### 09.01.05

**SANS and SAXS Characterization of Block Copolymer/Bioinspired Mineral Nanocomposite Gels.** P. Thiagarajan<sup>a</sup>, Umai Kanapathipillai<sup>b</sup> and Surya Mallapragada<sup>b</sup>, <sup>a</sup>Argonne National Lab, Argonne, IL 60439, <sup>b</sup>Dept. of Chemical and Biological Engineering and Ames Laboratory, Iowa State Univ., Ames, IA 50011.

We investigated the gels of a family of pentablock copolymers based on Pluronic<sup>®</sup> triblock copolymers conjugated with end blocks such as anionic poly(acrylic acid) and zwitterionic poly(sulfobetaine) as templates for the synthesis of bioinspired calcium phosphate nanocrystals. The pH dependent ionization of the end blocks and the temperature and concentration dependent phase behavior of the middle Pluronic, together, enable tuning of the structure and the templating property of the gels. We used Small angle neutron and X-ray scattering to characterize the length scales and the structural organization of the block copolymer and the inorganic nanoparticle phases, respectively. In the case of neat Pluronic<sup>®</sup> F127 gel and that used as a template for the synthesis of calcium phosphate at pH 1 and 3, SAXS showed the FCC ordering in the polymer phase. At pH 1 the effect of templating of F127 is reflected in a higher d spacing of the FCC phase. The gels of the neat pentablock copolymer with poly(2-diethylaminoethyl methacrylate) end blocks exhibit broad peaks. At pH 1 we observe a similar increase in d spacing of the first order peak in the presence of calcium phosphate, demonstrating the templating effect of the gel. At pH 3 the neat pentablock gel shows poor ordering and in the presence of inorganic only the first order peak is seen. However, strong SAXS signals are observed, indicating the aggregation of inorganic nanocrystals, that swamped the signal from the polymer phase. To circumvent this problem we successfully exploited the complementarity of the SAXS and SANS to characterize a number of neat and inorganic templated pentablock

polymer gels and delineated the structural features of inorganic and phases, respectively. In this presentation the effects of the chemical structure of the end blocks, polymer concentration and pH on the structural features of the neat and inorganic laden gels will be discussed.

Work benefited from the use of 12-ID at APS and IPNS funded by the U.S. DOE, BES, under contract No. DE-AC02-06CH11357 to U Chicago Argonne, LCC. Ames Laboratory is operated for the U.S. DOE by Iowa State University under contract No DE-AC02-07CH11358.

#### 09.01.06

**Characterization of Proteins Entrapped in Sol-Gel Materials Using Small Angle Neutron Scattering.** Hugh O'Neill, Guangming Luo, Volker Urban, Qiu Zhang, Alexis Rae Del Castillo, Center for Structural Molecular Biology, Chemical Sciences Div., Oak Ridge National Laboratory, TN 37831.

The entrapment of proteins using the sol-gel route provides a means to retain its native properties and artificially reproduce the molecular crowding and confinement experienced by proteins in the cell allowing investigation of the physico-chemical and structural properties of biomolecules at the biotic/abiotic interface. The biomolecules are spatially separated and "caged" in the nano-structured gel matrix but solutes can freely permeate the matrix. In this study, small angle neutron scattering was used to investigate the conformation of perdeuterated *Aequorea coerulescens* green fluorescent protein (GFP) entrapped in silica sol-gels to gain insight into the effects of caging and crowding on protein structure. It was also of interest to determine the effect of the protein on the structure of the silica gel. A series of gels were prepared with and without GFP. By matching the contrast of the silica gel to the solvent it was possible to overcome the coherent scattering background contribution that arises from the gel matrix. A structural model of GFP, based on the scattering contribution of the protein under such conditions, will be presented. The structural properties of the silica gel matrix were characterized in the absence and presence of protein using a mass fractal model.

Oak Ridge Natl. Lab. is managed and operated by UT-Battelle, LLC for the U. S. Department of Energy under contract No. DE-AC05-00OR22725. The submitted manuscript has been authored by a contractor of the U.S. Government under Contract DE-AC05-00OR22725. Accordingly, the U.S. Government retains a nonexclusive royalty-free license to publish or reproduce the published form of this contribution, or allow others to do so, for U.S. Government purposes.

#### 09.01.07

**Understanding Shear Induced Collapse of Entropically Stabilized Lamellar Phases.** P.D. Butler<sup>1</sup>, V. Stöppelkamp<sup>2</sup>, L. Porcar<sup>1,3,4</sup>, W.A. Hamilton<sup>5</sup>, <sup>1</sup>NCNR, <sup>2</sup>Technische Univ. München, <sup>3</sup>Univ. of Maryland, <sup>4</sup>ILL, <sup>5</sup>ANSTO.

Dilute lamellar phases have been known for many decades. Helfrich explained nicely how the bilayer undulations produce an effective pressure on their neighbors so that these systems can be seen as entropically stabilized. Since then theories have predicted that the lamellar phase must cease to exist at high shear rates when the undulations are damped to the point that the necessary periodic separation can no longer be supported. However it is difficult to obtain strong, direct evidence for this collapse as the shear rates at which it would take place are not normally experimentally accessible. Recently we showed that by using sugar as an inert viscosity enhancer, the collapse could be clearly demonstrated with the lowest volume fractions of membrane "collapsing" at the predicted shear rates. For higher concentrations however, some deviation from theory occurred. To better understand the details of the collapse requires a shear dependent structural study. This presents another experimental

challenge as the ideal technique involves neutron scattering through a shear cell. However, the lamellar orientation is such that the beam must traverse the cell tangentially and the considerable hydrogen in the sugar provides a high background signal while simultaneously substantially attenuating the scattering of interest. We have developed a new system using deuterated glycerol as the viscosity enhancer. Not only is the problem of measuring tangentially significantly alleviated, but higher viscosities than with sugar are achievable. We discuss the new system and present simultaneous viscosity and SANS data through the lamellar phase collapse. Finally, some preliminary work using the DANSE SliceView prototype to elucidate the collapsed structure is presented.

## 09.02 Macromolecular Dynamics

### 09.02.01

**The Impact of Collective Molecular Dynamics on Physiological and Biological Functionalities of Artificial and Biological Membranes.** Maikel C. Rheinstädter, Dept. of Physics and Astronomy, Univ. of Missouri-Columbia, Columbia, MO 65211.

We use neutron, X-ray and light scattering techniques to determine dynamical and structural properties of artificial and biological membranes. The combination of various techniques enlarges the window to length scales from the nearest-neighbor distances of lipid molecules to more than  $10^6$  m, covering time scales from about 0.1 ps to 1 s. The main research objective is to quantify collective molecular fluctuations in these systems and to establish relationships to physiological and biological functions of the bilayers, such as transmembrane transport. The motivation for this project is twofold: 1) By understanding fundamental properties of bilayers at the microscopic and mesoscopic level, we aim to tailor membranes with specific properties such as permeability and elasticity. 2) By relating dynamical fluctuations to physiological and biological functions, we can gain a deeper understanding of the bilayers on a molecular scale that may help optimizing the transmembrane transport of certain drugs. We show how bilayer permeability, elasticity and inter protein excitations can be determined from the experiments.

M.C. Rheinstädter et al., Phys. Rev. Lett. 93, 108107 (2004); Phys. Rev. Lett. 97, 048103 (2006); Phys. Rev. E 75, 011907 (2007); J. Vac. Soc. Technol. A 24, 1191 (2006).

### 09.02.02

**XPCS Studies of Nanoparticle Motion within Glassy Polymer Melts.** Robert Leheny, Hongyu Guo, Gilles Bourret, R. Bruce Lennox, Mark Sutton, James Harden, Physics & Astronomy, Johns Hopkins Univ., Baltimore, MD.

We report x-ray photon correlation spectroscopy (XPCS) experiments to investigate the motion of nanometer-scale gold particles within polystyrene melts of molecular weight between 2K and 100K g/mol. The gold particles, with radius of approximately 2 nm, are dispersed in a highly dilute concentration (volume fraction 0.0004) and are functionalized with polystyrene chains to stabilize them against aggregation. At high temperature above the glass transition of the polystyrene, the dynamic structure factor measured with XPCS indicates diffusive motion of the nanoparticles with a diffusion coefficient that obeys a Vogel-Fulcher temperature dependence, as expected for polymer melts near the glass transition. When the melts are quenched to lower temperature, the nature of the observed dynamics changes. Specifically, the XPCS results indicate non-diffusive motion that can be modeled as strain in the melt in response to localized stress relaxation. These dynamics evolve with time following the quench, suggesting that they are coupled to aging

of the polymer.

Such non-diffusive motion has been observed previously in disordered soft solids, such as colloidal gels and concentrated emulsions, and in several polymer systems including block copolymers, nanocomposites, and filled elastomers. However, in these previous polymeric materials, complicating factors such as mesophase ordering and particle-particle interactions have been identified as likely playing a role in creating the internal stress that drives the strain-like motion. Our observation of such motion from a dilute concentration of stable nanoparticle tracers indicates that it is an intrinsic property of quenched melts.

### 09.02.03

**Dynamics of Threadlike Micelles Studied by Neutron Spin Echo.** Dobrin P. Bossev<sup>1</sup>, Wei-Ren Chen<sup>2</sup>, Paul D. Butler<sup>3</sup>, Lee Magid<sup>4</sup>; <sup>1</sup>Indiana Univ., Bloomington, IN, <sup>2</sup>Oak Ridge National Lab; <sup>3</sup>NIST, Center for Neutron Research; <sup>4</sup>Univ. of Tennessee.

Micellar morphology in aqueous solutions of ionic surfactant is strongly dependent on the nature and the concentration of the present counterions. Cationic surfactants such as cetylpyridinium (CPyX) can be directed to form micelles with cylindrical cross-section by varying the counterions, X. Some organic counterions that penetrate the micellar interface, especially substituted chloro- and hydroxybenzoates (salicylates) and tosylate, produce very large, semi-flexible threadlike micelles organized in a branched network. Such morphologies are of great interests since they result in solutions with strong viscoelastic behavior. In this study we have used neutron spin echo (NSE) spectroscopy to investigate the dynamics of threadlike micelles of CPy surfactant combined with salicylate and Cl<sup>-</sup> ions at different surfactant concentrations and counterion environment. Using Zilman-Granek theory we can extract the persistent length and calculate the micellar flexibility of linear, branched and entangled threadlike micelles. These results are compared to those from a nonionic surfactant (C<sub>12</sub>E<sub>3</sub>) that forms micelles with cylindrical morphology but without pronounced viscoelastic behavior.

### 09.02.04

**Protein Dynamics in the Crystalline State.** Jeremy C. Smith, Oak Ridge National Laboratory, Oak Ridge, TN 37831.

The combination of X-ray crystallography, neutron scattering and computer simulation to elucidate motions in proteins will be examined.

### 09.02.05

**Dynamical Coupling Between Hydration Water and Proteins: A Comparison of Membrane and Soluble Proteins.** K. Wood<sup>\*,‡,£</sup>, D. Tobias<sup>°</sup>, G. Zaccari<sup>\*</sup>, M. Weik<sup>#</sup>, <sup>#</sup>Inst. de Biologie Structurale, Grenoble, France, <sup>\*</sup>Inst. Laue Langevin, Grenoble, France; <sup>‡</sup>Max-Planck-Inst. für Biochemie, Martinsried, Germany; <sup>°</sup>Univ. of California, Irvine, USA.

The relationship between the dynamics of a protein and its environment is important for the understanding of protein function in a cellular context. The dynamics of specific components of a complex system can be explored by combining neutron spectroscopy with isotope labelling. Here we studied deuterated systems, hydrated in H<sub>2</sub>O and the corresponding hydrogenated systems in D<sub>2</sub>O, to study separately hydration water and macromolecular dynamics, respectively. We present data on the maltose binding protein, a soluble protein, where we find a dynamical transition in the hydration water at 210 K triggers a transition in the protein at the same temperature, implying a tight

coupling between the two entities (1). A similar study performed on the purple membrane revealed a different scenario for the dynamical relationship between a membrane protein, bacteriorhodopsin, and its hydration water (2): a transition occurs at 200 K in the water, and in the protein at 250 K. For both the soluble and membrane protein studies presented, molecular dynamics simulations at temperatures spanning the observed transitions reproduced well the experimental data (1,2). The simulations then allow an investigation at the microscopic level of the observed transitions: the hydration water transitions observed are due to the onset of translational diffusion. The results suggest an important role of lipids in the dynamical control of membrane proteins.

1. Wood, K., Frölich, A., Paciaroni, A., Moulin, M., Hartlein, M., Zaccai, G., Tobias, D. J. & Weik, M. *in preparation*.

2. Wood, K., Plazanet, M., Gabel, F., Kessler, B., Oesterhelt, D., Tobias, D. J., Zaccai, G. & Weik, M. (2007) *Proc Natl Acad Sci U S A (in press)*.

## 09.02.06

**Comparison of Relaxation Dynamics in Saturated and Unsaturated Oriented Lipid Bilayers.** Hirsh Nanda<sup>1</sup>, Victoria Garcia-Sakai<sup>2</sup>, Susan Krueger<sup>1</sup>, Joseph E. Curtis<sup>1</sup>, <sup>1</sup>NIST Center for Neutron Research, National Inst. of Standards and Technology, Gaithersburg, MD 20899, <sup>2</sup>ISIS Pulsed Neutron & Muon Source, Rutherford Appleton Laboratory, Chilton, Didcot OX11 0QX, UK.

Neutron scattering provides a technique for directly probing the dynamical processes of membrane systems. Backscattering in particular is sensitive to time scales on the order of picoseconds to nanoseconds and length scales of angstroms to nanometers. Mobility in this regime can inform upon local interactions responsible for material properties and dynamical transitions in lipid membranes. The interpretation of backscattering spectra however, can be greatly augmented by molecular dynamics (MD) simulations. These models can provide detailed insights into the molecular underpinnings of dynamical relaxations. In this work, we present a comparison of DOPC and DMPC lipid dynamics characterized in both the liquid and gel phases, with neutron backscattering and MD simulations. Key differences in phase transition behavior between the two lipids are discussed. Insights into the different dynamic properties of the two lipid systems are gained from simulation and experiment. Finally, the use of coarse grain models to model lipid dynamics on longer length and time scales is briefly discussed.

## 10.01 Cool Structures

### 10.01.01

**Using X-ray and Neutron Diffraction to Study Complexes of Cyanuric Acid with Group I Metals: Neutron Crystallography from an X-ray Perspective.** Gary S. Nichol,<sup>a,b</sup> William Clegg,<sup>b</sup> Matthias J. Gutmann,<sup>c</sup> Duncan M. Tooke.<sup>b</sup> <sup>a</sup>Dept. of Chemistry, Univ. of Arizona, Tucson, AZ, USA, <sup>b</sup>School of Natural Sciences (Chemistry), Newcastle Univ., Newcastle upon Tyne, UK; <sup>c</sup>ISIS Neutron Facility, Rutherford Appleton Laboratory, Chilton, Oxfordshire, UK.

We have been interested in structural studies of cyanuric acid (CYH) for some time, in particular the coordination chemistry of CYH and CY<sup>-</sup> with the s-block metals<sup>1</sup> and weak hydrogen bonding studies in molecular complexes with high values of Z'.<sup>2</sup>

We found that s-block metal complexes of CY<sup>-</sup> exhibit a wide range of chemical and crystallographic ranging from small crystal size (requiring data collection at the Synchrotron Radiation Source) through twinning, disorder and finally in the case potassium

complexes, problems of simple chemical identity caused by charge balance issues.

For one of the complexes the chemical formula was proposed from X-ray diffraction studies as 1.5K<sup>+</sup>:2CY<sup>-</sup> as a result of crystallographically-imposed mirror symmetry, with a disordered hydrogen atom assumed to be a likely solution to our problem of unbalanced charges. Neutron diffraction studies were carried out to determine the behaviour of this supposedly disordered hydrogen. Unexpected results, along with some thoughts on neutron diffraction from an X-ray perspective, will be discussed.

G.S. Nichol, W. Clegg, M.J. Gutmann and D.M. Tooke, *Acta Cryst.*, 2006, B62, 5, 798–807. G. S. Nichol and W. Clegg, *Cryst. Growth Des.*, 2006, 6, 2, 451–460.

### 10.01.02

**Novel Cationic Copper Coordination Networks Constructed from 4, 4'-Bisimidazolybiphenyl Ligand.** Liangming Hu, Elinor Spencer, Carla Slebodnick, Brian E. Hanson, Dept. of Chemistry, Virginia Tech, Blacksburg, VA.

The reaction of copper nitrate with 4, 4'-bisimidazolebiphenyl (BIB) in the presence of phosphoric acid leads to the formation of two new hybrid network structures. The BIB ligand is relatively rigid and has only rotational flexibility about the long axis of the molecule. The first structure consists of a novel cationic copper phosphate 8-ring that encapsulate a hydroxide ion. The structure of the 8-ring consists of 4 copper (II) ions and 4 phosphorus atoms. These rings are linked into chains by parallel BIB ligands. The second structure, formed at higher pH, is constructed from similar 8-rings that are linked into a chain by fusing the 8-rings at one copper site. These two new copper compounds show simple paramagnetic behavior. An additional copper - BIB framework with sulfate will also be discussed.

### 10.01.03

**Pressure Induced Coordination Changes in K-Co-Oxomolybdates.** J.M. Engel<sup>ad</sup>, H. Ahsbahs<sup>b</sup>, H. Ehrenberg<sup>cd</sup>, H. Fuess<sup>d</sup>, <sup>a</sup> Virginia Tech Crystallography Laboratory, Blacksburg, VA, USA, <sup>b</sup>Inst. for Mineralogy, Petrology & Crystallography, Marburg, Germany, <sup>c</sup>Inst., for Complex Materials, IFW Dresden, Dresden, Germany, <sup>d</sup>Inst. for Materials Science, Darmstadt Univ. of Technology, Darmstadt, Germany.

Pressure-induced phase transitions with coordination changes and a one-to-one correspondence between the atomic sites of both phases are pseudoreconstructive: on one hand, bonds are broken, characteristic for reconstructive phase transitions. On the other hand, no diffusion of atoms takes place, which is typical for displacive phase transitions. During a systematic study of K-Co-oxomolybdates, high-pressure single-crystal experiments on K<sub>2</sub>Co<sub>2</sub>(MoO<sub>4</sub>)<sub>3</sub> and K<sub>4</sub>Co(MoO<sub>4</sub>)<sub>3</sub> have been carried out. The structures of several high-pressure phases of these compounds could be solved and refined and show pseudoreconstructive phase transitions. At ambient pressure K<sub>2</sub>Co<sub>2</sub>(MoO<sub>4</sub>)<sub>3</sub> and K<sub>4</sub>Co(MoO<sub>4</sub>)<sub>3</sub> belong to the class of ortho-oxomolybdates with [CoO<sub>6</sub>]-octahedra connected via edge sharing to form tetramers and dimers, respectively. The tetramers or dimers are cross-linked by [MoO<sub>4</sub>]-tetrahedra but the [MoO<sub>4</sub>]-tetrahedra are not connected to each other.

The high-pressure phase of K<sub>2</sub>Co<sub>2</sub>(MoO<sub>4</sub>)<sub>3</sub> includes [MoO<sub>5</sub>]-pyramids and [MoO<sub>6</sub>]-octahedra, in addition to [MoO<sub>4</sub>]-tetrahedra. The behaviour of K<sub>4</sub>Co(MoO<sub>4</sub>)<sub>3</sub> is more complex with three new high-pressure phases between ambient pressure and 7.9(1) GPa. The structures of these phases thus exhibit a stepwise increase in Mo coordination from tetrahedra via pyramids to octahedra with increasing pressure.

**10.01.04**

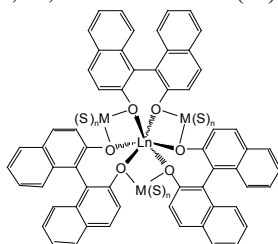
**Structural Variation Within Homo- and Heterometallic Uranium(VI) Phosphonocarboxylates.** Karah E. Knope<sup>a</sup>, Christopher L. Cahill<sup>a,b</sup>, <sup>a</sup>Dept. of Chemistry, George Washington Univ., Washington, DC, 20052, <sup>b</sup>Geophysical Laboratory, Carnegie Inst. of Washington, Washington, DC, 20015.

Uranium(VI) containing materials represent a structurally diverse class of compounds. The crystal chemistry is dominated by the  $\text{UO}_2^{2+}$  cation wherein the oxygen atoms of this moiety are nominally terminal. Through the judicious choice of organic linkers or the addition of second metal centers, we have assembled a catalog of uranium (VI) containing inorganic/organic hybrid materials that exhibit a range of structural motifs and topologies. Presented here is a survey of novel homo- and heterometallic uranium phosphonocarboxylates synthesized under hydrothermal conditions. These materials illustrate the influence of structural features such as metal-ligand coordination, intermolecular interactions, and incorporation of transition metal cations (including cation-cation interactions) on the dimensionality and overall topology of the resulting architectures.

**10.01.05**

**Structural Studies of Lanthanide Binolate Complexes Important as Catalysts in Asymmetric Synthesis.** Patrick J. Carroll, Dept. of Chemistry, Univ. of Pennsylvania, Philadelphia, PA.

Structure determinations of a series of Lanthanide Binolate complexes,  $\text{M}_3(\text{solv})_n(\text{BINOLate})_3\text{Ln}$ : ( $\text{M} = \text{Li}, \text{Na}, \text{K}$ ;  $\text{Ln} = \text{lanthanide(III)}$ ),  $\text{solv} = \text{THF}, \text{py}, \text{DMEDA}, \text{TMEDA}$ ; BINOLate = dianion formed by deprotonation of 1,1'-binaphthyl-2,2'-diol and derivatives presented numerous crystallographic challenges (crystal instability,  $Z' > 1$ , disorder, trigonal and hexagonal space groups, heavy atom chiral structure determination). These complexes are important catalysts in a large number of asymmetric syntheses and are themselves complicated molecules with intricate geometries.

**10.01.06**

**Complex Packing Motifs Encountered in a  $\beta$ -cyclodextrin/Adamantine Inclusion Compound.** G.D. Enright, K.A. Udachin, J.A. Ripmeester, Steacie Inst. for Molecular Sciences, National Research Council, Ottawa ONT., Canada.

$\beta$ -cyclodextrin has been shown to form 1:1 inclusion compounds with a number of different guest species. Initial studies of  $\beta$ -cyclodextrin with adamantane had revealed that the crystals as formed were orthorhombic ( $P2_12_12$ ) with four cyclodextrin and four adamantane molecules in the asymmetric unit ( $Z' = 4$ ). The host cyclodextrin molecules are stacked in columns with the adamantane guests located in cavities between the donut-shaped host molecules. Within a column three out of four consecutive host molecules are aligned with their primary hydroxyl groups on the same side. Every fourth host molecule is flipped so that the primary hydroxyl group is on the opposite side. This flipped molecule forms a hydrogen-bonded dimer with a neighboring molecule. Recently we had an opportunity to reexamine crystals that had been stored in water for several years. Remarkably all the crystals examined had been transformed to a triclinic form with  $Z' = 6$  and close to 600 non-hydrogen atoms in the asymmetric unit. The host molecules are still arranged in columns but all host molecules form H-bonded dimers with an adjacent molecule. The host:guest ratio still appears to be 1:1 but the guests

are disordered over seven distinct sites within the channels formed by the cyclodextrin columns.

**10.01.07**

**New Hosts for Fullerenes.** M.M. Olmstead, J.U. Franco, J.M. Hammons, Dept. of Chemistry, Univ. of California, Davis, CA 95616 USA.

The design of curved hosts for the organization of fullerenes into predictable or ordered structures continues to be a challenge. While porphyrins have had good success as cocrystallization agents for fullerenes, their van der Waals interactions primarily consist of  $\pi$ - $\pi$  interactions between curved and flat surfaces. Endohedral fullerenes, in particular, still tend to exhibit significant disorder in both the orientation of the cage atoms and in the positions of the interior atoms when cocrystallized with porphyrins. The interaction between the convex fullerene surface and an appropriate concave host is potentially stronger, and the position of external dipoles may have beneficial effects on the removal of disorder. Toward this end, we have examined a series of curved host molecules that are derivatives of and variations on the bi-saddled molecule Ni(TMAA), first described as a cocrystallizing agent for [60]fullerene by Raston et al. in 1998. One of our modified molecules forms an ordered, layered structure with [60]fullerene. Several other modified molecules have interesting structures in their own right, showing classical hydrogen bonding as well as non-classical interactions, the strength of which may preclude their ability to accommodate fullerenes in cocrystals.

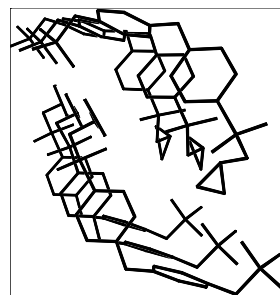
**10.01.08**

**Crystal Packing in the Thiirane-based Gelatinase Inhibitor (*S*)-4-(4-(thiiran-2-ylmethylsulfonyl)phenoxy)phenyl methanesulfonate, a System with  $Z' = 6$ .** Bruce C. Noll, Mijoon Lee, Dusan Heseck, Mayland Chang, Shahriar Mobashery, Dept. of Chemistry and Biochem., Univ. of Notre Dame, Notre Dame, IN.

We have shown that a novel class of thiirane inhibitors is highly selective in inhibition of gelatinases, enzymes important in cancer progression and metastasis. For mechanistic and structure-function studies, we have prepared over 100 derivatives, a number of which have been crystallized for structure determination.

Of more than 400 000 structures reported in the Cambridge Structural Database, only 269 possess  $Z' \geq 6$ .

In our studies of (*S*)-4-(4-(thiiran-2-ylmethylsulfonyl)phenoxy)phenyl methanesulfonate, we discovered the pure enantiomers crystallized in  $P1$  with  $Z' = 6$ . Five of the six independent molecules appear identical, while the sixth differs in the orientation of the thiirane moiety. The structure of the racemic mixture crystallizes in  $P1$  with  $Z' = 1$ . The relationships



between the molecules will be examined in some detail to attempt to understand the causes leading to this somewhat rare result.

## 13.01 Incommensurate & Modulated Structures

### 13.01.01

**Introduction to Modulated Structures.** Lee M. Daniels, Christer Svensson, Rigaku Americas Corp., The Woodlands, TX, and Materials Chemistry, Lund Univ., Lund, Sweden.

The ease with which we collect diffraction data with area detectors has simplified the lives of crystallographers, but also has revealed that non-traditional diffraction effects are not as uncommon as we once thought. Diffuse scattering, twinning, and incommensurate modulations appear regularly during otherwise routine crystallographic analyses. Modulated structures arise from a variety of different phenomena, and each of these can be thought of as some kind of perturbation of the short-range order that is assumed in a traditional 3-dimensional crystal structure. A beginner's description of these effects will be given, along with examples, and a straightforward, understandable approach to indexing and refining the main and satellite reflections will be described.

### 13.01.02

**Crystallographic Computing System Jana2006.** M. Dusek, V. Petricek, Lukas Palatinus, Inst. of Physics of the ASCR, v.v.i., Na Slovance 2, 182 21 Prague, Czech Republic.

Jana2006 has been developed for more than 25 years as a crystallographic tool focused to solution, refinement and interpretation of difficult, especially modulated structures. It calculates structures having up to three modulation vectors from powder as well as single crystal data measured with X-ray or neutron diffraction. The input diffraction data can be unlimitedly combined, the combination of powder neutron data with single crystal X-ray data being a typical example.

The structure solution can be done using the built-in charge flipping algorithm or by calling an external direct methods program. Jana2006 can handle multiphase structures (for both powder and single crystal data), merohedric twinning as well as twinning leading to partial overlap of diffraction spots, commensurate and composite structures. It can be used for investigation of structure families derived from a basic commensurate structure. It contains powerful transformation tools for symmetry (group-subgroup relations), cell parameters and commensurate-supercell relations. Wide scale of constrains and restrains is available including a powerful rigid body approach and possibility to define a local symmetry affecting only part of the structure. Multipole refinement is also available. The latest development of Jana2006 concerns magnetic structures.

The lecture will introduce Jana2006. The basic features and style of work will be demonstrated using typical examples.

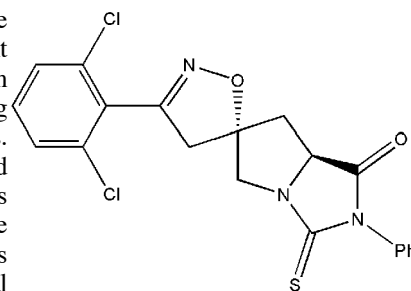
This research is supported by the grant 202/06/0757 of the Grant agency of the Czech Republic.

### 13.01.03

**New Software Tools for Indexing and Processing of Modulated Structures.** Michael Ruf<sup>a</sup>, Marilyn Olmstead<sup>b</sup>, Trixie Wagner<sup>c</sup>, Andreas Schönleber<sup>d</sup>, <sup>a</sup>Bruker AXS Inc. Madison, WI, <sup>b</sup>Dept. of Chemistry, Univ. of California, Davis, CA, <sup>c</sup>Novartis Institutes for BioMedical Research, Basel, Switzerland, <sup>d</sup>Laboratory for Crystallography, Univ. of Bayreuth, Germany.

Modulated structures distinguish themselves by their lack of conventional lattice periodicity. Their diffraction patterns exhibit

additional satellite reflections which prevent the structure's elucidation using traditional indexing and processing methods. Indexing modulated structures by integers requires more than three indices (3+d). This loss of the 3-dimensional periodicity necessitates



the concept of (3+d)-dimensional superspace in which periodicity is recovered and atoms are treated as d-dimensional atomic domains [1]. The aperiodic structure in real space is then interpreted as a cut through this (3+d) dimensional structure in superspace.

The use of two-dimensional detectors (CCD and IP) has now become a standard in crystallography laboratories. These detectors are not only great tools for experts in the field of modulated structures, but they also allow researchers to collect incommensurately modulated datasets without knowledge of the problem at hand, only to face difficulties during structure determination when applying conventional methods. With the high throughput of modern facilities we see more and more modulated structures.

The presentation focuses on new software tools for handling datasets of modulated structures, discussing several aspects of indexing, selecting q-vectors, data integration, and scaling procedures using a dataset of the spirooxazolineproline derivative below. We will also present the compound's superspace structure.

[1] Jansen, T., Janner, A., Looijenga-Vos, A., de Wolff, P.M. (1992), *International Tables for Crystallography*, Vol. C, IUCr / Kluwer Academic Publishers, Dordrecht, The Netherlands, pp. 797–835.

### 13.01.04

**Generating and Visualizing One-dimensional Incommensurate Structural Modulations.** Branton J. Campbell, Harold T. Stokes, Brigham Young Univ., Dept. of Physics & Astronomy, Provo, UT.

Phase transitions that result in incommensurate structural modulations are widely observed in crystalline solids and are relevant to a broad range of physical phenomena in magnetic, electronic, optical, and structural materials. While the (3+1)-dimensional superspace-group symmetries associated with one-dimensional modulations have been tabulated, the order parameters that produce these modulations have not been explored in detail. Using group-theoretical methods, we have developed a unique and exhaustive enumeration of the isotropy subgroups belonging to irreducible representations of the 230 crystallographic space groups at all incommensurate k-points. As a practical matter, we will demonstrate that anyone with a Java-enabled web browser can take advantage of these developments to generate and interactively visualize almost any incommensurate modulation involving occupancies or displacements, and save it to a CIF for subsequent refinement against single-crystal or powder diffraction data. These capabilities are now part of the online ISODISPLACE software tool, which requires little or no knowledge of group-theory from the user.

### 13.01.05

**There and Back Again: A Crystallographer's Tale of Modulated Protein Crystals.** J.J. Lovelace, J. C. Porta, Gloria E.O. Borgstahl, Eppley Inst. for Research in Cancer and Allied Diseases, Omaha, NE 68198.

Knowledge of the structure of actin in its various conformations

is essential for understanding the dynamics of cell motility. A key regulator of actin polymerization is profilin, an abundant protein that associates with actin in a 1:1 complex that serves as a precursor for actin filament formation. Several structures of actin, in the monomeric state and in complexes with actin binding proteins, such as profilin, have been solved. Several models of actin filaments and their function have been discussed, but the low resolution structural data cannot validate any of these.

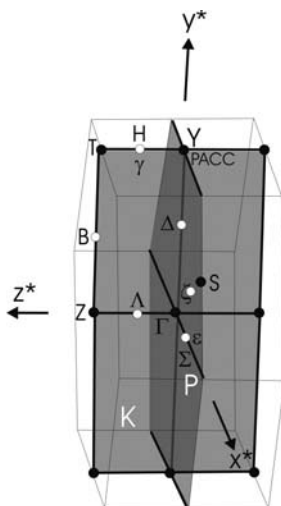
Slightly acidic pH is known to dissociate profilin from actin and to stabilize actin filaments. When profilin:actin crystals are transferred to an acidic pH, they exhibit a modulated diffraction pattern. It has been speculated that these modulated crystals contain actin filaments, or an intermediate state of actin filament formation.

This epic tale will detail our successes and failures as we have pursued solving the structure of modulated profilin:actin crystals. This modulation was first observed in the early 1990's but was shelved as there was no way of processing the data at that time. With recent advances in the field of modulated crystallography for small molecules and vast improvements in computing power, we thought it was time to revisit this problem. We have worked through the problems associated with reproducing the original data and can now purify, crystallize and modulate the complex at will. We were able to get the unit cell and q-vector from room temperature modulated images. The q-vector suggests the modulation is incommensurate. Most recently we have been able to cryo-trap the modulated state and have a low resolution average structure from that data.

### 13.01.06

**Predicting Possible Modulated Phases in the Layered Perovskite-Like  $A_2BX_4$  Structures of Propylammonium Tetrachlorometallates.** I.P. Swainson, Canadian Neutron Beam Centre, NRC, Chalk River, ON, Canada.

Propylammonium (PA) tetrachlorometallates show complex behavior (phases  $\alpha$ - $\beta$ - $\gamma$ - $\delta$ - $\epsilon$ - $\zeta$ ) on cooling, including re-entrant commensurate, and multiple incommensurate phases, characterized by radically differing modulation wavevectors. The layer-perovskites are characterised by layers of corner-bonded octahedra separated by layers of amine cations. An examination of tilt and buckling modes of a plane of untilted octahedra (modelling the  $\alpha$ -phase), performed using the Rigid Unit Mode (RUM) approximation, reveals sheets of pure tilts at  $\{\xi, \frac{1}{2}, \zeta\}$  and buckling modes at every wavevector. These RUMs are a class of acoustic modes, characterized as a modulation of the layers: tilts are a special case involving no displacement and yield commensurate phases, whereas buckling modes contain elements of tilting and translation of the octahedra, and generally yield incommensurate phases. The tilted  $Cmca$  structure of the re-entrant  $\beta$ - and  $\delta$ -phases can be viewed as the parent structure of all the incommensurate phases. This has a much restricted set of buckling modes with wavevectors lying in only two planes that intersect at a line of tilts. All the wavevectors of the incommensurately modulated phases ( $\gamma, \epsilon, \zeta$ ) lie in the planes. The eigenvectors of the tilts are examined to determine the corresponding irreducible representations; those of the connecting buckling modes were determined by compatibility relations. Possible



space groups were deduced from the codes isotropy and iso(3+1)d. This shows that the connectivity of the inorganic component determines the possible modes of distortion of the entire system, and thereby delimits the possible incommensurate structures.

### 13.01.07

**Disordered and Modulated Vanadium Oxide Structures.** Peter Y. Zavalij, Dept. of Chemistry and Biochemistry, Univ. of Maryland, College Park, MD 20742, USA.

There has been much interest recently in vanadium oxides and their intercalates due to their application in oxidative catalysis and often unique magnetic and electrochemical properties. The vanadium oxide frameworks have rich crystal-chemistry [1] and intercalation chemistry due to the variety of vanadium coordination polyhedra and wide range of oxidation states. This work presents disordered structure of two ammonium trivanadates, and temperature effect on the disorder. In both structures only orientation of ammonium ions is disordered that has not been noticed in prior routine structure determination. Interestingly, when cooled down, one structure becomes ordered with twice larger unit cell, while the other one turns into incommensurate structure with two-dimensional modulation. Another structure, tetramethyl ammonium tetravanadate, shows 1D incommensurate modulation at room temperature but becomes 2D commensurate structure at low temperature.

This presentation also details integration and refinement technique of modulated structures. Comparison of the modulation in vanadium oxide structures with known isostructural metal oxide frameworks reveals that framework metal and intercalated species drastically affect type of modulation.

1. Zavalij P.Y. and Whittingham M.S. *Acta Cryst.*, B55, 627-663 (1999).

### 13.01.08

**Study of Structure-property Relationship in Novel Inorganic Compounds with Disorder and/or Long Range Order.** Olivier Gourdon, Delphine Gout, Gordon J. Miller, Thomas Proffen, Eric Bauer, Joe D. Thompson.

For decades we have limited our knowledge of the atomic structure of materials to the average structure. However the *real* materials possess atomic arrangements which are usually more complicated and deviate from this standard description.

The interest of disorder structures and long range order structures is to possess interesting properties (from anti ferromagnetism to superconductivity, giant magnetocalorimetry...) and usually the properties are governed or linked to their atypical structure (*local structure/defect or modulated waves*). For these materials a traditional crystallographic approach fails BUT we have now tools and the knowledge to treat the deviation from the average structure.

The goal of this presentation is to discuss the different tools which allowed us to understand the different range order and especially to highlight the special aspect of the aperiodicity. Numerous examples will be used to emphasize our structural descriptions.

Recently, we have investigated by both neutron and X-ray diffraction the crystal structures of a series of  $La_{1-x}Ce_xIn_3$  ( $x=0.02, 0.2, 0.5, 0.8$ ) intermetallic compounds. Our results emphasize atypical atomic displacement parameters (ADP) for the In and the rare-earth (R.E.) sites. Depending of the  $x$  value, the In ADP presents either "an ellipsoidal" elongation (La rich compounds) or a "butterfly-like" distortion (Ce rich compounds). These deformations have been understood by theoretical techniques based on the band theory and

are the result of hybridization between conduction electrons and  $4f$ -electrons.

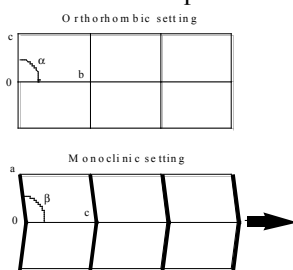
Another example will be the crystallographic reinvestigation of the  $\gamma$ -brass (Cu-Zn) binary system using neutron diffraction. This study shows that the  $\gamma$ -brass structure is not unique but part of a family of intergrowth compounds. (3+1) D description has been used to solve the structures and a 1D quasicrystal description has been proposed.

## 13.02 Solid State Transformations & Reactions

### 13.02.01

**Concomitant Polymorphism and Twinning of Dichloro-bis( $\eta^5$ -tert-butylcyclopentadienyl)titanium(IV).** Ilia A. Guzei, Håkon Hope, Amitabha Mitra, Univ. of Wisconsin-Madison and Univ. of California-Davis, USA.

The title compound (I) crystallizes in the orthorhombic space group  $P2_12_12_1$  ( $a=10.7028$  Å,  $b=12.8508$  Å,  $c=6.5844$  Å,  $V=905.62$  Å<sup>3</sup>) at 298 K (phase I). The Ti complex resides on the two-fold axis with  $Z'=2$ . Complex (I) undergoes two sharp enantiotropic phase transitions upon cooling. The first transformation occurs at 293 K to yield a unit cell with a doubled  $c$  axis ( $a=10.5539$  Å,  $b=12.8757$  Å,  $c=13.0817$  Å,  $V=1777.66$  Å<sup>3</sup> at 175 K) and the orthorhombic space group  $P2_12_1$  (phase II). The doubling of the unit cell volume results in the addition of a translational component to the two-fold rotational symmetry in the  $c$  direction, and now the complex is in a general position. The second transition takes place at 147 K to convert the single crystal into a merohedrally twinned crystal with two monoclinic components of half the size ( $a=6.5486$  Å,  $b=12.7403$  Å,  $c=10.5529$  Å,  $\beta=92.327^\circ$ ,  $V=879.71$  Å<sup>3</sup> at 100 K) in the monoclinic space group  $P2_1$  (phase III). The Ti complex remains in a general position. The concomitant phase transition and twinning necessarily result in the loss of symmetry along the  $a$  and  $c$  axes and can be thought of as taking the  $c$  axis in phase II and “pulling” (shifting) it in the positive direction to generate the twinning in phase III (see diagram). The unique angle widens as the temperature is lowered. The variable temperature study of the selected crystal was conducted in an automated mode on a Bruker SMART APEX2 diffractometer with Cu  $K\alpha$  radiation while the exact transition temperatures were manually pinpointed with Mo  $K\alpha$  radiation.



### 13.02.02

**The Syntax, Chemistry and Crystallography of Solid-state Reactions in Molecular Crystals: Visiting the Past to Understand the Present.** Bruce M. Foxman, Dept. of Chemistry, Brandeis Univ., Waltham, MA 02454.

Solid-state reactions offer both an exceptional opportunity and a distinct challenge. In optimal cases, irradiation or thermolysis of crystals can lead to unusual stereospecific intermolecular reactions that cannot be accomplished in solution. The challenge lies in discovering new classes of materials capable of solid-state reactivity, and in determining the both the chemical and crystallographic principles which govern their behavior. While solid-state reactions are rare, there are valuable search protocols to discover new reactions

or (better still) new *classes* of reactions. The presentation will first review certain critical studies from a limited number of senior scientists in order to define the scope and terminology of solid-state reactions as well as approaches to designing, discovering and understanding extant or new solid-state reactions. This is a *required* exercise in view of certain recent publications which demonstrate a lack of understanding of major concepts. We will focus on reactions of four main types: (i) one-phase topotactic reactions (**T1**); (ii) topotactic reactions involving two or more phases (**Tn**); (iii) reactions in which a single crystal becomes polycrystalline (**SP**); (iv) reactions in which a single crystal produces (at least initially) an amorphous product (**SA**). Topotactic reactions are single crystal-to-single crystal reactions (SCSCRs) where the daughter phase(s) is(are) aligned in an explicit three-dimensional fashion with respect to the mother phase. The largest class of SCSCRs are those where the space group of the original unit cell does not change, and the lattice parameters change smoothly over time. Examples of all these cases will be discussed, using recent examples from the solid-state reactivity of metal complexes of carboxylates and phosphines as well as diacetylenes. A new type of process, radiation-induced twinning in a combined **SA/T2** reaction, occurs as part of the solid-state polymerization of an acetylenedicarboxylate salt.

### 13.02.03

**Novel Supramolecular Approaches to Design Photoreactive Multi-component Assemblies: From Single to Concomitant Topochemical [2+2] Photoreactions.** A. Briceño. Laboratorio de Síntesis y Caracterización de Nuevos Materiales, Centro de Química, Inst. Venezolano de Investigaciones Científicas, (IVIC), Apartado 21827, Caracas, 1020-A, Venezuela. abriceno@ivic.ve.

Recently, we have reported the ability of *multivalent templates* based on hydrogen bonded metal complexes as design strategy to direct [2+2] photocycloaddition of stilbenes in the solid state. We have shown that multivalent metal-ligand interactions provide a simple and direct mean to induce the self-assembly of metal-organic building blocks bearing distinctive ligands with variable multiple binding donor-acceptor sites. Such binding capacity can be finely modulated to afford an interesting range of structural diversity, having the adequate geometrical parameters needed for the solid-state photoreactivity of active centers (Double bonds). This approach has produced unprecedented examples of supramolecular isomers with different reactivity in the solid state and examples of concomitant harmonisation of hydrogen bonding and metal-templated to mediate [2+2] photodimerisation reactions in the solid state with quantitative yields. More recently, we have used the modular assembly approach to combine potentially reactive unsaturated molecules (Nitrogen heterocyclic and carboxylic acid) through directional supramolecular synthons. This strategy allows the possibility of obtaining novel hydrogen bonded assemblies, which can exhibit unusual reactivity patterns in the solid state where, for example, concomitant topochemical [2+2] photoreactions result in a single structure and/or a heterodimer. An examination of the structures of these assemblies reveal common trends in the hydrogen bonding patterns, which will be discussed in detail.

This work was supported by FONACIT-Venezuela through grant LAB-97000821.

### 13.02.04

**Characterisation of Solid-state Structural Phase Transitions.** Ross J. Angel, Eleda M. Johnson, Jing Zhao, Fabrizio Nestola\*, Virginia Tech Crystallography Laboratory, 3076 Derring Hall, Virginia Tech, Blacksburg VA 24060, \*Now at Dip. di Geoscienze, Univ. di Padua.

Structural phase transitions are a pervasive class of phase transformations in which the two phases have a well-defined structural relationship such that the space-group symmetry of one is a sub-group of the symmetry of the other. Analysis of the symmetry relationship immediately provides constraints upon the possible structural changes at the transition, and upon the thermodynamic character of the transition. Many such transitions can be characterized within the framework of mean-field theories such as that due to Landau. These allow the complete thermodynamic characterization of the phase transition, and the evolution of physical properties of the system, to be related to the structural changes accompanying the transition.

In the presentation, worked analyses will be presented for examples of structural phase transitions in perovskites, silicate minerals, and small molecule systems. Particular emphasis will be placed upon the evolution of unit-cell parameters through the phase transitions, from which the symmetry-breaking, and non-symmetry-breaking, spontaneous strains can be calculated. These strains provide a direct and unambiguous measure of the thermodynamic character of the transition. Structural data will be used to show that the order-parameter evolution derived from the spontaneous strains does reflect the internal evolution of the structure. In addition, when measured as a function of pressure, the variation of cell parameters can be used to also determine the elastic softening accompanying such phase transitions.

### 13.02.05

**Isotopic H/D Structural Phase Transition in Ammonium Copper Tutton Salt.** A.J. Schultz,<sup>a</sup> P.M.B. Piccoli,<sup>a</sup> M.A. Hitchman<sup>b</sup>, C.J. Simmons,<sup>c</sup> <sup>a</sup>IPNS, Argonne National Laboratory, Argonne, IL 60439, USA, <sup>b</sup>Dept. of Chemistry, Univ. of Tasmania, Hobart, Tasmania 7001, Australia, <sup>c</sup>Div. of Natural Sciences, Univ. of Hawaii at Hilo, Hilo, HI 86720, USA.

Ammonium copper Tutton salt,  $(\text{NH}_4)_2[\text{Cu}(\text{H}_2\text{O})_6](\text{SO}_4)_2$ , is a unique system in which the interplay of the Jahn-Teller expression and the hydrogen-bonding network determines which of two dimorphs is adopted (1-4). The direction of the Jahn-Teller distortion, in which two opposite water ligands have elongated Cu-O bonds relative to the other four bonds, switches by  $90^\circ$  between the two dimorphs. Adoption of one dimorph or the other can be controlled by the isotopic H/D ratio. In addition, application of pressure on the perdeuterated salt,  $(\text{ND}_4)_2[\text{Cu}(\text{D}_2\text{O})_6](\text{SO}_4)_2$ , causes the structure to switch reversibly between the two packing motifs (1,2). From a previously published EPR study, the direction of the Jahn-Teller distortion in the crystalline salt appeared to change quite abruptly at  $\sim 50\%$  deuteration with no evidence of an intermediate phase (2). In addition to previous studies at 0, 42 and 100% deuteration (1,3), we have now examined the structure at 57, 75 and 82% deuteration using single crystal neutron diffraction, and observe the structural transition between 75% and 82% deuteration. These results will be discussed in the context of the deuterium isotope effect on the hydrogen bonded network involved in the cooperative Jahn-Teller switch.

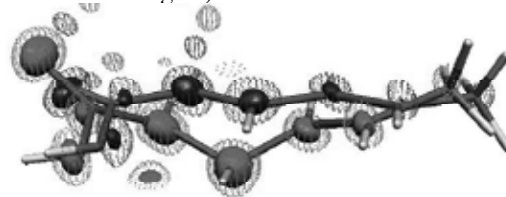
Work at Argonne was supported by the DOE Office of Science-BES under contract DE-AC02-06CH11357.

- (1) C. J. Simmons *et al.* (1993). *J. Am. Chem. Soc.* 115, 11304-11311.
- (2) W. Rauw *et al.* (1996). *Inorg. Chem.* 35, 1902-1911.
- (3) R. W. Henning *et al.* (2000). *Inorg. Chem.* 39, 765-769.
- (4) A. J. Schultz *et al.* (2003). *Cryst. Growth Des.* 3, 403-407.

### 13.02.06

**Competitive Isomerization and Dimerization Reactions: A New Look at Stereochemical Requirements for [2+2] Addition.** S.-L. Zheng, O. Pham, C.M.L. Vande Velde, M. Gembicky, P. Coppens, Dept. of Chemistry, State Univ. of New York, Buffalo, NY, 14260.

The supramolecular solid is an eminently suitable medium for the study of photochemical processes in solids.<sup>1</sup> Following work on the single-crystal-to-single-crystal photo-isomerizations of olefin acids in *C*-ethylcalix[4]resorcinarene frameworks;<sup>2</sup> we describe the competitive *E/Z* isomerization and [2+2] dimerization in co-crystals of 1,1,6,6-tetrahexaphenyl-2,4-diyne-1,6-diol and sorbic acid. At 90K both *E/Z* isomerization and dimerization occur, but the conversion percentages are limited. At 280K the dimerization reaction, which requires a  $\sim 1.8\text{\AA}$  lateral shift of the reacting molecules, dominates, and the reaction is very fast. The temperature dependence of the dimerization reaction has been observed earlier for crystals of 2-benzyl-5-benzylidenecyclopentanone, in which a similar large offset occurs.<sup>3</sup> From the data available at present it appears that the offset of the reacting double bonds must be included in criteria for solid-state dimerization. In our studies results are visualized by photodifference maps, an example of which is shown in the figure<sup>4</sup> (see Figure: 1 min. exposure at 280K, blue: -4.5, light blue: -3.0, orange: 3.0, red:  $2.0\text{ e}\text{\AA}^{-3}$ , the second reacting molecule is center-of-symmetry related and located below the figure).



Support of this work by NSF (CHE0236317) is gratefully acknowledged.

1. P. Coppens, *et al.*, *Zeitschr. fuer Kristallogr.* (2008) In Press.
2. S.-L. Zheng, *et al.*, *Acta Crystallogr.* (2007) **B63**, 644-649; *Chem. Com.* (2007) 2735-2737; *Chem. Eur. J.* (2008) **14**, 706-713.
3. K. Honda *et al.*, *J. Am. Chem.Soc.* (1999) 121, 8246-8250. I. Turowska-Tyrk, *Chem. Phys. Lett.* (2002) **361**, 115-120.
4. *XD2006-A Computer Program Package for Charge Density Analysis* (2006).

## 13.03 Structural Biology in Neurological Disorders

### 13.03.01

**Structural Neurology: A New Approach to the Understanding, Treatment and Prevention of Neurologic Disorders.** Dagmar Ringe, Gregory A. Petsko, Rosenstiel Basic Medical Sciences Research Center, Brandeis Univ. MS 029, Waltham, MA 02454.

The rapid aging of the population in most developed countries will eventually produce a world in which almost a third of its inhabitants will be over 60 years of age. Coincidentally, 60 is the age at which the incidence of neurodegenerative diseases such as Parkinson's Disease, Alzheimer's Disease and stroke begin to rise exponentially. Effective treatments are lacking for these and nearly all of the major neurologic disorders, which taken together cost the U.S. over \$330 billion per year. We have set up a program to bring the techniques of structure-guided drug discovery to bear on a number of these diseases. The program combines human genetics, studies in model organisms, mechanistic enzymology, computational approaches, and X-ray crystallography of validated targets to provide novel therapeutic approaches. A highlight of our strategy is the use of pharmacological chaperones to increase the steady-state concentration of neuroprotective proteins – we are not only limited to finding inhibitors of neurotoxic ones. We will give examples of this approach in the treatment of Gaucher Disease and the prevention of Parkinson's and Alzheimer's Diseases.

**13.03.02****Crystal Structure of JNK3 in the DFG Loop out Conformation.**

G. Toth<sup>§</sup>, S. Lovell<sup>\*</sup>, H. Kim<sup>\*</sup>, J. Wu<sup>§</sup>, K. Powell<sup>§</sup>, H. Sham<sup>§</sup>, I. Griswold-Prenner<sup>§</sup>, <sup>§</sup>Elan Pharmaceuticals, Inc., 800 Gateway Blvd., South San Francisco, CA 94080, <sup>\*</sup>deCODE biostructures, Inc. 7869 NE Day Rd. W., Bainbridge Island, WA 98110.

In neurodegenerative diseases, the molecular mechanism of progressive neuronal cell loss is unclear; although, in many cases it may be associated with activation of the c-Jun N-terminal kinase (JNK) pathway. *In vivo* knockout studies of the JNK3 gene suggest that JNK3 is an appropriate target for the development of therapeutics for the treatment of neurodegenerative diseases such as Alzheimer's and Parkinson's diseases. Several ATP site inhibitors of JNK3 have been developed and their co-crystal structures with JNK3 reported. Most of these inhibitors, however, suffer either from lack of selectivity or from poor pharmacokinetic properties, such as low CNS penetration. In all of the reported complex crystal structures, the DFG loop motif was observed in the *in* position. In an effort to determine how an allosteric inhibitor binds to JNK3, we co-crystallized JNK3, a peptide derived from JNK interacting protein 1 (JIP1), and BIRB-796, a potent allosteric p38 kinase inhibitor. BIRB-796 binds to JNK3 in a similar manner as to p38 kinase, by stabilizing the DFG loop in an *out* conformation. Visual inspection and computational analyses of the crystal structure suggest that differences in two pairs of residues, Met115(JNK3) – Leu72(p38) and Met146(JNK3) – Thr96(p38), are most likely responsible for the higher affinity of BIRB-796 to p38 compared to JNK3 kinase. Furthermore, no difference in pocket shape, size and electrostatics was observed in the pocket created by the flip out of the DFG loop between JNK3 and p38 kinase.

**13.03.03****From Folding on Ribosomes to Misfolding of Alpha-Synuclein in Parkinson's Disease: Insights from NMR Spectroscopy.**

John Christodoulou<sup>1,2</sup>, <sup>1</sup>Inst. of Structural Molecular Biology, Div. of Structural Molecular Biology, Univ. College London, and School of Crystallography, Birkbeck College, Gower St., London, UK, <sup>2</sup>Dept. of Chemistry, Univ. of Cambridge, Cambridge, UK.

Structural biology pursuits in protein folding and misfolding are aimed towards understanding the conformations of polypeptide chains ranging from the intermediate states sampled during the vectorial synthesis on ribosomes to those observed in protein misfolding where in several disease states amyloid fibrillar deposits are observed.

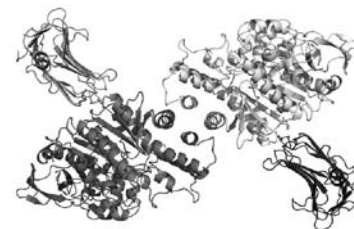
NMR spectroscopy is a powerful tool in such studies as it can provide structural and dynamical information of such disordered states. In this talk, the use of NMR to characterize the co-translational folding of protein chains while they are being created on ribosomes is described. This work is allowing us to structurally probe the relationship between biosynthesis and folding. The dynamic structural properties of alpha-synuclein, the primary component of amyloid fibrillar deposits found in Parkinson's disease brains is also discussed. We probe the intrinsically disordered native state of alpha-synuclein and its membrane-bound form as well as oligomeric states (including fibrils) of alpha-synuclein and the close homologue, beta-synuclein. The combined use of NMR spectroscopy together with newly developed ensemble molecular dynamics (MD) simulations have allowed us to probe the topology of these proteins including their cellular interactions, e.g. with chaperones, calmodulin and to consider strategies to prevent aggregation and its devastating consequences.

1)Structure and Dynamics of a ribosome-bound nascent chain by NMR spectroscopy Hsu, S.-T.D., Fucini, P., Cabrita, L.D., Launay, H., Dobson, C.M., Christodoulou, J., *P.N.A.S.* (2007)

104, 16516-16521. 2)Heteronuclear NMR investigations of dynamic regions of intact *E. coli* ribosomes, Christodoulou, J., Larsson, G., Fucini, P., Connell, S., Pertinhez, T.A., Hanson, C.L., Redfield, C., Nierhaus, K.H., Robinson, C.V., Schleucher, J., Dobson, C.M., *P.N.A.S.* (2004), 101, 10949-10954. 3)Mapping long-range interactions in  $\alpha$ -synuclein using spin-label NMR and ensemble molecular dynamics simulations Dedmon, M.M., Lindorff-Larsen, K., Christodoulou, J., Vendruscolo, M., Dobson, C.M., *J. Am. Chem. Soc.* (2005) 127, 476-477. 4)Molecular determinants of the aggregation of  $\alpha$ -synuclein and  $\beta$ -synuclein Rivers, R.C., Kumita, J.R., Tartaglia, G.G., Dedmon, M.M., Pawar, A., Vendruscolo, M., Dobson, C.M., Christodoulou, J., *Protein Science* (2008) *in press*.

**13.03.04****Structural Insights into Neuronal Transporters.** Paul Shaffer, Eric Gouaux.**13.03.05****Structures of Synaptic Proteins Neuroligin-1 and the Neuroligin-1/Neurexin-1 $\beta$  Complex Reveal Specific Protein-protein and Protein-Ca<sup>2+</sup> Interactions.** D. Araç, A.A. Boucard, E. Özkan, P. Strop, E. Newell, T.C. Südhof, A.T. Brunger, Howard Hughes Medical Inst., Stanford Univ., Stanford, CA, 94305, USA.

Neurexins and neuroligins provide trans-synaptic connectivity by the Ca<sup>2+</sup>-dependent interaction of their alternatively spliced extracellular domains. Neuroligins specify synapses in an activity-dependent manner, presumably by binding to neurexins (1) and mutations in these genes may be among the causes for autism and mental retardation. Here, we present the crystal structures of neuroligin-1 in isolation and in complex with neurexin-1 $\beta$  (2). Neuroligin forms a constitutive dimer, and two neurexin monomers bind to two identical surfaces on the opposite faces of the neuroligin dimer to form a heterotetramer. The neuroligin-1/neurexin-1 $\beta$  complex exhibits a nanomolar affinity, and includes a large binding interface that contains bound Ca<sup>2+</sup>. Alternatively spliced sites in neurexin-1 $\beta$  and in neuroligin-1 are positioned nearby the binding interface, explaining how they regulate the interaction. Structure-based mutations of neuroligin-1 at the interface disrupt binding to neurexin-1 $\beta$ , but not the folding of neuroligin-1, and confirm the validity of the binding interface of the neuroligin-1/neurexin-1 $\beta$  complex. These mutants reduce the affinity for the complex by up to three orders of magnitude, so they could be used as molecular tools to determine the function of the interaction of neuroligin with neurexin *in vivo*. Our results provide molecular insights for understanding the role of cell-adhesion proteins in synapse function.



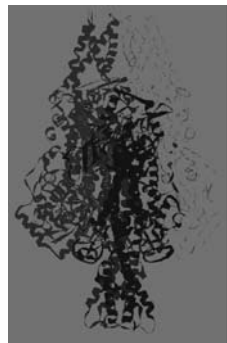
1. Chubykin, A.A., *et al.* (2007) Activity-dependent validation of excitatory versus inhibitory synapses... *Neuron* 54, 919-931.

2. Arac, D., *et al.* (2007) Structures of Neuroligin-1 and the Neuroligin-1/Neurexin-1 $\beta$  Complex ... *Neuron* 56, 992-1003.

**13.03.06****Clinical and Pre-clinical Evaluation of Structure Based Phenylketonuria Therapeutics.** Raymond C. Stevens, Dept. of Molecular Biology, The Scripps Research Inst., 10550 North Torrey Pines Rd., La Jolla, CA 92037, USA.

Phenylketonuria (PKU) leads to an inability to dispose of phenylalanine consumed in a normal diet due primarily to inactive phenylalanine hydroxylase enzyme (PAH, EC 1.14.16.1). As a consequence, mental retardation can occur if treatment with a phenylalanine-restricted diet is not followed. During the past several years during the clinical development of Kuvan, we have been evaluating the genotype-phenotype relationship of the patient mutations with response to

Kuvan. In addition, development of alternate treatments, particularly for the more severe forms of PKU that are not responsive to Kuvan, are desirable.



In order to produce a protected form of the enzyme phenylalanine ammonia lyase (PAL) as an enzyme substitution therapeutic and one that possesses better specific activity, less proteolytic susceptibility, prolonged survival *in vivo*, and reduced immunogenicity, we determined the 3-dimensional structure of *Rhodospiridium toruloides* PAL to 1.6 Å (Figure 1), performed PAL engineering based on its structure, and chemically modified the enzyme. The enzyme has completed pre-clinical development.

Figure 1. 3-dimensional structure of the Phenylalanine Ammonia Lyase enzyme at 1.6 Å resolution. The enzyme is a tetramer, with the active site composed of residues from different monomers.

This work was funded by The Scripps Research Institute, U01 grant from NINDS and a fellowship from the Michaux Family Foundation for PKU.

## 13.04 Diffraction Studies of Correlated Electron Systems

### 13.04.01

**Magnetically Induced Ferroelectricity in Frustrated Quantum Magnets.** Michel Kenzelmann<sup>\*1,2</sup>, <sup>1</sup>Laboratory for Solid State Physics, ETH Zurich, CH-8093 Zurich, Switzerland, <sup>2</sup>Laboratory for Neutron Scattering, ETH Zurich & Paul Scherrer Institute, CH-5232 Villigen, Switzerland.

Magnetic insulators with competing exchange interactions can give rise to strong fluctuations and qualitatively new ground states. The proximity of such systems to quantum critical points can lead to strong cross-coupling between magnetic long-range order and the nuclear lattice. Case in point is a new class of multiferroic materials in which the magnetic and ferroelectric order parameters are directly coupled, and a magnetic field can suppress or switch the electric polarization [1]. Our neutron measurements reveal that ferroelectricity is induced by magnetic order and emerges only if the magnetic structure creates a polar axis [2-5]. The spin dynamics and the field-temperature phase diagram of the ordered phases provide evidence that competing ground states are essential for ferroelectricity. The origin of the magneto-electric coupling most probably arises from strain derivatives of the isotropic exchange interactions and anisotropic exchange couplings such as Dzyaloshinskii-Moriya interactions.

[1] T. Kimura et al, *Nature* **426**, 6962 (2003).

[2] G. Lawes et al, *Phys. Rev. Lett.* **95**, 087205 (2005).

[3] M. Kenzelmann et al, *Phys. Rev. Lett.* **95**, 087206 (2005).

[4] M. Kenzelmann et al, *Phys. Rev. B* **74**, 014429 (2006).

[5] M. Kenzelmann et al, *Phys. Rev. Lett.* **98**, 267205 (2007).

### 13.04.02

**Interplay Between the Short-Range Polar Order and Low-Frequency Lattice Dynamics in Relaxor Ferroelectrics.** P.M. Gehring<sup>1</sup>, C. Stock<sup>2</sup>, G. Xu<sup>3</sup>, W. Chen<sup>4</sup>, Z.-G. Ye<sup>4</sup>, H. Cao<sup>5</sup>, J.-F. Li<sup>5</sup>, D. Viehland<sup>5</sup>, H. Luo<sup>6</sup>, <sup>1</sup>NIST Center for Neutron Research, Gaithersburg, MD, USA, <sup>2</sup>ISIS Facility, Rutherford Appleton Lab, Chilton Didcot, Oxon, UK, <sup>3</sup>Brookhaven National Lab, Upton, NY, USA, <sup>4</sup>Simon Fraser Univ., Burnaby, BC, Canada, <sup>5</sup>Virginia Tech, Blacksburg, VA, USA, <sup>6</sup>Shanghai Inst. of Ceramics, Shanghai, China.

Lead-based relaxor ferroelectric materials exhibit the largest reported piezoelectric coefficients and strain. While of obvious

interest to the industrial community, these compounds exhibit rich and complex physical properties that are of equal interest from a materials science perspective. Based on a perovskite structure of the form  $PbB''B''O_3$ , these relaxor materials possess quenched chemical short-range order that gives rise to random fields, intense diffuse scattering, and heavily damped, low-frequency TA and soft TO modes. The diffuse scattering is both electric-field and temperature dependent and appears to be onset at the same temperature where the phonon damping is maximal. Doping with  $PbTiO_3$ , a conventional soft mode ferroelectric, increases both the piezoelectric character as well as the  $q$ -integrated diffuse scattering intensity until the morphotropic phase boundary, beyond which both drop precipitously<sup>[1]</sup>. This indicates a direct connection between the exceptional piezoelectricity and the short-range polar order. Evidence of a strong coupling between TA phonons polarized along  $\langle 110 \rangle$  and the diffuse scattering is consistent with this finding and suggests a possible mechanism for the exceptional piezoelectricity<sup>[2]</sup>.

[1] M. Matsuura, K. Hirota, P.M. Gehring, Z.-G. Ye, W. Chen, and G. Shirane, *Phys. Rev. B* **74**, 144107 (2006).

[2] Guangyong Xu, Jinsheng Wen, C. Stock, and P.M. Gehring, submitted to *Nature Materials*.

### 13.04.03

**Spin and Charge/orbital Ordering in Nearly Half-doped Manganites.** J.A. Fernandez-Baca, Neutron Scattering Science Div., Oak Ridge National Laboratory\*, Oak Ridge, TN 37831, USA.

Neutron scattering is ideal to study the study the spin and charge/orbital ordering (CO-OO) in the CMR and related manganites that results from the strong interplay of spin, lattice and orbital degrees of freedom. In this talk I will review this subject and will focus in the nearly half-doped perovskite manganite  $Pr_{0.55}(Ca_{0.8}Sr_{0.2})_{0.45}MnO_3$  (PCSMO). On cooling from room temperature, PCSMO first enters into a CO-OO state below  $T_{CO}$  and then becomes an isotropic CE-type long-range ordered antiferromagnet below  $T_N$ . At temperatures above  $T_N$  but below  $T_{CO}$  ( $T_N < T < T_{CO}$ ), the spins in PCSMO form highly anisotropic smectic liquid-crystal-like texture with ferromagnetic (FM) quasi-long-range ordered one-dimensional zigzag chains weakly coupled antiferromagnetically.<sup>1</sup> Such a magnetic smectic-like phase results directly from the spin-orbit interaction and demonstrates the presence of textured 'electronic soft' phases in doped Mott insulators.

\*Oak Ridge National Laboratory is managed by UT/Battelle, LLC for the US DOE under contract DE-AC05-00OR22725. <sup>1</sup>Ye et al, *Phys. Rev. B* **72**, 212404 (2005).

### 13.04.04

**Short-range Charge and Spin Superlattices in Layered Perovskite Oxides.** Igor Zaliznyak, Andrei Savici, Genda Gu, Hideki Yoshizawa, Naoki Sakiyama, Ying Chen, Hye Jung Kang, CMPMS, Brookhaven National Laboratory, Upton, NY 11973.

Charge and spin ordering (CO/SO) are ubiquitous features of doped strongly correlated transition metal oxides. A number of competing mechanisms are at the origin of these phases - from charge density wave formation and spin-exchange to Jahn-Teller instability and electrostatic interactions (crystal strain) underlying general tendency of complex alloys to adopt superlattices whose unit cell incorporates all different ionic species existing in the material.

In most cases these superlattices are short-range ordered. The structure of the corresponding diffuse scattering pattern provides an important insight into the mechanism of CO/SO phase formation. Here we report on charge- and spin-ordered patterns appearing in cobalt-based relatives of high- $T_c$  cuprate superconductors, strongly

correlated oxides  $\text{La}_{1-x}\text{Sr}_x\text{Co}_2\text{O}_4$  ( $x = 0.5; 0.61$ ) and  $\text{Pr}_{1-x}\text{Ca}_x\text{Co}_2\text{O}_4$  ( $0.39 < x < 0.73$ ), which were investigated by elastic neutron scattering. We compare the measured pattern of magnetic diffuse scattering with predictions of several simple models of disorder truncating the superlattice coherence.

### 13.04.05

**Three Dimensional Magnetic Correlations in  $\text{LuFe}_2\text{O}_4$ .** A.D. Christiansen<sup>1</sup>, M.D. Lumsden<sup>1</sup>, M. Angst<sup>1</sup>, Z. Yamani<sup>2</sup>, W. Tian<sup>1†</sup>, R. Jin<sup>1</sup>, S.E. Nagler<sup>1</sup>, B.C. Sales<sup>1</sup>, D. Mandrus<sup>1,1</sup>. Oak Ridge National Laboratory, Oak Ridge, TN USA, <sup>2</sup>National Research Council, Canadian Neutron Beam Center, Chalk River, Ont., Canada, <sup>†</sup>Present address Ames Laboratory, Iowa State Univ., Ames, IA.

$\text{LuFe}_2\text{O}_4$  has recently attracted much attention due to a novel electronically driven ferroelectric transition and concomitant indications of coupling between magnetic degrees of freedom and a large spontaneous polarization. To examine the behavior of  $\text{LuFe}_2\text{O}_4$  in further detail, we have performed polarized and unpolarized neutron diffraction experiments on high quality single crystal specimens. These measurements reveal two phase transitions involving magnetic degrees of freedom below 300 K (see fig. 1). Below 240 K we observe magnetic reflections indicating that the magnetic interactions are 3-dimensional in character. This magnetic ordering may be understood in terms of a symmetry allowed ferrimagnetic structure of the parent R-3m space group with a propagation vector of  $(1/3 \ 1/3 \ 0)$ . Below 175 K many of the magnetic Bragg peaks become significantly broadened and a broad diffuse component to the magnetic scattering becomes evident. In addition, a new set of satellites is observed indexed as  $(1/3 \pm \delta \ 1/3 \pm \delta \ 3L/2)$  where  $\delta \sim 0.27$ . Polarized neutron diffraction measurements indicate that these satellites have a substantial magnetic component.

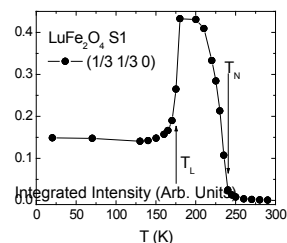


Fig. 1. Integrated intensity for the  $(1/3 \ 1/3 \ 0)$  magnetic peak. Phase transitions are indicated at 240 K ( $T_N$ ) and 175 K ( $T_L$ ).

## 13.05 Modern Teaching Tools for 21st Century Science

### 13.05.01

**Educating Virtual APS Users: On-line Educational Materials for Powder Diffraction Crystallography.** Brian H. Toby, Advanced Photon Source, Argonne National Laboratory, Argonne IL 60439.

There are good arguments both for and against people making use of synchrotron and neutron facilities without traveling to them. However, this discussion is largely moot, as the transition to remote access is happening, regardless. Even if it were not, with the dramatic decrease in measurement times, users will not spend a week or two doing measurements at a national lab, where they can learn analysis techniques at a leisurely pace from a Jim Jorgensen, Alan Hewat or Dave Cox: a world-class expert who also supervises the beamline. As mail-in measurements become common for powder diffraction crystallography at user facilities, and even more acutely as few universities provide student with the needed crystallography background, how will newcomers to the techniques become educated? Workshops with a broad agenda, such as the annual X-ray Neutron school at Argonne provide a good introduction, but not enough of the needed tools.

At the APS, we have been preparing audio-visual web based (read as “canned”) lectures to provide users with some skills needed for crystallographic analysis of powder diffraction data. This talk will discuss what we are doing and some of the strengths and failings of this approach.

### 13.05.02

**Crystallography and Scientific Inquiry.** Bernhard Rupp, q.e.d. life science discoveries, Livermore, CA 94551.

A recent rush of retractions of protein structures published in high impact journals shows that not all is well in the way macromolecular crystallography is taught to students. As a consequence, misinformation and uncritical use of sophisticated and increasingly powerful methods propagates to the next generation. The negative impact of severely incorrect structures extends beyond mere nuisance: crystallographic structure models carry great persuasive power - a wrong structure in a vanity journal contradicting correct experimental findings makes it quite impossible for others to obtain funding for their work.

With great power of modern crystallography comes great responsibility for its appropriate use. The idea that crystallography is just a basic analytical technique is gravely mistaken and only amplifies the risk of uncritical use of increasingly powerful crystallographic methods. The complexity of teaching a field that encompasses fundamental mathematics, physics, and probability theory in addition to the biological knowledge necessary to analyze and interpret the results with an array of bioinformatics tools have been addressed in a white paper by the ACA Education Committee/USNCCr in 2005. A closer inspection of incorrect structures shows that an even deeper and more concerning general disregard for the process of scientific inquiry leads to wrong structures and misinterpretations. These findings should be taken as an encouragement to teach crystallography in a larger framework consistently emphasizing the role of evidence and probability in inference methods. Examples range from crystallization propensities to maximum likelihood in phasing and refinement to evidence-based examination of ligand structures. In such a curriculum, even if the details of crystallographic theory are long forgotten, the fundamentals of proper inquiry and inference will remain invariably useful for the student.

### 13.05.03

**An Interactive Tutorial to Teach Diffraction Physics Related to Crystal Structure Determination.** R.B. Neder, Kristallographie und Strukturphysik, Univ. Erlangen, Erlangen, Germany.

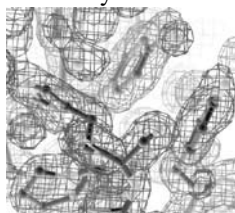
Modern crystal structure determination programs work extremely well in an almost black box mode. Students using these programs may end up with the correct list of atom coordinates, yet will not understand why and how the program derived the crystal structure. As a consequence possible pitfalls will only be understood after a several and painful failures. I have developed several interactive tutorials that are used within a classroom setting but are equally well suited for a self guided study. The tutorials start at basic aspects like, among many others, the atomic form factor, the relative orientation of planes and reciprocal space vectors  $hkl$ . Several tutorials cover the phase problem by illustrating the effect of one or two atoms in a unit cell onto the structure factor. The next group of tutorials focuses on the structure determination itself. Here students can for example, investigate the effect of the intensity and phase on the resulting electron density. Other tutorials in this group illustrate the physical reasons behind structure determination by illustrating triple phase relationships and the influence of symmetry on intensity statistics.

Finally several tutorials ask the students to solve simple structures in a well laid out step by step process. The use of these tutorials has markedly improved the students understanding of the crystal structure determination process. The tutorials are available on-line at: <http://lks.physik.uni-erlangen.de/diffraction/>

### 13.05.04

**Exploiting Advances in Cyberinfrastructure to Provide Practical Experience in Crystallography.** K.A. Kantardjieff<sup>1,2</sup>, <sup>1</sup>Dept. of Chemistry and Biochemistry, <sup>2</sup>Keck Center for Molecular Structure, Cal State Univ., Fullerton, CA 92834.

With the migration of academic crystallography from a research specialty to a technique employed by a wide community of users, training and instruction in crystallography have been increasingly relegated to non-curricular resources, such as web-based tutorials. While web-based tutorials are often well-constructed and can provide an extremely valuable resource to the broader scientific community, such tutorials generally do not provide the practical experience needed to appreciate the value of crystallographic information and to correctly interpret and judge the quality of crystallographic results. Now, however, we can exploit advances in networking, web-based tools and other facets of cyberinfrastructure to effectively broaden access to instrumentation, data handling, and data analysis. This has the potential to develop in the wider user community a sufficient working knowledge of the field, enabling them to answer specific research questions, to collaborate with those having greater expertise, to utilize crystallographic results as the basis for or validation of their own work, and to critically review published structures or those being submitted for publication. The opportunities and challenges to delivering training and instruction in crystallography using various facets of cyberinfrastructure, and their pedagogical implications, will be discussed.



### 13.05.05

**The Interactive Lectures for the School & College Instructors.** Kodess, B.N, Kodess, P.B, Sidorenko, F.A., Kodes P.I., ICS&E, Denver, CO, PIRAE, VNIIMS, Moscow.

The interactive lectures were developed [IUCr, 2005, *J. Mat. Edu.*,1999]. These lectures are intended for Instructors and use by them as the introduction in Science for different age's students and freshmen.

For the students of age of 10-12 years and older the collections of the minerals and the models of crystals are demonstrated and then they make the model of crystals themselves out of the paper (e.g. cutting diamond). The atom models are used – from simple inorganic materials to organic macromolecules. The animation and show of the functional characteristics are used for providing better understanding. Among them are mechanical (e.g. strength - for application in different constructions, optical (including use in lasers), selectivity and thermostability (use for creation of drug and others). Furthermore, youngest students can also observe and describe the process of crystal growing with the help of a special solution, designed for fortnight of observing.

The proposed type of study helps to increase efficiency of the study tasks and assists to prevent the professional burnout of the Instructors. It will reveal that this interactive lecture keeps students' attention much longer and increases the volume of informationz given to them into the fascinating world of substance study. They let the educators

decide the task of motivation increase in the study of Science and also help to develop ecological awareness. It is important that on lectures appears the additional interaction between instructors and students, based on cooperation. This type of interaction develops activity and creative motivation of students, and in the school they reducing the risk of professional burnout and fading of educators. This work is partly supported by fund's funds of ISTC, CRDF and RFFI.

## 13.06 Molecular Magnets

### 13.06.01

**Molecule-based Magnets: New Chemistry and New Materials for this Millennium.** Joel S. Miller, Dept. of Chemistry, Univ. of Utah, Salt Lake City, UT 84112.

Molecule-based materials exhibiting the technologically important property of bulk magnetism have been prepared and studied in collaboration with many research groups worldwide frequently exhibit supramolecular structures. These magnets are prepared via conventional organic chemistry methodologies, but unlike classical inorganic-based magnets do not require metallurgical processing. Furthermore, these magnets are frequently soluble in conventional solvents (*e. g.*, toluene, dichloromethane, acetonitrile, THF) and have saturation magnetizations more than twice that of iron metal on a mole basis as well as in some cases coercive fields exceeding that of Co<sub>5</sub>Sm. Also magnets with critical temperatures exceeding room temperature have been prepared. In addition to an overview of magnetic behavior, numerous examples of structurally characterized magnets made from molecules will be presented. These will include [M<sup>III</sup>(C<sub>5</sub>Me<sub>5</sub>)<sub>2</sub>][A], [Mn<sup>III</sup>(porphyrin)][A] (A = cyanocarbon etc. electron acceptors) as well as M[TCNE]<sub>x</sub>, which for M = V is a room temperature magnet, which can be fabricated as a thin film magnet. A new class of magnets of [Ru<sup>III</sup>(O<sub>2</sub>CR)<sub>4</sub>]<sub>3</sub>[M<sup>III</sup>(CN)<sub>6</sub>] (M = Cr, Fe; R = Me, *t*-Bu) composition will also discussed. For R = Me an interpenetrating cubic (3-D) lattice forms and the magnet exhibits anomalous hysteresis, saturation magnetization, out-of-phase,  $\chi''(T)$ , AC susceptibility, and zero field cooled-field cooled temperature-dependent magnetization data. This is in contrast to R = *t*-Bu, which forms a layered (2-D) lattice. These will be discussed.

We thank the numerous crystallographers that have and continue to make major contributions to this work, including, A.M. Arif, J.C. Calabrese, R.L. Harlow, J.-H. Her, A.L Rheingold, P.W. Stephens among others as well as the continued partial support by the DO DMS (Grant #DE-FG03-93ER45504 and #DE-FG02-01ER45931), the NSF (Grant #0553573), and the AFOSR (Grant No. F49620-03-1-0175).

### 13.06.02

**The Role of Halide-Halide Exchange Coupling in Low Dimensional Copper Halide Quantum Magnetic Systems.** Roger D. Willett, Dept. of Chemistry, Washington State Univ., Pullman, WA 99164, USA.

Magnetic exchange pathways between metal ions normally involve coupling via bridging ligands. However, with copper(II) halide systems, significant, or even dominant, coupling occurs via halide-halide contacts between halocuprate species. These so-called 'two-halide' exchange pathways are a result of the extensive delocalization of the magnetic spin density into the halide valence orbitals. This has led to a variety of significant low dimensional spin 1/2 quantum magnets, such as 2d AFM systems and AFM ladder systems.



Halogen-Halogen Contacts Between Cu<sub>2</sub>X<sub>6</sub><sup>2-</sup> Dimers

This talk will focus on the role of two-halide exchange pathways in  $\text{Cu}_2\text{X}_6^{2-}$  dimer systems, where these interactions have previously been largely overlooked.

### 13.06.03

**[4x4] Grids by Designed Self-Assembly:  $\text{Mn}^{\text{II}}_{16}$ ,  $\text{Cu}^{\text{II}}_{16}$ ,  $\text{Co}^{\text{II}}_{16}$  and  $\text{Ni}^{\text{II}}_{16}$  Magneto-structural Investigations.** L.N. Dawe, L.K. Thompson, Dept. of Chemistry, Memorial Univ., St. John's, NL, A1B 3X7, Canada.

Tetrapotic bis-hydrazone ligands have been prepared, and produce  $[4x4]M_{16}$  grids ( $M = \text{Mn}(\text{II})^{1,2}$ ,  $\text{Cu}(\text{II})^2$ ,  $\text{Co}(\text{II})$ ,  $\text{Ni}(\text{II})$ ) by self-assembly reactions with metal salts. The metal centers are linked via a combination of  $\mu\text{-O}_{\text{hydrazone}}$  and  $\mu\text{-NN}_{\text{pyridazine}}$  bridges, with predominantly antiferromagnetic behavior exhibited in all cases. Structures were obtained by single crystal x-ray diffraction studies from which suitable magnetic models were derived. In particular,

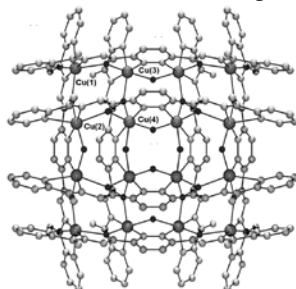


Fig.1:  $[4x4] \text{Cu}^{\text{II}}_{16}$  grid

structural data revealed that each six-coordinate copper ion in the  $\text{Cu}^{\text{II}}_{16}$  grid (Fig. 1) displayed Jahn-Teller distortion, leading to some orbitally orthogonal bridging connections.<sup>3</sup> Multiple intra-grid magnetic exchange pathways were present and were modeled by taking the molecular symmetry and orthogonal connections into account. These results and those for  $\text{Mn}^{\text{II}}_{16}$ ,  $\text{Co}^{\text{II}}_{16}$  and  $\text{Ni}^{\text{II}}_{16}$  will be discussed.

1. Dey, S.K., Thompson, L.K., Dawe, L.N. *Chem. Commun.* 2006, 4967-4969.
2. Dey, S.K., Abedin, T.S.M., Dawe, L.N., et al. *Inorg. Chem.*, **2007**, (46), 7767-7781.
3. Dawe, L.N., Thompson, L.K. *Angew. Chem.*, **2007** (46), 7440-7444.

### 13.06.04

**Hydrogen-bonding and Exchange in Benzimidazole-Functionalized Organic Radical Solids.** Paul M. Lahti, Dept. of Chemistry, Univ. of Massachusetts, Amherst, MA, USA.

Radicals can be crystallographically assembled to some extent by formation of 1-D hydrogen-bonding NH to N chains in organic radicals functionalized with 2-benzimidazolyl groups. Both tert-butyl nitroxide and 4-nitroxylphenyl radical groups show nearly the same crystallography (BABI, PhBABI). Additional crystallographic contacts depend upon functionalization of the benzimidazole aryl ring. Asymmetric aryl functionalization breaks up pi-stacking and CH to aryl herringbone 'T-type' interactions, and changes NH to N hydrogen bonding to NH to ON hydrogen bonding, so that the radical spin itself is directly involved with the hydrogen bond (CIBABI, Me<sub>2</sub>BABI) to form crystallographic dyads, but no crystallographic chains. BABI forms an ordered antiferromagnetic (AFM) phase at 1.7 K, PhBABI exhibits AFM exchange as a spin bilayer or spin ladder; CIBABI and Me<sub>2</sub>BABI exhibit AFM spin pairing. A nitronyl nitroxide radical group functionalized with tetrafluorobenzimidazole forms 1-D chains with NH to N and NH to ON interactions (F4BImNN), similar to crystallography of the nonfluorinated analogue described by other workers (BImNN, Yoshioka et al.) but with different interchain packing. F4BImNN acts as a quasi-1D ferromagnet that forms an ordered AFM phase at 0.7 K. F4BImNN and BImNN form organic alloys with hydrogen-bonding that is very similar to that of the individual components, showing similar magnetic behavior above 1.8 K but different solid phase EPR spectral behavior as a function of temperature.

BABI: Y. Miyazaki, et al. *J. Phys. Chem. B* 106 (2002) 8615. PhBABI: Y. Miyazaki, A. Inaba, M. Sorai, P. S. Taylor, P. M. Lahti, submitted (2007). CIBABI, Me<sub>2</sub>BABI: J. R. Ferrer, et al. *Chem. Mater.* 13 (2001) 2447. BImNN: N. Yoshioka, et al. *Chem. Lett.* (1997) 251. F4BImNN: H. Murata, et al. *J. Am. Chem. Soc.*, 130, (2008) 186. F4BImNN/BImNN alloy: H. Murata, et al. *Chem. Mater.* 19 (2007) 4111.

### 13.06.05

**Hydrogen Bond Mediated Magnetic Superexchange: Deuterium Isotope Effect in  $\text{CuF}_2(\text{H}_2\text{O})_2(\text{pyrazine})$ .** John A. Schlueter<sup>a</sup>, Kylee A. Funk<sup>a</sup>, Jamie L. Manson<sup>b</sup>, Sonal Brown<sup>c</sup>, Janice L. Musfeldt<sup>d</sup>, <sup>a</sup>Materials Science Div., Argonne National Laboratory, Argonne, IL 60439, <sup>b</sup>Dept. of Chemistry and Biochemistry, Eastern Washington Univ., Cheney, WA 99004, <sup>c</sup>Dept. of Chemistry, Univ. of Tennessee, Knoxville, TN, 37996.

The title compound contains linear copper pyrazine chains similar to those observed in  $\text{Cu}(\text{NO}_3)_2(\text{pyz})$ . A significant difference between these two structures is that in the title compound, strong F...H-O hydrogen bonds tether the chains together to yield a 2D square lattice. The copper  $d_{x^2-y^2}$  magnetic orbitals are confined to this  $\text{CuF}_2\text{O}_2$  plane. Long-range magnetic ordering is observed below 2.6 K which is about 25 times higher than in  $\text{Cu}(\text{NO}_3)_2(\text{pyz})$ . A deuterium isotope effect on the magnetic ordering temperature provides further evidence that the strongest magnetic coupling occurs through hydrogen bonding within this 2D plane. Spectroscopic studies also support the fact that hydrogen bonding plays an important role in the magnetic coupling in this system.

Crystal data:  $a = 7.6926(6) \text{ \AA}$ ,  $b = 7.5568(6) \text{ \AA}$ ,  $c = 6.8970(5) \text{ \AA}$ ,  $\beta = 111.065(3)^\circ$ ,  $V = 374.14(5) \text{ \AA}^3$ ,  $Z = 8$ ,  $T = 298 \text{ K}$ , space group  $P2_1/c$ .

This work was supported by the U.S. Department of Energy, Office of Science, Basic Energy Sciences, at Argonne National Laboratory, an U.S. Department of Energy Office of Science laboratory, operated by UChicago Argonne, LLC, under contract DE-AC02-06CH11357. The U.S. Government retains for itself and others acting on its behalf a nonexclusive, royalty-free license in this contribution, with the rights to reproduce, to prepare derivative works, and to display publicly.

### 13.06.06

**Hydrogen Bonding and Multiphonon Structure in Copper Pyrazine Coordination Polymers.** J.L. Musfeldt, S. Brown, J. Cao, M.M. Conner, A.C. McConnell, H.I. Southerland, J.L. Manson, J.A. Schlueter, M.D. Phillips, M.M. Turnbull, C.P. Landee, Dept. of Chemistry, Univ. of Tennessee, Knoxville, TN.

We report a systematic investigation of the temperature dependent infrared vibrational spectra of a family of chemically related coordination polymer magnets based upon bridging bifluoride ( $\text{HF}_2^-$ ) and terminal fluoride ( $\text{F}^-$ ) ligands in copper-pyrazine complexes including  $\text{Cu}(\text{HF}_2)(\text{pyz})_2\text{BF}_4$ ,  $\text{Cu}(\text{HF}_2)(\text{pyz})_2\text{ClO}_4$ , and  $\text{CuF}_2(\text{H}_2\text{O})_2(\text{pyz})$ . We compare our results with several one- and two-dimensional prototype materials including  $\text{Cu}(\text{pyz})(\text{NO}_3)_2$  and  $\text{Cu}(\text{pyz})_2(\text{ClO}_4)_2$ . Unusual low temperature hydrogen bonding, local structural transitions associated with stronger low-temperature hydrogen bonding, and striking multiphonon effects that derive from coupling of an infrared-active fundamental with strong Raman-active modes of the pyrazine building-block molecule are observed. Based on the spectroscopic evidence, these interactions are ubiquitous to this family of coordination polymers and may work to stabilize long range magnetic ordering at low temperature. Similar interactions are likely to be present in other molecule-based magnets.

## 13.08 Catalysis Studies Using SAXS & High Energy Scattering with PDF

### 13.08.01

#### Resonant X-ray PDF Studies of Catalytic Gold Nano-Particles.

T. Egami<sup>1,2,3</sup>, W. Dmowski<sup>1</sup>, S. Dai<sup>3</sup>, S.H. Overbury<sup>3</sup>, <sup>1</sup>Dept. of Materials Science and Engineering, Univ. of Tennessee, Knoxville, TN 37996, <sup>2</sup>Dept. of Physics and Astronomy, Univ. of Tennessee, Knoxville, TN 37996, <sup>3</sup>Oak Ridge National Laboratory, Oak Ridge, TN 37831.

Nan-scale gold particles supported on oxides are known to exhibit exceptional catalytic activity in many important reactions, for example oxidation of CO. However, many aspects of the Au-oxide interface structure and chemical nature of active gold particles are not well known. In addition, exposure to high temperature causes slow degradation of the catalyst due to particle coarsening. We used resonant X-ray atomic pair-density function (PDF) analysis to study the local atomic structure of Au nano-particles supported on titania and silica. The measurements were performed at the gold  $L_3$  absorption edge to determine the gold differential PDF in order to study the atomic environment of Au atoms, since the total PDF is dominated by the PDF of the oxide support. The results indicate that there are some distinct atomic correlations between nano-crystalline gold and the  $TiO_2$  support. The correlations appear as an additional PDF peak in the second nearest neighbor shell of Au. This extra bonding may as well modify the chemical state of Au resulting in, for example, preferred binding of CO. We also studied Au particle coarsening on silica substrate *in situ* at high temperatures, using high energy X-ray scattering and an area detector to determine the temperature evolution of Au PDF up to 850 C.

This work was supported by the National Science Foundation through grant DMR04-04781 and by the Office of Basic Energy Sciences, U.S. Department of Energy.

### 13.08.02

#### *In situ* Grazing Incidence Small Angle X-ray Scattering: An Advanced Characterization Technique for Catalyst Surfaces.

C. Revenant<sup>1</sup>, F. Leroy<sup>2</sup>, G. Renaud<sup>1</sup>, R. Lazzari<sup>3</sup>, A. Letoublon<sup>4</sup>, T. Madey<sup>5</sup>, <sup>1</sup>CEA/Grenoble, France, <sup>2</sup>CRMCN, Marseille, France, <sup>3</sup>INSP, Paris, France, <sup>4</sup>INSA, Rennes, France, <sup>5</sup>State Univ. of New Jersey, NJ, USA.

Catalytic nanomaterials have properties which are intimately linked to their structure and morphology. Widely used characterization techniques are imaging techniques such as Transmission Electron Microscopy, near field microscopies like Scanning Tunneling Microscopy, and Atomic Force Microscopy. If these techniques most often provide the required information, it may be advantageous, in some cases, to complement these real space imaging techniques with X-ray measurements. Indeed, X-rays present several advantages. First, an averaged statistics over the whole sample is performed, thus sampling in the same way as for the catalytic properties. In addition, *in situ* and real time experiments can be performed in various environments (from ultra-high vacuum to high pressure gases). Thus, the Grazing Incidence Small Angle X-Ray Scattering (GISAXS) technique has emerged as a powerful tool to analyze the morphology and distribution of islands on a substrate.

A setup allowing simultaneous GISAXS and Grazing Incidence X-Ray Diffraction (GIXD) in ultra-high vacuum at different stages [1] has been developed. The capability of such X-ray techniques will be illustrated with an example of faceted Pt/W(111) surface upon thermal annealing [2]. A full characterization of the nano-faceted surface has been obtained through quantitative GISAXS analysis [3].

[1] G. Renaud, R. Lazzari, C. Revenant, *et al.*, Science 300 (2003) 1416.

[2] C. Revenant, F. Leroy, G. Renaud, R. Lazzari, A. Letoublon, T. Madey, Surf. Sci. 601 (2007) 3431.

[3] C. Revenant, F. Leroy, R. Lazzari, G. Renaud, and C.R. Henry, Phys. Rev. B 69 (2004) 35411.

### 13.08.03

#### *In-situ* Combined GISAXS and TPR Studies of Size Selected Nanocatalysts: A New Approach to Investigate Size Effects in Catalysis.

Sungsik Lee<sup>a</sup>, Yu Lei<sup>a,b</sup>, Byeongdu. Lee<sup>a</sup>, Randall E. Winans<sup>a</sup>, Kristian Sell<sup>c</sup>, Ingo Barke<sup>c</sup>, Armin Kleibert<sup>c</sup>, Viola von Oyenhausen<sup>c</sup>, Karl-Heinz Meiwes-Broer<sup>c</sup>, Stefan Vajda<sup>a</sup>, <sup>a</sup>Argonne National Laboratory, Argonne, IL, USA, <sup>b</sup>Univ. of Illinois, Chicago, IL, USA, <sup>c</sup>Inst. für Physik, Univ. Rostock, Rostock, Germany.

Fundamental studies of size effects in catalysis require monodisperse catalytic particles dispersed on technically relevant oxide supports, as well as analytical techniques which allow for *in situ* monitoring of particle size and catalytic activity under realistic reaction conditions.

In this paper, we report on a unique combination of experimental methods which enable us to 1) fabricate highly uniform catalytic particles at the sub-nanometer to few tens of nanometer scale, 2) to image the catalytic particles under reaction conditions using *in situ* GISAXS and 3) evaluate catalytic performance using temperature programmed reaction (TPR) experiments.

The powerful potential of the developed approach will be illustrated on the direct epoxidation of propylene on size-selected silver nanocatalysts, starting with a  $Ag_3$  cluster and ending with 25 nm size particles. As revealed by GISAXS, during the catalytic reaction, the catalyst shape changes in a complex manner; TPR results show catalytic activity and selectivity to be strongly dependent on cluster size and temperature.

The work at Argonne National Laboratory was supported by the US Department of Energy, Contract DE-AC-02-06CH11357 with UChicago Argonne, LLC, Operator of Argonne National Laboratory. S.V. gratefully acknowledges the support by the Air Force Office of Scientific Research.

### 13.08.04

#### Combining WAXS/(SAXS) with Spectroscopic Measurements to Follow Catalysts in Action. A.M. Beale, B.M. Weckhuysen, Inorganic Chemistry & Catalysis, Dept. of Chemistry, Faculty of Sciences, Sorbonnelaan 16, 3584 CA, Utrecht, The Netherlands.

X-ray diffraction (XRD) is routinely employed to study bulk catalysts 'in action'. [1] Combining this technique with other scattering methods such as Small Angle X-ray Scattering (SAXS/WAXS) and/or with spectroscopic techniques (e.g. X-ray Absorption Spectroscopy (XAS)), results in the formation of powerful setups with the potential to unravel new insight into the behaviour of solid-state materials under reaction conditions. Much of the published literature focuses on the combination of one technique with XRD (often XAS) although more recently there has been an increasing trend to combine multiple (> 2) techniques into one setup. [2] Recently we and others reported the first results obtained from a combined SAXS/WAXS/XAS setup. [3] In this work we illustrated the insight that could be obtained into the formation processes of a zeolite type material. More recently we have expanded the gamut of multiple technique setups to follow the deactivation behaviour of important iron molybdate catalysts during methanol to formaldehyde conversion; first, using a combination of XRD/XAS/UV-Vis, to study how the active  $Fe_2(MoO_4)_3$  phase deactivates and subsequently we use a combination of SAXS/WAXS/XAS/UV-Vis to assess the stability of a novel iron molybdate material.

[1] - Weckhuysen, B. M. (Ed.), *In-situ spectroscopy of catalysts*, American Scientific Publishers Stevenson Ranch, 2004.

[2] - S. J. Tinnemans, J. G. Mesu, K. Kervinen, T. Visser, T. A. Nijhuis, A. M. Beale, D. E. Keller, A. M. J. van der Eerden, B. M. Weckhuysen, *Catal. Today* 113, 3, (2006)

[3] - A. M. Beale, A. M. J. van der Eerden, S. D. M. Jacques, O. Leynaud, M. G. O'Brien, F. Meneau, S. Nikitenko, W. Bras, B. M. Weckhuysen, *J. Am. Chem. Soc.* 128, 12386, (2006).

### 13.08.05

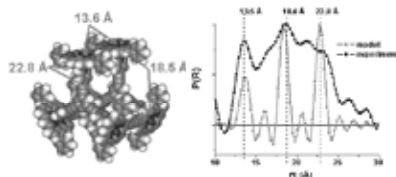
**Watching Nanoparticles Grow: The Mechanism and Kinetics for the Formation of TiO<sub>2</sub>-Supported Platinum Nanoparticles.** Peter J. Chupas,<sup>1</sup> Karena W. Chapman, <sup>1</sup>Guy Jennings,<sup>1</sup> Peter L. Lee<sup>1</sup>, Clare P. Grey<sup>2</sup>, <sup>1</sup>X-ray Science Div., Advanced Photon Source, Argonne National Laboratory, Argonne, IL, 60439, <sup>2</sup>Dept. of Chemistry, Stony Brook Univ., Stony Brook, NY 11794.

Highly-dispersed supported metal nanoparticles find widespread application in catalysis, including in hydrocarbon reforming and polymer-electrolyte-membrane fuel cells. Pivotal to the development of catalytic materials with controlled reactivity, is the understanding of the fundamental mechanisms that drive the formation of catalytic nanoparticles. A key step towards this goal is the ability to discriminate between the separate processes including the initial reaction of the precursors and the subsequent nanoparticle sintering. Recently, the Pair-Distribution-Function (PDF) method has emerged as a powerful technique to probe the structure of nano-scale materials, with atomic-scale resolution across the entire length scale of the nanoparticle, although to date this has been limited to studies of static materials prepared *ex situ*, i.e., in advance of the measurement. Here we use *in situ* time-resolved PDF methods to monitor the structural evolution and kinetics associated with the formation of Pt<sup>0</sup> nanoparticles from Pt<sup>4+</sup> ions.

### 13.08.06

**Solution Phase X-ray Scattering: Structural Characterization of Supramolecular Porphyrin Assemblies.** K.L. Mulfort,<sup>1,2</sup> S. J. Lee,<sup>1</sup> D.M. Tiede,<sup>2</sup> J.T. Hupp<sup>1</sup>, <sup>1</sup>Dept. of Chemistry, Northwestern Univ., <sup>2</sup>Chemistry Div., Argonne National Laboratory.

Much of modern synthetic chemistry is intent on mimicking the complexity, both in structure and function, of known natural systems for applications such as light harvesting and selective oxidative catalysis. In this pursuit, self-assembly has become an extremely powerful technique in synthetic schemes as these target structures increase in complexity to provide more specific functions with greater efficiency. We are particularly interested in coordinative self-assembly of metalloporphyrin based supramolecular systems. These assemblies are built through relatively weak metal-N coordination bonds, which allows for structural "self-healing" to yield the thermodynamically most favored structure, while the redundancy of many metal-N bonds throughout the assembly provides structural integrity. One of the major drawbacks of this field is the accurate and unambiguous structure determination. Characterization of these assemblies by traditional (i.e. solid-state) crystallographic techniques is not trivial and often irrelevant to the intended function. Therefore, the solution phase structure, as opposed to that in the solid state, will provide a good understanding of the structure-function relationship of these materials.



We will present the complete solution phase structural characterization

of two porphyrin-based supramolecular systems: a series of porphyrin prisms and a series of catalytic porphyrin box structures. SAXS analysis gives us the overall size (radius of gyration,  $R_g$ ) of the discrete assembly which we can distinguish from its components as well as higher oligomeric species. Additionally, scattering at higher  $q$ -values (WAXS) and the subsequent PDF analysis resolves metal-metal distances that are characteristic markers for identifying the structure of the assembly. Furthermore, WAXS and associated PDF patterns also provide a unique measure of the solution state configurational dispersion of the assembly and structure at the solvent-solute interface.

## 13.09 Emerging Opportunities for X-ray and Neutron Scattering: New Sources and New Techniques

### 13.09.01

**Synchrotron Science at SLAC/Stanford - the LCLS and Other Recent Developments.** Keith Hodgson, SLAC, Stanford Univ., Menlo Park, CA.

The Stanford Linear Accelerator Center (SLAC) has a diverse program in the development and applications of accelerator-based synchrotron radiation resources and provides these to a large user community. The portfolio of accelerators includes the currently operational 3rd generation storage ring called SPEAR3 and by mid 2009, the world's first x-ray free electron laser, called the Linac Coherent Light Source (LCLS), will begin first operations. This talk will highlight some of the recent developments and plans for instruments and techniques that will take advantage of the unique properties of these light sources to enable discovery science in the coming decade. It will also present plans for the longer term evolution of the synchrotron science program at SLAC.

Synchrotron-related operations, R&D and construction at SLAC are primarily supported by the DOE Office of Basic Energy Sciences.

### 13.09.02

**Coherence and Ultra-short Pulses for Structure Determination: New Storage Ring and FEL Facilities at DESY in Hamburg - Petra-III, FLASH, and XFEL.** J.R. Schneider, Deutsches Elektronen-Synchrotron DESY and Stanford, Linear Accelerator Center SLAC, Menlo Park, CA 94025 USA.

The DORIS III and PETRA III storage ring synchrotron radiation facilities at DESY will be operated in tandem for experiments needing either high flux or high brightness. PETRA III, currently under construction, is designed for reaching an emittance of 1 nmrad at 6 GeV electron energy and will provide micro-beams with a high degree of coherence. Research priorities, the planned instrumentation for 14 undulator beamlines and the status of the construction will be presented.

X-ray free-electron lasers provide laterally coherent beams in flashes of 100 femtoseconds or less of very high intensity: At FLASH, DESY's free-electron laser for the spectral range of the VUV and soft X-rays, one gets, in flashes of 10 femtosecond duration, as many photons per second as we get today from the best storage ring facilities. FLASH is operated as a user facility since summer 2005 and some of the results obtained so far, including the first steps towards single molecule imaging will be presented.

Finally the science case, the layout and the status of the European XFEL Facility project in Hamburg will be discussed and put into perspective with the hard X-ray FEL facilities at SLAC, USA, and Spring-8 in Japan.

**13.09.03**

Steve Dierker. No abstract submitted.

**13.09.04**

**Serial Crystallography for the Cornell ERL.** J.C.H. Spence, B. Doak, U. Weierstall, K. Schmidt, P. Fromme, D. De Ponte, R. Kirian, M. Hunter, H. Chapman\*, D. Shapiro\*\*, Physics, ASU, Tempe, AZ USA 85287, \*FLASH, DESY, Hamburg, Germany, \*\*Advanced Light Source, LBNL, Berkeley, CA.

Recently we have developed a gas-focussed droplet-beam injector to provide a single-file high-brightness stream of particles (such as proteins) across the Cornell ERL (1). This is currently being tested at the ALS, and first results from half-micron crystallites of Photosystem 1 protein will be shown (2). Patterns from 50nm gold balls doped into a beam of sub-micron uncharged water droplets will also be shown.

Detailed calculations for the ERL for scattering from aligned single proteins, including inversion to a charge-density map using iterative phasing (3), give an exposure time of 150 seconds per orientation (4). For a continuous single stream of molecules whose spacing is slightly greater than the X-ray beam diameter, the exposure time is the same as that from a single, stationary, immortal molecule. (The transit time does not allow significant radiation damage). Data is collected continuously below the damage threshold until it is statistically significant for each orientation. An on-demand version of a piezo-driven variant is under development which can be synchronized with FLASH and LCLS.

In earlier work (5), we have proposed the use of an intense CW IR laser to align this single-file stream of hydrated proteins using the induced dipole moment, in a manner akin to a laser wrench. Plans for our first experiments in March 2008 on detection of diffraction (prior to destruction) of protein crystallites from femtosecond pulses at FLASH will also be outlined.

1. U.Weierstall et al Expts in Fluids (2008); D. De Ponte et al in prep.
2. D.Shapiro et al (2008). in prep.
3. H.Chapman et al. J. Opt. Soc Am 23, 1179 (2006)
4. D.Starodub et al. J. Synch Res. 15, 62 (2008).
5. D.Starodub et al. J. Chem Phys. 123, 244304 (2005)

**13.09.05**

**New X-ray Scattering Opportunities with an Upgraded Advanced Photon Source.** Dennis M Mills, Deputy Associate Laboratory Director for Scientific User Facilities and Deputy Director, X-Ray Science, Advanced Photon Source Argonne National Laboratory,\* Argonne, IL 60439 USA.

The staff of the Advanced Photon Source (APS) is in the process of developing plans for an upgrade to the accelerator complex to maintain our forefront position as a hard x-ray user facility. Although we have looked carefully at the possibility of a storage ring upgrade, the performance that can be attained falls short of our goals (expectations) and so we are exploring the possibility of an energy recover linac (ERL) to be associated with the existing storage ring. Radiation at 1 Å (12 keV) generated by an ERL will be highly coherent and have important implications on certain techniques such as coherent imaging, coherent scattering (structural analysis of non-crystalline materials, x-ray photon correlation spectroscopy) and micro-/nano-probes. The impact on these fields and others will be discussed.

\* Use of the Advanced Photon Source was supported by the U. S. Department of Energy, Office of Science, Office of Basic Energy Sciences, under Contract No. DE-AC02-06CH11357.

**13.09.06**

**Bigger, Better, Faster, More: The ESRF Upgrade Programme.** E.P. Mitchell, European Synchrotron Radiation Facility, 6 rue Jules Horowitz, BP-220, 38043 Grenoble Cedex, France.

When the ESRF opened its first beam line in 1994, it was the world's first insertion device based ("third-generation") synchrotron radiation source. The user community, and with it the number of third-generation light sources, have been growing steadily since then. However a point has been reached where an evolutionary extension of its capabilities is increasingly difficult due to the physical limitations of the infrastructure. An ambitious plan for a ten-year Upgrade Programme has therefore been developed which aims at improving all areas of science under investigation at the ESRF. However, particular emphasis is given to five scientific themes that have been identified as the core programmes for the following decade: Nanoscience and Nanotechnology, Structural and Functional Biology and Soft Matter, Pump-and-Probe Experiments and Time-Resolved Science, Science at Extreme Conditions, and X-ray Imaging.

The components of the Upgrade are:

- Reconstruction of about one half of the currently 31 beamlines, with an emphasis on nanofocussing;
- Improvements to the accelerator complex including longer straight sections to increase the capacity for further beamlines, plus preparation of a longer-term design for a new, higher brightness lattice;
- Instrumentation developments, particularly new detectors, nano-compatible engineering and sample manipulation;
- Extensions to the experimental hall totalling 21,000 m<sup>2</sup> permitting up to sixteen beamlines to be doubled in length to up to 140 m, and to house new infrastructure.

Many new developments under the ESRF Upgrade Programme are relevant to other synchrotron light sources and would benefit



from being carried out in collaboration with partners. For the various user communities, the initiation and development of science-driven partnerships with other institutes and facilities is planned as a core aspect of the ESRF's future

programme. These partnerships will facilitate access to the ESRF by user communities who are new to research with synchrotron light and for established users provide coordinated "one-stop-shop" access to complementary facilities.

**13.09.07**

**Facilities for X-ray Scattering, Diffraction, and Crystallography at the Canadian Light Source.** Michel N. Fodje, Canadian Light Source, Saskatoon, Canada.

The Canadian Light Source is one of the largest scientific projects in Canada, with seven beamlines now in operation and six new beamlines under construction or commissioning. Scientific research at the CLS can be loosely grouped into three subject areas -- Materials Science, Environmental science, and Life Sciences. The CLS has strong and growing capabilities in X-Ray scattering, diffraction and Crystallography techniques. The 08ID1 and 08B1 beamlines are part of the Canadian Macromolecular Crystallography Facility (CMCF) which will allow data collection from very small crystals with very large unit cells in a highly automated manner. The Hard X-ray Micro Analysis (HXMA) beamline 06ID1 currently enables ambient temperature, high pressure powder diffraction with support for surface

diffraction and micro-diffraction in development. The 07B2 beamline combines X-ray fluorescence and Laue X-ray diffraction to study microscopic samples. This beamline will also allow remote control by users. The 10ID2 beamline enables the use of resonant elastic and inelastic X-ray scattering (REIXS) together with spectroscopic techniques to study self-assembling nanostructures, ferromagnetic systems, and quantum materials. The CLS is also currently planning a third phase of beamline development which will include the Brockhouse X-ray diffraction and scattering sector for materials research, 04ID. This facility will enable structural characterization of materials by microcrystallography, high-resolution powder diffraction at extreme conditions, as well as small-angle and wide-angle X-ray scattering.

### 13.09.08

**Diamond: Diffraction And Many Other New Directions for UK Science.** Elizabeth Duke, Diamond Light Source, Harwell Science and Innovation Campus, Chilton, Oxfordshire. OX11 0DE UK.

The latest sparkling gem in the diadem of British Science is Diamond, the United Kingdom's new third generation synchrotron source, built to assist in the solution of hard scientific problems. Part of the glitter comes not just from the extraordinary brightness of the source, but from the way new scientific research facilities have been built in close proximity – something which is already paying dividends as I will endeavour to highlight.

Diamond (<http://www.diamond.ac.uk>) is a 561m circumference 3GeV machine which has been optimised for producing X-rays of energy between 100eV and 20keV. Operation started in 2007 with the machine and eight Phase 1 beamlines. Six of these eight are dedicated to various forms of hard X-ray diffraction and include three for macromolecular crystallography (MX), one for materials and magnetism, one for the study of materials at extreme conditions and one for non-crystalline diffraction. The other two cover nanoscience and microfocus spectroscopy. Construction of a further fourteen Phase 2 beamlines is well underway. An overview of the machine and the non-MX beamlines highlighting some of the latest results will be presented.

There are 6 beamlines dedicated to MX on Diamond, three in Phase 1, two in Phase 2 and one in Phase 3. The three Phase 1 beamlines are broadly similar, concentrating on meeting the demand for synchrotron beamtime from the vibrant UK MX community though one of them includes containment facilities to permit data collection on Category 3 pathogens. The first of the Phase 2 MX beamlines is a microfocus beamline capable of achieving a focus at the sample position of 5micron. All four beamlines are rapidly tunable from 5-25keV using X-rays from canted in-vacuum undulator insertion devices. The final Phase 2 MX beamline is a fixed wavelength beamline targeting high throughput work and that which does not require MAD capability. The Phase 3 beamline, still in the early design stages will be optimised for data collection at softer energies, primarily driven by a desire to optimise experimental techniques for sulphur-SAD. An outline of the designs of the beamlines plus the latest results will be presented.

### 13.09.09

**Neutron Scattering Opportunities at ORNL's New and Upgraded Neutron Facilities: The Spallation Neutron Source and High Flux Isotope Reactor.** K.W. Herwig, Neutron Scattering Science Div., Oak Ridge National Laboratory, Oak Ridge, TN 37831.

Neutron scattering techniques provide a non-destructive, highly penetrating probe of both the structure and dynamics of condensed

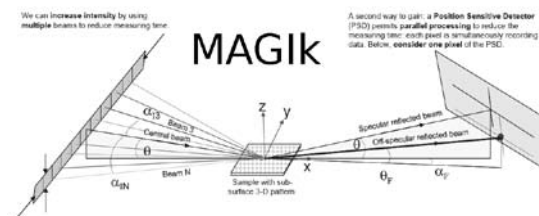
matter. The \$1.4B Spallation Neutron Source (SNS) at the Oak Ridge National Laboratory was the largest U.S. civilian science research facility construction project and was completed in June 2006. It is currently ramping up in power and instrumentation to fulfill its science mission. There are four operating neutron scattering instruments with an additional 7 to be added in 2008. The ORNL High Flux Isotope Reactor (HFIR) has recently completed significant upgrades which greatly extend its capabilities. This talk will present an overview of the SNS and HFIR facilities and neutron scattering instrumentation with an emphasis on new and novel SANS, reflectometry, and diffraction capabilities.

### 13.09.10

**Two Novel Reflectometers for the Expanded NCNR Cold Neutron Guide Hall: CANDoR and MAGIk.** Brian B. Maranville, Charles Majkrzak, Norman Berk, NIST Center for Neutron Research (NCNR), Gaithersburg, MD.

For specular reflectivity, the conventional scheme at a continuous source uses a monochromatic beam and a single matched pair of entrance and exit slits to define the Q-vector of the scattered neutrons. This greatly reduces the beam intensity from what is available in the guide. At a pulsed source, a larger fraction of the available wavelengths are used, but the integrated intensity of the source is lower. In the CANDoR instrument, we will get the advantages of both approaches. Multiple independent polychromatic cold neutron beams will be focused on the sample, and the reflected beam will be separated by wavelength and angle into a bank of 324 detectors. The intensity at each detector is to first order the same as in the conventional scheme, so that an increase of several orders of magnitude in measurement efficiency is possible.

Off-specular neutron reflectivity allows measurement of the in-plane magnetic and chemical order of thin films simultaneously. In conventional reflectivity setups the beam is defined as an extended



line (along the y-axis as seen in the figure), effectively integrating over one of the spatial

dimensions. Resolving the third dimension through collimation of the incident beam to a single point leads to an unacceptable loss of orders of magnitude in intensity. In MAGIk, we will construct a new type of instrument currently under development by several groups<sup>[1-3]</sup> and ourselves in which incoming neutrons are tagged according to the incident and/or reflected angle in the y-direction, thereby resolving information along this axis. Several tagging methods are considered, including spin-precession<sup>[1]</sup> and programmable attenuators.

[1] R. Pynn *et al.*, *Rev. Sci. Instr.* **73**, 2948 (2002)

[2] R. Pynn *et al.*, *Rev. Sci. Instr.* **76**, 053902 (2005)

[3] G.P. Felcher *et al.*, *Physica B (Cond. Matt.)* **336** (2003)

### 13.09.11

**Recent Developments at the ISIS Facility.** Richard M. Ibberson, ISIS Facility, STFC, Rutherford Appleton Laboratory, Harwell Science & Innovation Campus, Didcot, Oxfordshire, OX11 0QX, UK.

Activity and recent developments at the ISIS Facility, a world-class pulsed-neutron and muon source, will be described and plans for its ongoing utilization given. In particular, progress on the ISIS Second Target Station and its evolving instrument suite will be reviewed.

Developments to the Target Station 1 crystallography instrument suite will also be presented. Most notably, results and new capabilities on the high-resolution powder diffractometer (HRPD), following the recent installation of a high-reflectivity supermirror guide, will be reviewed along with upgrade plans for the medium-resolution high-flux (POLARIS) and high-pressure (PEARL/HiPr) diffractometers.

### 13.09.12

**Time Resolved Atomic-Resolution Laue Studies at the AR Ring at KEK.** M. Pitak, M. Gembicky, S. Zheng, P. Coppens, SUNY at Buffalo, NY, USA, M. Messerschmidt, DESY, Hamburg, Germany, SLAC-Stanford, Menlo Park, CA, USA, S.-I. Adachi, Inst. of Materials Structure Science, KEK & ERATO, JST., Tsukuba, Ibaraki Japan, S. Koshihara, ERATO and Frontier Research Center, Tokyo Inst. of Technology, Meguro-ku, Tokyo, Japan.

The NW14 beamline at PF-AR, KEK, Japan is dedicated to time-resolved studies at high-resolution and is filled with a single 60mAm pulse.<sup>1</sup> Several laser-pump/X-ray probe datasets on metalloorganic complexes were collected with 3-10 pulses per frame and different undulator gaps (11-13 mm). The effect of the reversible light-induced changes in the crystal are visible in modest spot broadening in the on-, but not in the alternately collected off-frames. To reduce the effect of uncertainties in the lambda curves, which represent the spectral distribution as well as variations in X-ray absorption and other effects with wavelength,<sup>2</sup> the fractional changes on illumination, or *response ratios* for each reflection, are derived before symmetry-equivalents are averaged. Spot integration and scaling are performed with PRECOGNITION™.<sup>3</sup> The relative scaling of on- and off- the plates is of particular importance in the derivation of reliable response ratios. Results are compared with those of previous monochromatic time-resolved studies. The use of the Laue technique is of particular importance if non-reversible processes such as chemical reactions in solids are to be studied.

Experiments funded by the US Department of Energy (DEFG02-02ER15372). Facilities made available by the ERATO Non-equilibrium Dynamics Project, JST.

S. Nozawa *et al.*, *J. Synchr. Rad.* (2007), 14, 313-319.

<sup>2</sup> K. Moffat, *Int. Tables for Cryst.* (2006), Vol. F, Chapter 8.2.

<sup>3</sup> Z. Ren, Precognition™ (5.0), Renz Research, Inc. 2006.

### 13.09.13

**Macromolecular Powder Diffraction. Structure Solution via Molecular Replacement.** Jennifer Doebbler, Robert Von Dreele, Advanced Photon Source, Argonne National Laboratory, 9700 S. Cass Ave, Argonne, IL.

Macromolecular powder diffraction is a burgeoning technique for protein structure solution — ideally suited for cases where no suitable single crystals are available. Over the past seven years, pioneering work by Von Dreele, *et al.*, and Margiolaki, *et al.*, demonstrated the viability of the approach for several protein structures. Among these initial powder studies, molecular replacement solutions of insulin and turkey lysozyme, themselves, into alternate space groups were accomplished. Pressing the technique further, Margiolaki, *et al.*, executed the first molecular replacement of an unknown protein structure: the SH3 domain of ponsin.

To demonstrate that cross-species molecular replacement of larger structures is also possible, we present the solution of HEWL using the 60% identical human lysozyme (PDB code: 1LZ1) as the search model. Due to the high incidence of overlaps in powder patterns, especially as structures get larger, we have used extracted intensities from five data sets taken at different salt concentrations in a multi-pattern Pawley refinement. This work also serves to expand upon

the previous by presenting a full-scale multi-species analysis combined with a fold matching scheme. It should be noted that since the generated maps are highly biased by the model, the use of chemical restraints becomes highly important to allow for least-squares refinement of the structure by fitting to the diffraction data itself. Extension to higher molecular weight structures, to test the limit of this technique is ongoing. Use of the APS was supported by the DOE/OS/BES under contract number W-31-109-ENG-38.

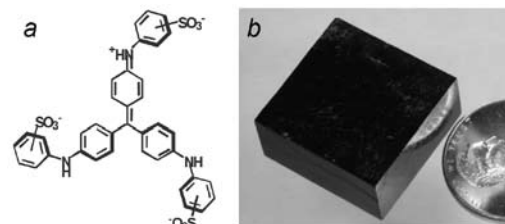
## 13.10 Supramolecular Chemistry: Organic Crystals from Assembly to Function

### 13.10.01

**More about Eligio Perucca, Primo Levi, Induced Optical Activity, and Enantioselective Adsorption to Crystals.** Bart Kahr,<sup>a</sup> Yonghong Bing,<sup>a</sup> John Freudenthal,<sup>a</sup> Werner Kaminsky,<sup>a</sup> Davide Viterbo,<sup>b</sup> <sup>a</sup>Dept. of Chemistry, Univ. of Washington, Seattle WA 98195, USA, <sup>b</sup>Dip. di Scienze e Tecnologie Avanzate – Univ. del Piemonte Orientale “A. Avogadro”, I-15100 Alessandria, Italy.

This presentation is an update to our 2007 ACA lecture in Salt Lake City, “Eligio Perucca first observed induced optical activity in 1919”. We present further analyses of sodium chlorate crystals grown in the presence of an equilibrium mixture of triarylmethane dyes. These crystals gave the first evidence of induced optical activity and of the enantioselective adsorption of a racemic mixture to a crystal, milestones in molecular chirality that were attributed to others many years later. New methods of analyses are brought to bear on the question of just what Perucca observed in his unknown but nevertheless groundbreaking paper including Stokes-Mueller imaging polarimetry.

Perucca's mixed crystals are shown to be nothing short of a linear crystal optics laboratory that when properly analyzed reveal



the complex interplay of linear birefringence, linear dichroism, circular birefringence, and circular dichroism. In Salt Lake City, we established that Perucca was a memorable tyrant, a personality trait that when combined with published reports of his relationship with the author/chemist Primo Levi led to the easy conclusion that he was something even less appealing. Here, we reinvestigate the wartime relationship of Perucca and Levi, and show that Perucca was not only a stereochemical pioneer, but a man of principle.

We thank the US-NSF (CHE-0349882) for support of this research.

### 13.10.02

**Correlation of Biomineral Crystal Growth Modification with Impurity Adsorption Kinetics.** Ryan E. Sours, Randall C. Mazzarino, Tissa J. Thomas, Chemistry Dept., Towson Univ., Towson, MD 21252 USA.

During a chromatographic separation, the time it takes for a molecule to elute from the column is determined by the relative amount of time spent adsorbed onto the stationary phase versus the time spent free in the mobile solvent phase. The more time spent adsorbed onto the stationary phase, the longer the retention time for that molecule.

During crystal growth, the extent of growth modification caused by an impurity is likely related to the lifetime of that impurity on the crystal surface. Thus, if biomineral crystals are used as the chromatographic stationary phase, the relative retention time for an individual molecule should correlate with its effectiveness as a growth modifier for that particular crystal. Molecules with longer retention times (longer surface lifetimes) should be better growth modifiers than those with short retention times.

Calcite (calcium carbonate) and whewellite (calcium oxalate monohydrate) were chosen for initial investigation. HPLC columns were packed with the relevant crystal phase and single-component runs were performed with a variety of organic impurities. Based on relative retention times, peak shapes, and modeling calculations, adsorption kinetics for the impurities were determined and compared to previously determined efficacies for crystal growth modification.

### 13.10.03

**Surface and Microwave Methods for the Selection of Pharmaceutical Polymorphs.** Venkat R. Thalladi, Dept. of Chemistry and Biochemistry, Worcester Polytechnic Inst., 60 Prescott St., Worcester, MA 01605 USA.

Polymorphism, the ability of a compound to adopt multiple solid-state arrangements, is critical to pharmaceutical drug development and formulation. Polymorphs, be they thermodynamic or metastable, exhibit distinct advantages and limitations. For example, thermodynamic polymorphs display prolonged phase stability; metastable forms have desirable dissolution properties. Selective growth of both types of polymorphs is therefore essential to the rational design of suitable drug formulation. In this talk, we describe two techniques currently being developed in our group for the selective growth both types of polymorphs. These techniques involve the crystallization of active ingredients in the presence of attractive and repulsive surface templates, and microwave radiation.

### 13.10.04

**What do Polymorphs Teach us About Crystal Nucleation and Growth?** Lian Yu, Jing Tao, Ye Sun, Hanmi Xi, Shuang Chen, Jun Huang, M.D. Ediger, Univ. of Wisconsin, School of Pharmacy and Dept. of Chemistry, Madison, WI.

The ability of a liquid to crystallize as multiple polymorphs is a phenomenon of industrial importance and an opportunity to study crystal nucleation and growth. Using polymorphs to study crystallization follows the tradition of using polymorphs to test principles of thermodynamics and structure-property relations. We have used polymorphs to study the nucleation of one crystalline phase on the advancing growth front of another. The fast-nucleating polymorph is not necessarily the product of crystallization, but may nucleate another, faster-growing polymorph. We have also used polymorphs to study the diffusionless crystal growth that is abruptly activated in certain fragile organic liquids near the glass transition temperature. For the ROY system, currently the top system for the number of coexisting polymorphs of solved structures, diffusionless growth exists for some polymorphs but not others, with those showing the growth mode being denser and more isotropically packed.

### 13.10.05

**Cross-Nucleation and Polymorph Selection: Unravelling the Competition Between Kinetics and Thermodynamics.** Jerome Delhommelle, Caroline Desgranges, Dept. of Chemical Engineering, Univ. of South Carolina.

Controlling polymorphism, that is, in which structure atoms (or molecules) crystallize, still remains an unsolved problem. Since polymorphs generally have different physical properties, understanding this phenomenon is crucial for many applications. In this work, we use molecular dynamics simulations to study the early stages of the crystallization process in supercooled liquids of spherical particles. We present a few results obtained recently in our group:

- we propose the first molecular mechanism for the experimental observation of cross-nucleation between polymorphs [1],
- we demonstrate how cross-nucleation can be controlled and, more generally, how the control of polymorphism can be achieved for a simple Lennard-Jones fluid [2],
- we provide some insight into the molecular mechanisms underlying polymorph selection in charge-stabilized colloidal suspensions [3],
- we elucidate the pathway to crystallization of Aluminum and analyze the differences with the crystallization mechanism of a simple fluid [4],
- we provide numerical evidence for a structural evolution of alpha-N2 critical nuclei into beta-N2 crystallites [5].

[1] C. Desgranges and J. Delhommelle, *J. Am. Chem. Soc.* 128, 10368 (2006).

[2] C. Desgranges and J. Delhommelle, *Phys. Rev. Lett.* 98, 235502 (2007).

[3] C. Desgranges and J. Delhommelle, *J. Am. Chem. Soc.* 128, 15104 (2006).

[4] C. Desgranges and J. Delhommelle, *J. Am. Chem. Soc.* 129, 7012 (2007).

[5] J. M. Leyssale, J. Delhommelle and C. Millot, *J. Am. Chem. Soc.* 126, 12286 (2004).

### 13.10.06

**An *in situ* Atomic Force Microscopy Study of Monosodium Urate Crystal Growth.** Clare M. Yannette, Jennifer A. Swift, Dept. of Chemistry, Georgetown Univ., Washington, DC 20057.

The occurrence of gout has long been associated with the crystallization of monosodium urate (MSU) in the synovial fluid of the joints. However, little is known about the nucleation of this material or the growth rates and mechanisms of its individual surfaces. The goals of this work are (1) to investigate the surface topography of MSU crystals and (2) to obtain a molecular-level understanding of its growth rates and mechanisms. *In situ* atomic force microscopy (AFM) has been used to characterize the surface topology and determine the growth rates and mechanisms of single crystal MSU as a function of fundamental solution parameters such as pH, supersaturation, and temperature.

Synthetic MSU crystals are grown in the lab from aqueous solutions containing uric acid and sodium chloride. Topographical images of MSU (010) display stacks of multi-layers in air as well as mono- and multi-layer steps in fluid. Surface layer growth rates have been obtained from slow scan axis disabled images. Under the range of supersaturation investigated, layer growth proceeds at a constant rate of 1 nm/sec. In addition to the layer growth observed, the adsorption and expansion of two-dimensional islands is also evident. In order to learn more about the birth and spread of MSU islands on the surface, dynamic light scattering is employed to determine the particle size of MSU islands in solution. At this point, the mechanism(s) of growth for MSU appear to include both layer by layer growth and growth by two-dimensional nucleation.

**13.10.07**

**Reaction Crystallization Mechanisms for Screening and Synthesis of Cocrystals.** Naír Rodríguez-Hornedo, Sarah J. Nehm, Adivaraha Jayasankar, David J. Good, L. Sreenivas Reddy, Dept. of Pharmaceutical Sciences, Univ. of Michigan, Ann Arbor, MI 48109 (nrh@umich.edu).

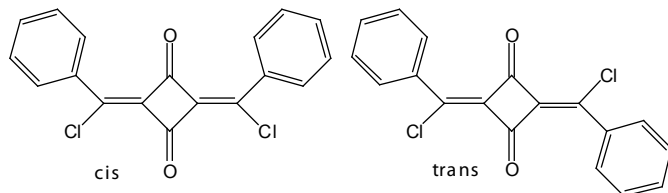
Cocrystals offer the advantage of generating solid forms of active pharmaceutical ingredients (APIs) with other molecular components and produce materials with strikingly different and advantageous properties. Much of the research in this field has focused on the application of supramolecular chemistry concepts to the design of cocrystals while the mechanisms for cocrystal formation are not well understood.

This talk will present liquid and solid-state driven methods for cocrystal formation. The phase transformation of API to cocrystal has been shown to depend on solution and cocrystal chemistry where non-stoichiometric concentrations of cocrystal reactants lead to thermodynamically favorable conditions for cocrystallization (Nehm et al., *Crystal Growth & Design*, 2006; Rodríguez-Hornedo et al., *Molecular Pharmaceutics*, 2006). A reaction crystallization method (RCM) for cocrystal screening and synthesis based on the above principles is applied to various systems including the generation of cocrystals by moisture sorption.

**13.10.08**

**Polymorphism and Isomer Cocrystals of Dimers of Phenylpropionyl Chloride.** Raymond E. Davis, Vincent M. Lynch, Dept. of Chem. & Biochemistry, Univ. of Texas, Austin, TX 78712.

Crystallization from a mixture of the isomers (below) of dimers of phenylpropionyl chloride leads to a variety of crystal forms. Dimerization of phenylpropionyl chloride (Wasserman, E. R., Ph.D. Dissertation, Harvard University, 1949) gave brick-red crystalline material, then thought to be a single compound. Monoclinic crystals obtained (R.E. Davis, 1967) by slow evaporation of a benzene contain only the *trans* isomer at an inversion center: *C2/c* (No. 15),  $Z = 4$ ,  $a = 19.311$ ,  $b = 4.791$ ,  $c = 15.801$ ,  $\beta = 96.55^\circ$ . This result was at variance with the observation of a dipole moment of 2.7 D. A recent  $^{13}\text{C}$  NMR spectrum analysis (Wasserman, H. H., private communication) indicated that the material was a 60-40 mixture of two very similar compounds. Thermal gradient sublimation has now yielded red plates of a triclinic polymorph of the *trans* isomer with the molecule at an inversion center: *P-1* (No. 2),  $Z = 1$ ,  $a = 3.799$ ,



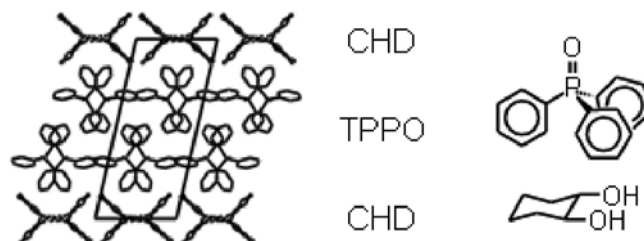
$b = 9.173$ ,  $c = 10.623 \text{ \AA}$ ,  $\alpha = 79.77$ ,  $\beta = 80.86$ ,  $\gamma = 87.60^\circ$ . The thermal gradient sublimation also produced red triclinic needles that contained a mixture of the isomers in the ratio 2 *cis* : 1 *trans*, with the *trans* molecule at an inversion center: *P-1* (No. 2),  $Z = 3$ ,  $a = 3.804$ ,  $b = 11.576$ ,  $c = 24.63 \text{ \AA}$ ,  $\alpha = 100.54$ ,  $\beta = 94.52$ ,  $\gamma = 96.78^\circ$ . Molecular packing in the three crystal forms will be discussed.

**13.10.09**

**An Unexpected Co-Crystal with a Variable Degree of Order: 1:1 *rac*-1,2-Cyclohexanediol/Triphenylphosphine Oxide.** C.P. Brock, M.A. Siegler, Y. Fu, G.H. Simpson, D.P. King, S.Parkin, Dept. of

Chemistry, Univ. of Kentucky, Lexington, KY 40506.

A 1:1 co-crystal of *rac*-*trans*-1,2- $\text{C}_6\text{H}_{10}(\text{OH})_2$  (hereafter, CHD) and  $(\text{C}_6\text{H}_5)_3\text{PO}$  (or, TPPO) has been found that is unusual because there are no strong interactions between the two kinds of molecules, which are segregated into layers. Neither pure CHD nor pure TPPO has any obvious packing problem that would make formation of an inclusion complex likely. The TPPO layers are very much like those found in two of the four known polymorphs of pure TPPO. The H-bonded ribbons of CHD are similar to those found in other *vic*-diol crystals. The co-crystals are triclinic (*P1-bar*), but the deviations from monoclinic symmetry (*C2/c*) are small. The deviations arise from incomplete enantiomeric disorder of the R,R and S,S diols. The magnitudes of the deviations depend on the solvent from which the crystal is grown. When the structure is refined as triclinic the deviations of the occupancy factors from 0.50 mirror the deviations from monoclinic symmetry because information about the partial



R,R/S,S ordering is transmitted from one diol layer to the next through the very pseudosymmetric TPPO layer. Analyses suggest individual CHD layers are at least mostly ordered. The degree of order seems to be established at the time the crystal is grown and is unlikely to change with heating or cooling. Thermal data suggest the existence of the co-crystal is a consequence of kinetic rather than thermodynamic factors. Reasons for this surprising failure of fractional crystallization will be discussed.

**13.10.10**

**A Thermodynamic Understanding of the Stability of Co-Crystals.** Matthew L. Peterson, TransForm Pharmaceuticals, Lexington MA 02421 USA, Mark A. Oliveira, Roger J. Davey, Univ. of Manchester, Manchester UK, M139PL, mark.oliveira@postgrad.manchester.ac.uk.

Relative Enthalpy of Formation of Pharmaceutical Co-crystals. Pharmaceutical co-crystals have become an important area of focus for the pharmaceutical industry in recent years. Co-crystals are crystalline materials that consist of different molecular and electrically neutral species held together by non-covalent forces. There are many questions that remain to be answered about the fundamental science of their formation and stability. The enthalpies of formation of carbamazepine, cyheptamide, and dihydrocarbamazepine co-crystals have been determined by solution calorimetry as part of this investigation. The calculation used a Hess cycle to compare the enthalpy of solutions measured for the co-crystals and their constituents. Factors affecting the enthalpy of solution such as enthalpy of dilution and the enthalpy of mixing of unlike solutes have been investigated. The difference in the enthalpy of the crystal forms is affected by the difference in the intermolecular bonding. The number of hydrogen bonds per unit cell per molecule, type of hydrogen bonds, crystal density, and packing configuration was considered in the analysis of the data. Comparison of this data with the enthalpy of formation provides a clue about the relative strengths of hydrogen bonding versus van der Waals forces. Comparison of these three closely related systems provides a direct measure of the magnitude of the effect that slight differences in intermolecular structure have on intermolecular forces in the crystals.

**13.10.11****Managing Supramolecular Assemblies using Molecular Shape.**

K.A. Wheeler, Dept. of Chemistry, Eastern Illinois Univ., Charleston, IL 61920 USA.

The manner in which molecules organize into energetically favorable collections often relates to complementary electrostatic non-bonded contacts and best fit scenarios. Because of this, it is not surprising that most investigations in this area make use of robust metal-center and hydrogen-bond contacts. Less well studied, but no less important to the overall molecular recognition process, are chemical features that produce less manageable motifs via ill-defined or weak contacts. Molecular shape is one such feature. The quasiracemate approach has proven useful for exploring the utility of molecular shape to crystal packing and may eventually provide insight to what extent molecular topology influences supramolecular chemistry and can molecular shape be used predictively to construct reliable molecular frameworks? Recent results offer new insight into the utility and structural tendencies of materials that exhibit quasiracemic behavior.

**13.10.12****Formation and Characterization of Polymer-Reinforced Porous Single Crystals.** Lara A. Estroff, Hanying Li, Miki Kunitake, Materials Science and Engineering, Cornell Univ., Ithaca, NY.

In this work, we characterize the internal structure of calcite crystals grown in an agarose hydrogel and show that the gel-grown calcite crystals, like biogenic calcite crystals, incorporate the organic matrix. The gel fibers are uniformly distributed within the crystals, without changing the regular rhombohedral morphology of calcite crystals. Etching of the gel-grown crystals with distilled water reveals an interpenetrating network of gel fibers and crystalline material. TEM examination of microtomed slices shows directly the porous internal structures of the crystals. Both electron-back scattered diffraction (EBSD) and selected area electron diffraction (SAED) demonstrate that the structures are single crystals of calcite.

We will also discuss the mechanism of gel incorporation during crystal growth. The effects of gel concentration, gel strength, and the concentration of calcium ions on the amount of incorporated gel were investigated by SEM and TGA. The results show that: 1) The amount of incorporated agarose increases roughly linearly with increasing gel concentration; 2) Crystals grown in a weaker gel (agarose IX) do not incorporate the organic matrix; 3) The amount of incorporated agarose initially increases and then reaches a constant value with increasing concentration of calcium ions. Based on these results, we propose the following mechanism: The gel network causes the growing crystals to incorporate the gel fibers by blocking mass transport to the growth fronts. Counter to this force, the crystallization pressure acts on the gel fibers to push them away. If the gel network is weak, the fibers will be pushed away by the pressure, while if the gel network is strong, the pressure will expand the gel network and the growing crystals will incorporate the fibers. The degree of expansion of the network decreases with increasing supersaturation (calcium concentration). This work provides an in vitro platform to study the biomineralization of calcite and a potential approach to fabricate single crystals coupled with large internal surface areas.

**13.10.13****Serendipity in Drug Development: Discovery and Development of Stable Crystalline Forms of Active Pharmaceutical Ingredients.**

Narayan Variankaval, Materials Characterization and Technology Assessment, Merck Research Laboratories, Rahway, NJ.

This presentation will present the serendipitous discoveries of crystal forms in Merck and their implications in drug development. Three cases will be discussed - (a) crystalline HCl salts of an MC4R agonist, (b) crystalline free base of an ER-beta inhibitor and (c) the discovery of the crystalline phosphate salt monohydrate of sitagliptin, marketed as Januvia by Merck. In each case emphasis will be placed on the nature of the isolation process and more importantly structure-property-function relationships that enabled these forms of the active ingredient to be successfully formulated into drug products. In all these cases crystal structures were solved either from single-crystals or from high resolution powder diffraction data using simulated annealing algorithms. The role played by serendipity in a time of high-throughput approaches for crystal form screening will be highlighted throughout.

**13.10.14**

**Structure and Thermal Behavior of Metal Citraconates.** G. Díaz de Delgado,<sup>a</sup>T. González,<sup>b</sup>A. Briceño,<sup>b</sup><sup>a</sup>Laboratorio de Cristalografía, Facultad de Ciencias, Univ. de Los Andes, Mérida 5251, Venezuela, <sup>b</sup>Laboratorio de Síntesis y Caracterización de Nuevos Materiales, Centro de Química, Inst. Venezolano de Investigaciones Científicas, Caracas 1020-A, Venezuela. diaz@ula.ve.

Metal carboxylates continue to be important materials for a variety of reasons. They are extensively used as precursors in the preparation of metal oxides with potential catalytic activity and in the hydro- and solvothermal synthesis of new metal coordination polymers with hybrid organic-inorganic frameworks. However, the organic moiety may undergo rearrangements, decomposition, and/or reactions during the process making it important to establish its thermal behavior. Recent attempts to obtain metal citraconates by hydrothermal synthesis have been unsuccessful when using citraconic (methyl maleic) acid in the reaction mixture. However, mixed ligand compounds containing the citraconate moiety have been prepared using itaconic acid as a reagent. In this contribution we describe the structure and thermal behavior in the solid state of some metal citraconates, in particular, Sodium citraconate monohydrate (1) and sodium hydrogen citraconate (2). Compound (1) is Monoclinic, C2/m, with  $a=10.967(3)$ ,  $b=6.811(2)$ ,  $c=10.207(3)$  Å,  $\beta=88.23(2)^\circ$ ,  $Z=4$ . Compound (2) is Monoclinic, P2<sub>1</sub>/c, with  $a=12.003(4)$ ,  $b=5.395(2)$ ,  $c=10.213(4)$  Å,  $\beta=111.12(2)^\circ$ ,  $Z=4$ . Both materials decompose upon heating to produce a mixture of methane, ethane, ethene, propane, propene, and butane. <sup>1</sup>H-NMR spectra indicates the formation of sodium methacrylate as a product of partial decomposition upon heating. This is in agreement with the weight loss processes and the transitions observed in the TGA and DSC curves.

This work was supported by FONACIT-Venezuela through grant LAB-97000821.

**13.10.15**

**Structural and Magnetic Properties of [Cu(HF<sub>2</sub>)(pyrazine)<sub>2</sub>]SbF<sub>6</sub> (1) and a Defect-rich Analog [Cu<sub>2</sub>F(HF)(HF)(pyrazine)<sub>4</sub>](SbF<sub>6</sub>)<sub>2</sub> (2).** Jamie L. Manson<sup>a</sup>, Heather I. Southerland<sup>a</sup>, Brendan Twamley<sup>b</sup>, John A. Schlueter<sup>c</sup>, Kylee A. Funk<sup>c</sup>, <sup>a</sup>Dept. of Chemistry and Biochemistry, Eastern Washington Univ., Cheney, WA 99004, <sup>b</sup>Univ. Research Office, Univ. of Idaho, Moscow, ID 83844, <sup>c</sup>Materials Science Div., Argonne National Laboratory, Argonne, IL 60439.

The title compounds contain 2D [Cu(pyrazine)<sub>2</sub>]<sup>2+</sup> square layers that are linked along the *c*-axis by HF<sub>2</sub><sup>-</sup> anions to yield 3D frameworks. SbF<sub>6</sub><sup>-</sup> ions occupy the interior sites. While 1 has a higher Néel temperature,  $T_N$ , of 4.3 K and stronger intra-layer magnetic interactions, 2 displays a markedly lower  $T_N$  of 1.7 K and quasi-1D magnetic behavior. The differences in behavior can be rationalized

by the defect nature of 2 where every-other  $\text{HF}_2^-$  bridge is broken and successive alternation of the magnetic  $d_{x^2-y^2}$  orbitals leads to a reduced spin dimensionality. These materials have been studied in detail by various experimental and theoretical methods, the results of which will be presented.

Crystal data: (1)  $a = b = 9.7200(6)$  Å,  $c = 6.9414(9)$  Å,  $V = 655.8(1)$  Å<sup>3</sup>,  $Z = 2$ ,  $T = 298$  K, space group  $P4/nmm$ ; (2)  $a = 13.589(2)$ ,  $b = 19.974(3)$  Å,  $c = 19.893(3)$  Å,  $V = 5399.6(11)$  Å<sup>3</sup>,  $Z = 8$ ,  $T = 298$  K, space group  $Cmca$ .

This work was supported by an award from Research Corporation (JLM) and the U.S. Department of Energy, Office of Science, Basic Energy Sciences, at Argonne National Laboratory, a U.S. Department of Energy Office of Science laboratory, operated by UChicago Argonne, LLC, under contract DE-AC02-06CH11357. The U.S. Government retains for itself and others acting on its behalf a nonexclusive, royalty-free license in this contribution, with the rights to reproduce, to prepare derivative works, and to display publicly.

### 13.10.16

**Architectural Diversity and Elastic Networks in Hydrogen-bonded Host Frameworks: From Molecular Jaws to Cylinders to Embedded Capsules.** Michael D. Ward, Molecular Design Inst., Dept. of Chemistry, New York Univ., New York, NY 10003.

Guest-free guanidinium organomonosulfonates (GMS) and their inclusion compounds display a variety of lamellar crystalline architectures distinguished by different “up-down” projections of the organomonosulfonate residues on either side of a two-dimensional (2D) hydrogen-bonding network of complementary guanidinium ions (G) and sulfonate moieties (S), the so-called GS sheet. Using a combinatorial library of 24 GMS hosts and 26 guest molecules, a total of 304 inclusion compounds out of a possible 624 possible host-guest combinations were realized, revealing a remarkable capacity of the GMS hosts to form inclusion compounds despite the facile formation of the corresponding guest-free compounds and the absence of “predestined” inclusion cavities like those in related guanidinium organodisulfonate host frameworks. The GS sheets in the inclusion compounds behave as “molecular jaws” in which organomonosulfonate groups projecting from opposing sheets clamp down on the guest molecules, forming ordered interdigitated arrays of the host organic groups and guests. Both the guest-free and inclusion compounds display a variety of architectures that reveal the structural integrity of two-dimensional GS sheet and the unique ability of these hosts to conform to the steric demands of the organic guests. Certain GMS host-guest combinations prompt formation of tubular inclusion compounds in which the GS sheet curls into cylinders with retention of the 2D GS network. The cylinders assemble into hexagonal arrays through interdigitation of the organosulfonate residues that project from their outer surfaces, crystallizing in high symmetry trigonal or hexagonal space groups. This unique example of network curvature and structural isomerism between lamellar and cylindrical structures, with retention of supramolecular connectivity, is reminiscent of the phase behavior observed in surfactant microstructures and block copolymers. The large number of host-guest combinations explored here permits grouping of the inclusion compound architectures according to the shape of the guests and the relative volumes of the organomonosulfonate groups, enabling more reliable structure prediction for this class of compounds than for molecular crystals in general. More recent results that demonstrate the introduction of molecular capsules embedded in these frameworks also will be described.

### 13.10.17

**Metallosupramolecular Architectures Based on Metal(II)-betadiketonates and Small Polyfunctional Molecules as Building Blocks.** N. Judaš, Laboratory of General and Inorganic Chemistry, Dept. of Chemistry, Faculty of Science, Univ. of Zagreb, Horvatovac 102a, HR-10 000 Zagreb, Croatia.

$\beta$ -Diketonate ligands (*i.e.* acetylacetonone,  $\alpha$ -benzylacetylacetonone and dibenzoylmethane) were used to prepare coordinatively unsaturated  $\text{M}^{\text{II}}$ -betadiketonate complexes (where  $\text{M}^{\text{II}} = \text{Cu}^{\text{II}}, \text{Ni}^{\text{II}}, \text{Co}^{\text{II}}$ ). It has been previously shown that this class of compounds exhibit the intriguing ability to act as hosts for both small and bulky molecules (*e.g.* solvent molecules and fullerenes).<sup>1</sup> In addition, metal(II)-betadiketonates were recently recognized as building blocks for 1D hydrogen-bonded coordination polymers.<sup>2</sup> In particular,  $\beta$ -diketonates were used as chelating ligands for  $\text{Cu}^{\text{II}}, \text{Co}^{\text{II}}$  and  $\text{Ni}^{\text{II}}$  to direct their self-assembly process with ditopic molecular linkers towards the formation of 1D polymers.

In this contribution the design, synthesis and structural analysis of 2D hydrogen-bonded structures based on infinite 1D coordination polymers, which are composed of metal(II)-betadiketonates (where  $\text{M}^{\text{II}} = \text{Cu}^{\text{II}}, \text{Ni}^{\text{II}}, \text{Co}^{\text{II}}$ ) and small polyfunctional ligands such as hexamethylenetetramine, pyrazine, 4,4'-bipyridine, nicotinamide and pyridine will be described. Specifically, it will be shown how an appropriate polyfunctional ligand can orchestrate the self-assembly process of 1D coordination polymers into 2D hydrogen-bonded networks. The structural analysis was performed *via* single-crystal X-ray diffraction.

The research is supported by Ministry of Science, Education and Sport of the Republic of Croatia (grant No. 119-1193079-1084).

1) D. V. Soldatov, *J. Chem. Cryst.* 36 (2006) 747-768.

2) C. B. Aakeröy, N. Schultheiss & J. Desper, *Inorg. Chem.* 44 (2005) 4983-4991.

### 13.10.18

**Crystallisation Methods for the Synthesis of Coordination Polymer Complexes.** Elinor C. Spencer<sup>a</sup>, J.A.K. Howard<sup>b</sup>, <sup>a</sup>Dept. Geosciences, Virginia Tech, Blacksburg, VA 24061, USA, <sup>b</sup>Dept. Chemistry, Durham Univ., South Rd., Durham DH1 3LE, UK.

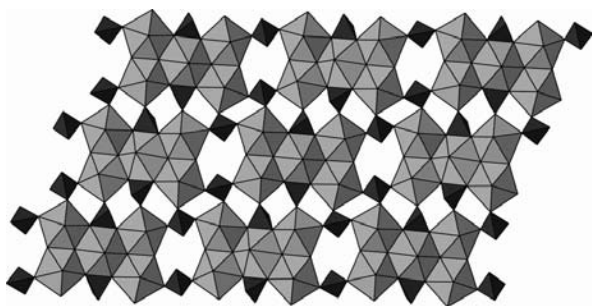
Vapour diffusion and low-concentration crystallisation techniques have been successfully employed in the synthesis of several novel mixed metal-organic 1-D coordination polymer complexes incorporating copper and lead ions, and a variety of dicarboxylate ligands. Additionally, the vapour diffusion method has been used to produce an unusual bimetallic ring structure comprising cobalt ions and 2,2'-diphenyldicarboxylate. The crystal structures of all complexes have been elucidated using single-crystal X-ray diffraction, and these will be presented.

### 13.10.19

**Hydrolysis of  $\text{PF}_6^-$  as a Route to Uranium Phosphates.** Nicholas Deifel<sup>1</sup>, K. Travis Holman<sup>2</sup>, Christopher L. Cahill<sup>1</sup>, <sup>1</sup>The George Washington Univ., Dept. of Chemistry, Washington, DC 20052, <sup>2</sup>Georgetown Univ., Dept. of Chemistry, Washington, DC 20057.

The study of uranyl ( $\text{UO}_2^{2+}$ ) phosphates is of interest due to relevance to the long-term stewardship of spent nuclear fuel. These materials are traditionally synthesized via hydrothermal routes wherein phosphate anions are introduced via preformed alkali metal phosphates, phosphoric acid or as a complex oxide such as  $\text{P}_2\text{O}_5$ . We report an alternative route, namely the hydrolysis of the hexafluorophosphate anion ( $\text{PF}_6^-$ ) to yield phosphate bearing phases. Using the aforementioned *in situ* formation of phosphate anions over the course of a synthesis (vs. the use of a pre-formed building unit)

has resulted in several uranium phosphate phases and, notably, a new uranium phosphate anionic sheet-type with an unprecedented pentameric secondary building unit (1) and a new phosphate fluoride (2). Compound 1,  $[(\text{UO}_2)_5(\text{PO}_4)_4\text{F}_4]$  ( $\text{H}_{10}\text{C}_{10}\text{N}_2$ )<sub>3</sub>, was made by combining uranium(VI) oxynitrate with tetrabutylammonium  $\text{PF}_6^-$  and 4,4' bipyridyl under hydrothermal conditions. The resulting structure crystallizes in the spacegroup  $P-1$  and is a layered uranium phosphate anionic sheet with protonated 4,4' bipyridyl in the interlayer. Compound 2,  $\text{UFPO}_4$ , was synthesized as the above in the absence of an organic and crystallizes in the spacegroup  $Cmca$ . It is densely packed and consists of eight coordinate  $\text{U}^{4+}$  cations linked through corner and edge sharing phosphate tetrahedra and bridging fluorine atoms. Presented will be a systematic overview of crystal structures resulting from this hydrolysis, as well as some noteworthy crystallographic challenges displayed by these materials such as twinning and disorder.



## 13.11 Biological Applications of SAXS and SANS

### 13.11.01

**Small Angle Scattering Studies of Cationic Driven Folding of RNA.** R.M. Briber<sup>1</sup>, S. Moghaddam<sup>1,2</sup>, J.-H. Roh<sup>1</sup>, G. Caliskan<sup>3</sup>, S. Chauhan<sup>3</sup>, L. Guo<sup>4</sup>, D. Thirumalai<sup>2</sup>, S. Woodson<sup>3</sup>, <sup>1</sup>Dept. of Mat. Sci. & Eng., <sup>2</sup>Inst. for Physical Science & Tech Univ. of Maryland, College Park, MD, <sup>3</sup>T.C. Jenkins Dept. of Biophysics, Johns Hopkins Univ., Baltimore, MD, <sup>4</sup>Advanced Photon Source, Argonne National Lab, Argonne, IL.

Small Angle X-Ray Scattering (SAXS) from RNA aqueous solutions has been used to observe the size of the Azoarcus ribozyme as a function of  $\text{Mg}^{2+}$  concentration. The equilibrium pathway for Azoarcus folding in the presence of  $\text{Mg}^{2+}$  involves collapse to an intermediate state  $I_C$  at about 0.5mM  $\text{Mg}^{2+}$  and folding to the final native tertiary structure, N, which occurs at about 2mM  $\text{Mg}^{2+}$ . Our results have shown there is a collapse to a compact state for Azoarcus that corresponds to the  $I_C$  state and we see no large changes in  $R_g$  for the  $I_C \rightarrow N$  transition. We have studied the effect of tertiary interactions on the collapse transition by disrupting of the interactions through mutations. Our measurements indicate that the tertiary interactions play an important role in the stabilization of the collapsed state with the midpoint of the collapse transition increasing significantly and the transition becoming less cooperative. More recent work on the kinetics of folding as measured by stopped-flow SAXS has found that there are two kinetic process present during the folding process. The first is a relatively fast process with a time constant  $\tau \sim 2-4$  msec where the Azoarcus RNA collapses from the unfolded state with  $R_g \sim 6.5$  nm to a compact state with 3.8 nm. The second process is relatively slow with  $\tau \sim 500$  msec - 50 seconds where the molecule folds to the native state with  $R_g$  of 3.1 nm. The SAXS measurements were carried out at Argonne National Lab Advanced Photon Source BioCAT beamline ID18.

### 13.11.02

**Combining Small Angle Scattering and NMR Restraints for Structural Refinement of Macromolecular Complexes in Solution.** Frank Gabel, Inst.de Biologie Structurale, 41, rue Jules Horowitz, 38027 Grenoble, France.

One of the greatest challenges in modern structural biology is the topology characterization of multi-domain macromolecular complexes that govern a major part of important cellular functions. Due to steric properties and inter-domain flexibility, crystallization of such complexes is not always easily accomplished. Amongst the most promising approaches to this problem are multi-disciplinary methods, e.g., by combining X-ray crystallography of single domains with small angle X-ray or neutron scattering (SAXS/SANS) from entire complexes.

Although some progress has been made in the recent years, in many cases these combinations suffer from the ambiguity of how to position high-resolution domain structures with the proper orientations into the low-resolution envelopes provided by the SAXS/SANS. Nuclear magnetic resonance (NMR) residual dipolar couplings (RDCs) can provide such rotational restraints that define domain orientations within larger complexes. Additional contact information between individual domains may be supplemented by NMR chemical shift perturbations.

We present several examples of structural refinement of biomacromolecules in solution by a combination of NMR and SAXS/SANS and discuss their precision and accuracy.

### 13.11.03

**Analyzing Flexible Proteins Using Small Angle X-ray Scattering.** E. Mylonas, P. Bernadó, M. Petoukhov, D. I. Svergun, EMBL Hamburg, C/O DESY, Notkestrasse 85, 22603 Hamburg, Germany.

The number of natively unfolded proteins or proteins with long flexible linkers that have been identified and studied during the recent years is persistently increasing. They are involved in various biologically significant functions such as transcriptional/translation regulation, cell cycle control, modulation of the assembly of other proteins, neuron development etc and are most common in higher organisms. Structural analysis of flexible macromolecular systems is a difficult task since high resolution techniques are barely applicable. However solution small angle X-ray scattering (SAXS) can be applied and two different approaches can be utilized to analyze the data. Information from other methods such as NMR, EM or FRET can also be introduced in the modeling process as additional restraints. The simplest of the two approaches is to produce a SAXS-constrained model which represents on average the shape of the particle in solution e.g. in order to elucidate the relative position of the domains of a multidomain protein. This can be done with existing software that is also used for folded proteins. Of course, such an approach ignores the intrinsic flexibility of the molecules. Using the recently developed Ensemble Optimization Method (Bernadó et al., 2007) it is possible to fit a SAXS curve to multiple models selected from a randomly generated pool. This approach can provide information about the conformational space a protein can explore.

Bernadó, P., Mylonas, E., Petoukhov, M. *et al.* (2007). *Journal of the American Chemical Society* 129, 5656-5664.

### 13.11.04

**Biological Small Angle Scattering/diffraction Facility Beamline 4-2 at SSRL.** Thomas M Weiss, M. Niebuhr, P. Liu, H. Tsuruta, SSRL/SLAC, Stanford Univ., Menlo Park CA.

Beamline 4-2 at the Stanford Synchrotron Radiation Laboratory (SSRL) is a small angle x-ray scattering/diffraction facility dedicated

to structural studies on mostly non-crystalline biological systems and has been operational for over a decade. The facility is currently undergoing an extensive instrumental upgrade of both optics and in-hutch instrumentation to take full advantage of the high brightness beam produced by the third generation storage ring SPEAR3. The instrument will deliver a photon flux of  $3 \times 10^{12}$  photon/s at the sample in the energy range 5-17keV at 500mA ring current. The optional multilayer monochromator increases the flux level by more than an order of magnitude.

The instrument features a pin-hole geometry camera with seven sample-to-detector distances ranging from 0.2m to 3.5m, providing access to the Q-range  $0.003\text{-}4.2 \text{ \AA}^{-1}$  (at 11keV). A newly acquired CCD area detector, optimized for high photon detection efficiency, low noise and improved baseline stability, is expected to provide reliable solution scattering data at low sample concentrations even at high Q values. Several specialized sample handling devices are available, including a stopped-flow rapid mixer for time-resolved studies in the millisecond to minute scale. Our high throughput solution scattering setup, which incorporates a capillary solution cell, a liquid dispenser and a motorized sample selector, is being developed for fully automated data collection. A single-axis goniostat is integrated for single crystal, fiber and grazing-incidence studies and a special sample chamber with accurate temperature and humidity control is available for lipid studies.

A customized version of the Blu-ICE/DCS software is used to control the entire instrument providing an intuitive graphical user interface for the experiment.

### 13.11.05

**Resolution of the Unfolded State.** Gregory Beaucage, Dept. of Chemical and Materials Engineering, Univ. of Cincinnati, Cincinnati OH 45221.

The unfolded states in proteins and nucleic acids remain weakly understood despite their importance to protein folding; misfolding diseases (Parkinson's & Alzheimer's); natively unfolded proteins (~ 30% of eukaryotic proteins); and to understanding ribozymes. Research has been hindered by the inability to quantify the residual (native) structure present in an unfolded protein or nucleic acid. Here, a scaling model is proposed to quantify the degree of folding and the unfolded state (Beaucage, 2004, 2007). The model takes a global view of protein structure and can be applied to a number of analytic methods and to simulations. Three examples are given of application to small-angle scattering from pressure induced unfolding of SNase (Panick, 1998), from acid unfolded Cyt c (Kataoka, 1993) and from folding of Azoarcus ribozyme (Perez-Salas, 2004). These examples quantitatively show 3 characteristic unfolded states for proteins, the statistical nature of a folding pathway and the relationship between extent of folding and chain size during folding for charge driven folding in RNA.

Beaucage, G., Biophys. J., in press (2007). Beaucage, G., Phys. Rev. E. 70, 031401 (2004). Kataoka, M., Y. Hagihara, K. Mihara, Y. Goto J. Mol. Biol. 229, 591 (1993). Panick, G., R. Malessa, R. Winter, G. Rapp, K. J. Frye, C. A. Royer J. Mol. Biol. 275, 389 (1998). Perez-Salas U. A., P. Rangan, S. Krueger, R. M. Briber, D. Thirumalai, S. A. Woodson, Biochemistry 43 1746 (2004).

### 13.11.06

**SAXS Validation of Molecular Dynamics and Docking Based Conformational Sampling.** Kenneth A. Frankel<sup>a</sup>, Martin Pelikan<sup>b</sup>, Robert P. Rambo<sup>a</sup>, Gregory Hura<sup>a</sup>, John A. Tainer<sup>a,c</sup>, Michal Hammel<sup>a</sup>, <sup>a</sup>Lawrence Berkeley National Laboratory, <sup>b</sup>Univ. of Missouri, <sup>c</sup>Scripps Research Inst.

Proteins often adopt flexible multiple domain conformations or form multidomain complexes. These proteins are often not readily amenable to conventional structural analysis such as X-ray crystallography or NMR. Here we perform a systematic exploration of the use of small angle X-ray scattering (SAXS) measurements to filter candidate protein structures for the purpose of protein structure prediction. SAXS is used to potentially validate the predicted structures and to determine the set of most probable atomic models.

In our first strategy, molecular dynamics (MD) simulations are used to explore conformational space. A common strategy is to perform the MD simulation on the domain linkers at very high temperature (~1500K), where the additional kinetic energy prevents the molecule from becoming trapped in a local minimum. Molecular modeling on the interdomain linkers determines the conformational distribution follow by fitting of the theoretical SAXS profile for each conformer to the experimental data. A genetic algorithm could then be applied to analyze the presence of multiple conformations contributing to the experimental scattering profile.

Protein crystal structures are generally monomeric, however biologically active samples and proteins in solution often form multimers. In our second strategy, docking searches are used to predict the interface of dimers and higher-order multimers. We start with a known monomeric structure or a set of structures calculated by protein-folding software. The docking search returns a set of candidate structures that are subsequently validated by fit of the theoretical SAXS profiles to the experimental data. This method can be of potential use to validate predictions from protein folding software.

We present examples of molecular dynamics and docking calculations on test data sets. These examples show the viability of the methods. The software package (alias: BILBO) performing the SAXS validation of MD and docking predicted models is freely available from the authors.

This work was supported by the USDOE under Contract Number DE-AC02-05CH11231.

### 13.11.07

**Molecular Envelopes from SAXS and Single-Molecule Diffraction Experiments at an XFEL.** D.K. Saldin, V. L. Shneerson, R. Fung, A. Ourmazd, Univ. of Wisconsin-Milwaukee.

It has been shown by Stuhrmann [1] that the use of spherical harmonic expansions allows the determination of the expansion coefficients  $f_{lm}$  of a molecular envelope  $F(\omega)$ , where  $\omega$  is an angular coordinate, from small angle X-ray scattering (SAXS) data of an ensemble of randomly oriented molecules. The method involves expressing the spherical harmonic expansion coefficients of the scattered amplitudes  $A_{lm}$  in terms of corresponding expansion coefficients  $f_{lm}^{(q)}$  of the  $q$ th power of  $F(\omega)$ . Owing to the difficulty of numerically evaluating  $f_{lm}^{(q)}$  for higher values of  $l$  and  $q$ , Svergun and Stuhrmann [2] proposed a recursion formula, from which the higher-order coefficients are calculated from lower-order ones. This formalism follows from evaluations of radial integrals of the shape function from power series representations of spherical Bessel functions. We show and demonstrate with practical numerical calculations that difficulties with this formalism may be circumvented by performing analytically the radial integrals with entire Bessel function kernels.

Finally, we show how a further extension of this formalism may allow a more accurate determination of the molecular shape function from diffraction patterns of molecules in random orientations, as envisaged in proposed experiments [3,4] at a future 4th generation

X-ray free electron laser (XFEL) to determine the structures of individual proteins.

- [1] H. B. Stuhmann, *Z. Phys. Chem.* 72, 177 (1970).  
 [2] D. I. Svergun and H. B. Stuhmann, *Acta Cryst. A* 47, 736 (1991).  
 [3] K. J. Gaffney and H. N. Chapman, *Science* 316, 1444 (2007).  
 [4] V. L. Shneerson, A. Ourmazd, and D. K. Saldin, in press (arXiv:0710.2561).

### 13.11.08

**Crystallographic and Small Angle Scattering Studies of the Bacteriophage T4 Replication Complex.** Jennifer D. Hinerman\*, B. Leif Hanson\*, Timothy Mueser\*, \*Dept. of Chemistry, Univ. of Toledo, Toledo OH.

The organization and coordination of DNA replication machinery at the replication fork is important for accurate, efficient DNA synthesis in all organisms. *Bacteriophage T4* provides an attractive model system for determining the architecture of the replication fork and the mechanisms responsible for controlling and coordinating DNA synthesis on the two strands. Interactions between the proteins in the replisome and primosome are key to successful lagging strand replication. Understanding how these complexes interact at the replication fork begins with determining how the T4 gp59 helicase assembly protein (59 protein) recognizes and functions at the fork. The T4 gp32 single-stranded DNA binding protein (32 protein) protects lagging strand single-stranded DNA generated by recombination and replication processes. The 59 protein interacts with replication fork DNA and 32 protein to facilitate the loading of the T4 gp41 helicase (41 helicase) onto the protected DNA. ITC data indicate the 59 protein complexes to the 32-B truncation (32-B, N-terminal deletion) with an affinity of 10  $\mu$ M. The structures of 59 protein and the 32 core have been previously published. Crystallographic studies of protein-protein and protein-DNA complexes of 59 protein, 32 protein and 32 truncations are underway. Successful crystallization of a 32 truncation (32-B) yielded crystal diffraction to 2.9 Å. Small angle scattering experiments (SAXS, APS ChemMatCARS with D. Cookson; SANS, CSMB BioSANS at ORNL with W. Heller and V. Urban) were performed to investigate the interactions between 59 protein with 32 protein and 32-B protein. Models of the binary complexes and the structure of 32-B will be presented.

## 13.12 Powder Challenges

### 13.12.01

**Electron Density at High Pressure from Maximum Entropy Analysis.** John S. Tse, Univ. of Saskatchewan, Saskatoon, Canada.

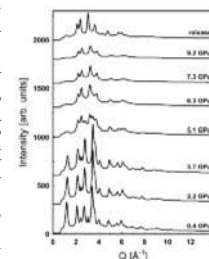
The nature of chemical bonding in materials changes dramatically under pressure. The study of the electron topology will be helpful to identify phase transition mechanism and provide information on the electron structure. We have performed an analysis of high resolution x-ray diffraction patterns of Ba8Si46 clathrate collected from ambient to 30 GPa obtained in a diamond anvil cell using He as a quasihydrostatic pressure transmitting medium using the Maximum Entropy Method. The results indicate unambiguously that the homothetic phase transition at about 17 GPa is due to an extensive rehybridization of the Si atoms leading to a transfer of valence electrons from the bonding to the interstitial region.

Additional and supporting evidence is obtained from a similar study on pure Si. The results show that high resolution and high  $q$  data of materials at high pressure can be obtained using synchrotron radiation and may be useful for the extraction of bonding information with the Maximum Entropy Method.

### 13.12.02

**Structural Changes in Nano-crystalline Mackinawite (n-FeS) at High-pressure.** L. Ehm<sup>1</sup>, F. M. Michel<sup>1</sup>, S.M. Antao<sup>2</sup>, P.J. Chupas<sup>2</sup>, P.L. Lee<sup>2</sup>, C.D. Martin<sup>2</sup>, S. Shastri<sup>2</sup>, J.B. Parise, <sup>1</sup>State Univ. of New York, Dept. of Geosciences, Stony Brook, NY 11794, <sup>2</sup>X-ray Science Div., Argonne National Laboratory, Argonne IL 60439.

Iron sulfides are of major importance in geological, environmental and planetary science. The phase relations in this system are complex and not fully resolved. Recently, it has been shown that synthetic nano-crystalline FeS, similar to that formed in marine sediments from reaction of iron and hydrogen sulfide produced by sulfate-reducing microorganisms adopts the mackinawite structure. The determination of the atomic structure of n-FeS is now possible due to the availability of intense, focused, high-energy synchrotron radiation. These new experimental facilities allow the collection of X-ray total scattering data in pressure cells with good statistics at high reciprocal space values (i.e. 15-20 Å<sup>-1</sup>). The pair distribution function (PDF) is obtained by Fourier transformation of the total elastic scattering data, contains information of the short-, intermediate, and long-range distribution of interatomic distances. The high-pressure behavior of n-FeS with particle sizes of 6, 7, and 8 nm has been investigated by high-energy X-ray total scattering and PDF analysis. An irreversible first-order phase transition from tetragonal mackinawite to orthorhombic FeS-II was observed at about 3 GPa. The transition is induced by the closure of the van-der-Waals gap in the layered mackinawite structure. A grain size effect on the transition pressure and the compressibility was observed. The n-FeS study is an example of a broad class of nano-crystalline minerals where the total scattering approach provides significant new information on the structure.



We would like to thank NSF (DMR-0452444) and DOE (DE-FG02-03ER46085) for financial support.

### 13.12.03

**Guest Atom Disorder in sII and sH Krypton Clathrate Hydrates.** B.C. Chakoumakos<sup>1</sup>, Ling Yang<sup>1</sup>, D.D. Klug<sup>2</sup>, C.A. Tulk<sup>1</sup>, D. Martin<sup>3</sup>, Lars Ehm<sup>3</sup>, J.B. Parise<sup>3</sup>, <sup>1</sup>Neutron Scattering Science Div., Oak Ridge National Lab, Oak Ridge, TN, USA; <sup>2</sup>National Research Council of Canada, Steacie Inst. for Molecular Sciences, Ottawa ON, Canada, <sup>3</sup>Stony Brook Univ., Dept. of Geosciences, Stony Brook, NY, USA.

Kr clathrate hydrate sII was cold-loaded (77K) into a piston cylinder press, warmed to 240K and compressed to 18 kbar, resulting in the formation of sH clathrate. The sample was then quenched to 77K at 18 kbar and recovered to ambient pressure. At the APS sector 11-ID-B X-ray powder diffraction data ( $\lambda=0.137024$  Å) were collected at 40K to  $Q_{\max} = 11$  Å<sup>-1</sup>. Models for Rietveld analysis included only O and Kr atoms. The Kr atoms were initially positioned at the centers of the cages and their isotropic displacements and site occupancies were varied. After a best fit was obtained, the Kr atoms were variously removed from the models, and difference Fourier maps calculated to examine the electron density distribution in the cages. In the small cage of sII the electron density resides at the center, however, for the large cage the electron density is located distinctly off-center, with a tetrahedral arrangement of density at 0.7 Å from the cage center. A subsequent refinement with a split-site model provides a better fit. A similar analysis for sH shows the difference density at the cage center positions for the small and medium cages; however for the large barrel-shaped cage, the electron density is distributed into an equatorial girdle and two symmetry related peaks towards either end

of the barrel.

Oak Ridge National Laboratory is supported by the Division of Materials Sciences, U.S. D.O.E. (contract DE-AC05-00OR22725 with UT-Battelle, LLC).

### 13.12.04

**A New Hexagonal Phase for Pressure-Quenched Xe Clathrate Hydrate.** Ling Yang,<sup>1,2</sup> C.A. Tulk,<sup>1</sup> D.D. Klug,<sup>3</sup> L. Ehm,<sup>4</sup> D. Martin,<sup>4</sup> B.C. Chakoumakos,<sup>1</sup> J.J. Molaison<sup>1</sup>, J.B. Parise<sup>4</sup>, <sup>1</sup>Neutron Scattering Science Div., <sup>2</sup>Center for Nanophase Materials Science, Oak Ridge National Laboratory, Oak Ridge, TN 37831, <sup>3</sup>National Research Council of Canada, Ottawa, Ontario, Canada K1A 0R6, <sup>4</sup>Stony-Brook Univ., Stony Brook, New York, NY 11794.

Xe clathrate hydrate of structure type I (sI) was first synthesized at 250 K and 300 psi from powdered ice. The temperature stabilized samples were then cold loaded (at 77 K) into a piston cylinder device and compressed to 20 Kbar to transform to the well-known hexagonal phase (sH), then the pressure was released and the sample recovered in the liquid nitrogen. The quench-recovered sample was characterized with high energy (115 Kev,  $\lambda = 0.137 \text{ \AA}$ ) synchrotron X-ray scattering at APS, sector 11-1B, in both high resolution and PDF modes. A Le Bail fit of the quench-recovered phase with space group  $P6/mmm$  gives a good fit, ( $R_{wp} = 0.02$ ), and the lattice parameters obtained ( $a = 11.989$ ,  $c = 11.504 \text{ \AA}$ ) are significantly different than those for the conventional sH ( $a = 11.753$ ,  $c = 10.130 \text{ \AA}$ ). This new phase (sH<sub>q</sub>) can be well modeled with the hexagonal clathrate hydrate structure that has been previously reported for Br<sub>2</sub> (Harris 1932) and (CH<sub>3</sub>)<sub>3</sub>N (Panke 2003). Using the energy optimized coordinates of the ideal framework provided by Kosyakov et al. (1994), the X-ray diffraction pattern of the sH<sub>q</sub> can be fitted well ( $R_{wp} < 0.04$ ). The transformation of the sH at high pressure to the pressure-quenched sH<sub>q</sub> can be visualized as the splitting of the large cage in sH into two symmetry equivalent smaller cages in sH<sub>q</sub>.

Oak Ridge National Laboratory is supported by the Division of Scientific User Facilities, U. S. Department of Energy.

### 13.12.05

**High Energy X-ray Diffraction from Aerodynamically Levitated Silicate Melts.** C.J. Benmore<sup>1</sup>, M.C. Wilding<sup>2</sup>, J.K.R. Weber<sup>1,3</sup>, Q. Mei<sup>3</sup>, <sup>1</sup>Argonne National Laboratory, IL, 60439, USA, <sup>2</sup>Univ. of Wales, Aberystwyth, Cerdigion SY23 3BZ, UK, <sup>3</sup>Materials Development, Inc., Arlington Heights, IL 60004, USA.

Containerless high energy x-ray diffraction measurements on silicate liquids have been performed on laser heated droplets suspended in an aerodynamic levitator system. The use of large area detectors has enabled liquid structure factors in the Al<sub>2</sub>O<sub>3</sub>-SiO<sub>2</sub> and MgO-SiO<sub>2</sub> systems to be obtained over a wide Q-range at temperatures >2000°C in minutes. Pure silica is found to maintain strong directional bonds and a high degree of intermediate range order in the liquid state, consistent with SiO<sub>2</sub> having a weak glass transition. The addition of alumina to SiO<sub>2</sub> results in a rapid a breakdown of the corner shared SiO<sub>2</sub> intermediate range ordered network, and the (Si and Al) cations are found on average to be surrounded by four oxygens across the entire compositional range. This is consistent with the presence of a significant number of tetrahedral oxygen triclusters (three cations bonded to a single oxygen) acting as a charge balance mechanism in high Al<sub>2</sub>O<sub>3</sub> content aluminosilicate melts. Magnesium silicate liquids on the other hand reveal a structural transition from a polymerized silicate network to a disordered MgO<sub>n</sub> network with increasing MgO content, similar but not identical to, that found in the glassy state. These structural changes are associated with increasing liquid fragility from SiO<sub>2</sub> (strong) towards the fragile Forsterite (Mg<sub>2</sub>SiO<sub>4</sub>) and Mullite (Al<sub>6</sub>Si<sub>2</sub>O<sub>13</sub>) compositions.

This work was supported by the U.S. DOE, at the XSD and IPNS Divisions, Argonne National Laboratory under contract number DE-AC02-06CH11357.

## 13.13 Materials for Energy Applications

### 13.13.01

**The Prediction of Structure and Properties for Rechargeable Li Battery Electrode Materials.** G. Ceder, Dept. of Materials Science & Engineering, Massachusetts Inst. of Technology, Cambridge, MA.

The prediction of crystal structure is becoming the Achilles heel of *ab initio* computational materials design. While significant progress has been made on improving the prediction of properties with computational quantum mechanics, such results are often meaningless when calculated on an incorrect structure. Hence, the promise of virtual materials design can only be realized if methods to predict structure can be developed. I will use the application of Li-storage electrodes for rechargeable batteries to illustrate how crystal structure determines important properties such as voltage, charging rate capability, and capacity fade, and how these properties can be predicted.

I will also show how an unusual, but efficient solution to the structure prediction problem can be obtained by merging ideas from heuristic approaches and *ab initio* methods: In the same way that scientist build empirical rules by observation of experimental trends, we have developed machine learning approaches that extract knowledge from a database of experimental and computed information, and uses this to rapidly direct accurate quantum mechanical techniques to the lowest energy crystal structure of a material. *Knowledge* is captured in a Bayesian probability network that relates the probability to find particular crystal structure at a given composition to structure and energy information at other compositions. We show that this approach is highly efficient in finding the ground states of materials.

### 13.13.02

**Bulk Materials for Thermoelectric Power Generation.** Michael A. McGuire, Materials Science and Technology Div., Oak Ridge National Laboratory.

Coupling between flows of electrical and thermal energy in thermoelectric (TE) materials allows for the direct conversion between heat and electricity. This allows small reliable devices to be constructed to provide electrical power in remote locations, or to recover energy from waste heat by turning it directly into electricity. Using such devices, heat from automobile engines or exhaust systems can be used to power onboard electrical components, which could decrease the load on the alternator and ultimately increase fuel efficiency. Efficient TE devices require materials with not only a strong coupling between charge and heat currents (the Seebeck coefficient,  $S$ ), but also low electrical resistivity ( $\rho$ ) and low thermal conductivity ( $\kappa$ ). In bulk crystalline materials these three transport properties are intimately related to the crystal structure. Optimizing  $S$ ,  $\rho$ , and  $\kappa$  simultaneously in a given compound and the discovery of new materials with good combinations of these properties are two of the greatest challenges which must be overcome for the development of efficient TE power generation devices. I will introduce the basic concepts of TE device design and applications, and review some of the best materials currently used for power generation. I will then address some new materials and classes of compounds that show promise for future development, emphasizing throughout the importance of the understanding of relationships between crystal structure and transport properties.

**13.13.03****Structural Aspects of Coordination Polymers for Gas Storage.**

Craig M. Brown<sup>1</sup> Yun Liu<sup>1,2</sup>, Dan A. Neumann<sup>1</sup>, <sup>1</sup>NIST Center for Neutron Research, 100 Bureau Dr., Gaithersburg, MD, <sup>2</sup>Dept. of Materials and Engineering, Univ. of Maryland, College Park, MD.

Storing Hydrogen molecules in porous media based on a physisorption mechanism is one possible approach to reach the US Department of Energy targets for on-board hydrogen storage. Although the storage capacities of coordination polymers have progressed significantly over recent years, some technological obstacles pose challenges for their future improvement. These include the generally low H<sub>2</sub> adsorption enthalpy limiting room temperature applications and the lack of understanding of surface packing density hindering the efficient improvement of H<sub>2</sub> adsorption uptake.

To improve the H<sub>2</sub> affinity in coordination polymers, our previous work has shown that the coordinatively unsaturated metal centers (CUMCs) can greatly enhance the H<sub>2</sub> binding strength. A study of MOF-74 will be presented, showing that its open Zn<sup>2+</sup> ions bind H<sub>2</sub> strongly and are identified as being responsible for the large initial H<sub>2</sub> adsorption enthalpy of 8.4 kJ/mol. In all, there are four H<sub>2</sub> adsorption sites in MOF-74 identified by neutron powder diffraction. These four hydrogen adsorption sites are closely packed in MOF-74 and form a one dimensional nanoscale tube structure. We will present a series of gas adsorption studies in MOF-74 aimed at elucidating the nature of the metal-hydrogen interactions in these materials.

**13.13.04****Temperature and Pressure Dependent Structural Changes of MIL-53, A Potential H<sub>2</sub> Storage Material.**

Jae-Hyuk Her<sup>1,2</sup>, Yun Liu<sup>1,2</sup>, Craig Brown<sup>1</sup>, Dan Neumann<sup>1</sup>, Anne Dailly<sup>3</sup>, <sup>1</sup>NIST Center for Neutron Research, 100 Bureau Dr., Gaithersburg, MD 20899, <sup>2</sup>Dept. of Materials & Engineering, Univ. of Maryland, College Park, MD 20742, <sup>3</sup>GM Corp., Chemical & Environmental Science Lab., 30500 Mound Rd., Warren, MI 48090.

Aluminum terephthalate (MIL-53) has attracted researchers' interest due to its potential application as a physisorption-based hydrogen storage material. However, its structural information under non-ambient environments is not completely understood. To elucidate the storage mechanism and shed insight on the apparent hysteresis in the isothermal hydrogen adsorption, we have studied the MIL-53 structure at various temperatures and under several hydrogen (deuterium) pressures using neutron powder diffraction.

The bare material showed an unexpected phase transition with an extremely large hysteresis effect between ~100 K and ~300 K. The previously known open-pore structure (Imma:HT-phase) begins to collapse into a closed-pore structure (C2/c:LT-phase) at about 100 K and gradually transforms as temperature decreases. Observations of similar structural transitions have been reported only in the cases of solvation, where there is significant solvent-framework interaction.

To further illustrate the effects of structure on the isotherm at 77 K, we loaded D<sub>2</sub> gas into MIL-53 progressively up to 4.5 bars. The applied pressure was observed to induce a transition from the closed LT-phase to a more opened structure while maintaining the monoclinic symmetry (C2/c). At a pressure of 4.5 bars, the closed LT-phase was almost completely absent and did not recover after the pressure was reduced to 1.5 bars. From this work, two D<sub>2</sub> loading sites were identified by Rietveld refinement, corresponding to 3.8 mass percent (H<sub>2</sub> equivalent) if fully occupied, consistent with previous reports.

**13.13.05****Methane Storage in Nanoporous Metal-Organic Frameworks and Novel Phase Transition of Confined Methane.** Hui Wu, Dept. of Materials Science and Engineering, Univ. of Maryland, 2135 Chemical & Nuclear Engineering, College Park, MD 20742.

Nanoporous metal-organic frameworks (MOFs) are promising materials for methane storage. Using Rietveld refinement of neutron powder diffraction and difference Fourier analysis, we for the first time directly determined the methane sorption sites in two prototypical MOF materials: zeolitic imidazolate framework-8 (ZIF8, Zn<sub>6</sub>(N<sub>2</sub>C<sub>4</sub>H<sub>5</sub>)<sub>12</sub>) and metal-organic framework-5 (MOF5, Zn<sub>4</sub>O<sub>13</sub>(C<sub>8</sub>H<sub>4</sub>)<sub>3</sub>). We found that the methane adsorption are affected by both the available binding sites and the local framework geometry. Therefore, optimization of binding energy, accessible adsorption sites and free pore volume is the key in designing new materials for methane storage. The primary methane adsorption sites are associated with the organic linkers in ZIF8 and metal oxides clusters in MOF5. Methane molecules on these primary sites possess well-defined orientations, implying relatively strong binding with the framework. At low temperature, additional methane molecules can populate on the secondary sites and be confined in the framework. An unusual first-order phase transition at ~ 60 K is observed for the confined methane in both ZIF8 and MOF5. Such novel phase transition are originated from the partial ordering of the confined methane in the framework pores. Removal of the methane molecules from the host lattice at higher temperature recovers the original symmetry of the framework. This suggests that, besides having exceptional adsorption properties, MOFs also provide fascinating opportunities for investigating the phase behavior of physically and biologically fundamental small molecules such as H<sub>2</sub>O, CH<sub>4</sub>, and NH<sub>3</sub> in nano-confinement environment.

**13.13.06****Crystal Chemistry, Crystallography, and Thermoelectric Properties of Compounds in the Ca-Sr-Co-O System.**

W. Wong-Ng<sup>1</sup>, G. Liu<sup>1</sup>, E. Thomas<sup>1</sup>, M. Otani, N. Lowhorn<sup>1</sup>, J.A. Kaduk<sup>2</sup>, <sup>1</sup>Ceramics Div., National Inst. of Standards and Technology, Gaithersburg, MD, <sup>2</sup>INEOS Technologies, Naperville, IL.

In response to soaring energy demand, increasing global attention to research and development of thermoelectric materials has developed in recent years. The discovery of the novel thermoelectric oxides has been of great interest to the thermoelectric community, particularly to those who are interested in high-temperature applications, such as the automobile industry, because of the stability of oxides at high temperature. One specific family, the layered cobaltites that include Ca<sub>2</sub>Co<sub>3</sub>O<sub>6</sub> and Ca<sub>3</sub>Co<sub>4</sub>O<sub>9</sub> has attracted considerable attention because of the coexistence of large Seebeck coefficient and low resistivity. These compounds also have high electronic anisotropy. This paper discusses the crystal chemistry, crystallography, and thermoelectric property measurements of several series of compounds in the ternary oxide system, Ca-Sr-Co-O. The phase diagram of this system will also be described.

**13.13.07****Structure of a Fluorous Metal-Organic Framework with High Gas Storage Capacities.** Xiaoping Wang, Chi Yang, Mohammad A. Omary, Dept. of Chemistry, Univ. of North Texas, Denton, TX.

Crystal structure of a fluorinated metal-organic framework, {Ag<sub>2</sub>[Ag<sub>4</sub>Tz<sub>6</sub>]}<sub>n</sub> (where Tz = 3,5-bis(trifluoromethyl)-1,2,4-triazolate), **FMOF-1**, has been studied by single crystal X-ray crystallography. It represents the first example of a fluorinated MOF

that has the perfluorinated metal–triazolate clusters serve as building blocks. The resulting crystal structure shows extended 3D open frameworks consisting of 6–connected tetranuclear  $[Ag_4Tz_6]$  clusters linked by 3–coordinate Ag(I) centers. The architectural stability and porosity of **FMOF–1** is confirmed by the high volumetric nitrogen, oxygen and hydrogen storage capacities at various temperature and pressure conditions. Most significantly, the hydrogen adsorption isotherm reveals a hysteretic adsorption/desorption of  $H_2$  within **FMOF–1**, which would permit  $H_2$  to be adsorbed at high pressures but stored at lower pressures.

## 13.14 Microcrystals

### 13.14.01

**In situ Study of Nanotemplate-Induced Growth of Protein Microcrystals by Submicron GISAXS.** Claudio Nicolini, Sailish Tripathi, Eugenia Pechkova, Nanoworld Institute, Univ. of Genova and Fondazione Elba, Italy.

The early steps of growth and nucleation of Lysozyme and Thaumatine microcrystals with classical and protein nanotemplate-based hanging vapor diffusion methods are studied *in situ* using submicron beam GISAXS (nGISAXS) at the ID 13 of the European Synchrotron Radiation Facility (ESRF). Out-of-plane cuts in the Yoneda regions of 2D scattering profiles point to the detection of ultrasmall crystals well before the detection by light microscopy. Crystal formation with of nanotemplate occurs quite earlier than with the classical method. The data are discussed with distinct modes of crystal nucleation and growth for the two proteins, in correlation with Raman Spectroscopy and Atomic Force Microscope.

### 13.14.02

**High Resolution Electron Diffraction of 3D Protein and Pharmaceutical Nano-crystals.** J.P. Abrahams<sup>a</sup>, D.G. Georgieva<sup>a</sup>, H.W. Zandbergen<sup>b</sup>, S. Nicolopoulos<sup>c</sup>, J. Portillio<sup>d</sup>, <sup>a</sup>Dept. of Biophysical & Structural Chemistry, Leiden Univ., 2300 RA Leiden, The Netherlands, <sup>b</sup>Inst. for Metal Research, Delft Univ. of Technology, 2628 CJ Delft, The Netherlands, <sup>c</sup>Nanomegas SPRL, Bruxelles, Belgium, <sup>d</sup>Serveis Científicotecnics, Univ. de Barcelona, Safaris s/n 08028, Spain.

Relative to the number of elastic scattering events, X-rays are three orders of magnitude more damaging to organic molecules than electrons, so for structure determination of 3D nano-crystals of proteins and other damage-prone molecules, electron diffraction is an attractive alternative. For 2D protein crystals, electron diffraction is the only option, but 3D protein crystals present additional problems that have so far frustrated the promise electrons hold in this respect. Here we report that these problems can, to a certain extent, be overcome by combining modern flash-freezing techniques, low dose diffraction conditions and precession of the electron beam. Our procedures, specifically aimed at gathering high-resolution, 3D reciprocal space data, allowed electron diffraction up to 2.2 Å resolution of 3D protein nano-crystals (lysozyme) and up to 1 Å resolution of penicillin-type nano-crystals and the collection of largely complete 3D data sets.

### 13.14.03

**Recording Data from Multiple Protein Microcrystals Using Laue Diffraction.** Sterling Cornaby<sup>1,2</sup>, David Schuller<sup>1</sup>, Doletha M. E. Szebenyi<sup>1</sup>, Detlef Smilgies<sup>1</sup>, Quan Hao<sup>1,2</sup>, Donald Bilderback<sup>1,2</sup>; <sup>1</sup>Cornell High Energy Synchrotron Source, <sup>2</sup>Applied and Engineering Physics, Cornell Univ., Ithaca, NY.

Many proteins of biological importance form only microcrystals (10  $\mu\text{m}$  or less). Using a strong, micron-sized, X-ray beam (such as that from an Energy Recovery Linac (ERL)), good diffraction can be obtained from a single microcrystal, but radiation damage leads to rapid degradation of diffraction quality with time. To obtain a complete, high quality dataset, multiple crystals must be used. We have developed a method for rapidly collecting data from a set of identically grown crystals, using the Laue technique. Diffraction patterns were collected from groups of protein crystals, some as small as 20  $\mu\text{m}$  across, mounted on MicroMesh™ grids, using a “pink beam” at the CHESS D1 station. The bandpass of the beam was 30%, from 10 to 13 keV. This bandwidth was set with two rhodium coated mirrors and a silicon nitride x-ray transmission mirror fabricated from a silicon wafer at the Cornell nanofabrication facility. The wide bandpass beam was then focused to a 13  $\mu\text{m}$  spot size with a single bounce monochromator optic, which is achromatic, achieving a flux density of  $\sim 3 \times 10^8$  photons/sec/ $\mu\text{m}^2$ . A structure was obtained from a set of 17 Laue images from 3 lysozyme crystals, using molecular replacement, and refined to an  $R_{\text{free}}$  under 30%. We believe that this approach will lead to a new avenue for solving protein structures using  $< 10 \mu\text{m}$  crystals and an ERL source.

### 13.14.04

**Dedicated Tuneable Microfocus Beamline I24 at the Diamond Light Source: Prospects for Microcrystallography on Membrane Proteins.** G. Evans, A. Wagner, Diamond Light Source, Harwell Innovation Campus, Didcot OX11 0DE, UK.

The I24 beamline at Diamond Light Source in the UK is the first dedicated tuneable microfocus beamline for macromolecular crystallography. It is scheduled to host its first users in July 2008 and is currently in the final stages of construction and early stages of commissioning.

The beamline aims to address the challenges presented by crystallographic studies on membrane proteins and large multi-protein complexes where crystal samples, once obtained, are notoriously weakly diffracting and typically small in size. The talk will discuss the design considerations for the beamline and present first results from commissioning. Developments being undertaken with the Diamond Membrane Protein Laboratory to help in the manipulation and characterization of microcrystals and in the analysis of diffraction data from such samples will also be presented.

### 13.14.05

**Protein Crystallography with a Micrometre-sized Synchrotron-radiation Beam.** Gebhard Schertler, Laboratory of Molecular Biology, Cambridge, CB2 0QH, Cambridge, UK.

For the first time, protein microcrystallography has been performed with a focused synchrotron-radiation beam of 1 micrometre using a goniometer with a sub-micrometre sphere of confusion. The crystal structure of xylanase II has been determined with a flux density of about  $3 \times 10^{10}$  photons/sec/1 micrometre<sup>2</sup> at the sample. Two sets of diffraction images collected from different sized crystals were shown to comprise data of good quality, which allowed a 1.5 Å resolution xylanase II structure to be obtained. The main conclusion of this experiment is that a high-resolution diffraction pattern can be obtained from 20 micrometre<sup>3</sup> crystal volume, corresponding to about  $2 \times 10^8$  unit cells. Despite the high irradiation dose in this case, it was possible to obtain an excellent high-resolution map and it could be concluded from the individual atomic B-factor patterns that there was no evidence of significant radiation damage. The photoelectron escape from a narrow diffraction channel is a possible

reason for reduced radiation damage as indicated by Monte Carlo simulations. These results open many new opportunities in scanning protein microcrystallography and make random data collection from microcrystals a real possibility, therefore enabling structures to be solved from much smaller crystals than previously anticipated as long as the crystallites are well ordered.

### 13.14.06

#### Can Radiation Damage be Reduced with a 1-Micron Beam?

R.F. Fischetti<sup>1</sup>, R. Sanishvili<sup>1</sup>, D. Yoder<sup>1</sup>, Stefan Vogt<sup>2</sup>, Gerold Rosenbaum<sup>3</sup>, V. Nagarajan<sup>1</sup>, M. Becker<sup>1</sup>, S. Xu<sup>1</sup>, J.L. Smith<sup>1,3</sup>, <sup>1</sup>GM/CA-CAT, Advanced Photon Source and Biosciences Div., Argonne National Laboratory, Argonne, IL 60439, <sup>2</sup>Experimental Facilities Div., Advanced Photon Source Argonne National Laboratory, Argonne, IL 60439, <sup>3</sup>Life Sciences Inst., Dept. of Biological Chemistry, Univ. of Michigan, Ann Arbor, MI 48109.

Last year we announced the development of our “mini-beam” with a 5-micron cross section and low angular divergence (<100 microradians) that enabled micro-diffraction experiments on the two GM/CA-CAT insertion device beamlines. The small beam has several advantages: data of higher signal-to-noise quality can be collected from small crystals by better matching the beam size to the crystal size, one can select the best part of an inhomogeneous crystal, and one can use a rastering technique to record a complete data set with minimal radiation damage. These approaches have been used successfully to solve several structures [1,2].

Recently, we have employed a long focal length Fresnel Zone Plate (FZP) to provide a focused beam of ~1-micron cross section at the sample position. Recent theoretical calculations suggest that radiation damage from the reabsorption of photoelectrons may be reduced in the volume probed by such a small beam [3]. We will present the results of a radiation damage study to test this theory.

<sup>1</sup>Pablo D. Jadzinsky, Guillermo Calero, Christopher J. Ackerson, David A. Bushnell, Roger D. Kornberg, *Science* 318, 430-433 (2007).

<sup>2</sup>Vadim Cherezov, Daniel M. Rosenbaum, Michael A. Hanson, Soren G.F. Rasmussen, Foon Sun Thian, Tong Sun Kobilka, Hee-Jung Choi, Peter Kuhn, William I. Weis, Brian K. Kobilka, Raymond C. Stevens, *Science* 318, 1258-1265 (2007)

<sup>3</sup>Colin Nave and Mark A. Hill (2005), *J. Synchrotron Rad.*, 12, 299–303

## 13.15 Diffuse Scattering Studies of Local Structure in the Solid State

### 13.15.01

**Interplay of Spin-orbital-charge and Lattice Degrees of Freedom in Cobaltites.** Despina Louca, Dept. of Physics, Univ. of Virginia, Charlottesville, VA.

To understand the multi-functionality of complex transition metal oxide systems and the underlying mechanisms that give rise to intriguing effects, it is necessary to understand the intricate interplay of four degrees of freedom: spin – electronic – lattice – orbital. While not all degrees of freedom may be simultaneously active, understanding and defining the competing interactions between the existing degrees of freedom and how they couple together can shed light on fundamental physical questions. This could lead to functional control of technologically important materials with important industrial applications by manipulating and controlling external parameters. An example from the perovskite family will be used, the cobaltites, to address the role of complexity, phase competition and structural inhomogeneities. The cobaltites display several important characteristics that are commonly found in strongly correlated electron systems.

### 13.15.02

**Diffuse Scattering Studies of Local Structure in Crystals with Precipitates.** R.I. Barabash, G.E. Ice, Materials Science and Technology Div., Oak Ridge National Laboratory, USA.

The statistical kinematical theory of diffuse scattering is reviewed. The scattering from different defect distributions is modeled by nonperiodic potentials. The averaged part of the potential is responsible for Bragg scattering, while fluctuating parts of the potential results in diffuse scattering. Fluctuating parts of the potential are analyzed in the framework of the fluctuation wave method. Long and short fluctuation waves of the defect concentration and static displacements are taken into account. The shape function of coherent precipitates is discussed. Distortions of the lattice and changes of the scattering factor due to precipitates cause asymmetry of the diffuse scattering distribution. A comparison with the single defect approximation approach is performed. Experimental and simulated Huang scattering intensity maps are used to perform quantitative characterization of the defects structure and distribution.

Research is sponsored by the Division of Materials Science and Engineering, Office of Basic Energy Science U.S. Department of Energy. Synchrotron measurements on Unicat beamline 34-IDE and 33 BM at the Advanced Photon Source (APS), was also supported by the U.S. Department of Energy, Office of Science.

### 13.15.03

**Study of the Local Distortions of RETe<sub>3</sub> (RE=rare earth) in the Charge-density-wave State Using the Atomic Pair Distribution Function Analysis.** H.J. Kim\*, E.S. Bozin, S.J.L. Billinge, Dept. of Physics and Astronomy, Michigan State Univ., East Lansing, MI, C.D. Malliakas, M.G. Kanatzidis, Dept. of Chemistry, Northwestern Univ., Evanston, IL, Th. Proffen, Lujan Neutron Scattering Center, Los Alamos National Laboratory, Los Alamos, NM 87545.

The charge-density-wave (CDW) state is one of the fundamental broken-symmetry ground states of metals [1] that is commonly found in complex materials. In RETe<sub>3</sub> (RE=rare earth) a simple, single-q, Fermi-surface nesting driven incommensurate CDW (IC-CDW) is found in 2-D tellurium square-net. The atomic pair distribution function (PDF) analysis [2], based on total scattering approach, was carried out to probe the local distortions of CeTe<sub>3</sub>, SmTe<sub>3</sub>, and HoTe<sub>3</sub> in the CDW state. Our PDF study on CeTe<sub>3</sub> suggests that the IC-CDW in CeTe<sub>3</sub> at 300K consists of commensurate CDW domains separated by discommensurations, rather than being a uniform incommensurate CDW as seen crystallographically [3]. The evolution of local Peierls distortions with temperature was studied both in the CDW and normal state of HoTe<sub>3</sub> as well as in the CDW state of SmTe<sub>3</sub>. These recent results will also be addressed.

[1] G. Gruner, *Density Waves in Solids*, Perseus Publishing, Cambridge, MA, 1994.

[2] T. Egami & S. J. L. Billinge, *Underneath the Bragg Peaks: Structural Analysis of Complex Materials*, Pergamon Press Elsevier, Oxford, England, 2003.

[3] H. J. Kim et al., *Phys. Rev. Lett.* 96, 226401 (2006).

\*current address : Lujan Neutron Scattering Center, Los Alamos National Laboratory

### 13.15.04

**The Null-matrix Method Applied on a NiPt Alloy.** J.A. Rodriguez, Univ. of Maryland/NIST, Gaithersburg, MD, S.C. Moss, Dept. of Physics, Univ. of Houston, Houston, TX, J.L. Robertson, Oak Ridge National Laboratory, Oak Ridge, TN, J.R.D. Copley, D.A. Neumann, NIST Gaithersburg, MD 20899, J. Major, Max Planck Inst. fur Metallforschung, 70569 Stuttgart, Germany.

The Null-matrix consists of a composition whereby all effects depending on the average lattice scattering vanish. The only remaining contributions to the diffuse scattering are the Short Range Order (SRO) and Size Effect (SE) terms. Such data permit the extraction

of the SRO parameters (concentration correlations) as well as the displacement parameters (concentration-displacement correlations). We will show the example of a NiPt alloy. Using the Disk Chopper Spectrometer (DCS) at NIST, we have investigated a Null-Matrix Crystal 62Ni 0.52 Pt 0.48, (62Ni has a negative scattering length, nearly equal in magnitude to Pt). Using the Krivoglaz-Clapp-Moss theory, we obtain the effective pair interactions between near neighbors in the alloy from the extracted SRO parameters. The results can be used by theorists to model the alloy in the context of the electronic theory of alloy phase stability, including a preliminary evaluation of the local species-dependent displacements.

### 13.15.05

**X-ray Diffuse Scattering Study of Nano-Scale Lattice Modulation in  $\text{YBa}_2\text{Cu}_3\text{O}_{7-x}$ .** X. Liu<sup>1</sup>, Z. Islam<sup>2</sup>, S. K. Sinha<sup>1</sup>, S.C. Moss<sup>3</sup>, J.C. Lang<sup>2</sup>, U. Welp<sup>4</sup>, <sup>1</sup>Dept. of Physics, Univ. of California, San Diego, La Jolla, CA, <sup>2</sup>Advanced Photon Source, Argonne National Laboratory, Argonne, IL, <sup>3</sup>Dept. of Physics and Texas Center for Superconductivity, Univ. of Houston, Houston, TX, <sup>4</sup>Materials Science Div., Argonne National Laboratory, Argonne, IL.

High temperature superconducting cuprates are intrinsically inhomogeneous due to the dopant atoms. How these dopants perturb the local lattice and the electronic ground state, and their role in transport properties are of great interest. X-ray diffuse scattering studies on optimally doped  $\text{YBa}_2\text{Cu}_3\text{O}_{7-x}$  ( $x=0.08$ ) revealed that the oxygen vacancies cluster to form kinetically limited 4-unit-cell superlattice with  $q_0 = (0.25, 0, 0)$ , along the shorter Cu-Cu bonds. This corresponds to the presence of O-ordered "ORTHO-IV" phase patches in the  $\text{YBa}_2\text{Cu}_3\text{O}_7$  matrix. Long-range strains emanating from these modulated regions are also observed. Quantitative modeling indicates that the strain fields are anisotropic and much stronger along the shorter Cu-Cu bond direction, which may play an important role in the anisotropic transport properties of  $\text{YBa}_2\text{Cu}_3\text{O}_{7-x}$ . Furthermore, modeling of the total diffuse scattering reveals a secondary lattice modulation along the 1-D Cu-O chains to reside only within the O-ordered "ORTHO-IV" phase patches with a wavevector  $q_1 = (0, \sim 0.2, 0)$ , which is consistent with the Fermi-Surface nesting vector,  $(0, 2k_F \sim 0.22, 0)$ , for the chains, according to positron annihilation spectroscopy measurements photoemission results and band structure calculations.

Research at UCSD in the groups of S.K.S. is supported by the U.S. Department of Energy/Basic Energy Sciences through Grant No. DE-FG02-03ER46084. Use of the Advanced Photon Source is supported by the DOE, Office of Science, under Contract No. DE-AC02-06CH11357.

### 13.15.06

**Local Structure of Complex Phases of  $\text{NaNbO}_3$  by Neutron PDF.** D.C. Mitchell<sup>1</sup>, W. Dmowski<sup>1</sup>, Th. Proffen<sup>2</sup>, T. Egami<sup>1,3,4</sup>, <sup>1</sup>Dept. of Materials Science and Engineering, Univ. of Tennessee, Knoxville, TN 37996, <sup>2</sup>LANSCE, Los Alamos National Laboratory, Los Alamos, NM, <sup>3</sup>Dept. of Physics and Astronomy, Univ. of Tennessee, Knoxville, TN 37996, <sup>4</sup>Oak Ridge National Laboratory, Oak Ridge, TN 37831.

$\text{NaNbO}_3$  has a simple chemical formula and belongs to the aristotype perovskite structure. However, it is probably the most structurally complex ferroelectric known. We carried out pulsed neutron diffraction measurements using the NPDF diffractometer at LANSCE in Los Alamos National Laboratory from 8 K up to 930 K. We analyzed data using both the standard crystallographic Rietveld refinement and the atomic pair distribution function (PDF) analysis. In this temperature range  $\text{NaNbO}_3$  undergoes several phase transitions changing macroscopic symmetry and electric properties.

However, the PDF data suggests more gentle changes in the local atomic structure. For polar phases there is a clear split in the Nb-O peak at 2 Å indicating the displacement of Nb atom in the oxygen octahedron and its contribution to the local polarization. This split vanishes above 750 K. At low temperatures Na atoms are also displaced from the ideal perovskite position forming short bonds with oxygen. This bonding is much weaker at room temperature and probably becomes randomized. However, even in the cubic paraelectric phase there is an indication of Na displacements from the ideal position, which is evident from the large temperature factors in the Rietveld refinement and also from the asymmetric peak profiles in the PDF.

## 13.16 Time Resolved Scattering

### 13.16.01

**Structural Dynamics of Myoglobin Investigated by Time-resolved Laue Crystallography.** D. Bourgeois, Inst. de Biologie Structurale, UMR 5075, CNRS/CEA/UJF, Grenoble Cedex, France and ESRF, Grenoble Cedex, France.

Structural dynamics are essential in controlling protein function. Cavity networks have been discovered in proteins, that modulate structural dynamics trajectories and are functionally relevant. In globins these cavities have been assigned a role in ligand migration and docking. This raised renewed interest for time-resolved structural investigations of myoglobin (Mb), the "hydrogen atom of biology". Photo-dissociation of MbCO generates a non-equilibrium population of protein structures relaxing over a time-range extending from ps to ms. This process triggers ligand migration to matrix cavities, associated to the control of geminate rebinding. This presentation will focus on time-resolved Laue diffraction studies on the triple mutant YQR-Mb (Leu29Tyr, His64Gln, Thr67Arg), that aim at following with near-atomic resolution the sequence of structural events associated with protein relaxation in the time window 0.1-300 ns. The slow ligand binding and little fast-geminate recombination in YQR-Mb allowed to highlight the fact that, upon CO photolysis, motions of secondary structures (E-helix, CD turn) lag significantly (100-300 ns) behind local rearrangements around the heme, which occur promptly ( $\leq 3$  ns). The photo-dissociated ligand populates the Xe-binding cavity distal to the heme by 100 ps, essentially before any globin relaxation, and migrates to the Xe1 proximal site in phase with E-helix and CD turn relaxation. The heme relaxation towards the deoxy configuration is heterogeneous, with a ps phase and a slower phase extending over ns. Such complex relaxation of YQR-Mb reflects re-equilibration among conformational substates known to play an essential role in controlling protein function.

### 13.16.02

**Time-Resolved Small-Angle X-ray Scattering Study of Protein Folding.** S. Takahashi, T. Konuma, Y. Goto, and T. Fujisawa, Inst. for Protein Research, Osaka Univ., Osaka 565-0871, Japan and Graduate School of Engineering, Gifu Univ., Gifu 501-1193, Japan.

To understand the mechanism of protein folding, the time-resolved changes in protein compactness in protein folding were systematically investigated by small-angle x-ray scattering (SAXS). Our system is based on the continuous-flow rapid mixing device that can mix two solutions within several hundreds of microseconds, and the beamline at SPring8 designed for X-ray scattering of biological macromolecules (BL45XU-SAXS). We characterized the folding dynamics of cytochrome *c*, apomyoglobin, single-chain monellin and heme oxygenase. The four proteins showed the common folding

mechanism termed “collapse and search”, in which the collapse occurring within several hundreds of microseconds precedes the formation of the native structure occurring in the time domain from milliseconds to seconds. The collapsed conformations demonstrated the scaling relationship between radius of gyration ( $R_g$ ) and chain length with a scaling exponent of  $0.35 \pm 0.11$ , which suggests that the collapse is caused by the coil-globule transition of polymers. We are currently investigating the folding dynamics of  $\beta$ -lactoglobulin by time-resolved SAXS technique. The protein forms a well-known intermediate that possesses a significant amount of non-native helices. Our preliminary results showed that the intermediate is collapsed. The detailed investigation on the formation and disappearance processes of the non-native helices would reveal the relationship between the helix formation and compaction in protein folding.

### 13.16.03

**The Kinetics and Mechanisms of Pressure-Jump Induced Phase Transitions of Lyotropic Lipid Mesophases and Proteins.** Roland Winter, Dept. of Chemistry, Physical Chemistry I - Biophysical Chemistry, Technical Univ. Dortmund, Otto-Hahn Str. 6, D-44227 Dortmund, Germany.

Besides the lamellar lipid bilayer, various non-lamellar lipid phases (hexagonal, micellar, cubic), have become a subject of increased research interest. These lyotropic self-assembled structures are of central importance to the structure and function of cell membranes and play a pivotal role in surfactant-based technologies. The inverse bicontinuous cubic phases have also attracted considerable biotechnological interest, such as for protein crystallization and drug delivery. Moreover, cellular traffic, in particular membrane fusion, budding and fission, must eventually proceed via structural routes that are closely linked to those which occur during lyotropic phase transitions. Identifying and understanding such transformations in model systems will therefore be of central importance to our understanding of endo- and exocytosis and to the design of lipid packaging for effective drug delivery. Much is known about amphiphile-water mixtures in equilibrium but, as yet, little is known about their kinetic and non-equilibrium behavior. The kinetic and structural aspects of the lamellar to inverse bicontinuous cubic phase transition have been investigated using various lipid systems. Transitions in both the forward and reverse directions are effected by means of rapid pressure-jumps and the subsequent structure monitored using Time-Resolved X-Ray Diffraction (TRXRD). The data obtained is analysed with reference to established models, such as for biological cell fusion. The technique has also been applied for studying protein folding reactions. We present data on the pressure-induced un/refolding of proteins using Synchrotron SAXS and FT-IR spectroscopy, which monitor changes in the tertiary and secondary structural properties of the proteins upon pressurization or depressurization. Finally, recent advances in using pressure for studying misfolding and aggregation (amyloidogenesis) of proteins will be discussed. Our approach reveals new insights into the pre-aggregated regime as well as mechanistic details about concurrent aggregation pathways and the differential stability of the protein aggregates.

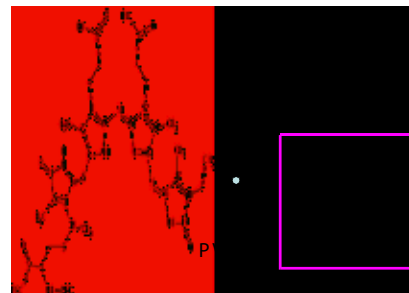
### 13.16.04

**The Z/E Isomerization in Biliproteins.** M. Schmidt<sup>1</sup>, A. Patel<sup>2</sup>, W. Reuter<sup>3</sup>. <sup>1</sup>UW-Milwaukee, Milwaukee, USA, <sup>2</sup>Syracuse Univ., Syracuse, USA, <sup>3</sup>Fa. John, Meckenheim, Germany.

Time-resolved macromolecular crystallography unifies kinetics with structure determination. Chemical reactions in biological macromolecules can be observed in real-time and on the atomic

length scale. As an introduction, photo-flash experiments on <sup>1,29</sup>W-Myoglobin<sup>1</sup> are presented. When compared to the wild-type myoglobin, these experiments clarify the most important migration pathway of small gas-molecules through the protein matrix.

Conformational changes can be particularly well studied using photoactive proteins since they can be conveniently triggered by light. Of special interest are stable photo-optical switches, which can be actively switched back and forth. The  $\alpha$ -subunit of the bili-protein



Phycoerythrocyanin (PEC) constitutes one of these switches. Here, the bile-chromophore phycoviolobilin undergoes a reversible *Z*- to *E*-isomerization.  $\alpha$ -PEC is a role model for similar reactions in the well-known phytochromes which are the most important photo-receptors in plant and other organisms. The *Z*- to *E*-transition is characterized for the first time using conventional static crystallographic methods<sup>2,3</sup>. However, an authentic, detailed description how this molecular photo-switch works is only possible when time-resolved methods are employed.

[1] Schmidt, M., Nienhaus, K., Pahl, R., Krasselt, A., Nienhaus, U., Parak, F. and Srajer, V. (2005) PNAS USA 13, 11704-11709. [2] Schmidt, M., Patel, A., Zhao, Y. and Reuter, W. (2007) Biochemistry 46, 416-423. [3] Schmidt, M., Krasselt, A. and Reuter, W. (2006) BBA 1764, 55-62.

### 13.16.05

**Time-Resolved Solution X-ray Scattering Studies on the Allosteric Transition of *E. coli* Aspartate Transcarbamoylase.** H. Tsuruta<sup>1</sup>, J. Xia<sup>2</sup>, W. Guo<sup>2</sup>, E.M. O'Day<sup>2</sup>, E.R. Kantrowitz<sup>2</sup>, <sup>1</sup>SSRL/SLAC, Stanford Univ., Menlo Park, CA 94025, <sup>2</sup>Dept. of Chemistry, Boston College, Chestnut Hill, MA 02467.

*E. coli* aspartate transcarbamoylase is a dodecameric allosteric enzyme which undergoes a large quaternary structure change upon homotropic and heterotropic allosteric transitions. We will report the direct observation of the kinetics of the quaternary structural transitions promoted by *L*-aspartate in the presence of carbamoyl phosphate and the bi-substrate analog *N*-phosphonoacetyl-*L*-aspartate, recorded at 5ms time-resolution in the temperature range 5-25 °C. Advanced synchrotron radiation instrumentation permitted the use of near physiological solution conditions without the use of ethylene glycol which was required in the past but recently found to dramatically influence enzyme activity. Both the very fast transition from T to R and the reverse transition from R to T after all available substrates have been consumed were observed with high data statistics. It appears that the two-state transition model accounts for the quaternary structural transition even at the earliest stage we have so far recorded. We have also investigated the effects of allosteric effectors on the kinetics. ATP increases the rate of T→R transition and shortens the duration in which the enzyme is in the R steady state. The latter observation is in apparent contradiction to the notion of ATP as an activator. CTP alters both T→R and R→T transitions significantly and the enzyme does not reach the same level of steady-state structural state, compared to the identical conditions without CTP. We observed, for the first time, that UTP alone shortens the duration of the steady-state dramatically in contrast to previous studies in which UTP had only synergic effects in the presence of CTP.

**13.16.06**

**Sub-nanosecond Intermediate of PYP Photocycle Captured by Time-Resolved X-ray Crystallography.** H. Ihee, Y.O. Jung, Center for Time-Resolved Diffraction, Dept. of Chemistry (BK21), KAIST, Daejeon, 305-701, Republic of Korea.

Since the geometrical isomerization within the chromophore pocket of a protein is spatially restricted via media constraints such as hydrogen bonding network and confined space, the usual one-bond-flip mechanism observed in the gas and solution phases no longer holds and instead the volume-converting mechanism has been hypothesized. Previous studies on photoactive yellow protein (PYP) predicted that a twisted form of chromophore by volume-converting model in picoseconds regime, but its exact 3D structure has been elusive. Here we report the earliest intermediate structure ( $I_T$ ) of *trans-cis* isomerization in PYP and detailed atomic motions by picosecond X-ray crystallography. The  $I_T$  intermediate is distorted such that the planarity of chromophore is broken while all three original hydrogen bonds are still intact, and resembles a theoretically predicted transition-state. Hydrogen bonds networking make this distorted structure stable as an intermediate rather than a transition state detectable with time-resolved crystallography. The carbonyl oxygen of  $I_T$  is along the pathway connecting the ground state and the next intermediate ( $I_{CB}$ ) via the bicycle-pedal motion.

We thank ESRF for access to beamline ID09B. This work was supported by Creative Research Initiatives (Center for Time-Resolved Diffraction) of MOST/KOSEF.

**13.16.07**

**Time-Resolved Methods for Fiber Diffraction of Muscle.** T.C. Irving, CSRRI, Dept. BCPS, Illinois Inst. of Technology, 3101 S. Dearborn, Chicago IL, 60616, USA.

X-ray fiber diffraction is the best method to obtain simultaneous structural and functional information from physiological preparations on the required millisecond and sub-millisecond time scale. Third generation sources have provided some unique opportunities and new challenges, especially with detectors, for this relatively old field of study. In this overview talk, I will highlight three studies that exemplify what is now possible with the small-angle instrument at the BioCAT beamline 18ID at the Advanced Photon Source, Argonne National Labs. These will include studies of stretch activation in the indirect flight muscle of *Drosophila* (Dickinson et al., 2005. *Nature*, 433:330-333), studies of the molecular basis for the adjustment of muscle force to the load (Piazzesi, et al., 2007. *Cell* 131, 784-795) and studies of lattice behavior during contraction of live cardiac muscle (Farman et al., 2007. *Biophys J.* 92(9):L73-5).

BioCAT is a National Institutes of Health-supported Research Center RR-08630.

## AW.01 Etter Early Career Award

**AW.01.01**

**Manipulating Hydrogen Bonds in Crystalline Solids: From Etter's Rules to Anion Recognition.** Radu Custelcean, Chemical Sciences Div., Oak Ridge National Laboratory, Oak Ridge, TN.

Hydrogen bonds play critical roles in Nature, from controlling the structure and properties of water to ensuring the cohesion and functionality of complex biological structures. It is therefore of little surprise that researchers working in diverse fields have long attempted to utilize these interactions for deliberate assembly of materials and nanostructures with desired architectures and functions. While conceptually simple, this task is difficult to execute due to the notoriously difficult problem of predicting and controlling the assembly of hydrogen bonds in the solid state, as these relatively

weak interactions may assume alternative patterns with comparable probability of formation. Building on the seminal work of Etter, who in the late 80s formulated empirical "rules" for predicting the intermolecular association of common H-bonding groups, we took on the challenge of assembling functional crystalline solids from simple urea and thiourea H-bonding units. After investing some efforts into understanding the basic electronic and steric factors governing the association of these groups in the solid state, we are now at the point where we can successfully employ them for the design and synthesis of new materials with predetermined functionality. Of particular interest to us is the intriguing possibility of using ureas and thioureas for functionalization of crystalline frameworks rather than their assembly, which requires different design strategies that prevent these groups from self-association. The application of this approach to design and synthesis of functional crystalline materials for anion recognition and separation will be presented.

**AW.01.02**

**Crystal Growth of Bis-Diphenyl Ureas on Silica Templates.** Christina A. Capacci, Jennifer A. Swift, Georgetown Univ., Dept. of Chemistry, 37th & O Sts. NW, Washington, DC 20057

Controlling polymorphism remains a long standing concern for solid state chemists. Historic solutions to this problem have included the introduction of tailor-made additives and crystal growth in polymers, gels or on Langmuir-Blodgett films. Our approach utilizes rationally designed self-assembled monolayers which function as a 2D-template. By engineering a 2D surface with complementary chemical and/or geometric interactions with specific crystal planes, the selective growth of crystal phases can be achieved. Previous work<sup>[1]</sup> has focus on gold-thiol monolayers. The present study focuses on crystal growth in the presence of templates made from 3-X-propyl and 4'-X-phenyl propyl silanes self-assembled on silica. Changes in crystal morphology, nucleation density, orientation and phase selectivity will be described.

[1] Hiremath, R.; Basile, J.A.; Vamey, S. W.; Swift, J.A., *J. Am. Chem. Soc.*, 2005, **127**, 18321-18237.

**AW.01.03**

**Synthesis of Materials in the  $AA'W_3O_{12}$  Family using a Non-Hydrolytic Sol-Gel Process.** Tamam Baiz, Cora Lind, Dept. of Chemistry, The Univ. of Toledo, Toledo, OH 43606, USA.

Negative thermal expansion (NTE) materials, which shrink upon heating, have been a topic of great interest in recent years. Incorporating NTE compounds into composites will allow the synthesis of materials with more desirable expansion coefficients. With these materials, a mismatch of thermal expansion between bonded materials, which could result in cracks, stresses or separation, can be avoided. One family of materials that has been known to show NTE is the tungstate family  $A_2W_3O_{12}$ , where A can be a variety of trivalent cations. However, little research has been carried out on systems containing two differently charged cations instead of just trivalent cations.

In the research presented here, the target is the development of systems where the A site contains two differently charged ions, leading to the synthesis of materials of the type  $AA'W_3O_{12}$  (A= Mg, Zn; A'= Zr, Hf). Previously in the Lind group, heterosystems of this type have been explored via a ball-milling technique, followed by high temperature treatments. Reported herein are the results of a study aimed at synthesizing these materials using a much lower temperature route, known as the non-hydrolytic sol-gel method (NHSG). Samples were characterized using variable temperature powder X-ray diffraction and scanning electron microscopy.

**AW.01.04**

**Adventures in Fullerene Crystallography: A Basketful of Egg-Shaped Fullerenes and a Glimpse of What May Come.** Christine M. Beavers, Marilyn M. Olmstead, Christopher J. Chancellor, Alan L. Balch, Dept. of Chemistry, Univ. of California, Davis, CA 95616.

The collection of endohedral fullerenes that have been crystallographically characterized at UC Davis has grown in the last year. The egg-shaped non-IPR fullerene  $Tb_3N@C_{84}$  was debuted in 2006 as the first structure of a fullerene that has available IPR (isolated pentagon rule) isomers, but instead forms a non-IPR isomer.<sup>1</sup> Following close on the heels of their more famous sibling,  $Tm_3N@C_{84}$  and  $Gd_3N@C_{84}$  are now ready to emerge onto the scene and flaunt their rule-breaking ways.

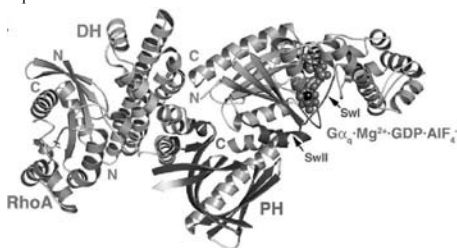
The arms race that is fullerene crystallography is not slowing down. The search for the biggest fullerene structure has led to an obvious junction; the crystals just don't diffract as well when the cages get larger. The obvious answer: more power! The higher flux available at the Advanced Light Source has allowed us to elucidate the structure of the largest fullerene yet,  $C_{94}$ , as well as give us another glimpse into the non-IPR world.

1. Beavers, C.M.; Zuo, T.; Duchamp, J.C.; Harich, K.; Dorn, H.C.; Olmstead, M.M.; Balch, A.L.,  $Tb_3N@C_{84}$ : An Improbable, Egg-Shaped Endohedral Fullerene that Violates the Isolated Pentagon Rule. *Journal of the American Chemical Society* **2006**, 128, (35), 11352-11353.

**AW.01.05**

**Structural Insights into the Activation of RhoA by G<sub>q</sub>-Coupled Receptors.** Aruna Shankaranarayanan<sup>1,2</sup>, Susanne Lutz<sup>3</sup>, Cassandra Coco<sup>2</sup>, Marc Ridilla<sup>1</sup>, Mark Nance<sup>1</sup>, Christiane Vettel<sup>3</sup>, Doris Baltus<sup>3</sup>, Chris Evelyn<sup>4</sup>, Richard Neubig<sup>4</sup>, Thomas Wieland<sup>3</sup>, John Tesmer<sup>1,4</sup>, <sup>1</sup>Life Sciences Inst., Univ. of Michigan, Ann Arbor, MI, <sup>2</sup>Dept. of Chemistry & Biochemistry, Inst. for Cellular & Molecular Biology, Univ. of Texas, Austin, TX, <sup>3</sup>Inst. of Experimental & Clinical Pharmacology & Toxicology, Univ. of Heidelberg, Mannheim, Germany, <sup>4</sup>Dept. of Pharmacology, Univ. of Michigan, Ann Arbor, MI.

$G_{\alpha_q}$ -coupled receptors play an important role in a broad range of physiological events including cardiovascular development and function. p63RhoGEF is a guanine nucleotide exchange factor, that functions as a  $G_{\alpha_q}$  effector and signals the activation of RhoA. To examine the mechanism of  $G_{\alpha_q}$ -mediated activation, we have determined the crystal structure of the  $G_{\alpha_q}$ -p63RhoGEF-RhoA complex, which reveals that  $G_{\alpha_q}$  interacts with both the Dbl homology (DH) and pleckstrin homology (PH) domains of p63RhoGEF with its C-terminal helix and its effector binding site, respectively. The structure predicts that  $G_{\alpha_q}$  potentially relieves auto inhibition mediated by the PH domain of p63RhoGEF by fixing the relative orientation of the DH and PH domains in a manner that allows RhoA to engage the DH domain. We show that  $G_{\alpha_q}$  activates p63RhoGEF-related family members Trio and Kalirin, revealing that there exists an evolutionarily conserved family of RhoA activators responsive to G<sub>q</sub>-coupled receptors. Comparison of the  $G_{\alpha_q}$ -p63RhoGEF-RhoA structure with other recently determined complexes reveals emerging themes of how PH domains and  $G_{\alpha_q}$  subunits engage their protein targets at the cell membrane.



Lutz & Shankaranarayanan *et al*, *Science* 2007

**AW.01.06**

**Cholix Toxin, a Novel ADP-ribosylating Factor from *Vibrio cholerae*.** René Jørgensen, Alexandra E. Purdy, Robert J. Fieldhouse, Matthew S. Kimber, Douglas H. Bartlett, A. Rod Merrill, Univ. of Guelph, Gordon St., Guelph, ON, Canada.

The ADP-ribosyltransferases are a class of enzymes that display activity in a variety of bacterial pathogens responsible for causing diseases in plants and animals including those affecting mankind, such as diphtheria, cholera and whooping cough. We report the characterization of a novel toxin from *Vibrio cholerae*, which we call cholix toxin. The toxin is active against mammalian cells ( $IC_{50} = 4.6 \pm 0.4$  ng/mL) and crustaceans (*Artemia* nauplii  $LD_{50} = 10 \pm 2$   $\mu$ g/mL). Here we show that this toxin is the third member of the diphthamide-specific class of ADP-ribose transferases and that it possesses specific ADP-ribose transferase activity against ribosomal eukaryotic elongation factor 2. We also describe the high-resolution crystal structures of the multi-domain toxin and its catalytic domain at 2.1 and 1.25 Å resolution, respectively. The new structural data show that cholix toxin possesses the necessary molecular features required for infection of eukaryotes by receptor-mediated endocytosis, translocation to the host cytoplasm, and inhibition of protein synthesis by specific modification of elongation factor 2. The crystal structures also provide important insight into the structural basis for activation of toxin ADPRT activity. These results indicate that cholix toxin may be an important virulence factor of *Vibrio cholerae* that likely plays a significant role in the survival of the organism in an aquatic environment.

**AW.01.07**

**A New Detergent System for Membrane Protein Crystallization: 1.4 Å Crystal Structure of the Membrane Protein PagP in SDS/MPD.** J.A. Cuesta-Seijo<sup>3</sup>, G.G. Privé<sup>1,2,3</sup>, <sup>1</sup>Dept. of Medical Biophysics, Univ. of Toronto, <sup>2</sup>Dept. of Biochemistry, Univ. of Toronto, <sup>3</sup>Div. of Cancer Genomics & Proteomics, Ontario Cancer Inst., Univ. Health Network, MaRS Center, Toronto Medical Discovery Tower; Toronto, Ontario M5G 1L7, Canada.

SDS is usually a strongly denaturing detergent, but the cosolvent MPD changes the properties of SDS into a much milder detergent. In our earlier studies, SDS/MPD has been shown to stabilize and refold a panel of soluble and membrane proteins as judged by activity assays and spectral properties<sup>1</sup>. The SDS/MPD detergent system is used here to crystallize PagP, an 8-stranded  $\beta$ -barrel protein from the outer membrane of gram negative bacteria. PagP was overexpressed into inclusion bodies and the SDS/MPD system was used both for refolding and crystallization of PagP. The resulting structure, refined to 1.4 Å, is similar to the crystal structure of PagP in the detergent LDAO. Several SDS molecules are seen in the crystal structure bound to grooves in the membrane exposed surface of the protein. The use of SDS/MPD for refolding allowed for a simpler purification procedure and increased the amount of protein available by 1-2 orders of magnitude. The crystallization and the resulting structure shows that SDS in the presence of MPD can be used for the crystallization of native states of membrane proteins.

<sup>1</sup>Catherine Michaux, Neil C. Pomroy and Gilbert G Privé. Refolding SDS-Denatured Proteins by the Addition of Amphipathic Cosolvents. *J Mol Biol.* 2008 Feb 1;375(5):1477:88

**AW.01.08**

**ER  $\alpha$ -Glucosidase I: Expression, Purification, and Preliminary Crystallography.** M.K. Barker<sup>1</sup>, D.R. Rose<sup>1,2</sup>, <sup>1</sup>Dept. of Medical Biophysics, Univ. of Toronto, <sup>2</sup>Div. of Cancer Genomics &

Proteomics, Ontario Cancer Inst., University Health Network, Toronto, ON M5G1L7 Canada.

Many proteins on the eukaryotic cell surface are covalently linked to complex carbohydrates, leading to a heterogeneously sugar-coated cell. The process of protein N-glycosylation begins in the endoplasmic reticulum (ER) with the transfer of a standard N-glycan,  $\text{Glc}_3\text{Man}_9\text{GlcNAc}_2$ , to an asparagine residue of a nascent protein. The terminal glucose residue is subsequently cleaved by the transmembrane enzyme  $\alpha$ -Glucosidase I (GluI), followed by further processing in the ER and Golgi. Recent studies on the *S. cerevisiae* homolog of GluI have determined several key residues within the catalytic domain, located in the ER-luminal C-terminal region (Faridmoayer *et al.*, 2007). However, despite current interest in GluI the structure is presently unknown, largely due to the lack of an overexpression system which gives sufficient protein yields for structural investigations.

We have cloned a transmembrane-deleted construct of the *S. cerevisiae* GluI into pPICZ $\alpha$ A, a secreted-expression vector for the methylotrophic yeast *Pichia pastoris*. The expression has been optimized and GluI is purified from the supernatant using nickel-affinity chromatography prior to gel filtration chromatography. The purified final yield of active GluI is three milligrams of protein per litre of growth culture. Initial crystal screens have given several hits which are currently being optimized for quality of crystal diffraction. This poster will describe the ongoing work towards gaining a structure of this key member of the N-glycosylation pathway.

## AW.02 Patterson Award: Advances in Macromolecular Phasing and their Impact to Structural Biology

### AW.02.01

**Resolution of Phase Ambiguity in Macromolecular Crystallography: 25 Years Later.** Bi-Cheng Wang, Dept. of Biochemistry and Molecular Biology, Univ. of Georgia, GA 30602.

In the early 1980s, *de novo* structure determinations of macromolecules were mostly accomplished by the technique of multiple isomorphous replacement (MIR) where diffraction data sets from two or more isomorphous heavy atom derivatives were required, in addition to the native data set. Although the phasing power of the single isomorphous replacement (SIR) method was recognized as early as the 1960s, SIR data alone were not routinely used, because of the phase ambiguity problem associated with the SIR data. By analyzing the nature of the SIR phase ambiguity and later the phase ambiguity associated with single-wavelength anomalous scattering (SAS) data, I realized that an electronic density map produced by SIR or SAS data alone contained a perfect protein image plus some random noise (see below and Figs 1a,1b, Wang, Meth. Enzymology, 115, 90-112, 1985).

$$2 \times \rho_{\text{SIR}} = \rho_{\text{Protein}} + (\text{Noise})_{\text{SIR}} \quad 2 \times \rho_{\text{SAS}} = \rho_{\text{Protein}} + (\text{Noise})_{\text{SAS}}$$

This realization made me feel that a properly designed “noise filtering” process should be able to transform, in most cases, a SIR or SAS map into a perfect protein density map without the need of additional experimental data from either different heavy atom derivatives or data collected at different wavelengths. A computer software suite (ISIR/ISAS) was written to demonstrate the potential for protein structure determination by SIR or SAS data alone, including the use of the weak SAS signals from the sulfur atoms in the CYS or MET residues of the unlabeled native protein. I am very pleased to see the recent growing interest in protein structure determinations using the SAS (or SAD) data, and occasionally by sulfur phasing. In this talk, I

will reminisce about some of the theoretical aspects of work done in the early 1980s, initial structures solved by the ISIR/ISAS program, and the future perspectives on routine sulfur phasing.

### AW.02.02

**Evolution of Phase Evaluation from MAD and SAD Measurements.** Wayne A. Hendrickson, Howard Hughes Medical Institute, Dept. of Biochemistry and Molecular Biophysics, Columbia Univ., New York, NY 10032.

Resonance between x-ray waves and electronic orbitals in atoms leads to perturbations in x-ray scattering, known as anomalous scattering. The effect of anomalous scattering on the phases of diffracted waves (Bijvoet, *Proc. Acad. Sci. Amst. B52*, 313, 1949) has proved useful since the early days of protein crystallography (Blow, *Proc. Roy. Soc. A247*, 302, 1958). Initially, anomalous scattering was used to supplement the phase information from multiple isomorphous replacement (MIR) experiments, giving the improvement to MIRAS. Then, first in application to rubredoxin, measurements from single isomorphous replacements with anomalous scattering (SIRAS) proved to suffice (Herriott *et al.*, *J. Mol. Biol.*, **50**, 391, 1970). The advance to use of anomalous scattering without isomorphous replacement came in the analysis of crambin (Hendrickson & Teeter, *Nature* **290**, 107, 1981), owing success to accurate  $\text{CuK}\alpha$  measurements of small Bijvoet differences from sulfur anomalous scattering. In hindsight, this analysis is seen to be the first by single-wavelength anomalous diffraction (SAD). For crambin, the inherent phase ambiguity of SAD was resolved from the partial-structure contribution of sulfur atoms. Density modification approaches (Wang, *Methods Enzymol.* **115**, 90, 1985) provided a more general method for resolution of phase ambiguity; and this has been transformative, leading to the current dominance of SAD analyses in *de novo* macromolecular phasing. Arguably, however, the most crucial impetus to preeminence of anomalous scattering approaches came from synchrotrons. The spectral continuum of synchrotron radiation opened access to the resonance edges where anomalous scattering is greatest. This prompted the development and ascendance of multiwavelength anomalous diffraction (MAD) for phasing (Hendrickson, *Trans. Amer. Cryst. Assn.* **21**, 11, 1985; Hendrickson, *Science* **254**, 51, 1991), and it now permits optimized SAD experiments. MAD ultimately displaced MIR in predominance for *de novo* structure determinations and SAD has now replaced MAD. The evolution continues – less now in analytical methods and more in delivery of efficacious resonant centers.

### AW.02.03

**Wang Limit.** Z. Dauter, Macromolecular Crystallography Laboratory, NCI, Argonne Natl. Lab, Argonne, IL 60438, USA.

The term “Wang limit” of the Bijvoet ratio equal to 0.6 % was not introduced by B.C. Wang, but was used by others as amount of anomalous signal sufficient to solve a structure by single-wavelength anomalous phasing. Actually, Wang never suggested that this value constitutes the border limit for application of his phasing method, he just showed that accurate data containing so low anomalous signal can be successfully used for structure solution. The amount of anomalous signal expected in diffraction data can be estimated from the crystal content, but in practice its usefulness depends crucially on the accuracy of measured intensities. The progress in data collection methodology achieved within last decade made it practical to utilize very small anomalous signals, for example of sulfur atoms present in native protein crystals, often at the level of a fraction of a percent. The expectations of Wang from early 1980s turned out to be very realistic and the practically achieved “Wang limit” value gradually diminishes.

**AW.02.04**

**S and Cr, the Power Couple Next Door.** E.F. Pai, Y. Liu, A. Dong, Depts. of Biochemistry, Medical Biophysics, and Molecular Genetics, Univ. of Toronto, Div. of Cancer Genomics & Proteomics, Ontario Cancer Inst./Princess Margaret Hospital, Toronto, ON, Canada.

With the Structural Genomics Consortium across the street, we took advantage of the existence of crystals that were available in their native form but could not be produced from Se-Met modified versions of the proteins. For simplicity, we collected diffraction data on our standard rotating anode home source, which was re-equipped with a Cr anode and Cr-specific optics. We sampled a range of crystals varying in molecular weight, sulfur content, diffraction power and signal to noise ratio. Our goal was to test whether parameters could be identified that indicated the probability with which those “problem crystals” could be rescued by S-SAD. In line with our “practicability” focus, we also tested some modifications to the standard procedures. The results of our SAD experiences will be discussed.

**AW.02.05**

**Neutron Direct Methods: Have Structure Applications Involving Neutrons Come of Age?** Herbert A. Hauptman, David A. Langs, Hauptman Woodward Medical Research Inst., 700 Ellicott St., Buffalo, NY 14203.

Crystallographers for many years believed that direct phasing methods could not be readily applied to neutron diffraction data for organic structures because hydrogen introduces negative features in the density map relative to other common elements. The positivity of  $\rho(r)$  was thought to be a necessary condition for the mathematical validity of the direct phasing process. Replacing hydrogen by deuterium gets around this problem, but surprisingly does not enhance direct methods solution rates, in spite of the fact that the probabilistic weights of the phase invariants of the D-structures are significantly larger than those for the negatively scattering H-structures. The reasons for this are now better understood.

Given that the above observations concern the application of direct methods to a single native set of neutron data, one may wonder whether similar unforeseen phasing advantages might occur in SIR macromolecular phasing applications to neutron data, as compared to our general experiences using X-ray data. Structural applications that consider several different methods for pursuing neutron SIR phasing will be described.

Research support from the Human Frontier Science Program is gratefully acknowledged.

**AW.02.06**

**Direct Methods and Solvent Flattening.** Hai-fu Fan, Beijing National Laboratory for Condensed Matter Physics, Inst. of Physics, Chinese Academy of Sciences, Beijing 100080, China.

A direct method of breaking enantiomorphous phase ambiguity was proposed in 1965 and substantially improved in 1985. It succeeded in the test of solving a small protein with experimental SAD data in 1990. Combination of the direct method and solvent flattening resulted in dramatically increasing of phasing power. This led to successful SAD phasing of moderate-sized proteins with data at 2~3Å resolution since the middle of 1990s. In recent years, a dual-space iterative procedure involving direct-method phasing, solvent flattening, model building and structure refinement has been proposed and extensively tested. The technique has been proved very efficient in automatic solution of protein structures with SAD/SIR data at lower than atomic resolution and in partial-structure extension with or without SAD/SIR information. Typical applications will be given

in detail. These include: (i) Automatic solution of a 1206-residue protein using anomalous scattering signals from 22 sulfur atoms in the SAD data at 2.1Å resolution collected with Cu-K $\alpha$  X-rays; (ii) Test of SAD phasing at different resolutions from 2.1Å down to 4.0Å; (iii) Combination of SOLVE/RESOLVE, OASIS and DM in SAD/SIR phasing for low resolution, low redundancy and “not-good-quality” data; (iv) Molecular-replacement model completion starting with a model amount to ~20% of the whole structure.

**AW.02.07**

**Molecular Machines, Tropical Diseases and the Power of Llamas.** Wim G. J. Hol, Dept. of Biochemistry, Univ. of Washington, Seattle, WA.

Multi-protein molecular machines are often dynamic assemblies which perform a large number of steps in the right way at the right moment. Examples are (i) the invasion machinery of the malaria parasite, (ii) the “editosome” from the sleeping sickness parasite, and (iii) the Type 2 Secretion System (T2SS) of a wide variety of pathogenic bacteria. The T2SS from *Vibrio cholerae* and from enterotoxigenic *E. coli* (ETEC) secrete critical virulence factors including cholera toxin (CT) and the heat-labile enterotoxin (LT). ETEC is responsible for the death of about 800,000 children annually in the poorer areas of the world. Over the years we have elucidated crystal structures of many components from these three machineries, including domains from twelve T2SS proteins and T2SS subcomplexes. For a number of these structure determinations, the use of single-chain antibodies from camelids appeared to be very helpful in crystal growth by decreasing flexibility of the target protein and by providing additional crystal contact surfaces.

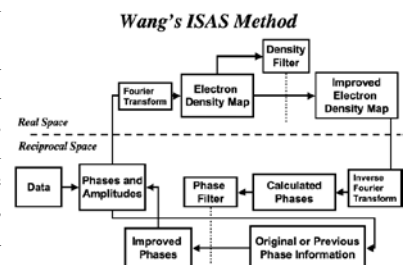
**AW.02.08**

**The First *de novo* Structure Determinations using Wang’s ISAS Technique.** J.P. Rose, Dept. of Biochemistry and Molecular Biology, Univ. of Georgia, Athens, GA 30602 USA.

As a young post-doc new to protein crystallography, the Veterans Hospital in Pittsburgh in the early 1980’s was an exciting place. It was during this time that B.C. Wang, faced with the problem of a protein that formed only a single platinum derivative, developed what was to become the first practical method for macromolecular structure determination from SIR or SAS data, a process he called noise filtering (also referred to as solvent flattening), that resurrected the technique of density modification.

The ISIR technique yielded many new structures and variants of the approach were included in many popular phasing packages, however limitations in X-ray optics, crystal cooling, detectors and data reduction algorithms at that time limited the application of Wang’s noise filtering to single wavelength anomalous scattering data.

The talk will focus on the use Wang’s ISAS technique in the structure determination of bovine neuromalous scattering signal provided by a non-covalently bound iodinated hormone mimic, the structure determination of human ferrochelatase using the iron anomalous scattering signal provided by the ferrochelatase iron-sulfur cluster and the structure determination of the photoprotein obelin using the sulfur anomalous scattering signal provided by the native protein alone.



## TR.01 TRANSACTIONS SYMPOSIUM

### Complementary Methods for Structure/Function Studies of Biomolecules

#### TR.01.01

**In Crystallo UV-visible Spectroscopy.** D. Bourgeois, Inst. de Biologie Structurale, UMR 5075, CNRS/CEA/UJF, 41 rue Jules Horowitz, 38027 Grenoble Cedex 1, France and ESRF, 6 rue Jules Horowitz, BP 220, 38043 Grenoble Cedex, France.

Structural biology at synchrotron sources relies increasingly on complementary methods that are applied to the same sample. Microspectrophotometry in the UV-visible range is a method of choice to assess the relevance of crystallographic structures, monitor chemical changes induced by the X-ray beam, characterize colored ligands, or identify trapped intermediates states [1]. Based on the development of the so-called "Cryobench" laboratory at the European Synchrotron Radiation Facility, Grenoble, France, the principles of in-crystallo UV-visible spectroscopy will be recalled. The possibility to record fluorescence lifetimes and Raman spectra from single crystals will be emphasized [2, 3]. The example of superoxide reductase, a non-heme iron enzyme involved in superoxide detoxification will be detailed. In this case, the combination of kinetic crystallography and Raman spectroscopy was determinant in assessing the relevance of trapped iron-peroxyde intermediate species [4].

[1] T. De la Mora-Rey, et al, *Curr. Opin. Struc. Biol.* (2007), 17, 580-586

[2] A. Royant, et al, *J. Appl. Cryst.* (2007), 40, 1105-1112

[3] P. Carpentier, et al, *J. Appl. Cryst.* (2007), 40, 1113-1122

[4] G. Katona, et al, *Science*, (2007), 316, 449-52

#### TR.01.02

**Photoreduction of Metalloprotein Active Sites by Synchrotron Radiation.** Britt Hedman<sup>1</sup>, Mary C. Corbett<sup>2</sup>, Matthew J. Latimer<sup>1</sup>, Thomas L. Poulos<sup>3,4</sup>, Irina F. Sevrioukova<sup>3</sup>, Keith O. Hodgson<sup>1,2</sup>, <sup>1</sup>Stanford Synchrotron Radiation Laboratory, SLAC, Stanford Univ., 2575 Sand Hill Rd., MS 69, Menlo Park, CA 94025, <sup>2</sup>Dept. of Chemistry, Stanford Univ., Stanford, CA 94305, <sup>3</sup>Depts. of Molecular Biology & Biochemistry, <sup>4</sup>Physiology & Biophysics, and Chemistry, Univ. of California, Irvine, CA 92697.

X-ray damage to protein crystals is assessed on the basis of the degradation of diffraction intensity, yet this measure is not sensitive to the rapid changes that occur at photosensitive groups, such as the active sites of metalloproteins. X-ray absorption spectroscopy (XAS) has been used to study the x-ray dose-dependent photoreduction of crystals of the [Fe<sub>2</sub>S<sub>2</sub>]-containing metalloprotein, putidaredoxin. A dramatic decrease in the rate of photoreduction, followed through changes in the XAS edge structure, is observed in crystals cryocooled with liquid helium at 40 K as compared to those cooled with liquid nitrogen at 110 K, showing structural changes consistent with active site cluster reduction at 110 K, but not at 40 K, even after an eight-fold increase in dose. Comparing structural results from EXAFS to those from crystallography on this and similar proteins, show that x-ray induced photoreduction has impacted the crystallographic data and subsequent structure solutions. These results indicate the importance of using LHe-based cooling for metalloprotein crystallography in order to limit changes at the metalloprotein active sites. The study also illustrates the need for direct measurement of redox states of the metals, through XAS, simultaneously with the crystallographic measurements.

The work was performed at SSRL with support from the NIH NCRR BTP program and the US DOE BER. SSRL operations are funded by the US DOE BES.

#### TR.01.03

**XANES Measurements of the Rate of Radiation Damage to Selenomethionine Side Chains.** James Holton, Biochemistry and Biophysics/Physical Biosciences, UCSF/LBNL, Berkeley, CA.

X-ray absorbance near-edge spectroscopy (XANES) is already a widely used technique at protein crystallography beamlines for determining the best photon energies to use for MAD or SAD experiments. However, XANES can also be used to probe specific chemical changes in the sample and provide complimentary information to crystallographic data. In this study, the x-ray induced cleavage of selenomethionine (SeMet) at cryogenic temperatures was examined and the rate of this damage reaction was found to be influenced by the chemical and physical condition of the sample. Lowering the pH, especially with ascorbic or nitric acids, had a protective effect (reducing the reaction rate) and amorphous samples reacted more slowly than samples that contained crystals of water ice. Low temperature also had a protective effect and the damage rate decreased monotonically with decreasing sample temperature (down to 93 K). In one protein crystal the SeMet damage rate was the same as that of the free amino acid, but the longest SeMet lifetime measured was found in crystals of a different protein. This protection was found to arise from the folded structure of the molecule. The progression of this damage reaction was not linear with time but rather with dose (the energy deposited by the x-ray beam per unit mass of sample). The dose at the half-reaction point ranged from 5 to 43 MGy (kJ/g). These rates were 34- to 3.8-fold higher than the rate at which Se atoms interact directly with X-ray photons, so the energy driving this reaction must be migrating to the Se site from other atoms (a secondary effect). The wide range of decay rates can be explained if the damaging species is a charged quasiparticle that follows the electric field lines around protein molecules.

#### TR.01.04

**Dynamics of Soluble and Membrane Proteins and their Surroundings.** Douglas Tobias, Dept. of Chemistry, Univ. of California, Irvine, Irvine, CA 92697, dtobias@uci.edu.

Protein motions occur over many decades of time, from femtoseconds to seconds and longer. It is well recognized that fast (picosecond to nanosecond) atomic fluctuations are usually required for protein function. At room temperature and in native environments, these fluctuations are liquid-like, while at low temperature and in non-native environments, they appear to be glass-like. A large number of experimental and simulation studies have led to the conclusion that the solvent environment of a protein has a profound influence on protein dynamics, and it is often said that protein motion is slaved to solvent motion. In addition to being of great current fundamental interest, a detailed description of the connection between protein and solvent motion is necessary for understanding the regulation of protein function by changing environmental conditions in cells, and it also has potential biotechnological applications. This talk will review our molecular dynamics simulation studies of the environmental dependence of fast protein dynamics, as well as related neutron spectroscopic investigations. Particular attention will be paid to a detailed description of the dynamics of protein hydration water, and the coupling between solvent and protein dynamics. Specific examples to be presented include dry and hydrated soluble proteins, soluble proteins in glass-forming solvents, and a membrane protein (bacteriorhodopsin) in its natural, multi-component membrane environment, as well as reconstituted in a single-component lipid bilayer. It will be shown that soluble protein motions are directly coupled to the aqueous solvent, and that the situation is more complex in membranes where protein dynamics couple directly to both water and lipid motions, and the lipids, in turn, are dynamically coupled to the water through a different mechanism than the protein.

**TR.01.05**

**Neutron Protein Crystallography.** Leighton Coates, Spallation Neutron Source, Oak Ridge National Laboratory, 1 Bethel Valley Road, Oak Ridge, TN 37831.

The major hurdles holding back neutron protein crystallography since its inception are now starting to be removed. Recently, a number of successful studies have been conducted at the LANSCE based protein crystallography station (PCS) and the LADI III instrument at the Institut Laue Langevin (ILL) examples of which will be given.

The construction of the Spallation Neutron Source (SNS) at Oak Ridge National Laboratory (ORNL) provides a unique opportunity for the design and construction of a dedicated neutron macromolecular diffractometer. MaNDI (Macromolecular Neutron Diffractometer) is currently being designed and built at the SNS and will start operations in around 2012 being only the second time-of-flight based dedicated macromolecular crystallography instrument in North America [1]. The instrument will benefit from the latest advances in detector technology as well as from the order of magnitude gain in neutron intensity that the SNS will provide.

These improvements coupled with many others will greatly reduce the crystal size requirement and data collection time making neutron macromolecular crystallography studies viable for many more protein systems and other complexes. Recent advances in the development of refinement software for use with neutron macromolecular diffraction data will also be highlighted.

[1] A.J. Schultz, P. Thiyagarajan, J.P. Hodges, C. Rehm, D.A.A. Myles, P. Langan and A.D. Mesecar, Conceptual design of a macromolecular neutron diffractometer (MaNDI) for the SNS *J. Appl. Cryst.* (2005). 38, 964-974.

**TR.01.06**

**Neutron Diffraction Studies of Membranes and Membrane Proteins as Multilayers.** David Worcester, Biology Div., Univ. of Missouri-Columbia & CNBT Project, NCNR, Gaithersburg, MD, Ella Mihailescu, Stephen H. White, Dept. of Physiology and Biophysics, UC-Irvine, CA.

Biomembrane studies by neutron diffraction from multilayers have been greatly aided by the new diffractometer/reflectometer AND/R at NCNR. These studies utilize deuterium labeled components such as peptides with selected amino acids deuterated, or lipids with deuterium covalently incorporated at specific sites. Small proteins or peptides can also be obtained in fully deuterated form by expression in cell cultures with D<sub>2</sub>O. Recent studies will be presented for both low-resolution analysis and one-dimensionally oriented microcrystals from multilayered samples that provide data to nearly atomic resolution. Sample preparation is described that allows measurements to be made from the same sample using neutrons, X-rays, FTIR and oriented circular dichroism spectroscopy. Research supported in part by the National Institute of General Medical Sciences.

**TR.01.07**

**Combining High-Resolution Structures with Small-Angle Scattering and Neutron Contrast Variation Data for Studying of Protein Complexes in Solution.** Jill Trehwella, School of Molecular and Microbial Biosciences, Univ. of Sydney, Australia.

Small-angle solution scattering yields low-resolution structural information that complements high-resolution techniques such as crystallography and NMR. The ever increasing desire to understand more complex biological systems, has brought about a recent surge in interest in the technique, greatly facilitated by developments in sources, instrumentation, and 3D modelling algorithms. Modelling

3D structures from solution scattering data is an appealing idea; however, the solution may not be uniquely determined by a single scattering profile. This ambiguity can be resolved, in part, through the inclusion of neutron contrast variation data<sup>1</sup>. We have been using this approach to study bio-molecular signalling and regulation, specifically looking at the protein interactions controlling bacterial sporulation<sup>2</sup> and more recently in those involved in cardiac muscle function<sup>3,4</sup>. This presentation will describe the strengths and limitations of these approaches in the context of understanding bio-molecular structure and function. It will also compare and contrast what can be done with small-angle X-ray scattering for which contrast variation is not generally feasible using examples drawn from our studies of IP3<sup>5</sup> signalling and transcriptional regulation<sup>6</sup>.

1. Whitten, Cai, Trehwella in press *J Appl Cryst.* 2007

2. Whitten, Jacques, Hamouda, Hanley, King, Guss, Trehwella, Langley *J Mol Biol* 368, 407, 2007.

3. Howarth, Meller, Solaro, Trehwella, Rosevear *J Mol Biol* 373, 706, 2007.

4. Jeffries, Whitten, Harris, Trehwella, J. submitted 2007

5. Chan, Whitten, Jeffries, Bosanac, Mal, Ito, Michikawa, Mikoshiba, Trehwella, Ikura *J Mol Biol* 373, 1269, 2007.

6. Taraban, Zhan, Matthews, Swint-Kruse, Trehwella in press *J Mol Biol*

**TR.01.08**

**Real-time Small-Angle X-ray Scattering Study of Assembly and Disassembly Cycles of Cyanobacterial Circadian Clock Proteins.**

S. Akiyama, PRESTO, Japan Science and Technology Agency, 418 Honcho, Kawaguchi, Saitama 3320012, Japan, RIKEN SPring8 Center, Harima Inst., 111, Kouto, Sayo, Hyogo 6795148, Japan.

Incubation of three clock proteins, KaiA, KaiB, and KaiC, with ATP induces a KaiC phosphorylation cycle that is a potential circadian clock pacemaker in cyanobacterium *Synechococcus elongatus* PCC 7942. To take a structural snapshot of the oscillator, we followed the dynamic oscillatory processes of the Kai proteins using real-time small-angle x-ray scattering techniques. The scattering pattern of a ternary mixture robustly oscillated with a period of approximately 24 h, indicating a repeated assembly and disassembly of the Kai complexes. In the presentation, we will discuss the size and shape of these clock complexes.

**TR.01.09**

**Use of SAXS to Interrogate a Known Crystal Structure as a Basis for Modeling the HIV Defense Factor APOBEC3G.**

Joseph E. Wedekind<sup>a</sup>, Jason D. Salter<sup>a</sup>, Ryan P. Bennett<sup>a</sup>, Jolanta Krucinska<sup>a</sup>, Richard E. Gillilan<sup>b</sup>, Harold C. Smith<sup>a</sup>, <sup>a</sup>Dept. of Biochemistry & Biophysics, Univ. of Rochester SMD, Rochester, NY 14642, <sup>b</sup>Macromolecular Structure Facility at the Cornell High Energy Synchrotron Source (MacCHESS), Cornell Univ., Ithaca, NY 14853, joseph.wedekind@rochester.edu

APOBEC3G (hA3G) is an anti-viral protein expressed in CD4+ T cells. Its mode of action entails deamination of dC to dU in the context of first-strand HIV DNA. Such nucleobase 'editing' confers hypermutation to the viral genome, incapacitating it for subsequent infection. hA3G activity demands the absence of the HIV protein Vif, which recruits hA3G to an E3 ligase complex leading to its degradation. Interest in the function of hA3G, its interaction with Vif, and production of a crystallographically affable construct, prompted us to characterize hA3G by SAXS. Initial efforts focused on a dimeric variant that revealed an elongated shape ( $D_{\text{Max}} = 14$  nm) with an  $R_G$  of 4.6 nm. These results were unexpected since prior deaminase crystal structures exhibited tetragonal envelopes ( $D_{\text{Max}} = 7.8$  nm) with  $R_G$  values of 2.5 nm. Although no crystal structure has been reported for hA3G, that of a distant family member, A2, has been described.

A2 comprises an elongated (1.3 nm) 'dimer-of-dimers' in its ASU, and has been used broadly to model hA3G. However, the dimeric hA3G scattering profile does not concur with that of tetrameric A2 ( $\chi = 3.3$ ). As such, we prepared a monomeric form of hA3G with an  $R_G$  of 3.3 nm ( $D_{\text{max}} = 8$  nm). Significantly, the scattering profile of this 47 kDa subunit also fit poorly to both of the 42 kDa dimeric A2 subunit arrangements in its ASU ( $\chi = 6.4$  & 5.3). These results have implications for hA3G versus A2 oligomer similarity and suggest the potential to assess such modeling templates by SAXS.

#### TR.01.10

**Trapping an Invisible DNA Repair Intermediate for NMR and Crystallography.** James T. Stivers, Dept. of Pharmacology and Molecular Sciences, Johns Hopkins Medical School, 725 North Wolfe St., Baltimore, MD 21205.

The efficient enzymatic detection of damaged bases concealed in the DNA double helix is an essential step during DNA repair in all cells. Emergent structural and mechanistic approaches have provided glimpses into this enigmatic molecular recognition event in several systems. A ubiquitous feature of these essential reactions is enzyme binding to the damaged base in a very unstable extrahelical binding mode. This presentation will describe a combined approach that uses chemistry, solution NMR and X-ray crystallography to characterize the dynamics and structure of an enzyme-bound extrahelical base that is present at an equilibrium population of only one part in 100,000 enzyme-DNA complexes. The findings suggest that enzymes recognize damaged bases by trapping extrahelical conformers that arise from thermal breathing motions of the DNA duplex.

#### TR.01.11

**Merging Crystallography and Spectroscopy to Define Docking at the Proteasome via Rpn13.** Xiang Chen, Patrick Schreiner, Leah Randles, Naixia Zhang, Koraljka Husnjak, Suzanne Elsasser, Daniel Finley, Ivan Dikic, Michael Groll, and Kylie Walters.

An estimated 90% of all proteins are degraded via the proteasome, a 2.5 MDa complex composed of a 20S catalytic subunit capped by one or two 19S regulatory components. Proteins are generally marked for proteasomal degradation by covalently attached ubiquitin chains; however, how the proteasome recognizes its ubiquitinated substrates is not understood. We have identified Rpn13 as a novel ubiquitin receptor intrinsic to the proteasome and have merged x-ray crystallography with NMR spectroscopy to determine how this protein binds polyubiquitin. Our Rpn13:monoubiquitin structure unveils a new ubiquitin recognition mode in which loops are used to bind ubiquitin. By using fluorescence spectroscopy, we find this non-canonical ubiquitin-binding mode to yield the strongest binding affinity to date for a ubiquitin receptor associated with proteasomal degradation. Our merger of crystallography with spectroscopy resulted in a highly efficient, cost effective strategy for defining the Rpn13:ubiquitin protein complex and afforded much insight into Rpn13's function in the proteasome.

#### TR.01.12

**Structural Aspects of HIV-1 Entry Using NMR, X-ray Crystallography and Docking Techniques.** Carole A. Bewley,<sup>a</sup> Son N. Lam,<sup>a</sup> Chih-Chin Huang,<sup>b</sup> Priyamvada Acharya,<sup>b</sup> Syed Hussan,<sup>a</sup> Peter D. Kwong<sup>b</sup>, <sup>a</sup>Laboratory of Bioorganic Chemistry, National Institute of Diabetes and Digestive and Kidney Diseases and <sup>b</sup>Vaccine Research Center, National Institutes of Health.

To better understand the structural basis for entry of HIV into

target cells, ideally we would solve high resolution structures of complexes for each relevant interaction between virus and target cell. However, this has not proven to be possible for the surface envelope glycoproteins of HIV. To overcome the intractable qualities of these proteins, we have been using in combination NMR, X-ray crystallography and modeling techniques to derive what we believe are accurate models of the interactions between HIV Envelope and key portions of its coreceptors, namely the GPCRs CXCR4 and CCR5. Approaches used to generate these structures and models will be discussed as well as their validation by NMR and other biochemical and biophysical techniques.

**MP001**

**The PSI Structural Genomics Knowledgebase.** Helen M. Berman<sup>1</sup>, Paul Adams<sup>2</sup>, Andras Fiser<sup>3</sup>, Adam Godzik<sup>4</sup>, Andrei Kouranov<sup>1</sup>, Rajesh Nair<sup>5</sup>, Christine Orengo<sup>6</sup>, Burkhard Rost<sup>5</sup>, Wendy Tao<sup>1</sup>, Torsten Schwede<sup>7</sup>, Raship Shah<sup>1</sup>, John Westbrook<sup>1</sup> <sup>1</sup>Dept. of Chemistry & Chemical Biology, Rutgers, State Univ. of New Jersey, Piscataway, NJ, <sup>2</sup>Berkeley Structural Genomics Center, Lawrence Berkeley National Lab, Berkeley, CA, <sup>3</sup>Dept. of Biochemistry & Seaver Center for Bioinformatics, Albert Einstein College of Medicine, Bronx, NY, <sup>4</sup>The Burnham Inst., La Jolla, CA, <sup>5</sup>Columbia Univ., New York, NY, <sup>6</sup>Univ. College London, London, UK, <sup>7</sup>Div. of Bioinformatics, Biozentrum, Univ. of Basel, Basel, Switzerland.

The Protein Structure Initiative (PSI) has been successful in producing over 2500 protein structures in a high throughput manner. The strategies used for target selection by PSI centers have resulted in the determination of significantly more novel structures than from structural biology in general. In addition, new technologies for all aspects of the structure determination and analysis pipeline have been developed.

The PSI Structural Genomics Knowledgebase (PSI SG KB) is designed to turn the products of the PSI effort into knowledge that is important for understanding living systems and disease. The PSI SG KB Portal allows access to the structures, annotations, technologies, and models that are the products of the PSI. A description of how this resource will enable further biological discovery will be given. The PSI SG KB is funded by the NIH.

**SP002**

**Crystal Structure of the Heterotrimer Core of the *S. cerevisiae* AMPK Homolog SNF1.** Michael J. Rudolph, Gabriele A. Amodeo, Liang Tong, Dept. of Biological Sciences, Columbia Univ., New York, NY 10027, USA.

AMP-activated protein kinase (AMPK) is a crucial enzyme for maintaining energy homeostasis in eukaryotes. It is regulated by the intracellular ratio of AMP:ATP. When this ratio is high, indicating a low energy state, AMPK is activated, whereas it is inhibited when the ratio is low. Upon activation, AMPK upregulates a number of catabolic processes while simultaneously downregulating energy-consuming processes. AMPK is an attractive target for drug discovery against obesity, type-II diabetes, among other diseases.

The AMPK homolog in *S. cerevisiae* is known as SNF1. We report here the crystal structure at 2.6 Å resolution of the heterotrimer core of SNF1. An interesting difference between SNF1 and mammalian AMPK is SNF1 does not appear to be activated by AMP in vivo. However, our data suggest that SNF1 still has the capacity to bind AMP. The glycogen binding domain (GBD) in the b subunit (Sip2) interacts with Snf4 in the heterotrimer, but should still be able to bind carbohydrates. Our structure is supported by a large body of biochemical and genetic data on this complex. Most importantly, the structure reveals that part of the regulatory sequence (RS) in the a subunit (Snf1) is sequestered by Snf4, demonstrating a direct interaction between the a and g subunits and suggesting that our structure may represent the heterotrimer core of SNF1 in its activated state.

Structure of the heterotrimer core of SNF1. The positions of AMP as observed from our studies and β-cyclodextrin as bound in rat GBD

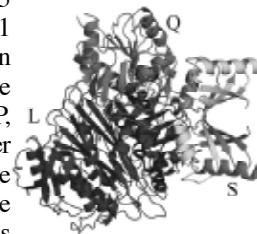
are shown for reference.

Amodeo GA\*, Rudolph MJ\*, and Tong L. Crystal structure of the heterotrimer core of *Saccharomyces cerevisiae* AMPK homologue SNF1. *Nature* 449, 492 (2007) \*These authors contributed equally to this work.

**TP003**

**Formylglycinamide Ribonucleotide Amidotransferase from *Thermotoga maritima*: Structural Insights into the Complex Formation.** Mariya Morar, Steven E. Ealick, Dept. of Chemistry and Chemical Biology, Cornell Univ., Ithaca, NY 14853.

In the fourth step of the purine biosynthetic pathway, formyl glycinamide ribonucleotide (FGAR) amidotransferase, also known as PurL, catalyzes the conversion of FGAR, ATP, and glutamine to formyl glycinamide ribonucleotide (FGAM), ADP, Pi, and glutamate. Two forms of PurL have been characterized, large and small. Small PurL, present in Gram-positive bacteria and archaea, contains the FGAM synthetase activity and forms a complex with two additional gene products, PurQ and PurS. The structure of PurS is known, however the function remains to be elucidated, while PurQ, whose structure has not been reported, contains the glutaminase activity. In *Bacillus subtilis*, the formation of the PurLQS complex is dependent on glutamine and ADP by an unknown mechanism. We determined the structure of the PurLQS complex from *Thermotoga maritima* to 3.5 Å resolution. The structure reveals a 2:1:1 stoichiometry of PurS:Q:L, respectively. In the complex, TmPurL contains a nucleotide bound in an auxiliary site, modeled as ADP, and TmPurQ contains a glutamyl thioester intermediate covalently bound in the active site. Comparison of TmPurLQS with the reported structures of TmPurL, as well as the large PurL from *Salmonella typhimurium* reveals conformational changes in TmPurL attributed to the complex formation. A mechanism of recruitment of PurQ and PurS to the complex by PurL with the assistance of small molecules is proposed based on these observations. The PurS dimer shows flexibility thought to be important for the catalytic coupling between PurL and PurQ, and for the formation of the ammonia channel between them. A potential path for the ammonia channel is identified.

**MP004**

**Instantly Identify Protein Crystals.** G. Ravich, Vu Tran, Korima Inc., Carson CA 90746 USA.

The Korima PRS-1000 UV Microscope instantly reveals the presence of protein crystals in hanging or sitting drop crystallization plates. This technique utilizes the natural fluorescence of folded proteins, which is primarily due to the aromatic residue of tryptophan. A short arc mercury lamp filtered at 280nm excites protein crystals through an ultraviolet microscope objective. Emissive radiation in the 350nm region is collected by the same objective lens and imaged into a UV sensitive camera. The system presents both a UV and visible image simultaneously side by side. Differentiating protein crystals from salt crystals is easy, salt crystals do not fluoresce. Viewing the results not only saves the researcher from pursuing further trials it also eliminates the need for time consuming screening by x-ray diffraction.

Fluorescence takes place independent of the focal plane. The PRS-1000 is configured to provide the necessary excitation in the field of view such that protein crystals regardless of where there may form will fluoresce with high contrasting signaling.

Membrane protein crystals fluoresce without any noticeable interference due to the presence of detergents. Lipidic cubic phase

membrane protein crystals are also revealed even when their crystallization results in micro crystals below 5 micron. All of the described protein crystals are imaged and identified without radiation damage.

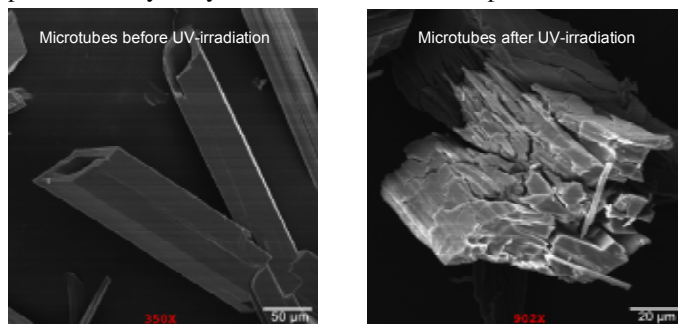
The photos were provided by Jeff Abramson Lab at UCLA.

### SP005

**A Single-crystalline Photoreactive Cocrystal with a Rectangular Cross-section.** Dejan-Krešimir Bučar, Leonard R. MacGillivray, Dept. of Chemistry, Univ. of Iowa, Iowa City, IA.

Since the discovery of carbon nanotubes, nano- and microscaled tubular structures have attracted immense attention due to their applications in optoelectronics, catalysis, biotechnology and drug delivery. Recent research in this field has mainly focused on inorganics and macromolecules, while significantly less attention has been paid to the design of single-crystalline tubular structures based on small organic molecules. At the same time, the design of such structures based on more than one organic component remains unexplored.

We have recently discovered that the 1:1 cocrystals of resorcinol and trans-1,2-bis(4-pyridyl)ethylene (4,4'-bpe) grown from acetonitrile exhibit a rectangular tubular structure. Single crystal X-ray diffraction studies of the tubes revealed a structure characteristic for single crystals. Given that the 4,4'-bpe molecules in the crystalline tube conform to the topochemical postulates, we have carried out a photoreactivity study in which the tubes were exposed to broad-band



UV-irradiation for 24 hours. NMR studies of the irradiated sample revealed quantitative formation of rctt-tetrakis(4-pyridyl)cyclobutane in the solid state. SEM studies of the reacted solid showed that the tubular structure lost integrity during the photoreaction. Specifically, the single crystals cracked to form a polycrystalline sample. To our knowledge, this is the first example of photoactive rectangular single-crystalline microtubes.

### MP006

**SAS Analysis in 2D and the DANSE Project.** Mathieu Doucet<sup>1</sup>, Paul Butler<sup>1,2</sup>, <sup>1</sup>The Univ. of Tennessee, <sup>2</sup>The National Institute of Science and Technology, Center for Neutron Research.

Small Angle Scattering is now a relatively mature technique which has had an enormous impact on all of materials science as it reveals structure on the nanoscale. To date however, almost all quantitative work has used modeling techniques which assume that the structures in the system have no preferential spatial orientation (so-called isotropic scattering) and can therefore be analyzed in 1 dimension. The data however are usually taken as a 2dimensional cut in reciprocal space. Increasingly, SAS is being applied to systems under some external, often orienting, field. Analysis of the resultant anisotropic scattering patterns has typically been limited to a qualitative discussion, perhaps quantifying the degree of orientation, or at best, to a 1D analysis of

the structure in 2 orthogonal directions. As part of the NSF funded DANSE project, the SANS subproject has been working on producing code to make quantitative analysis in 2D routine. We are developing C libraries which will eventually be used within the full DANSE framework but which can and are being used outside the framework either in our prototypes or incorporated into standard packages such as the next release of the NIST IGOR package. The current SliceView prototype extends the usual 1D analytical models to 2D while work is being done to understand how to simulate complex shapes in 2D which have no analytical expressions. We show how bypassing the traditional computation of the density pair-correlation function has little speed consequence in 1D but speeds up the computation in 2D by orders of magnitude. Error estimates are usually ignored even in 1D and are also discussed. More information about the project and the current SliceView prototype are available from our website at [danse.chem.utk.edu](http://danse.chem.utk.edu).

### TP007

**Nitrile-Halogen Contacts in Benzylidene-anilines Revisited: The Influence of the Substitution Pattern.** W.H. Ojala, K.M. Lystad, J.M. Spude, B.C. MacQueen, Chemistry Dept., Univ. of St. Thomas, St. Paul, MN 55105, C.R. Ojala, Chemistry Dept., Normandale Community College, Bloomington, MN 55431.

In an effort to identify pairs of “bridge-flipped” isomeric benzylideneanilines ( $R-CH=N-R'$  and  $R-N=CH-R'$ ) that assume identical molecular packing arrangements in their respective crystals for use in future cocrystallization experiments, we have been examining benzylideneanilines substituted with both a nitrile group and a halogen atom to determine whether a Lewis acid-Lewis base interaction of the form  $-C\equiv N:\cdots X-$  occurring in both isomers of the pair would encourage the formation of isostructural isomers through the formation of similar structural motifs (e.g. chains or dimers) in the separate isomers. From our previous four pairs of isomers defining the  $2-C\equiv N-4'-X$  ( $X = F, Cl, Br, I$ ) series, our focus has turned to other substitution patterns. In contrast to that series, in which the intermolecular nitrile-halogen contact is found only where  $X = I$  (consistent with the relative strength of iodine as a Lewis acid), we find nitrile-halogen contacts in the  $2-C\equiv N$ -benzylidene-2'-X-aniline structures in which  $X = Br, Cl, \text{ or } I$ ; all three compounds are isostructural. Yet, although we find a nitrile-halogen contact in the 2-I-benzylidene-2'-C≡N-aniline structure as well, this compound is not isostructural with its bridge-flipped isomer. No close nitrile-halogen contacts are found in the 4-C≡N-benzylidene-2'-I-aniline, 2-C≡N-benzylidene-3'-I-aniline, or 3-Br-benzylidene-2'-C≡N-aniline structures, in which intermolecular interactions other than  $-C\equiv N:\cdots X-$  are presumably structure-defining.

Acknowledgment is made to the Donors of the American Chemical Society Petroleum Research Fund for support of this research.

### SP008

**A New Class of Organic Ligands Based on Cyclobutane: Design, Total Synthesis and Applications Thereof.** Dejan-Krešimir Bučar, Quanli Chu, Phuong V. Dau, Stacy C. Sommerfeld, Claude L. Mertzenich, Leonard R. MacGillivray, Dept. of Chemistry, Univ. of Iowa, Iowa City, IA, USA.

Metallosupramolecular chemistry has attracted tremendous attention in material sciences in the last 25 years. Recent advances in this area gave rise to functional materials, which were successfully used for gas-storage and separation purposes, as well as in catalysis. Interestingly, the research in this area is exclusively based on organic ligands that contain backbones based on five- and six-

membered rings (e.g. benzene and cyclopentadiene). At the same time, metallosupramolecular assemblies based on ligands that have a cyclobutane ring as backbones remained virtually unexplored (Bučar et al. *Eur. J. Inorg. Chem.* 2007, 4559).

With this in mind, we have developed a methodology that allows the synthesis of cyclobutane-based ligands predetermined for the design and construction of metallosupramolecular assemblies with nanometer-sized cavities and voids. The synthesis of such ligands is based on post-synthetic modifications of synthons derived from a template-directed synthesis in the solid state (MacGillivray et al. *J. Am. Chem. Soc.* 2000, 122, 7817). In particular, bromo-stilbazoles were used to obtain bromo-phenyl-containing cyclobutane derivatives, which were subjected to palladium-catalyzed coupling reactions (i.e. Suzuki reactions) to yield ligands with extended pyridine handles. In this contribution, we present the solid-state synthesis of several bromo-phenyl-containing cyclobutane derivatives, the products of their post-synthetic modifications, and their potential applications in metallosupramolecular chemistry. The synthesized materials were studied via single crystal X-ray diffraction and <sup>1</sup>H NMR spectroscopy.

### MP009

**Molecular Basis of Passive Immunotherapy of Alzheimer's Disease.** Chris Dealwis, Anna S. Gardberg, Dept. of Pharmacology, School of Medicine, Case Western Reserve Univ., Cleveland, Ohio.

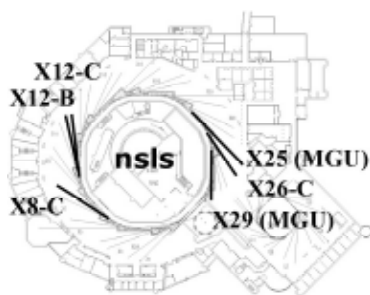
Amyloid aggregates of the A $\beta$  peptide are implicated in the pathology of Alzheimer's disease. Anti-A $\beta$  monoclonal antibodies (mAbs) have been shown to reduce amyloid plaques in vitro and in animal studies. Consequently, passive immunization is being considered for treating Alzheimer's, and anti-A $\beta$  mAbs are now in phase II trials. We report the isolation of two new mAbs (PFA1 and PFA2) that recognize A $\beta$  monomers, protofibrils, and fibrils, as well as the structures of their antigen binding fragments (Fabs) in complex with the A $\beta$ (1-8) peptide DAEFRHDS. The immunodominant EFRHD sequence forms salt-bridges, hydrogen-bonds, and hydrophobic contacts, including interactions with a striking WWDD motif of the Fabs. We also show that a similar sequence (AKFRHD) derived from the human protein GRIP1 is able to cross-react with both PFA1 and PFA2 and, when co-crystallized with PFA1, binds in an identical conformation to A $\beta$ (1-8). Since such cross-reactivity has implications for potential side effects of immunotherapy, our structures provide a template for designing derivative mAbs that target A $\beta$  with improved specificity and higher affinity.

### TP010

**The PXRR, a Resource for Macromolecular Crystallography at the NSLS.** D.K. Schneider, A. Héroux, A.M. Orville, H.H. Robinson, A.M. Saxena, A. Soares, R.M. Sweet, Biology Dept., L. Berman, NSLS Dept., Brookhaven National Laboratory, Upton, NY.

The PXRR mission includes providing visiting and remote scientists with state-of-the-art data collection and structure-solving capabilities.

To achieve our mission we provide for rapid access to six PXRR beamlines at the NSLS, continuing facility development, innovation of new methods, as well as support and training of visiting scientists. Our flexible beamtime scheduling mechanism often yields time



at either insertion device beamline (X25 or X29) within days. It also enables moving samples from one beamline to another in order the better to match data collection requirements with particular beamline capabilities.

In addition to our popular mail-in crystallographic collaborations, we also have begun supporting remote data collection. All six beamlines are fully integrated with our data-collection and data base program PXDB to facilitate data management and experiment tracking. Three of our beamlines support cryogenic automounters and are particularly well suited for high volume screening and remote operations. A new micro-diffractometer has just been installed on our premier X25 ID beamline to support data collection from a 20-50 micrometer x-ray beam. To support concurrent x-ray diffraction and spectroscopic analysis, we have installed an in-beam single crystal spectrophotometer at beamline X26-C. These new capabilities, and other proposed developments, motivate our planning of an entirely new experimental MX facility to exploit the unique capabilities anticipated at NSLS-II. We are eager to work with you towards this exciting future.

This work is supported by the NCRF of the National Institutes of Health, and the OBER of the US Department of Energy.

### SP011

**Racemic Polymorphs of 2-[Methyl(phenyl)amino]nicotinic Acid.** Sihui Long,<sup>+</sup> Sean Parkin,<sup>+</sup> Maxime Siegler,<sup>+</sup> Carolyn P. Brock,<sup>+</sup> Tonglei Li<sup>+</sup>, <sup>+</sup>Dept. of Pharmaceutical Sciences, <sup>+</sup>Dept. of Chemistry, Univ. of Kentucky, Lexington, KY.

Four polymorphs (I, II, III and IV) have been discovered for a chiral diarylamine, 2-[methyl(phenyl)amino]nicotinic acid (2-MPNA), as colorless crystalline solids by crystallization from solution under different conditions. One hydrate and one salt of 2-MPNA were also obtained. Structures of all six crystals were determined by X-ray diffraction at 90 K. The unit cell parameters are as following. Form I (Cc): a = 11.711(2), b = 8.6444(17), c = 11.664(2)Å,  $\beta$  = 104.17(3)°, V = 1144.8(4)Å<sup>3</sup>; form II (Pca21): a = 14.3290(2), b = 8.9360(3), c = 26.5210(7)Å, V = 3395.85(15)Å<sup>3</sup>; form III (Pc): a = 13.316(3), b = 8.8408(18), c = 14.282(3)Å,  $\beta$  = 91.60(3)°, V = 1680.7(6)Å<sup>3</sup>; form IV (P21): a = 8.6871(7), b = 44.926(4), c = 14.282(3)Å,  $\beta$  = 90.113(4)°, V = 5556.9(8)Å<sup>3</sup>; H (P21/n): a = 7.155(1), b = 7.595(1), c = 21.868(4)Å,  $\beta$  = 90.73(1)°, V = 1188.3(3)Å<sup>3</sup>; S (P21/n): a = 6.8955(14), b = 13.5839(3), c = 13.7170(3)Å,  $\beta$  = 102.60(3)°, V = 1253.9(4)Å<sup>3</sup>. Examination of the crystal structures of four racemic polymorphs reveals 17 crystallographically independent molecules in the asymmetric units (Z' = 1, 3, 3, 10 for forms I, II, III, and IV, respectively), and the number increases to 19 when both the hydrate (Z' = 1) and salt (Z' = 1) are considered. Concomitant polymorphism has been discovered for forms I and IV. All four polymorphs have similar hydrogen-bonding arrangements which are different from those in the hydrate and salt.

### TP012

**Low Resolution SAXS Study of Human FEZ1: A Natively Unfolded Protein.** J.C. Silva<sup>1,3</sup>, D.C.F. Lanza<sup>1,2</sup>, E.M. Assmann<sup>1</sup>, A.J.C., Quaresma<sup>1,2</sup>, G.C. Bressan<sup>1,2</sup>, J. Kobarg, I.L. Torriani<sup>1,2</sup>, <sup>1</sup>Laboratório Nacional de Luz Síncrotron, Campinas, SP, Brazil, <sup>2</sup>I. de Biologia., UNICAMP, Campinas, SP, Brazil, <sup>3</sup>I. de Física, UNICAMP, Campinas, SP, Brazil.

The Fasciculation and Elongation protein Zeta 1 (FEZ1) is the mammalian orthologue of the *Caenorhabditis elegans* protein UNC-76, necessary for axon growth. Human FEZ1 interacts with Protein Kinase C (PKC) and several regulatory proteins involved in functions

ranging from microtubule associated transport to transcriptional regulation. Theoretical predictions and results from spectroscopic studies and limited proteolysis experiments suggest that FEZ1 could belong to the class of natively unfolded proteins. It is already known that proteins with multiple functions have frequently a disordered intrinsic structure. It is well known that high resolution structures of proteins with a low degree of compactness are hard to obtain and small angle X-ray scattering (SAXS) is the most adequate technique to obtain dimensional parameters. SAXS experiments of 6xHis-FEZ1(1-392) and of the N terminal fragment 6xHis-FEZ1(1-227) in solution confirmed both their dimerization as well as their open extended shapes, compatible with partially unfolded proteins. Low resolution 3D conformational models of very large or partially unstructured molecules do not permit an unambiguous determination of the spatial positions of secondary structure elements, but allow the description of the overall molecular shape. Ab-initio calculations depict the natively unfolded characteristics of these macromolecules, the full-length protein and the N-terminal construct, which appear to explore a large conformational space. The overall shapes and some details of the 3D dimer arrangements will be presented.

### MP013

**Applications of High Throughput Solution X-ray Scattering (SXS).** Greg Hura, Michal Hammel, Robert Rambo, Shelley Claridge, Angeli Mennon, Paul Alivisatos, Mike Adams, John Tainer, Lawrence Berkeley National Lab, Berkeley, CA.

Several techniques, both experimental and computational, exploit the deep and broad survey of bio-macromolecular structures made available by X-ray crystallography and NMR. Results from these techniques have provided insights into the structures of macromolecules which have not yet been probed by or remain intractable to atomic resolution techniques. Solution X-ray scattering (SXS) has matured to probe details down to 10<sup>2</sup> resolution. This resolution is sufficient to elucidate a great deal of the architecture of macromolecules, how they interact and exchange products along a pathway. SXS may be powerfully combined with information from atomic resolution and computational structure prediction methods. We have developed a high throughput national user facility. Complete SXS data collection (including a buffer blank and a 3 fold serial dilution) requires 10 minutes for a macromolecule of interest. We have also developed a data analysis tree which requires minimal human intervention and in some cases may be complete in 30 minutes. Further, our web accessible data storage utility BioIsis ([www.bioisis.net](http://www.bioisis.net) <<http://www.bioisis.net/>>) allows direct access to data at all stages of analysis. We demonstrate this strategy on 16 proteins from *Pyrococcus furiosus* previously prepared for a crystallographic based structural genomic effort. The strategy described here is being applied to large scale natively purified complexes from both *Pyrococcus furiosus* and *Sulfolobus solfataricus*. In addition we describe the results from a high throughput screen for the purpose of producing enzymatically accessible nano-gold labeled DNA. SXS is an excellent tool for investigating the properties of macromolecules designed through nano-technology.

### MP015

**Determining the Telomere-Binding Properties of Glyceraldehyde-3-Phosphate Dehydrogenase (GAPDH).** Neil Demarse, John Baatz, Eleanor Spicer, Besim Ogretmen, Christopher Davies, Medical Univ. of South Carolina, Charleston, SC.

Glyceraldehyde-3-phosphate dehydrogenase (GAPDH) is a well-known and ubiquitous glycolytic enzyme that also exhibits several

non-glycolytic activities, including DNA repair, membrane fusion, apoptotic signaling, tRNA transport and microtubule bundling. GAPDH binds to telomeres, and in human A549 non small-cell lung adenocarcinoma cells, overexpression of GAPDH protects telomeres from chemotherapeutic agents. Thus, the inhibition of GAPDH-telomere binding may provide a new means to treat non small-cell lung cancer. We have thoroughly analyzed the chemical characteristics of the interaction between GAPDH and a synthetic telomeric DNA oligomer, 5'-(TTAGGG)<sub>3</sub>-3', using gel shift assays, blue native-PAGE, ChIP assays and X-ray crystallography. GAPDH preferentially binds a single stranded (ss) telomeric DNA oligomer with a K<sub>d</sub> of 40nM, and GAPDH requires the nucleic acids T1, G5 and G6 (5'-TTAGGG-3') of the telomere repeat for binding. The stoichiometry of the interaction was calculated to be two oligomers of DNA per GAPDH tetramer. To determine whether the active site of GAPDH overlaps with the ssDNA binding site, we performed competition assays and showed that the GAPDH cofactor, NAD<sup>+</sup>, competes with the ss-telomeric oligomer in a dose-dependent manner. Additionally, site-directed mutagenesis of the GAPDH active-site residue Cys149 to alanine, which is adjacent to the NAD<sup>+</sup>-binding site and involved in hydride transfer to NAD<sup>+</sup>, eliminated binding to the ss-telomeric DNA. Using high-resolution crystal data, we developed a putative model of GAPDH binding to ss-DNA. Future experiments will use non-DNA binding mutant to determine the in vivo role of GAPDH in A549 cells. We will determine the effect on telomere-length in response to the chemotherapeutic agents and reveal whether GAPDH binds to telomeres in non-cancerous lung epithelial cell lines. The evidence derived from these experiments could allow for the development of drugs that target the protective effect of GAPDH on telomeres in order to increase the efficacy of chemotherapeutic agents already used to treat non small-cell lung cancer.

### SP016

**New Protein Fold Revealed by A 1.65 Å Resolution Crystal Structure of *Francisella tularensis* Pathogenicity Island Protein IglC.** Ping Sun,<sup>1</sup> Brian P. Austin,<sup>1</sup> Florian D. Schubot,<sup>2</sup> David S. Waugh,<sup>1</sup> <sup>1</sup>Macromolecular Crystallography Laboratory, Center for Cancer Research, National Cancer Institute at Frederick, P.O. Box B, Frederick, MD, <sup>2</sup>Present Address: Dept. of Biological Sciences, Virginia Polytechnic Inst. and State Univ., Blacksburg, VA.

*Francisella tularensis* is a highly infectious Gram-negative intracellular pathogen that causes the fulminating disease tularemia and is considered to be a potential bioweapon. *F. tularensis* pathogenicity island proteins play a key role in modulating phagosome biogenesis and subsequent bacterial escape into the cytoplasm of macrophages. The 23 kDa pathogenicity island protein IglC is essential for the survival and proliferation of *F. tularensis* in macrophages. Seeking to gain some insight into its function, we determined the crystal structure of IglC at 1.65 Å resolution. IglC adopts a β-sandwich conformation that exhibits no similarity with any known protein structure.

### TP017

**Structure of the Hypothetical Protein PF0899 from *Pyrococcus furiosus* at 1.85 Å Resolution.** <sup>1</sup>M. Gary Newton, <sup>1</sup>L.L. Clancy Kelley, <sup>1</sup>B.D. Dillard, <sup>1</sup>W. Tempel, <sup>1</sup>L. Chen, <sup>2</sup>N. Shaw, <sup>1</sup>D. Lee, <sup>1</sup>F.J. Sugar, <sup>1</sup>F.E. Jenney Jr, <sup>1</sup>H.S. Lee, <sup>1</sup>C. Shah, <sup>1</sup>F.L. Poole III, <sup>1</sup>M. Adams, <sup>3</sup>J.S. Richardson, <sup>3</sup>D. Richardson, <sup>2</sup>Z.-J. Liu, <sup>1</sup>B.-C. Wang, <sup>1</sup>J. Rose, <sup>1</sup>Southeast Collaboratory for Structural Genomics, Dept. of Biochem. & Molecular Biology, Univ. of Georgia, Athens, GA, USA, <sup>2</sup>National Laboratory of Biomacromolecules, Inst. of Biophysics, Chinese Academy of Sciences, Beijing, People's Republic of China,

<sup>3</sup>Dept. of Biochemistry, Duke Univ., Durham, NC, USA.

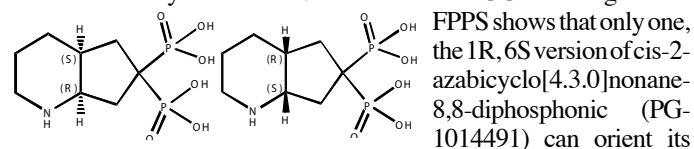
The hypothetical protein PF0899\* is a 95-residue peptide from the hyperthermophilic archaeon *Pyrococcus furiosus* that represents a gene family with six members. *P. furiosus* ORF PF0899 has been cloned, expressed and crystallized and its structure has been determined by the Southeast Collaboratory for Structural Genomics (<http://www.secs.org>). The structure was solved using the SCA2Structure pipeline from multiple data sets and has been refined to 1.85 Å against the highest resolution data set collected (a presumed gold derivative) with a crystallographic R factor of 21.0% and R(free) of 24.0%. The refined structure shows some structural similarity to a wedge-shaped domain observed in the structure of the major capsid protein from bacteriophage HK97, suggesting that PF0899 may be a framework structural protein.

Work supported by the National Institutes of Health (GM62407), the Georgia Research Alliance and the University of Georgia Research Foundation. \*See Kelley et al., *Acta Cryst.* (2007). F63, 549-552.

### MP018

**The Mode of Binding of Nitrogen Containing Bisphosphonates in Farnesyl Pyrophosphate Synthase.** Barnett, BL,<sup>1</sup> Dunford, JE,<sup>2</sup> Lundy, MW,<sup>1</sup> Dao, X,<sup>2</sup> Evdokimov, A,<sup>3</sup> Walter, RL,<sup>3</sup> Meckel, M.,<sup>3</sup> Song, X,<sup>4</sup> Boeckman, Jr, RK,<sup>4</sup> Ebetino, FH,<sup>3</sup> <sup>1</sup>Univ. of Cincinnati, Cincinnati, OH, <sup>2</sup>Oxford Univ., Oxford, UK, <sup>3</sup>Procter & Gamble Pharm, Mason, OH, <sup>4</sup>Univ. of Rochester, Rochester, NY.

Two major components of the in vivo mechanism of action of the bone loss inhibitor class of nitrogen containing bisphosphonates (N-BPs) are their ability to target bone mineral (bone affinity) and their subsequent inhibition of a specific biochemical target within the osteoclast, the enzyme Farnesyl Pyrophosphate Synthase (FPPS). From recently available crystal structures of the human FPPS enzyme ligated with N-BPs, it is clear that differences in inhibitory potency are based on key interactions of the N-BPs within the geranyl pyrophosphate (GPP) binding site. The most potent FPPS inhibitors seem to form strong hydrogen bonds between the bisphosphonate nitrogen and the hydroxyl of Thr 201 -OH and the backbone carbonyl (C=O) of Lys 200. Protein crystallography of a mirror image pair of conformationally restricted N-BPs within the GPP binding site of



nitrogen in the region of the binding site necessary for hydrogen bonds to these peptidic residues. Isolated enzyme inhibition studies with human FPPS confirmed that PG-1014491 was the more potent inhibitor with a 50% inhibitory concentration (IC<sub>50</sub>) of 15 nM vs 359 nM for the poorly oriented N-BP enantiomer PG-1014493. In vivo studies have also demonstrated corresponding potency differences. The role of the Lys 201 and Thr 200 hydrogen bonding sites is further established for the N-BPs and these findings help validate the role of FPPS as the key biochemical target for the N-BPs.

### TP019

**SCrALS - Service Crystallography at the Advanced Light Source: A Collaborative Access Project for Chemical Crystallography.** Jeanette A. Krause<sup>1</sup>, Allen G. Oliver<sup>2</sup>, <sup>1</sup>Dept. of Chemistry, Univ. of Cincinnati, Cincinnati, OH, 45221, <sup>2</sup>Dept. of Chemistry & Biochemistry, Univ. of California-Santa Cruz, Santa Cruz, CA 95064.

The SCrALS (Service Crystallography at ALS) project aims to provide collaborative access to synchrotrons for chemical

crystallography. Synchrotron sources generate a more brilliant beam with a significantly higher X-ray photon flux; thus analysis of previously undesirable samples, such as those too small or poorly diffracting for in-house laboratory systems, is now possible. The SCrALS project operates as a mail-in service with data collected during regular scheduled beam runs.

Samples submitted through the SCrALS project come from a variety of uniquely different research programs yielding fascinating structural information. This presentation will highlight some of the crystallographic results that would otherwise not have been possible without access to the more intense beam provided by a synchrotron source.

Contact the authors for more information on the SCrALS project: [jeanette.krause@uc.edu](mailto:jeanette.krause@uc.edu) or [aoliver@chemistry.ucsc.edu](mailto:aoliver@chemistry.ucsc.edu).

### SP020

**Temperature Induced Phase Transformations in Relaxor Ferroelectrics Lead Scandium Tantalate and Ba-doped Lead Scandium Tantalate.** Bernd Maier<sup>1</sup>, Boriana Mihailova<sup>1</sup>, Carsten Paulmann<sup>1</sup>, Thomas Malcherek<sup>1</sup>, Joerg Ihringer<sup>2</sup>, Martin Gospodinov<sup>3</sup>, Rainer Stosch<sup>4</sup>, Bernd Guettler<sup>4</sup>, Ulrich Bismayer<sup>1</sup> <sup>1</sup>Univ. Hamburg, Hamburg, Germany, <sup>2</sup>Univ. Tuebingen, Tuebingen, Germany, <sup>3</sup>Bulgarian Academy of Sciences, Sofia, Bulgaria, <sup>4</sup>Physikalisch-Technische Bundesanstalt, Braunschweig, Germany.

X-ray diffraction and Raman spectroscopic studies in a wide temperature range on perovskite-type relaxors PbSc<sub>0.5</sub>Ta<sub>0.5</sub>O<sub>3</sub> (PST) and Pb<sub>0.78</sub>Ba<sub>0.22</sub>Sc<sub>0.5</sub>Ta<sub>0.5</sub>O<sub>3</sub> (PBST) are presented. The temperature evolution of phonon anomalies and the pseudo-cubic unit cell parameter for both PST and PBST reveals the existence of a critical temperature T\* between the Burns temperature T<sub>B</sub> and the temperature of the dielectric-permittivity maximum T<sub>m</sub>. T\* is associated with coupling of initially nucleated polar sub-clusters and their aggregation into larger polar nanoclusters. The temperature range between T<sub>B</sub> and T\* is characterized by coupling between adjacent off-centered BO<sub>6</sub> octahedra to form initial polar clusters, while the range between T\* and T<sub>m</sub> is characterized by coupling between off-centered B-cations from adjacent polar clusters. Off-centered Pb atoms exist even above T<sub>B</sub> and their coherence length governs the coupling between polar regions comprising B-cation off-centered shifts and directs the formation of proper or relaxor ferroelectric state.

### MP021

**Structural Investigation of the Mechanism of Human Brain Aspartoacylase.** Johanne Le Coq, Radhika Malik, Ronald E. Viola, Dept. of Chemistry, Univ. of Toledo, Toledo, OH 43606 USA.

Canavan disease is a fatal neurological disorder caused by the malfunctioning of a single metabolic enzyme. Aspartoacylase catalyzes the deacetylation of *N*-acetyl-L-aspartic acid (NAA) to produce acetate and L-aspartate, and is the only brain enzyme that has been shown to effectively metabolize NAA. Although the exact role of this enzymatic reaction has not yet been completely elucidated, the metabolism of NAA appears to be necessary in the formation of myelin lipids and defects in this enzyme lead to this neurological disorder. The structure of human brain aspartoacylase has now been determined in complex with a stable tetrahedral intermediate analog, N-phosphonomethyl-L-aspartate. This potent inhibitor forms multiple interactions between each of



its heteroatoms and the substrate binding groups arrayed within the active site. The binding of the catalytic intermediate analog induces the conformational ordering of several substrate binding groups thereby setting up the active site for catalysis. The highly ordered binding of this inhibitor has allowed assignments to be made for substrate binding groups that have been confirmed by mutagenesis studies, and provides strong support for a carboxypeptidase-type mechanism for the hydrolysis of the amide bond of the NAA substrate. This work is supported by a grant from the NIH (NS045664).

### TP022

**New Developments for Neutron and X-Ray Diffraction Studies at RT of Type III AntiFreeze Protein.** A. Mitschler<sup>1</sup>, Matthew Blakeley<sup>2</sup>, I. Haertlein<sup>2</sup>, M. Haertlein<sup>2</sup>, C. Mueller-Dickmann<sup>3</sup>, A. Popov<sup>3</sup>, E. Howard<sup>1</sup>, A. Podjarny<sup>1</sup>, <sup>1</sup>IGBMC, 1 rue Laurent Fries, Illkirch, France, <sup>2</sup>ILL, 6 rue Jules Horowitz, Grenoble, France, <sup>3</sup>ESRF, 6 rue Jules Horowitz, Grenoble, France.

Type III Antifreeze Proteins (AFPs) are small globular monomeric proteins (66 aa, M.W.=7kDa), which are highly homologous. Their shared antifreeze property is linked to a network of hydrogen bonding between a specific lattice plane on ice and several conserved, polar and solvent accessible amino acids located along a flat Ice-Binding Surface (IBS).

We shall present our developments:

1) - Neutron Laue data collection on the new LADI III (ILL) on an *ab-initio* fully deuterated “tiny” crystal (volume = 0.12 mm<sup>3</sup>, resolution = 2 Å), including production of fully deuterated protein, crystallization by macro-seeding in D<sub>2</sub>O. The ratio resolution/volume is similar to the Human Aldose Reductase [1].

2) - X-ray diffraction at Synchrotron ESRF beamline ID29 on a fully deuterated crystal of the same crystallization batch at a resolution of 1.05 Å, necessary to carry out a joint Neutron – X-ray refinement like for Human Aldose Reductase h-AR [2].

3) Specific H labelling on Leucine and Isoleucine of the fully deuterated protein, in order to create a contrast useful for specific phasing methods for neutron diffraction data. (Human Frontier Science Program).

<sup>1</sup>Hazemann, Blakeley et al., Acta Cryst. (2005), D61,1413 – 141.

<sup>2</sup>Blakeley, Ruiz et al., accepted by PNAS, January 2008.

### SP023

**Surface Characterization of Uric Acid Crystals by Chemical Force Microscopy.** Janeth Presores, Jennifer Swift, Dept. of Chemistry, Georgetown Univ., Washington, DC, 20057.

Kidney stones are heterogeneous aggregates of crystals of different compounds. Anhydrous uric acid is one of the most common building blocks. Laboratory grown crystals of uric acid adopt a plate-like habit in which the largest face is (100). Surface adhesion is important in key steps of kidney stone formation including crystal growth and crystal aggregation. As a model for how different biomolecules attach to surfaces of uric acid *in vivo*, in this study we quantify the adhesion force between chemically modified AFM cantilever tips and the (100) surface of single uric acid crystals. The adhesion forces obtained suggest that interaction between the AFM probe and the crystal both depend on the chemical functionality of the tip and the pH of the solution where the measurements are performed. Chemical force microscopy used in the study provides molecular-level insight into uric acid crystal surfaces and their likely interaction with biomolecules.

### TP024

**Detergent-Associated Solution Conformations of Membrane Proteins Studied by Small-Angle X-Ray Scattering.** William T. Heller<sup>1</sup>, Yiming Mo<sup>1</sup>, Byung-Kwon Lee<sup>2</sup>, Jeffrey M. Becker<sup>2</sup>, <sup>1</sup>Ctr. for Structural Molecular Biology, Oak Ridge Natl. Lab., Oak Ridge, TN 37831; <sup>2</sup>Dept. of Microbiology, Univ. of Tennessee, Knoxville, TN 37996.

Membrane proteins present major challenges for structural and functional studies. Detergents used to solubilize and extract membrane proteins from the native membrane are assumed to leave the protein properly folded with a belt of detergent encompassing the membrane-spanning segments of the structure. Small-angle x-ray scattering was used to probe the detergent-associated solution conformations of three membrane proteins, namely bacteriorhodopsin (BR), the Ste2p G-protein coupled receptor from *S. cerevisiae*, and the *E. coli* porin OmpF. Contrary to the traditional model of a detergent-associated membrane protein, the helical proteins BR and Ste2p are unfolded and associated with detergent micelles, while OmpF is embedded in a disk-like micelle. The comparison provided by the BR and Ste2p, both members of the 7TM family of helical membrane proteins, suggests a possible mechanism for why BR, like other rhodopsins, can readily refold properly to crystallize, while Ste2p can not do so from a detergent-associated state.

This work was supported by the LDRD Program of Oak Ridge Natl. Lab., managed and operated by UT-Battelle, LLC for the U. S. Department of Energy under contract No. DE-AC05-00OR22725, and NIH GM-022087 from the Natl. Inst. of General Medical Sciences. The submitted manuscript has been authored by a contractor of the U.S. Government under Contract DE-AC05-00OR22725. Accordingly, the U.S. Government retains a nonexclusive royalty-free license to publish or reproduce the published form of this contribution, or allow others to do so, for U.S. Government purposes.

### MP025

**Independence of U2AF Activity on Interdomain Linker Composition.** Jermaine L. Jenkins<sup>1</sup>, Haihong Shen<sup>2</sup>, Michael R. Green<sup>2</sup>, Clara L. Kielkopf<sup>1</sup>, <sup>1</sup>Dept. Biochemistry and Biophysics, Univ. of Rochester School of Medicine, Rochester, NY, <sup>2</sup>Programs in Gene Function and Expression and Molecular Medicine, Univ. of Massachusetts Medical School, Worcester, MA.

Despite low primary sequence similarity, the splicing factors U2AF<sup>65</sup>, SXL, and PTB recognize Py-tract sequences with various arrangements of tandem RNA recognition motifs (RRM)s. The two RRM of SXL are tightly interacting with one another and the bound Py-tract (PDB code 1B7F). In contrast, the N-terminal RRM1 and RRM2 domains of PTB lack detectable intramolecular interactions (PDB codes 2AD9/2ADB). Site-specific crosslinking experiments establish that the two RRM of U2AF<sup>65</sup> exhibit dynamic behavior and slide across longer Py-tracts [Banerjee *et al.* (2000) *RNA* 6:901]. Accordingly, our recent structure of a U2AF<sup>65</sup> variant with a shortened interdomain linker shows that two RRM independently interact with distinct RNA sites (PDB code 2G4B) [Sickmier *et al.* (2006) *Mol. Cell* 23:49]. This co-crystallized U2AF<sup>65</sup> functions comparably to wild-type protein when tested using *in vitro* RNA splicing assays and RNA binding experiments. Here, we further corroborate that U2AF<sup>65</sup> RRM1 and RRM2 interact with RNA independently, by substituting the U2AF<sup>65</sup> interdomain linker with the corresponding region between PTB RRM1 and RRM2. The activity of the U2AF<sup>65</sup> variant with the PTB linker was tested using *in vitro* RNA splicing assays, fluorescence anisotropy assays, and isothermal titration calorimetry. The results support the view that the RNA binding mode of the U2AF<sup>65</sup> RRM1 and RRM2 domains is similar to the N-terminal PTB RRM, and distinct from SXL.

**SP026**

**New Neutron Beamlines.** C. Hoffmann, Oak Ridge National Laboratory, Oak Ridge, TN.

Neutron scattering is a “gentle” probe for “soft”, organic materials as well as highly penetrating to investigate materials in special and well defined environments.

The Oak Ridge National Laboratory (ORNL) is hosting two powerful neutron sources for neutron scattering investigations, a pulsed Spallation Neutron Source (SNS) and the newly upgraded High Flux Isotope Reactor (HFIR). A range of neutron scattering instruments optimized for elastic (structural) and inelastic (motional) analyses under controlled conditions are currently at various stages of construction, completion, or already in operation and will become fully available to the user community in a few years time frame.

This presentation will highlight the opportunities for wide and small angle diffraction on current and future instrumentation. The SNS and HFIR instrument suite will comprise up to 24 instruments: numerous diffractometers for wide and small angle scattering, investigating single crystal and poly-crystalline samples, various spectrometers for molecular motion and vibration modeling and reflectometers for thin film investigation of lipid layers and molecular magnetic materials; HFIR will also house a number of triple axis spectrometers. Showcases of molecular and macromolecular structural and motional analyses will be discussed.

More information on SNS and HFIR can be found on the ORNL Neutron Sciences web site at <http://neutrons.ornl.gov>.

This research is supported by UT Battelle, LLC under Contract No. DE-AC05-00OR22725 for the U.S. Department of Energy, Office of Science.

**MP027**

**Motion Control of the Iron-sulfur-protein in bc1 Complex from *Rhodobacter Sphaeroides*.** Lothar Esser<sup>1</sup>, Maria Elberry<sup>2</sup>, Chang-An Yu<sup>2</sup>, Linda Yu<sup>2</sup>, Di Xia<sup>1</sup>, <sup>1</sup>National Institutes of Health, National Cancer Institute, Bethesda, MD 20892, <sup>2</sup>Dept. of Biochemistry and Molecular Biology, Oklahoma State Univ., Stillwater, OK 74078.

Ubiquinol/ubiquinone cytochrome c oxidoreductase (cytochrome bc<sub>1</sub>, bc<sub>1</sub>) is a membrane-embedded enzyme of paramount importance in the vast majority of life forms. Its primary function is to (re-)oxidize membrane soluble ubiquinol to ubiquinone and secondarily it couples this process to proton translocation across the membrane, maintaining the membrane potential required for various cellular activities. Cytochrome bc<sub>1</sub> is a dimeric multi subunit membrane protein complex with two substrate-binding sites located within the cytochrome b subunit but on opposite sides of the membrane. Remarkably, for every two electrons removed from the substrate ubiquinol, bc<sub>1</sub> transports four protons across the membrane against the existing proton gradient. The details of this mechanism are subject of intense research but it appears that the large-scale oscillatory motion of the 14 kDa head domain of the Iron-Sulfur-Protein (ISP) subunit is of fundamental importance. To study the mechanism of this enzyme, we have crystallized wild-type and mutant *Rhodobacter Sphaeroides* bc<sub>1</sub> (Rsbc<sub>1</sub>) with a number of inhibitors. Here we focus on the characterization of Rsbc<sub>1</sub> in complex with famoxadone. Famoxadone has considerable commercial importance in crop protection and the complex structure offers insights into ways to combat resistant strains that inevitably arise. Furthermore, the structure offers valuable information regarding the motion control mechanism of the ISP. It appears that indeed, the motion of the ISP can be arrested without direct ISP – substrate (here famoxadone) interaction.

**SP028**

**Altered Dimer Interface Decreases Stability in an Amyloidogenic Protein.** James Thompson<sup>BS</sup>, Elizabeth M. Baden,<sup>\*</sup> Francis Peterson,<sup>U</sup> Brian Volkman,<sup>U</sup> Marina Ramirez-Alvarado,<sup>\*A</sup>, <sup>\*</sup>Dept. of Biochemistry & Molecular Biology, Mayo Clinic College of Medicine, Rochester, MN 55905, <sup>U</sup>Dept. of Biochemistry, Medical College of Wisconsin, Milwaukee, WI 53226, <sup>B</sup>Dept. of Physiology & Biomedical Engineering, Mayo Clinic College of Medicine, Rochester, MN 55905.

Amyloidoses are devastating and currently incurable diseases in which the process of amyloid formation causes fatal cellular and organ damage. The molecular mechanisms underlying amyloidoses are not well known. We address the structural basis of immunoglobulin light chain amyloidosis, which results from deposition of light chains produced by clonal plasma cells. We compare light chain amyloidosis protein AL-09 to its wild type counterpart, the  $\lambda$ I O18/O8 light chain germline. Crystallographic studies indicate that both proteins form dimers. However, AL-09 has an altered dimer interface that is rotated 89.6° from the  $\lambda$ I O18/O8 dimer interface. The three non-conservative mutations in AL-09 are located within the dimer interface, implicating these mutations in the decreased stability of this amyloidogenic protein. Moreover, AL-09 forms amyloid fibrils more quickly than  $\lambda$ I O18/O8 in vitro. These results support the notion that properly formed light chain dimers may be protective against amyloid formation, opening a new direction into rational drug design for amyloidogenic proteins.

**TP029**

**Crystal Structure of Maltase-Glucoamylase as a Basis for Controlling Blood Glucose Levels.** D. R. Rose, L. Sim, Ontario Cancer Inst. and Dept. of Medical Biophysics, Univ. of Toronto, Toronto, Ontario M5G 1L7.

A clinical challenge in treating Type II Diabetes is the control of glucose release from the digestion of starch in the intestine. Two enzymes are responsible for post-amylase starch processing, maltase-glucoamylase (MGAM) and sucrase-isomaltase (SIM). Understanding the structure/function characteristics of these activities, including their specificities for different starch structures, is a goal in the development of anti-Diabetic compounds, and in the understanding of the nutritional efficiency of food sources.

Each of the enzymes MGAM and SIM is made up of duplicated glycosyl hydrolase (GH) family 31 catalytic domains with overlapping but different substrate specificities. We have begun our study of these enzymes by determining the crystal structure of the N-terminal MGAM GH31 domain (ntMGAM) in complex with a number of glycosidase inhibitors.

This presentation will include results describing the basis for differential specificity of the structurally-related MGAM and SIM catalytic domains, as well as insights into the mechanism of inhibition of their activities. The potential of improving the efficacy of the compounds based on the structural analysis will be discussed.

**MP030**

**Micropatterned Flexible Crystallization Plates: Parameters and Applications.** R.M. Baur, R.E. Thorne, Physics Dept., Cornell Univ., Ithaca, NY 14853 USA.

A new design for a non-rigid crystallization tray is presented. Trays consist of a thin flexible polypropylene film imprinted with microstructures via hot embossing onto a photolithographically-patterned template. Micropatterned rings improve droplet uniformity and stability over conventional well design, simplifying image analysis and providing reliable droplet shape and positioning even if the tray is tilted or inverted. This, together with the x-ray transparency of the polypropylene film, permits *in situ* diffraction studies. Alternately, crystals can be harvested by conventional methods. Crystals that have adhered to the surface and that would be difficult to harvest from a rigid well plate could be freed by gently flexing the film, or the section of film holding the crystal could be cut out for mounting.

**TP031**

**Design of Porous Solids From 2-D and 3-D Coordination Frameworks Utilizing Imidazolylbenzoic Acids.** Lisa S. Lee, Yu Wang, John C. MacDonald, Dept. of Chemistry & Biochemistry, Worcester Polytechnic Inst., Worcester, MA 01609 USA.

We are investigating the design and synthesis of coordination frameworks of molecules in an effort to create new families of porous crystalline solids. Molecules with metal binding sites can be designed to self-assemble via metal coordination into coordination polymers that form a range of 2-D and 3-D architectures. We are targeting porous solids constructed from two related families of organic molecules: 4-(1*H*-imidazol-1-yl)benzoic acids and 4-(1*H*-benzo[*d*]imidazol-1-yl)benzoic acids. The synthesis, characterization and properties of these molecules and framework materials composed of metal ion complexes of these molecules are discussed.

**MP033**

**Structural Impact of Three Parkinsonism-Associated Missense Mutations of Human DJ-1.** Mark A. Wilson, Mahadevan Lakshminarasimhan, Marien T. Maldonado, Wenbo Zhou, Anthony L. Fink, Dept. of Biochemistry, Redox Biology Center, Univ. of Nebraska-Lincoln & Univ. of California-Santa Cruz.

In this study we show that three different Parkinsonism-associated missense mutations (A104T, E163K and M26I) in the human protein DJ-1 subtly perturb the structure of the protein without causing major folding defects or loss of functionally critical dimerization. Atomic resolution X-ray crystallography shows that the A104T substitution introduces water and a discretely disordered residue into the core of the protein, E163K disrupts a key salt bridge with R145, and M26I causes packing defects in the core of the dimer. All three missense mutations destabilize DJ-1 in solution as determined by DSC. The deleterious effect of each Parkinsonism-associated mutation on DJ-1 is dissected by analysis of engineered substitutions (M26L, A104V, and E163K/R145E) that partially alleviate each of the defects introduced by the A104T, E163K and M26I mutations. In total, our results suggest that the protective function of DJ-1 can be compromised by diverse perturbations in its structural integrity, especially in more highly oxidized forms of the proteins.

**TP034**

**Design and Performance of the New Supermirror Guide on HRPD at ISIS.** R.M. Ibberson, K.S. Knight, L.C. Chapon, P.G. Radaelli, ISIS Facility, STFC-Rutherford Appleton Lab, Harwell Science & Innovation Campus, Didcot, Oxfordshire, U.K.

The 100 m long high-resolution powder diffractometer, HRPD, at the ISIS Facility has been upgraded recently with the installation of a high-reflectivity supermirror guide. Flux gains are substantial compared with the old instrument and are between a factor ~10 to 40 times greater across the incident wavelength range for the instrument. The new guide has an increased radius of curvature thus transmits shorter wavelength neutrons that were previously cut off and making it feasible to access even shorter *d*-spacings. The intrinsically high instrumental resolution,  $\Delta d/d$  better than  $1 \times 10^{-3}$  and effectively constant across the whole diffraction pattern, is retained.

This presentation will describe the unique geometric design of the new guide and compare the predicted performance, based on simulated data from Monte Carlo calculations, with observed experimental results. New capabilities of HRPD will be illustrated by recent results drawn from the current commissioning programme on the instrument.

**MP036**

**Transport Across the Bacterial Membrane: Structural and Functional Aspects of the Two Partner Secretion System.** V. Villeret and B. Clantin, Inst. de Biologie de Lille, Inst. Pasteur de Lille, Lille 59021 France.

The superfamily of Omp85/TpsB membrane proteins includes essential proteins such as the Toc75, Sam50/Tob55 and Omp85/YaeT homologs, which are the cores of large hetero-oligomeric complexes involved in protein transport across, and insertion of  $\beta$ -barrel proteins into, the outer membrane of chloroplasts, mitochondria and Gram-negative bacteria. It also includes TpsB transporters, which are components of the « Two-Partner Secretion » (TPS) systems in Gram negative bacteria (1). TPS systems secrete large, mostly  $\beta$ -helical proteins called « TpsA » that serve as virulence factors.



FhaC, the outer-membrane transporter that secretes the *Bordetella pertussis* adhesin filamentous haemagglutinin (FHA) is one of the most characterized TPS system. The structures of FhaC (2-5) and of FHA (6) have been determined, providing structural insights into this secretion process. The structural and functional data on the FhaC/FHA system will be presented. They allow to propose a model for transport of FHA across the outer membrane, which may apply more generally to the secretion of TpsA proteins by their dedicated TpsB transporters.

In conclusion, we have determined the first crystal structure of a member of the Omp85-TpsB transporter superfamily. It offers molecular insights into how proteins get into and across cellular membranes.

1. Mazar J. and Cotter P.A. *Trends Microbiol* (2007) 15, 508-15.
2. Clantin B. *et al. Science* (2007) 317: 957-61.
3. Tommassen J. *Science* (2007) 317 : 903-04.
4. Research Highlight. *Nature Reviews Microbiology* (2007) 5, 747.
5. Research Highlights. *Nature Structural and Molecular Biology* (2007)14, 795.
6. Clantin B. *et al. PNAS* (2004) 101, 6194-6199.

secretion process. The structural and functional data on the FhaC/FHA system will be presented. They allow to propose a model for transport of FHA across the outer membrane, which may apply more generally to the secretion of TpsA proteins by their dedicated TpsB transporters. In conclusion, we have determined the first crystal structure of a member of the Omp85-TpsB transporter superfamily. It offers molecular insights into how proteins get into and across cellular membranes.

1. Mazar J. and Cotter P.A. *Trends Microbiol* (2007) 15, 508-15.
2. Clantin B. *et al. Science* (2007) 317: 957-61.
3. Tommassen J. *Science* (2007) 317 : 903-04.
4. Research Highlight. *Nature Reviews Microbiology* (2007) 5, 747.
5. Research Highlights. *Nature Structural and Molecular Biology* (2007)14, 795.
6. Clantin B. *et al. PNAS* (2004) 101, 6194-6199.

### SP037

**Crystal Structure of the Human iNOS CaM-FMN Domain in Complex with Ca<sup>2+</sup>-Calmodulin.** Chuanwu Xia<sup>1</sup>, Ila Misra<sup>1</sup>, Takashi Iyanagi<sup>2</sup>, Jung-Ja P. Kim<sup>1</sup>, <sup>1</sup>Dept. of Biochemistry, Medical College of Wisconsin, WI, <sup>2</sup>Biometal Science Lab, RIKEN Spring-8 Center, Harima Inst., Hyogo, Japan.

Nitric Oxide synthases (NOSs) catalyze the conversion of L-arginine to nitric oxide and citrulline. There are three NOS isozymes depending on their physiological roles: neuronal NOS, endothelial NOS, and inducible NOS (iNOS). The NOSs consist of an N-terminal P450-like oxygenase domain and the C-terminal reductase domain, and they are linked by a calmodulin (CaM) binding peptide. CaM is required for NO production and its binding is dependent of Ca<sup>2+</sup>. Unlike the other two NOS isozymes, iNOS is induced at the transcriptional level and CaM is bound tightly to the enzyme independent of the exogenous [Ca<sup>2+</sup>]. We have cloned, crystallized and solved the structure of the CaM-binding peptide/FMN binding domain of human iNOS complexed with CaM and Ca<sup>2+</sup>. The cloned protein is able to reduce cytochrome *c*, when reconstituted with the FAD/NADPH domain. The crystals belong to the P<sub>2</sub> space group, with unit cell dimensions of 36.6 Å, 160.8 Å, 127.8 Å and β= 90.4°. The relative orientations between the FMN domain and the bound CaM in each of the four molecules in the ASU are very different, suggesting that CaM-binding regulates the electron transfer from FMN to heme by adjusting the relative orientation/distance of the two cofactors. In addition, relative orientations of the N- and C-terminal domains of CaM are also different among the four molecules, showing the flexibility between the two domains of CaM. The work was supported by NIH grant GM52682.

### TP038

**Structure-Function Studies of Enzymes Associated with Synthesis of Glycopeptide Antibiotics.** R. Shi<sup>1</sup>, S.S. Lamb<sup>2</sup>, S. Bhat<sup>1</sup>, A. Proteau<sup>1</sup>, T. Sulea<sup>3</sup>, G. D. Wright<sup>2</sup>, A. Matte<sup>3</sup>, M. Cygler<sup>1,3</sup>, Dept. of Biochemistry, McGill Univ., Montréal, Québec, Canada, <sup>2</sup>Antimicrobial Research Centre, Dept. of Biochemistry and Biomedical Sciences, McMaster Univ., Hamilton, Ontario, Canada, <sup>3</sup>Biotechnology Research Instr., NRCC, Montréal, Québec, Canada.

Over the past decade, antimicrobial resistance has emerged as a major public-health crisis. Glycopeptide antibiotics (GPAs) such as vancomycin and teicoplanin are clinically important for the treatment of Gram-positive bacterial infections. We have determined the crystal structures of a sulfotransferase StaL and a methyltransferase MtfA, two tailoring enzymes in the biosynthesis of glycopeptide antibiotics (GPA). StaL is a PAPS-dependent sulfotransferase capable of sulfating the cross-linked heptapeptide substrate, yielding the product A47934, a unique teicoplanin-class GPA. The sulfonation reaction catalyzed by StaL constitutes the final step in A47934 biosynthesis. StaL is the

second prokaryotic sulfotransferase to be structurally characterized. MtfA is a SAM-dependent N-methyltransferase responsible for the methylation of the N-terminus of chloroeremomycin, a vancomycin-class GPA. Although the binding site architecture of PAPS (for StaL) or SAM (for MtfA) displays high similarity to related enzymes, both enzymes contain a large binding cavity for the antibiotic substrate. Both StaL and MtfA are dimers and possess novel dimerization motifs, different from other related enzymes that have so far been structurally characterized. We have applied molecular modeling to investigate the binding mode of the antibiotic substrates. Based on the structural analysis and modeling results, a series of putative active site residues have mutated and kinetically characterized. In addition to the conserved residues, several other residues important for substrate binding or catalysis have been identified. (CIHR GSP-48370).

### MP039

**SAXS, Lee-Richards Surfaces and a Simplified Command Set for Maps.** H.J. Bernstein, I. Awuah Asiamah, G. Darakev, N. Darakev, J. Jemilawon N. Jia, P. Kamburov, G. McQuillan, G. Todorov, Dowling College, Oakdale, NY 11769, USA.

Electron density maps are both essential experimental data in crystallography and also an important tool for molecular visualization. The simpler the interface used to generate, load, and manipulate maps, the easier it is to focus on the science involved. Building on the map commands in DINO, CCP4mg and PyMOL, we present a new, simpler Structural Biology Extensible Visualization Scripting Language (SBEVSL) map command set that facilitates generation of surfaces for low-resolution bead models of proteins and approximations to Lee-Richards surfaces of higher resolution structures as contour meshes and surfaces of simple Gaussian pseudo-densities. The command set includes support for loading both experimental and calculated maps with masking based on other maps, including Gaussian pseudo-densities approximating the effect of the PyMol carve feature.

This work is part of the combined efforts of the SBEVSL groups at Dowling College and Rochester Institute of Technology. The people at Dowling are: Isaac Awuah Asiamah, Darina Boycheva, Georgi Darakev, Nikolay Darakev, Philip Gozo, John Jemilawon, Nan Jia, Petko Kamburov, Greg McQuillan, Daniel O'Brien, Georgi Todorov, Herbert J. Bernstein. The people at RIT are: Scott E Mottarella, Brett Hanson, Charles Westin, Corey Wischmeyer, Paul A Craig. Work supported in part by grant 1R15GM078077-01 from NIGMS.

### SP040

**Unusual Commonality and Phase Transformations within the Six Crystal Forms of an Active Pharmaceutical Ingredient.** Michael A. Galella, Solid State Chemistry, R&D, Bristol-Myers Squibb Co., Princeton, NJ 08543.

A pharmaceutically active molecule has been shown to crystallize in multiple crystal forms, including neat and solvate forms. The crystal structures of some of these forms exhibit marked similarities, especially in the intermolecular arrangement of the *ab* planes. Four of the solvated crystal structures are members of two structurally distinct solvate families. The structural differences that distinguish solvate families will be illustrated. Furthermore, a temperature induced phase transition between two ethyl acetate solvate polymorphs was observed by variable temperature single crystal x-ray diffraction. This result suggests that the other solvates of this family may undergo a similar transformation.

### TP041

**Modulation of Intensity in Neutron Spectroscopy.** Markus Bleuel, Roland Gahler\*, Ed Land, Jyotsana Lal, IPNS, Argonne National

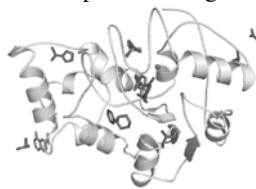
Laboratory, USA, \*Institut Laue-Langevin, France.

The use of a neutron spin echo (NSE) spectrometer in a small angle neutron scattering (SANS) geometry at a pulsed source allows experiments where both the spatial and the time domain will be completely scanned within each neutron pulse, without moving parts inside the instrument. Particularly the new MISANS instrument, a new design for an instrument to be built at the spallation neutron source (SNS), combines high NSE energy resolution for quasi-elastic measurements with a SANS q-resolution. Furthermore the MIEZE (modulation of intensity by zero effort)-technique used in this spectrometer allows the measurement of magnetic samples with a polarized neutron beam and spin-incoherent scattering samples as well as the use of a SANS-area detector (consisting of time resolving scintillation photo multipliers) without loss of signal due to depolarization of the neutron beam which is a huge problem for other NSE-instruments. We present first experiments at the Intense Pulsed Neutron Source (IPNS) to explore this novel techniques in order to optimize it for the pulsed neutron beam and the capabilities of the instrument for science are discussed.

#### MP042

**Fragment-Based Cocktail Crystallography Combined with *in silico* Chemical Screening to Target Uracil-DNA Glycosylase of *Leishmania*.** E.T. Larson<sup>1,2</sup>, W. Deng<sup>1,2</sup>, S. Shibata<sup>1,2</sup>, Z. Zhang<sup>1,2</sup>, L. Xiao<sup>1,2</sup>, N. Mueller<sup>1,2</sup>, A. Napuli<sup>1,2</sup>, F. Zucker<sup>1,2</sup>, F.S. Buckner<sup>1,3</sup>, W.C.E. Van Voorhis<sup>1,3</sup>, W.G.J. Hol<sup>1,2</sup>, E. Fan<sup>1,2</sup>, C.L.M.J. Verlinde<sup>1,2</sup>, E.A. Merritt<sup>1,2</sup>, <sup>1</sup>MSGPP, <sup>2</sup>Biochemistry Dept, <sup>3</sup>Div. of Tropical Disease, Univ. of Washington School of Medicine, Seattle, WA.

The Medical Structural Genomics of Pathogenic Protozoa Consortium (www.msgpp.org) investigates enzymes from essential pathways of several pathogenic protozoa as potential therapeutic targets. These eukaryotic parasites have a devastating impact on human health worldwide and development of new drugs to fight these debilitating and often fatal diseases is needed. Target proteins are subjected to a 3-pronged attack via crystallographic, computational, and biophysical screening of small molecule libraries. One such potential target is uracil-DNA glycosylase (UDG), a critical component of DNA repair. DNA repair is especially important to these parasites because their complex life cycle involves dramatic environmental changes that cause genotoxic stress. Importantly, many trypanosomes have highly similar UDG sequences so results may be relevant to many parasites of the family Trypanosomatidae. To identify small, interacting molecules, crystals of *L. naiffi* UDG were soaked in a series of 70 cocktails of 6 to 10 compounds each, designed such that individual constituents can be distinguished by their electron density. Through cocktail crystallography, several compounds have been identified that bind in the active site and along the DNA-interaction surface. These structures provide the starting point for further exploration of chemical space for possible inhibitors via *in silico* modeling and computational screening. In parallel with physical screening, these methods serve as a guide for structure-based inhibitor design.



#### SP043

**A Multiple-Data-Set Data Collection Strategy for A Better Data Set Within a Fixed X-ray Dose.** B.C. Wang, Z.J. Liu\*, L. Chen, G. Rosenbaum, J. Chrzas, Z.-Q. Fu, J. Rose, Dept. of Biochem. & Molecular Biology, SER-CAT, Univ. of Georgia, Athens, GA, \*Currently: Inst. of Biophysics, Chinese Academy of Sciences, Beijing, China.

Within a fixed X-ray dose, what is the best strategy to collect a data set from a given crystal that will increase the structure solvability? Do we need to do a long exposure for each diffraction image so that we may “visualize” the diffraction spots better to get better data?

On the contrary, we have found that a better data set can be produced, if a shorter exposure time is used for each image and repeat the data collection a number of times using the same crystal. This means that a better data set can be obtained, within an equivalent total exposure time, from merging multiple data sets of shorter exposures, even if the images from each data set give somewhat weaker “visible” spots!

This is the proposed Multiple-Data-Set Data Collection Strategy. Both the theoretical and practical aspects of this strategy will be discussed.

#### SP044

**Crystal Structure of Type II Restriction Endonuclease PabI Revealed Novel DNA Binding Fold and DNA-Recognition Mode.** K. Miyazono<sup>1,7</sup>, M. Watanabe<sup>2,7</sup>, J. Kosinski<sup>3</sup>, K. Ishikawa<sup>2,5</sup>, M. Kamo<sup>1</sup>, T. Sawasaki<sup>4</sup>, K. Nagata<sup>1</sup>, J.M. Bujnicki<sup>3</sup>, Y. Endo<sup>4</sup>, M. Tanokura<sup>1,5</sup>, I. Kobayashi<sup>2,5,6</sup>, <sup>1</sup>Dept. of Applied Biological Chem., Univ. of Tokyo, Japan, <sup>2</sup>Dept. of Medical Genome Sciences, Univ. of Tokyo, Japan, <sup>3</sup>Lab of Bioinformatics & Protein Eng., Int'l Inst. of Molecular & Cell Biology, Poland, <sup>4</sup>Dept. of Applied Chem., Ehime Univ., Japan, <sup>5</sup>Biophysics & Biochem., Univ. of Tokyo, Japan, <sup>6</sup> Inst. of Medical Science, Univ. of Tokyo, Japan,

PabI is a restriction endonuclease found in *Pyrococcus abyssi* through comparison of closely related genomes. PabI was predicted to have a novel structure by the analysis of amino acid sequence. Additionally, unlike most restriction enzymes, PabI is able to cleave a target DNA without Mg<sup>2+</sup>. To reveal structural basis of PabI, we determined its three-dimensional structure by X-ray crystallography. We expressed PabI in a wheat-germ cell-free translation system. The structure of PabI was determined by the SAD method using selenomethionine derivative at 3.0 Å resolution. Structural analysis of PabI showed that this enzyme adopts a novel protein fold as predicted. PabI forms homodimer by a formation of extended anti-parallel  $\beta$ -sheet that is curved to form an extended groove, which is the unique architecture of PabI. We named this unique substructure “half pipe”. Mutational and *in silico* DNA binding analyses have assigned the “half pipe” region as the double-strand DNA binding site.



Miyazono, Watanabe et al. Nucleic Acids Research 2007 35(6):1908-18.

#### SP045

**Crystal Structures of Human and *S. aureus* Pyruvate Carboxylase and Molecular Insights into the Carboxyltransfer Reaction.** Song Xiang, Liang Tong, Columbia Univ., New York, NY.

Pyruvate carboxylase (PC) catalyzes the biotin-dependent production of oxaloacetate and has important roles in gluconeogenesis, lipogenesis, insulin secretion and other cellular processes. PC contains the biotin carboxylase (BC), carboxyltransferase (CT) and biotin-carboxyl carrier protein (BCCP) domains. We report here crystal structures at 2.8 Å resolution of full-length PC from *Staphylococcus aureus* and the C-terminal region (missing only the BC domain) of human PC. A conserved tetrameric association is observed for both enzymes, and our structural and mutagenesis studies reveal a novel domain, the PC tetramerization (PT) domain, that is important for this oligomerization. A BCCP domain is located in the active site of the CT domain, providing the first molecular insights into how biotin participates in the carboxyltransfer reaction.

**TP046****First Complex of Biphenyl Dioxygenase with a PCB: Crystal Structure of Biphenyl dioxygenase with 2, 6 di Chlorobiphenyl.**

Kumar, P.<sup>1,2</sup>, Gómez-Gil, L.<sup>2</sup>, Barriault, D.<sup>4</sup>, Sylvestre, M.<sup>4</sup>, Eltis, L.D.<sup>2</sup>, Bolin, J.T.<sup>3</sup>, Indian Inst. of Technology Roorkee-247667, India<sup>1</sup>; Depts. of Microbiology and Biochemistry, Life Sciences Inst., Univ. of British Columbia, Vancouver, BC V6T 1Z3, Canada<sup>2</sup>; Dept. of Biological Sciences, Purdue Univ., West Lafayette, IN, USA<sup>3</sup>; Inst. National de Recherche Scientifique (INRS-Inst. Armand-Frappier), Pointe-Claire, Quebec H9R 1G6, Canada<sup>4</sup>

Biphenyl dioxygenase (BPDO) catalyzes the aerobic transformation of biphenyl and various polychlorinated biphenyls (PCBs). It is an enzyme of interest because of its potential to oxidize toxic pollutants and to catalyze oxygenation reactions for the manufacture of fine chemicals. The first crystal structure of a BPDO•PCB complex was determined at 2.6 Å resolution using enzyme purified from *Pandoraea pnomenus* B-356 (BPDO-B356) and 2, 6 dichlorobiphenyl (PCB10). Biochemical data show that BPDO-B356 is one of the more potent PCB-degrading BPDOs. Structural comparison revealed conformational changes in the binding pocket upon PCB10 binding. It is noteworthy that the coordination of the active site Fe (II) changes upon PCB10 binding. Movements of ligands may be required to avoid steric clashes with PCB10, may also be important for control of dioxygen binding, and may influence substrate preferences. An important structural variation relative to other BPDOs involves a loop region, residues 249-262, which forms the entrance to the PCB binding pocket.

**MP047**

**An Electron Paramagnetic Resonance Study of the Jahn-Teller Effect in Copper Doped Cadmium-Histidine.** Michael J. Colaneri, Jacqueline Vitali, Brenda Marmol, Dept. of Chemistry & Physics, State Univ. of New York College, Old Westbury, NY 11568, Dept. of Physics, Cleveland State Univ., Cleveland, OH 44115.

Electron Paramagnetic Resonance (EPR) spectroscopy has detected a Jahn-Teller effect in a copper-histidine complex. At low temperature (less than 160K), the EPR spectra of Cu<sup>2+</sup>-doped Cd<sup>2+</sup>-histidine crystals display two copper patterns, each related by a crystalline two-fold axis that runs through the cadmium ion in the host and between its two coordinating histidine molecules. Drastic changes occur in the EPR spectra between 160K and 230K. At temperatures higher than 230K and up to room temperature, the EPR spectrum consists of only a single copper species, with rhombic g and A hyperfine tensors. The higher temperature resonances display a strong dependence of line-width with the copper hyperfine component. EPR line-widths are being fit at various temperatures using the software package PeakFit and will be used to determine the energy state profile of the complex. A previous interpretation of the temperature dependent EPR from powder samples used a dynamic model where the copper ion hops between two symmetry related histidine binding sites, with a critical temperature of roughly 180K. However, subsequent single crystal EPR experiments have shown a 1:1 conversion from the low temperature to high temperature patterns over a very narrow temperature range. These recent findings suggest a static Jahn-Teller distortion about the copper complex.

**SP048**

**Hydrogen Bonded Intercalation of Unsaturated Pyridyl Compounds into 1D-Coordination Polymers.** T. González,<sup>a</sup> A. Briceño,<sup>a</sup> G. Díaz de Delgado,<sup>b</sup> <sup>a</sup>Laboratorio de Síntesis y Caracterización de Nuevos Materiales, Centro de Química, Inst.

Venezolano de Investigaciones Científicas (IVIC), Caracas 1020-A, Venezuela. <sup>b</sup>Lab. de Cristalografía, Facultad de Ciencias, Univ. de Los Andes, Mérida 5251, Venezuela. tegonzal@ivic.ve.

In the last years, there has been a growing interest in the self-assembly of flexible networks. Such structures can exhibit reversible dynamic behaviors (shrinking and breathing) in response to external perturbations. The design of hydrogen bonded coordination frameworks represent an important approach to the preparation of new supramolecular metal assemblies. This strategy allows the possibility for generating coordination polymers of different dimensionality (1, 2 and 3-D) by combining crystal engineering tools (hydrogen bonds and metal coordination). Such coordination architectures can display multiple binding donor-acceptor sites on their supramolecular periphery. This feature can be exploited to intercalate secondary molecular units through self-complementary hydrogen bonded synthons between coordination arrays. In this context, as part of our interest in the study of potentially photoreactive metal assemblies, in this contribution we explore the use of 1-D coordination polymers bearing carboxylic groups as potential hydrogen bonded templates of unsaturated organic molecules based on pyridyl derivatives, with geometrical parameters appropriate for the solid-state photoreactivity of the double bonds between neighboring molecules. An examination of the structures of these assemblies reveals common structural trends in the solid state, which will be discussed in detail in this contribution.

This work was supported by FONACIT-Venezuela through grant LAB-97000821.

**MP049**

**Studying Local Structural Aspects of Metal-Insulator Transition in Cu(Ir<sub>1-x</sub>Cr<sub>x</sub>)<sub>2</sub>S<sub>4</sub> Using Total Scattering X-ray Atomic Pair Distribution Function.** E.S. Bozin, A.S. Masadeh, H.J. Kim, P. Juhas, S.J.L. Billinge, Dept. of Physics and Astronomy, Michigan State Univ., East Lansing, MI 48824, J.F. Mitchell, Material Science Div., Argonne National Laboratory, Argonne, IL 60439.

A thiospinel CuIr<sub>2</sub>S<sub>4</sub> exhibits a metal-insulator (MI) transition at T=230 K, with simultaneous spin-dimerization and charge-ordering [1]. The transition can also be driven by extended exposure to the x-rays at low T [2, 3]. Total x-ray scattering study of CuIr<sub>2</sub>S<sub>4</sub> was carried out using 100 KeV synchrotron beam and rapid acquisition pair distribution function (RAPDF) approach. The RAPDF results indicate consistency of the local and average structure at high T. At 100 K long x-ray exposure melts the long-range order (LRO) of the dimerization pattern, without affecting the local structure, in agreement with diffuse scattering result [3]. The dependence of the LRO related superlattice peak intensity on the exposure time reveals that the melting occurs within approximately 15 seconds of exposure under experimental conditions used. At 100 K the LRO is recovered without temperature increase quickly after the cessation of the beamtime exposure. Results on Cr doped samples will be addressed as well.

[1] P.G. Radaelli *et al.*, Nature 416, 155 (2002). [2] V. Kiryukhin *et al.*, Phys. Rev. Lett. 97, 225503 (2006). [3] H. Ishibashi *et al.*, Phys. Rev. B 66, 144424 (2002). This work is supported by the NSF under grant DMR-0703940. ANL is supported under DOE contract No.DE-AC02-06CH11357.

**TP050**

**Combined Charge-Density, Time-Resolved Photocrystallographic and Theoretical Study of the Properties of K<sub>2</sub>(methylviologen)[Pt<sub>2</sub>(P<sub>2</sub>O<sub>5</sub>H<sub>4</sub>)<sub>4</sub>].** Milan Gembicky, Katarina Matuszyna, Mateusz Pitak, Marc Messerschmidt, Philip Coppens, Dept. of Chemistry, SUNY Buffalo, NY, 14260 USA.

It is now possible to apply different advanced crystallographic techniques in a comprehensive analysis of the properties of complex solids. The  $[\text{Pt}_2(\text{P}_2\text{O}_5\text{H}_2)_4]^{4+}$  ion forms a series of salts with widely different luminescence properties. The title compound<sup>1</sup>  $\text{K}_2(\text{methylviologen})[\text{Pt}_2(\text{P}_2\text{O}_5\text{H}_2)_4]$  ( $\text{K}_2\text{MV}(\text{Ptpop})$ ) is a mixed salt in which the luminescence of the Ptpop anion is strongly quenched by electron transfer to the methylviologen acceptor. Its 90K lifetime is 0.3  $\mu\text{s}$ , compared with 15  $\mu\text{s}$  for the n-BuN<sup>4+</sup> salt. Net ionic charges in the crystal are found to be less than the formal charges of the ions, indicating that partial charge transfer occurs even in the ground state. Time-resolved measurements of the excited state structure will be discussed and compared with earlier measurements on other salts of the same anion. Electron transfer integrals have been calculated with B3LYP/6-31G\*\* and compared with those in  $\text{MV}_2\text{Ptpop}$  in which the luminescence is fully quenched<sup>2</sup>.

Research funded by the US Department of Energy (DEFG02-02ER15372) and the National Science Foundation (CHE0236317).

1. Gerlits, Oksana O., (2005), 292 pp. Ph.D. Thesis, State Univ. of New York, Buffalo, NY, USA. 2. Matuszyna, Katarina, Gerlits, Oksana O., Coppens, Philip, Inorg. Chem, to be submitted.

### MP052

#### Targeting DNA Replicative Proteins from Hyperthermophilic and Psychrophilic Archaea for Structure Determination.

Miranda L. Byrne, Ronny C. Hughes, Damien Marsic, Edward Meehan, and Joseph D. Ng, Laboratory for Structural Biology, Univ. of Alabama, Huntsville, Huntsville, AL 35899.

The process of DNA replication in all organisms is complex and requires the concerted action of multiple proteins in order to achieve faithful replication of the genomic template. Organisms that thrive in extreme conditions such as high heat or extreme cold must also contend with additional outside influences in their quest to faithfully replicate their genome. In order to examine the molecular basis which allows these organisms to survive, we seek to clone, express, crystallize, and determine the crystallographic structure of several proteins involved in the DNA replication machinery from a hyperthermophilic marine archaeon *Thermococcus thio-reducens* and a psychrophilic archaeon *Methanococcoides burtonii* DSM 6242. To-date, the crystal structure of a family B DNA polymerase from *T. thio-reducens* (TtpolB) has been solved to 2.0 Å. The protein crystals belong to the monoclinic space group P2<sub>1</sub>, with the unit cell parameters a = 111.699 Å, b = 75.455 Å, c = 112.825 Å,  $\beta = 90.769^\circ$ . An initial structure of the homotrimeric proliferating cell nuclear antigen (PCNA) or sliding clamp from the psychrophilic archaea *M. burtonii* DSM 6242 has also been determined to 2.5 Å. The protein crystals belong to the trigonal hexagonal space group R3 with the unit cell parameters a = b = 102.531 Å, c = 97.149 Å. Structural analysis among the selected targets relative to their counter temperature homologs reveals high topological equivalence with variable sequence identity. Molecular regions that may be important for thermal stability are identified and discussed.

### TP053

**Homodimeric Structure and dsRNA Cleavage Activity of the C-terminal RNase III Domain of Human Dicer.** D. Takeshita<sup>1</sup>, S. Zenno<sup>2</sup>, K. Saigo<sup>3</sup>, M. Tanokura<sup>1</sup>, <sup>1</sup>Dept. of Appl. Biol. Chem., Grad. Sch. of Agric. & Life Sci., Univ. of Tokyo, Tokyo, Japan, <sup>2</sup>Dept. Bioeng., Maebashi Inst. Tech., Gunma, Japan, <sup>3</sup>Dept. of Biophys. Biochem., Grad. Sch. of Sci., Univ. of Tokyo, Tokyo, Japan

In many eukaryotes, small RNAs trigger gene silencing in a sequence-specific manner. Dicer plays a role in the production of small RNAs, short interfering RNAs (siRNAs) and microRNAs (miRNAs). Dicer contains two RNase III domains (RNase IIIa and RNase IIIb) that

are responsible for the dsRNA processing. The crystal structure of the C-terminal RNase III domain (RNase IIIb) of human Dicer was determined at 2.0 Å resolution. Homodimeric structure of RNase IIIb was observed, and gel-filtration chromatographic analysis indicated that the RNase IIIb domain exists as a stable dimer. The dimeric mode is similar to the dimers of bacterial RNase III domains and two RNase III domains of Giardia Dicer. Biochemical analysis revealed that the RNase IIIb is active in processing of dsRNA, and generate short dsRNAs with 2 nt 3' overhang, which is characteristic of RNase III products. Structural and functional analyses of RNase IIIb domain of human Dicer revealed evolutionary conservation needed for catalysis, and its divergence of structure.

### MP054

#### Using RasMol, PyMol and Jmol with the Structural Biology Extensible Visualization Scripting Language (SBEVSL).

P. A. Craig\*, S. E. Mottarella\*, C. Wischmeyer\*, H. J. Bernstein<sup>^</sup>, I. Awuah Asiamah, D. Boycheva<sup>^</sup>, G. Darakev<sup>^</sup>, N. Darakev<sup>^</sup>, P. Gozo<sup>^</sup>, J. Jemilawon<sup>^</sup>, N. Jia<sup>^</sup>, P. Kamburov<sup>^</sup>, G. McQuillan<sup>^</sup>, D. O'Brien<sup>^</sup>, G. Todorov<sup>^</sup>, \*Rochester Institute of Technology, Rochester NY 14623, <sup>^</sup>Dowling College, Oakdale, NY 11769.

There are many useful molecular graphics programs, but moving among them can be challenging. The Structural Biology Extensible Visualization Scripting Language (SBEVSL) project is working to simplify the task of starting a graphics presentation under one package, e.g. RasMol or Jmol and then moving to another package, such as PyMOL or CCP4mg for, say, better renderings of certain features without having to redo all the work of selecting orientations and types of displays. For some uses, the scripting language can be used a block box, much the way we use Postscript for text documents, but, where feasible, SBEVSL is designed to be comprehensible to scientists by using simple menu-click-like commands and reasonable defaults. RasMol, PyMol and Jmol are being given "native" SBEVSL support and external translators will allow the approach to be applied with other packages, such as CCP4mg.

This work is part of the combined efforts of the SBEVSL groups at Dowling College and Rochester Institute of Technology. The people at Dowling are: Isaac Awuah Asiamah, Darina Boycheva, Georgi Darakev, Nikolay Darakev, Philip Gozo, John Jemilawon, Nan Jia, Petko Kamburov, Greg McQuillan, Daniel O'Brien, Georgi Todorov, Herbert J. Bernstein. The people at RIT are: Scott E Mottarella, Brett Hanson, Charles Westin, Corey Wischmeyer, Paul A Craig.

Work supported in part by grant 1R15GM078077-01 from NIGMS.

### TP055

**New Opportunities for Powder Diffraction at SNS.** Ashfia Huq, Jason Hodges, Spallation Neutron Source, Oak Ridge National Laboratory, Oak Ridge TN 37831.

POWGEN3 is a third-generation time-of-flight powder diffractometer at the Spallation Neutron Source. The instrument is optimized for both parametric studies of materials under a wide range of conditions (T, P, H, flowing gases, etc) and ab-initio crystal structure determinations of complex solid-state materials with asymmetric unit-cells of the order  $\sim 1,500 \text{ \AA}^3$ . In this presentation we will present the new opportunities this instrument will provide the user community with an emphasis on the sample environment that are being designed to be used for routine operation and time resolved data collection under special environmental conditions.

ORNL/SNS is managed by UT-Battelle, LLC, for the U.S. Department of Energy under contract DE-AC05-00OR22725. Work at ANL supported by the U.S. DOE, Basic Energy Sciences--Materials Sciences, under Contract W-31-109-ENG-38.

**SP056**

**A Magic Triangle? Experimental Phasing of Macromolecules with a Triiodo Benzene Derivative.** Tobias Beck, George M. Sheldrick, Lehrstuhl fuer Strukturchemie, Georg-August-Univ., D-37077 Goettingen, Germany.

Experimental phasing of macromolecules by methods that utilize the anomalous dispersion of certain atoms requires that these atoms are actually present and well-ordered in the crystal lattice. Although some structures can be solved with intrinsic anomalous scatterers (e.g. sulfur and metals), there is a need for compounds that can be used as derivatives for proteins and introduce external anomalously scattering atoms.

The compound 5-amino-2,4,6-triiodoisophthalic acid, which has three anomalously scattering atoms and also three functional groups for hydrogen bonding, was synthesized and utilized as a heavy atom derivative for protein structure solution. It was cocrystallized with several test proteins and X-ray data were collected. Examples of SAD-phasing using these data will be presented. An implementation in programs for heavy atom location, similar to the search for 'super-sulfurs',<sup>1</sup> is possible since the three iodine atoms present in the molecule form an equilateral triangle that can be easily identified in the SAD or SIRAS map.

<sup>1</sup>Debreczeni, J.E., Girmann, B., Zeeck, A., Kraetzner, R., Sheldrick, G.M. (2003). *Acta Cryst.* D59, 2125-2132.

**MP057**

**Structure of Protein MMP1218 from *Methanococcus maripaludis* S2.** Norma Duke, Brittany Conrad, Rory Mulligan, Minyi Gu, Andrzej Joachimiak, Argonne National Laboratory, Argonne, IL.

The x-ray crystal structure of protein MMP1218, C-terminal residues 74-415, has been solved to 2.0Å resolution. Though it was formally referred to as a "conserved hypothetical protein" (NCBI CAF30774.1), further examination of this entry states it to be an "LOR/SDH bifunctional enzyme conserved region". This protein belongs to BIG\_908.1, and is the first structural representative of this mega-family. The structure contains a dimer in the asymmetric unit, and belongs to tetragonal space group P412112; a=b=119.6Å, c=161.7Å ; R=19.1%, Rfree=21.7%. Comparison of this result to other known macromolecular structures will be examined.

Results shown in this report are derived from work performed at Argonne National Laboratory, Structural Biology Center at the Advanced Photon Source. Argonne is operated by UChicago Argonne, LLC, for the U.S. Department of Energy, Office of Biological and Environmental Research under contract DE-AC02-06CH11357.

**SP058**

**Structure and Function of Achaean Enzyme 5-Formaminoimidazole-4-carboxamide-1-β-D-ribofuranosyl 5'-Monophosphate Synthetase.** Yang Zhang<sup>1</sup>, Robert H. White<sup>2</sup>, Steven E. Ealick<sup>1</sup>, <sup>1</sup>Dept. of Chemistry and Chemical Biology, Cornell Univ., Ithaca, NY 148531, <sup>2</sup>Dept. of Biochemistry, Virginia Polytechnic Inst. and State Univ., Blacksburg, VA 24061.

Purine biosynthesis requires ten enzymatic steps in higher organisms while prokaryotes require an additional enzyme for step six. In most organisms steps nine and ten are catalyzed by the *purH* gene product, a bifunctional enzyme with both 5-formaminoimidazole-4-carboxamide-5'-monophosphate ribonucleotide (FAICAR) synthase and inosine monophosphate (IMP) cyclohydrolase activity. Recently it was discovered that Archaea utilize different enzymes to catalyze steps nine and ten. An ATP-dependent FAICAR synthetase is encoded by the *purP* gene and IMP cyclohydrolase is encoded by

the *purO* gene. We have determined the X-ray crystal structures of FAICAR synthetase from *Methanocaldococcus jannaschii* complexed with various ligands, including the tertiary substrate complex and product complex. The enzyme belongs to the ATP-grasp superfamily and is predicted to use a formylphosphate intermediate. In addition, we have determined in three crystal forms the structures of a functionally unclassified PurP ortholog from *Pyrococcus furiosus*. With approximately 50% sequence identity, *P. furiosus* PurP is structurally homologous to *M. jannaschii* PurP but does not catalyze the FAICAR synthetase reaction. A phylogenetic analysis was performed to explore the possible role of this functionally unclassified PurP.

**TP059**

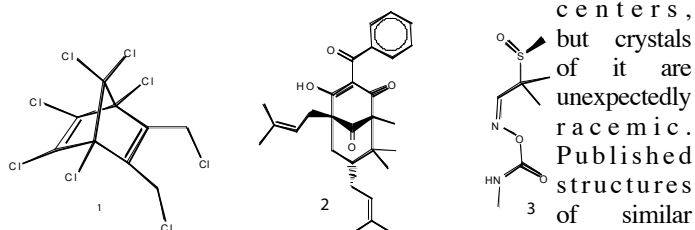
**Structural and Mutational Studies of Anthocyanin Malonyltransferases Establish the Features of BAHD Enzyme Catalysis.** Hideaki Unno, Fumiko Ichimaida, Hirokazu Suzuki, Seiji Takahashi, Yoshikazu Tanaka, Atsushi Saito, Tokuzo Nishino, Masami Kusunoki, Toru Nakayama, Dept. of Applied Chemistry Faculty of Engineering, Nagasaki Univ., Nagasaki, Japan.

The BAHD family is a class of acyl-CoA-dependent acyltransferases that are involved in plant secondary metabolism and show a diverse range of specificities for acyl acceptors. Anthocyanin acyltransferases make up an important class of the BAHD family and catalyze the acylation of anthocyanins that are responsible for most of the red-to-blue colors of flowers. Here, we describe crystallographic and mutational studies of three similar anthocyanin malonyltransferases from red chrysanthemum petals: anthocyanidin 3-O-glucoside-6"-O-malonyltransferase (Dm3MaT1), anthocyanidin 3-O-glucoside-3", 6"-O-dimalonyltransferase (Dm3MaT2), and a homolog (Dm3MaT3). Mutational analyses revealed that seven amino acid residues in the N- and C-terminal regions are important for the differential acyl-acceptor specificity between Dm3MaT1 and Dm3MaT2. Crystallographic studies of Dm3MaT3 provided the first structure of a BAHD member, complexed with acyl-CoA, showing the detailed interactions between the enzyme and acyl-CoA molecules. The structure, combined with the results of mutational analyses, allowed us to identify the acyl-acceptor binding site of anthocyanin malonyltransferases, which is structurally different from the corresponding portion of vinorine synthase, another BAHD member, thus permitting the diversity of the acyl-acceptor specificity of BAHD family to be understood.

**MP060**

**Adventures in Chirality.** Frank R. Fronczek, Dept. of Chemistry, Louisiana State Univ., Baton Rouge, LA, 70803.

Several structures will be presented in which some aspect of their chirality is interesting, unusual, or instructive. Compound 1 crystallizes in space group P4<sub>1</sub>2<sub>1</sub>2 and has been referred to using the oxymoron "enantiopure meso". This presents some nomenclature ambiguities. Examples of kryptoracemates (enantiopure crystals with pairs of enantiomers in the asymmetric unit) will be given. Compound 2 is a natural product from St. John's Wort, and contains three asymmetric

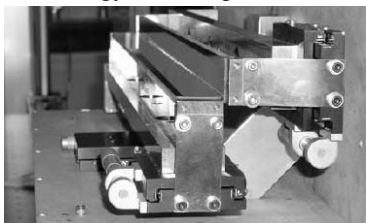


compounds from the same genus are sometimes racemic (without comment) and sometimes not. Compound 3 crystallizes from partially-resolved solution as partially-resolved crystals having  $Z'=2$  in  $P2_1$ . One molecule is ordered (enantiopure), and the other is disordered with a 80:20 mix of enantiomers. Absolute configuration determination was possible; Flack parameter -0.13(9). Experiences with Hooft's method of determining absolute structure (ACA Salt Lake City, 10.02.07) will also be described.

### TP061

**Nondispersive Kirkpatrick-Baez Neutron Supermirror Optics.** G.E. Ice<sup>1</sup>, C.A. Tulk<sup>1</sup>, J.J. Molaison<sup>1</sup>, P.Z. Takacs<sup>2</sup>, K.H. Andersen<sup>3</sup>, T. Bigault<sup>3</sup>, <sup>1</sup>Oak Ridge National Laboratory, Oak Ridge, TN USA 37831, <sup>2</sup>Brookhaven National Laboratory, Upton, NY USA 11973, Inst. Laue-Langevin, 38042 Grenoble Cedex 9, France.

Supermirror optics are inherently nondispersive and efficiently reflect a wide neutron bandpass. When used in a Kirkpatrick-Baez design, they can doubly-focus neutrons to a small focal spot with on-sample brilliance near the source brilliance limit, and with total flux scaled to the scattering angle of the mirror. The supermirror maximum reflection angle and the reflectivity below this angle are conditioned respectively by the total number of coated layers and the quality of the interfaces. This allows KB supermirror optics to focus efficiently and still leaves room for environmental chambers or other sample mounting hardware. In this presentation we describe the performance of 1st and 2nd generation KB neutron supermirror systems and describe advanced metrology used to produce ultra-perfect mirror surfaces capable of focusing to <25 micron-diameter. The mirrors described are optimized for thermal neutrons, but the advantages of supermirror focusing are even more compelling for cold neutrons.



Coupled with more powerful neutron sources and better neutron detectors, this emerging class of optics will enable experiments on previously impossibly small samples where signal and signal-to-background are important, and will enable experiments where small beams are essential to resolve inherent sample inhomogeneities.

Research in part at the ILL, ESRF and SNS. G.E.I. supported by the DOE, Division of Basic Energy Sciences and Engineering, P.Z.T. supported by the DOE, Nuclear and Particle Physics, C.A.T and J.J.M. supported by DOE Division of Scientific Facilities, K.A and T. Bigault supported by the Institut Laue-Langevin. This submission has been authored in part by scientists under contract to the Department of Energy. The U.S. Government retains a nonexclusive, license to publish or reproduce this submission.

### SP062

**Structural Basis for the Iron Uptake Mechanism of *Helicobacter pylori* Ferritin.** Ki Joon Cho, Ji-Hye Lee, Hye Jeong Shin, In Seok Yang, Seung Taik Lim, Kyung Hyun Kim, Korea Univ., Seoul, Korea.

Ferritin is essential for iron storage and release and gastric colonization of *Helicobacter pylori*, and protects the bacteria from acid-amplified iron toxicity. In an effort to gain understanding of iron uptake and release mechanisms, we have determined the crystal structures of *H. pylori* ferritin (Hpf) in apo, low- and high-iron bound forms and at acidic pH. A pair of histidine residues His93 and His96 located in proximity to the ferroxidase center was identified as a putative metal binding site, which may provide a novel entry pathway for iron translocation to the center. His149 at the entrance of 4-fold symmetry channels was found to induce conformational changes upon binding

of Fe ions, which are tightly coupled to Fe translocation. Hpf may have evolved in the human stomach to possess dual uptake mechanisms for iron through the histidine gates near the ferroxidase center and the 4-fold channel.

### TP065

**A Cobalt Beacon in the Active Site of Human Carbonic Anhydrase II.** Balendu Avvaru<sup>1</sup>, Daniel Arenas<sup>2</sup>, Chingkuang Tu<sup>3</sup>, David B. Tanner<sup>2</sup>, Mavis Agbandje-McKenna<sup>1</sup>, David N. Silverman<sup>1,3</sup>, Robert McKenna<sup>1</sup>, <sup>1</sup>Dept. of Biochem. & Molecular Biology, College of Medicine, <sup>2</sup>Dept. of Physics, <sup>3</sup>Dept. of Pharmacology & Therapeutics, College of Medicine, Univ. of Florida, Gainesville, FL 32610.

It has been well established that amino acids in the active site of an enzyme influence the local pH. We hypothesize that the pH of crystallization may not reflect the true pH of the active site. In order to address this, crystal structures of human carbonic anhydrase II (HCA II) with Co<sup>+2</sup> substituted active sites were studied from pH 5.5 to 12 using x-ray crystallography and visible spectroscopy. The structural and kinetic aspects of these results will be presented.

### MP066

**pKa Predictions of Turkey Ovomuroid Third Domain via a New CHARMm Based Generalized Born algorithm: A Validation Study Comparing Experimental Versus Predicted.** Francisco Hernandez-Guzman, Velin Spassov, Accelrys, 10188 Telesis Ct. Suite 100, San Diego, CA.

Understanding the protonation state of amino acids in the context of three dimensional structures is critical to structure function studies. *In Silico* structure based drug design, protein engineering, molecular dynamics and protein modeling in general, heavily depend on the proper assignment and placement of hydrogens for titratable residues at a specific pH. A major limitation of structures determined by X-ray crystallography is that in general the resolution is not high enough to resolve the position and presence of hydrogens. Therefore, either additional difficult experimental techniques must be performed, or computational methods may be used for proper hydrogen assignment. In this work, we introduce a validation study done for a newly developed CHARMm based Generalized Born method for predicting protonation state of titratable residues. The algorithm is called GBpK and has been developed for accurate prediction of protein ionization states, as well as pI prediction, pK shift estimations, titration curve calculations, pH dependent proton assignment, proton placement optimization and side chain flips of asparagines and glutamines based on the CHARMm energy function. For the validation study we focused on the widely studied Turkey Ovomuroid Third Domain and we use an ensemble of 50 NMR structures (10MU.pdb). To further test the method, we also include a comparison of having a system containing all hydrogens versus only using explicit polar hydrogens. The experimental to predicted correlation coefficient of titratable residues shows an impressive  $R^2 = 0.95$  for an all hydrogen system, and  $R^2 = 0.97$  for a protein system having only polar hydrogens with RMSD deviations of 0.90 and 0.66 respectively.

### TP067

**A High-Field (30-45 Tesla) Pulsed Magnet Instrument for X-Ray Studies of Materials at The Advanced Photon Source.** Zahirul Islam, Advanced Photon Source, Argonne National Laboratory, Argonne, IL, Jacob Ruff, Dept. of Physics & Astronomy, McMaster Univ., Hamilton, ON, Canada, Yasuhiro Matsuda, Inst. for Materials Research, Tohoku Univ., Sendai, Japan, Zhe Qu, Physics Dept., Tulane Univ., New Orleans, LA, Hiroyuki Nojiri, Inst. for Materials

Research, Tohoku Univ., Sendai, Japan, Shunsuke Yoshii, Inst. for Materials Research, Tohoku Univ., Sendai, Japan, Bruce Gaulin, Dept. of Physics and Astronomy, McMaster Univ., Hamilton, ON, Canada, Zhiqiang Mao, Physics Dept., Tulane Univ., New Orleans, LA, Jonathan Lang, Advanced Photon Source, Argonne National Laboratory, Argonne, IL.

High-field pulsed magnets for synchrotron x-ray applications are not the solution to all problems requiring high magnetic fields, but, they are the only solution to many that are of great interest. We present an extremely high-field pulsed magnet system for x-ray studies of materials at the Advanced Photon Source (APS). The high-field environment capabilities provided by this instrument for scattering and spectroscopy studies are unique in the United States. Currently, 30 Tesla in split-coil magnets and ~45 Tesla solenoids are available for scattering and spectroscopic experiments, respectively. They have been developed at Tohoku University using high-tensile-strength and high conductivity CuAg wires. Pulsed fields (1-5 ms in duration) are generated using a configurable bipolar capacitor bank (3kV, up to 4.5 mF). These low-energy small-bore coils are mounted on the cold finger of a closed-cycle He cryostat capable of a repetition rate of ~10-20 minutes for peak fields in the range of 20-30 Tesla. Time-resolved scattering data are typically collected using a fast APD detector. Results from preliminary scattering studies of structural fluctuations in a geometrically frustrated magnet will be presented and future opportunities in experiments and instrumentation will be discussed. Use of the Advanced Photon Source is supported by the U. S. Department of Energy, Office of Science, under Contract No. DE-AC02-06CH11357.

#### SP068

**Structure of the *Nitrosomonas europaea* Rh Protein.** Xin Li\*, Sanjay Jayachandran<sup>†</sup>, Hiep-Hoa Nguyen<sup>†</sup>, Michael K. Chan\*, \*Ohio State Biophysics Program, Depts. of Biochemistry and Chemistry, Ohio State Univ., Columbus, OH 43210, <sup>†</sup>TransMembrane Biosciences, Pasadena, CA 91107.

Amt/MEP/Rh proteins are a family of integral membrane proteins implicated in the transport of NH<sub>3</sub>, CH<sub>2</sub>NH<sub>2</sub>, and CO<sub>2</sub>. While Amt/MEP proteins are agreed to transport ammonia (NH<sub>3</sub>/NH<sub>4</sub><sup>+</sup>), the primary substrate for Rh proteins has been controversial. Initial studies suggested that Rh proteins also transport ammonia, but more recent evidence suggests that they transport CO<sub>2</sub>. Here we report the first structure of an Rh family member, the Rh protein from the chemolithoautotrophic ammonia-oxidizing bacterium *Nitrosomonas europaea*. This Rh protein exhibits a number of similarities to its Amt cousins, including a trimeric oligomeric state, a central pore with an unusual twin-His site in the middle, and a Phe residue that blocks the channel for small molecule transport. However, there are some significant differences, the most notable being the presence of an additional cytoplasmic C-terminal  $\alpha$  helix, an increased number of internal proline residues along the transmembrane helices, as well as a specific set of residues that appear to link the C-terminal helix to Phe blockage. This latter linkage suggests a mechanism in which binding of a partner protein to the C-terminus could regulate channel opening. Another difference is the absence of the extracellular  $\pi$ -cation binding site conserved in Amt/Mep structures. Instead, CO<sub>2</sub> pressurization experiments identify a CO<sub>2</sub> binding site near the intracellular exit of the channel whose residues are highly conserved in all Rh proteins, except those belonging to the Rh30 subfamily.

#### MP069

**Structural Studies on Vitamin B<sub>6</sub> Catabolism.** Kathryn M. McCulloch<sup>1</sup>, Tathagata Mukherjee<sup>1</sup>, Tadhg P. Begley<sup>1</sup>, Steven E. Ealick<sup>1</sup>, <sup>1</sup>Dept. of Chemistry and Chemical Biology, Cornell Univ., Ithaca, NY 14853.

Pyridoxine, also known as vitamin B<sub>6</sub>, is an essential cofactor that is involved in a myriad of reactions within the cell. The biosynthetic pathway for vitamin B<sub>6</sub> has been thoroughly studied. However, the catabolism of vitamin B<sub>6</sub> has received less attention. A few microorganisms have been identified that can grow solely on vitamin B<sub>6</sub>, including *Mesorhizobium loti* MAFF303099. The proposed catabolic pathway is composed of seven enzymatic reactions and we have determined the structures of two enzymes from this pathway.

The decarboxylation of the intermediate 3-hydroxy-2-methylpyridine-4,5-dicarboxylate has been shown to be catalyzed by the gene product of mlr6971, 3-hydroxy-2-methylpyridine-4,5-dicarboxylate decarboxylase (HMPDdc) to form 3-hydroxy-2-methylpyridine-5-carboxylate (MHPC). HMPDdc had previously been annotated as a possible epimerase based on sequence similarity. We have determined the structure of HMPDdc to 1.9 Å using SAD phasing. HMPDdc belongs to the class II aldolase superfamily and unexpectedly crystallized with a metal ion bound within the active site. Based on the structure of HMPDdc, we were able to propose a mechanism for this decarboxylation reaction.

Recently, the gene encoding the enzyme which catalyzes the subsequent reaction has been identified. MHPC is converted to 2-(acetamidomethylene)succinate (2-AMS) by the flavin-dependent enzyme 2-methyl-3-hydroxypyridine-5-carboxylate oxygenase (MHPCO). Previous studies on MHPCO have shown that two oxygen atoms are incorporated into 2-AMS. MHPCO is of interest as it catalyzes an oxidative ring opening without the use of any metal cofactor. We have determined the structure of MHPCO bound to FAD and the structure of MHPCO bound to FAD and the substrate MHPC at 2.1 Å using SAD phasing.

#### TP070

**Structural Studies of Type III Restriction Endonuclease *EcoRII*-DNA Complexes.** Liqing Chen<sup>1</sup>, Li Qiu<sup>1</sup>, Michal Szczypek<sup>2</sup>, Monika Reuter<sup>2</sup>, Edward J. Meehan<sup>1</sup>, <sup>1</sup>Laboratory for Structural Biology, Dept. of Chemistry, Graduate Programs of Biotechnology, Univ. of Alabama, Huntsville, AL, USA, <sup>2</sup>Inst. of Virology, Humboldt Univ. Medical School (Charité), Berlin, Germany.

*EcoRII* is a type III restriction endonuclease that interacts with two copies of the DNA sequence 5'CCWGG (W = A or T), one being the target for cleavage, the other serving as allosteric effector. *EcoRII* has two functional domains, an N-terminal effector domain and a C-terminal catalytic domain. After we solved the *EcoRII* structure and proposed a putative autoinhibition/activation mechanism, the detailed interactions of *EcoRII* with its effector and substrate DNAs remain unknown. Therefore, cracking down the *EcoRII*-DNA complex structure through x-ray crystallography becomes our next challenge.

The binding of *EcoRII* to DNA substrate was confirmed by the native gel electrophoresis results. It was intriguing to find that actually two types of stable *EcoRII*-DNA complex were formed. The association constants for both complexes was estimated around 10<sup>8</sup>-10<sup>9</sup> M<sup>-1</sup>. Previous *EcoRII* crystallization experience and biochemical investigation of *EcoRII* binding and cleavage activities revealed the profound role of Mg<sup>+2</sup>. To avoid undesired DNA substrate cleavage in the presence of Mg<sup>+2</sup> within many crystallization screening formulations, we expressed and purified several inactive *EcoRII*

mutants that bind DNA substrates tightly. Co-crystallization of these mutants as well as the wild type and active mutants with various DNA oligomers are under intensive investigation and will be presented.

Supported in part by NSF-EPSCoR to the Laboratory for Structural Biology, University of Alabama in Huntsville. Work in Berlin was supported by Deutsche Forschungsgemeinschaft.

### SP071

**Structure of SARS-CoV nsp9 G104E.** Zachary J. Miknis<sup>1</sup>, Timothy C. Umland<sup>1,2</sup>, L. Wayne Schultz<sup>1,2</sup>, <sup>1</sup>Dept. of Structural Biology, Univ. at Buffalo, Buffalo, NY 14203, <sup>2</sup>Hauptman Woodward Inst., Buffalo, NY 14203.

Following the emergence of SARS-CoV in late 2002, considerable efforts have been made towards studying viral proteins related to genome reproduction and viral packaging. One of the earliest determined structures was nsp9, a non-specific RNA/DNA binding dimer consisting of seven B strands and one alpha helix. The helix contains a conserved GXXXG known to be a dimerization motif in both transmembrane and soluble proteins. The motif was targeted for mutagenesis to study its role in nsp9 dimerization and the consequences for viral reproduction and structure. Previous data indicated that the dimer of nsp9 is required for viability and that mutations at the G100E or G104E disrupt the dimer in solution.

Diffraction quality crystals were obtained with the nsp9 G104E mutant, which diffracted to 2.6 Å resolution and were solved using molecular replacement. Interestingly, the helix-helix dimer interface targeted by G104E was observed in the crystal via non-crystallographic symmetry with significant structural distortions as compared to wild-type structures. A string of four monomers in the asymmetric unit is propagated along the B axis of the crystal to generate a helix-like string of nsp9 sheet-sheet dimers which exposes a near continuous patch of positive charge along the surface of the helix.

Structures of wild-type nsp9 and the G104E mutant were used for generating mutants to map the RNA binding surface of nsp9. Surface arginine and lysines were initially targeted, followed by residues involved in coordinating sulfate and phosphate ions in the crystal structures. Binding affinities were calculated using fluorescence anisotropy measurements of RNA-protein interactions. Several mutants have lower affinity for RNA, providing an initial binding surface.

### MP072

**A Neutron Sensitive Anger Camera for Neutron Scattering Instruments.** Richards, John, Cooper, Ronald, Visscher, Theodore, Donahue, Cornelius, Detector Sciences Group, Spallation Neutron Source, 1 Bethel Valley Rd., Oak Ridge, TN 37830 USA.

In the material sciences determining the structure of materials with large unit cells is an important area of research. At neutron scattering facilities the range of the unit cells which can be studied is limited by the position resolution of the detector systems. Time resolved detectors with 1mm resolution are needed to further this area of research. To meet these requirements we have developed a neutron sensitive Anger camera using position sensitive photomultiplier tubes, pixel mapping optics, and a novel anode gain matching scheme. The design of the camera, its operational parameters, and some preliminary data will be presented on this poster.

### TP073

**Polysaccharide Structures: A Heuristic Journey from Laboratory Sources to Synchrotron Radiation.** Srinivas Janaswamy, Rengaswami Chandrasekaran, Whistler Center for

Carbohydrate Research, Purdue Univ., West Lafayette, IN 47907, janaswam@purdue.edu

Biopolymer realm encompasses a great variety of globular proteins, viruses, polypeptides, polynucleotides and polysaccharides. A thorough understanding of their assembly, biological activities, functions and mechanisms is very much in need. In this set, polysaccharides form an important class due to their abundant food and pharmaceutical applications. Despite their plenitude, very few of them are structurally characterized. One of the main reasons could be polysaccharides are not amenable for traditional structure solution techniques. They can at best be coaxed to form partially ordered semi-crystalline specimens and oriented fibers with some lateral ordering.

Traditionally, in the laboratory experiments the intensity data from polysaccharide fibers are collected on flat photographic films. The fiber, in the camera, is maintained at required humidity by flushing a study stream of helium gas bubbled through a saturated solution. Undoubtedly this data collection strategy has yielded several canonical polysaccharide structures. Albeit, this approach suffers from some technical problems, such as (1) the intensity from laboratory generators is not really high, consequently the duration of data collection extends to as long as 24hrs and beyond, (2) due to such long exposures the background noise also gets accumulated posing difficulty in analyzing low intensity reflections especially from weakly diffracting fibers, and (3) fiber can not be examined at all positions along the fiber axis, to name a few. These glitches can now be overcome effectively by the availability of synchrotron radiation. BioCAT and BioCARS beamlines at Argonne National Laboratory, Chicago, IL are very much helpful in this regard. The duration for the total data collection is as low as 2 seconds as the incident intensity is very high compared to laboratory generators.

### SP074

**High Resolution Crystal Structures of the HIV-1 Protease and the I54V Mutant Reveal Tetrahedral Reaction Intermediates.**

Y. Tie<sup>1</sup>, A.Y. Kovalevsky,<sup>1</sup> A.A. Chumanevich,<sup>1</sup> C.H. Shen<sup>1</sup>, J.M. Louis<sup>2</sup>, R.W. Harrison<sup>1,3</sup>, I.T. Weber<sup>1,4</sup>, <sup>1</sup>Biology Dept., <sup>3</sup>Computer Science Dept. and <sup>2</sup>Chemistry Dept., Molecular Basis of Disease Program, Georgia State University, Atlanta, GA 30303, <sup>2</sup>Laboratory of Chemical Physics, National Inst. of Diabetes and Digestive and Kidney Diseases, The National Institutes of Health, Bethesda, MD.

HIV-1 protease (PR) is the target for several important antiviral drugs used in AIDS therapy. The drugs bind inside the active-site cavity of PR where normally the viral poly-protein substrates are bound and hydrolyzed during maturation of the infectious viral particle. We report high resolution crystal structures of wild-type PR and the multi-drug resistant variant with I54V mutation in complex with a self-processed peptide at resolutions of 1.2-1.5 Å. Both the *gem-diol* tetrahedral reaction intermediate (TI) and the reaction products were observed. Distinctive interactions are observed for the TI binding in the active site cavity of PR<sub>WT</sub> and PR<sub>I54V</sub>. The mutant PR<sub>I54V</sub>/TI complex has lost water-mediated hydrogen bond interactions with the amides of Ile 50/50' in the flap. Hence, the structures provide insight into the mechanism of drug resistance arising from this mutation. The structures also illustrate intermediate states in the hydrolysis reaction. One of the *gem-diol* hydroxide groups in the PR<sub>WT</sub>-TI complex forms a very short hydrogen bond with the outer carboxylate oxygen of the catalytic Asp25. Quantum calculations based on this TI structure are consistent with protonation of the inner carboxylate oxygen of Asp25', in contrast to several theoretical studies. Further analysis and comparison of these structures with PR complexes with clinical inhibitors will help design novel drugs with new binding modes

**TP075****Toward a Joint X-ray/Neutron Refinement of the Cysteine Peptidase Papain: The Room Temperature X-ray Structure.**

A.S. Gardberg<sup>1</sup>, H.M. O'Neill<sup>1</sup>, E. Snell<sup>2</sup>, D.A.A. Myles<sup>1</sup>, <sup>1</sup>Center for Structural Molecular Biology, ORNL, Oak Ridge, TN, <sup>2</sup>Hauptman-Woodward Medical Research Inst., Buffalo, NY.

Cysteine peptidases (CPs) comprise the ~20 families of peptidases dependent on a cysteine residue at the active site. The best known family of CPs is C1; enzymes of this family appear in all protozoa, plants, and animals. While many principles of CP activity have been thoroughly studied, the molecular basis for CP substrate hydrolysis remains poorly understood.

The enzyme used in this study is papain, a member of the C1 family and the archetypal CP. Papain is obtained from papaya fruits; its utility in tenderizing meat has been known for thousands of years. Papain finds immunological utility in the cleavage of immunoglobulins into Fc and FAB fragments, and medical use in the treatment of stings and chronic wounds. Earlier work reported the crystallization of papain from ethanol/methanol solutions, revealing that papain comprises 2 major structural domains. Papain activation is believed to depend on the formation of a thiolate-imidazolium pair between residues Cys25 and His159 at the cleft between domains.

In this study we have obtained crystals from a new aqueous condition containing PEG, buffer, and sodium thiosulfate. In this condition, papain crystallizes in a low-solvent-content unit cell. A 1.60 Å X-ray data set was collected at 300 K in 4 h on a copper-source diffractometer. Results show that a thiosulfate moiety is bound to the active site cysteine, Cys25. Efforts to optimize crystal size for ultra-high resolution X-ray diffraction and neutron diffraction data collection are ongoing. By locating the hydrogen atoms at the active site, we hope to determine the protonation state of His159 and obtain a clearer picture of papain activation and substrate hydrolysis.

**SP076****Crystallization of the *Drosophila* Tgo Basic-helix-loop-helix-PAS Domain.** Dongli Wang, Robert Rose, Biochemistry Dept., North Carolina State Univ., 128 Polk Hall, Raleigh, NC 27695.

bHLH (basic-helix-loop-helix) proteins constitute a large transcription factor family which fulfill diverse roles in cellular differentiation and proliferation. bHLH factors function as homo- and heterodimers, and the function is regulated in part through selection of dimerization partners. The bHLH-PAS (Per-Arnt-Sim) subgroup contains a second PAS dimerization domain adjacent to the HLH dimerization domain. Selection between dimerization partners is determined by the two adjacent PAS domains, referred to as PASA and PASB. To characterize modifications of the HLH dimerization domain and how the PAS domain selects between dimerization partners, we are studying the bHLH-PAS protein *Drosophila* Tgo. Tgo, and its mammalian ortholog Arnt, are ubiquitously expressed proteins that dimerize with other bHLH-PAS proteins. In *Drosophila*, Tgo heterodimerizes with Sim, Trh, Sima and Ss, while each of these bind only Tgo and not one another. Tgo heterodimers regulate *Drosophila* midline development ... Tgo can form homodimers *in vitro* as well. Currently there are only structures of individual PAS domains, and no crystal structure demonstrating the interaction between bHLH-PAS heterodimers. Therefore the structural basis for selection of binding partners for PAS proteins is not well understood either.

Our goal is to crystallize Tgo heterodimers to determine how bHLH-PAS proteins select dimerization partners, and how the PAS domain might affect DNA binding. So far in our lab, we have cloned and purified *Drosophila* Tgo (bHLH-PAS). From crystal trials using

the robot at the Hauptman-Woodward Institute, we have obtained promising initial crystals of Tgo. We are currently optimizing these conditions.

**TP077****Novel Substrate Binding Modes by the Bacterial (outer membrane) Cobalamin Transporter BtuB.** Peter S. Horanyi, Michael D. Purdy, James M. Vergis, Christian Banchs, Michael C. Wiener, Univ. of Virginia Dept. of Molecular Physiology and Biological Physics, Charlottesville, VA 22908.

In Gram-negative bacteria, BtuB is the outer membrane active transporter responsible for uptake of corrin-containing compounds (corrinoids) such as cobalamins and cobinamides. BtuB is an example of the TonB-dependent transporter family, which utilizes the inner membrane proton-motive force to affect transport across the outer membrane. We have characterized structurally and functionally the interactions of multiple corrinoids with BtuB. To date, all structures of these substrate-transporter complexes contain substrate bound to the extracellular face of the transporter. We have recently observed an additional novel periplasmic binding site that may provide unique insight into the mechanism of transport.

[Research supported by NIH Grant 2R01GM079800]

**MP078****Facilitating Low Volume Protein Crystallography Set-ups Using the Mosquito® Liquid Handler.** Joby Jenkins, Rob Lewis, Jas Sanghera, Chloe Milburn, TTP LabTech Ltd, Melbourn Science Park, Melbourn, Hertfordshire, SG8 6EE, UK.

A prerequisite for efficient high throughput protein crystallisation screening is the accurate pipetting and positioning of the low volume drops used in hanging and sitting drop setups. Screening the many different conditions under which a protein crystal may form lends itself to automation, since it requires hundreds of similar experiments to be set up to find the few 'hits'. Automated solutions exist for low volume pipetting, however, the variable viscosities of protein and reservoir/screen solutions present significant challenges for many liquid handling systems. Another challenge is that of drop positioning. The mosquito® (TTP LabTech) offers fast positive displacement pipetting for accurate and reproducible aspiration and dispensing throughout the 50 µL - 1.2 µL range, producing CVs of <8% at 50 µL irrespective of viscosity. This, plus its columnar arrangement of pipettes, allows it to automate hanging drop as well as sitting drop set-ups. Mosquito's micropipettes are also disposable, thus guaranteeing zero cross contamination where required.

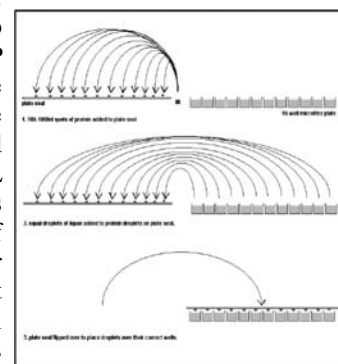


Figure: Automated hanging drop setup

**SP079****Temperature Dependent Studies of Protein Crystals: Lattice Disorder, Radiation Sensitivity, and the Glass Transition.** Matthew Warkentin, Robert Thorne, Dept. of Physics, Cornell Univ., 219 Clark Hall, Ithaca, NY 14853.

We have measured unit cell parameters, mosaicities, B-factors, crystal perfection, and radiation sensitivity for four model systems

-- Lysozyme, Trypsin, Thaumatin and Ribonuclease A -- as a function of temperature. Unlike in previous temperature-dependent studies, data is continuously collected from an individual crystal as it cools from 300 K to 100 K. B factors and mosaicity increase and large scale crystal perfection (as probed by X-ray topography) degrades between 240 K and 180 K. These parameters show more modest evolution between 180 K and 100 K, where solvent and protein motions have frozen out. Similarly, most of the decrease in radiation sensitivity occurs between 240 K to 180 K. This confirms that the glass transition in the solvent + mobile protein system is responsible for the dramatically increased crystal lifetimes at 100 K. Radiation damage studies may thus allow quantitative study of solvent and protein motions.

#### MP080

**Crystal Structure of *Pseudomonas aeruginosa* PilY1, a Protein Required for Bacterial Motility and Infection.** Jillian Orans<sup>†</sup>, Ryan W. Heiniger<sup>‡</sup>, Michael D.L. Johnson<sup>\*</sup>, Matthew C. Wolfgang<sup>‡</sup>, Matthew R. Redinbo<sup>\*†</sup>, Dept. of Chemistry<sup>†</sup>, Dept. of Biochemistry and Biophysics<sup>\*</sup>, and Dept. of Microbiology and Immunology<sup>‡</sup>, Univ. of North Carolina at Chapel Hill, Chapel Hill, NC, 27599.

*Pseudomonas aeruginosa* is an opportunistic pathogen that significantly impacts humans with compromised immune systems, and is chronic in cystic fibrosis patients. *Pseudomonas* infection requires attachment to the host cell via a type IV pilus. PilY1 is the putative pilus tip adhesin protein; it has also been implicated in twitching motility and pilus biogenesis, both of which are necessary for the colonization of host cells. We present the crystal structure of the C-terminal half of pilY1 (residues 613-1161) determined using SeMet SAD phasing and refined to 2.1 Å. Structural elucidation required the mutation of 22 leucines residues to methionine to identify three additional methionines for sufficient phasing power. The structure reveals a unique and modified incomplete β-propeller with an extended β-strand incorporated into two distinct propeller blades. Through site-directed mutagenesis and functional assays we have identified specific regions of the protein essential for both pilus biogenesis and twitching motility. These results have important implications in the design of compounds to specifically inhibit *Pseudomonas* infection.

#### TP081

**Structural Perspective on the Lead Optimization of Anticancer Prodrug PABA/NO.** R.C. Kalathur, J.E. Saavedra, L.K. Keefer, X. Ji, Center for Cancer Research, National Cancer Inst., Frederick, Maryland, 21702.

Human glutathione S-transferase P1 (GSTP1), one of the cytosolic GSTs that belong to a family of the phase II xenobiotic metabolizing enzymes, detoxifies a wide variety of electrophilic compounds including exogenous xenobiotics such as mutagens, anticancer agents, and their metabolites. Therefore, GSTP1 is believed to play an important protective role in tumor cell pathogenesis and survival, and the overexpression of GSTP1 has been linked to drug resistance to cancer chemotherapeutic agents. Our structure-based design of prodrugs intended to release cytotoxic levels of nitric oxide in GSTP1-overexpressing cancer cells yielded PABA/NO, which exhibited anticancer activity both *in vitro* and *in vivo* with a potency similar to that of cisplatin (Findlay et al., *Mol. Pharmacol.* 65: 1070-1079, 2004). However, PABA/NO is not 100% GSTP1 specific. It can also be activated by other classes of GSTs, including GSTA1 that is abundant in liver. Here, we present the structural perspective on the optimization of PABA/NO, showing how the three-dimensional

structures of GSTP1, in its ligand-free form, in complex with a glutathione (GSH) analog, and in complex with both PABA/NO and the GSH-analog guide the improvement of isozyme selectivity of the prodrug.

This research was supported by the Intramural Research Program of the NIH, National Cancer Institute, Center for Cancer Research.

#### MP082

**Automated Sample Handling, Data Collection and Structure Solution with ACTOR.** A.R. Criswell, A. Dowell, R. Bolotovsky, J.W. Pflugrath, C. Yang, Rigaku Americas Corp., The Woodlands, TX, USA, 77381.

Systems for automatic sample mounting and diffraction data collection have matured in recent years. Many such automated systems automate the full process from crystalline samples of unknown quality to correctly traced electron density maps. Enabling these methods are reliable hardware for sample handling, tracking methods to identify samples accurately, and software for sample analysis, data collection and processing, and structure solution. Recent developments in the ACTOR system include optional hardware and software for RFID sample tracking and new hardware designs. Additionally, the ACTOR software has expanded to include an automated structure solution pipeline, formerly offered as part of the MIFit software. These software modules expand the capabilities of ACTOR to use 'bind and grind' and SAD methods for structure solution. We will describe these new hardware and software developments and evaluate their efficacy and reliability in identifying satisfactory samples and producing correct protein structures.

#### TP083

**Prospectives for Macromolecular Structure Determination via Neutron Isomorphous Replacement Data.** David A. Langs, Hongliang Xu, Herbert A. Hauptman, Hauptman-Woodward Medical Research Institute, 700 Ellicott St., Buffalo, NY 14203 USA.

The idea to use the difference in scattering between hydrogen and deuterium as a tool to determine macromolecular structure is not particularly new. But from the very beginnings experimentalists have been severely handicapped by the weak strengths of neutron beams generated from nuclear fission processes, the daunting task of preparing fully deuterated biological samples to avoid high background scattering and the unsolved challenge to prepare sophisticated partially hydrogenated derivatives that would be required for traditional isomorphous replacement phasing methods. But methods for expressing deuterated proteins to service both NMR and neutron crystallographic studies have been perfected over the past 10 years and strategies to selectively hydrogenate certain amino acids in these perdeuterated proteins sequences are currently under investigation in a number of laboratories. With the advent of high intensity spallation technology beamlines many groups could be well positioned to contemplate using D/H substitution for SIR structure solution. This presentation will call attention to some of the unforeseen phasing problems that might arise as a consequence of making such applications using neutron diffraction data.

Research support from the Human Frontier Science Program is gratefully acknowledged

#### SP084

**Crystal Structures of the Human Ceramide Activator Protein Saposin D at 1.3 and 2.0Å.** K. Popovic<sup>1</sup>, G.G. Prive<sup>1,2,3</sup>, <sup>1</sup>Dept. of Medical Biophysics, Univ. of Toronto, <sup>2</sup>Dept. of Biochemistry, Univ. of Toronto, <sup>3</sup>Div. of Cancer Genomics & Proteomics, Ontario

Cancer Inst., Univ. Health Network, MaRS Center, Toronto Medical Discovery Tower; Toronto, Ontario M5G 1L7, Canada.

Sphingolipids (SLs) are essential components of eukaryotic cell membranes taking part in cell adhesion, cell growth, cell regulation, intracellular trafficking, interaction with signal molecules and toxins. Typically, two proteins are involved in the lysosomal breakdown of a SL: an acid hydrolase and an activator protein. If either of



these proteins is functionally absent, the corresponding lipid substrate accumulates and is stored within tissues of the body. Saposin D is a sphingolipid activator protein required for the lysosomal breakdown of ceramide to a fatty acid and sphingosine by acid ceramidase. We have determined the crystal structure of saposin D in two different crystal forms at 1.3 Å and 2.0 Å, resulting in a total of six crystallographically independent views of this small 80 amino acid protein. All of the structures are highly similar, and reveal the form of the saposin fold previously seen in the crystal structures of saposins A and C, as opposed to the saposin B. Saposin D is slightly more compact than the related saposins A and C due to slight repositioning of the “stem” and “hairpin” regions of the protein.

#### MP085

**Three-Dimensional Models of KaiA-KaiC and KaiB-KaiC Protein Complexes and Functional Insights into the Cyanobacterial Circadian Clock.** R. Pattanayek,<sup>1</sup> D.R. Williams,<sup>2</sup> S. Pattanayek,<sup>1</sup> T. Mori,<sup>3</sup> Y. Xu,<sup>3</sup> C.H. Johnson,<sup>3</sup> P.L. Stewart,<sup>2</sup> M. Egl<sup>1</sup>, Depts. of <sup>1</sup>Biochemistry, <sup>2</sup>Molecular Physiology and Biophysics, <sup>3</sup>Biological Sciences, Vanderbilt Univ., Nashville, TN.

The circadian clock of the cyanobacterium *Synechococcus elongatus* can be reconstituted *in vitro* by mixing recombinant KaiA, KaiB and KaiC proteins with ATP, producing KaiC phosphorylation and dephosphorylation cycles that have a regular rhythm with a ca. 24-h period and are temperature-compensated. KaiA enhances KaiC phosphorylation and is antagonized by KaiB. We have used X-ray crystallography, negative-stain and cryo-EM, biochemical and mutagenetic data to build 3D-models of the KaiA-KaiC and KaiB-KaiC clock protein complexes. The KaiA dimer interacts with the KaiC homo-hexamers via the flexible C-terminal region of the latter. A second, potentially more transient interaction concerns an apical loop region of KaiA and the inter-subunit ATP-binding cleft in KaiC. Two KaiB dimers bind to the C-terminal half of KaiC and the interaction results in splaying of the C-terminal domains of KaiC subunits. The model of the KaiB-KaiC complex also provides a rationalization of the earlier observation that KaiA and KaiB simultaneously bind to KaiC during the dephosphorylation phase. The two complexes and insights into clock function and regulation of phosphorylation based on them will be discussed.

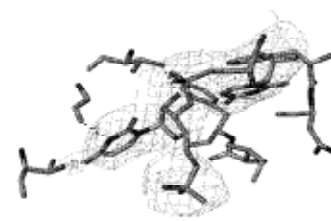
Support by the National Institutes of Health (R01 GM73845 to ME, R01 GM67152 to CHJ, and F32 GM71276 to DRW) is gratefully acknowledged.

#### TP086

**Crystal Structure of Vaccinia Virus Poly(A) Polymerase–vp39 Heterodimer with a Specific UU Oligonucleotides.** C.Z. Li, H.Y. Li, S.F. Zhou, T. Poulos, P.D. Gershon\*, Dept. of Molecular Biology & Biochemistry, Univ. of California, Irvine, CA, 92697.

Addition of the poly(A) tail to mRNA is an important step in all organisms, including poxviruses which encode their own poly(A) polymerase (PAP). The poxvirus PAP (VP55) is very unusual and

mechanistically highly novel, insofar as it (a) moves along the poly(A) tail during tail addition, (b) has a processivity factor (VP39) that confers a dramatic increase in processivity after the first 30 nt of the tail have been added, allowing 200–250 nt tails



to be added. The crystal structure for the VP55-VP39 heterodimer is published (1), but not for complexes with RNA. Initiation of poly(A) tail addition requires a nucleic acid primer containing the sequence: UUN<sub>15</sub>U for VP55 and UUN<sub>25</sub>U for VP55-VP39. The downstream U binding site has been known for 10 years, via a photocrosslinking approach in which the UU binding site was refractory to analysis. Here, a series of short, UU containing oligonucleotides were used. A 3.35 Å heterodimer structure (hopefully soon to be improved) in space group P1, with the cell dimensions of  $a=70.222\text{Å}$ ,  $b=77.876\text{Å}$  and  $c=107.446\text{Å}$  was soaked with a UU containing oligonucleotide, revealing the specific binding site for UU on the VP55 surface, around residues F47, T109 and T116, a site previously assigned for binding a second ATP molecule. With regard to uridylyte recognition: The first U base was hydrogen bonded to T116 and T113, the second base was stacked with F47. The 3' phosphate was clearly seen in the structure. The first base and ribose interacted with determinants of binding for the ATP di/triphosphate.

(1) C. M. Moure, B. R. Bowman, P. D. Gershon and F. A. Quiocho, Crystal structures of the vaccinia virus polyadenylate polymerase heterodimer: insight into ATP selectivity and processivity, *Mol. Cell*, 2006, 22, 339-348. \*Correspondence: pgershon@uci.edu We thank Stanford Synchrotron Research Lab for access to beamline 9-2. This research is supported by NIH (GM51953).

#### MP087

**Overcoming the Incommensurability Between Curved Surfaces and Azimuthal Alignments of Divergently Stacked Diamond Unit Cells in Epitaxially Oriented Overgrowth.** Boris Udovic, Sezanska 11, SL-6210 Sezana, Slovenia, boris.udovic@email.si

The cutting edges of high speed rotating gas-turbine fan-blades at the compressive inlet of the first stage of air jet-engines are exposed to heavy wear regimes by smashing impacts against flaying solid objects, debris and erosive Harmattan, El-Ghibli etc. sandy winds. In addition, the mechanical depletion of protective hard coatings as DLC-CVD is furthermore enhanced if the radius of the circle of curvature reaches lower values at the sharpest side of the blade borderline. Properly, the mechanical failure at curved surfaces is unavoidable because of accumulative effects of driving distortional forces for crack initiation at the level of the periodic interfacial potential energy between geometrically incommensurable curved line of the substrate and the epitaxially overgrown diamond cells (cubic system, hexoctahedral symmetry, space group  $Fd\bar{3}m$ ). The disregistry between the atoms on either side of the curved-straight interface lengthens the repeat period of the function energy, which reaches the potential minima by redirecting the azimuthal angle of twist. The orthogonal pile-up of diamond-CVD stacked unit cells is modified in the fashion of long divergent columnar grains grown along radially emerging lines which are perpendicular to the curved interfacial line. The observed *highly textured* topology of DLC films is more precisely a geometrically *fractured* than *nano-structured* spatial property. A 3D spider-like web mesophase of carbon chains that permeate the inter-crystallite voids and strengthen the curved hard coating films is synthesized *via* isolobal reactions by desymmetrization of frontier orbitals of suitable diradical linkers with sewing actions that preserves the  $sp^3$  relationship between glassy-carbon atoms to a great extent.

**TP088****Submicron-Resolution Three-Dimensional X-Ray Microscopy.**

B.C. Larson, Materials Science & Technology Div., Oak Ridge National Laboratory, P. O. Box 2008, Oak Ridge, TN 37830.

X-ray structural microscopy using polychromatic x-ray microbeams at 3<sup>rd</sup> generation synchrotron sources provides the capability to measure local crystal orientations, grain-sizes, grain morphologies, and both intra- and inter-granular misorientations with submicron spatial resolution in three dimensions. Measurements can be performed over length scales varying from the submicron resolution of the technique to hundreds of microns. This range encompasses critical mesoscopic length scales, as determined by materials microstructure features such as polycrystal grain size and deformation induced dislocation patterning. This presentation will show examples of x-ray structural microscopy for nondestructive investigations of polycrystalline grains in aluminum and dislocation tensors in elastically and plastically bent Si. The present capabilities of the 3D x-ray microscopy facility developed by ORNL on Sector 34 of the Advanced Photon Source at Argonne National Laboratory will be discussed and the outlook for sub-100 nm microscopy capabilities will be presented.

Research sponsored by the U. S. Department of Energy Office of Science, Basic Energy Sciences Division of Materials Sciences and Engineering; the APS is supported by the Department of Energy Office of Science.

**SP089****Structure-function Studies of the BTB Domain from Zinc-finger Transcription Factors.**

P.J. Stogios<sup>1</sup>, J.A. Cuesta-Seijo<sup>2</sup>, L. Chen<sup>2</sup>, N.C. Pomroy<sup>2</sup>, G.G. Privé<sup>1,2</sup>. <sup>1</sup>Dept. of Medical Biophysics, Univ. of Toronto, Toronto, Canada, <sup>2</sup>Ontario Cancer Inst., Toronto, Canada.

The BTB domain is a widely distributed motif with 183 examples in the human genome. 43 of these BTB domains are found in proteins that also contain Zinc Finger motifs, most of which have been characterized as transcription repressors. The domain is thought to mediate homo-dimerization, hetero-dimerization and oligomerization of these proteins. As well, specific BTB domains in this family have been shown to interact with components of chromatin remodeling complexes, including nuclear co-repressor proteins and histone deacetylases. Using a BTB-ZF family-wide focus, we have used x-ray crystallography, cross-linking studies, analytical ultracentrifugation, dynamic light scattering and native gel electrophoresis to study the structure and interactions of BTB domains. We determined the structures of 4 BTB domains and show each is homo-dimeric in structure and solution. The FAZF and Miz-1 BTB domains show novel structural rearrangements, including altered domain swapping state. The Kaiso BTB domain oligomerizes in crystal structure. The BTB domain is able to select for binding to a peptide from the co-repressor SMRT, as we show this interaction does not occur in 5 of 6 BTB domains other than BCOR. These results show that in a general sense, the BTB domain provides a conserved structure that mediates homo-dimerization of BTB-ZF transcription factors. Specific examples show altered domain swapping state or higher-order oligomerization. Lastly, the BTB domain is able to provide selectivity for co-repressor binding. These results provide a framework for further studies into the hetero-dimerization, oligomerization, and peptide-binding, and transcription repression functions of the BTB domain.

**TP090****Crystal Structure of Human Checkpoint Kinase 2 in Complex with a Potent & Selective Inhibitor.**

George T. Lountos<sup>1,4,5</sup>, Andrew G. Jobson<sup>3,4,6</sup>, Joseph E. Tropea<sup>1,4,5</sup>, Di Zhang<sup>1,4,5</sup>, Robert Shoemaker<sup>2,4,5</sup>, Yves Pommier<sup>3,4,6</sup>, David S. Waugh<sup>1,4,5</sup>,

<sup>1</sup>Macromolecular Crystallography Laboratory, <sup>2</sup>Screening Technologies Branch, <sup>3</sup>Laboratory of Molecular Pharmacology, <sup>4</sup>Center for Cancer Research, <sup>5</sup>National Cancer Institute, Frederick, MD 21702, <sup>6</sup>National Cancer Inst., Bethesda, MD 20892.

Chk2 is a checkpoint kinase involved in the ATM-Chk2 checkpoint pathway. This pathway is activated by genomic instability and DNA damage and results in either apoptosis or arrest of the cell cycle to allow DNA repair to occur. Studies have demonstrated that Chk2 is endogenously activated in precancerous lesions with genomic instability and in cancer cells grown in culture. Chk2 has been identified as a tumor suppressor and a promising target for anti-cancer drug design. Currently, the number of selective Chk2 inhibitors remains limited. Our primary rationale for development of Chk2 inhibitors is focused on two areas. Selective inhibition in p53-defective tumor cells may provide chemo/radiosensitization as Chk2 is activated in tumor cells by a wide range of chemotherapeutic drugs and ionizing radiation. Thus, selective inhibition of Chk2 could increase the therapeutic indices of DNA-targeted agents in p53-defective tumors. Furthermore, inhibition of Chk2 in normal cells may also protect normal tissues from p53-induced apoptosis. We have initiated a drug design effort targeting Chk2 by screening over 100,000 compounds in the Open Repository Library and identified a bis-guanylhydrazone, NSC109555, as a potent and selective inhibitor with an IC<sub>50</sub> = 240 nM. A 2.05 Å co-crystal structure of Chk2 complexed with NSC109555 has been solved and provides an important first step in a structure-based drug design effort to provide a rational approach for developing novel inhibitors of Chk2.

**SP091****A Simulation Study of Scattering from Molecular Models with Random Physical Variations, Applied to Protein Models Derived from SAXS Data.**

S.H. Sillau<sup>1</sup>, M. J. van der Woerd<sup>2</sup>, F.J. Breidt<sup>1</sup>, <sup>1</sup>Dept. of Statistics, <sup>2</sup>Dept. of Biochemistry & Molecular Biology, Colorado State Univ., Fort Collins, CO 80523.

The aim of biological SAXS is to determine low resolution molecular structures of proteins in solution by analyzing their scattering patterns. The theoretical scattering intensity as a function of angle is analytically expressed in the Debye formula, which involves individual atomic structure factors and inter-atom distances for the molecule of interest.

Empirical scattering intensities show random variation, with variability increasing at higher resolutions. A natural stochastic model for scattering is a Poisson process model, under which variation of observed intensities about the theoretical intensity would be inversely proportional to theoretical intensity multiplied by angle. At low resolution, this model can explain the observed empirical variation, but at high resolution, it under-predicts the empirical variation.

An alternative explanation for the empirical variation is that the random variation about the theoretical intensity curve is due not only to Poisson counting statistics, but also due to physical variations in the molecular model. We investigated this alternative via simulation to see if we could qualitatively replicate some of the features of experimental intensity curves.

For each model, we repeatedly simulated a random molecule and computed the theoretical intensity curve. The results show that variation in the observed intensities for such randomly-varying models is consistent with those seen in actual data. These results will lead to a better understanding of the data distribution, which serves as the basis for a qualitative descriptor for protein models based on likelihood measures of goodness of fit, derived from SAXS data.

**TP092**

**Time Resolved SAXS and Contrast Variation SANS for the Study of an AAA+ ATPase.** B. Tracy Nixon,<sup>1</sup> Saikat Chowdhury,<sup>1</sup> Baoyu Chen,<sup>1</sup> Tatyana Sysoeva,<sup>1</sup> Liang Guo,<sup>2</sup> <sup>1</sup>Penn State, Univ. Park, PA 16802, <sup>2</sup>Argonne National Lab, Argonne, IL 60439.

The scientific community is still learning how the ubiquitous AAA+ ATPase molecular motors perform mechanical work. Previously, we reported solution structures revealing a large conformational change upon binding ATP that allows one such ATPase, the NtrC1 transcriptional activator of *Aquifex aeolicus*, to bind to the sigma factor of bacterial RNA polymerase. Our recently solved crystal structure of a mutant with ATP bound has confirmed this conformational change. Meanwhile, we have initiated time resolved SAXS to characterize kinetic details of this process, by using a new detector and stop flow device to capture SAXS profiles every 10 msec upon mixing ATPase with the ATP analog ADP-BeF<sub>3</sub>. Derived radius of gyration suggest completion of the structural transition from apo to the ATP state within about 500 msec. Detailed analyses with SVD and global fitting suggest the presence of at least one intermediate in this process. Similarly collected kinetic data for binding ADP-AIF<sub>x</sub> and ADP will characterize conformational changes associated with entering the transition state for ATP hydrolysis and moving to the post-hydrolysis state after release of phosphate, respectively. Finally, we have begun combining SAXS and contrast-varied SANS to determine solution structures of individual components in the complex transcription initiation machinery composed of RNA polymerase, promoter DNA and ATPase. These seminal studies will provide kinetic information and structural details of how these ATPases activate transcription and thereby control beneficial and harmful activities of many species of bacteria.

Work funded by NIH. The BioCAT is an NIH supported Research Center.

**SP093**

**Structural Studies of HLA-B14 and HLA-B27 Subtypes Differently Associated with Ankylosing Spondylitis.** P. Kumar<sup>1</sup>, A. Vahedi-Faridi<sup>2</sup>, E. Merino<sup>3</sup>, J.A. López de Castro<sup>3</sup>, W. Saenger<sup>2</sup>, A. Volz<sup>1</sup>, B. Uchanska-Ziegler<sup>1</sup>, A. Ziegler<sup>1</sup>, <sup>1</sup>Inst. für Immunogenetik, Charité - Universitätsmedizin Berlin, 14195 Berlin, Germany, <sup>2</sup>Inst. für Kristallographie, Freie Univ. Berlin, 14195 Berlin, Germany, <sup>3</sup>Centro de Biología Molecular Severo Ochoa, Univ. Autónoma de Madrid, 28049 Madrid, Spain.

The HLA class I subtype pairs, B\*2705/B\*2709, and B\*1402/B\*1403, exhibit differential association with ankylosing spondylitis (AS). B\*2705 and B\*1403 are associated with AS, whereas B\*2709 and B\*1402 are not. These pairs differ only by a single amino acid exchange (Asp116His and Leu156Arg, respectively). To understand the molecular interactions underlying the differential disease association of the two HLA pairs, we study the differences in presentation of common ligand peptides by the four HLA subtypes. We have obtained crystal structures of B\*1402, B\*2705 and B\*2709 complexed to a common natural ligand, pCatA (IRAAPPPLF), all at 1.8 Å resolution, and of B\*1402 in complex with pLMP2 (RRRWRLTV), a viral antigen possibly involved in AS pathogenesis, at 2.5 Å resolution. Structures of B\*2705:pLMP2 and B\*2709:pLMP2 were previously determined by us. The orientation of the pCatA peptide in the HLA binding grooves is nearly identical despite the presence of 18 residues distinguishing B\*2705 and B\*1402. The pLMP2 peptide is presented in similar conformations in B\*1402:pLMP2 and B\*2705:pLMP2, despite differential anchoring of an Arg at peptide position 5, while, in contrast, in B\*2709:pLMP2, pLMP2 is displayed in a drastically different conformation. The results with pCatA and B\*1402/B\*2705:pLMP2 provide

an explanation for the existence of HLA-B14/B27 cross-reactive T cells, and have implications for negative T cell selection within the thymus.

**TP094**

**1.85 Å Structure of a Modified 8R-Lipoxygenase from the Soft Coral *Plexaura Homomalla* Suggests a New Substrate Binding Mode for Animal Lipoxygenases.** D.B. Neau<sup>\*</sup>, N.C. Gilbert<sup>#</sup>, S.G. Bartlett<sup>#</sup>, A. Dassey<sup>#</sup>, M.E. Newcomer<sup>#</sup>, <sup>\*</sup>Center for Advanced Microstructures and Devices and <sup>#</sup>Dept. of Biological Sciences, Louisiana State Univ., Baton Rouge, LA 70803 USA.

Animal lipoxygenases produce an array of chiral hydroperoxy derivatives from membrane-derived arachidonic acid. Individual lipoxygenase enzymes show a high degree of regiospecificity and stereospecificity. While the position of the catalytic machinery is conserved in the enzyme family, the diversity of product specificity appears to require differences in the mode of substrate binding among isozymes. A new 1.85 Å structure of a modified 8R-lipoxygenase (8R-LOX) from the soft coral *Plexaura homomalla* suggests a mode of substrate binding that has not been considered previously. In light of this new potential binding mode, we can reinterpret the results of some previously conflicting mutation experiments and suggest refinement to the current general model for animal lipoxygenase catalysis.

**MP095**

**Magnetic Annealing Effects on the Local Environment in Fe<sub>20</sub>Ni<sub>80</sub> Alloy.** Y.S. Puzyrev, G.E. Ice, P. Zschack, Oak Ridge National Lab., Oak Ridge, TN.

We measure diffuse x-ray scattering from permalloy Fe<sub>20</sub>Ni<sub>80</sub> single crystal. This single crystal was annealed in magnetic field of 2000 Gauss along <100> crystallographic direction. Measurements were made on beamline 33-ID at the Advanced Photon Source using a wavelength dispersive spectrometer to suppress Compton, Fluorescence and Resonant Raman backgrounds. Data was collected over a large volume in reciprocal space and measurements were made at three energies to maximize, invert, and minimize the x-ray scattering contrast between Fe and Ni. We recovered short-range order (SRO) parameters and atomic displacements (AD) for the crystal. Symmetry of the short-range order peaks and scattering redistribution indicates that the magnetic field induces anisotropic local SRO domains.

**TP096**

**Dissecting the Insulin Promoter by X-ray Crystallography and Small Angle Scattering.** A. Longo<sup>1,2</sup>, V. Urban<sup>1</sup>, R. Rose<sup>2</sup>, <sup>1</sup>Oak Ridge National Laboratory, Oak Ridge, TN 37831, <sup>2</sup>North Carolina State Univ., Raleigh, NC 27695.

Insulin is exclusively expressed in the beta-cells of the pancreatic islets. Expression is regulated by the cooperative binding of several transcription factors on a large promoter region of more than 350 bps. A short region of 50 bps called a mini-enhancer has been shown to retain beta-cell-specific gene expression through the synergistic interaction between the homeodomain Pdx1 and the basic helix-loop-helix E47-NeuroD1 [1].

In an attempt to characterize the structural basis for the interaction between transcription factors on the minienhancer we have solved the crystal structures of the DNA binding domains of Pdx1 [2] and of the E47-NeuroD1 heterodimer [3] bound to their respective

DNA binding sites. Using the crystallographic models we designed computational models of Pdx1 and E47-NeuroD1 bound to the mini-enhancer. Such models will be used to interpret small angle scattering data that we collected on the ternary complex. We are also carrying out preliminary crystallization studies of the complex. The unique combination of the two techniques will allow us to describe the insulin promoter mini-enhancer structure.

[1] Ohneda, et al. (2000) The homeodomain of PDX-1 mediates multiple protein-protein interactions in the formation of a transcriptional activation complex on the insulin promoter, *Mol Cell Biol* 20, 900-11.

[2] Longo, et al. (2007) Structural basis for induced fit mechanisms in DNA recognition by the Pdx1 homeodomain, *Biochemistry*, 46, 2948-2957

[3] Longo, et al. Crystal structure of E47-NeuroD1/Beta2 bHLH domain-DNA complex: heterodimer selectivity and recognition. *Biochemistry* in press  
V.U. acknowledges support by the U.S. Department of Energy, under Contract No. DE-AC05-00OR22725 with ORNL, managed and operated by UT-Battelle, LLC.

### SP097

#### Crystal Structure of Trioxacarcin A Covalently Bound to DNA.

Roland Pfoh, George M. Sheldrick, Lehrstuhl für Strukturchemie, Georg-August Univ., 37077 Göttingen, Germany.

Trioxacarcins are a group of antibiotics that can be isolated from marine streptomycetes. They are cytotoxic against various cancer cell lines, active against Gram-positive and Gram-negative bacteria and show high anti-malaria activity<sup>1</sup>. Trioxacarcin A forms a stable complex with double stranded DNA making a covalent bond to the N7 position of guanine. Cleavage of this DNA-trioxacarcin complex at 100 degree Celsius results the natural product gutingimycin<sup>2</sup> by guanine abstraction, and an abasic DNA. The structure of trioxacarcin A covalently bound to an oligonucleotide was determined to 1.78 Å resolution. Experimental phases were obtained by MAD experiments using brominated oligonucleotides. In the crystal structure the alkylation of d(AACCGGTT) occurs at the guanine that is followed by a thymine. In the resulting duplex this thymine is flipped out and trioxacarcin intercalates at the 3'-side of the alkylated guanine.

<sup>1</sup>Maskey RP et al. (2004) *J Antibiot* 57:771-779.

<sup>2</sup>Maskey RP et al. (2004) *Angew Chem Int Ed* 43:1281-1383.

### TP098

#### Crystal Structures of Different Inhibited and Redox Forms of Cytochrome *c* Oxidase Show Changes in Proton Pathways.

Ling Qin, Jian Liu, Martyn A. Sharpe, Denise A. Mills, Carrie Hiser, R. Michael Garavito, Shelagh Ferguson-Miller. Mich. St. Univ., Biochem & Molecular Biology, E. Lansing, MI, USA.

Well-ordered crystals of native and mutant forms of cytochrome *c* oxidase (CcO) from *Rhodobacter sphaeroides* (*Rs*), containing the two catalytic subunits (PDB entry 2GSM) are reproducibly obtained in the presence of the inhibitor cadmium. Crystal structures have been solved in various redox states and for several mutant forms. Changes are seen upon reduction of both two subunit and four subunit crystals, which are reversed by re-oxidation and which are different from those reported in the reduced form of 13-subunit bovine CcO (PDB entry 1V55). Since the changes are reversible and solubilized crystals are fully active, it seems that these are not structural changes enroute to a denatured form, but may in fact represent an intermediate in the redox process. The major change occurs in the position of the heme *a*<sub>3</sub> porphyrin ring and the region below it, impacting on the structure of the K-proton channel. The changes could relate to the proposal that the K-channel is gated so as to supply protons only during certain steps of the redox cycle. Comparison of the water arrangement in high resolution structures of various mutant and redox forms suggests that different intermediate

redox states may be trapped in different crystal forms where proton uptake is blocked by mutation or inhibitors. A mutant that has a shortened C-terminal of subunit I and the D-path mutant D132A, which are both inhibited in proton uptake, show loss of occupancy of some water positions in the D-path. These waters are postulated to be part of a protonatable water cluster suggested to stabilize, and be stabilized by, the reduction of heme *a*. (supported by NIH GM26916; MTTT-CST-CTA 085P1000817; MSU REF03-016).

### MP099

#### Phase Equilibria and Crystal Chemistry of the BaO-Nb<sub>2</sub>O<sub>5</sub> and BaO-WO<sub>3</sub>-Nb<sub>2</sub>O<sub>5</sub> Systems.

C.J. Rawn<sup>1,2</sup>, W.B. Goodwin<sup>1</sup>, A.M. dos Santos<sup>3</sup>, J. Muth<sup>4</sup>, <sup>1</sup>Dept. of Materials Science and Engineering, Univ. of Tennessee, Knoxville, TN, <sup>2</sup>Materials Science and Technology Div., Oak Ridge National Laboratory, Oak Ridge, TN, <sup>3</sup>Neutron Scattering Sciences Div., Oak Ridge National Laboratory, Oak Ridge, TN, <sup>4</sup>Farragut High School, Knoxville, TN.

Structures in the BaO-Nb<sub>2</sub>O<sub>5</sub> and BaO-Nb<sub>2</sub>O<sub>5</sub>-WO<sub>3</sub> system are of interest due to their promising dielectric properties and potential applications in the field of wireless communications. There are 41 crystal structures for BaO-Nb<sub>2</sub>O<sub>5</sub> binary compounds reported in the Inorganic Crystal Structure Database (ICSD), however, no crystal structure has been reported for the compound Ba<sub>4</sub>Nb<sub>2</sub>O<sub>9</sub>. Several studies have suggested both low- and high-temperature polymorphs for the compound; there are at least six Powder Diffraction File cards that describe the X-ray powder diffraction pattern. In an attempt to determine the crystal structure Ba<sub>4</sub>Nb<sub>2</sub>O<sub>9</sub> was synthesized using traditional solid-state techniques. To understand the polymorphic β to β' phase transition some samples have been fired at 1200 °C and above. A sample of the ternary composition Ba<sub>6</sub>Nb<sub>2</sub>WO<sub>14</sub> was fired at 1300 °C and X-ray diffraction data showed single phase Ba<sub>4</sub>Nb<sub>2</sub>O<sub>9</sub>. This result suggests a large region of solid solubility for Ba<sub>4</sub>Nb<sub>2</sub>O<sub>9</sub> once WO<sub>3</sub> is added. There are three BaO-Nb<sub>2</sub>O<sub>5</sub>-WO<sub>3</sub> ternary crystal structures reported in the ICSD: Ba<sub>9</sub>Nb<sub>6</sub>WO<sub>27</sub>, Ba<sub>4</sub>Nb<sub>2</sub>WO<sub>12</sub>, and Ba<sub>3</sub>Nb<sub>0.66</sub>W<sub>1.33</sub>O<sub>8.66</sub>. Attempts have been made to synthesize these three ternary compounds using traditional solid state synthesis.

### SP100

#### X-ray Crystallographic Studies of Chlorite Dismutase.

B.R. Goblirsch\*, B.R. Streit#, J.L. DuBois#, C.M. Wilmot\*, \*Univ. of Minnesota, Minneapolis, MN 55455, #Univ. of Notre Dame, Notre Dame, IN 46556.

Perchlorate (ClO<sub>4</sub><sup>-</sup>) and its reduced oxy-anionic derivatives have been classified by the Environmental Protection Agency as "top ten" pollutants. Environmental persistence of these toxic compounds is aided by their high solubility and stability. As such, bioremediation represents a viable alternative to more traditional cleanup methods.

Microbial perchlorate reduction is sequentially carried out by two enzymes. Perchlorate reductase catalyzes the four electron reduction of perchlorate to chlorite (ClO<sub>2</sub><sup>-</sup>).<sup>1</sup> Chlorite is subsequently dismutated into chloride ions and molecular oxygen by chlorite dismutase (CLD). Mechanistic studies and secondary structure analysis suggest CLD is a novel member of the *b*-type hemoprotein family. I will discuss these data, and present the progress that has been made towards elucidating the structure of CLD from *Dechloromonas aromatica* RCB via Fe-MAD phasing.

1. Coates, J.D. & Achenbach, L.A. Microbial perchlorate reduction: rocket-fueled metabolism. *Nature reviews* 2, 569-580 (2004).

**TP101**

**Allosteric Regulation in the Bacterial GTPase BipA Revealed Through Structural and Biochemical Studies.** Victoria L. Robinson, Raymond S. Brown, Tobias P. Neef, Megan deLivron, Dept of Molecular & Cell Biology, Univ. of Connecticut, Storrs, CT

BipA, also known as TypA, is a highly conserved prokaryotic GTPase that functions at a basal level to regulate numerous essential actions in bacteria. It is a member of the translational family of bacterial GTPases, which also includes EF-G, EF-Tu, IF2 and LepA. Although its exact cellular function remains elusive, BipA is thought to control stress and virulence events that secure bacterial survival and successful invasion of the host. Consequently, BipA represents a novel target for antimicrobial development. As part of an interdisciplinary approach to answer fundamental questions about the mechanism of action of BipA, including its interaction with the ribosome, we have solved the crystal structure of *Salmonella typhimurium* BipA to 2.7 Å resolution by selenium SAD phasing. The protein crystallizes in space group P2<sub>1</sub> with two copies in the asymmetric unit. Twenty-four selenium atoms were found using SOLVE and initial model built using RESOLVE. In agreement with sequence homology, the first four domains in BipA resemble those previously described for domains I, II, III and V in the EF-G/EF-2 family of translation factors, whereas the C-terminal domain of BipA is unique. Biochemical studies demonstrate that the majority of the ribosome binding determinants are localized to this region of the protein. Structural and biochemical data will be presented which describes how interdomain interactions contribute to the biological activities of the protein. In particular, we have discovered that conformational changes in the GTPase domain, brought about by nucleotide binding and hydrolysis, influence the positioning of the C-terminal domain of BipA, which in turn, regulates ribosome association by the protein.

We thank beamlines X-6A and X-25 at the NSLS. This work is supported by the University of Connecticut Research Foundation and an American Heart Association Scientist Development Grant (# 0635519T) awarded to V.L.R.

**MP102**

**Wavelength-Shifting Fiber Scintillation Neutron Detectors for POWGEN3 & VULCAN at SNS.** Lowell Crow, Neutron Facilities Development Div., Oak Ridge National Lab, Oak Ridge, TN 37830

We have constructed and tested wavelength-shifting fiber scintillation neutron detector modules for initial commissioning of the POWGEN3 powder diffractometer and the Vulcan engineering diffractometer at the Spallation Neutron Source (at Oak Ridge National Laboratory). Both instruments are scheduled for commissioning in 2008.

The design is based on a successful prototype [1]. POWGEN3 and VULCAN require neutron detector systems with large, narrow pixels (about 5mm x 50 mm), good efficiency at up to about 0.5 eV, and areas of several square meters. The detector uses a 6LiF/ZnS:Ag scintillation screen for neutron conversion. The light is collected using a two-layer grid of wavelength-shifting plastic optical fibers with 1 mm diameter. 308 vertical fibers are spaced 2.5 mm apart, and 152 horizontal fibers are also spaced 2.5 mm apart. The detector has an area of 780 mm X 400 mm with an active area of nearly 95%. The vertical fiber ends are mapped to an array of 20 photomultiplier tubes (PMTs) in a 2Cn coincidence pattern. This pattern encodes the 5 mm wide horizontal pixels. Each horizontal fiber is mirrored at one end, and the other end conducts light to a PMT; bundling of these fibers defines the vertical pixels. The detector operates in coded coincidence, requiring signals from one PMT corresponding to a vertical pixel and two PMTs corresponding to a horizontal pixel. The PMT output is converted to digital signals using fast comparators,

and the neutron identification and position encoding are processed digitally. The ~0.3 m<sup>2</sup> module is an integrated unit, with scintillator, grid, PMTs, and digital processors mounted in a single frame.

[1] M. L. Crow, J. P. Hodges, and R. G. Cooper, Nucl. Instr. Meth. A 529 (2004) 287.

**TP103**

**Determining the Structure of Individual Macromolecules and Nanoparticles with XFEL Sources.** Abbas Ourmazd, Russell Fung, Valentin Shneerson, Univ. of Wisconsin-Milwaukee.

Determining the structure of single macromolecules is a grand challenge targeted by 4th generation (XFEL) sources under construction [1]. Algorithms are now available to recover the structure of a single macromolecule by inverting its 3D diffracted intensity distribution [2,3,4]. A central challenge, however, concerns the reconstruction of the 3D diffracted intensity distribution from an ensemble of 2D diffraction patterns, each of which emanates from an unknown or imperfectly controlled orientation of the molecule or nanoparticle. Using a train of 500 kDa biological molecules and pulses from an X-ray Free Electron Laser (XFEL), 10<sup>9</sup> scattered photons can be collected in about an hour. If the orientation of each 2D diffraction pattern were known, this would be ample to recover the molecular structure. However, each 2D diffraction pattern contains a mean photon count (MPC) of 0.01 per pixel in the high-q region. Suggested approaches to determining the orientation of diffraction patterns require a 10<sup>3</sup> times higher MPC. Even classification of patterns into orientational classes so as to boost the signal through averaging requires a flux, which exceeds that delivered by XFEL's by two orders of magnitude [5].

We describe how the 3D scattered intensity distribution can be reconstructed from an ensemble of 2D diffraction patterns with an MPC of 0.01 per pixel, as expected from 4th generation (XFEL) sources, and consider the prospects for going toward the MPC delivered by 3rd generation sources. (See also <http://www.uwm.edu/~ourmazd/>)

[1] K.J. Gaffney, H.N. Chapman, Science 316, 1444 (2007)

[2] J. R. Fienup, Appl. Opt. 21, 2758 (1982)

[3] J. Miao et al., PNAS 98, 6641 (2001)

[4] J.C.H. Spence et al., Acta Cryst. A61, 237 (2005)

[5] V. Shneerson et al., in press (arXiv:0710.2561)

**SP104**

**The Crystal Structure of the siRNA Binding Domain of an Argonaute Protein from the Novel Hyperthermophilic Archaeon *Thermococcus thioreducens*.** R.C. Hughes, M.L. Byrne, J.D. Ng, The Laboratory for Structural Biology, Univ. of Alabama in Huntsville, 301 Sparkman Dr. Huntsville, AL 35899 USA.

The crystal structure of the PAZ domain of a piwi-argonaute protein from the hyperthermophilic archaeon *Thermococcus thioreducens* has been determined to 2.8 Å resolution. The protein crystals belong to the primitive orthorhombic space group P2<sub>1</sub>2<sub>1</sub>2<sub>1</sub> with the unit cell parameters a=36.83Å, b=58.71Å and c=61.81Å. The structure was determined via molecular replacement using the *Pyrococcus furiosus* argonaute as the initial search model. The structure of this protein exhibits a high degree of structural conservation when compared to argonaute proteins from higher eukaryotes despite low sequence homology. Work is currently underway to characterize the siRNA binding activity of the PAZ domain. In addition, crystallization optimization and initial diffraction is being conducted in effort to obtain the structure of the full-length protein.

The development of a mini-pipeline structural genomics was supported in part by NSF STTR-05605 and NSF-EPSCoR (EPS-0447675). Crystallographic data was collected at APS on the SERCAT beamline.

**TP105**

**The Structural and Kinetic Implications of Glu 106 Mutations on Proton Shuttling in Human Carbonic Anhydrase II.** K. Sippel<sup>1</sup>, J. Quirit<sup>1</sup>, C. K. Tu<sup>2</sup>, A. Savoy<sup>1</sup>, J. Domsic<sup>1</sup>, D. Silverman<sup>1,2</sup>, M. Agbandje-McKenna<sup>1</sup>, R. McKenna<sup>1</sup>, Dept. of Biochemistry<sup>1</sup>, and Dept. of Pharmacology and Physiology<sup>2</sup>, College of Medicine, Univ. of Florida, Gainesville, FL 32608 USA.

The conserved residue, Glu 106, of Carbonic Anhydrase II (CAII) has been implied to play an important role in the proton shuttling capacity of the active site. Three mutants, E106H, E106S, and E106D, have been investigated structurally and kinetically. The conservative mutation, E106D, maintained wild-type activity, while E106H and E106S demonstrated increasingly impaired function. Crystallographic studies indicate positional variation and the addition of water molecules, as well as revealing new and interesting information regarding the conformation of His 64, the primary proton shuttling residue. These results, taken in combination, show an insightful picture into the active site dynamics of hCA2.

**MP106**

**Determination of Hydrogen Positions in Prehnite Using Powder Neutron Diffraction.** T. A. Detrie<sup>1</sup>, N. L. Ross<sup>1</sup>, M. D. Welch<sup>2</sup>, R. J. Angel<sup>1</sup>, <sup>1</sup>Dept. of Geosciences, Virginia Tech, Blacksburg, VA 24061, <sup>2</sup>Mineralogy, The Natural History Museum, Cromwell Rd., London, SW7 5BD, UK.

Neutron diffraction has become a well-established technique for structural studies of earth materials, especially for the determination of atomic positions of hydrogen in minerals, because the presence of heavier atoms has often been thought to preclude the location of H by X-ray single-crystal diffraction. Many previous neutron diffraction studies on minerals used deuterated samples to aid in the identification of the location of the hydrogen atoms. However, in many minerals, the exchange rate of hydrogen/deuterium (H/D) is unknown and there is a risk that incomplete exchange may result in nearly contrast-matched H:D (2:1) values, making H(D) invisible to neutrons.

In this study, powder neutron diffraction data were collected on a natural sample of prehnite,  $\text{Ca}_2\text{Al}(\text{AlSi}_3\text{O}_{10})(\text{OH})_2$ , at room temperature using the neutron time-of-flight diffractometer POLARIS at the ISIS facility, Rutherford-Appleton Laboratory, U.K. Structure refinement was performed by the Rietveld method.

Single-crystal X-ray diffraction data were collected on a single crystal of prehnite at room conditions with an Oxford Diffraction Xcalibur diffractometer with  $\text{MoK}\alpha$  radiation. Data were refined using Shelxl and the hydrogen atoms were located in difference Fourier maps. The results of the X-ray and neutron refinements were in good agreement, including the location of the hydrogen atom, confirming that hydrogen can be located in minerals by X-ray diffraction and by neutron diffraction of undeuterated samples.

**TP107**

**CORELLI: A Novel Instrument for Efficient Single Crystal Diffraction with Elastic Discrimination.** Stephan Rosenkranz, Raymond Osborn, Materials Science Div., Argonne National Laboratory, Argonne, IL 60439 USA.

Many emerging phenomena of high technological and scientific interest are governed by complex disorder and nanoscale self-organization e.g. in the form of stripes, phase separation, or dimerization, which result from the competition between interactions with incompatible order. Examples include high

temperature superconductivity, colossal magnetoresistance, relaxor ferroelectricity, and negative thermal expansion. Single crystal diffuse neutron scattering provides a very powerful probe of such disorder in crystalline materials on the 1-10nm length scale. Accurate modeling of such structures requires measurements over a large volume of reciprocal space with sufficient energy resolution to separate quasi-static diffuse scattering from vibrational and other inelastic scattering. This capability will be provided by CORELLI, a novel diffraction instrument, which utilizes the cross correlation method to obtain efficient elastic discrimination. We will discuss the new capabilities and opportunities this instrument will provide for determining complex disorder and short range correlations.

Work supported by US DOE BES-DMS DE-AC02-06CH11357

**SP108**

**Crystal Structure of the Isolated IQGAP1 GAP-related Domain.** V.B. Kurella<sup>1</sup>, C. Bryan<sup>1</sup>, J. Ricks<sup>1</sup>, H. Bellamy<sup>2</sup>, D.K. Worthylake<sup>1</sup>, <sup>1</sup>Dept. of Biochemistry and Molecular Biology, LSU Health Sciences Center, New Orleans, LA, <sup>2</sup>Center for Advanced Microstructures and Devices, LSU, Baton Rouge, LA.

IQGAP is a 190 kD molecular scaffold that contains several domains required for interaction with numerous proteins. One of these domains is homologous to the Ras GTPase-activating protein (GAP) domains of p120RasGAP and neurofibromin. However, instead of binding to active Ras and accelerating hydrolysis of bound GTP, the IQGAP1 GAP-related domain (GRD) binds to active forms of Cdc42 and Rac1 and *preserves* their GTP-bound states. We report here the crystal structure of the isolated IQGAP1 GRD. Despite quite low sequence conservation, the overall structure of the GRD is very similar to the structures of the RasGAP and neurofibromin, but there are significant differences. Instead of a catalytic "arginine finger" seen in RasGAP and neurofibromin, the GRD possesses a conserved threonine. Threonine 1046 resides in an  $\alpha$ -helical secondary structure element whereas in RasGAP and neurofibromin, the catalytic arginine is within a more flexible loop region. In addition, residues 1099 – 1129 of IQGAP1 have no structural equivalent in RasGAP, and are seen to form an extension at one end of the GRD. Since the sequence of residues 1099-1129 is conserved between IQGAP1 homologs, this region may confer a functionality particular to IQGAP-family GRDs. Assuming a similar mode of interaction as seen in the Ras-RasGAP (transition state) complex, we have created an energy-minimized model of Cdc42-GTP bound to the GRD. The model indicates that steric clash between threonine 1046 with the phosphate-binding loop and other subtle changes mediated by IQGAP1 residues effectively disrupt the proper geometry required for GTP hydrolysis.

**TP109**

**The Crystal Structures of *Enterococcus* Aminoglycoside (2'') Phosphotransferase variants Ib and Ic, Enzymes Implicated in Antibiotic Resistance.** Clyde Smith<sup>1</sup>, Paul Young<sup>2</sup>, Laura Byrnes<sup>1</sup>, Ted Baker<sup>2</sup>, <sup>1</sup>SSRL, Stanford, CA, <sup>2</sup>School of Biological Sciences, Univ. of Auckland, New Zealand.

The emergence of bacteria resistant to important classes of antibiotics has become a major clinical problem over the last few years, and now almost all antibacterial compounds in use today have associated examples of resistant bacterial isolates. In the United States, *Enterococci* are among one of the most common resistant bacteria isolated in nosocomial infections. The synergistic use of ampicillin or vancomycin with an aminoglycoside (kanamycin or gentamicin), has long been the optimal therapy for enterococcal infections, but many previously susceptible strains have since

acquired resistance to the aminoglycosides. Resistance arises by gene transfer from other bacteria, these genes coding for enzymes that deactivate the antibiotics by chemically altering specific groups on the drug. We have determined the structures of two aminoglycoside phosphotransferases, APH(2'')-Ib and APH(2'')-Ic.

We have crystallized APH (2'')-Ib as the gentamicin complex, the AMP complex and a ternary AMPPNP/streptomycin complex. The APH(2'')-Ic enzyme, although related to the Ib enzyme, has a 400-fold preference for GTP over ATP, and we have solved the structure of the GDP complex of the enzyme. The APH(2'') enzymes have a two-domain fold very similar to the protein kinases. Gentamicin binds in a cleft in the C-domain between a conserved central core and a variable helical subdomain. Streptomycin (an inhibitor) also binds in the same site but in a conformation which precludes phosphorylation. Comparison of the gentamicin and streptomycin complexes shows how the enzyme is able to distinguish between the 4,6-disubstituted aminoglycosides (substrates) and the 4,5-disubstituted molecules (inhibitors).

### MP110

**Magnetic Structural Changes of Cobalt Oxide under High Pressure.** A.M. dos Santos, C.A. Tulk, J.J. Molaison, B.C. Chakoumakos, Neutron Scattering Science Div., Oak Ridge National Laboratory, Oak Ridge TN 37831.

Cobalt monoxide orders antiferromagnetically at 290K with a tetragonal distortion. More interestingly, the magnetic spin is not oriented along the tetragonal unique axis, but at an angle of about 27° (and at 8° from the (111) plane) corresponding approximately to the [113] direction<sup>1</sup>. This exceptional occurrence is likely due to a competition of effects between the Jahn-Teller distortions of the high spin d<sup>7</sup> ion with the spin orbit coupling resulting from its unquenched angular momentum. While some explanations were suggested for such a unique feature such as multiple k-vector<sup>1</sup> – later disproved<sup>2</sup> –, asymmetric cation-cation superexchange<sup>3</sup>, and non collinear alignment of the spin and orbital angular momentum<sup>4</sup>, experimental evidence for the cause is still lacking.

The effect of pressure on the transition temperature of cobalt monoxide was investigated *in-situ* through neutron diffraction. Pressure was applied by a Paris-Edinburgh cell specially designed for this type of experiment. The presented work allowed not only the pressure calibration of the high pressure setup but to monitor the increase of the Néel temperature with pressure to 8 GPa, as well as carefully investigate the evolution of the magnetic structure with pressure, and therefore shed some light on the origin of the unusual magnetic structure of this compound.

Research sponsored by the LDRD Program of Oak Ridge N. Lab., managed by UT-Battelle, LLC for the U.S. Dept. of Energy under Contract No. DE-AC05-00OR22725.

<sup>1</sup>Van Laar B., Phys. Rev. 138, A854 (1965)

<sup>2</sup>Herrmann Ronzaud D., Burlet P., Rossatmignod J., J. Phys. C – Solid State 11, 2123 (1978)

<sup>3</sup>Yamada T., Nakanish O., J. Phys. Soc. Japan 36, 1304 (1974)

<sup>4</sup>Hope D.A.O., Cheetham A.K., J. Solid State Chem. 72, 42 (1988)

### SP111

**Crystal Structure of Conserved Domains of *Streptococcus mutans* Adhesion Protein Antigen I/II Reveals a Polyproline-type II Helix Interacting with an Extended  $\alpha$ -helix.** Matt Larson<sup>1</sup>, Kanagalghatta Rajashankar<sup>2</sup>, Lawrence Delucas<sup>3</sup>, Suzanne Michalek<sup>4</sup>, Jeannine Brady<sup>5</sup>, Champion Deivanayagam<sup>3</sup>, <sup>1</sup>Dept. of Physiology and Biophysics, <sup>3</sup>Dept. of Vision Sciences, <sup>4</sup>Dept. of Microbiology, Univ. of Alabama, Birmingham AL 35294, <sup>5</sup>Dept.

of Oral Biology, Univ. of Florida, Gainesville, FL 32610, <sup>2</sup>NE-CAT Advanced Photon Source, Argonne National Lab, Argonne, IL.

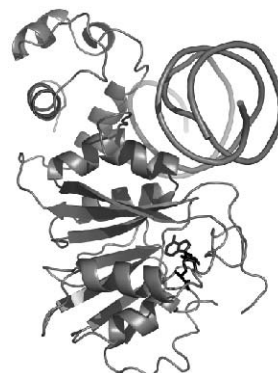
A fragment of *Streptococcus mutans* (*S. mutans*) Antigen I/II containing the third alanine-rich repeat, the variable region, and the first proline-rich repeat (A3VP1) was crystallized and the structure solved. The protein crystals grown belong to the P2<sub>1</sub> spacegroup with a cell dimensions of a = 60.719, b = 153.057, c = 49.675 Å, and  $\alpha = 90$ ,  $\beta = 89.97$ , and  $\gamma = 90$  degrees. A complete dataset was collected with 1.8 Å resolution and solved using molecular replacement. The protein structure reveals the association of the proline-rich domain forming an unusually long single polyproline type II helix wrapped with the alanine-rich domain as an extended  $\alpha$ -helix. The interaction between the extended  $\alpha$ -helix and the polyproline helix is primarily mediated through hydrophobic interactions. Isothermal titration calorimetric studies on the nature of the interaction between the alanine-rich domain and the proline-rich domains showed both high binding affinity and high enthalpy changes, and indicated the formation of a stable 1:1 complex. Circular dichroism(CD) spectroscopy studies using several domain truncations of Antigen I/II were used to compare the secondary structure in solution versus the crystal structure. Protein binding studies implicate the polyproline-helix in binding to the human tooth surface receptor Salivary Agglutinin Glycoprotein (SAG) via interactions with scavenger receptor domains. These results support a role in the initial pathogenesis of bacterial tooth adhesion involving the novel extended conformational region of the Antigen I/II protein of *S. mutans*.

### TP112

**Crystal Structure of an RNA Methyltransferase in Complex with RNA and S-adenosylhomocystine.** C. Tu, J.E. Tropea, B.P. Austin, D.S. Waugh, D.L. Court, X. Ji, Center for Cancer Research, National Cancer Inst., National Institutes of Health, Frederick, MD 21702 USA.

KsgA is a universally conserved rRNA methyltransferase, of which orthologs have been found in all species, from bacteria to humans. Mutations in *ksgA*, which result in the loss of dimethylation at A1518 and adjacent A1519 in 16S ribosomal RNA, are the most common mode of resistance to the antibiotic kasugamycin (Ksg) in *E. coli* and other bacteria. The crystal structure of apo-KsgA from *E. coli* was reported by O'Farrell *et al.* (PDB code: 1QYR). Here we present the crystal structure of KsgA from a hyperthermophilic bacterium, in its ligand-free form and in complex with RNA with and without bound cofactor S-adenosylhomocystine (SAH). The overall scaffold of apo-KsgA resembles its ortholog in *E. coli*. Our structures show significant conformational changes of the protein upon ligand binding. Most of the highly conserved residues in KsgA are involved in the binding of either the RNA or SAH. The unique C-terminal domain of KsgA is also functionally important. A catalytic mechanism for this ancient enzyme is proposed that is in agreement with available biochemical data. The structure of the ternary complex also provides a framework for the design of novel antibiotics against the Erm family of RNA methyltransferases, which share a similar protein fold and SAH binding pocket with KsgA.

X-ray diffraction data were collected at the 22-ID beamline of SER-CAT, Advanced Photon Source, Argonne National Laboratory. This research was supported by the Intramural Research Program of the NIH, National Cancer Institute, Center for Cancer Research.



**MP113**

**Time-of-Flight Neutron Crystallography at the Protein Crystallography Station at Los Alamos National Laboratory.** S.Z. Fisher, A.Y. Kovalevsky, M. Mustyakimov, M.J. Waltman, B.P. Schoenborn, P. Langan, Bioscience Div. B-8, Los Alamos National Laboratory, Los Alamos, NM 87545.

The PCS (Protein Crystallography Station) at Los Alamos Neutron Science Center (LANSCE) is a unique facility in the USA that is designed and optimized for detecting and collecting neutron diffraction data from macromolecular crystals. PCS utilizes the spallation neutron source at LANSCE to enable time-of-flight measurements. This increases the neutron flux on the sample by using a wavelength range (0.6 to 7 Å) that is optimal for studying macromolecular crystal structures. These features combine to make measurements of smaller crystals (<1 mm<sup>3</sup>) possible as well as cut down on data collection time. The main advantage of using neutrons versus X-rays for structure determination, is that neutrons are scattered equally well from hydrogen as the other more electron-rich atoms. Often the most important features of enzyme catalysis involves proton or hydrogen transfer and even medium-resolution neutron data can be used to observe these fine details. Recent projects and studies conducted at PCS include initial diffraction and/or neutron structure determinations of diisopropyl fluorophosphatase (DFPase), endothiasepsin, haemoglobin, and rubredoxin. The current status and progress of these projects will be discussed, as well as anticipated experiments for the upcoming run cycle.

**TP114**

**MacCHESS Initiatives: Serving Structural Biology, Preparing for an ERL.** D. Szebenyi, R. Cerione, M. Cook, U. Englich, R. Gillilan, S. Gruner, Q. Hao, X. Hong, I. Kriksunov, Q. Liu, W. Miller, D. Schuller, S. Smith, MacCHESS, Cornell Univ., Ithaca, NY 14853.

MacCHESS ("Macromolecular diffraction at CHESS") is an NIH/NCRR funded facility at the Cornell High Energy Synchrotron Source; our research initiatives seek to benefit users of both current storage ring X-ray sources and future Energy Recovery Linacs (ERLs). Projects include:

**Microcrystallography** – X-ray microfocus capillaries, precision crystal-positioning devices, excellent crystal viewing optics, and helium-based background reduction allow users to collect data from ever-smaller crystals, or to locate well-diffracting regions of larger imperfect crystals. A recent experiment used an array of small crystals, recording a few Laue images from each and merging them to create a complete dataset.

**Pressure cryocooling** - A new method for cryocooling crystals under pressure reduces both cooling-induced degradation and the need for penetrating cryoprotectants, and can stabilize mobile ligands. We offer pressure-cooling as a service to CHESS users, while continuing to develop the method. Related work seeks to improve crystal quality using novel protocols for temperature control.

**SAXS and low resolution phasing** - Small angle X-ray scattering at CHESS is under active development; the data are used to (1) follow large-scale conformational changes and (2) to determine a molecular envelope as a starting point in phasing.

**Soft X-ray beamline** - Custom multilayer optics give a bending magnet station a flux comparable to that of the wiggler stations; the target 6-10 KeV energy range is suitable for SAD experiments on many metalloproteins.

**Other R&D** includes automatic sample handling and crystal centering,

novel detectors (some customized for microcrystallography), and continued upgrades to station equipment.

**SP115**

**The Crystal Structure of TTHA0415, a Putative ACP Reductase from *Thermus thermophilus* at 1.9Å Resolution.** J.T. Swindell<sup>1</sup>, L. Chen<sup>1</sup>, A. Ebihara<sup>2</sup>, A. Shinkai<sup>2</sup>, S. Kuramitsu<sup>2</sup>, S. Yokoyama<sup>2</sup>, Z.-Q. Fu<sup>1,3</sup>, J. Chrzas<sup>1,3</sup>, J.P. Rose<sup>1,3</sup>, B.C. Wang<sup>1,3</sup>. <sup>1</sup>Southeast Collaboratory for Structural Genomics, Dept. of Biochemistry and Molecular Biology, <sup>2</sup>Southeast Regional Collaborative Access Team, Univ. of Georgia, Athens, GA, USA, <sup>3</sup>RIKEN Structural Genomics/Proteomics Initiative (RSGI), Yokohama, Japan.

Open-reading frame 415 in the genome of the hyperthermophile *Thermus thermophilus* (TTHA0415) encodes a 245-residue protein whose sequence suggests it may be an 3-oxoacyl-[acyl-carrier protein] (ACP) reductase. The protein was cloned, expressed and crystallized by the RIKEN Structural Genomics/Proteomics group, when a homologous structure was not known. In collaboration with the Southeast Collaboratory for Structural Genomics (SECSG), data to 1.7Å resolution were collected on the Southeast Regional Collaborative Access Team (SER-CAT) bending magnet beamline 22BM at the Advanced Photon Source, Argonne National Laboratory. The structure was solved by the automated molecular replacement module of SGXPro using a SECSG structure of a putative ACP reductase from *Clostridium thermocellum* (2HQ1) as a search model. The structure has been refined to 1.9Å resolution with an R value of 19.1% and Rfree of 22.9%. Details of the structure and a comparison with other ACP reductases will be presented.

Work was supported in part with funds from the NIH (GM62407).

**TP116**

**A Key Metabolic Enzyme as an Attractive Target for Antibiotic Development.** Ronald E. Viola, Xuying Liu, Alexander Pavlovsky, Chris Faehnle, Dept. of Chemistry, Univ. of Toledo, Toledo, OH 43606 USA.

The biosynthetic pathway derived from aspartate is unique to plants and microorganisms, producing four of the amino acids required for protein synthesis. In addition, metabolites produced by this pathway are involved in general methylation reactions, bacterial cell-wall cross-linking, sporulation and quorum sensing. This pathway presents several potential targets for antibiotic development, since disruption will have devastating consequences for the survival of a microorganism. We have determined structures of a key enzyme in this pathway, ASA dehydrogenase, from several Gram-negative and Gram-positive infectious organisms, including structures of enzyme-substrate, enzyme-inhibitor, enzyme-intermediate, and mutant enzyme complexes. These structures support a common catalytic mechanism despite a wide range of sequence homologies between various species; however, differences in the mode of coenzyme binding and intersubunit communication provide attractive targets for the design and potential development of selective lead compounds for new antibiotics.

**MP117**

**Development of a Compact Crystal Positioning System for the TOPAZ Single Crystal Diffractometer at the Spallation Neutron Source.** M.J. Frost, C. Hoffmann, Oak Ridge National Laboratory, Oak Ridge, TN. M. Austin, P. Carmen, E. Miller, L. Mosier, R. Viola, Square One Systems Design, Jackson, WY.

A precise, versatile, and automated method of orienting a sub-millimeter crystal in a focused neutron beam is required for efficient operation of the TOPAZ Single Crystal Diffractometer at the Spallation Neutron Source at Oak Ridge National Laboratory. To fulfill this need, a Compact Crystal Positioning System (CCPS) is under development in collaboration with Square One Systems Design in Jackson, Wyoming. Versatility is achieved using a design that incorporates six linear axes and one rotational axis of motion in a tripod, while maintaining precision by using piezo-electric motors with a high spatial resolution. The motions of the linear actuators are combined to mimic a two-axis goniometer. The final system will have these attributes and be vacuum/cryogenically compatible. NI LabVIEW provides a means of system automation while at the same time accommodating the modular nature of the SNS sample environment control software for straightforward system integration.

This research is supported by DOE Small Business Research Initiative grant number DE-FG02-05ER84257 and by UT Battelle, LLC under Contract No. DE-AC05-00OR22725 for the U.S. Department of Energy, Office of Science.

**TP118**

**An Open And Flexible Robotic System Designed Towards Autonomous Protein Crystal Harvesting.** Robert Viola<sup>1</sup>, Peter Carmen<sup>1</sup>, Jace Walsh<sup>1</sup>, Echo Miller<sup>1</sup>, Mark Balas<sup>3</sup>, Cameron Wright<sup>3</sup>, John O'Brien, Bernhard Rupp<sup>2,3</sup>, <sup>1</sup>Square One Systems Design, Jackson, WY 83002, <sup>2</sup>q.e.d. life science discoveries, Livermore, CA 94551, <sup>3</sup>Univ. of Wyoming, Laramie, WY 82071.

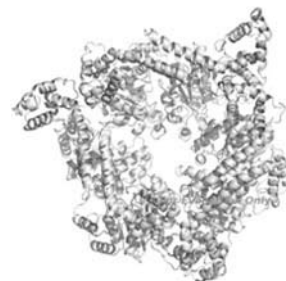
Recent advances in micromanipulation robotics and micro-fabrication have made it possible to seriously consider automation of protein crystal harvesting. Based on the experience gained during the development of an operator-assisted (and now operator-assisting) universal micromanipulation robot (UMR) prototype, we discuss the progress and challenges ahead for the design of a fully autonomous, integrated system capable of the reliable harvesting of protein microcrystals. Harvesting of micron-sized objects requires a sophisticated mechanical system, and autonomy means that a capable real-time machine vision system embedded in powerful control software must be developed. The vision system and the mechanical system interact and feedback in a complex way, and the demands on the optical system pose additional and formidable design challenges. Real time image processing interfaced with mechanical control and feedback are at the cutting edge of technology, and the conceptual design of autonomous systems represents a research frontier in mechatronics. We expect that the current operator-assisting UMR will systematically evolve into a system endowed with progressively increasing autonomy. While one cannot demand that an autonomous system will be capable of addressing *all and every* possible harvesting situations, it will handle the majority of cases while significantly increasing the reliability of protein micro-crystal harvesting and the reproducibility of cryo-cooling. In addition, advanced micromanipulation robotics will likely open the field to new science and emerging crystallization technologies of potentially far reaching impact.

Work sponsored by NIH STTR Phase II Grant No. 2 R42 GM073278-02A1.

**SP119**

**The Structure of a DnaB-Family Replicative Helicase and its Interactions with Primase.** Ganggang Wang<sup>1</sup>, Michael G. Klein<sup>1</sup>, Etienne Tokonzaba, Yi Zhang, Lauren G. Holden, Xiaojiang S. Chen, Molecular and Computational Biology, Univ. of Southern California, CA 90089, USA. <sup>1</sup>These authors contributed to the work equally.

Helicases are essential enzymes for DNA replication, a fundamental process in all living organisms. The DnaB family are hexameric replicative helicases that unwind duplex-DNA and coordinate with RNA primase and other proteins at the replication fork in prokaryotes. Here, we report the full-length crystal structure of G40P, a DnaB family helicase. The hexamer complex reveals a unique architectural feature and a novel assembly mechanism. The hexamer has two-tiers: a 3-fold symmetric N-terminal tier and a 6-fold symmetric C-terminal tier. Monomers with two different conformations, termed cis and trans, come together to provide a topological solution for the unusual dual symmetry within a hexamer. Structure-guided mutational studies suggest an important role for the N-terminal tier in binding primase and regulating primase-mediated stimulation of helicase activity. This study provides insights into the structural and functional interplay between G40P helicase and DnaG primase.



We thank the staff at LBL's ALS BL8.2.1, BL8.2.2, BL4.2.2 and APS 19id in Argonne National Laboratory for assistance in data collection.

**TP120**

**Structure of the Catalytic Trimer of *Methanococcus jannaschii* Aspartate Transcarbamoylase in an Orthorhombic Crystal Form.** Jacqueline Vitali<sup>1</sup>, Michael J. Colaneri<sup>2</sup>, <sup>1</sup>Dept. of Physics, Cleveland State Univ., Cleveland, OH 44115, <sup>2</sup>Dept. of Chemistry and Physics, SUNY College, Old Westbury, NY 11568.

The catalytic trimer of *Methanococcus jannaschii* aspartate transcarbamoylase is extremely heat stable, maintaining 75% of its activity after heat treatment for 60 min at 75° C. This paper reports the structural analysis of an orthorhombic form of the enzyme containing four crystallographically independent trimers in the asymmetric unit. Data for two crystals were measured at beamline X12B of the NSLS at BNL and were merged and scaled with the HKL software package to give a complete data set (99.5%) at 3.0 Å resolution with  $R_{\text{sym}} = 0.095$ . The space group is P212121 and the cell constants are  $a = 87.13$ ,  $b = 167.93$  and  $c = 319.41$  Å. The structure was solved with EPIC and refined with CNS to  $R = 0.215$  and  $R_{\text{free}} = 0.269$  (10% of data). In this structure the catalytic subunits associate in pairs to form two similar staggered complexes, each with an inter-trimer distance of 33.8 Å. This quaternary arrangement of trimers is similar to that previously observed in a monoclinic form of the enzyme. Each trimer has a sulfate at the center of its three CP domains in the central channel. These sulfates probably came from the crystallization medium. Other structural elements potentially contributing to the thermostability include: (i) changes in the amino acid composition such as a decrease in the thermolabile residues Gln and Asn, an increase in the charged residues Lys and Glu, an increase in Tyr and a decrease in Ala residues; (ii) shortening of the N-terminus and shortening of three loops; (iii) a larger number of salt bridges, in particular, the improvement of ion-pair networks.

**MP121**

**TOPAZ, the Next Generation of Single-Crystal Neutron Diffraction at the Spallation Neutron Source.** C. Hoffmann, M.J. Frost, J. Thomison, L. Davis, M. Overbay, Oak Ridge National Laboratory, Oak Ridge, TN.

Single crystal neutron diffraction in structure analysis allows for high resolving power of light elements in close proximity to heavy elements, unlike more traditional X-Ray crystallography. However, neutron diffraction has as of late been a very time consuming process. By using the high-power Spallation Neutron Source at Oak Ridge National Laboratory and a highly efficient beam transport system, TOPAZ will be able to accommodate sub-millimeter sized crystals such as those used in X-Ray Crystallography. In addition, the large detector area will allow for fewer crystal positions per sample, thus reducing the overall time for each experiment. The wavelength range will be 0.5-4.0 Å and accommodate unit cells in the range of ~50Å with moderate complexity. Various sample environments will be available including cryogenic cooling, heating, and magnetic fields. The magnetic field environment coupled with the planned polarized neutron option will allow for future experiments investigating magnetic structure transitions in materials. TOPAZ will be commissioned in Spring 2009 and begin participation in the user program by Fall 2009.

This research is supported by UT Battelle, LLC under Contract No. DE-AC05-00OR22725 for the U.S. Department of Energy, Office of Science.

**TP122**

**Probing the Molecular Interface of Cellulose and Lignin in Biomass.** Barbara R. Evans<sup>1</sup>, Hugh M. O'Neill<sup>1,2</sup>, Volker Urban<sup>1,2</sup>, Dean A. Myles<sup>1,2</sup>, <sup>1</sup>Chemical Sciences Div., Oak Ridge National Laboratory, Oak Ridge, TN, <sup>2</sup>Center for Structural Molecular Biology, Oak Ridge National Laboratory.

Lignocellulosic biomass offers an abundant renewable feedstock for conversion to fuels, but its recalcitrance to deconstruction and hydrolysis requires the use of costly, energy-intensive pretreatments. New fundamental understanding of biomass structure and aggregation at the molecular level is required to improve pretreatment and conversion methods. Neutron scattering and diffraction could provide this molecular-scale structural information. We conducted a D<sub>2</sub>O exchange, neutron contrast variation study with small-angle neutron scattering (SANS) on purified samples of the biomass components cellulose and lignin. The calculated and observed D/H match points were determined, and these data were then used to understand the SANS patterns obtained from pretreated biomass that contains cellulose and lignin. The experiments detected the nanometer-scale characteristics of conformation and aggregation of the component polymers revealing molecular structural differences between two types of purified lignin, and between microcrystalline cellulose and steam-exploded wood.

This research was funded by the LDRD Seed Money Program of Oak Ridge Natl. Lab., managed and operated by UT-Battelle, LLC for the U. S. Department of Energy under contract No. DE-AC05-00OR22725. The submitted manuscript has been authored by a contractor of the U.S. Government under Contract DE-AC05-00OR22725. Accordingly, the U.S. Government retains a nonexclusive royalty-free license to publish or reproduce the published form of this contribution, or allow others to do so, for U.S. Government purposes.

**SP123**

**Structural Characterization of a Novel Redox-Sensitive Transcriptional Regulator Involved in *Pyrococcus furiosus* Sulfur Response.** H. Yang<sup>1,2</sup>, G. Lipscomb<sup>1</sup>, B.C. Wang, R.A. Scott, Dept. of Biochemistry and Molecular Biology, Univ. of Georgia,

Athens, GA 30602 USA. <sup>1</sup>These authors contributed equally to this work. <sup>2</sup>Current Address: MVVB, ID, NCIRD, CCID, CDC, Atlanta, GA 30333 USA.

The archaeal basal transcription apparatus is eukaryotic in nature while transcriptional regulation appears to occur primarily through bacteria-like mechanisms; however, only a small number of archaeal transcriptional regulators have been characterized in detail. This work describes the structural characterization of the novel transcriptional regulator SurR of the hyperthermophilic archaeon *Pyrococcus furiosus* and the discovery of its redox-sensitive switch. SurR was found to both activate and repress the transcription of genes involved in the primary response of *P. furiosus* to elemental sulfur (S<sup>0</sup>), and SurR was determined to have binding sites upstream of almost all genes which were both up- and down-regulated only 10 min after S<sup>0</sup> addition to a growing culture according to DNA microarray expression profiling experiments. The crystal structure of SurR revealed the presence of a disulfide bond at the CxxC motif in the N-terminal winged helix-turn-helix (HTH) DNA binding domain. This motif was found to act as a redox switch sensitive to colloidal sulfur, such that oxidation of SurR abolishes its sequence-specific DNA binding affinity. The crystal structure of a mutant protein in which both cysteine residues of the CxxC motif were replaced with alanine indicated that the CxxC switch controls the DNA binding affinity of SurR by modulating the conformation of the HTH DNA-binding domain. This novel transcriptional regulator, termed SurR for sulfur response regulator, is likely a relevant participant in transcriptional regulation pathways related to *P. furiosus* S<sup>0</sup> metabolism, exerting transcriptional control in the reduced state and releasing from its cognate DNA when becoming oxidized in the presence of S<sup>0</sup>.

PDB IDs: 2QLZ, 2QUF

We thank SER-CAT at APS for data collection. This work was supported by National Institutes of Health grant GM42025 and National Science Foundation grant MCB 96-31093 to R.A.S.

**TP124**

**Structural Basis for Substrate Recognition by Executioner Caspases.** I.T. Weber<sup>1,2</sup>, B. Fang<sup>1</sup>, J. Agniswamy<sup>1</sup>, A.A. Chumanevich<sup>1</sup>, R.W. Harrison<sup>3,1</sup>, <sup>1</sup>Biology Dept., <sup>2</sup>Chemistry Dept., and <sup>3</sup>Computer Science Dept., Molecular Basis of Disease Program, Georgia State Univ., Atlanta, GA 30303, USA.

The executioner caspases play an important role in inducing apoptosis, and are targets for pharmacological modulation of cell death in diverse diseases. Decreased cell death is desirable for treatment of stroke, nerve crush injury, myocardial infarction, neuromuscular and neurodegenerative diseases, while activation of cell death would be advantageous in cancer therapy. Caspases cleave many known and unknown cellular proteins in pathways leading to cell death. Caspase-3 and 7 show a preference for hydrolyzing the peptide bond after the sequence motif DEVD in studies on short peptides. However, many protein substrates of caspases are cleaved at non-canonical sites relative to the reported recognition motifs. Therefore, the structural basis for recognition of different peptide sequences has been examined for caspase-3 and -7. Crystallographic analysis revealed that caspases can bind tetrapeptides (P1-P4) of non-optimal sequences with favorable interactions within the S1-S4 protein subsites (1). Strongly inhibiting peptide aldehydes bound caspase-7 with little structural variation. In contrast, complexes with weaker inhibitors showed larger conformational variation and adaptation of the peptide side chains and the caspase residues, especially in S2 and S4. A new S5 subsite was identified in caspase-3 that bound hydrophobic P5 in pentapeptides, unlike most tested caspases (2). Moreover, a novel peptide binding site was observed on the surface

of caspase-7, which may have a role in regulation of activity. These results should be considered in the design of selective small molecule inhibitors.

1. Agniswamy et al. (2007) FEBS J. 274:4752-4765.
2. Fang et al. (2006) J. Mol. Biol. 360:654-666.

### MP125

**IMAGINE – Neutron Laue Diffractometer at the High Flux Isotope Reactor (HFIR).** Flora Meilleur<sup>1,3</sup>, Dean Myles<sup>2</sup>, Bryan Chakoumakos<sup>3</sup>, Christina Hoffmann<sup>3</sup>, Chris Tulk<sup>3</sup>, Leighton Coates<sup>3</sup>, <sup>1</sup>Dept. of Biochemistry, North Carolina State Univ., Raleigh, NC, <sup>2</sup>Center for Structural Molecular Biology, ORNL, Oak Ridge, TN, <sup>3</sup>Neutron Scattering Science Div., ORNL, Oak Ridge, TN.

The time required to collect neutron diffraction data from small or weakly scattering samples is often prohibitive on conventional monochromatic diffractometers. The need to improve and accelerate the data collection rates for such work inspired development in the early 1990's of a novel neutron Laue Diffractometer (LADI) instrument at the ILL. Essential differences in the design of LADI compared to conventional diffractometers included (1) the use of a Quasi-Laue diffraction geometry, and (2) the use of a large cylindrical neutron image-plate detector. This combination provides a ten-fold to hundred-fold gain in efficiency over conventional monochromatic neutron diffractometers.

We propose to construct and operate a neutron image-plate single crystal diffractometer at the HFIR which will provide atomic resolution information on chemical, organic, metallo-organic and protein single crystals. The instrument will benefit communities with interest in pharmaceuticals, minerals and other inorganic crystals, small molecules, molecular organo-metallic crystals and metal-organic frameworks molecular crystal structures, and will enable the neutron crystal structure of some smaller proteins to be determined at or near atomic resolutions (1.5 Å).

We will give an overview of the IMAGINE project at the HFIR. The instrument capabilities will be illustrated with recent data collected from protein crystals on the Laue diffractometer at the ILL.

Oak Ridge National Laboratory is managed by UT-Battelle, LLC, for the U.S. Department of Energy under Contract DE-AC05-00OR22725.

### SP126

**X-ray Crystallographic Studies of Pig Sarcosine Dehydrogenase.** Wei Yong, Ila Misra, Jung-Ja P. Kim, Medical College of Wisconsin, WI 53222.

Sarcosine dehydrogenase (SDH) is a monomeric, mitochondrial matrix protein (MW ~100 KD) containing a covalently bound FAD. SDH catalyzes the oxidative demethylation of sarcosine (N-methylglycine) to glycine. The oxidized methyl group is then transferred to tetrahydrofolate forming 5, 10-methylenetetrahydrofolate. The electron transfer flavoprotein (ETF) links sarcosine oxidation to the main mitochondrial electron transport system. The deficiency of SDH in humans is genetically transmitted and is the cause of an amino acid metabolism disorder called sarcosinemia. The crystal structure of pig sarcosine dehydrogenase has been determined to 2.5 Å resolution. SDH structure has two domains, FAD binding domain and tetrahydrofolate binding domain. The two active sites, the sarcosine binding site and the tetrahydrofolate binding site in SDH are ~40 Å apart, connected by an irregular channel. Detailed analysis of the structure and its relationship to its function will be discussed.

This work was funded by NIH GM-29076 (JJK). Data were collected at SBC-CAT beam-line 19-ID at Advanced Photon Source, Argonne National Labs, IL.

### TP127

**Analyzing *B. stearotherophilus* Tryptophanyl-tRNA Synthetase (TrpRS) Catalytic Activity using Multiple Mutant Cycles.** Violetta Weinreb, Li Li, Charles W. Carter, Jr., Dept of Biochem. Biophys., CB 7260, UNC Chapel Hill, Chapel Hill, NC.

*B. stearotherophilus* TrpRS structures provide the most complete structural characterization of conformational changes related to catalysis by an aminoacyl-tRNA synthetase. The <sub>192</sub>KMSKS<sub>196</sub> motif and the opposing loop containing K111 bind exclusively to the triphosphate and are the two most mobile elements in the catalytic cycle. Lysine residues K192 and K111 make key interactions to the PP<sub>i</sub> leaving group via two of the three phosphate oxygen atoms that bind to the catalytic Mg<sup>2+</sup> ion. Molecular Dynamics simulations suggest that these interactions activate the Mg<sup>2+</sup> ion by weakening its interactions, which we have shown to. The catalytic contribution of Mg<sup>2+</sup> accelerates amino acid activation by 10<sup>5</sup>, and is coupled by the lysine interactions to an endergonic twist of the anticodon-binding domain relative to the active site. To clarify these sources of TrpRS catalytic activity, we investigated lysine-metal interactions quantitatively, determining effects of lysine to alanine and lysine to glutamine mutants in multi-variant thermodynamic cycles with Mn<sup>2+</sup> for Mg<sup>2+</sup> substitution by [ATP]-dependent Michaelis-Menten kinetics. K111 and K192 are strongly coupled to the metal. Interaction of both Lysine residues with the pyrophosphate leaving group in the transition state suggests a catalytic contribution from the untwisting domain movement. Coupling was also observed for a remote mutation, F37I, which affects both k<sub>cat</sub> and the use of Mn<sup>2+</sup>. These interactions are consistent with effective strain on the scissile Pα-O-Pβ linkage, arising from an unfavorable conformation necessary to assemble the active site around ATP that is resolved by (exergonic) untwisting during the catalytic step. Supported by NIGMS.

### MP128

**A High Pressure Diffractometer at the Spallation Neutron Source.** J.J. Molaison, C.A. Tulk, A.F. Moreira dos Santos, G.E. Ice, Oak Ridge National Laboratory, Oak Ridge, TN 37831 USA.

The Spallation Neutrons And Pressure (SNAP) diffractometer, a high flux, medium resolution instrument, will be used to study a variety of powdered and single-crystal samples under extreme pressure and temperature. The increased neutron flux coupled with large volume pressure cells using large synthetic single-crystal opposed anvils significantly extends the pressure range currently accessible with the technique of neutron diffraction. The goal is to routinely achieve pressures of 50 to 100 GPa for an ~1-mm<sup>3</sup> sample. In addition, recent advances in next generation detectors will allow the incident beam-focusing optics, pressure chamber, and detector array to be highly integrated, providing a flexible facility for materials studies under extreme conditions.

G. E. Ice's research is supported in part by the DOE Division of Materials Sciences and Engineering. Oak Ridge National Laboratory is managed by UT-Battelle, LLC under DOE contract DE-AC05-00OR22725.

### SP129

**The Tale of a Four-electron Oxidoreductase.** Chandra J. Duncan<sup>1</sup>, C. Nicklaus Steussy<sup>1</sup>, Tim Schmidt<sup>1</sup>, Louise V. Wrensford<sup>2</sup>, Victor W. Rodwell<sup>2</sup>, John W. Burgner II<sup>1</sup>, Cynthia V. Stauffacher<sup>3</sup>, <sup>1</sup>Dept. of Biological Sciences, Purdue Univ., West Lafayette IN 47907, <sup>2</sup>Dept. of Chemistry, Albany State Univ., Albany GA 31705, <sup>3</sup>Dept. of Biochemistry, Purdue Univ., West Lafayette IN 47907, <sup>4</sup>Dept. of Biological Sciences & Purdue Cancer Center, Purdue Univ., West Lafayette IN 47907.

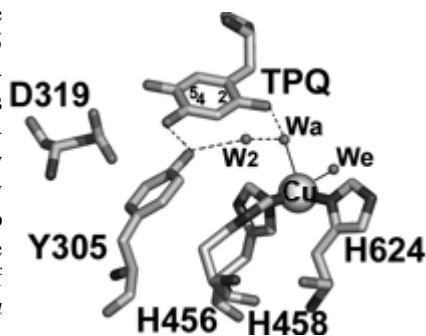
HMG-CoA reductase is a critical enzyme in isoprenoid biosynthesis and a drug target both for the control of cholesterol in humans and for antibiotics targeted at gram-positive pathogens. This enzyme has an interesting reaction mechanism, as it catalyzes two reactions to convert HMG-CoA to mevalonate using two successive hydride transfers from NADH without release of an intermediate species. In different stages of the reaction, a C-terminal three-helix flap domain repetitively opens and closes, bringing critical residues into the active site. We now have analyzed more than a dozen high resolution static structures with various ligands, slow substrates and products in both productive and non-productive complexes. Productive complexes have demonstrated that the reaction can run in the crystal, so we have also begun time resolved Laue experiments to follow the mechanism directly. The static structures have produced snapshots along the reaction pathway that show large changes in domain orientation as well as detailed changes in active site residues and substrate conformation that tie together structural information with biochemical results. With these results we can create both a movie and story about how the enzyme, substrates, and cofactors work together to catalyze this four-electron reduction reaction.

### TP130

**X-ray Crystal Structures of N-semiquinone and Iminoquinone Forms of *Hansenula polymorpha* Copper Amine Oxidase.** C.M. Wilmot\*, B.J. Johnson\*, P. Cedervall\*, B.R. Goblirsch\*, J.P. Klinman#, Univ. of Minnesota, Minneapolis, MN 55455, and Univ. of California, Berkeley, CA 94720.

At their active sites copper amine oxidases (CAOs) contain both a mononuclear copper ion as well as a protein derived quinone cofactor, 2,4,5-trihydroxyphenylalanine quinone (TPQ). Catalytic activation of molecular oxygen in CAOs has been proposed to involve either a Cu(II)-aminoquinol intermediate or a Cu(I)-N-semiquinone intermediate. These forms exist in equilibrium in the reduced enzyme.

Methylamine reduction of *Hansenula polymorpha* CAO crystals at different pHs in a low O<sub>2</sub> environment has enabled three distinct forms of the enzyme to be freeze-trapped for x-ray structure determination at 1.7 - 2.15 Å resolution. The identities of the species present in each crystal were confirmed by single crystal UV/visible microspectrophotometry. Methylamine reduction at acidic or neutral pHs revealed protonated and deprotonated forms of the oxidized iminoquinone that are accompanied by a bound dioxygen species. However, methylamine reduction at pH 8.5 has revealed a copper-ligated cofactor that is proposed to be the N-semiquinone observed by microspectrophotometry in this crystal, leading to novel implications for the catalytic mechanism of *Hansenula polymorpha* CAO.



H. polymorpha CAO active site

This work was funded by NIH GM-66569 (CMW) and GM-25765 (JPK). BJJ was supported by NIH Training Grant GM-008700. Data were collected at SBC-CAT beam-line 19-ID at the Advanced Photon Source, Argonne National Labs, IL.

### MP131

**The Effect of Homopolymer on the Morphology and Domain Size of Diblock Copolymer/Nanoparticle Complexes in a Selective Solvent.** Vilas G. Pol,<sup>†,\*</sup> Chieh-Tsung Lo,<sup>‡</sup> Byeongdu Lee,<sup>‡</sup> R.E. Winans,<sup>‡</sup> P. Thiyagarajan<sup>†</sup>, <sup>†</sup>Intense Pulsed Neutron Source and <sup>‡</sup>X-ray Science Div., Argonne National Laboratory, Argonne, IL 60439.

Solvent selectivity is an important parameter that determines the phase behavior of block copolymer solutions and hence its role has to be considered in solution-based synthetic routes for tailoring morphologies of nanocomposites. We carried out small angle neutron scattering (SANS) studies on the phase behavior of complexes of poly(styrene-*b*-2-vinylpyridine) (PS-PVP) with PS homopolymers (2-15k) and thiol-terminated polystyrene (PS) stabilized Au nanoparticles [ANPs] or their mixture with different PS content in toluene-*d* [selective solvent] as a function of homopolymer concentration and temperature. In the bulk PS-PVP/ANPs/PS homopolymer composite, PS homopolymer was used to increase the conformational entropy and swell the preferred domains to enable the ANPs to redistribute uniformly, causes the phase transformation. In comparison between PS homopolymer and ANPs, ANPs also reduce the degree of segregation of the system and induce the order-disorder transition that is not seen in PS-PVP/ PS homopolymer complex in the selective solvent within the temperature of our study. The domain spacing of PS-PVP/ANPs/ PS homopolymer complex in a selective solvent shows a strong function of PS homopolymer concentration and temperature. The decrease of domain spacing with increasing temperature is attributed to the increase in compatibility between two microdomains, which allows the lateral expansion at the interface and hence reduces the expansion perpendicular to the interface. The increase in the domain spacing with the addition of PS homopolymer shows fairly linear relationship that is different from scaling behavior of the PS-PVP/ANPs complex with the addition of ANPs or a solvent.

Work benefited from the support by the U.S. Department of Energy, Office of Science, Office of Basic Energy Sciences, under contract DE-AC02-06CH11357.

### SP132

**Optimization of Inhibitors of the Human Cytoplasmic Protein Tyrosine Phosphatase.** Kristoff T. Homan<sup>1</sup>, Deepa Balasubramaniam<sup>1</sup>, Olaf Wiest<sup>2</sup>, Paul Helquist<sup>2</sup>, Cynthia V. Stauffacher<sup>1</sup>, <sup>1</sup>Dept. of Biological Sciences, Purdue Univ., West Lafayette, IN 47907, <sup>2</sup>Dept. of Chemistry and Biochemistry, Univ. of Notre Dame, Notre Dame, IN 46556.

Inhibition of the human cytoplasmic protein tyrosine phosphatase (HCPTP) provides a mechanism to down regulate the metastatic phenotype present in human epithelial tumors caused by the removal of phosphorylation of the EphA2 receptor tyrosine kinase. Inhibitors for each isoform of HCPTP have been identified by *in silico* screening of small molecule libraries as well as through rational design. *In vitro* kinetic analysis has verified the discovery of low micro-molar inhibitors of HCPTP, which are the most potent inhibitors of HCPTP reported to date. Common structural elements have been identified among these computationally identified inhibitors that agree with rationally designed elements. Co-crystallization of inhibitor-enzyme complexes is now proceeding in order to gain detailed structural information of inhibitor binding which is necessary to guide future inhibitor optimization. A higher resolution (1.29 Å) structure of HCPTP-B has been solved in a new crystallographic packing arrangement. Even though no inhibitor is present bound to HCPTP-B, there are several structural changes which impact the conformational space available to inhibitors. Additional studies include the enzymatic analysis of mutants of both isoforms of

HCPTP, further kinetic studies at multiple pHs, and well as the development of an assay using a different substrate in order to better describe the activity and specificity of this enzyme. Each of these studies will direct inhibitor development as well as elucidate the future of isoform-specific inhibitors of HCPTP.

### TP133

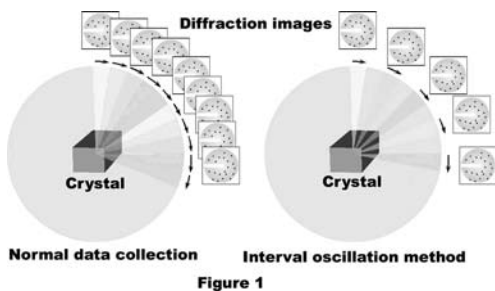
**Evaluation of a Novel Rotation Method to Suppress Absolute Radiation Damage to Protein Crystals.** Kunio Hirata<sup>1</sup>, Go Ueno<sup>1</sup>, Kazuya Hasegawa<sup>2</sup>, Tetsuya Shimizu<sup>1</sup>, Takashi Kumazaka<sup>1,2</sup>, Masaki Yamamoto<sup>1</sup>, <sup>1</sup>RIKEN SPring-8 Center, Harima Inst., <sup>2</sup>JASRI/SPring-8.

The novel data collection method which can reduce absolute exposure time to crystal will be introduced. The method named as 'interval oscillation method' represents oscillation data collection by skipping every other diffraction image (Figure 1). Reflection intensities to be appeared in the skipped ranges are estimated from partially observed reflections on its neighbor frames [1,2] according to Equation 1.

$I_{\text{estimate}}(h) = I_{\text{obs}}(h) / P_{\text{calc}}(h)$  (Equation 1)  $h$ : reflection index,  $I$ : reflected intensity,  $P$ : reflection partiality

The method enables us to reduce absolute X-ray exposure time to a sample crystal down to 1/2 or more less compared to the normal rotation method.

In this method, precision of estimated partiality of each reflection dominate results of crystal structure analysis. Making the best of collected diffraction frames from wider oscillation ranges, approximate crystal orientation can be determined. According to the orientation matrix, penetration length of each reflection onto Ewald



A basic concept of the 'interval oscillation method'

collected in the normal procedure and made virtual ones without even-numbered frames. The virtual datasets were processed with this method using MOSFLM suite. The results will be discussed via both MR and SAD phasing.

Some applications of the method especially for protein micro crystallography will be also introduced.

- [1] R. Bolotovskiy et al, *J. Appl. Cryst.* (1998). 31, 708-717  
[2] K. Hirata et al, *J. Synchrotron Rad.* 11 (60-63), 2004

### MP134

**Neutron Diffraction of Polydysprosium Models of Polygadolinium Complexes with High *In Vitro* MRI Relaxivities.** Dale C. Swenson<sup>1</sup>, Paula M. B. Piccoli<sup>2</sup>, Chang-Tong Yang<sup>1</sup>, Arthur J. Schultz<sup>2</sup>, Louis Messerle<sup>2</sup>. <sup>1</sup>Dept. of Chemistry, Univ. of Iowa, Iowa City IA 52242, <sup>2</sup>Intense Pulsed Neutron Source, Argonne National Laboratory, Argonne IL 60439.

We have discovered a new class of amino-acid-chelated polygadolinium complexes with very high MRI (magnetic resonance imaging) relaxivities. Relaxivity in MRI contrast agents

has a sixth-order dependence on Gd<sup>3+</sup>-H distance, among other physicochemical parameters. Since Gd has a high neutron absorption cross-section, we have studied polydysprosium analogs in order to measure the Dy<sup>3+</sup>-H distances to  $\mu_3$ -OH and inner sphere water ligands. We report here results of neutron diffraction single crystal experiments using the IPNS SCD at Argonne National Laboratory to obtain data from the perchlorate salts of three model complexes: [Dy<sub>2</sub>(ala)<sub>4</sub>(OH)<sub>8</sub>]<sup>6+</sup>, [Dy<sub>2</sub>(val)<sub>4</sub>(OH)<sub>8</sub>]<sup>6+</sup>, and [Dy<sub>4</sub>( $\mu_3$ -OH)<sub>4</sub>(val)<sub>6</sub>(OH)<sub>6</sub>(ClO<sub>4</sub>)<sub>4</sub>]<sup>6+</sup>. The data from Dy<sub>2</sub>(val)<sub>4</sub> and Dy<sub>4</sub>( $\mu_3$ -OH)<sub>4</sub>(val)<sub>6</sub> were of insufficient quality to perform neutron-only refinement, so a joint X-ray-neutron refinement was done using the GSAS program (Larson and Von Dreele, 2000). Data from the Dy<sub>2</sub>(ala)<sub>4</sub> sample allowed a neutron-only refinement. All hydrogen atoms were located in difference Fourier maps. Those of highest import were refined with anisotropic displacement parameters. Some valine and alanine C-H distances were restrained in the refinements. H-bond geometries are reported. The Dy<sup>3+</sup>-H distances to inner sphere waters range from 2.81 to 3.11 Å. The Dy<sup>3+</sup>-H distances for the  $\mu_3$ -OH ligands range from 2.73 to 3.01 Å. Comparisons to other X-ray and neutron diffraction studies on mononuclear lanthanide aquo-complexes will be given.

Work at ANL was supported by the U.S. DOE BES, under contract DE-AC02-06CH11357. Work at UI was supported by DOD's CDMRP under contract W81XWH-06-1-0155.

Larson, A.C.; Von Dreele, R.B. *General Structure Analysis System--GSAS*, Los Alamos National Laboratory, 2000.

### SP135

**The Molecular Basis of MAP Kinase Regulation by HePTP.** D.A. Critton<sup>§</sup>, B.L. Brown<sup>‡</sup>, A. Tortajada<sup>§</sup>, R. Page<sup>§</sup>, <sup>§</sup>Dept. of Molecular Biology, Cell Biology and Biochemistry, Brown Univ., Providence, RI 02912. <sup>‡</sup>Dept. of Molecular Pharmacology, Physiology and Biotechnology, Brown Univ., Providence, RI 02912.

Disruptions in the tight regulation of T cell activation and differentiation are correlated with numerous immunological cancers including acute leukemia. The increasing prevalence of these cancers is associated with increased exposure to oxidative environmental toxins, which can target and inhibit cysteine-based tyrosine phosphatases (CBTPs). Immunological cancers are also associated with constitutive activation of tyrosine kinases, especially the extracellular signal-regulated kinases (Erk). Hematopoietic tyrosine phosphatase (HePTP) is a non-receptor CBTP that regulates the activities of the MAP kinases Erk and p38, both by protein targeting and by active dephosphorylation. HePTP and its MAP kinase substrates engage in a unique, *reciprocal* interaction, with HePTP dephosphorylating Erk and p38 at their activation loops, and with Erk and p38 phosphorylating HePTP at two distinct sites. In order to investigate these processes at atomic detail, we have produced an HePTP: Erk2-specific 'toolkit,' including 1. HePTP substrate trapping mutants (STMs) whose activities are severely compromised yet are still able to bind target substrates; 2. functional mutants that reflect distinct biological states of the HePTP:Erk2 complex; and 3. efficient methods for activating Erk2 to study the different HePTP: Erk2 complexes, i.e. the active dephosphorylation complex. Using this new biological toolkit together with x-ray crystallography, we are characterizing the multiple transient conformations of the HePTP: Erk2 interaction that drive T cell activation at atomic detail.



This work was supported through funding to RP from NIH-5P20RR016457-07 and an ACS Research Scholar Grant.

**TP136**

**An Automated Pipeline for Doing Molecular Replacement Including Search Model Discovery And Preparation.** Ronan Keegan, Martyn Winn, Peter Briggs, Wanjuan Yang, CCP4, STFC Daresbury Laboratory, Warrington, UK.

MrBUMP (Molecular replacement with Bulk Model Preparation) is a new automated molecular replacement program from CCP4. With a little input from a user in the form of a structure factor file (MTZ file) and a sequence file it is designed to source a large number of appropriate search models by using various on-line resources, prepare the search models for molecular replacement and carry out molecular replacement for each of the search models against the target data. It is very much a brute-force approach to the problem and is useful in difficult cases when it may produce a solution given by an efficacious combination of model and preparation method that would be missed otherwise. In more easily solved cases the benefit is simply that of convenience. MrBUMP is an automation framework built upon many of the tried and trusted structure solution programs from the CCP4 suite. The program is also designed to make use of computational cluster resources in order to speed up its processing. It is included in CCP4 6.1, the latest release of the popular protein crystallography software suite.

**MP137**

**New Opportunities for Simple Access to Automated Crystal Handling at the NSLS.** Alexei S. Soares, Mary Carlucci-Dayton, Howard Robinson, Robert Sweet, Dieter Schneider, Biology Dept., Brookhaven National Lab, Upton, NY.

Synchrotron users increasingly employ crystal handling automation to augment the flexibility and speed of their work. To support these efforts, the Protein Crystallography Research Resource (PxRR) initiated programs to provide needed equipment and training both onsite and remotely. Here we describe these access modes in detail, along with complimentary training material and an opportunity for hands-on familiarization and demonstration of all necessary parts and tools.

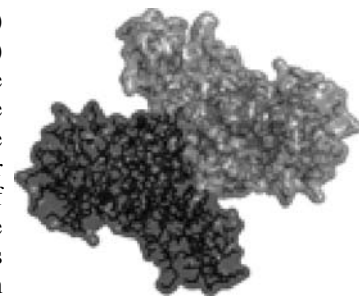
The PxRR automation program deploys cryogenic robotic specimen mounting systems based on the hybrid pneumatic/stepper motor system developed at the Lawrence Berkeley National Laboratory (LBNL). This design was selected for its minimal footprint, inherent safety, and reliable random access to a large selection of specimens. An overview of the mechanical and software capabilities is presented, along with a summary of reliability and usage statistics.

**SP138**

**The Role of the Dimeric Interface in the Catalytic Mechanism of Human Manganese Superoxide Dismutase.** John F. Domsic<sup>1</sup>, Jiayin Zheng<sup>2</sup>, Patrick S. Quint<sup>1</sup>, Diane E. Cabelli<sup>3</sup>, David N. Silverman<sup>2</sup>, Robert McKenna<sup>1</sup>, <sup>1</sup>Dept. of Biochemistry and Molecular Biology and <sup>2</sup>Dept. of Pharmacology and Therapeutics, Univ. of Florida, Gainesville, FL 32610; <sup>3</sup>Dept. of Chemistry, Brookhaven National Laboratory, Upton, NY 11973.

Manganese superoxide dismutases (MnSODs) are enzymes that occur ubiquitously in nature and share high sequence homology between organisms. These enzymes catalyze the disproportionation of superoxide in a two step mechanism. The result is a reduction and subsequent oxidation of the active site manganese, and the formation of molecular oxygen and hydrogen peroxide. During the second step, a product-inhibited state may form in which a superoxo-complex forms with the manganese. This product inhibition occurs

in both the dimeric (prokaryotic) and the tetrameric (eukaryotic) MnSODs. Kinetically, the eukaryotic MnSODs are the more product-inhibited of the two forms. To gain a better understanding of the basis of differential product inhibition we examined two sets of mutations at the dimeric interface of human MnSOD (hMnSOD) via x-ray

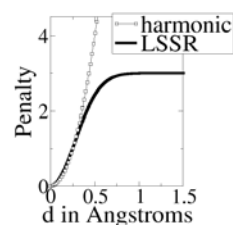


crystallography and kinetic analysis. The first mutation was at Glu162, a residue which acts as a second shell ligand of the neighboring monomer's manganese. Mutation to alanine or aspartate resulted in a great reduction of catalysis that was caused by a decrease in the stability (E162D) or complete loss (E162A) of the second shell ligand interaction with the manganese. The second mutation examined the role Phe66 which is involved in a dimeric interaction near the active site rim. Phe66 interacts with the adjacent monomer's Gln119 in hMnSOD, and this interaction is flip-flopped in the eukaryotic SODs. Mutation to alanine or leucine results in an enzyme that has an overall decrease in activity. Interestingly, however, the F66L enzyme shows an overall decrease in the level of product inhibition. This is explained due to a relaxation of the active site environment which prevents a build-up of the product-inhibited state.

**TP139**

**Refinement with Local Structure Similarity Restraints (LSSR) Enables Exploitation of Information from Related Structures and Facilitates use of NCS.** O.S. Smart, M. Brandl, C. Flensburg, P. Keller, W. Paciorek, C. Vornrhein, T.O. Womack, G. Bricogne, Global Phasing Ltd., Sheraton House, Cambridge CB3 0AX, UK.

We have developed a novel restraint procedure that can be used in maximum-likelihood refinement to exploit information that the structure under consideration is similar to another. This similarity can be to an already solved structure, the "target". For instance a high-resolution apo structure can be used as a target when refining a lower-resolution ligand-soak structure. Alternatively the similarity could be between two or more chains within the structure being refined and thus can enforce NCS. The restraint is defined by considering the distance  $r_{AB}$  between pairs of atoms  $A, B$  within the chain to be restrained. All pairs of atoms that are not bonded and have  $r_{AB} < 5.5 \text{ \AA}$



are considered. Structural similarity implies that the distance  $r'_{AB}$  between the corresponding atoms in the other chain or target structure will in general be close to  $r_{AB}$ . LSSR imposes for each atom pair a penalty on the difference in distances  $d = r_{AB} - r'_{AB}$ . For targeting to an external structure,  $r'_{AB}$  remains constant in the refinement, whereas for NCS it will vary.

The LSSR functional form is not harmonic but instead plateaus as  $d$  gets large, thus automatically allowing differences to be accommodated if the X-ray data so demand. Because LSSR are local, there is no need to separate out domains. These features make it easy to use compared to conventional harmonic superposition-based NCS treatments which often require elaborate segmentations. BUSTER refinement with LSSR results in lower  $R_{\text{free}}$  and an improved  $R_{\text{work}} - R_{\text{free}}$  gap. The method is particularly applicable to the refinement of protein-ligand complexes.

**MP140****SAXSess – An Analytical Tool for Nanostructured Biomaterials.**

P. Kotnik<sup>1</sup>, H. Schnablegger<sup>1</sup>, O. Glatter<sup>2</sup>, Ch. Moitzi<sup>2</sup>, <sup>1</sup>Anton Paar GmbH, A-8054 Graz, Austria; <sup>2</sup>Univ. of Graz, Graz, Austria.

Small-angle X-ray scattering (SAXS) is a well-established method for structural investigations in the size regime between 1 and 100 nm.



With the new laboratory instrument, SAXSess, structural information can be acquired, such as (1) size distribution, (2) particle shape and internal structure, (3) surface-to-volume ratio and (4) degree of crystallinity.

One unique feature of the SAXSess system is its ability to simultaneously and continuously measure from small to wide-angles (of up to 40°) without changing the instrumental set-up. Therefore the nanostructure and the phase state of a sample can be analysed in a single run.

Thus, a huge variety of applications are addressed in quality control and research. The most prominent systems and application fields are

Nanoparticles: proteins, viruses, drug-delivery systems, paints, micelles, vesicles

Biomaterials: collagene, keratine, wood, cellulose, biomineralization products (bones, sea shells, etc.)

Polymers: block copolymers, semi-crystalline polymers

Drug Delivery: characteri-zation of nano-devices (micelles and vesicles),

Screening of storage conditions: determination of the porosity and the degree of crystallinity,

Stability of dispersions: particle sizing of colloidal dispersions.

In this presentation we will show a few examples of the above mentioned application areas.

**SP141**

**Crystal Structure of *Streptococcus pneumoniae* Nicotinamidase with Bound Inhibitor Provides Insight into Mechanism of Catalysis.** Jarrod B. French<sup>1,3</sup>, Anthony A. Sauve<sup>2,3</sup>, Steven E. Ealick<sup>1,3</sup>, <sup>1</sup>Dept. of Chemistry and Chemical Biology, Cornell Univ., Ithaca, NY, <sup>2</sup>Pharmacology Dept., Weill Medical College of Cornell Univ., New York, NY, <sup>3</sup>Tri-Institutional Training Program in Chemical Biology.

The conversion of nicotinamide to nicotinic acid is an important step in the NAD<sup>+</sup> recycling pathway in micro-organisms. This conversion is catalyzed by a class of enzymes called nicotinamidases, which have been determined to be essential for the viability of many parasitic microbes. These enzymes are absent in mammals however, making them a potential target for a novel class of antibiotics. In addition, nicotinamidases have been shown to regulate Sirtuins, a family of enzymes that are purported to play a role in lifespan extension.

With the goal of better understanding the mechanism of catalysis of this enzyme, we have determined the X-ray crystal structure of the *Streptococcus pneumoniae* nicotinamidase unliganded and in complex with the inhibitors nicotinaldehyde and 5-methoxy-nicotinaldehyde. The geometry of the inhibitors and the bond distances in the active site suggest that a covalent intermediate forms between the ligand and the catalytic cysteine. Our structures also reveal that the active site contains a metal ion with octahedral geometry. In addition to contacts with the enzyme, the metal co-ordinates the pyridyl nitrogen of the ligand and to a water molecule, or with two water

molecules in the absence of ligand. We suspect that the metal ion serves to both orient the substrate and to activate the water molecule for nucleophilic attack.

The nicotinamidase structures that we present here allow us to describe a likely mechanism of catalysis for this enzyme.

**TP142**

**CCP4 Diffraction Image C++ Library.** Francois Remacle, Graeme Winter, STFC Daresbury Laboratory, Keckwick Lane, Warrington, WA4 4AD, Cheshire, UK.

This C++ library, dealing with X-ray diffraction images of protein crystal was originally part of XIA, a data reduction automation project. Since it appeared that it could be useful to have it as a separate entity, it was decided to include this library with the other CCP4 core libraries and therefore make it available publicly with CCP4 version 6.1. The purpose of the library is to have a single way of handling diffraction image whatever detector it comes from. Currently it can support several detector formats (MAR, ADSC, RIGAKU, BRUKER, OXFORD-DIFFRACTION, CBF).

In addition to providing access to standard header information, it contains also operations or calculations that can be performed on the image raw data or on peaks found in the image. The latest operation being developed is an automatic method to calculate a mask for the backstop area and the arm of the backstop (if any).

In addition to C++, this library has interface to make it usable from Python, Tcl-Tk and Java (as a JNI interface) to be as flexible for developers who would like to use its functionalities.

**MP143**

**Small-Angle Neutron Scattering of Microemulsion Systems Containing pH-Degradable Surfactants for Protein Encapsulation and Drug Delivery.** D.G. Hayes, J.A. Gomez del Rio, V.S. Urban, J.S. Lin, Dept. of Biosystems Engineering, Univ. of Tennessee, Knoxville, TN 37996 USA.

Microemulsion systems are potentially useful in biotechnology as hosts for multiphasic biocatalysis, membrane mimics, drug delivery vehicles, and for extraction-based protein purification. A major problem with their utility for these applications is the difficult recovery of microemulsion-encapsulated biomolecules. Our group has addressed this problem by employing pH-degradable cyclic ketal, or 1,3-dioxolane, alkyl ethoxylate surfactants synthesized in the laboratory. These surfactants must be accompanied by an additional surfactant to form suitable microemulsion systems.

This poster will provide an overview of our research on the application of these microemulsion systems for protein extraction-based purification and drug delivery, and describe the use of SANS to characterize the microemulsion phases formed in the absence and presence of by the cyclic ketal surfactant. Bicontinuous microemulsion phases undergo structural changes upon encapsulation of proteins.

**SP144**

**A Study of Protocatechuate 3,4-Dioxygenase Mutants and Substrate Interactions.** Rebecca D. Hoeft, Ke Shi, Zu-Yi Gu, Jeff Digre, C. Kent Brown, Cathleen A. Earhart, Douglas H. Ohlendorf, Biochemistry, Molecular Biology and Biophysics, Univ. of Minnesota, Minneapolis, MN.

Protocatechuate 3,4-dioxygenase is a nonheme, iron containing enzyme that catalyzes the intradiol oxidative cleavage of 3,4-dihydroxybenzoic acid to  $\beta$ -carboxy-*cis,cis*-muconic acid via

incorporation of molecular oxygen into the aromatic ring of the substrate. In an attempt to further understand the factors involved in substrate turnover and mechanism, a series of second sphere residue mutants has been created and structurally and kinetically examined. These crystals diffract to high resolution and show clearly that alterations of these second sphere residues can dramatically affect the interactions with substrate and substrate analogs. A detailed structural and kinetic comparison of these mutants will be presented.

#### TP145

**Automated Crystallographic Structure Refinement in PHENIX.** Pavel V. Afonine, Ralf W. Grosse-Kunstleve, Peter H. Zwart, Nigel W. Moriarty, Paul D. Adams, Lawrence Berkeley National Lab, Berkeley, CA 94720 USA.

Crystallographic structure refinement is a vital step in improving and completing initial atomic models for further analysis. New or improved crystallographic algorithms, implemented using highly efficient programming tools, can provide a very high level of automation and robustness during structure refinement. *phenix.refine* is a general purpose state of the art refinement module of PHENIX project<sup>1,2</sup>. Recent developments include specialized tools for the refinement of macromolecules at subatomic resolutions ( $< 0.9\text{\AA}$ ) where the bonding electron density becomes visible and must be accounted for in the model<sup>3</sup>. Key features of *phenix.refine* include:

Automatic handling of most data formats;

Individual coordinates refinement using minimization or simulated annealing;

Highly optimized and automated rigid body refinement;

Atomic displacement parameter (ADP) refinement: individual isotropic or anisotropic, grouped, TLS or any mixture;

Occupancy refinement (grouped, individual, constrained for alternative conformations);

Automatic NCS detection and use in refinement as restraints;

Automatic twinning detection and use in refinement;

Various refinement targets (maximum-likelihood, maximum-likelihood with experimental phase information, and amplitude least-squares);

Robust mask-based bulk-solvent correction and anisotropic scaling;

$\sigma_A$ -weighted map output;

Refinement using X-ray data, neutron data or joint refinement with both;

Refinement at ultra-high resolution using an Inter Atomic Scattering model.

One of distinct features of *phenix.refine* is that any number and combination of the strategies listed above can be applied to any selected part of a model and performed in one refinement run.

Program availability: [www.phenix-online.org](http://www.phenix-online.org).

1. Adams PD, Gopal K, Grosse-Kunstleve RW, Hung L-W, Ioerger TR, McCoy AJ, Moriarty NW, Pai RK, Read RJ, Romo TD, Sacchettini JC, Sauter NK, Storoni LC, Terwilliger TC. *J. Synchrotron Rad.* (2004), 11:53-55.

2. Afonine PV, Grosse-Kunstleve RW & Adams PD. CCP4 newsletter, July 2005; 8.

3. Afonine PV, Grosse-Kunstleve RW, Adams PD, Lunin VY & Urzhumtsev A. *Acta Cryst.* (2007). D63, 1194-1197.

#### MP146

**Reconstruction of Molecular Envelopes by SAXS has Implications for Molecular Modeling of APOBEC3G and the APOBEC-1 Complementation Factor (ACF).** Jason D. Salter<sup>1</sup>, Jolanta Krucinska<sup>1</sup>, Ryan P. Bennett<sup>1</sup>, Chad A. Galloway<sup>1</sup>,

Richard E. Gillilan<sup>2</sup>, Harold C. Smith<sup>1</sup>, Joseph E. Wedekind<sup>1</sup>, <sup>1</sup>Dept. of Biochemistry and Biophysics, Univ. of Rochester School of Medicine and Dentistry, Rochester, NY 14642, <sup>2</sup>Macromolecular Structure Facility at the Cornell High Energy Synchrotron Source, Cornell Univ., Ithaca, NY 14853.

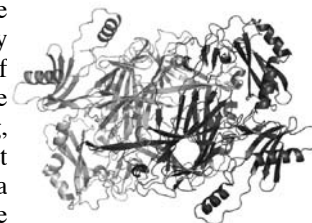
Apobec3G (A3G) is a cellular cytidine deaminase with antiretroviral activity that protects CD4<sup>+</sup> T-cells from HIV-1 infection by deaminating deoxycytidine to deoxyuridine on single-stranded viral DNA during reverse transcription. However, the HIV-1 viral infectivity factor (vif) protein is capable of directly binding and targeting A3G for polyubiquitination and proteasomal degradation leaving CD4<sup>+</sup> T-cells vulnerable to HIV infection. High and low resolution molecular models of A3G may facilitate design of anti-retroviral therapeutics. Here SAXS was used to reconstruct the molecular envelopes of A3G prepared in both dimeric and monomeric forms. Unexpectedly, the catalytically active A3G dimer has an elongated shape ( $D_{\text{max}} = 140\text{\AA}$ ,  $R_G = 46\text{\AA}$ ), with an apparently small dimeric interface. Here, the A3G molecular envelopes will be compared spatially to crystallographic models of both free cytidine deaminases and APOBEC2, a related member of the APOBEC family, to assess their potential for modeling A3G.

ACF is an RNA binding protein comprising three RRM that together with APOBEC-1 form a core editosome responsible for deaminating cytidine to uridine at position 6666 of ApoB mRNA, thereby controlling production of full length versus truncated ApoB protein, which is important for fatty acid metabolism. Here, we present the restored molecular envelope of the N-terminal RRM of ACF as well as a comparison to other RRM-containing proteins.

#### SP147

**Structural Insights into Substrate Specificity in Copper Amine Oxidases from *Hansenula polymorpha*.** V.J. Klema\*, C.M. Chang<sup>#</sup>, B.J. Johnson\*, M. Mure<sup>#</sup>, J.P. Klinman<sup>#</sup>, C.M. Wilmot\*, \*Univ. of Minnesota, Minneapolis, MN 55455, <sup>#</sup>Univ. of California, Berkeley, CA 94720.

Copper amine oxidases (CAOs) catalyze the oxidative deamination of primary amines to their corresponding aldehydes. As well as a copper ion, these ubiquitous enzymes utilize the novel organic cofactor 2,4,5-trihydroxyphenylalanine quinone (TPQ), which is formed by post-translational modification of an active site tyrosine residue. The reaction mechanism is ping-pong, in which the formation of product aldehyde leaves the enzyme in a two electron reduced state. The reoxidation requires molecular oxygen, which is reduced to hydrogen peroxide to regenerate the resting enzyme. Ammonia is also released during this half of the cycle.



Previously a CAO from the yeast *Hansenula polymorpha* had been characterized, whose preferred substrates were small aliphatic primary amines (HPAO-1). A second CAO has now been identified from the same organism (HPAO-2), with a 34% sequence identity to HPAO-1. We have shown that HPAO-2 has a substrate preference for aromatic amines. A 2.0 $\text{\AA}$  resolution crystal structure of HPAO-2 refined to  $R(\text{cryst}) = 0.160$ ,  $R(\text{free}) = 0.203$ , and a FOM of 0.971 provides structural insight into the kinetic and substrate differences between these two yeast CAOs.

This work was funded by NIH GM-66569 (CMW) and GM-25765 (JPK). Data were collected at SBC-CAT beam-line 19-ID at the APS, Argonne National Labs, IL.

## TP148

**PrimeX: An Integrated Protein Crystal Structure Refinement Package with Powerful Real-Space Tools For Automation.**

Jeffrey A. Bell, Schrödinger, 120 West Forty-Fifth St., 29<sup>th</sup> Floor, Tower 45, New York, NY 10036 USA.

PrimeX provides an integrated graphical and computational environment for the complete refinement of molecular replacement structures. The full-featured graphics program, Maestro, has been augmented with the structure manipulation tools required by protein crystallographers. The Maestro Project Table provides a summary of refinement progress. Protein geometry and fit to density are assessed in Maestro to aid in finding model errors. All major computational functions can be accessed through an easy-to-use graphical interface as well as through the command line.

Reciprocal-space refinement extends well-validated maximum likelihood methods with the use of the all-atom force field OPLS-AA. The more accurate all-atom view of chemical structure is advantageous for geometric restraint, as well as for analysis and validation. The result is a high-quality model that is accurate and well-suited for use in computational chemistry operations such as library screening. Simulated annealing refinement extends the radius of convergence of reciprocal-space minimization.

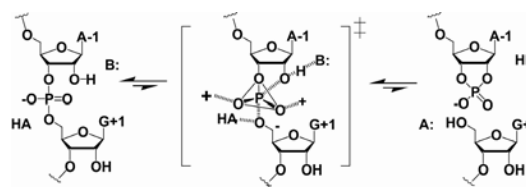
Real-space building of segments of polypeptide into electron density provides a very powerful tool for model correction, combined with a separate tool specifically for side chain fitting. Ligand placement into electron density also provides a measure of protein-ligand chemical complementarity.

The combination of the protein analysis tools with real- and reciprocal-space methods in PrimeX provides the basis for powerful automation of protein crystal structure refinement. Such automation can be especially useful in an industrial environment that requires the refinement of large numbers of molecular replacement solutions.

## SP149

**Trapping a Pre-Ligation Hairpin Ribozyme Complex by Use of 5'-Deoxy-5'-Fluoro-Guanosine.** Robert C. Spitale<sup>2</sup>, Joseph E. Wedekind<sup>1,2</sup>, <sup>1</sup>Dept. of Biochemistry & Biophysics, Univ. of Rochester School of Medicine & Dentistry, Rochester, NY, <sup>2</sup>Dept. of Chemistry, Biological Chemistry Cluster, Univ. of Rochester, Rochester, NY 14642, joseph.wedekind@rochester.edu.

Ribozymes process genetic transcripts in all three kingdoms of life. Yet despite the essentiality of these macromolecular machines, little is known about the chemical principles they employ to accomplish their respective biological reactions. The hairpin ribozyme is a small RNA motif that catalyzes reversible phosphodiester bond cleavage between residues A-1 and G+1 of its cognate substrate (Scheme 1). Several investigations have suggested this reaction proceeds by nucleobase-assisted general acid/base chemistry. However, the recent discovery of ordered water molecules in the hairpin ribozyme active site demonstrated how solvent molecules could: (i) provide electrostatic stabilization of the transition state, and (ii) contribute to specific acid/base chemistry. Such results mandated new efforts to provide a more comprehensive description of the hairpin ribozyme reaction coordinate (Scheme 1). The equilibrium of this reaction favors ligation over cleavage, and no high-resolution, homogeneous complexes exist for the pre-ligation state. As such, we undertook the design and synthesis of 5'-Deoxy-5'-Fluoro-Guanosine (5FG), an inert isostere of guanosine. Incorporation of fluorine at the 5'-position of G+1 should allow trapping of the 2',3'-cyclic phosphate, thereby producing a pre-ligation mimic. This structure should lead to a better understanding of the catalytic



**Scheme 1:** The Hairpin Ribozyme Reaction

strategies utilized by ribozymes for rate acceleration. Progress on the incorporation of 5FG into RNA, kinetic characterization of this complex, and elucidation of the crystal structure will be presented.

## TP150

**A More Automated Approach to Data Collection for Macromolecular Crystallography.** Billy K. Poon, Peter H. Zwart, Paul D. Adams, Nicholas K. Sauter, Lawrence Berkeley National Lab, Berkeley, CA.

With the advances in structure refinement software that can automatically solve structures and the increasing use of robotics at synchrotron beamlines for data collection, high throughput crystallography is becoming much more automated. However, one aspect of crystallography that still requires a certain level of human intervention is processing the collected data. Web-Ice (Gonzalez A, Moorhead P, McPhillips SE, Song J, Sharp K, Taylor JR, Adams PD, Sauter NK, and Soltis SM, (2008) J. Appl. Cryst. 41(1), in press), jointly developed at the Stanford Synchrotron Radiation Laboratory and the Lawrence Berkeley National Laboratory, aims to address this issue by providing beamline users with a unified, graphical user interface that couples the low level control of the beamline hardware with the processing software (DISTL, LABELIT, MOSFLM) responsible for converting raw diffraction images into data sets suitable for refinement. Web-Ice can also perform automated crystal screening for selecting the best samples and calculate the optimal strategy for data collection. Recent and future developments include automatic handling of ice rings at varying two theta angles, automatic selection of the appropriate space group, and automatic data integration and scaling. Through Web-Ice, the beamline user can be more efficient at the synchrotron by allowing the software to handle the decision making for data collection in routine cases, while retaining the flexibility for more difficult data sets by providing a more user friendly interface for tweaking various parameters and customization of scripts for the data processing software.

## SP151

**Preliminary Neutron and Ultrahigh Resolution X-ray Single Crystal Diffraction Studies of the Aspartic Proteinase Endothiapepsin Co-crystallized with a Gem-diol Inhibitor PD-135,040.** Han-Fang Tuan, Leighton Coates, Grinnell College, 1115 8th Ave, Grinnell, IA 50112 USA.

Aspartic proteinases are a class of enzymes widely distributed among fungi, plants, vertebrates and viruses. They are involved in numerous disease conditions, including hypertension, amyloid disease, malaria, and AIDS.

Aspartic proteinase inhibitors have a proven therapeutic effect in the treatment of AIDS. The aspartic proteinase class of enzyme is comprised of two structurally similar domains, each contributing an aspartic acid residue to form a catalytic dyad that cleaves the substrate peptide bond. The enzyme used in these studies is endothiapepsin, a member of the aspartic proteinase family, which is composed of 330 amino acid residues, with roughly 170 residues in each domain. The crystallographic studies of the catalytic mechanism of aspartic

proteinases have largely been done on enzyme-inhibitor complexes that mimic the putative transition-state intermediate. The gem-diol class of inhibitors mimic both of the hydroxyl groups that are thought to exist in the transition-state. In this study, endothiapepsin has been co-crystallized with a gem-diol inhibitor PD-130,040 in a low solvent content unit cell (39%), which is unprecedented for this enzyme-inhibitor complex. This enables atomic resolution ( $1.0 \approx$ ) X-ray single crystal diffraction data to be collected at 100K on beamline ID14-2 at the ESRF synchrotron. Bond length analysis from this atomic resolution X-ray data set was used to deduce the protonation states of the two catalytic aspartates. Results show that one aspartate, Asp215, is protonated on the outer oxygen while the other aspartate, Asp32, is negatively charged when the inhibitor is bound. A room temperature (298K) X-ray single crystal diffraction data set was collected on an in house rotating anode X-ray generator. A room temperature (298K) neutron single crystal diffraction data set was collected at the Protein crystallography station (PCS) beamline at the LANSCE spallation neutron source. These data sets will be used for joint X-ray/neutron refinement to visualize the hydrogen/deuterium atoms at the active site. Through locating the catalytic hydrogen atoms in this complex, we will get a clearer understanding of the catalytic mechanism of aspartic proteinases.

### TP152

**New Algorithms for Single Crystal Photometry.** M.R. Pressprich, Avid Programming, Oregon, WI 53575 USA.

A new program has been developed for integrating single crystal reflection data collected with area detectors. A particular goal is accommodating marginal protein crystals.

The least squares positioning model fits the following geometrical degrees of freedom using analytical derivatives:

- Orientation of the crystal relative to the goniometer mounting bracket.
- Rotational misorientation of the detector relative to the incident beam.
- Rotational misorientation of the scan axis relative to the incident beam.
- Translational misalignment of the crystal, scan axis and detector.
- Unit cell angles and dimensions.

For a single domain crystal the model includes 19 refinable degrees of freedom. Parameters are coupled for refinement of twinned or split crystals.

The image background analysis applies Kalman filtering to separate signal from noise. Predicted background estimates are derived by in-plane Fourier analysis and corrections are made by statistically robust frame-to-frame updating of pixels beyond reflection domains.

Reflection intensities are determined from profile fitting and synthetic aperture (simple summation) photometry. Profile fitting implies that the reflection intensity is determined by adjusting a model profile to best fit the observed reflection shape after background subtraction, and is preferred for weak reflections in the presence of significant background. Synthetic aperture photometry involves summing the background corrected pixels lying within a model profile perimeter, and is generally favored for intense reflections. The extent of the reflection (its support) is determined from the beam spectrum and cross fire, the crystal size, and the detector point spread function.

This research was partially supported by Bruker AXS.

### MP153

**SAXS Measurements of Nanoscale Condensation Phenomena in Supercritical Jets.** A.R. Sandy, S. Narayanan, J. Ilavsky, J. Wang, The Advanced Photon Source, Argonne National Laboratory, Argonne, IL 60439, K.C. Lin, Taitech Inc., Beaver Creek, OH 45430, M. Ryan, Universal Technology Corp., Dayton, OH 45432, C. Carter, Air Force Research Laboratory, Wright-Patterson AFB OH 45433.

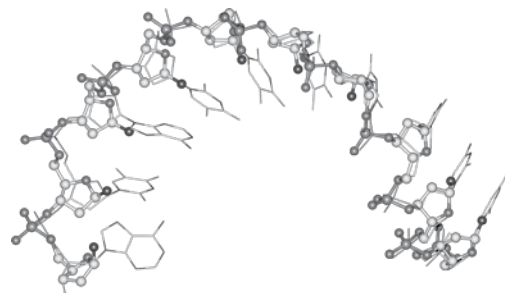
We have developed a time-resolved SAXS set-up optimized for studying condensation phenomena at the nanoscale within the plumes of supercritical jets. The combination of 1) an intense and well-collimated x-ray beam from the Advanced Photon Source, 2) a short x-ray path length gas injection cell with Kapton windows capable of sustaining high quiescent internal pressures, 3) a gas injection process stable over  $\approx 3-4$  seconds and 4) a Pilatus time-resolved area detector situated 3.5 m from the scattering center behind a precisely positioned direct-beam beamstop allows for efficient study of the homogeneous nucleation process inside such optically-opaque supercritical jets. The set-up has been applied to the study of supercritical ethylene gas injected, over a range of injection conditions, via small diameter ( $\approx 0.5$  mm) nozzles into quiescent nitrogen gas. For a particular set of injection parameters and at an axial location of 1.0 mm from the nozzle exit, we find that the droplet diameter is around 60-80 nm and that the condensed liquid is mainly distributed within the core of the plume. At the periphery of the jet plume, liquid volume fraction is substantially lower and droplet size is smaller. We have also studied the axial dependence of the nucleated phase. Generally, we find that the liquid volume fraction decreases exponentially with the axial distance from the nozzle exit and that the injection conditions with higher temperatures generate less liquid as expected based on optical shadowgraph measurements [1]. Use of the Advanced Photon Source was supported by the U. S. Department of Energy, Office of Science, Office of Basic Energy Sciences, under Contract No. DE-AC02-06CH11357.

[1] Lin, K.-C., Cox-Stouffer, S. K., Jackson, T. A., "Structures and Phase Transition Processes of Supercritical Methane/Ethylene Mixtures Injected Into a Subcritical Environment," *Combustion Science and Technology*, Vol. 178, 2006, pp. 129-160.

### SP154

**Towards an Automated System for Building Nucleic Acids.** J. Hattne, V.S. Lamzin, EMBL Hamburg,  $\frac{c}{o}$  DESY, Building 25A, Notkestr. 85, 22603 Hamburg, Germany.

X-ray structures of DNA and RNA, either on their own or in complex with protein, are often of high biological importance and may, due to their diffraction properties, prove challenging to the crystallographer. In practice, nucleic acids have to be modelled manually, since truly automatic methods are not yet available. This is a time-consuming and error-prone process. Here we present a pattern-recognition procedure, which determines the location and orientation of the nucleobases, as well as the position of the backbone phosphates in electron density maps. Depending on data quality, the r.m.s. positional error is around 0.6 Å at a resolution higher than 3.0 Å. Coupling the protein chain-tracing algorithms previously implemented in ARP/wARP with DNA/RNA-specific stereochemical information results in an almost complete polynucleotide backbone model (see figure, where



the automatically constructed backbone is shown in a ball-and-stick representation, and the final deposited structure is rendered in thin lines). The procedure assumes no particular conformation of the strands, nor does it require the presence of base pairing or base stacking. Although prominent in DNA, these are features often absent in RNA. The backbone model and the recognised nitrogenous bases together set the stage for an objective and automated system for building nucleic acids.

### TP155

**Absorption Correction Based on a 3D Model Reconstruction from Visual Images.** R.M.F. Leal<sup>1,2,3</sup>, S.C.M. Teixeira<sup>2,3</sup>, V. Rey-Bakaikoa<sup>1</sup>, V.T. Forsyth<sup>2,3</sup>, E. Mitchell<sup>1</sup>, <sup>1</sup>ESRF, Rue Jules Horowitz Grenoble France, <sup>2</sup>Institut Laue Langevin, Rue Jules Horowitz Grenoble France, <sup>3</sup>EPSAM&ISTM, Keele Univ. Staffordshire ST5 5BG England.

We describe the results of a feasibility study for the application of absorption corrections to macromolecular crystallographic X-ray diffraction data using a 3D crystal model generated photographically. The model allows path lengths through crystal, solvent and crystal mount system to be determined. The approach has been tested on the macromolecular crystallography beamline ID23-1 at the ESRF in Grenoble using a model insulin system with the standard mini diffractometer facilities which incorporate high quality camera systems for sample alignment. Data from the insulin crystal at low incident beam energy were recorded and processed using this approach. A comparison of the resulting data is made against those treated using an empirical method, and show significant improvement. The methods described here are of general interest, particularly for long wavelength X-ray work, and may also be applied to account for absorption effects in neutron crystallography.

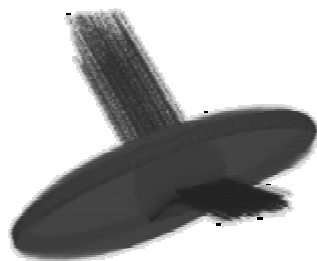
R. Leal, S. Teixeira, V. Rey, T. Forsyth, E. Mitchell (2007). "Absorption Correction based on a 3D Crystal and Support Model". Journal of Applied Crystallography. Submitted. R. Leal, S. Teixeira, V. Rey-Bakaikoa, E. Mitchell and T. Forsyth, "Absorption correction based on a 3D crystal and support model", Acta Cryst. (2007). A63, s78-s79

### MP156

**Measuring Nanoscale Perturbation of Polymer Matrix in Polymer Nanocomposites Using X-ray Photon Correlation Spectroscopy.** R. Aravinda Narayanan<sup>1</sup>, A. Sandy<sup>2</sup>, S.S. Sternstein<sup>3</sup>, P. Thiyagarajan<sup>4</sup>, <sup>1</sup>Chemical Sciences, Oak Ridge Nat'l Lab, Oak Ridge, TN, <sup>2</sup>Advanced Photon Source, Argonne Nat'l Lab, Argonne, IL, <sup>3</sup>Dept. of Matls Sci & Eng, Rensselaer Polytechnic Inst., Troy, NY, <sup>4</sup>Intense Pulsed Neutron Source, Argonne Nat'l Lab, Argonne, IL.

Polymer nanocomposites exhibit novel thermo-mechanical properties. For instance, the glass-transition temperature ( $T_g$ ) and viscosity of the composite can have values lower than that of the bulk polymer, thus spectacularly violating Einstein's theory of viscosity of dispersions according to which the addition of particles to a polymer should always increase the viscosity. These properties are a complex product of nanoparticle-polymer interfacial interactions, interfacial area, and inter-particle distances. It can be theorized

that the effect of all these factors is to perturb the polymer matrix. However, challenges in measuring perturbation of the polymer at the nanoscale have forced qualitative explanations based on an analogy with ultra-thin films where a similar effect on  $T_g$  is observed, and computer simulations focusing



on particular aspects of the complex problem. Here, we propose a unique quantitative measure of polymer perturbation and extract it from nanoscale interfacial relaxation dynamics studies on a series of repulsive and attractive interfaces in silica - (poly) vinyl acetate nanocomposites, using x-ray photon correlation spectroscopy. An important finding is that the perturbation length scale extends to a few hundred nanometers exceeding the inter-particle distance which suggests overlap of perturbations from many particles causing dramatic changes in bulk properties.

### SP157

**Computational Construction of a Class Ia Aminoacyl-tRNA Synthetase Minimal Catalytic Domain: *M. thermoautotrophicus*-LeuRS.** Ozgun Erdogan, Steven Lewis, Brian Kuhlman, Charles W. Carter, Jr., Dept. of Biochemistry, UNC, Chapel Hill, NC.

Aminoacyl tRNA synthetases are divided into two classes depending on the amino acid they activate. The class Ia Leu-tRNA synthetase from *M. thermoautotrophicus* actually interacts with the class IIa Pro-tRNA synthetase of the same species, enhancing its rate of tRNA aminoacylation five-fold, suggesting that these enzymes share complementary molecular surfaces. There is preliminary evidence that amino acid activation may be catalyzed by a minimal catalytic domain (MCD) obtained by deleting from the native genes the insertions responsible for most of the evolutionary variability, while keeping the conserved, catalytic signature sequences<sup>1</sup>. In order to see to what extent these enzymes make use of surfaces of the Minimal Catalytic Domains (MCDs) in such an interaction, we have constructed the MCD of LeuRS *M. Thermoautotrophicus* computationally using Rosetta design software. As there is no structural information for this protein, LeuRS from other organisms were compared, and the most appropriate match was decided from sequence alignments. Removal of inserted domains from the homologous structure, while keeping all signature sequences, left us with three discrete regions. The three disjoint regions were connected with loops designed by Rosetta to construct the MCD. Redesign of exposed surfaces was done using Rosetta and surface area differences calculated by AreaMol. The constraint was to keep the residues whose environments have been changed by removing insertion domain. To protect the active site from mutations by Rosetta, residues from the ligand binding pockets were identified by superimposition of the structure onto another LeuRS crystal structure bound to leucyl-sulfoamyl adenylate and the conserved Class I signature sequences. The resulting LeuRS MCD design was a peptide with 131 amino acids long. Supported by NIGMS 78227.

<sup>1</sup>Pham, Y. et al. *Mol. Cell* **25**, 851-862 (2007).

### TP158

**Distant Homology Detection Using a Length and Structure-based Sequence Alignment Tool (LESTAT).** Marianne M. Lee\*, Ralf Bundschuh\*<sup>‡</sup>, Michael K. Chan\*<sup>‡</sup>, \*The Ohio State Biophysics Program, <sup>†</sup>Dept. of Physics, <sup>‡</sup>Depts. of Biochemistry & Chemistry, The Ohio State Univ., Columbus, OH 43210.

A new machine learning algorithm, LESTAT (Length and Structure-based sequence Alignment Tool) has been developed for detecting protein homologs having low sequence identity. LESTAT is an iterative profile-based method that runs without reliance on a predefined library and incorporates several novel features that enhance its ability to identify remote sequences. To overcome the inherent bias associated with a single starting model, LESTAT utilizes three structural homologs to create a profile consisting of structurally conserved positions and block separation distances.

Subsequent profiles are refined iteratively using sequence information obtained from previous cycles. Additionally, the refinement process incorporates a “lock-in” feature to retain the high scoring sequences involved in previous alignments for subsequent model building and an enhancement factor to complement the weighting scheme used to build the position specific scoring matrix. A comparison of the performance of LESTAT against PSI-BLAST for seven systems reveals that LESTAT exhibits increased sensitivity and specificity over PSI-BLAST in six of these systems, based on the number of true homologs detected and the number of families these homologs covered. Notably, many of the hits identified are unique to each method – presumably resulting from the distinct differences in the two approaches. Taken together, these findings suggest that LESTAT is a useful complementary method to PSI-BLAST in the detection of distant homologs.

### MP159

**Influence of Matrix Block Copolymer Structure on the Dynamics of Domain-specific Nanoparticles.** D.A. Bohnsack<sup>†‡</sup>, V.G. Pol<sup>†</sup>, B. Lee<sup>‡</sup>, Alec Sandy<sup>‡</sup>, R.E. Winans<sup>‡</sup>, P. Thiyagarajan<sup>†</sup>, Intense Pulsed Neutron Source (†) and X-ray Sciences Div. (‡), Argonne National Laboratory, Argonne, IL 60439 USA.

Gold nanoparticles have been synthesized with an oligomeric stabilizing layer that imparts an enthalpic driving force for the particle to reside within a specific block of a phase-separated block copolymer (BCP) matrix. The addition of these nanoparticles, as well as low molecular weight linear homopolymers, alters the phase-separated morphology of the BCP system as determined through small-angle X-ray scattering. In addition to changing the domain sizes, the addition of nanoparticles leads to an order-order transition and a shift in the dominant phase morphology from cylindrical to lamellar domains. X-ray photon correlation spectroscopy measurements have been used to show that the equilibrium dynamics of these enthalpically confined nanoparticles is dependent on the BCP phase morphology. Observed changes in relaxation times are correlated to the increase in number of translational degrees of freedom available to the particle in a two-dimensional lamellar phase compared to a one-dimensional cylindrical phase. Additionally, the inhomogeneous medium in which the particles translate gives rise to anomalous diffusion, approaching the ballistic limit for random motion.

This work benefited from the use of facilities at IPNS and 8-ID, Advanced Photon Source, ANL supported by the U.S. Department of Energy, Office of Science, Office of Basic Energy Sciences, under Contract No. DE-AC02-06CH11357.

### SP160

**A 1.6 Å Resolution Crystal Structure of *cis*-3-Chloroacrylic Acid Dehalogenase Reveals An Additional Active Site Residue - R117.** Youzhong Guo,<sup>§‡</sup> Hector Serrano,<sup>‡</sup> William H. Johnson, Jr.,<sup>‡</sup> Christian P. Whitman<sup>‡</sup>, Marvin L. Hackert,<sup>§</sup> <sup>‡</sup>Div. of Medicinal Chemistry, College of Pharmacy, <sup>§</sup>Dept. of Chem. & Biochem., Inst. for Cell and Molecular Biology, Univ. of Texas, Austin, TX 78712.

*trans*- and *cis*-1, 3-Dichloropropenes are active ingredients in widely used fumigants such as **Telone II**. The environmentally toxic dichloropropenes can be degraded by a number of soil bacteria such as *Pseudomonas pavonaceae*. The bacterial degradation of the 1,3-dichloropropene depends on a hydrolytic dehalogenation reaction catalyzed by both *cis*- and *trans*-3-chloroacrylic acid dehalogenases. *cis*-3-Chloroacrylic acid dehalogenase is a member of the 4-OT family characterized by a conserved  $\beta$ - $\alpha$ - $\beta$  motif and a catalytic N-terminal proline. Pro-1, Arg-70, Arg-73, and Glu-114 had initially been implicated as key catalytic residues in the *cis*-CaaD mechanism by amino acid sequence alignment with known members of the 4-OT

family. Mutagenesis studies confirmed their importance prior to the availability of crystal structures. His-28 and Tyr-103 were identified as additional key catalytic residues based on recent crystal structures, and combined with the earlier results, led to a working hypothesis for the catalytic mechanism. We have now independently solved higher resolution crystal structures of both native and an inactivated form of *cis*-CaaD. Our structures showed density for additional C-terminal residues and identified another active site residue, Arg-117. The importance of Arg-117 for activity has been confirmed by mutagenesis and kinetic studies on the R117A mutant. Furthermore, our structure shows a distinctly different conformation for the enzyme inactivated by (*R*)-Oxirane-2-carboxylate than that in the published structure, and adds to our understanding of the catalytic mechanism of *cis*-CaaD. A summary of these results will be presented.

This work is supported in part by grants from The Welch Foundation (F 1219, F1334).

### TP161

**A Rasmol to PyMOL Translator.** Scott Mottarella, Brett Hanson, Charles Westin, Paul Craig, Herbert Bernstein, Biological Sciences, Rochester Inst. of Technology, 85 Lomb Memorial Dr., Rochester, NY 14623 USA.

For many educators and scientists, PyMOL is the application of choice for preparing images and animations of their structures because of the beauty and quality of the images. However, many are most familiar with the scripting languages associated with RasMol, Chime and Jmol. The long-range goal of our Structural Biology Extensible Visualization Scripting Language project is to make the multiple molecular visualization tools available to the broadest possible audience, where each user can use many programs, with knowledge of the scripting language for only one of those programs. The first step has been a comparison of the command sets for RasMol and PyMOL, followed by creation of a plug-in for PyMOL that will accept RasMol script files, translate the commands into PyMOL script and execute the commands. The process involves searching for recognized, valid, RasMol script commands and performing its PyMOL equivalent, either as a single command or as a series of commands that produce the same result. Future plans include expansion to additional molecular visualization programs and the preparation of a web site to provide script translation among the various programs. The project is funded in part by NIGMS grant #1R15GM078077.

### MP162

**16 K Synchrotron X-ray Charge Density Study of Coordination Polymer,  $\text{Co}_3(\text{C}_8\text{H}_4\text{O}_4)_4(\text{C}_4\text{H}_{12}\text{N}_2)(\text{C}_5\text{H}_{11}\text{NO})_3$  at ChemMatCARS, Sector 15, Advanced Photon Source.** Y.S. Chen,<sup>1</sup> H.F. Clausen,<sup>2</sup> J. Overgaard,<sup>2</sup> B.B. Iversen<sup>2</sup>, <sup>1</sup>ChemMatCARS, Univ. of Chicago, Advanced Photon Source, Argonne, IL, USA, <sup>2</sup>Dept. of Chemistry, Univ. of Aarhus, Aarhus, Denmark.

The charge density of coordination polymer  $\text{Co}_3(\text{C}_8\text{H}_4\text{O}_4)_4(\text{C}_4\text{H}_{12}\text{N}_2)(\text{C}_5\text{H}_{11}\text{NO})_3$ , 1, has been determined from multipole modeling of structure factors obtained from single crystal synchrotron X-ray diffraction measurements at 16 K. The crystal structure formally contains a negatively charged framework with cations and neutral molecules in the voids. However, the charge density suggests that the framework is close to neutral, and qualitative conclusions based on formal charge counting, e.g. about guest inclusion properties, therefore will be in error. There are considerable differences in the charge distributions of the three unique benzene dicarboxylic acid linkers, which are widely used in coordination polymers. This documents that the electrostatic properties of coordination polymer

cavities, and thereby their inclusion properties, are highly tunable. Orbital population analysis reveals both Co sites to be high spin  $\text{Co}^{2+}$  ions, and the electron density topology shows that the tetrahedrally coordinated Co atom has an atomic volume which is 15% larger than the octahedrally coordinated Co atom. The crystal structure has both ferro-magnetic and antiferromagnetic interactions, but no direct metal – metal bonding is evidenced in the charge density. The magnetic ordering therefore takes place through super-exchange in the oxygen bridges and the aromatic linkers. Bonding analysis of the experimental charge density reveal that two oxygen atoms, O(1) and O(11), have significant covalent contributions to the metal-ligand bonding, whereas all other oxygen atoms have closed shell interactions with the metals. This suggests that it is these two oxygen atoms which are the key mediators of the magnetic ordering.

### SP163

**Is TCR-MHC Recognition the Result of T Cell Receptor Evolution or Selection in the Thymus?** Peter J. Miller<sup>1</sup>, David S. Riddle<sup>2</sup>, Jeffrey A. Frelinger<sup>2</sup>, Edward J. Collins<sup>1,2</sup>, <sup>1</sup>Dept. of Biochemistry and Biophysics, <sup>2</sup>Dept. of Microbiology and Immunology, Univ. of North Carolina, Chapel Hill, NC 27599.

T cell receptor (TCR) recognizes foreign peptides presented in the context of major histocompatibility complex molecules (MHC). Intriguingly, crystal structures of TCR-MHC complexes have revealed a conserved docking orientation between the two molecules. One explanation for this phenomenon is that the TCR has evolved to recognize MHC, and therefore the preference of the TCR to bind MHC is germline encoded. The other main hypothesis is that the conserved binding orientation is the result of T cell selection in the thymus, and the influence of other T cell surface molecules involved, such as the co-receptor CD8. TCR is a heterodimer with each chain being comprised of a constant and variable domain. During T cell development one of a number of variable gene segments may be used in conjunction with the a or b constant domains. Each variable gene segment encodes two of the three binding loops (complementarity-determining region (CDR) loops 1 and 2) and the third loop (CDR3) is encoded by recombination of that variable gene segment with additional gene segments. Therefore, to examine any conservation of binding, we must examine complexes of the same MHC bound to TCRs with the same variable segments. Within the existing set of co-crystal TCR-MHC structures determined, there are a few TCR with the same b variable domain bound to the same MHC molecule. If TCR-MHC recognition is germline encoded, then one would expect to see the same residues making contact between the TCR b chain and the MHC, but there are none. Therefore, we hypothesized that if MHC recognition is indeed germline encoded, then it must lie within the TCR a chain. In order to examine this directly, we are determining crystal structures of TCRs with the same alpha chain (Va2) bound to the same MHC (H-2K<sup>b</sup>).

### TP164

**From Sample to Structure: The Development and Integration of High-throughput Technologies to Provide X-ray Data for Structural Solution.** Joseph Luft<sup>1</sup>, Edward Snell<sup>1</sup>, Aina Cohen<sup>2</sup>, Jennifer Wolfley<sup>1</sup>, Meriem Said<sup>1</sup>, Raymond Nagel<sup>1</sup>, Christina Veatch<sup>1</sup>, M. Elizabeth Snell<sup>1</sup>, S. Michael Soltis<sup>2</sup>, Michael Malkowski<sup>1</sup>, George DeTitta<sup>1</sup>, <sup>1</sup>Hauptman-Woodward Inst., Buffalo NY, <sup>2</sup>Stanford Synchrotron Radiation Laboratory, Menlo Park, CA.

A high-throughput crystallization screening service has been in operation for 8 years screening over 9600 macromolecules from the biological and structural genomics communities. Technologies are being developed to include optimization and X-ray data collection

from the resulting crystals in a highly automated manner. At the heart of the screening process lies a carefully constructed set of 1536 crystallization cocktails. The cocktail design enables chemical space analysis of the crystallization results. This analysis readily identifies solubility trends, vectors for crystal optimization, and exposes promising un-sampled areas of chemical space. After analysis, optimization proceeds directly from screening in a rapid, highly-parallel fashion. The optimization protocol simultaneously fine-screens chemical and temperature-dependent phase behavior in regions of chemical space that immediately surround the screening hit. A capillary tip crystal production method is being developed for *in-situ* X-ray data collection without physical manipulation of the crystals. Crystal production is designed for compatibility with the Stanford Automated Mounting (SAM) system developed at SSRL, allowing for remote data collection. A SAM emulator is being constructed at the crystallization laboratory to facilitate a rapid diffraction-based feedback loop for the optimization. The technologies developed will be incorporated into the current crystallization screening service, already available to the community at large. We gratefully acknowledge NIH U54 GM074899.

### MP165

**The Structure of Bicyclo[2.2.1]hept-5-ene-2,3-diylbis(methylene)dimethanesulfonate.** Daniel S. Jones, Dawn A. Revis, Matthew D. Brooker, Markus Eitzkorn, Dept. of Chemistry, The Univ. of North Carolina at Charlotte, Charlotte, NC 28223 USA.

The title compound was isolated as an intermediate in the synthesis of a triene; the triene may serve as a precursor for a molecular pincer. The title compound crystallizes in space group  $P2_1/a$  with  $a = 9.057(1)$  Å,  $b = 11.327(1)$  Å,  $c = 13.882(2)$  Å, and  $\beta = 101.55(1)^\circ$ .  $R(\text{obs})$  for 2028 observed reflections is 0.063.

Possible disorder models for the structure will be discussed.

### SP166

**DCoH Stability Regulates HNF-1 $\alpha$  Activity in Diabetes.** Helen Rho, Chasity N. Jones, Robert B. Rose, Dept. of Molecular & Structural Biochemistry, NCSU, Raleigh, NC 27695.

Dimerization cofactor of HNF-1 $\alpha$  (DCoH) is a bifunctional protein involved in metabolic and transcriptional regulation. As a coactivator it stabilizes dimers of the transcription factor hepatocyte nuclear factor-1 $\alpha$  (HNF-1 $\alpha$ ). Preliminary results from transient transfection assays indicate that DCoH may stabilize HNF-1 $\alpha$  mutations associated with diabetes. In order to interact with HNF-1 $\alpha$ , DCoH switches its oligomeric state from a tetramer to a dimer. To address how DCoH regulates HNF-1 $\alpha$  activity, we are investigating the dynamics of DCoH/ HNF-1 $\alpha$  complex formation by measuring the relative stability of homo- and heterotetramers.

Surprisingly, DCoH must cofold with HNF-1 $\alpha$  in order to form a complex due to hyperstability of the homotetramer. To characterize this stability, we compared DCoH with the less stable homolog DCoH2. DCoH2 can interact with HNF-1 $\alpha$  *in vitro* by mixing the proteins. Both homologs adopt identical folds with the greatest differences at the surface and tetrameric interface. The structure of a point mutation in DCoH1, T51S, indicates that the decrease in stability of the DCoH2 homotetramer results from ordering a water molecule at the tetramer interface. The decreased stability of the DCoH1-T51S homotetramer, as measured via a His<sub>6</sub>-pull-down assay with HNF-1 $\alpha$ , confirmed that this mutation destabilizes the homotetramer. This structure partially explains the decreased stability of the DCoH2 homotetramer and provides insight into HNF-1 $\alpha$  regulation by DCoH in diabetes.

Data were collected at SERCAT beam line 22-ID at the APS, Argonne National Labs, IL. This research is supported by ADA 7-03-JF-34 and NSF MCB-0643830.

**TP167**

**Single-column Purification of Native Proteins to Homogeneity for Structural Studies – The IMAC/TAGZyme Process.** Helena Block<sup>a</sup>, Jan Kubicek<sup>a</sup>, Jörg Labahn<sup>b</sup>, Frank Schäfer<sup>a\*</sup>, <sup>a</sup>QIAGEN GmbH, Qiagen Strasse 1, 40724 Hilden, Germany, <sup>b</sup>Inst. of Structural Biology (IBI-2), Research Center Jülich, 52425 Jülich, Germany.

We describe an efficient strategy to produce high-quality proteins of native structure by using a single IMAC chromatography column and exoproteolytic 6xHis-Tag removal via the TAGZyme system followed by a subtractive IMAC purification step to remove protease and impurities. Quality assays approved a high purity of the obtained recombinant human proteins such as the monomeric cytokine Interleukin-1 beta (IL-1 $\beta$ ) and trimeric Tumor Necrosis Factor alpha (TNF $\alpha$ ).

IL-1 $\beta$  was analysed in further detail and the final preparation was apparently free of host cell proteins, endotoxins, protease, and aggregates. The N-terminal amino acid sequence of IL-1 $\beta$  was in full agreement with its natural mature form. The homogeneity of the product was further shown by X-ray structure determination which confirmed the previously solved structure of the protein. We propose the IMAC/TAGZyme process as a general strategy for preparation of proteins for structural studies as well as for production of biopharmaceuticals.

**MP168**

**Crystal Structures that Change Across Interfaces.** A. David Rae, Research School of Chemistry, Australian National Univ., Canberra, Australia. rae@rsc.anu.edu.au

Two simple examples of structures changing across interfaces are twins and stacking faults. In the interface region a different structure occurs compared to the structure on either side of the interface. Crystals where this interfacial region extends for multiple layers are being observed but often ignored for the lack of a program that allows the coexistence of prototype structures and refinable rules for the creation of the observed diffraction patterns. Often the possibilities can be derived from an idealized, maybe disordered, parent structure of higher symmetry, but this need not be so. Commensurability need not extend to three dimensions and may be approximate only, requiring lattice distortion at an interface. Chemical composition need not be the same for each prototype structure. Packing arguments can be used to show that many of these crystals should contain perfectly ordered layers but have different rules for relating adjacent layers. The asymmetric units for different prototype structures may be only be approximately related by simple rules and comprehensive constraint and restraint options are then useful. Different crystals will vary in population-type parameters and co-refinement of different crystals at the same temperature is useful. The author is completing his refinement program RAELS08 to refine such structures and will discuss what he hopes is a comprehensive set of options to choose from when refining crystals that change across interfaces but contain essentially well defined prototypes.

**SP169**

**Homology Exploration with ProMOL.** Corey Wischmeyer, Paul Craig, Herbert Bernstein, Biological Sciences, Rochester Inst. of Technology, 85 Lomb Memorial Dr., Rochester, NY 14623 USA.

The ProMOL plugin for PyMOL is an intuitive user interface that gives users access to many of the complex tools that exist within PyMOL, without requiring that the user learn to program in Python. Among its many tools, ProMOL features a motif-matching interface

that can compare enzyme active sites based on the relative positions of the catalytic residues. Tools found in ProMOL can be used to compare any structure with more than 30 known catalytic active site motifs, which were drawn from the Catalytic Site Atlas (<http://www.ebi.ac.uk/thornton-srv/databases/CSA/>). The motif analysis tool can be fine tuned to narrow or expand the three dimensional search space for active site alignment. Alignment results for enzyme classes across different taxonomic categories will be presented and compared, along with suggestions for implementing more effective alignment strategies with the motif tool in ProMOL. The project is funded in part by NIGMS grant #1R15GM078077.

**TP170**

**The PX Scanner: New Developments Enabling Complete Low Temperature Data Collection.** J. Duncan, Oxford Diffraction Ltd, 68 Milton Park, Abingdon, Oxfordshire, OX14 4RX UK.

The PX scanner is a unique instrument from Oxford Diffraction enabling the collection of X-ray data from protein crystals, in-situ, in the crystallisation plate. The capabilities of the PX Scanner now extend to a complete identification and data collection system for protein crystals in-situ. Previously, X-ray data collection in the PX Scanner has been limited to a 6° omega scan of the crystals in the crystallisation plate at room temperature. Recently, we have been able to collect full 360° data sets using the PX Scanner. In order to achieve this new level of functionality we have designed a novel Phi axis which allows crystals to be inserted directly into the X-ray beam in the PX Scanner. For low temperature data collection we have built a new cryo-cooling instrument specifically designed for use with the PX Scanner. The PX Scanner now represents a single instrument providing a complete crystal screening solution. Promising crystals can be identified optically and selected for in-situ data collection in the crystallisation plate. If diffraction is promising from crystals in-situ they can be looped out and placed on the Phi axis tip, flash frozen in the PX Scanner cryo-stream ready for low temperature data collection.

**MP171**

**Crystalline Structure Determination and Low Temperature Study of Diethylcarbamazine Citrate: An Anti-Filariasis Drug.** C.C.P. da Silva<sup>1</sup>, J. Ellena<sup>1</sup>, S.B. Honorato<sup>2</sup>, A.P. Ayala<sup>2</sup>, J.S. Mendonça<sup>3</sup>, L.M.U. Mayer<sup>3</sup>, N. Boechat<sup>3</sup>, <sup>1</sup>Laboratorio de Cristalografia, Inst. de Física de São Carlos-USP, São Carlos (SP), Brazil. <sup>2</sup>Dept. de Física, Univ. Federal do Ceará, Fortaleza (CE), Brazil. <sup>3</sup>FioCruz-Fundação Oswaldo Cruz, Inst. de Tecnologia em Fármacos-FarManguinhos, Rio de Janeiro (RJ), Brazil.

The title compound, C<sub>10</sub>H<sub>21</sub>N<sub>3</sub>O<sub>7</sub>, known as diethylcarbamazine (DEC) citrate, is one of the active pharmaceutical ingredients most used in the treatment of the *Lymphatic filariasis*<sup>1</sup>. As no one structure is available by single crystal X-ray diffraction in the literature, we report its crystal structure, determined at room temperature (293K), and compare the results with the low temperature structure (150K). The DEC citrate crystallizes, at room temperature, in the monoclinic space group P2<sub>1</sub>/c, with an adopted chair conformation in the heterocyclic ring of the DEC molecule. The crystal packing is stabilized by the presence of one strong O-H...O intermolecular interaction between the DEC molecule and the citrate and by two N-H...O intermolecular interactions. The crystal interaction of DEC citrate forms intercalated layers of these two molecules in the packing, along *a*. The low temperature study, performed at 150K, showed the presence of a phase transition and a slight, but notable, increase in the magnitude of the unit cell parameters,

leading to changes in the structure of the DEC molecule, specially in the  $O=CNC_2$  group. These results indicate that DEC citrate presents two different crystal structure distortions, that still need to be confirmed by others crystallographic methods.

[1] R. P. Tripathi\*, D. Katiyar, N. Dwivedi, B.K. Singh and J.Pandey (2006); *Current Medicinal Chemistry*, 13, 3319-34.

### SP172

**New Technique of Manipulating a Protein Crystal.** Kazufumi Takano, Tomoya Kitatani, Shigeru Sugiyama, Hiroyoshi Matsumura, Hiroaki Adachi, Satoshi Murakami, Tsuyoshi Inoue, Yusuke Mori, Osaka Univ., SOSHO Inc., JST-CREST, Suita 565-0871, Japan.

We have developed a new device of manipulating a protein crystal, Crystal Catcher. The Crystal Catcher directly captures a crystal with an adhesive. The easy and stable removing of a protein crystal from the drop has been achieved using the Crystal Catcher. The crystal picked up on the Crystal Catcher is positioned in the cryostream on the goniometer and flash-cooled. The capturing and mounting are effective for various protein crystals including membrane protein crystals without causing significant damage. Furthermore, the background noise in XRD analysis reduces because nylon loop and cryoprotectant surrounding a crystal are absent. This new approach will replace nylon loops to pick up protein crystals.

### MP173

**Intramolecular Hydrogen Bonds Involving Adjacent OH and  $CH_2OH$  Groups: Neutron Diffraction, Data Mining, and Computational Studies.** C.H. Schwalbe,<sup>1</sup> D.L. Rathbone,<sup>1</sup> T.F. Koetzle,<sup>2</sup> A.J. Schultz,<sup>2</sup> S.R. Sagineedu,<sup>3</sup> J. Stanslas<sup>3,4</sup>, <sup>1</sup>School of Life & Health Sciences, Aston Univ., Aston Triangle, Birmingham UK, <sup>2</sup>IPNS Div., Argonne National Lab, Argonne, IL, USA, <sup>3</sup>Dept. of Biomedical Sciences, Faculty of Medicine & Health Sciences, <sup>4</sup>Natural Products Lab, Inst. of Bioscience, Univ. Putra Malaysia, Serdang, Selangor, Malaysia.

Andrographolide is a biologically active natural product with neighboring OH and  $CH_2OH$  groups on a decalin ring. Our neutron diffraction study confirms that the OH group is the donor and  $O(H)CH_2$  the acceptor in an intramolecular hydrogen bond (IHB). However, an X-ray study of a derivative acetylated at a remote OH group showed the reverse pattern. A CSD search for adjacent cyclic C atoms, one bearing OH and the other  $CH_2OH$ , with normalized H atoms and  $O...O$  distance  $\leq 2.95$  Å, yielded 61 matching fragments: 32 with  $CH_2OH...OH$  contacts  $\leq 2.3$  Å, 21 with similar  $OH...O(H)CH_2$ , the remainder with weaker or no IHB. Attached to a 6-membered ring, usually as the cis isomer,  $CH_2OH$  was donor in 24 and OH in 16 fragments. On a 5-membered ring, always cis, these numbers were 8 and 3. Structures of cis-1-hydroxy-2-hydroxymethylcyclohexane and -cyclopentane optimized in the 6-31G\* basis set favor the  $CH_2OH...OH$  form over the  $OH...O(H)CH_2$  by 0.5 and 7.7 kJ/mol respectively, i.e. the energy preference for  $CH_2OH...OH$  is stronger with a 5-membered ring. Cluster analysis with dSNAP shows main clusters matching the IHB types without clear subclustering by ring size.

Work supported by the U.S. Department of Energy, Office of Basic Energy Sciences, under contract DE-AC02-06CH11357, and the Malaysian Ministry of Science, Technology and Innovation (MOSTI) grant no. 5450293.

### SP174

**Desktop Minstrel UV<sup>TM</sup>: A Novel Protein Crystal Monitoring Automation System Using UV Fluorescence Microscopy.** Jian Xu, Craig Sterling, Michael Willis, Rigaku Automation, 5999 Avenida Encinas, Suite 150, Carlsbad, CA 92008.

Identifying protein crystals in crystallization droplets has long been considered a challenging step in the field of protein crystallography. Although there are numerous automated crystallization robots readily available, none have been able to successfully monitor crystal growth by distinguishing protein crystals from non-protein crystals and detecting crystals from drops that are otherwise difficult to see with visible light. In order to fulfill this critical need, Rigaku has developed a novel protein crystal monitoring automation system, the Desktop Minstrel UV<sup>TM</sup>, which uses UV fluorescence microscopy. The system includes an ultraviolet microscope with at least one ultraviolet light emitting diode, providing illumination with the wavelength matching the absorption of the fluorescing amino acids, such as tryptophan. To greatly decrease photo-damage to the protein crystals, the fluorescing light illuminated on the sample is reduced to the minimum and is then digitally recorded by a camera with a CCD sensor. We have conducted crystallization experiments with various proteins in order to evaluate this system. The resulting UV images from these experiments clearly reveal the protein crystals from non-protein crystals, such as salts. In addition, this UV crystal monitoring system is built upon the platform of Rigaku's state-of-art imaging automation technology, the Desktop Minstrel<sup>TM</sup>, which makes the evaluation of a large number of crystallization experiments possible. The Desktop Minstrel UV enables researchers to accurately harvest protein crystals for data collection or design follow-up experiments.

### TP175

**A Novel, High-throughput System to Enhance Protein Solubility, Stability and Crystallization.** L.J. DeLucas, L. Nagy, D. Johnson, T. Lewis, Center for Biophysical Sciences and Engineering, Univ. of Alabama at Birmingham, W.W. Wilson, Dept. of Chem., Mississippi State Univ., C.S. Henry, Dept. of Chem., Colorado State Univ.

The crystallization of proteins as well as the solubilization and stabilization of proteins represent examples of protein solution phenomena that are inextricably linked to the thermodynamics of protein-protein interactions. In the case of crystallization, aggregation is prerequisite for the formation of a nucleus, a critical sized ordered aggregate capable of sustaining ordered growth. Conversely, physical stability of pharmaceutical formulations generally depends on suppression of aggregation. In either case, it is ultimately protein-protein interactions in a specified solvent condition that dictates the process outcome. A quantitative measure of protein-protein interactions is given by the second virial coefficient, B. The second virial coefficient is a thermodynamic term representing the summation of all forces (i.e. charge-charge, dipole-dipole, Van der Waals, etc.) between two bodies in a dilute solution. Published data clearly show a strong correlation of the second virial coefficient versus solubility and/or crystallization properties for proteins. Development of a high-throughput, self-interaction chromatography system (shown in figure) capable of measuring B for 150 solution conditions in 8 hours (with 20  $\mu$ g of total protein) will be presented. The system incorporates a predictive algorithm and two different incomplete factorial screens (one for protein solubilization/stability and a second for crystallization). Validation data for several different proteins will be presented demonstrating the utility of this technology to improve protein solubility, polydispersity and crystal quality.



**MP176**

**The Three-dimensional Network Polymer Formed by the Hydrothermal Reaction of Mercaptotriazole and Zinc Thiocyanate.** Urs Geiser, John A. Schlueter, Materials Science Div., Argonne National Laboratory, Argonne, IL 60439, USA.

We previously reported that the hydrothermal reaction of 2-aminotriazole (AmTAZ) with zinc thiocyanate results in the decomposition of the thiocyanate ion and the formation of the cubic cage network polymer  $[Zn_6(AmTAZ)_6S_2](NO_3)_3$  (solvent) (**1**). This salt contains triangular building blocks with a central sulfide ion surrounded by three zinc centers that are bridged by AmTAZ mono-anions. The fourth zinc coordination site is taken up by the single AmTAZ nitrogen atom of an adjacent building block.

Here we report that when AmTAZ is replaced by mercaptotriazole under otherwise identical reaction conditions, at least some of the thiocyanate survives and is incorporated into the resulting product. On the other hand, the mercapto group is eliminated, and the crystallized salt,  $Zn_4S(TAZ)_3(SCN)_3$  (**2**), contains unsubstituted triazolate (TAZ), and its charge is balanced without the addition of unbound anions.

The rhombohedral crystal structure of **2** contains the homologous triangular building block as **1**, which is also connected to three other blocks via TAZ bridges into a three-dimensional network (distorted simple cubic topology). In contrast to **1**, the sulfide center is additionally coordinated to a bulky  $Zn(NCS)_3$  group that protrudes and essentially fills the cavity of the network but does not otherwise coordinate to it.

This work was supported by the U.S. Dept. of Energy, Office of Science, Basic Energy Sciences, at Argonne National Laboratory, an U.S. Department of Energy Office of Science laboratory, operated by UChicago Argonne, LLC, under contract DE-AC02-06CH11357.

**SP177**

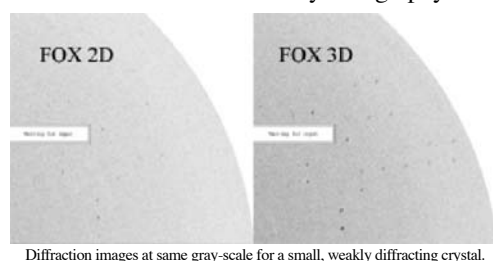
**The State of the Art in X-ray Optics – The FOX Family of Ellipsoidal Single Reflection Optics.** Brett Kraabel, Vincent Roger, Olivier Pacaud, Peter Høghøj, Xenocs SA, 19, rue François Blumet, F-38360 Sassenage, France, info@xenocs.com

Xenocs is the world leader in X-ray multilayer single reflection optics with the FOX 2D optics introduced in 2003, which currently provide the brightest possible beam for any given X-ray source. Now Xenocs announces the launch of the FOX 3D x-ray optics, the first true ellipsoidal single Bragg reflection optics on the market, as a stand-alone optic and in combination with the GeniX microfocus X-ray source.

The two main advantages of the FOX 3D optics are wider active areas enabling larger collection angles in both dimensions (up to 4 degrees in the sagittal direction, for example) and improved focusing properties. These improvements enhance both integrated flux and spot definition – and therefore beam brightness – and are of particular importance for applications requiring high flux and/or small spots.

We present data for several such applications (protein crystallography, X-ray reflectometry (XRR), and microdiffraction) to show the advantages offered by the FOX 3D optics over not only all double-reflection optics but even FOX 2D. Protein crystallography data

comparing a FOX 3D to a FOX 2D optic is presented for both a large, well diffracting crystal and a small weakly diffracting crystal. The results show that the FOX



3D optics prove their worth for smaller or more weakly diffracting crystals, where the mean  $I/d(I)$  increased by over 100%. For XRR or microdiffraction, we discuss the advantages of using optics with large collection angles to focus the maximum monochromatic flux on a small spot. Finally, for SAXS we present results obtained by combining a FOX optic with a microfocus source.

**TP178**

**Augmenter of Liver Regeneration and Probing for Interacting Proteins.** Q.J.T. Florence, B. Dillard, P. Horanyi, J.T. Swindell, H. Xu, B.C. Wang, J.P. Rose, Dept. of Biochemistry and Molecular Biology, Univ. of Georgia, Athens, GA 30602, USA.

ALR (Augmenter of Liver Regeneration) from *Rattus norvegicus* is a sulfhydryl oxidase, that catalyses the formation of disulphide bonds using molecular oxygen and releasing hydrogen peroxide as a by-product. Despite the knowledge of the reaction it catalyses, the question of why ALR performs this function has yet to be answered. In *Saccharomyces cerevisiae*, the ALR homolog Erv1 (Essential for Growth and Respiration protein 1) was recently identified as being part of the mitochondrial intermembrane space import pathway, which imports proteins synthesized in the cytosol into the mitochondria. In this pathway, Erv1 interacts with Mia40 (mitochondrial intermembrane assembly protein 40) via disulphide bridges and catalyzes the formation of disulfide bonds within the complex. After this occurs, it is postulated that the final electron acceptor is cytochrome c, which oxidizes Erv1.

With this in mind, research has been conducted investigating proteins, which will possibly interact with ALR leading to the answer of why it is necessary. ALR and Mia40 from *Rattus norvegicus* have been recombinantly expressed and isolated using various purification techniques. The question of whether ALR interacts with cytochrome c and Mia40 has been investigated using Alphascreen technology, self-interaction chromatography, and capillary electrophoresis. From these experiments the biochemical characteristics of the interactions have been identified and possible solution conditions that should favor crystallization of the complexes have been determined.

**SP179**

**Time-of-Flight Neutron Diffraction Study of Human Deoxyhemoglobin.** A.Y. Kovalevsky,<sup>a</sup> T. Chatake,<sup>b</sup> T. Ishikawa,<sup>b</sup> N. Shibayama,<sup>c</sup> S.-Y. Park,<sup>d</sup> M. Mustyakimov,<sup>a</sup> P. Langan,<sup>a</sup> Y. Morimoto,<sup>b</sup> <sup>a</sup>Bioscience Div., Los Alamos National Laboratory, Los Alamos, NM, USA; <sup>b</sup>Kyoto Univ., Research Reactor Inst., Kumatori, Osaka, Japan; <sup>c</sup>Jichi Medical Univ., Dept. of Physiology, Shimotsuke, Tochigi, Japan; <sup>d</sup>Yokohama City Univ., Graduate School of Integrated Science, Tsurumi, Yokohama, Japan.

Human hemoglobin (Hb), an  $\alpha_2\beta_2$  tetramer comprised of two identical heterodimers  $\alpha\beta$ , is an efficient oxygen transport system that allows the oxygen to be delivered to tissues throughout the human body. It exists in the low-affinity T state just before an oxygen molecule binds to its active site (heme) and is converted to the high-affinity R state once oxygenized. It is known that the binding to and release of oxygen from Hb are modulated by protons and inorganic anions. However, the X-ray analysis is largely incapable of providing details on hydrogen atom positions even when ultra-high resolution data are available. In contrast, neutrons scatter off hydrogen (deuterium) as well as off carbon, nitrogen and oxygen atoms, and therefore, can be located in structures of moderate resolution of  $\sim 2 \text{ \AA}$ . A large crystal of deoxyHb ( $\sim 12 \text{ mm}^3$ ) was grown and used for room-temperature neutron diffraction experiment at Protein Crystallography Station (PCS) of Los Alamos Neutron Scattering Center (LANSCE). A

data set was collected to 1.8 Å resolution using the time-of-flight quasi-Laue technique. The data processing, structure refinement and analysis will be discussed in conjunction with room-temperature X-ray structure.

### TP180

**Robotic Crystallization and Iterative Optimization of Precipitant Concentration.** S. Majeed<sup>1</sup>, L. Chen<sup>1</sup>, C. Hood<sup>1</sup>, G. Ofek<sup>1</sup>, K. Shakir<sup>2</sup>, T. Zhou<sup>1</sup>, G.J. Nabel<sup>1</sup>, P.D. Kwong<sup>1</sup>, <sup>1</sup>Vaccine Research Center, NIH, Bethesda MD 20892, <sup>2</sup>Formulatrix, Inc., Waltham MA 02451.

Numerous successes have been reported with robotic crystallizations that use predefined screens. Such use of predefined screens contrasts with historical methods of crystallization, which generally incorporated experimental feedback to place the protein under study close to its precipitation point, where crystallization is most likely. In this experiment, we sought to integrate robotic screening with iterative optimization of precipitant concentration. A robotic system was developed that permitted experimentally determined solubility behavior to be incorporated into tailored sparse matrices. Three commercial screens defining 160 conditions were used as a basis set of crystallization conditions. Five test proteins were analyzed, three that crystallized readily and two that crystallized less frequently. For readily crystallized proteins, a broad sampling of three or four precipitant concentrations was sufficient to elicit crystallization, and further optimization appeared to be of minimal benefit. For difficult to crystallize proteins, however, further optimization doubled the number of basis set conditions producing crystals. Thus the efficacy of precipitant optimization was found to be dependent on the frequency with which a particular protein crystallized. We applied these results to three cases that had failed to produce suitable crystals with predefined screens – the z13 antibody, the Ebola viral spike, and several HIV-1 gp120-antibody complexes. In all three cases, iterative optimization enhanced crystallization. Our robotic developments, now incorporated into RockMaker software, generate tailored precipitant-point-optimized screens, which enhance the crystallization of difficult to crystallize proteins.

### MP181

**Novel Lanthanoid Chloride – Methanol Adduct Crystals,  $\text{LnCl}_3(\text{CH}_3\text{OH})_x(\text{H}_2\text{O})_y$  as New Scintillators for Gamma-ray and Neutron Detectors.** J.O. Ramey<sup>1</sup>, B.C. Chakoumakos<sup>2</sup>, R. Custelcean<sup>3</sup>, J.A. Kolopus<sup>1</sup>, Rongying Jin<sup>1</sup>, L.A. Boatner<sup>1</sup>, John Neal<sup>1</sup>, Dariusz Wisniewski<sup>1</sup>, <sup>1</sup>Center for Radiation Detection Materials and Systems, <sup>2</sup>Neutron Scattering Science Div., <sup>3</sup>Chemical Sciences Div., Oak Ridge National Laboratory, Oak Ridge, TN 37831.

The exploration of lanthanoid chloride methanol adducts as possible scintillation materials for radiation detection has revealed at least two new families of crystal structures, one based on an edge-sharing  $\text{LnCl}_3$  dimer, e.g.,  $\text{CeCl}_3(\text{CH}_3\text{OH})_4$ , and the other based on an infinite edge-sharing chain, e.g.,  $\text{PrCl}_3(\text{CH}_3\text{OH})_2(\text{H}_2\text{O})$ . Undoubtedly, other distinct crystal structures will be found in our ongoing efforts, given the volume changes due to the lanthanide contraction and the variation in water content. Large single crystals (> several cubic cm) can be grown. In the examples realized so far, the Ln adopts eight-fold coordination in a square-prism. In particular,  $\text{CeCl}_3(\text{CH}_3\text{OH})_4$  represents the first example of a metal-organic scintillator for use in both gamma-ray and neutron detection with a light yield of over 16,000 photons/MeV, an energy resolution of ~11% at 662 keV, and a decay time of 64 nsec. We anticipate that a number of similar cerium metal organic adducts can now be synthesized and identified whose performance as a scintillator for radiation detection applications may

well exceed that of  $\text{CeCl}_3(\text{CH}_3\text{OH})_4$ .

Research supported by the DOE Office of Nonproliferation Research and Development, NA-22, in the National Nuclear Security Administration and by the Division of Materials Sciences and Engineering, Office of Basic Energy Sciences, US Department of Energy, under contract DE-AC05-00OR22725 with Oak Ridge National Laboratory, managed and operated by UT-Battelle, LLC.

### SP182

**Long Range Magnetic Cooperativity Through Extended Structural Motifs? Introducing Intermolecular  $\pi$ - $\pi$  Interactions into  $[3 \times 3] \text{Mn}^{\text{II}}$ , and  $\text{Cu}^{\text{II}}$ , Grids.** L.N. Dawe and L.K. Thompson. Dept. of Chemistry, Memorial Univ., St. John's, NL, A1B 3X7, Canada.

Previously reported tritopic bis-hydrazone ligands with terminal pyridine, pyridazine and pyrimidine groups have produced  $[3 \times 3] \text{M}_9$  grids<sup>[1]</sup> ( $\text{M} = \text{Mn}(\text{II}), \text{Cu}(\text{II}), \text{Zn}(\text{II})$ ) in high yield, that have been characterized magnetically and structurally by single crystal x-ray diffraction. The metal centers are linked by  $\mu$ -O<sub>hydrazone</sub> bridges and exhibit antiferromagnetic behavior, except for the  $\text{Cu}^{\text{II}}$  cases, which are dominated by intramolecular ferromagnetic interactions. In an attempt to organize grid molecules into extended 2D arrays, ligands with a variety of quinoline-type endpieces were synthesized. Upon self-assembly with appropriate metal salts, a regular  $[3 \times 3] \text{Mn}^{\text{II}}$  was produced, as well as a unique  $3 \times [1 \times 3] \text{Mn}^{\text{II}}$  rectangle<sup>[2]</sup> (Fig.1), and two  $[3 \times 3] \text{Cu}^{\text{II}}$  grids<sup>[3]</sup> that exhibit extended intermolecular 'face to face' and 'face to end'  $\pi$ - $\pi$  interactions. In one case, this destroys the normally observed octahedral  $\text{Cu}^{\text{II}}$  Jahn-Teller distortions, resulting in a distinctive antiferromagnetic  $[3 \times 3] \text{Cu}^{\text{II}}$  grid. The structural results of this investigation will be presented.

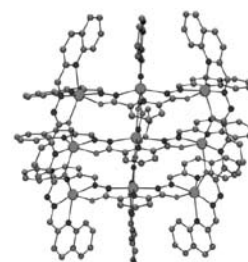


Fig. 1: A  $3 \times [1 \times 3] \text{Mn}^{\text{II}}$  rectangle

[1] Dawe, L.N. et al. *J. Mater. Chem.*, 2006, 16, 2645, and references therein.

[2] Dey, S.K., Abedin, T.S.M., Dawe, L.N., et al. *Inorg. Chem.*, 2007, 46, 7767.

[3] Dawe, L.N., Abedin, T.S.M., Thompson, L.K. *Dalton Perspective*, 2008. In press.

### TP183

**Surface Entropy Reduction Approaches to Manipulate Crystal Forms of  $\beta$ -Ketoacyl Acyl Synthase II from *Streptococcus pneumoniae*.** G. Parthasarathy, R. Cummings, J.W. Becker, S.M. Soisson, Merck Research Laboratories Rahway, NJ, USA.

We undertook a series of experiments with the  $\beta$ -ketoacyl acyl carrier protein synthase II protein (FabF) from *Streptococcus pneumoniae* (spFabF) to evaluate the capability of surface entropy reduction (SER) to manipulate protein crystallization. Previous work has shown that this protein crystallizes in two forms. The triclinic form contains four molecules in the asymmetric unit (a.u.) and diffracts to 2.1 Å resolution, while the more desirable, primitive orthorhombic form, contains one molecule in the a.u. and diffracts to 1.3 Å. We wished to evaluate the effect of SER mutations that were specifically engineered to avoid perturbing crystal packing interfaces employed by the favorable, primitive orthorhombic crystal form, while potentially disrupting a surface of the protein employed by the less desirable triclinic crystal form. Two mutant proteins were engineered, each harboring five SER mutations. Extensive crystallization screening produced crystals of each mutant, but only under conditions different from the native protein. One of the mutant proteins yielded crystals that are of a new form (centered orthorhombic), despite the fact that the interfaces employed by the primitive orthorhombic form of the native protein were specifically unaltered. Structure determination at

1.75 Å resolution reveals that one of the mutations, E383A, appears to play a key role in disfavoring the less desirable triclinic crystal form and in generating a new surface for a packing interaction that stabilizes the new crystal form.

#### MP184

**Comparative Structural Chemistry of Metal Salts of Different Isomeric Aminonaphthalenesulfonates.** Philip J. Squattrito, Dane J. Genter, Spring M. Downer, Kristin Kirschbaum, Eric J. Yearley, A. Alan Pinkerton, Dept. of Chemistry, Central Michigan Univ., Mt. Pleasant, MI, 48859 and Dept. of Chemistry, Univ. of Toledo, Toledo, OH, 43606.

This paper presents recently obtained structural results of metal salts of several isomeric amine-substituted naphthalenesulfonate anions with a view towards discerning trends in the type of layered structure observed as a function of the substitution pattern of the anion. Salts of 5-aminonaphthalene-1-sulfonate as well as the 4,1; 5,2; and 6,2 isomers have been crystallized with various divalent first row transition metals, alkaline earths and alkali metals. The structures are composed of alternating layers of metal complexes and sulfonate anions. In some cases the metal ions are coordinated directly by the amine N or sulfonate O atoms, while in others the cations are fully hydrated. In the latter cases the layers are linked by extensive networks of hydrogen bonds between the amine, sulfonate and water moieties. The anions always pack so that the amine and sulfonate groups line the surfaces of the layer where these favorable interactions can be maximized. For structures with similar metal complexation, the thickness of the anion layers (as measured by the perpendicular distance between planes of metal ions) is clearly dependent on the positioning of the functional groups on the naphthalene ring. Extra water molecules of crystallization are sometimes found in the hexaaquametal cation layers when the packing of the anions causes greater vertical or horizontal spacing of the cations. The systematic relationships among these structures will be highlighted along with unexpected coordination behaviors.

#### SP185

**The Synthesis and Structure of the Alkaline Earth Metal Salts of  $[\text{Au}(\text{SCN})_2]_2^{2-}$ .** Nathan L Coker<sup>1</sup>, A. Darren Back<sup>1</sup>, Cynthia Schroll<sup>1</sup>, Tonia L. Stroud<sup>1</sup>, Jeanette A. Krause<sup>2</sup>, <sup>1</sup>Dept. of Physical Sciences, Morehead State Univ., Morehead, KY 40351, <sup>2</sup>Dept. of Chemistry, Univ. of Cincinnati, Cincinnati, OH 45221.

Various salts of the gold complex have unexpected solid-state characteristics, namely monomeric, dimeric, and infinite polymer structures. For the tetraphenylphosphonium salt the anion is a non-emitting monomer whereas the tert-butyl-ammonium is a dimer and the alkali and ammonium salts form infinite one-dimensional polymers. The shift in the emission is directly influenced by the distance of the Au-Au interaction. In this work, the synthesis of the  $\{\text{Ba}[\text{Au}(\text{SCN})_2]_2\}_n$  and 18-crown-6- $\{\text{Ba}[\text{Au}(\text{SCN})_2]_2\}$  will be described and the 3-dimensional structure presented.

#### TP186

**In Vacuum and Thermal Flow-cells for Biological SAXS/WAXS at DND-CAT, 5ID-D.** Steven Weigand<sup>1</sup>, Benjamin Stillwell<sup>1</sup>, J. David Londono<sup>2</sup>, William E. Guise<sup>2</sup>, Denis T. Keane<sup>1</sup>, <sup>1</sup>DND-CAT Synchrotron Research Center, Northwestern Univ., <sup>2</sup>E.I. duPont de Nemours & Co., Wilmington, DE 19880.

The DuPont-Northwestern-Dow Collaborative Access Team (DND-CAT), has long been focused on studying industrial polymers by

simultaneous small and wide angle scattering (SAXS and WAXS). Recently the techniques supported at 5ID-D have been broadened to include capillary flow-cells for the collection of solution scattering (e.g. nano-particle suspensions or biological macromolecules).

The sample environment and detector configuration is well suited for studying the low resolution structure of biological macromolecules and complexes in solution. Over two continuous decades of momentum transfer vectors ( $q = 0.006\text{\AA}^{-1}$  to  $2\text{\AA}^{-1}$  at  $\lambda = 1.2\text{\AA}$ ) can be observed with some overlap between the two detectors. A temperature controlled automated sample changer and wash system allows several samples or a concentration series to be run without entering the 5ID-D enclosure. We have collected good data on as little as  $100\mu\text{l}$  of a  $1\text{mg/ml}$  protein sample.

#### MP187

**Present Status and Future Plan of Structural Biology Beamlines at SPring-8.** T. Kumasaka,<sup>1</sup> K. Hirata,<sup>2</sup> N. Shimizu<sup>1</sup>, M. Kawamoto,<sup>1</sup> K. Hasegawa,<sup>1</sup> S. Baba,<sup>1</sup> N. Okazaki,<sup>1</sup> A.-H. Teh,<sup>1</sup> G. Ueno,<sup>2</sup> T. Hikima,<sup>2</sup> A. Nisawa,<sup>2</sup> T. Shimizu,<sup>2</sup> M. Yamamoto,<sup>1,2</sup> <sup>1</sup>JASRI/SPring-8, <sup>2</sup>RIKEN SPring-8 Center, Hyogo 679-5198 Japan.

BL41XU produces a highest brilliant X-ray for protein crystallography at SPring-8 for obtaining high quality data from protein microcrystals ( $\sim 25\mu\text{m}$ ) using a microbeam ( $\sim 25\mu\text{m}$ ). The minimum beam size at sample position is  $25 \times 25\mu\text{m}^2$  by using K/B mirror system and the two sets of a quadrant slit. Photon flux and flux density of the  $25 \times 25\mu\text{m}^2$  beam at  $1\text{\AA}$  are  $3.0 \times 10^{11}$  photons/sec and  $4.8 \times 10^{14}$  photons/sec/mm<sup>2</sup>, respectively. To suppress the effect of radiation damage by the bright beam, several built-in functions are added to our data collection software BSS.

For routine data collection, "Mail-in data collection system" has been developed at bending magnet beamlines, BL26B1/B2 and BL38B1. It makes possible that distant users collect diffraction data without visiting SPring-8. The users only send samples to SPring-8 via courier service and can request measurement conditions and check results at their laboratory on the Web. The data collection for the samples is carried out with the automated beamline operation system using BSS and sample auto-changer SPACE. Smooth communication with the users is achieved by the data management system D-Cha. D-Cha provides GUI to deposit the experimental conditions for samples and to browse / download the collected data on web browser.

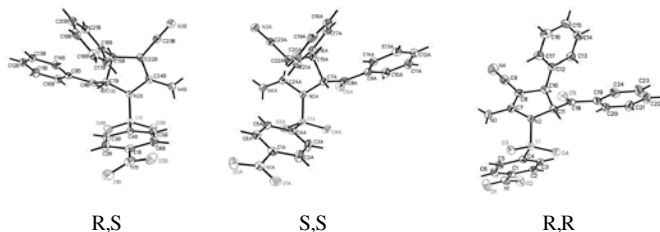
We are now constructing a new microbeam beamline BL32XU, where an in-vacuum undulator and a K/B mirror system will be installed. The flux density of the beam will reach  $10^{16}$  photons/sec/mm<sup>2</sup> at the wavelength of  $1\text{\AA}$  and minimum beamsizes will be expected to  $2 \times 1\mu\text{m}$  by a ray-trace calculation. This beamline will be opened from the spring of 2010 and adapted to microcrystals and multicroystal clusters.

#### SP188

**Crystal Structure of a Cis and Trans Isomers of a 2-Pyrroline Derivative and their Anti-cancer Properties.** Paul Tongwa,<sup>c</sup> Igor V. Magedov,<sup>a</sup> Giovanni Luchetti,<sup>a</sup> Artem S. Kireev,<sup>a</sup> Madhuri Manpadi,<sup>a</sup> Wim F. A. Steelant,<sup>a</sup> Severine van Slambrouck,<sup>a</sup> Mikhail Yu Antipin,<sup>c</sup> Tatiana V. Timofeeva<sup>c</sup> Alexander Kornienko,<sup>a</sup> <sup>a</sup>Dept. of Chemistry, NMTECH, Socorro, NM, 87701, <sup>c</sup>Dept. of Natural Sciences, NMHU, Las Vegas, NM 87701.

A novel multicomponent synthesis involving a reaction of various N-aryl- and N-alkylsulfonamido acetophenones with aldehydes and malononitrile has been used to obtain a variety of substituted 2-pyrrolines which are useful pharmaceutical agents. Reaction

products from multicomponent synthesis have been separated by crystallization from different solvents. It was found that synthesis gives a mixture of cis- and trans-products. The cis-isomer has a centro-symmetric space group of  $P21/n$ ,  $Z=4$ , while the trans-isomer has an acentric space group  $P21$ ,  $Z=8$  with four molecules in asymmetric unit. Molecules of the cis-product have an R,S-configuration of two chiral centers in pyrroline ring. In trans-product, all four molecules differ by orientation of substituents and two molecules out of four have R,R- and another two S,S-configuration of the chiral centers. Superposition of molecules of trans-product revealed that conformational differences are not very significant and that inverted R,R-form has molecular conformation close to S,S-



form. However, search for additional symmetry elements connecting all four molecules in crystal gave negative results. It gives us reason to suggest that in spite of acentric space group of trans-product, it is effectively a racemic mixture of two forms. Results of testing of cytotoxicity against cancer cells of these and similar materials will be discussed in connection with their molecular structure.

#### TP189

**Behaviour of Succinonitrile-Based Lithium Battery Solid Electrolytes under Non-Ambient Conditions.** P.S. Whitfield, A. Abouimrane, I.J. Davidson, Inst. for Chemical Process and Environmental Technology, National Research Council Canada, 1200 Montreal Rd., Ottawa, Ontario, K1A 0R6, CANADA.

The safety of lithium-ion batteries has recently been the subject of much interest due to a number of fires and recalls by battery manufacturers. Although an appropriate choice of electrode materials can improve the safety of battery systems, the use of a flammable and corrosive organic electrolyte will always be a concern. The development of a solid, non-flammable electrolyte for lithium-ion cells has been a goal for many years. Solid electrolytes based on succinonitrile have been found to possess ionic conductivities comparable to liquid electrolytes ( $10^{-3} \text{ Scm}^{-1}$ ) at room temperature.

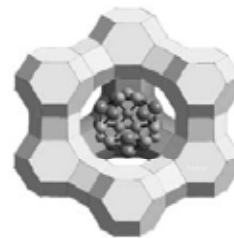
Previous studies have determined that solid crystalline adducts may be formed in succinonitrile-salt systems, which adversely affects the conductivity of the electrolyte. Compositions with lithium tetrafluoroborate and lithium bis(trifluoromethane) sulfonyl imide salts were studied to examine their phase behaviour within the temperature range of practical interest. The materials are extremely hygroscopic so were sealed in glass capillaries. The temperature of the capillary was controlled using a custom-built nitrogen gas-flow system. Correlations between the XRD and thermal analysis results provide insights into the differing performance of the various compositions. The best performing electrolyte composition at low temperature was found to possess a 'crystallinity-gap' where steric effects appear to poison crystallization even at low temperatures.

#### MP190

**Synchrotron X-ray Scattering Studies of Semiconductor Nanoclusters in Zeolites.** A.M.M. Abeykoon, S.C. Moss, W. Donner, Dept. of Physics, Univ. of Houston, M. Castro-Colin, Dept. of Physics Univ. of Texas at El Paso, E.A. Anokhina, A.J. Jacobson,

Dept. of Chemistry, Univ. of Houston.

When electrons and holes in a semiconductor are confined to ultra-small regions of space (typically 1-25 nm), the optical and electronic properties become strongly size-dependent. Such structures are called quantum dots, nanowires or nanoclusters, depending upon their shape and dimensionality. These nanostructures are of great interest for a variety of potential electronic, photochemical and nonlinear optical applications and are necessary for an analysis of the transition from molecular to bulk semiconductor properties. This talk will discuss the structure of HgSe and Se semiconductor nanoclusters encapsulated in both Nd-Y (spherical pore) and LTL (tubular pore) zeolites. The molecular structure of these systems was modeled by performing a Rietveld refinement on X-ray Bragg data. A remarkable feature in our X-ray diffraction patterns, continuous diffuse scattering under the Bragg peaks, will also be discussed along with forthcoming PDF results. We use the results of optical studies to complement our X-ray structural work.



#### SP191

**Are X-rays Damaging to Structural Biology? A Case Study with Xylose Isomerase.** Kristin Wunsch<sup>1</sup>, Mark van der Woerd<sup>2</sup>, Edward Snell<sup>1,3</sup>, <sup>1</sup>Hauptman-Woodward Medical Research Inst., 700 Ellicott St., Buffalo NY 14203, <sup>2</sup>Dept. of Biochemistry and Molecular Biology, Colorado State Univ., 1385 Centre Ave., Fort Collins, CO 80523, <sup>3</sup>Dept. of Structural Biology, SUNY Buffalo, 700 Ellicott St., Buffalo NY 14203.

Structural crystallography is a powerful technique for visualizing a macromolecule at atomic resolution. The resulting models are used to improve our understanding of macromolecule function. As more intense X-ray sources become available the amount of detail that can be seen increases. However, X-rays themselves cause detrimental physical effects on the sample through primary and secondary radiation damage. This can be mitigated, but not eliminated through cryocooling. In a case study with xylose isomerase, we demonstrate that high-resolution data can sometimes provide misleading results due to photo-induced structural changes. Crystals of xylose isomerase diffract to very high resolution, 0.87 Å and provide high-quality electron density maps. However, if we collect multiple, identical data sets sequentially with a lower individual X-ray dose, we see the progressive formation of alternative metal sites in the xylose isomerase enzyme and a variation in their occupancy as a function of the cumulative dose. The structure changes progressively during collection of the data sets and ultimately resembles the structure seen in the high-resolution data set, obtained at a corresponding cumulative dose. Some of the features in the high-resolution maps are actually dose-dependent artifacts of the exposure to X-rays used to reveal those features. Our model and therefore understanding of function is altered by the very method we use to obtain it. X-rays can be damaging to structural crystallography, just how damaging we do not yet know.

#### TP192

**Validation of UO<sub>2</sub> Defect Models by X-Ray Diffraction for Future Minor Actinide MOX Fuel Development.** H.M. Volz, C.R. Stanek, E.P. Luther, J.T. Dunwoody, K.J. McClellan, S.L. Voit, Los Alamos National Laboratory, Los Alamos, NM, 87545 USA.

As part of the Global Nuclear Energy Partnership Program (GNEP), research is being conducted on actinide-bearing fuels

for transmutation in a fast reactor. In particular, a series of small-scale fabrication and irradiation tests are being performed on minor actinide MOX fuels. Model development and validation has begun with UO<sub>2</sub> and will be extended to include transuranics in the future. Lanthanides are known to be carried through the electrochemical separations stream and their presence affects final oxide fuel specifications (density, stoichiometry, etc.). Moreover, changes in the lattice parameter due to lanthanide impurities in the UO<sub>2</sub> crystal structure may cause cracking during the sintering process. To understand and prevent this behavior, atomic scale modeling is being undertaken as part of process development. Atomistic simulations of various defect mechanisms in UO<sub>2</sub> have been performed, and show differences in expected lattice parameter variations with lanthanide concentration. Samples were prepared with various lanthanides in differing concentrations to validate these models with experimental data. Sealed tube X-ray powder diffraction data were collected, and full pattern Rietveld refinements with GSAS were performed. Results of these studies will be discussed, along with the implications of the defect modeling on the dominant solution mechanisms operating in the Ln:UO<sub>2</sub> system.

### SP193

**Modeling the Pre-nucleation Stage of a Solid-state Reaction.** Ivan Halasz, Ernest Meštrović, Hrvoj Vančik, Univ. of Zagreb, Dept. of Chemistry, Horvatovac 102a, 10000 Zagreb, Croatia.

Solid-state reactions have often been described in terms of crystal structures of reactant and product solid phases without structural insight into possible intermediate phases and the time evolution of the system. Time-resolved X-ray diffraction experiments have recently been used to characterize intermediate phases. In this contribution, we analyze the homogenous part of solid-state dimerization of *p*-bromonitrosobenzene to the corresponding azodioxibenzenes. We demonstrated that the nucleation and growth of the daughter phase is not concomitant with formation of the dimer molecules. In particular, the formation of the new phase is only observed after the chemical reaction has advanced to a small degree. In that way, the initial product of the reaction is a solid solution of dimeric molecules in the monomer crystal lattice. The observed reaction mechanism can be interpreted in context of favorable orientation of monomer molecules for the dimerisation reaction. Solid solution formation was studied in a time-resolved X-ray diffraction experiment on single crystals of the monomer. The time-dependent changes in X-ray reflection intensities were qualitatively reproduced by introducing translation and rotation on molecules within a model single crystal composed of 10×10×10 unit cells. The results, accompanied by DISCUS calculations, allow the description of structural changes in the parent crystal.

### TP194

**The Design of a Home Lab Beamline for Screening and Analysis of Microcrystals.** Daniel C. Franke, Bruker AXS, Inc., Frank von Delft, SGC Oxford.

Until recently, the major drawbacks towards getting useful diffraction data on a home source from microcrystals included insufficient X-ray brilliance and non ideal detectors causing people to have to go to the Synchrotron and wasting valuable synchrotron time on screening experiments. Advances in high brilliance sources and photon counting area detectors led us to investigate pushing the boundaries of traditional data collection to achieve useful data from extremely small crystals.

In this submission we will discuss a some of the considerations we have had to incorporate into the design of a system optimized for

microcrystalline protein samples; Generation of small (yet intense) positionally stable beams, new alignment procedures for ensuring beam location at the sample, selection of the ideal detector for the application and even an upgrade to the optical microscope to achieve higher resolutions and zooms so these crystals can be seen.

The resulting properties of the system are a beam that the user can select the size and divergence (at the sample position). The applications of such a system extend beyond just microcrystalline samples. We will be investigating crystals of varying sizes as well as studying different crystalline regions within the same crystal.

### SP195

**Temperature-Dependent X-Ray Scattering Studies of Spin Crossover Materials.** G.J. Halder, K.W. Chapman, P.J. Chupas, Materials and X-ray Science Divisions, Argonne National Laboratory, IL 60439, USA.

Spin crossover materials present a novel type of molecular switch that can exist in two different electronic states (high-spin or low-spin) with marked differences in geometry, magnetism and color. The potential bistability of their switching behavior has led to their development toward display and memory devices. More recently, the incorporation of guest-dependent spin crossover behavior into porous coordination networks (or metal-organic frameworks) has generated materials suitable for molecular sensing applications. Spin transitions are most commonly investigated magnetically, but temperature-dependent X-ray scattering techniques offer a wealth of complimentary structural details, such as the identification of phase transitions, and changes in lattice parameters and bond lengths. Here, we present variable temperature synchrotron powder diffraction and pair distribution function analyses of a selection of spin crossover materials.

### TP196

**Structure Determination of Multi-Component Systems from Pair Distribution Function.** Pavol Juhas, Phillip M. Duxbury, Simon J.L. Billinge, Physics and Astronomy, Michigan State Univ., East Lansing, MI.

The analysis of the atomic Pair Distribution Function (PDF) makes no requirement on perfect crystalline order in the material and as such it has become an essential tool for studying local deviations from the ideal crystal structure. However, it is not simple to obtain a complete structure image from the PDF data, and a typical data processing consists of tedious trial-and-error checking of a series of structure models. Our previous work [1] described a different way of extracting structure from PDF, where a structure of single-element molecule could be solved *ab-initio* from PDF data alone. We will demonstrate the extension of *ab-initio* PDF method to general, multi-component molecules and to periodic systems with large supercells.

[1] P. Juhas, D. M. Cherba, P. M. Duxbury, W. F. Punch, S.J.L. Billinge, *Ab initio* determination of solid-state nanostructure, Nature 440, 655-658 (2006).

### SP197

**High-pressure Crystallography of R-3c Rhombohedral Perovskites.** Jing Zhao<sup>1</sup>, Nancy L. Ross<sup>1</sup>, Ross J. Angel<sup>1</sup>, Serena C Tarantino<sup>2</sup>, Michael A. Carpenter<sup>3</sup>, <sup>1</sup>Virginia Tech Crystallography Laboratory, Virginia Tech, Blacksburg VA 24060, <sup>2</sup>Dip. di Scienze della Terra, Univ. Pavia, I-27100 Pavia, Italy, <sup>3</sup>Dept. of Earth Sciences, Univ. of Cambridge, England.

High-pressure crystallography, the evolution of crystal structure with pressure, provides very important information for understanding fundamental interactions between atoms or ions. It has been

demonstrated that the structural variation of *R-3c* rhombohedral perovskites under pressure can be generally described by the rotation angle of  $\text{BO}_6$  octahedra about the threefold axis, and that the octahedral rotation is controlled by the compressibility difference between the  $\text{BO}_6$  octahedra and  $\text{AO}_{12}$  polyhedra [1]. The rotation angle, as the order parameter of a generalized mean-field approach, may decrease with pressure and a continuous transition then happens from a rhombohedral to a cubic structure, e.g.  $\text{LaAlO}_3$  at 14 GPa [2]. However, a powder XRD study suggested that pressure induces a first-order phase transition from *R-3c* to *Imma* in  $\text{PrAlO}_3$  perovskite [3], which is different from the second-order phase transition of  $\text{LaAlO}_3$ . The question therefore arises; "is  $\text{PrAlO}_3$  an exception that shows a discontinuous transition in *R-3c* perovskites?" In this contribution, we report a structural study of  $\text{PrAlO}_3$  by high-resolution single-crystal XRD. Its high-pressure behavior is compared with other *R-3c* rhombohedral perovskites on the basis of the coupling relation between the octahedral  $\text{BO}_6$  and polyhedral  $\text{AO}_{12}$  groups.

[1] J. Zhao et al., *J. Phys: Cond. Matt.* 2004, 16, 8763.

[2] P. Bouvier and Kreisel J., *J. Phys: Cond. Matt.* 2002, 14, 3405.

[3] B. Kennedy et al., *Chem.Mater.*2002, 14, 2644.

### TP198

**Total X-ray Scattering from Dynamic, Biological Crystals.** Demian Riccardi, Dept. of Biochemistry, Qiang Cui, Dept. of Chemistry & Theoretical Chemistry Inst., George N. Phillips, Jr., Depts. Biochemistry & Computer Science, Univ. of Wisconsin, Madison, 433 Babcock Dr., Madison, WI 53706.

Biomolecular structures determined by typical X-ray crystallography experiments result in models that best reproduce the sharp Bragg intensities. These models correspond to the average electron density of the unit cell convoluted with the crystal lattice and are improved when the effects of atomic variations on the Bragg intensities are taken into account, via occupancies and temperature factors that correspond to uncorrelated motions. While this approach has been very successful, insights into the ensemble of states available to the crystal and dynamic transitions between these states are lost. Fortunately, much of this information can be regained by studying the diffuse scattering throughout reciprocal space that is due to symmetry-breaking, correlated motions within the crystal. Crystal motions ranging from uncorrelated, random atomic displacements to collective lattice vibrations yield distinct diffuse scattering patterns. In this study, the total X-ray scatter from several biological molecules is investigated where correlated motions are computed with an elastic network model. The effects of treating crystal environment explicitly are highlighted.

This work is funded by the NLM Grant 5T15LM007359.

### SP199

**Molecular Basis for Actin Reorganization by the Neuronal Protein SPAR.** B.L. Brown<sup>1</sup>, R. Page<sup>2</sup>, <sup>1</sup>Molecular Pharmacology, Physiology and Biotechnology, <sup>2</sup>Molecular Biology, Cell Biology and Biochemistry, Brown Univ., Providence, RI 02912 USA.

In the central nervous system, excitatory synaptic transmission primarily occurs at dendritic spines, small protrusions located on dendrites. Dysregulation of spine structure and motility has been implicated in a variety of pathologies including Down Syndrome, schizophrenia and drug addiction. Spine-associated RapGAP (SPAR) is a multidomain scaffolding protein that is enriched in mature dendritic spines and regulates spine dynamics and morphology through its interactions with the actin cytoskeleton and the small GTPase Rap2. Our aim is to use X-ray crystallography combined with

biochemical studies to determine the molecular basis by which SPAR mediates changes in spine structure through its interactions with its multiple effector proteins. To this end, individual SPAR domains are being expressed, purified, and characterized separately to determine the role each region plays in actin regulation. We have produced soluble mg quantities of the SPAR PDZ domain which is stable for up to 6 months at 4°C. Using NMR spectroscopy, we determined that the SPAR PDZ domain interacts with a Kalirin-7 C-terminal peptide, suggesting that it is a Class I PDZ domain. We have also produced soluble and well-folded amounts of the SPAR minimal interaction RapGAP domain. In conjunction, we have purified the GTPase Rap2 in order to characterize the interaction between the RapGAP domain and Rap2. These studies investigating SPAR structure and function will lay the groundwork for the development of novel therapies to treat diseases caused by abnormal spine structure and motility. This work was supported by the Rhode Island Foundation Medical Research Grant, #20050240 to RP and a Pharmacia Fellowship to BB.

### MP200

**Temperature and Vibration: Probing the Impact of a Cold-stream on Protein Crystallography Data Collection.** R. W. Alkire, N.E.C. Duke, F.J. Rotella, Structural Biology Center, Biosciences Division, Advanced Photon Source, Argonne National Laboratory, Argonne, IL 60439 USA.

Protein crystallography at a synchrotron source is rarely done without the aid of a low temperature device. While most of us take for granted that a cold-stream is there simply to provide a low temperature environment, the specifics are much more complex. Using an Oxford Cryostream 600 at 5l/s and 100K, we first mapped the temperature profile via a thermocouple mounted at the sample position. Using a silicon single crystal mounted in a loop, we looked at the reflection characteristics of a single reflection as a function of cold-stream position. With a sufficiently sensitive probe, this provides a comprehensive map of turbulence within the cold-stream. To complete the measurements, lysozyme data were collected at specific points in the cold-stream profile so that a complete crystallographic comparison could be made. While not every sample is susceptible to motion, knowledge of where turbulence occurs and how it impacts data collection can be useful knowledge to possess. As a by product of this work, we will also make some specific suggestions about different types of loops and how to minimize vibration.

This work was supported by the U. S. Department of Energy, Office of Biological and Environmental Research and Office of Basic Energy Sciences, under Contract DE-AC02-06CH11357.

### SP201

**Neutron Scattering Study of a Four-Leg Antiferromagnetic Heisenberg Spin Tube.** V.O. Garlea, A. Zheludev, L.-P. Regnault, J.-H. Chung, Y. Qiu, M. Boehm, K. Habicht, M. Meissner, E. Ressouche, B. Grenier, Oak Ridge National Lab, Oak Ridge, TN.

We report the results of elastic and inelastic neutron scattering studies carried out on the quasi-one-dimensional quantum spin-liquid system  $\text{Cu}_2\text{Cl}_4 \cdot \text{D}_8\text{C}_4\text{SO}_2$  (Sul- $\text{Cu}_2\text{Cl}_4$ ).

We show that, contrary to previously proposed models that relied on bond-alternating nearest neighbor interactions, the dominant interactions are actually next-nearest-neighbor couplings. The key magnetic interactions are established by superexchange across two-chlorine bridges, leading to the formation of uniform 4-leg spin tubes<sup>1</sup>. A partial geometric frustration of rung interactions induces a small incommensurability of short-range spin correlations. Neutron diffraction measurements carried out in the presence of a

magnetic field have shown that at a critical field ( $H_c \sim 4$  T),  $\text{Sul-Cu}_2\text{Cl}_4$  goes through a field-induced antiferromagnetic order with an incommensurate propagation vector.

<sup>1</sup>V. O. Garlea et al.: arXiv:0710.0891, Phys. Rev. Lett. -in press..

### MP202

**New Macromolecular Crystallography Beam Line Facilities at the Stanford Synchrotron Radiation Laboratory.** Herb Axelrod, Clyde Smith, Stanford Synchrotron Radiation Laboratory, Stanford Linear Accelerator Center, Menlo Park, CA 94025.

The Macromolecular Crystallography Group at the Stanford Synchrotron Radiation Laboratory operates several state-of-the-art beam lines. Four beam lines are currently open to users (BL9-2, BL9-1, BL11-1 and BL7-1). A new beam line, BL12-2, is being commissioned during 2008.

This beam line has an undulator source and will provide a microfocus beam. All the beam lines are equipped with an automated sample mounting system; in addition to SSRL cassettes, ALS-style pucks can also be used with this system. High throughput screening, automated data collection, autoindexing and strategy calculation are available via Blu-Ice and Web-Ice. Remote access to the beam lines is available and routinely used by many user groups.

### SP203

**Microwave Assisted Polymorph Selection in Pharmaceutical Drugs.** Jason R. Cox, Venkat Thalladi, Dept. of Chemistry and Biochemistry, Worcester Polytechnic Inst., 60 Prescott St. Worcester, MA 01606 USA.

Microwave assisted chemical processes – from organic synthesis to the fabrication of nanomaterials – have attracted much interest owing to the unique heating properties associated with microwave irradiation. Microwave heating is selective (for polar species), rapid, and volumetric. In this work we describe the use of microwave heating in the crystallization of some pharmaceutical drugs. We show that highly supersaturated solutions of acetaminophen, piracetam and other drugs can be readily obtained by rapid overheating under microwave irradiation. From these solutions, it is possible to obtain metastable polymorphs in quantitative yield and high purity. In multimorphic systems, it is also possible to grow different polymorphs by seeding. We present the hypotheses behind our new approach, experimental protocols, rationalization of results, and applications of this research.

### MP204

**BioCARS: A State-of-the-art Facility for Time-resolved Crystallography with 100ps Time Resolution.** R.W. Henning, T. Graber, V. Srajer, Y. Chen, Z. Ren, F. Schotte<sup>1</sup>, P. Anfinrud<sup>1</sup>, K. Moffat, Center for Advanced Radiation Sources, Univ. of Chicago, Chicago, IL 60637, <sup>1</sup>Nat'l Institutes of Health, Bethesda, MD 20892.

BioCARS, a national facility located at the Advanced Photon Source (APS), has a long history in conducting time-resolved Laue crystallography research with ns time resolution (user experiments since 2000). We have recently upgraded the undulator beamline (14-ID) to become one of the best facilities in the world for conducting experiments with 100ps time resolution. Improvements in both the x-ray and laser capabilities were required in order to extend experiments into the sub-ns time domain. The more intense and strongly focused x-ray beam was achieved by using a KB mirror pair

(Oxford/SESO) which provides a focal spot size of  $35 \times 90 \mu\text{m}^2$  (V x H). Additional intensity was obtained by using dual in-line undulators (U23 & U27). The high heat loads that can be achieved with this configuration required the development of a new water-cooled heat-load chopper. The continuously rotating, air-bearing based chopper intercepts the white beam upstream of the mirrors and reduces the heat load on the downstream components by ~99%. BioCARS ultra-fast rotating chopper (Julich) used for selection of X-ray pulses was modified so individual x-ray pulses (100 ps) could be isolated in the standard operating mode of the APS (24 bunch). This expands the experimental beamtime for time-resolved experiments to almost the entire APS run cycle. A new Spectra Physics picosecond laser system and beam transport optics have been installed and can deliver ~35ps tunable laser pulses to the sample position. Preliminary time-resolved experiments have demonstrated that a time-resolved signal can be detected in the picosecond time range.

### SP205

**Multicomponent Organic and Pharmaceutical Solid Solutions.** Marta Dabros, Venkat Thalladi, Dept. of Chemistry and Biochemistry, Worcester Polytechnic Inst., 60 Prescott St., Worcester, MA 01605.

Multicomponent organic alloys can be viewed as materials that exhibit new or superior functions relative to the individual components. Traditionally, organic alloys are formed by molecules of similar shapes and sizes. Creation of an alloy of an arbitrary organic compound is extremely difficult because most organic molecules possess intricate shapes and participate in directional intermolecular interactions. In this presentation, we illustrate a generic supramolecular approach that allows the creation of alloys of organic and pharmaceutical compounds (irrespective of their size and shape and other characteristics) that are capable of forming hydrogen bonds. Four different types of supramolecular synthons, hydroxy-pyridyl, hydroxy-amino, carboxy-amido, and carboxy-aminopyridyl are shown to form the solid solutions. Bimolecular and trimolecular assemblies are used as templates for the creation of these unique alloys. The components in these alloys range from halogenated and methylated benzoic acids, phenols, and anilines to nonaromatic cyclic diazines. The principal advantage of solid solutions is that their properties can be modulated by the gradual modification of the relative ratio of the components.

### TP206

**Time-resolved Macromolecular Crystallography at BioCARS, Sector 14, Advanced Photon Source.** V. Srajer<sup>1</sup>, T. Graber<sup>1</sup>, R. Henning<sup>1</sup>, S. Ruan<sup>1</sup>, Z. Ren<sup>1</sup>, Y.-S. Chen<sup>1</sup>, K. Moffat<sup>1</sup>, P. Anfinrud<sup>2</sup>, F. Schotte<sup>2</sup>, W. E. Royer<sup>3</sup>, J. Knapp<sup>4</sup>, <sup>1</sup>Center for Advanced Radiation Sources, Univ. of Chicago, Chicago IL, <sup>2</sup>NIDDK/NIH, Bethesda MD, <sup>3</sup>Univ. of Massachusetts Medical School, Worcester MA; <sup>4</sup>Univ. of Texas Medical Branch, Galveston, TX.

Time-resolved crystallography is the main core research activity at the BioCARS facility, sector 14, APS. The facility is funded by NCCR/NIH. The goal of time-resolved studies is to visualize structures of transient intermediates in biological molecules by taking X-ray snapshots of molecules in the crystal as they perform their function at room temperature. These studies provide direct information at the structural level and with atomic resolution about molecules in action, as in photocycles, signal transduction, ligand migration and docking, or protein relaxation following a trigger event. During the last ten years, the time-resolved crystallography evolved from pioneering efforts to a well established technique as it has been successfully demonstrated that small structural changes can be detected with ns and sub-ns time

resolution<sup>[1-9]</sup> and that 4D time-resolved crystallographic data can be analyzed by methods such as Singular Value Decomposition to determine the structures of intermediates and elucidate the reaction mechanism<sup>[3-4]</sup>. Recent upgrades of the 14-ID beamline and the laser facility will substantially improve the ability to conduct time-resolved experiments at the BioCARS facility. Examples of most recent time-resolved crystallographic studies conducted at BioCARS will also be presented.

[1] Schmidt *et al.* *PNAS* **102** 11704 (2005); [2] Ihee *et al.* *PNAS* **102** 7145 (2005); [3] Rajagopal *et al.* *Structure* **13**, 55 (2005); [4] Schmidt *et al.* *PNAS* **101**, 4799 (2004); [5] Schotte *et al.* *Science* **300**, 1944 (2003); [6] Bourgeois *et al.* *PNAS* **103**, 4924 (2006); [7] Srajer *et al.* *Biochemistry* **40**, 13802 (2001); [8] Knapp *et al.* *PNAS* **103**, 7649 (2006); [9] Key *et al.*, *Biochemistry* **46**, 4706 (2007).

### SP207

**Characterization of Polymorphic Compounds.** Ilana Goldberg, Jennifer Swift, Dept. of Chemistry, Georgetown Univ., 37<sup>th</sup> and O Streets NW, Washington, DC 20057.

There are wide varieties of polymorphic compounds; including biological macromolecules, pharmaceuticals, and many other small molecules. In this study, different polymorphic materials are characterized in order to understand their different crystal forms and to determine how one form might be selectively grown over another. One approach to controlling polymorphism at the nucleation stage is to crystallize these compounds in the presence of a rationally designed 2D template. 2D self-assembled gold-thiol monolayers (SAMs) have been shown to control the growth orientation of several small molecule compounds. In addition, they have the demonstrated ability to selectively reduce the number of polymorphic phases obtained and to promote the growth of previously unknown phases. The goal of the present work is to expand the range of compounds to include polymorphic macromolecules and high energy compounds. The application of both traditional (X-ray, Raman, etc.) and less traditional (Hirschfeld surfaces, X-ray topography, etc.) analytical methods to these polymorphic systems will be discussed.

### MP208

**Enhanced Micro-Diffraction Capabilities at GM/CA CAT.** V. Nagarajan, M. Hilgart, S. Pothineni, S. Xu, S. Stepanov, M. Becker, O. Makarov, N. Sanishvilli, C. Ogata, R.F. Fischetti, Biosciences Div., Argonne National Laboratory, Argonne, 60439.

Last year we presented our “mini-beam” capability whereby a beam as small as 5 microns allowed micro-diffraction experiments. This was achieved by combining focusing optics and a small aperture placed 30 mm before the sample position resulting in a beam with Gaussian cross section and low divergence. A number of groups have utilized this capability to successfully solve structures that would have otherwise not been possible. The demand for this capability has been increasing rapidly. To satisfy the experimental requirements of our users, several enhancements outlined below are being developed.

Many users desire the ability to switch back and forth between “full beam” and “mini-beam” depending on the size and nature of their crystals. We have designed and implemented a versatile system that allows the whole process to be completed in 15 min.

Refraction effects greatly hamper the ability to locate micro-crystals in loops and precisely center them at the intersection of the rotation axis and the X-ray beam. We have developed an automated rastering procedure that records diffraction patterns over a user-defined region of the sample in a two-dimension grid. A figure of merit is generated for each diffraction pattern indicating the best position to collect data.

A similar procedure has been developed using X-ray fluorescence.

Many crystals are radiation sensitive and decay rapidly in the X-ray beam. Walking along the crystal and collecting a few frames at each position is the only viable option to collect a complete data set. We are developing a procedure that would automatically collect a set of frames and translate along the crystal once the extents of the crystal are defined.

### SP209

**Monitoring the Dehydration of Uric Acid Dihydrate by PXRD and Thermal Methods.** Amanuel Z. Zellelow, Kun-Hae Kim, Ryan E. Sours, Jennifer A. Swift, Dept. of Chemistry, Georgetown Univ., 37<sup>th</sup> and “O” Sts. NW, Washington, D.C. 20057.

Uric acid is the most abundant crystalline organic component found in human kidney stones. Several different phases have been identified in physiological systems including anhydrous uric acid (UA), uric acid dihydrate (UAD), uric acid monohydrate, as well as assorted salts of the ionized form, urate. The UAD phase is less stable than the UA, and can undergo an irreversible dehydration both in air and in solution. The mechanism and kinetics of this dehydration process in air are analyzed through a combination of techniques including powder X-ray diffraction (PXRD), hot-stage light microscopy, differential scanning calorimetry (DSC), and thermogravimetric analysis (TGA). The influence of crystal size, shape, and impurity inclusion (dyes and small cations) as well as humidity in the dehydration process will be discussed.

### TP210

**Tobacco Mosaic Virus Assembly of Fibrous and Macroscopic Bundled Arrays Mediated by Surface Aniline Polymerization.** S.V. Pingali<sup>1</sup>, Z. Niu<sup>3</sup>, M.A. Bruckman<sup>3</sup>, S. Li<sup>3</sup>, L.A. Lee<sup>3</sup>, B. Lee<sup>2</sup>, Q. Wang<sup>3</sup>, P. Thiyagarajan<sup>1</sup>, <sup>1</sup>IPNS, <sup>2</sup>APS, Argonne National Lab, Argonne, IL, <sup>3</sup>Univ. of South Carolina, Columbia, SC.

One-dimensional (1D) polyaniline/tobacco mosaic virus (TMV) composite nanofibers were synthesized by the self-assembly of rod like TMV particles assisted by the polymerization of aniline on its surface. At near-neutral reaction pH (6.0 – 8.0), branched polyaniline formed on the surface of TMV prevented lateral association and therefore long 1D nanofibers were observed with high aspect ratios and excellent processibility. At a lower pH (4.0-5.0), transmission electron microscopy (TEM) analysis revealed that initially long nanofibers were formed and upon long reaction time resulted in bundled structures. This association of single nanofibers to form bundled structures is presumably mediated by the hydrophobic interaction of polyaniline on the surface of these composite nanofibers. In-situ time-resolved small-angle X-ray scattering study on the formation of polyaniline/TMV composite nanofibers at different reaction pH conditions (4.0, 5.0, 6.0 and 8.0) supported our mechanism. The polyaniline layer formed on the external surface of TMV is thicker for reaction at pH 4.0 than for reaction at pH 8.0. This novel strategy to assemble TMV into well-organized composites could be utilized in the fabrication of advanced materials for potential applications including electronics, optics, sensing, and biomedical engineering.

Work benefited from the use of IPNS and APS funded by DOE, BES under contract DE-AC02-06CH11357 to the UChicago Argonne, LLC and funding from U.S. ARO-MURI program, DoD-DURIP and the W. M. Keck Foundation to QW.

**SP211**

**The Structure of a Dimer Interface Deletion Mutation of the Yeast Prion Protein Ure2p, and its Effect on Fibril Formation and Thermal Stability.** W.J. Bauer, T.C. Umland, Hauptman Woodward Medical Research Inst. and State Univ. of New York at Buffalo, NY 14203 USA.

Proteinaceous infectious particles (prions) are responsible for causing a number of diseases in a variety of mammals, including bovine spongiform encephalopathy ("mad cow disease") in cattle and the Creutzfeldt-Jakob disease (CJD) in humans. Yeast prion proteins are non-Mendelian genetic elements that transmit a self-propagating infectious agent to progeny cells or mating partners, and can give rise to heritable phenotypes. Ure2p is a yeast prion protein that is responsible for regulating nitrogen catabolism but can also form fibrils by infectiously inducing conformational changes in other Ure2p proteins converting them to the prion state of Ure2p, known as [URE3]. A seven residue deletion mutation to the central helix at the dimer interface of the C-terminal, GST-like domain decreases the proteins propensity to form these fibrils. These residues have been denoted as a *prion-promoting region* in the context of the full-length Ure2p. Surprisingly, this significant deletion within a central element of the dimer interface did not prevent dimerization either in solution or in the crystal structure. Additionally, this mutation does not seem to have an affect on the overall thermal stability of the C-terminal domain as determined by differential scanning fluorimetry. Here we present a 2.6 Å resolution crystal structure of this deletion mutant and the effect the mutation has on the overall thermal stability of several different full-length and single domain constructs. Investigations into the cause of decreased fibril formation rate could reveal a possible mechanism by which prion proteins are able to spontaneously adopt alternate conformations.

**SP212**

**A Bacterial Anticomplement.** Michal Hammel, Georgia Syfroera, David Ricklin, Paola Magotti, John D. Lambris, and Brian V. Geisbrecht, Advanced Light Source, Lawrence Berkeley National Lab, Berkeley, CA.

The complement system generates a finely regulated, yet potent antimicrobial response, making it an attractive target for bacterial virulence factors. Most commonly, endogenous regulatory proteins of the complement system are usurped to switch off complement activation, but the widespread human pathogen *Staphylococcus aureus* can inactivate the complement cascade by a more direct means. Previous work has shown that the extracellular fibrinogen-binding protein (Efb-C) generated by *S. aureus* blocks the complement pathway by binding to the thioester-containing domain of the complement C3b protein; indeed, *S. aureus* strains that lack Efb-C display reduced virulence. We resolve the crystal structures for the C3-binding domain of Efb-C in its unbound state and in complex with the C3d domain of C3. Structure-based functional studies suggest that native C3 is bound by Efb-C in a way that alters its conformation. As a consequence, conversion to C3b is prevented, and participation in the subsequent activation of the complement cascade is also blocked. As well as binding native C3, Efb-C also had high affinity for C3b, again appearing to induce conformational changes, this time in the already activated form of the complement component. Effective targeting of the interface between Efb-C and the C3d domain by a small molecule could be useful in the treatment of *S. aureus* infection.

**TP213**

**Structure of Bacterial Multiheme Cytochromes at the Microbial-mineral Interface.**

Alexander Johs<sup>1</sup>, Wang Wei<sup>1</sup>, Baohua Gu<sup>1</sup>, John F. Ankner<sup>2</sup>, Dean A. Myles<sup>3</sup>, Liyuan Liang<sup>1</sup>, <sup>1</sup>Environmental Sciences Div., Oak Ridge National Laboratory; <sup>2</sup>Neutron Scattering Sciences Div., Oak Ridge National Laboratory; <sup>3</sup>Center for Structural Molecular Biology, Oak Ridge National Laboratory.

Electron transfer by dissimilatory metal-reducing bacteria (DMRB) is facilitated by a series of c-type cytochromes associated with the outer bacterial membrane. Recent studies on *Shewanella oneidensis* MR-1 identified multiheme cytochromes that are required for electron transfer to insoluble iron oxide minerals. It has been shown that two cytochromes (OmcA and MtrC) exposed on the cell surface of DMRB assemble to form a terminal reductase complex interacting with the mineral surface. A combined approach, employing neutron reflectometry using a bacterial-mineral interface model and other complementary biophysical methods, is used to obtain information on the structural organization of these multiheme cytochromes at the interface. The bacterial-mineral interface model is constructed by self-assembly of these cytochromes and phospholipids into biomimetic membranes on an iron oxide thin film representing the mineral interface. Neutron reflectometry provides structural data of this complex interface with sub-nanometer resolution.



## Keywords

2D ANALYSIS.....	SOFTWARE.....	ANALYSIS TOOLS.....	MP006
2D ARRAY.....	[3X3] METAL GRID.....	INTERMOLECULAR PI-PI INTERACTI.....	SP182
3D MODELING.....	CRYSTAL SHAPE.....	ABSORPTION CORRECTION.....	TP155
4-OT SUPERFAMILY.....	DEHALOGENASE.....	CIS-3-CHLOROACRYLIC ACID.....	SP160
A-BETA.....	ALZHEIMER'S.....	IMMUNOTHERAPY.....	MP009
AAA+ ATPASE.....	TRANSCRIPTION.....	SAXS/SANS.....	TP092
AB INITIO.....	BATTERY.....	CRYSTAL STRUCTURE.....	13.13.01
AB INITIO MOLECULAR DYNAMICS.....	TIME CORRELATION FUNCTIONS.....	QUANTUM-CLASSICAL DYNAMICS.....	06.01.04
ABC TRANSPORTERS.....	INTERMEDIATE.....	MEMBRANE PROTEIN.....	01.03.02
ABSOLUTE CONFIGURATION.....	ANOMALOUS DISPERSION.....		03.02.05
ABSOLUTE STRUCTURE.....	CHIRALITY.....	BAYESIAN STATISTICS.....	03.02.06
ABSOLUTE STRUCTURE.....	ENANTIOPURE.....	CHIRALITY.....	MP060
ABSORPTION CORRECTION.....	3D MODELING.....	CRYSTAL SHAPE.....	TP155
ABSORPTION, FLUORESCENCE, RAMAN.....	KINETIC PROTEIN CRYSTALLOGRAPHY.....	IN CRYSTALLO SPECTROSCOPY.....	TR.01.01
ACCELERATED MOLECULAR DYNAMICS.....	CONFORMATIONAL TRANSITIONS.....	PROTEIN ENERGY LANDSCAPE.....	01.07.04
ACF.....	SAXS.....	APOBEC.....	MP146
ACP REDUCATASE.....	THERMUS THERMOPHILUS.....	STRUCTURAL GENOMICS.....	SP115
ACTIVE PHARMACEUTICAL INGREDIENT.....	PHASE TRANSFORMATION.....	POLYMORPH.....	SP040
ACTIVE SITE PH.....	COBALT.....	CARBONIC ANHYDRASE.....	TP065
ADRENERGIC RECEPTOR.....	MEMBRANE PROTEIN.....	GPCR.....	01.03.07
AERODYNAMIC LEVITATION.....	SILICATE MELT.....	LIQUID STRUCTURE.....	13.12.05
ALIGNMENT.....	HOMOLOGY.....	PYMOL.....	SP169
ALL-ATOM CONTACTS.....	MOLPROBITY VALIDATION.....	STRUCTURE IMPROVEMENT.....	01.05.05
ALLOSTERIC SITE.....	KINASE.....	JNK3.....	13.03.02
ALLOSTERIC TRANSITION.....	X-RAY SCATTERING.....	ENZYMOLGY.....	13.16.05
ALLOYS.....	DIFFUSE SCATTERING.....	NEUTRON SCATTERING.....	13.15.04
ALPHA GLUCOSIDASE I.....	N-GLYCOSYLATION.....	PICHIA PASTORIS.....	AW.01.08
ALTERNATIVE METHODS.....	APOBEC3G.....	SAXS.....	TR.01.09
ALZHEIMER'S.....	IMMUNOTHERAPY.....	A-BETA.....	MP009
AMINO ACID ACTIVATION.....	PROTEIN ENGINEERING.....	EVOLUTION.....	01.06.05
AMINOACYL-TRNA SYNTHETASE.....	MULTIPLE MUTANT CYCLES.....	KINETICS.....	TP127
AMINOGLYCOSIDE.....	RESISTANCE.....	SUBSTRATE COMPLEXES.....	TP109
AMYLOID.....	POLYGLUTAMINE.....	POLYPROLINE.....	02.01.02
AMYLOID.....	FIBRE DIFFRACTION.....	NEUTRONS & X-RAYS.....	02.01.03
ANALYSIS TOOLS.....	2D ANALYSIS.....	SOFTWARE.....	MP006
ANALYTICAL METHODS.....	POLYMORPHISM.....	GOLD-THIOL MONOLAYERS.....	SP207
ANDROGRAPHOLIDE.....	INTRAMOLECULAR HYDROGEN BOND.....	DATABASE ANALYSIS.....	MP173
ANGER.....	CAMERA.....	NEUTRON.....	MP072
ANION RECOGNITION.....	HYDROGEN BONDING.....	CRYSTAL ENGINEERING.....	AW.01.01
ANKYLOSING SPONDYLITIS.....	MHC STRUCTURE.....	HLA-B27 AND HLA-B14.....	SP093
ANNEALING.....	FLASH-COOLING.....	CRYOPROTECTION.....	01.08.06
ANOMALOUS.....	SOURCES.....	OPTICS.....	03.01.04
ANOMALOUS DISPERSION.....	ABSOLUTE CONFIGURATION.....		03.02.05
ANOMALOUS SCATTERING.....	PHASE AMBIGUITY.....	MACROMOLECULAR CRYSTALLOGRAPHY.....	AW.02.01
ANOMALOUS SCATTERING.....	PHASING.....	MAD.....	AW.02.02
ANOMALOUS SCATTERING.....	NEUROPHYSIN FERROCHELATASE OBE.....	ISAS STRUCTURE DETERMINATION.....	AW.02.08
ANOMALOUS SIGNAL.....	WANG LIMIT.....	DIFFRACTION DATA.....	AW.02.03
ANTHOCYANIN MALONYLTRANSFERASE.....	BAHD FAMILY.....		TP059
ANTIBIOTIC DEVELOPMENT.....	ENZYME MECHANISM.....	METABOLIC PATHWAY.....	TP116
ANTICANCER PRODRUGS.....	PABA/NO.....	HGSTP1.....	TP081
ANTIFERROMAGNETISM.....	MULTIFERROICITY.....	FERROELECTRICITY.....	13.04.01
ANTIFERROMAGNETISM.....	HYDROGEN-BONDING.....	ORGANIC RADICALS.....	13.06.04
ANTIGEN I/II.....	ORAL.....	STREPTOCOCCUS MUTANS.....	SP111
APERIODIC STRUCTURES.....	SOFTWARE.....	JANA2006.....	13.01.02
APOBEC.....	ACF.....	SAXS.....	MP146
APOBEC3G.....	SAXS.....	ALTERNATIVE METHODS.....	TR.01.09
ARACHIDONIC ACID.....	LIPOXYGENASE.....		TP094
ARCHAEA.....	REPLICATION.....		MP052
ARCHAEOGLOBUS FULGIDUS 1382.....	SULFUR PHASING.....	MEDIUM-RESOLUTION.....	03.01.03
AREA DETECTORS.....	DETECTOR CALIBRATION.....	SOFTWARE.....	03.02.02
ARGONAUTE.....	PAZ.....	SIRNA BINDING DOMAIN.....	SP104
ARTHRITIS.....	PROTEIN KINASE.....	INFLAMMATION.....	04.01.06
ASPARTATE TRANSCARBAMOYLASE.....	CRYSTAL STRUCTURE.....	THERMOSTABILITY.....	TP120
ASPARTIC PROTEINASE.....	NEUTRON DIFFRACTION.....	ENDOTHAPEPSIN.....	SP151
ASPARTOACYLASE.....	MECHANISM.....	CANAVAN DISEASE.....	MP021
ASYMMETRIC SYNTHESIS.....	BINOLATE.....	LANTHANIDE.....	10.01.05
ATOMIC FORCE MICROSCOPY.....	MONOSODIUM URATE CRYSTALS.....	GROWTH KINETICS.....	13.10.06
ATOMIC FORCE/ELECTRON MICROSCOPY.....	COLLAGEN.....	FIBER DIFFRACTION.....	02.01.05
ATOMIC FORCE/ELECTRON MICROSCOPY.....	COLLAGEN.....	FIBER DIFFRACTION.....	02.01.06
ATOMIC PAIR DISTRIBUTION FUNCTION.....	METAL-INSULATOR TRANSITIONS.....	CUIR2S4 THIOSPINEL.....	MP049
ATP GRASP FAMILY.....	PURINE BIOSYNTHESIS.....		SP058
AUGMENTER OF LIVER REGENERATION.....	MITOCHONDRIAL INTERMEMBRANE AS.....		TP178
AUTISM.....	SYNAPTIC JUNCTION.....	SYNAPSE MATURATION.....	13.03.05

## Keywords

AUTOINHIBITION.....	RESTRICTION ENZYME ECORII.....	PROTEIN-DNA INTERACTION.....	TP070
AUTOMATED STRUCTURE SOLUTION.....	AUTOMATION.....	HIGH-THROUGHPUT CRYSTALLOGRAPHY.....	MP082
AUTOMATION.....	MACROMOLECULAR CRYSTALLOGRAPHY.....	STRUCTURE DETERMINATION.....	01.05.03
AUTOMATION.....	STRUCTURE BASED DRUG DESIGN.....	SOFTWARE.....	03.01.05
AUTOMATION.....	CRYSTALLISATION.....		MP078
AUTOMATION.....	HIGH-THROUGHPUT CRYSTALLOGRAPHY.....	AUTOMATED STRUCTURE SOLUTION.....	MP082
AUTOMATION.....	SERVICE.....		MP137
AUTOMATION.....	HIGH-THROUGHOUT.....	CRYSTALLIZATION.....	TP164
BACTERIAL TOXIN.....	MONO-ADP-RIBOSYLTRANSFERASE.....	VIBRIO CHOLERAEE.....	AW.01.06
BAHD FAMILY.....	ANTHOCYANIN MALONYLTRANSFERASE.....		TP059
BARIUM NIOBATES.....	MICROWAVE DIELECTRIC.....	PHASE EQUILIBRIA.....	MP099
BATTERY.....	CRYSTAL STRUCTURE.....	AB INITIO.....	13.13.01
BAYES'S THEOREM.....	OPTIMAL PARAMETER ESTIMATION.....		01.02.02
BAYESIAN STATISTICS.....	ABSOLUTE STRUCTURE.....	CHIRALITY.....	03.02.06
BEAMLINE.....	MACROMOLECULAR CRYSTALLOGRAPHY.....	SYNCHROTRON.....	13.09.08
BEAMLINE.....	PROTEIN CRYSTALLOGRAPHY.....		MP187
BENZYLIDENEANILINES.....	ISOSTRUCTURALISM.....	LEWIS ACID.....	TP007
BHLH-PAS.....	TGO.....		SP076
BIFUNCTIONAL.....	LOR/SDH.....	BIG_908.1.....	MP057
BIG_908.1.....	BIFUNCTIONAL.....	LOR/SDH.....	MP057
BILIPROTEIN.....	Z/E ISOMERIZATION.....		13.16.04
BINOLATE.....	LANTHANIDE.....	ASYMMETRIC SYNTHESIS.....	10.01.05
BIOFUELS.....	LIGNOCELLULOSE.....	SMALL ANGLE NEUTRON SCATTERING.....	TP122
BIOINFORMATICS.....	SUBSTRATE IDENTIFICATION.....		01.06.01
BIOLOGICAL MOLECULES.....	MACROMOLECULES.....	X-RAY SCATTERING.....	TP102
BIOMINERALIZATION.....	CALCITE.....	CALCIUM OXALATE MONOHYDRATE.....	13.10.02
BIOMINERALIZATION.....	CALCITE.....	HYDROGELS.....	13.10.12
BIOMOLECULES.....	XFEL.....	SAXS.....	13.11.07
BIOPHYSICS.....	SAXS.....	RNA.....	13.11.01
BIOSAXS.....	FLOW-CELL.....	SYNCHROTRON.....	TP186
BIOTERRORISM.....	FRANCISELLA TULARENSIS.....	IGLC.....	SP016
BIOTIN.....	PYRUVATE CARBOXYLASE.....		SP045
BIPHENYL DIOXYGENASE.....	PCB.....	STRUCTURE.....	TP046
BLOCK COPOLYMER.....	SANS.....	HOMOPOLYMER.....	MP131
BLOCK COPOLYMER.....	NANOPARTICLE.....	DYNAMICS.....	MP159
BONE LOSS INHIBITOR.....	FARNESYL PYROPHOSPHATE SYNTHASE.....	N CONTAINING BISPHOSPHONATE.....	MP018
BORN-OPPENHEIMER POTENTIAL.....	DINS.....	HYDROGEN BOND.....	06.01.05
BTB DOMAIN.....	PROTEIN-PROTEIN INTERACTIONS.....	ZINC FINGER TRANSCRIPTION FACTOR.....	SP089
BTUB.....	COBALAMIN.....	OUTER-MEMBRANE.....	TP077
CA-SR-CO-O.....	STRUCTURE AND PROPERTIES.....	THERMOELECTRIC.....	13.13.06
CALCITE.....	CALCIUM OXALATE MONOHYDRATE.....	BIOMINERALIZATION.....	13.10.02
CALCITE.....	HYDROGELS.....	BIOMINERALIZATION.....	13.10.12
CALCIUM OXALATE MONOHYDRATE.....	BIOMINERALIZATION.....	CALCITE.....	13.10.02
CALCIUM PHOSPHATE NANOCRYSTALS.....	SAXS AND SANS.....	PENTABLOCK COPOLYMER GELS.....	09.01.05
CALIXARENE.....	HYDROGEN BOND.....	INCLUSION.....	13.10.16
CALMODULIN.....	INOS.....		SP037
CAMERA.....	NEUTRON.....	ANGER.....	MP072
CANADIAN LIGHT SOURCE.....	X-RAY SCATTERING.....	CRYSTALLOGRAPHY.....	13.09.07
CANAVAN DISEASE.....	ASPARTOACYLASE.....	MECHANISM.....	MP021
CANCER THERAPY.....	KINASE INHIBITOR.....	STRUCTURE-BASED DRUG DESIGN.....	TP090
CARBON BLACK.....	HIERARCHICAL STRUCTURES.....	SMALL-ANGLE SCATTERING.....	09.01.02
CARBONIC ANHYDRASE.....	ACTIVE SITE PH.....	COBALT.....	TP065
CARBONIC ANHYDRASE.....	PROTON SHUTTLE.....	WATER NETWORK.....	TP105
CARBOXYLATE.....	TOPOTAXY.....	SOLID-STATE REACTION.....	13.02.02
CATALYST.....	NANO-PARTICLES.....	PAIR DISTRIBUTION FUNCTION.....	13.08.01
CATALYST.....	COMBINED TECHNIQUES.....	DIFFRACTION/SPECTROSCOPY.....	13.08.04
CATALYTIC INTERMEDIATE.....	PRESSURIZED OXYGEN.....	COFACTOR-LESS OXIDASE.....	01.04.06
CATALYTIC INTERMEDIATES.....	REDOX CHEMISTRY.....	COPPER AMINE OXIDASE.....	TP130
CATALYTIC NANOPARTICLES.....	PAIR DISTRIBUTION FUNCTION ANALYS.....	TIME-RESOLVED.....	13.08.05
CCP4.....	PROTEIN CRYSTALLOGRAPHY.....	COMPUTATIONAL.....	TP136
CCP4.....	X-RAY DIFFRACTION.....	IMAGING.....	TP142
CERAMIC.....	CHARGE FLIPPING.....	INORGANIC.....	04.01.03
CERAMIDE ACTIVATOR PROTEIN.....	SAD PHASING.....	SAPOSIN D.....	SP084
CHARGE AND SPIN ORDER.....	NEUTRON DIFFUSE SCATTERING.....	STRONGLY CORRELATED OXIDES.....	13.04.04
CHARGE DENSITY.....	SYNCHROTRON.....	POLYMER.....	MP162
CHARGE DENSITY WAVE.....	LOCAL STRUCTURE.....	PDF.....	13.15.03
CHARGE FLIPPING.....	INORGANIC.....	CERAMIC.....	04.01.03
CHARGE-DENSITY.....	ELECTRON TRANSFER.....	PHOTOCRYSTALLOGRAPHY.....	TP050
CHARGE/ORBITAL ORDERING.....	CMR MANANITES.....	NEUTRON SCATTERING.....	13.04.03
CHEMICAL CRYSTALLOGRAPHY.....	SYNCHROTRON RADIATION.....	SERVICE CRYSTALLOGRAPHY.....	TP019
CHEMICAL FINGERPRINTS.....	THERMOSTABILITY.....	LIGAND.....	01.08.04
CHEMICAL FORCE MICROSCOPY.....	URIC ACID.....	SURFACE CHARACTERIZATION.....	SP023
CHEMICAL TRAPPING.....	RIBOZYME.....	INHIBITOR.....	SP149

## Keywords

CHESS.....	MICROCRYSTALLOGRAPHY.....	PRESSURE-FREEZING .....	TP114
CHIRAL MOLCULES .....	NON-LINEAR OPTICAL PROPERTIES .....	ISOTHIOCYANATES .....	03.01.06
CHIRALITY.....	BAYESIAN STATISTICS .....	ABSOLUTE STRUCTURE .....	03.02.06
CHIRALITY.....	ABSOLUTE STRUCTURE .....	ENANTIOPURE.....	MP060
CIRCADIAN CLOCK.....	CYANOBACTERIA.....	KAIA KAIB KAIC.....	MP085
CIRCULAR DICHROISM.....	INDUCED OPTICAL ACTIVITY.....	ENANTIOSELECTIVITY .....	13.10.01
CIS-3-CHLOROACRYLIC ACID.....	4-OT SUPERFAMILY .....	DEHALOGENASE.....	SP160
CLATHRATE HYDRATE.....	GUEST DISORDER.....	RIETVELD REFINEMENT.....	13.12.03
CLATHRATE HYDRATE.....	X-RAY SCATTERING.....	HIGH PRESSURE .....	13.12.04
CLOCK.....	SAXS.....	TIME-RESOLVED .....	TR.01.08
CLUSTER ANALYSIS.....	VISUALIZATION .....	DATABASES .....	03.02.04
CMR MANANITES .....	NEUTRON SCATTERING.....	CHARGE/ORBITAL ORDERING .....	13.04.03
CO-CRYSTAL.....	FRACTIONAL CRYSTALLIZATION.....	DISORDER.....	13.10.09
CO-CRYSTAL.....			13.10.10
CO-CRYSTALLIZATION.....	INHIBITOR.....	KINETICS .....	SP132
CO2 CHANNEL .....	NH3 CHANNEL.....	MEMBRANE PROTEIN.....	SP068
COA.....	HMG-COA REDUCTASE.....	NADH.....	01.04.02
COBALAMIN.....	OUTER-MEMBRANE.....	BTUB.....	TP077
COBALT.....	CARBONIC ANHYDRASE.....	ACTIVE SITE PH.....	TP065
COCKTAIL CRYSTALLOGRAPHY.....	URACIL-DNA GLYCOSYLASE.....	STRUCTURE-BASED DRUG DESIGN .....	MP042
COCRYSTAL.....	SCREENING .....	PHARMACEUTICAL COCRYSTAL .....	13.10.07
COCRYSTAL.....	MORPHOLOGY.....	SOLID-STATE REACTIVITY.....	SP005
COCRYSTAL.....	SOLID SOLUTION.....	PHARMACEUTICAL.....	SP205
COFACTOR-LESS OXIDASE .....	CATALYTIC INTERMEDIATE .....	PRESSURIZED OXYGEN .....	01.04.06
COLD-STREAM .....	VIBRATION .....	TURBULENCE.....	MP200
COLLAGEN .....	FIBER DIFFRACTION.....	ATOMIC FORCE/ELECTRON MICROSCOPY.....	02.01.05
COLLAGEN .....	FIBER DIFFRACTION.....	ATOMIC FORCE/ELECTRON MICROSCOPY.....	02.01.06
COLLECTIVE MOLECULAR DYNAMICS.....	MEMBRANES .....	NEUTRON, X-RAY AND LIGHT SCATTERIN.....	09.02.01
COMBINED TECHNIQUES .....	DIFFRACTION/SPECTROSCOPY .....	CATALYST.....	13.08.04
COMPLEMENT .....	EFB.....	STAPHYLOCOCCUS AUREUS.....	MP212
COMPUTATIONAL.....	CCP4.....	PROTEIN CRYSTALLOGRAPHY .....	TP136
CONFORMATIONAL TRANSITIONS.....	PROTEIN ENERGY LANDSCAPE .....	ACCELERATED MOLECULAR DYNAMICS .....	01.07.04
COORDINATION CHANGE .....	STRUCTURE SYSTEMATICS .....	HIGH-PRESSURE.....	10.01.03
COORDINATION POLYMER .....	QUANTUM MAGNET .....	CRYSTAL STRUCTURE.....	13.10.15
COORDINATION POLYMER .....	FRAMEWORK SOLID.....		MP176
COORDINATION POLYMER COMPLEX.....	VAPOUR DIFFUSION.....	SINGLE CRYSTAL .....	13.10.18
COORDINATION POLYMERS.....	URANIUM.....	PHOSPHONOCARBOXYLATES.....	10.01.04
COORDINATION POLYMERS.....	PYRIDYL COMPOUND .....	SELF ASSEMBLY .....	SP048
COPPER AMINE OXIDASE.....	TOPAQUINONE.....	ENZYME KINETICS .....	SP147
COPPER AMINE OXIDASE.....	CATALYTIC INTERMEDIATES .....	REDOX CHEMISTRY .....	TP130
COPPER HALIDE DIMERS .....	MAGNETIC EXCHANGE .....		13.06.02
COPPER PYRAZINE.....	MAGNETIC COORDINATION POLYMER.....	ISOTOPE EFFECT .....	13.06.05
COPPER-HISTIDINE .....	JAHN-TELLER .....	EPR .....	MP047
CORRELATED ELECTRONS .....	MODULATED STRUCTURE.....	INTERMETALLICS .....	13.01.08
CORRELATED MOTIONS .....	ELASTIC NETWORK MODEL.....	CRYSTAL DYNAMICS.....	TP198
CR RADIATION.....	SULFUR SAD.....		AW.02.04
CROSS-NUCLEATION .....	MOLECULAR SIMULATION.....	POLYMORPHISM.....	13.10.05
CRYO-ELECTRON MICROSCOPY .....	VIRUS .....	FIBER DIFFRACTION.....	02.01.01
CRYOCRYSTALLOGRAPHY .....	RADIATION DAMAGE.....	TEMPERATURE DEPENDENCE .....	SP079
CRYOPROTECTION.....	ANNEALING .....	FLASH-COOLING .....	01.08.06
CRYSTAL DYNAMICS.....	CORRELATED MOTIONS .....	ELASTIC NETWORK MODEL.....	TP198
CRYSTAL ENGINEERING.....	ANION RECOGNITION .....	HYDROGEN BONDING.....	AW.01.01
CRYSTAL HARVESTING.....	ROBOTICS .....	MECHATRONICS.....	TP118
CRYSTAL OPTIMIZATION.....	PAPAIN .....	CYSTEINE PEPTIDASE .....	TP075
CRYSTAL PACKING.....			10.01.08
CRYSTAL SCREEN IMPROVEMENT.....	SOLUBILITY SCREEN.....		01.08.05
CRYSTAL SHAPE.....	ABSORPTION CORRECTION .....	3D MODELING.....	TP155
CRYSTAL STRUCTURE.....	COORDINATION POLYMER.....	QUANTUM MAGNET .....	13.10.15
CRYSTAL STRUCTURE.....	AB INITIO .....	BATTERY.....	13.13.01
CRYSTAL STRUCTURE.....	SARCOSINE DEHYDROGENASE .....		SP126
CRYSTAL STRUCTURE.....	RNA.....	NUCLEASE .....	TP053
CRYSTAL STRUCTURE.....	THERMOSTABILITY .....	ASPARTATE TRANSCARBAMOYLASE.....	TP120
CRYSTALLISATION .....	AUTOMATION .....		MP078
CRYSTALLIZATION.....	OPTIMIZATION.....	SCREENING.....	01.08.03
CRYSTALLIZATION.....	STRUCTURE-BASED DRUG DESIGN .....	INDUSTRIAL.....	04.01.07
CRYSTALLIZATION.....	PHARMACEUTICAL.....	HYDRATE.....	13.10.13
CRYSTALLIZATION.....	AUTOMATION .....	HIGH-THROUGHOUT.....	TP164
CRYSTALLIZATION.....	TECHNOLOGY.....	SOLUBILIZATION .....	TP175
CRYSTALLIZATION PREDICTION .....	STRUCTURAL GENOMICS .....	RESCUE STRATEGIES.....	01.08.01
CRYSTALLIZATION TRAY .....	MACROMOLECULAR CRYSTALLIZATION.....	DEVICE MANUFACTURE.....	MP030
CRYSTALLOGRAPHY .....	CANADIAN LIGHT SOURCE .....	X-RAY SCATTERING .....	13.09.07
CRYSTALLOGRAPHY.....	HEMOGLOBIN.....	TIME-RESOLVED .....	TP206
CRYSTALS GROWTH.....	STRENGTH, SELECTIVITY,.....	INTERACTIVE LECTURES.....	13.05.05

## Keywords

CUIR2S4 THIOSPINEL.....	ATOMIC PAIR DISTRIBUTION FUNCTION ..	METAL-INSULATOR TRANSITIONS .....	MP049
CUPRATES.....	NANO-SCALE LATTICE MODULATION .....	X-RAY DIFFUSE SCATTERING.....	13.15.05
CYANOBACTERIA.....	KAIA KAIB KAIC .....	CIRCADIAN CLOCK .....	MP085
CYBERINFRASTRUCTURE.....	TUTORIAL.....	TEACHING.....	13.05.04
CYCLODEXTRIN.....	HIGH Z'.....	INCLUSION.....	10.01.06
CYSTEINE PEPTIDASE.....	CRYSTAL OPTIMIZATION.....	PAPAIN.....	TP075
D*TREK.....	IMAGE PROCESSING.....	DIFFRACTION DATA .....	01.05.01
DATA COLLECTION.....	DATA QUALITY .....		01.02.01
DATA COLLECTION STRATEGY.....	X-RAY DOSE .....	MULTIPLE DATA SETS .....	SP043
DATA PROCESSING.....	RADIATION DAMAGE .....	DATA QUALITY .....	01.02.03
DATA QUALITY.....	DATA COLLECTION .....		01.02.01
DATA QUALITY.....	DATA PROCESSING .....	RADIATION DAMAGE .....	01.02.03
DATABASE ANALYSIS.....	ANDROGRAPHOLIDE.....	INTRAMOLECULAR HYDROGEN BOND.....	MP173
DATABASES.....	CLUSTER ANALYSIS.....	VISUALIZATION.....	03.02.04
DCOH.....	HNF-1ALPHA.....	TRANSCRIPTION .....	SP166
DECARBOXYLASE.....	PYRIDOXINE.....	OXYGENASE.....	MP069
DECAY.....	SEMET.....	FLUORESCENCE.....	TR.01.03
DEFECT MODEL.....	URANIUM OXIDE.....	RIETVELD.....	TP192
DEHALOGENASE.....	CIS-3-CHLOROACRYLIC ACID.....	4-OT SUPERFAMILY .....	SP160
DENDRITIC SPINES.....	PDZ DOMAIN.....	SPAR.....	SP199
DERIVATIZATION.....	SELENIUM.....	NUCLEIC ACID .....	03.01.02
DESIGNED SELF-ASSEMBLY.....	MAGNETO-STRUCTURAL RELATIONSHIP.....	[4X4] METAL GRIDS .....	13.06.03
DETECTOR.....	POWDER.....	NEUTRON .....	MP102
DETECTOR CALIBRATION.....	SOFTWARE.....	AREA DETECTORS .....	03.02.02
DETERGENT.....	SAXS.....	MEMBRANE PROTEIN.....	TP024
DEVICE MANUFACTURE.....	CRYSTALLIZATION TRAY.....	MACROMOLECULAR CRYSTALLIZATION .....	MP030
DFT OPTIMIZATION.....	FLAVIN INTERMEDIATE.....	SINGLE CRYSTAL MICROSPECTROPHO.....	01.04.08
DIABETES.....	METABOLISM.....	OBESITY.....	SP002
DIAMOND GROWTH ON CURVED SURFA.....	DIAMOND INCOMMENSURABILITY LINE.....	DIAMOND SPIDER-LIKE WEB MESOPHASE.....	MP087
DIAMOND INCOMMENSURABILITY LINE.....	DIAMOND SPIDER-LIKE WEB MESOPHASE.....	DIAMOND GROWTH ON CURVED SURFA.....	MP087
DIAMOND SPIDER-LIKE WEB MESOPHASE.....	DIAMOND GROWTH ON CURVED SURFA .....	DIAMOND INCOMMENSURABILITY LINE.....	MP087
DIFFRACTION.....	STRUCTURE DETERMINATION.....	TEACHING.....	13.05.03
DIFFRACTION.....	LOCAL STRUCTURE.....	DIFFUSE SCATTERING .....	TP107
DIFFRACTION DATA.....	D*TREK.....	IMAGE PROCESSING .....	01.05.01
DIFFRACTION DATA.....	ANOMALOUS SIGNAL.....	WANG LIMIT .....	AW.02.03
DIFFRACTION/SPECTROSCOPY.....	CATALYST.....	COMBINED TECHNIQUES .....	13.08.04
DIFFUSE SCATTERING.....	LOCAL STRUCTURE.....	PRECIPITATES.....	13.15.02
DIFFUSE SCATTERING.....	NEUTRON SCATTERING.....	ALLOYS.....	13.15.04
DIFFUSE SCATTERING.....	METALLIC ALLOY.....	X-RAY.....	MP095
DIFFUSE SCATTERING.....	DIFFRACTION.....	LOCAL STRUCTURE .....	TP107
DINS.....	HYDROGEN BOND.....	BORN-OPPENHEIMER POTENTIAL.....	06.01.05
DIRECT METHODS.....	SUBSTRUCTURE DETERMINATION .....	EXPERIMENTAL ERROR .....	01.05.06
DIRECT METHODS.....	NEUTRONS.....	SIR PHASING.....	AW.02.05
DIRECT METHODS.....	SOLVENT FLATTENING .....	DUAL-SPACE ITERATION .....	AW.02.06
DIRECT METHODS.....	NEUTRONS.....	SIR DATA.....	TP083
DISORDER.....	CO-CRYSTAL.....	FRACTIONAL CRYSTALLIZATION .....	13.10.09
DISORDERED STRUCTURE.....	MODULATED STRUCTURE.....	VANADIUM OXIDE.....	13.01.07
DISTANT HOMOLGY DETECTION.....	SEQUENCE ALIGNMENT.....	REMOTE HOMOLOGS.....	TP158
DJ-1.....	PARKINSONS DISEASE.....	OXIDATIVE STRESS .....	MP033
DMPC & DOPC.....	SIMULATION.....	LIPID DYNAMICS .....	09.02.06
DNA BINDING PROTEIN.....	RESTRICTION ENZYMES .....	NOVEL PROTEIN FOLD.....	MP044
DNA INTERCALATION.....	EXPERIMENTAL PHASING.....	TRIOXACARCIN A.....	SP097
DNA-PROTEIN COMPLEX.....	NMR SPECTROSCOPY.....	X-RAY CRYSTALLOGRAPHY .....	TR.01.10
DRUG DELIVERY.....	SAXS.....	NANOSTRUCTURES.....	MP140
DRUG DESIGN.....	FRAGMENT BASED.....	HIGH THROUGHPUT.....	04.01.08
DUAL-SPACE ITERATION.....	DIRECT METHODS.....	SOLVENT FLATTENING .....	AW.02.06
DYNAMICS.....	NEUTRON SCATTERING.....	MOLECULAR DYNAMICS SIMULATION .....	09.02.04
DYNAMICS.....	NANOSCALE.....	POLYMER NANOCOMPOSITES .....	MP156
DYNAMICS.....	BLOCK COPOLYMER.....	NANOPARTICLE.....	MP159
EFB.....	STAPHYLOCOCCUS AUREUS.....	COMPLEMENT.....	MP212
ELASTIC NETWORK MODEL.....	CRYSTAL DYNAMICS.....	CORRELATED MOTIONS .....	TP198
ELECTROLYTES.....	NON-AMBIENT DIFFRACTION .....	LITHIUM BATTERIES.....	TP189
ELECTRON DENISTY.....	MAXIMUM ENTROPY ANALYSIS.....	HIGH PRESSURE .....	13.12.01
ELECTRON DIFFRACTION.....	STRUCTURE ANALYSIS.....	MICROCRYSTALS.....	04.01.02
ELECTRON DIFFRACTION.....	PROTEIN.....		13.14.02
ELECTRON TRANSFER.....	PHOTOSYSTEM I.....	LIGHT-HARVESTING.....	01.03.05
ELECTRON TRANSFER.....	PHOTOCRYSTALLOGRAPHY.....	CHARGE-DENSITY .....	TP050
ENANTIOPURE.....	CHIRALITY.....	ABSOLUTE STRUCTURE .....	MP060
ENANTIOSELECTIVITY.....	CIRCULAR DICHROISM.....	INDUCED OPTICAL ACTIVITY .....	13.10.01
END-USERS.....	PDB FILES.....	MACROMOLECULAR STRUCTURE .....	01.07.01
ENDOTHIAEPSIN.....	ASPARTIC PROTEINASE.....	NEUTRON DIFFRACTION.....	SP151
ENERGY RECOVERY LINAC.....	SYNCHROTRON RADITION.....	X-RAY SCATTERING .....	13.09.05
ENZYME INHIBITION.....	SUBSTRATE SPECIFICITY .....	GLYCOSIDASE.....	TP029

## Keywords

ENZYME KINETICS.....	COPPER AMINE OXIDASE.....	TOPAQUINONE.....	SP147
ENZYME MECHANISM.....	METABOLIC PATHWAY.....	ANTIBIOTIC DEVELOPMENT.....	TP116
ENZYME MECHANISM KINETICS.....	STRUCTURE COMPARISONS.....	STRUCTURE-FUNCTION RELATIONSHI.....	SP144
ENZYME MOTION.....	MOLECULAR MOVIE.....	HMG-COA REDUCTASE.....	SP129
ENZYME SPECIFICITY.....	STRUCTURE-GUIDED DRUG DESIGN.....	LIGAND RECOGNITION.....	TP124
ENZYMOLGY.....	ALLOSTERIC TRANSITION.....	X-RAY SCATTERING.....	13.16.05
EPR.....	COPPER-HISTIDINE.....	JAHN-TELLER.....	MP047
ESRF.....	SYNCHROTRON.....	NANO.....	13.09.06
EVOLUTION.....	VIRUS.....	NON CRYSTALLOGRAPHIC SYMMETRY.....	01.03.03
EVOLUTION.....	PHYLOGENY.....	SUBSTRATE DETERMINATION.....	01.06.02
EVOLUTION.....	NUCLEAR RECEPTOR.....		01.06.04
EVOLUTION.....	AMINO ACID ACTIVATION.....	PROTEIN ENGINEERING.....	01.06.05
EVOLUTION.....	PROTEIN CLASSIFICATION.....	FOLDING.....	01.07.03
EXCITED STATE.....	LAUE DIFFRACTION.....	TIME RESOLVED.....	13.09.12
EXPERIMENTAL ERROR.....	DIRECT METHODS.....	SUBSTRUCTURE DETERMINATION.....	01.05.06
EXPERIMENTAL PHASING.....	MACROMOLECULES.....	HEAVY ATOME DERIVATIVES.....	SP056
EXPERIMENTAL PHASING.....	TRIOXACARCIN A.....	DNA INTERCALATION.....	SP097
FABF.....	SURFACE ENTROPY REDUCTION.....	KETOACYL ACYL CARRIER PROTEIN.....	TP183
FARNESYL PYROPHOSPHATE SYNTHASE.....	N CONTAINING BISPHOSPHONATE.....	BONE LOSS INHIBITOR.....	MP018
FERRITIN.....	HELICOBACTER PYLORI.....	IRON UPTAKE.....	SP062
FERROELCTRIC.....	LOCAL ATOMIC STRUCTURE.....	SODIMU NIOBATE.....	13.15.06
FERROELECTRIC.....	NEUTRON SCATTERING.....	RELAXOR.....	13.04.02
FERROELECTRIC.....	MULTIFERROIC.....	NEUTRON DIFFRACTION.....	13.04.05
FERROELECTRIC.....	TRANSITION.....	RELAXOR.....	SP020
FERROELECTRICITY.....	ANTIFERROMAGNETISM.....	MULTIFERROICITY.....	13.04.01
FGAM SYNTHETASE.....	PURINE BIOSYNTHESIS.....	MACROMOLECULAR COMPLEX.....	TP003
FIBER DIFFRACTION.....	CRYO-ELECTRON MICROSCOPY.....	VIRUS.....	02.01.01
FIBER DIFFRACTION.....	ATOMIC FORCE/ELECTRON MICROSCOPY.....	COLLAGEN.....	02.01.05
FIBER DIFFRACTION.....	ATOMIC FORCE/ELECTRON MICROSCOPY.....	COLLAGEN.....	02.01.06
FIBER DIFFRACTION.....	TIME RESOLVED.....	MUSCLE.....	13.16.07
FIBER DIFFRACTION.....	POLYSACCHARIDES.....	SYNCHROTON RADIATION.....	TP073
FIBRE DIFFRACTION.....	NEUTRONS & X-RAYS.....	AMYLOID.....	02.01.03
FLASH-COOLING.....	CRYOPROTECTION.....	ANNEALING.....	01.08.06
FLAVIN INTERMEDIATE.....	SINGLE CRYSTAL MICROSPECTROPHO.....	DFT OPTIMIZATION.....	01.04.08
FLOW-CELL.....	SYNCHROTRON.....	BIOSAXS.....	TP186
FLUORESCENCE.....	DECAY.....	SEMET.....	TR.01.03
FLUORESCENCE ANISOTROPY.....	RNA.....	SPLICING.....	MP025
FLUORINATED METALNORGANIC FRA.....	HYDROGEN STORAGE.....	GAS STORAGE.....	13.13.07
FLUX.....	OPTICS.....	X-RAY.....	SP177
FOCUSING.....	MICROBEAM.....	NEUTRON.....	TP061
FOLDING.....	EVOLUTION.....	PROTEIN CLASSIFICATION.....	01.07.03
FRACTIONAL CRYSTALLIZATION.....	DISORDER.....	CO-CRYSTAL.....	13.10.09
FRAGMENT BASED.....	HIGH THROUGHPUT.....	DRUG DESIGN.....	04.01.08
FRAMEWORK SOLID.....	COORDINATION POLYMER.....		MP176
FRANCISELLA TULARENSIS.....	IGLC.....	BIOTERRORISM.....	SP016
FREE ELECTRON LASER.....	PROTEINS.....	SERIAL CRYSTALLOGRAPHY.....	13.09.04
FREE-ELECTRON LASERS.....	SYNCHROTRON RADIATION.....		13.09.02
FULL DEUTERATION.....	JOINT REFINEMENT.....	NEUTRON DIFFRACTION.....	TP022
FULLERENE.....	HOSTS.....		10.01.07
FULLERENES.....	WHOLE MOLECULE DISORDER.....	SYNCHROTRON.....	AW.01.04
G40P.....	HEXAMER.....	HELICASE.....	SP119
GAQ-P63RHOGEF-RHOA COMPLEX.....	GPCR SIGNALING.....	MACROMOLECULAR CRYSTALLOGRAPHY.....	AW.01.05
GAS STORAGE.....	FLUORINATED METALNORGANIC FRA.....	HYDROGEN STORAGE.....	13.13.07
GENE REGULATION.....	RIBOSWITCH.....	METAL SENSING.....	01.01.04
GENERATOR.....	MICROFOCUS.....	INSTRUMENT.....	03.02.01
GENERATOR.....	MICROCRYSTAL.....	PROTEIN.....	TP194
GISAXS.....	TUNGSTEN.....	PLATINUM.....	13.08.02
GISAXS.....	SIZE SELECTED NANOCATALYST.....	SIZE EFFECT.....	13.08.03
GISAXS.....	NANOTEMPLATE.....	MICROCRYSTALS.....	13.14.01
GLASS TRANSITION.....	NANOPARTICLES.....	INTERNAL STRESS.....	09.02.02
GLYCOPEPTIDE ANTIBIOTICS BIOSYNTHESIS.....	SULFOTRANSFERASE.....	METHYLTRANSFERASE.....	TP038
GLYCOSIDASE.....	ENZYME INHIBITION.....	SUBSTRATE SPECIFICITY.....	TP029
GOLD(I) COMPLEXES.....	GOLD-GOLD INTERACTIONS.....	HYDROGEN-BONDED NETWORKS.....	SP185
GOLD-GOLD INTERACTIONS.....	HYDROGEN-BONDED NETWORKS.....	GOLD(I) COMPLEXES.....	SP185
GOLD-THIOL MONOLAYERS.....	ANALYTICAL METHODS.....	POLYMORPHISM.....	SP207
GPCR.....	ADRENERGIC RECEPTOR.....	MEMBRANE PROTEIN.....	01.03.07
GPCR SIGNALING.....	MACROMOLECULAR CRYSTALLOGRAPHY.....	GAQ-P63RHOGEF-RHOA COMPLEX.....	AW.01.05
GRAZING INCIDENCE.....	REFLECTOMETRY.....	NEUTRON.....	13.09.10
GROUP THEORY.....	STRUCTURAL DISTORTION.....	INCOMMENSURATE MODULATION.....	13.01.04
GROWTH.....	POLYMORPH.....	NUCLEATION.....	13.10.04
GROWTH KINETICS.....	ATOMIC FORCE MICROSCOPY.....	MONOSODIUM URATE CRYSTALS.....	13.10.06
GTPASE.....	RIBOSOME.....	VIRULENCE.....	TP101
GUEST DISORDER.....	RIETVELD REFINEMENT.....	CLATHRATE HYDRATE.....	13.12.03

## Keywords

H2 STORAGE	NEUTRON POWDER DIFFRACTION	PHASE TRANSITION	13.13.04
HAMMERHEAD RIBOZYME			01.01.02
HEAVY ATOME DERIVATIVES	EXPERIMENTAL PHASING	MACROMOLECULES	SP056
HELICASE	G40P	HEXAMER	SP119
HELICOBACTER PYLORI	IRON UPTAKE	FERRITIN	SP062
HEME	PROTON TRANSPORT	MEMBRANE PROTEIN	01.04.03
HEME	MONOOXYGENASE	METALLOPROTEIN	01.04.07
HEME	MEMBRANE PROTEIN	PROTON TRANSPORT	TP098
HEMOGLOBIN	TIME-RESOLVED	CRYSTALLOGRAPHY	TP206
HEPTP	PROTEIN TYROSINE PHOSPHATASE	SUBSTRATE-TRAPPING MUTANT	SP135
HEXAMER	HELICASE	G40P	SP119
HGSTP1	ANTICANCER PRODRUGS	PABA/NO	TP081
HIERARCHICAL STRUCTURES	SMALL-ANGLE SCATTERING	CARBON BLACK	09.01.02
HIGH PRESSURE	ELECTRON DENISTY	MAXIMUM ENTROPY ANALYSIS	13.12.01
HIGH PRESSURE	PHASE TRANSITION	TOTAL SCATTERING	13.12.02
HIGH PRESSURE	CLATHRATE HYDRATE	X-RAY SCATTERING	13.12.04
HIGH PRESSURE	LIPIDS	TR SAXS	13.16.03
HIGH PRESSURE	SPALLATION	NEUTRON DIFFRACTION	MP128
HIGH PRESSURE	RHOMBOHEDRAL PEROVSKITE	PHASE TRANSITION	SP197
HIGH THROUGHPUT	PROTEIN CRYSTALLIZATION	STRUCTURAL GENOMICS	03.01.01
HIGH THROUGHPUT	DRUG DESIGN	FRAGMENT BASED	04.01.08
HIGH THROUGHPUT	SCREENING	IN-SITU	TP170
HIGH Z'	INCLUSION	CYCLODEXTRIN	10.01.06
HIGH-FIELD PULSED MAGNET	X-RAY STUDIES IN HIGH MAGNETIC FIE	SPLIT-COIL GEOMETRY	TP067
HIGH-PRESSURE	SMALL-MOLECULAR	HYDROGEN BONDING	06.01.02
HIGH-PRESSURE	COORDINATION CHANGE	STRUCTURE SYSTEMATICS	10.01.03
HIGH-PRESSURE	MAGNETIC STRUCTURE	METAL OXIDES	MP110
HIGH-THROUGHOUT	CRYSTALLIZATION	AUTOMATION	TP164
HIGH-THROUGHPUT CRYSTALLOGRAPHY	AUTOMATED STRUCTURE SOLUTION	AUTOMATION	MP082
HIV MEMBRAN FUSION & VIRAL ENTRY	TRANSFERED NOE	NUCLEAR MAGNETIC RESONANCE SPE	TR.01.12
HIV-1 PROTEASE	REACTION INTERMEDIATE		SP074
HLA-B27 AND HLA-B14	ANKYLOSING SPONDYLITIS	MHC STRUCTURE	SP093
HMG-COA REDUCTASE	NADH	COA	01.04.02
HMG-COA REDUCTASE	ENZYME MOTION	MOLECULAR MOVIE	SP129
HMP-P SYNTHASE	THIAMIN BIOSYNTHESIS	RADICAL SAM SUPERFAMILY	01.01.01
HNF-1ALPHA	TRANSCRIPTION	DCOH	SP166
HOMOLOGY	PYMOL	ALIGNMENT	SP169
HOMOPOLYMER	BLOCK COPOLYMER	SANS	MP131
HOSTS	FULLERENE		10.01.07
HUMAN DEOXYHEMOGLOBIN	NEUTRON DIFFRACTION	PROTONATION STATE	SP179
HUMAN FEZ1	UNFOLDED PROTEIN	SAXS	TP012
HYBRID LRR	LEUCINE RICH REPEAT	TOLL-LIKE RECEPTOR	01.03.04
HYDRATE	CRYSTALLIZATION	PHARMACEUTICAL	13.10.13
HYDRATION WATER	NEUTRON SPECTROSCOPY		09.02.05
HYDROGELS	BIOMINERALIZATION	CALCITE	13.10.12
HYDROGEN	STORAGE	NEUTRON	13.13.03
HYDROGEN BOND	QUANTUM CHEMISTRY	NMR	06.01.03
HYDROGEN BOND	BORN-OPPENHEIMER POTENTIAL	DINS	06.01.05
HYDROGEN BOND	INCLUSION	CALIXARENE	13.10.16
HYDROGEN BOND H/D ISOTOPE EFFECT	JAHN-TELLER DISTORTION	NEUTRON DIFFRACTION	13.02.05
HYDROGEN BONDING	NEUTRON DIFFRACTION		06.01.01
HYDROGEN BONDING	HIGH-PRESSURE	SMALL-MOLECULAR	06.01.02
HYDROGEN BONDING	PROTON CONDUCTOR	NEUTRON SCATTERING SPECTROSCOPY	06.01.06
HYDROGEN BONDING	SINGLE CRYSTAL	NEUTRON DIFFRACTION	06.01.07
HYDROGEN BONDING	METAL(II)-BETADIKETONATES	POLYFUNCTIONAL LIGANDS	13.10.17
HYDROGEN BONDING	CRYSTAL ENGINEERING	ANION RECOGNITION	AW.01.01
HYDROGEN BONDING	POLYMORPHISM	RACEMIC	SP011
HYDROGEN POSITIONS	PREHNITE	POWDER NEUTRON DIFFRACTION	MP106
HYDROGEN STORAGE	GAS STORAGE	FLUORINATED METALNORGANIC FRA	13.13.07
HYDROGEN-BONDED NETWORKS	GOLD(I) COMPLEXES	GOLD-GOLD INTERACTIONS	SP185
HYDROGEN-BONDING	ORGANIC RADICALS	ANTIFERROMAGNETISM	13.06.04
HYDROGEN/METHANE STORAGE	METAL ORGANIC FRAMEWORKS	PHASE TRANSITION	13.13.05
HYDROTUNGSTITE	RIETVELD	QUANTUM CHEMISTRY	04.01.01
IDENTIFICATION	UV FLUORESENCE	PROTEIN RYSTALLIZATION	MP004
IGLC	BIOTERRORISM	FRANCISELLA TULARENSIS	SP016
IMAGE PROCESSING	DIFFRACTION DATA	D*TREK	01.05.01
IMAGING	UV	PROTEIN CRYSTAL	SP174
IMAGING	CCP4	X-RAY DIFFRACTION	TP142
IMMUNOTHERAPY	A-BETA	ALZHEIMER'S	MP009
IN CRYSTALLO SPECTROSCOPY	ABSORPTION FLUORESCENCE RAMAN	KINETIC PROTEIN CRYSTALLOGRAPHY	TR.01.01
IN VITRO SELECTION	RIBOZYME	LIGASE	01.06.06
IN-SITU	HIGH THROUGHPUT	SCREENING	TP170
INCLUSION	CYCLODEXTRIN	HIGH Z'	10.01.06

## Keywords

INCLUSION	CALIXARENE	HYDROGEN BOND	13.10.16
INCOMMENSURATE	MODULATED		13.01.01
INCOMMENSURATE	RIGID UNIT MODES	STRUCTURE PREDICTION	13.01.06
INCOMMENSURATE ANTIFERROMAGNET	QUANTUM SPIN-LIQUID	NEUTRON SCATTERING	SP201
INCOMMENSURATE MODULATION	GROUP THEORY	STRUCTURAL DISTORTION	13.01.04
INCOMMENSURATE MODULATION	PROFILIN:ACTIN	MODULATED PROTEIN	13.01.05
INCOMMENSURATE STRUCTURES	SOFTWARE		13.01.03
INDUCED OPTICAL ACTIVITY	ENANTIOSELECTIVITY	CIRCULAR DICHROISM	13.10.01
INDUSTRIAL	CRYSTALLIZATION	STRUCTURE-BASED DRUG DESIGN	04.01.07
INFERENCE	SCIENTIFIC INQUIRY	TEACHING CRYSTALLOGRAPHY	13.05.02
INFLAMMATION	ARTHRITIS	PROTEIN KINASE	04.01.06
INHIBITOR	KINETICS	CO-CRYSTALLIZATION	SP132
INHIBITOR	CHEMICAL TRAPPING	RIBOZYME	SP149
INORGANIC	CERAMIC	CHARGE FLIPPING	04.01.03
INORGANIC	SULFONATE	LAYERED	MP184
INOS	CALMODULIN		SP037
INSTRUMENT	GENERATOR	MICROFOCUS	03.02.01
INTEGRATION	PHOTOMETRY		TP152
INTERACTIVE LECTURES	CRYSTALS GROWTH	STRENGTH, SELECTIVITY	13.05.05
INTERFACES	PROBLEM STRUCTURES	REFINEMENT	MP168
INTERFERON REGULATORY FACTOR			01.01.03
INTERMEDIATE	MEMBRANE PROTEIN	ABC TRANSPORTERS	01.03.02
INTERMETALLICS	CORRELATED ELECTRONS	MODULATED STRUCTURE	13.01.08
INTERMOLECULAR PI-PI INTERACTIONS	2D ARRAY	[3X3] METAL GRID	SP182
INTERNAL STRESS	GLASS TRANSITION	NANOPARTICLES	09.02.02
INTRAMOLECULAR HYDROGEN BOND	DATABASE ANALYSIS	ANDROGRAPHOLIDE	MP173
IOTA-CARRAGEENAN	POLYMORPHISM	POLYSACCHARIDES	02.01.04
IQGAPI			SP108
IRES	TRANSLATION	RNA STRUCTURE	01.01.06
IRON UPTAKE	FERRITIN	HELICOBACTER PYLORI	SP062
ISAS STRUCTURE DETERMINATION	ANOMALOUS SCATTERING	NEUROPHYSIN FERROCHELATASE OBE	AW.02.08
ISOSTRUCTURALISM	LEWIS ACID	BENZYLIDENEANILINES	TP007
ISOTHIOCYANATES	CHIRAL MOLCULES	NON-LINEAR OPTICAL PROPERTIES	03.01.06
ISOTOPE EFFECT	COPPER PYRAZINE	MAGNETIC COORDINATION POLYMER	13.06.05
ITERATIVE OPTIMIZATION	TAILORED SCREENING	ROBOTIC CRYSTALLIZATION	TP180
JAHN-TELLER	EPR	COPPER-HISTIDINE	MP047
JAHN-TELLER DISTORTION	NEUTRON DIFFRACTION	HYDROGEN BOND H/D ISOTOPE EFFECT	13.02.05
JANA2006	APERIODIC STRUCTURES	SOFTWARE	13.01.02
JNK3	ALLOSTERIC SITE	KINASE	13.03.02
JOINT REFINEMENT	NEUTRON DIFFRACTION	FULL DEUTERATION	TP022
JOINT X-RAY NEUTRON REFINEMENT	RESULTS W/IMPLICATIONS MRI REX	NEUTRON DIFFRACTION RESULTS	MP134
KAIA KAIB KAIC	CIRCADIAN CLOCK	CYANOBACTERIA	MP085
KETOACYL ACYL CARRIER PROTEIN	FABF	SURFACE ENTROPY REDUCTION	TP183
KIDNEY STONES	URIC ACID DIHYDRATE		SP209
KINASE	JNK3	ALLOSTERIC SITE	13.03.02
KINASE INHIBITOR	STRUCTURE-BASED DRUG DESIGN	CANCER THERAPY	TP090
KINETIC PROTEIN CRYSTALLOGRAPHY	IN CRYSTALLO SPECTROSCOPY	ABSORPTION, FLUORESCENCE, RAMAN	TR.01.01
KINETICS	CO-CRYSTALLIZATION	INHIBITOR	SP132
KINETICS	AMINOACYL-TRNA SYNTHETASE	MULTIPLE MUTANT CYCLES	TP127
KSGA	SAH	RNA METHYLTRANSFERASE	TP112
LAMELLAR PHASE	RHEO-SANS	STRUCTURE	09.01.07
LANDAU THEORY	SPONTANEOUS STRAIN	PHASE TRANSITIONS	13.02.04
LANTHANIDE	ASYMMETRIC SYNTHESIS	BINOLATE	10.01.05
LAUE	MICROCRYSTALLOGRAPHY	X-RAY OPTICS	13.14.03
LAUE	PICOSECOND	TIME-RESOLVED	MP204
LAUE DIFFRACTION	TIME RESOLVED	EXCITED STATE	13.09.12
LAUE DIFFRACTOMETER	NEUTRON CRYSTALLOGRAPHY	MACROMOLECULE CRYSTALLOGRAPHY	MP125
LAYERED	INORGANIC	SULFONATE	MP184
LEUCINE RICH REPEAT	TOLL-LIKE RECEPTOR	HYBRID LRR	01.03.04
LEWIS ACID	BENZYLIDENEANILINES	ISOSTRUCTURALISM	TP007
LIGAND	CHEMICAL FINGERPRINTS	THERMOSTABILITY	01.08.04
LIGAND RECOGNITION	ENZYME SPECIFICITY	STRUCTURE-GUIDED DRUG DESIGN	TP124
LIGASE	IN VITRO SELECTION	RIBOZYME	01.06.06
LIGHT CHAIN AMYLOIDOSIS	LIGHT CHAIN VARIABLE DOMAIN		SP028
LIGHT CHAIN VARIABLE DOMAIN	LIGHT CHAIN AMYLOIDOSIS		SP028
LIGHT-HARVESTING	ELECTRON TRANSFER	PHOTOSYSTEM I	01.03.05
LIGNOCELLULOSE	SMALL ANGLE NEUTRON SCATTERING	BIOFUELS	TP122
LIKELIHOOD METHODS	SAXS	STATISTICS	SP091
LIPID DIFFRACTION	SMALL ANGLE SCATTERING	SOLUTION SCATTERING	13.11.04
LIPID DYNAMICS	DMPC & DOPC	SIMULATION	09.02.06
LIPIDS	TR SAXS	HIGH PRESSURE	13.16.03
LIPOXYGENASE	ARACHIDONIC ACID		TP094
LIQUID STRUCTURE	AERODYNAMIC LEVITATION	SILICATE MELT	13.12.05

## Keywords

LITHIUM BATTERIES.....	ELECTROLYTES.....	NON-AMBIENT DIFFRACTION.....	TP189
LOCAL ATOMIC STRUCTURE.....	SODIUM NIOBATE.....	FERROELECTRIC.....	13.15.06
LOCAL STRUCTURE.....	MOLECULAR MAGNETS.....	VIBRATIONAL SPECTROSCOPY.....	13.06.06
LOCAL STRUCTURE.....	PRECIPITATES.....	DIFFUSE SCATTERING.....	13.15.02
LOCAL STRUCTURE.....	PDF.....	CHARGE DENSITY WAVE.....	13.15.03
LOCAL STRUCTURE.....	DIFFUSE SCATTERING.....	DIFFRACTION.....	TP107
LOR/SDH.....	BIG_908.1.....	BIFUNCTIONAL.....	MP057
MACROMOLECULAR.....	REFINEMENT.....	RESTRAINTS.....	01.05.07
MACROMOLECULAR COMPLEX.....	SAXS.....	SANS.....	13.11.08
MACROMOLECULAR COMPLEX.....	FGAM SYNTHETASE.....	PURINE BIOSYNTHESIS.....	TP003
MACROMOLECULAR CRYSTALLIZATION.....	DEVICE MANUFACTURE.....	CRYSTALLIZATION TRAY.....	MP030
MACROMOLECULAR CRYSTALLOGRAPHY.....	STRUCTURE DETERMINATION.....	AUTOMATION.....	01.05.03
MACROMOLECULAR CRYSTALLOGRAPHY.....	SYNCHROTRON.....	BEAMLINE.....	13.09.08
MACROMOLECULAR CRYSTALLOGRAPHY.....	GAQ-P63RHOGF-RHOA COMPLEX.....	GPCR SIGNALING.....	AW.01.05
MACROMOLECULAR CRYSTALLOGRAPHY.....	ANOMALOUS SCATTERING.....	PHASE AMBIGUITY.....	AW.02.01
MACROMOLECULAR CRYSTALLOGRAPHY.....	MODEL BUILDING.....	NUCLEIC ACIDS.....	SP154
MACROMOLECULAR CRYSTALLOGRAPHY.....	NEUTRON SOURCES.....	NEURON SCATTERING.....	SP026
MACROMOLECULAR PHASING.....	SAD.....	SHELX.....	01.05.02
MACROMOLECULAR STRUCTURE.....	END-USERS.....	PDB FILES.....	01.07.01
MACROMOLECULE CRYSTALLOGRAPHY.....	LAUE DIFFRACTOMETER.....	NEUTRON CRYSTALLOGRAPHY.....	MP125
MACROMOLECULES.....	HEAVY ATOME DERIVATIVES.....	EXPERIMENTAL PHASING.....	SP056
MACROMOLECULES.....	X-RAY SCATTERING.....	BIOLOGICAL MOLECULES.....	TP102
MAD.....	ANOMALOUS SCATTERING.....	PHASING.....	AW.02.02
MAGNET.....			13.06.01
MAGNETIC COORDINATION POLYMER.....	ISOTOPE EFFECT.....	COPPER PYRAZINE.....	13.06.05
MAGNETIC EXCHANGE.....	COPPER HALIDE DIMERS.....		13.06.02
MAGNETIC STRUCTURE.....	METAL OXIDES.....	HIGH-PRESSURE.....	MP110
MAGNETO-STRUCTURAL RELATIONSHIP.....	[4X4] METAL GRIDS.....	DESIGNED SELF-ASSEMBLY.....	13.06.03
MANGANITES.....	NEUTRON POWDER DIFFRACTION.....	OXYGEN-VACANCY ORDERING.....	SP032
MAPS.....	SBEVSL.....	RASMOL.....	MP039
MATRIX.....	NUCLEATION.....	SEEDING.....	01.08.02
MAXIMUM ENTROPY ANALYSIS.....	HIGH PRESSURE.....	ELECTRON DENISTY.....	13.12.01
MAXIMUM-LIKELIHOOD STRUCTURE.....	SUBATOMIC RESOLUTION.....	PHENIX.....	TP145
MECHANISM.....	CANAVAN DISEASE.....	ASPARTOACYLASE.....	MP021
MECHATRONICS.....	CRYSTAL HARVESTING.....	ROBOTICS.....	TP118
MEDIUM-RESOLUTION.....	ARCHAEOGLOBUS FULGIDUS 1382.....	SULFUR PHASING.....	03.01.03
MEMBRANE PROTEIN.....	ZINC TRANSPORTER.....	PROTEIN STRUCTURE.....	01.03.01
MEMBRANE PROTEIN.....	ABC TRANSPORTERS.....	INTERMEDIATE.....	01.03.02
MEMBRANE PROTEIN.....	GPCR.....	ADRENERGIC RECEPTOR.....	01.03.07
MEMBRANE PROTEIN.....	HEME.....	PROTON TRANSPORT.....	01.04.03
MEMBRANE PROTEIN.....	CO2 CHANNEL.....	NH3 CHANNEL.....	SP068
MEMBRANE PROTEIN.....	DETERGENT.....	SAXS.....	TP024
MEMBRANE PROTEIN.....	PROTON TRANSPORT.....	HEME.....	TP098
MEMBRANE PROTEINS.....	MICROCRYSTALS.....	SYNCHROTRON BEAMLINES.....	13.14.04
MEMBRANE PROTEINS.....	NEUTRON DIFFRACTION.....	MEMBRANE STRUCTURE.....	TR.01.06
MEMBRANE STRUCTURE.....	MEMBRANE PROTEINS.....	NEUTRON DIFFRACTION.....	TR.01.06
MEMBRANE TRANSPORT.....	VIRULENCE FACTORS.....	TWO PARTNER SECRETION.....	MP036
MEMBRANES.....	NEUTRON X-RAY AND LIGHT SCATTERI.....	COLLECTIVE MOLECULAR DYNAMICS.....	09.02.01
MERGER CRYSTALLOGRAPHY & NMR.....	PROTEASOME.....	UBIQUITIN RECEPTOR.....	TR.01.11
METABOLIC PATHWAY.....	ANTIBIOTIC DEVELOPMENT.....	ENZYME MECHANISM.....	TP116
METABOLISM.....	OBESITY.....	DIABETES.....	SP002
METAL ACTIVE SITE.....	RADIATION DAMAGE.....	XAS.....	TR.01.02
METAL CITRACONATES.....	THERMAL DECOMPOSITION.....	SOLID STATE REACTIVITY.....	13.10.14
METAL ORGANIC FRAMEWORKS.....	PHASE TRANSITION.....	HYDROGEN/METHANE STORAGE.....	13.13.05
METAL OXIDES.....	HIGH-PRESSURE.....	MAGNETIC STRUCTURE.....	MP110
METAL SENSING.....	GENE REGULATION.....	RIBOSWITCH.....	01.01.04
METAL(II)-BETADIKETONATES.....	POLYFUNCTIONAL LIGANDS.....	HYDROGEN BONDING.....	13.10.17
METAL-INSULATOR TRANSITIONS.....	CUIR2S4 THIOSPINEL.....	ATOMIC PAIR DISTRIBUTION FUNCTION.....	MP049
METALLIC ALLOY.....	X-RAY.....	DIFFUSE SCATTERING.....	MP095
METALLOENZYME.....	SUPEROXIDE DISMUTASE.....		SP138
METALLOPROTEIN.....	HEME.....	MONOOXYGENASE.....	01.04.07
METALLOPROTEINS.....	RADIATION DAMAGE.....		SP191
METHANOL LNCL3 ADDUCTS.....	SCINTILLATORS.....	NEUTRON DETECTORS.....	MP181
METHYLTRANSFERASE.....	GLYCOPEPTIDE ANTIBIOTICS BIOSYNT.....	SULFOTRANSFERASE.....	TP038
MHC MOLECULE.....	T CELL RECEPTOR.....		SP163
MHC STRUCTURE.....	HLA-B27 AND HLA-B14.....	ANKYLOSING SPONDYLITIS.....	SP093
MICELLES.....	THREADLIKE.....	NEUTRON SPIN ECHO.....	09.02.03
MICO-DIFFRACTION.....	SINGLE CRYSTAL SPECTROSCOPY.....	SYNCHROTRON FACILITY.....	TP010
MICRO-CRYSTALS.....	MICRO-DIFFRACTION.....	RADIATION DAMAGE.....	13.14.06
MICRO-DIFFRACTION.....	RADIATION DAMAGE.....	MICRO-CRYSTALS.....	13.14.06
MICRO-DIFFRACTION.....	RASTERING.....	MINI-BEAM.....	MP208
MICROBEAM.....	SYNCHROTRON.....	MICROCRYSTALLOGRAPHY.....	13.14.05
MICROBEAM.....	NEUTRON.....	FOCUSING.....	TP061

## Keywords

MICROBEAM.....	X-RAY.....	MICROSTRUCTURE.....	TP088
MICROCRYSTAL.....	PROTEIN.....	GENERATOR.....	TP194
MICROCRYSTALLOGRAPHY.....	RIBOSWITCH.....	SAM.....	01.03.06
MICROCRYSTALLOGRAPHY.....	X-RAY OPTICS.....	LAUE.....	13.14.03
MICROCRYSTALLOGRAPHY.....	MICROBEAM.....	SYNCHROTRON.....	13.14.05
MICROCRYSTALS.....	PRESSURE-FREEZING.....	CHESS.....	TP114
MICROCRYSTALS.....	ELECTRON DIFFRACTION.....	STRUCTURE ANALYSIS.....	04.01.02
MICROCRYSTALS.....	GISAXS.....	NANOTEMPLATE.....	13.14.01
MICROCRYSTALS.....	SYNCHROTRON BEAMLINES.....	MEMBRANE PROTEINS.....	13.14.04
MICROEMULSIONS.....	PROTEIN PURIFICATION.....	SMALL-ANGLE NEUTRON SCATTERING.....	MP143
MICROFOCUS.....	INSTRUMENT.....	GENERATOR.....	03.02.01
MICROFOCUS BEAMLINE.....	SYNCHROTRON RADIATION.....	REMOTE ACCESS.....	MP202
MICROSTRUCTURE.....	MICROBEAM.....	X-RAY.....	TP088
MICROWAVE DIELECTRIC.....	PHASE EQUILIBRIA.....	BARIUM NIOBATES.....	MP099
MINI-BEAM.....	MICRO-DIFFRACTION.....	RASTERING.....	MP208
MITOCHONDRIAL INTERMEMBRANE AS.....	AUGMENTER OF LIVER REGENERATION.....		TP178
MIXED ISOMERS.....	POLYMORPHISM.....	MOLECULAR COCRYSTALS.....	13.10.08
MODEL BUILDING.....	NUCLEIC ACIDS.....	MACROMOLECULAR CRYSTALLOGRAPHY.....	SP154
MODULATED.....	INCOMMENSURATE.....		13.01.01
MODULATED PROTEIN.....	INCOMMENSURATE MODULATION.....	PROFILIN:ACTIN.....	13.01.05
MODULATED STRUCTURE.....	VANADIUM OXIDE.....	DISORDERED STRUCTURE.....	13.01.07
MODULATED STRUCTURE.....	INTERMETALLICS.....	CORRELATED ELECTRONS.....	13.01.08
MOFS.....			TP031
MOLECULAR COCRYSTALS.....	MIXED ISOMERS.....	POLYMORPHISM.....	13.10.08
MOLECULAR DYNAMICS.....	PROTEIN FLEXIBILITY.....	SAXS.....	13.11.06
MOLECULAR DYNAMICS.....	NEUTRON SPECTROSCOPY.....	PROTEIN DYNAMICS.....	TR.01.04
MOLECULAR DYNAMICS SIMULATION.....	DYNAMICS.....	NEUTRON SCATTERING.....	09.02.04
MOLECULAR MAGNETS.....	VIBRATIONAL SPECTROSCOPY.....	LOCAL STRUCTURE.....	13.06.06
MOLECULAR MOVIE.....	HMG-COA REDUCTASE.....	ENZYME MOTION.....	SP129
MOLECULAR RECOGNITION.....	QUASIRACEMIC MATERIALS.....	SUPRAMOLECULAR CHEMISTRY.....	13.10.11
MOLECULAR REPLACEMENT.....	POWDER DIFFRACTION.....	PROTEIN.....	13.09.13
MOLECULAR SIMULATION.....	POLYMORPHISM.....	CROSS-NUCLEATION.....	13.10.05
MOLPROBITY VALIDATION.....	STRUCTURE IMPROVEMENT.....	ALL-ATOM CONTACTS.....	01.05.05
MONO-ADP-RIBOSYLTRANSFERASE.....	VIBRIO CHOLERAE.....	BACTERIAL TOXIN.....	AW.01.06
MONOOXYGENASE.....	METALLOPROTEIN.....	HEME.....	01.04.07
MONOSODIUM URATE CRYSTALS.....	GROWTH KINETICS.....	ATOMIC FORCE MICROSCOPY.....	13.10.06
MORPHOLOGY.....	SOLID-STATE REACTIVITY.....	COCRYSTAL.....	SP005
MULTIFERROIC.....	NEUTRON DIFFRACTION.....	FERROELECTRIC.....	13.04.05
MULTIFERROICITY.....	FERROELECTRICITY.....	ANTIFERROMAGNETISM.....	13.04.01
MULTILAYER OPTICS.....	SINGLE CRYSTAL DIFFRACTION.....	X-RAY SOURCE.....	03.02.03
MULTIPLE DATA SETS.....	DATA COLLECTION STRATEGY.....	X-RAY DOSE.....	SP043
MULTIPLE MUTANT CYCLES.....	KINETICS.....	AMINOACYL-TRNA SYNTHETASE.....	TP127
MULTIPLE STRUCTURE ALIGNMENT.....	SENSE/ANTISENSE CODING.....		01.06.03
MULTIVALENT TEMPLATE.....	PHOTOCYCLOADDITION.....	TOPOCHEMISTRY.....	13.02.03
MUSCLE.....	FIBER DIFFRACTION.....	TIME RESOLVED.....	13.16.07
MUTAGENESIS.....	SARS.....	RNA BINDING.....	SP071
MYOGLOBIN.....	PROTEIN DYNAMICS.....	TIME-RESOLVED LAUE CRYSTALLOGR.....	13.16.01
N CONTAINING BISPHTHONATE.....	BONE LOSS INHIBITOR.....	FARNESYL PYROPHOSPHATE SYNTHASE.....	MP018
N-GLYCOSYLATION.....	PICHIA PASTORIS.....	ALPHA GLUCOSIDASE I.....	AW.01.08
NADH.....	COA.....	HMG-COA REDUCTASE.....	01.04.02
NANO.....	ESRF.....	SYNCHROTRON.....	13.09.06
NANO-PARTICLES.....	PAIR DISTRIBUTION FUNCTION.....	CATALYST.....	13.08.01
NANO-SCALE LATTICE MODULATION.....	X-RAY DIFFUSE SCATTERING.....	CUPRATES.....	13.15.05
NANOCLUSTERS.....	ZEOLITES.....	SEMICONDUCTOR.....	MP190
NANOFIBERS.....	TMV.....	TIME RESOLVED SAXS.....	TP210
NANOPARTICLE.....	POLYMER.....	NEUTRON SCATTERING.....	09.01.01
NANOPARTICLE.....	DYNAMICS.....	BLOCK COPOLYMER.....	MP159
NANOPARTICLES.....	INTERNAL STRESS.....	GLASS TRANSITION.....	09.02.02
NANOPARTICLES IN POLYMER MATRIX.....	SMALL ANGLE NEUTRON SCATTERING.....	POLYELECTROLYTE-PROTEIN COMPLEX.....	09.01.03
NANOSCALE.....	POLYMER NANOCOMPOSITES.....	DYNAMICS.....	MP156
NANOSTRUCTURES.....	DRUG DELIVERY.....	SAXS.....	MP140
NANOTECHNOLOGY.....	X-RAY SCATTERING.....	PROTEOMICS.....	MP013
NANOTEMPLATE.....	MICROCRYSTALS.....	GISAXS.....	13.14.01
NATIVELY UNFOLDED PROTEINS.....	RIBOZYME FOLDING.....	PROTEIN FOLDING.....	13.11.05
NCS.....	PROTEIN-LIGAND COMPLEX.....	REFINEMENT.....	TP139
NEGATIVE THERMAL EXPANSION.....	NON-HYDROLYTIC SOL-GEL PROCESS.....	POWDER DIFFRACTION.....	AW.01.03
NEUROLOGY.....	STRUCTURE-GUIDED DRUG DESIGN.....	PARKINSON'S DISEASE.....	13.03.01
NEURON SCATTERING.....	MACROMOLECULAR CRYSTALSTALLO.....	NEUTRON SOURCES.....	SP026
NEUROPHYSIN FERROCHELATASE OBE.....	ISAS STRUCTURE DETERMINATION.....	ANOMALOUS SCATTERING.....	AW.02.08
NEUTRON.....	SYNCHROTRON.....	SMALL MOLECULE.....	10.01.01
NEUTRON.....	SCATTERING.....	OPPORTUNITIES.....	13.09.09
NEUTRON.....	GRAZING INCIDENCE.....	REFLECTOMETRY.....	13.09.10
NEUTRON.....	HYDROGEN.....	STORAGE.....	13.13.03

## Keywords

NEUTRON.....	ANGER.....	CAMERA.....	MP072
NEUTRON.....	DETECTOR.....	POWDER.....	MP102
NEUTRON.....	TIME-OF-FLIGHT.....	PROTON TRANSFER.....	MP113
NEUTRON.....	FOCUSING.....	MICROBEAM.....	TP061
NEUTRON CONTRAST VARIATION.....	PROTEIN STRUCTURE AND FUNCTION.....	SMALL-ANGLE SCATTERING.....	TR.01.07
NEUTRON CRYSTALLOGRAPHY.....	MACROMOLECULE CRYSTALLOGRAPH.....	LAUE DIFFRACTOMETER.....	MP125
NEUTRON DETECTORS.....	METHANOL LNCL3 ADDUCTS.....	SCINTILLATORS.....	MP181
NEUTRON DIFFRACTION.....	HYDROGEN BONDING.....		06.01.01
NEUTRON DIFFRACTION.....	HYDROGEN BONDING.....	SINGLE CRYSTAL.....	06.01.07
NEUTRON DIFFRACTION.....	HYDROGEN BOND H/D ISOTOPE EFFECT.....	JAHN-TELLER DISTORTION.....	13.02.05
NEUTRON DIFFRACTION.....	FERROELECTRIC.....	MULTIFERROIC.....	13.04.05
NEUTRON DIFFRACTION.....	SANS.....	NEUTRON REFLECTOMETRY.....	13.09.11
NEUTRON DIFFRACTION.....	SINGLE CRYSTAL.....	SPALLATION NEUTRON SOURCE.....	MP117
NEUTRON DIFFRACTION.....	HIGH PRESSURE.....	SPALLATION.....	MP128
NEUTRON DIFFRACTION.....	ENDOTHAPEPSIN.....	ASPARTIC PROTEINASE.....	SP151
NEUTRON DIFFRACTION.....	PROTONATION STATE.....	HUMAN DEOXYHEMOGLOBIN.....	SP179
NEUTRON DIFFRACTION.....	FULL DEUTERATION.....	JOINT REFINEMENT.....	TP022
NEUTRON DIFFRACTION.....	PROTEIN CRYSTALLOGRAPHY.....		TR.01.05
NEUTRON DIFFRACTION.....	MEMBRANE STRUCTURE.....	MEMBRANE PROTEINS.....	TR.01.06
NEUTRON DIFFRACTION RESULTS.....	JOINT X-RAY NEUTRON REFINEMENT.....	RESULTS W/IMPLICATIONS MRI REX.....	MP134
NEUTRON DIFFUSE SCATTERING.....	STRONGLY CORRELATED OXIDES.....	CHARGE AND SPIN ORDER.....	13.04.04
NEUTRON OPTICS.....	SUPERMIRROR TECHNOLOGY.....	NEUTRON POWDER DIFFRACTION.....	TP034
NEUTRON POWDER DIFFRACTION.....	PHASE TRANSITION.....	H2 STORAGE.....	13.13.04
NEUTRON POWDER DIFFRACTION.....	OXYGEN-VACANCY ORDERING.....	MANGANITES.....	SP032
NEUTRON POWDER DIFFRACTION.....	NEUTRON OPTICS.....	SUPERMIRROR TECHNOLOGY.....	TP034
NEUTRON REFLECTOMETRY.....	NEUTRON DIFFRACTION.....	SANS.....	13.09.11
NEUTRON SCATTERING.....	NANOPARTICLE.....	POLYMER.....	09.01.01
NEUTRON SCATTERING.....	MOLECULAR DYNAMICS SIMULATION.....	DYNAMICS.....	09.02.04
NEUTRON SCATTERING.....	RELAXOR.....	FERROELECTRIC.....	13.04.02
NEUTRON SCATTERING.....	CHARGE/ORBITAL ORDERING.....	CMR MANANITES.....	13.04.03
NEUTRON SCATTERING.....	ALLOYS.....	DIFFUSE SCATTERING.....	13.15.04
NEUTRON SCATTERING.....	NEW INSTRUMENTATION.....	SINGLE CRYSTAL NEUTRON DIFFRACT.....	MP121
NEUTRON SCATTERING.....	INCOMMENSURATE ANTIFERROMAGNE.....	QUANTUM SPIN-LIQUID.....	SP201
NEUTRON SCATTERING SPECTROSCOPY.....	HYDROGEN BONDING.....	PROTON CONDUCTOR.....	06.01.06
NEUTRON SOURCES.....	NEURON SCATTERING.....	MACROMOLECULAR CRYSTALSTALLOG.....	SP026
NEUTRON SPECTROSCOPY.....	HYDRATION WATER.....		09.02.05
NEUTRON SPECTROSCOPY.....	PROTEIN DYNAMICS.....	MOLECULAR DYNAMICS.....	TR.01.04
NEUTRON SPIN ECHO.....	MICELLES.....	THREADLIKE.....	09.02.03
NEUTRON SPIN ECHO.....	QUASIE-ELASTIC.....	SMALL ANGLE NEUTRON SCATTERING.....	TP041
NEUTRON X-RAY AND LIGHT SCATTERING.....	COLLECTIVE MOLECULAR DYNAMICS.....	MEMBRANES.....	09.02.01
NEUTRONS.....	SIR PHASING.....	DIRECT METHODS.....	AW.02.05
NEUTRONS.....	SIR DATA.....	DIRECT METHODS.....	TP083
NEUTRONS & X-RAYS.....	AMYLOID.....	FIBRE DIFFRACTION.....	02.01.03
NEW INSTRUMENTATION.....	SINGLE CRYSTAL NEUTRON DIFFRACT.....	NEUTRON SCATTERING.....	MP121
NH3 CHANNEL.....	MEMBRANE PROTEIN.....	CO2 CHANNEL.....	SP068
NICOTINAMIDASE.....	PYRAZINAMIDASE.....		SP141
NITROBENZENE DIMERIZATION.....	ORGANIC SOLID-STATE REACTION.....	SOLID SOLUTION MODELING.....	SP193
NMR.....	HYDROGEN BOND.....	QUANTUM CHEMISTRY.....	06.01.03
NMR SPECTROSCOPY.....	X-RAY CRYSTALLOGRAPHY.....	DNA-PROTEIN COMPLEX.....	TR.01.10
NON CRYSTALLOGRAPHIC SYMMETRY.....	EVOLUTION.....	VIRUS.....	01.03.03
NON-AMBIENT DIFFRACTION.....	LITHIUM BATTERIES.....	ELECTROLYTES.....	TP189
NON-HYDROLYTIC SOL-GEL PROCESS.....	POWDER DIFFRACTION.....	NEGATIVE THERMAL EXPANSION.....	AW.01.03
NON-LINEAR OPTICAL PROPERTIES.....	ISOTHIOCYANATES.....	CHIRAL MOLCULES.....	03.01.06
NOVEL PROTEIN FOLD.....	DNA BINDING PROTEIN.....	RESTRICTION ENZYMES.....	MP044
NUCLEAR MAGNETIC RESONANCE SPECTRO.....	HIV MEMBRAN FUSION & VIRAL ENTRY.....	TRANSFERED NOE.....	TR.01.12
NUCLEAR MAGNETIC RESONANCE.....	SOLUTION.....	SMALL ANGLE SCATTERING.....	13.11.02
NUCLEAR RECEPTOR.....	EVOLUTION.....		01.06.04
NUCLEASE.....	CRYSTAL STRUCTURE.....	RNA.....	TP053
NUCLEATION.....	SEEDING.....	MATRIX.....	01.08.02
NUCLEATION.....	GROWTH.....	POLYMORPH.....	13.10.04
NUCLEIC ACID.....	DERIVATIZATION.....	SELENIUM.....	03.01.02
NUCLEIC ACIDS.....	MACROMOLECULAR CRYSTALLOGRAPH.....	MODEL BUILDING.....	SP154
OBESITY.....	DIABETES.....	METABOLISM.....	SP002
OPPORTUNITIES.....	NEUTRON.....	SCATTERING.....	13.09.09
OPTICS.....	ANOMALOUS.....	SOURCES.....	03.01.04
OPTICS.....	X-RAY.....	FLUX.....	SP177
OPTIMAL PARAMETER ESTIMATION.....	BAYES'S THEOREM.....		01.02.02
OPTIMIZATION.....	SCREENING.....	CRYSTALLIZATION.....	01.08.03
ORAL.....	STREPTOCOCCUS MUTANS.....	ANTIGEN I/II.....	SP111
ORGANIC LIGANDS.....	SOLID-STATE REACTIVITY.....	POST-SYNTHETIC MODIFICATION.....	SP008
ORGANIC RADICALS.....	ANTIFERROMAGNETISM.....	HYDROGEN-BONDING.....	13.06.04
ORGANIC SOLID-STATE REACTION.....	SOLID SOLUTION MODELING.....	NITROBENZENE DIMERIZATION.....	SP193
OSCILLATION.....	RADIATION DAMAGE.....	PROTEIN CRYSTALLOGRAPHY.....	TP133

# Keywords

OUTER-MEMBRANE.....	BTUB.....	COBALAMIN.....	TP077
OXIDATIVE STRESS.....	DJ-1.....	PARKINSONS DISEASE.....	MP033
OXYGEN-VACANCY ORDERING.....	MANGANITES.....	NEUTRON POWDER DIFFRACTION.....	SP032
OXYGENASE.....	DECARBOXYLASE.....	PYRIDOXINE.....	MP069
PABA/NO.....	HGSTP1.....	ANTICANCER PRODRUGS.....	TP081
PAGP.....	REFOLDING.....	SDS.....	AW.01.07
PAIR DISTRIBUTION FUNCTION.....	CATALYST.....	NANO-PARTICLES.....	13.08.01
PAIR DISTRIBUTION FUNCTION ANALYSIS.....	TIME-RESOLVED.....	CATALYTIC NANOPARTICLES.....	13.08.05
PAPAIN.....	CYSTEINE PEPTIDASE.....	CRYSTAL OPTIMIZATION.....	TP075
PARKINSON'S DISEASE.....	NEUROLOGY.....	STRUCTURE-GUIDED DRUG DESIGN.....	13.03.01
PARKINSONS DISEASE.....	OXIDATIVE STRESS.....	DJ-1.....	MP033
PAZ.....	SIRNA BINDING DOMAIN.....	ARGONAUTE.....	SP104
PCB.....	STRUCTURE.....	BIPHENYL DIOXYGENASE.....	TP046
PDB FILES.....	MACROMOLECULAR STRUCTURE.....	END-USERS.....	01.07.01
PDF.....	CHARGE DENSITY WAVE.....	LOCAL STRUCTURE.....	13.15.03
PDF.....	SPIN CROSSOVER.....	POWDER DIFFRACTION.....	SP195
PDF.....	STRUCTURE DETERMINATION.....		TP196
PDZ DOMAIN.....	SPAR.....	DENDRITIC SPINES.....	SP199
PENTABLOCK COPOLYMER GELS.....	CALCIUM PHOSPHATE NANOCRYSTALS.....	SAXS AND SANS.....	09.01.05
PF0899.....	UNCHARACTERIZED PROTEIN.....	PYROCOCCUS FURIOSUS.....	TP017
PHARMACEUTICAL.....	SURFACES AND MICROWAVE.....	POLYMORPHISM.....	13.10.03
PHARMACEUTICAL.....	HYDRATE.....	CRYSTALLIZATION.....	13.10.13
PHARMACEUTICAL.....	COCRYSTAL.....	SOLID SOLUTION.....	SP205
PHARMACEUTICAL COCRYSTAL.....	COCRYSTAL.....	SCREENING.....	13.10.07
PHASE AMBIGUITY.....	MACROMOLECULAR CRYSTALLOGRAPHY.....	ANOMALOUS SCATTERING.....	AW.02.01
PHASE EQUILIBRIA.....	BARIUM NIOBATES.....	MICROWAVE DIELECTRIC.....	MP099
PHASE TRANSFORMATION.....	POLYMORPH.....	ACTIVE PHARMACEUTICAL INGREDIENT.....	SP040
PHASE TRANSITION.....	TWINNING.....	VARIABLE TEMPERATURE EXPERIMENTS.....	13.02.01
PHASE TRANSITION.....	TOTAL SCATTERING.....	HIGH PRESSURE.....	13.12.02
PHASE TRANSITION.....	H2 STORAGE.....	NEUTRON POWDER DIFFRACTION.....	13.13.04
PHASE TRANSITION.....	HYDROGEN/METHANE STORAGE.....	METAL ORGANIC FRAMEWORKS.....	13.13.05
PHASE TRANSITION.....	HIGH PRESSURE.....	RHOMBOHEDRAL PEROVSKITE.....	SP197
PHASE TRANSITIONS.....	LANDAU THEORY.....	SPONTANEOUS STRAIN.....	13.02.04
PHASING.....	MAD.....	ANOMALOUS SCATTERING.....	AW.02.02
PHENIX.....	MAXIMUM-LIKELIHOOD STRUCTURE.....	SUBATOMIC RESOLUTION.....	TP145
PHOSPHONOCARBOXYLATES.....	COORDINATION POLYMERS.....	URANIUM.....	10.01.04
PHOTOCRYSTALLOGRAPHY.....	CHARGE-DENSITY.....	ELECTRON TRANSFER.....	TP050
PHOTOCRYSTALLOGRAPHY.....	PHOTOISOMERIZATION.....	PHOTODIMERIZATION.....	13.02.06
PHOTOCYCLOADDITION.....	TOPOCHEMISTRY.....	MULTIVALENT TEMPLATE.....	13.02.03
PHOTODIMERIZATION.....	PHOTOCRYSTALLOGRAPHY.....	PHOTOISOMERIZATION.....	13.02.06
PHOTOISOMERIZATION.....	PHOTODIMERIZATION.....	PHOTOCRYSTALLOGRAPHY.....	13.02.06
PHOTOMETRY.....	INTEGRATION.....		TP152
PHOTORECEPTOR.....	SIGNALLING.....	REACTION MECHANISM.....	01.04.01
PHOTOSYSTEM I.....	LIGHT-HARVESTING.....	ELECTRON TRANSFER.....	01.03.05
PHYLOGENY.....	SUBSTRATE DETERMINATION.....	EVOLUTION.....	01.06.02
PICHA PASTORIS.....	ALPHA GLUCOSIDASE I.....	N-GLYCOSYLATION.....	AW.01.08
PICOSECOND.....	TIME-RESOLVED.....	LAUE.....	MP204
PINCER.....	SULFONATE.....	TRIENE.....	MP165
PK PREDICTION.....	TITRATION CURVES.....	PROTEIN IONIZATION.....	MP066
PLATINUM.....	GISAXS.....	TUNGSTEN.....	13.08.02
POLYADENYLATE POLYMERASE.....	RNA COMPLEX.....	VACCINIA VIRUS PROTEIN.....	TP086
POLYELECTROLYTE-PROTEIN COMPLEX.....	NANOPARTICLES IN POLYMER MATRIX.....	SMALL ANGLE NEUTRON SCATTERING.....	09.01.03
POLYFUNCTIONAL LIGANDS.....	HYDROGEN BONDING.....	METAL(II)-BETADIKETONATES.....	13.10.17
POLYGLUTAMINE.....	POLYPROLINE.....	AMYLOID.....	02.01.02
POLYMER.....	NEUTRON SCATTERING.....	NANOPARTICLE.....	09.01.01
POLYMER.....	CHARGE DENSITY.....	SYNCHROTRON.....	MP162
POLYMER NANOCOMPOSITES.....	DYNAMICS.....	NANOSCALE.....	MP156
POLYMORPH.....	NUCLEATION.....	GROWTH.....	13.10.04
POLYMORPH.....	ACTIVE PHARMACEUTICAL INGREDIEN.....	PHASE TRANSFORMATION.....	SP040
POLYMORPHISM.....	POLYSACCHARIDES.....	IOTA-CARRAGEENAN.....	02.01.04
POLYMORPHISM.....	PHARMACEUTICAL.....	SURFACES AND MICROWAVE.....	13.10.03
POLYMORPHISM.....	CROSS-NUCLEATION.....	MOLECULAR SIMULATION.....	13.10.05
POLYMORPHISM.....	MOLECULAR COCRYSTALS.....	MIXED ISOMERS.....	13.10.08
POLYMORPHISM.....	SELF-ASSEMBLED MONOLAYERS.....	TEMPLATED GROWTH.....	AW.01.02
POLYMORPHISM.....	RACEMIC.....	HYDROGEN BONDING.....	SP011
POLYMORPHISM.....	GOLD-THIOL MONOLAYERS.....	ANALYTICAL METHODS.....	SP207
POLYPROLINE.....	AMYLOID.....	POLYGLUTAMINE.....	02.01.02
POLYSACCHARIDES.....	IOTA-CARRAGEENAN.....	POLYMORPHISM.....	02.01.04
POLYSACCHARIDES.....	SYNCHROTRON RADIATION.....	FIBER DIFFRACTION.....	TP073
POST-SYNTHETIC MODIFICATION.....	ORGANIC LIGANDS.....	SOLID-STATE REACTIVITY.....	SP008
POWDER.....	NEUTRON.....	DETECTOR.....	MP102
POWDER DIFFRACTION.....	PROTEIN.....	MOLECULAR REPLACEMENT.....	13.09.13
POWDER DIFFRACTION.....	NEGATIVE THERMAL EXPANSION.....	NON-HYDROLYTIC SOL-GEL PROCESS.....	AW.01.03

## Keywords

POWDER DIFFRACTION	PDF	SPIN CROSSOVER	SP195
POWDER DIFFRACTION	SPALLATION NEUTRON SOURCE		TP055
POWDER NEUTRON DIFFRACTION	HYDROGEN POSITIONS	PREHNITE	MP106
PRECIPITATES	DIFFUSE SCATTERING	LOCAL STRUCTURE	13.15.02
PREHNITE	POWDER NEUTRON DIFFRACTION	HYDROGEN POSITIONS	MP106
PRESSURE-FREEZING	CHESS	MICROCRYSTALLOGRAPHY	TP114
PRESSURIZED OXYGEN	COFACTOR-LESS OXIDASE	CATALYTIC INTERMEDIATE	01.04.06
PRION	YEAST	THERMAL STABILITY	SP211
PROBLEM STRUCTURES	REFINEMENT	INTERFACES	MP168
PROFILIN:ACTIN	MODULATED PROTEIN	INCOMMENSURATE MODULATION	13.01.05
PROGRAM	RESTRAINTS	REFINEMENT	TP148
PROLINE CATABOLISM	TWINNING	SUBSTRATE CHANNELING	01.01.05
PROTEASOME	UBIQUITIN RECEPTOR	MERGER CRYSTALLOGRAPHY & NMR	TR.01.11
PROTEIN	SANS	SOL-GEL	09.01.06
PROTEIN	MOLECULAR REPLACEMENT	POWDER DIFFRACTION	13.09.13
PROTEIN	ELECTRON DIFFRACTION		13.14.02
PROTEIN	GENERATOR	MICROCRYSTAL	TP194
PROTEIN CLASSIFICATION	FOLDING	EVOLUTION	01.07.03
PROTEIN COMPLEXES	ROSETTADOCK	STRUCTURE PREDICTION	01.07.05
PROTEIN CRYSTAL	IMAGING	UV	SP174
PROTEIN CRYSTALLIZATION	STRUCTURAL GENOMICS	HIGH THROUGHPUT	03.01.01
PROTEIN CRYSTALLOGRAPHY	BEAMLINE		MP187
PROTEIN CRYSTALLOGRAPHY	OSCILLATION	RADIATION DAMAGE	TP133
PROTEIN CRYSTALLOGRAPHY	COMPUTATIONAL	CCP4	TP136
PROTEIN CRYSTALLOGRAPHY	NEUTRON DIFFRACTION		TR.01.05
PROTEIN DESIGN	ROSETTA		SP157
PROTEIN DYNAMICS	TIME-RESOLVED LAUE CRYSTALLOGR	MYOGLOBIN	13.16.01
PROTEIN DYNAMICS	MOLECULAR DYNAMICS	NEUTRON SPECTROSCOPY	TR.01.04
PROTEIN ENERGY LANDSCAPE	ACCELERATED MOLECULAR DYNAMICS	CONFORMATIONAL TRANSITIONS	01.07.04
PROTEIN ENGINEERING	EVOLUTION	AMINO ACID ACTIVATION	01.06.05
PROTEIN ENGINEERING	PROTEIN THERAPETIC	PROTEIN STRUCTURE	13.03.06
PROTEIN FLEXIBILITY	SAXS	MOLECULAR DYNAMICS	13.11.06
PROTEIN FOLDING	NATIVELY UNFOLDED PROTEINS	RIBOZYME FOLDING	13.11.05
PROTEIN FOLDING	RAPID MIXING	SMALL ANGLE X-RAY SCATTERING	13.16.02
PROTEIN IONIZATION	PK PREDICTION	TITRATION CURVES	MP066
PROTEIN KINASE	INFLAMMATION	ARTHRITIS	04.01.06
PROTEIN PURIFICATION	SMALL-ANGLE NEUTRON SCATTERING	MICROEMULSIONS	MP143
PROTEIN RYSTALLIZATION	IDENTIFICATION	UV FLUORESENCE	MP004
PROTEIN STRUCTURE	MEMBRANE PROTEIN	ZINC TRANSPORTER	01.03.01
PROTEIN STRUCTURE	PROTEIN ENGINEERING	PROTEIN THERAPETIC	13.03.06
PROTEIN STRUCTURE AND FUNCTION	SMALL-ANGLE SCATTERING	NEUTRON CONTRAST VARIATION	TR.01.07
PROTEIN THERAPETIC	PROTEIN STRUCTURE	PROTEIN ENGINEERING	13.03.06
PROTEIN TYROSINE PHOSPHATASE	SUBSTRATE-TRAPPING MUTANT	HEPTP	SP135
PROTEIN-DNA INTERACTION	STRUCTURE AND FUNCTION		MP015
PROTEIN-DNA INTERACTION	AUTOINHIBITION	RESTRICTION ENZYME ECORII	TP070
PROTEIN-LIGAND COMPLEX	REFINEMENT	NCS	TP139
PROTEIN-PROTEIN INTERACTIONS	ZINC FINGER TRANSCRIPTION FACTOR	BTB DOMAIN	SP089
PROTEINS	SERIAL CRYSTALLOGRAPHY	FREE ELECTRON LASER	13.09.04
PROTEOMICS	NANOTECHNOLOGY	X-RAY SCATTERING	MP013
PROTON CONDUCTOR	NEUTRON SCATTERING SPECTROSCOPY	HYDROGEN BONDING	06.01.06
PROTON SHUTTLE	WATER NETWORK	CARBONIC ANHYDRASE	TP105
PROTON TRANSFER	NEUTRON	TIME-OF-FLIGHT	MP113
PROTON TRANSPORT	MEMBRANE PROTEIN	HEME	01.04.03
PROTON TRANSPORT	HEME	MEMBRANE PROTEIN	TP098
PROTONATION STATE	HUMAN DEOXYHEMOGLOBIN	NEUTRON DIFFRACTION	SP179
PURINE BIOSYNTHESIS	ATP GRASP FAMILY		SP058
PURINE BIOSYNTHESIS	MACROMOLECULAR COMPLEX	FGAM SYNTHETASE	TP003
PYMOL	SBEVSL	RASMOL	MP054
PYMOL	ALIGNMENT	HOMOLOGY	SP169
PYMOL	TRANSLATOR	RASMOL	TP161
PYRAZINAMIDASE	NICOTINAMIDASE		SP141
PYRIDOXINE	OXYGENASE	DECARBOXYLASE	MP069
PYRIDYL COMPOUND	SELF ASSEMBLY	COORDINATION POLYMERS	SP048
PYROCOCCUS FURIOSUS	SULFUR RESPONSE (SURR)	TRANSCRIPTIONAL REGULATOR	SP123
PYROCOCCUS FURIOSUS	PF0899	UNCHARACTERIZED PROTEIN	TP017
PYRUVATE CARBOXYLASE	BIOTIN		SP045
QUANTUM CHEMISTRY	HYDROTUNGSTITE	RIETVELD	04.01.01
QUANTUM CHEMISTRY	NMR	HYDROGEN BOND	06.01.03
QUANTUM MAGNET	CRYSTAL STRUCTURE	COORDINATION POLYMER	13.10.15
QUANTUM SPIN-LIQUID	NEUTRON SCATTERING	INCOMMENSURATE ANTIFERROMAGNET	SP201
QUANTUM-CLASSICAL DYNAMICS	AB INITIO MOLECULAR DYNAMICS	TIME CORRELATION FUNCTIONS	06.01.04
QUASIE-ELASTIC	SMALL ANGLE NEUTRON SCATTERING	NEUTRON SPIN ECHO	TP041
QUASIRACEMIC MATERIALS	SUPRAMOLECULAR CHEMISTRY	MOLECULAR RECOGNITION	13.10.11

## Keywords

RACEMIC.....	HYDROGEN BONDING .....	POLYMORPHISM.....	SP011
RADIATION DAMAGE .....	DATA QUALITY .....	DATA PROCESSING .....	01.02.03
RADIATION DAMAGE .....	MICRO-CRYSTALS .....	MICRO-DIFFRACTION.....	13.14.06
RADIATION DAMAGE .....	TEMPERATURE DEPENDENCE .....	CRYOCRYSTALLOGRAPHY .....	SP079
RADIATION DAMAGE .....	METALLOPROTEINS.....		SP191
RADIATION DAMAGE .....	PROTEIN CRYSTALLOGRAPHY.....	OSCILLATION .....	TP133
RADIATION DAMAGE .....	XAS .....	METAL ACTIVE SITE.....	TR.01.02
RADICAL SAM SUPERFAMILY .....	HMP-P SYNTHASE.....	THIAMIN BIOSYNTHESIS .....	01.01.01
RAMACHANDRAN DISTRIBUTIONS .....	STRUCTURAL BIOINFORMATICS .....	ROTAMERS.....	01.07.02
RAPID MIXING .....	SMALL ANGLE X-RAY SCATTERING.....	PROTEIN FOLDING .....	13.16.02
RASMOL .....	MAPS .....	SBEVSL .....	MP039
RASMOL .....	PYMOL .....	SBEVSL .....	MP054
RASMOL .....	PYMOL .....	TRANSLATOR .....	TP161
RASTERING.....	MINI-BEAM.....	MICRO-DIFFRACTION.....	MP208
REACTION INTERMEDIATE .....	TIME-RESSOLVED X-RAY CRYSTALLOG.....	X-RAY CRYSTALLOGRAPHY .....	13.16.06
REACTION INTERMEDIATE .....	HIV-1 PROTEASE .....		SP074
REACTION MECHANISM.....	PHOTORECEPTOR .....	SIGNALLING .....	01.04.01
REDOX CHEMISTRY .....	COPPER AMINE OXIDASE.....	CATALYTIC INTERMEDIATES .....	TP130
REFINEMENT.....	RESTRAINTS.....	MACROMOLECULAR .....	01.05.07
REFINEMENT.....	INTERFACES .....	PROBLEM STRUCTURES .....	MP168
REFINEMENT.....	NCS .....	PROTEIN-LIGAND COMPLEX.....	TP139
REFINEMENT.....	PROGRAM .....	RESTRAINTS .....	TP148
REFLECTOMETRY .....	NEUTRON .....	GRAZING INCIDENCE .....	13.09.10
REFOLDING .....	SDS .....	PAGP .....	AW.01.07
RELAXOR .....	FERROELECTRIC.....	NEUTRON SCATTERING .....	13.04.02
RELAXOR .....	FERROELECTRIC.....	TRANSITION .....	SP020
REMOTE ACCESS .....	MICROFOCUS BEAMLINE.....	SYNCHROTRON RADIATION.....	MP202
REMOTE HOMOLOGS .....	DISTANT HOMOLOGY DETECTION.....	SEQUENCE ALIGNMENT .....	TP158
REPLICATION .....	ARCHAEA.....		MP052
RESCUE STRATEGIES.....	CRYSTALLIZATION PREDICTION .....	STRUCTURAL GENOMICS .....	01.08.01
RESISTANCE .....	SUBSTRATE COMPLEXES .....	AMINOGLYCOSIDE .....	TP109
RESTRAINTS.....	MACROMOLECULAR .....	REFINEMENT.....	01.05.07
RESTRAINTS.....	REFINEMENT.....	PROGRAM .....	TP148
RESTRICTION ENZYME ECORII .....	PROTEIN-DNA INTERACTION .....	AUTOINHIBITION .....	TP070
RESTRICTION ENZYMES.....	NOVEL PROTEIN FOLD.....	DNA BINDING PROTEIN .....	MP044
RESULTS W/IMPLICATIONS MRI REX.....	NEUTRON DIFFRACTION RESULTS .....	JOINT X-RAY NEUTRON REFINEMENT .....	MP134
RHEO-SANS.....	STRUCTURE .....	LAMELLAR PHASE .....	09.01.07
RHOMBOHEDRAL PEROVSKITE .....	PHASE TRANSITION.....	HIGH PRESSURE .....	SP197
RIBOSOME .....	VIRULENCE .....	GTPASE .....	TP101
RIBOSWITCH.....	METAL SENSING .....	GENE REGULATION .....	01.01.04
RIBOSWITCH.....	SAM.....	MICROCRYSTALLOGRAPHY .....	01.03.06
RIBOZYME.....	LIGASE .....	IN VITRO SELECTION.....	01.06.06
RIBOZYME.....	INHIBITOR.....	CHEMICAL TRAPPING .....	SP149
RIBOZYME FOLDING .....	PROTEIN FOLDING .....	NATIVELY UNFOLDED PROTEINS .....	13.11.05
RIETVELD.....	QUANTUM CHEMISTRY.....	HYDROTUNGSTITE .....	04.01.01
RIETVELD.....	DEFECT MODEL.....	URANIUM OXIDE .....	TP192
RIETVELD ANALYSIS.....	SOREL CEMENT.....	XRPD.....	04.01.04
RIETVELD REFINEMENT.....	CLATHRATE HYDRATE.....	GUEST DISORDER .....	13.12.03
RIGID UNIT MODES .....	STRUCTURE PREDICTION .....	INCOMMENSURATE .....	13.01.06
RNA .....	BIOPHYSICS .....	SAXS .....	13.11.01
RNA .....	SPLICING .....	FLUORESCENCE ANISOTROPY .....	MP025
RNA .....	NUCLEASE .....	CRYSTAL STRUCTURE.....	TP053
RNA BINDING.....	MUTAGENESIS.....	SARS .....	SP071
RNA COMPLEX .....	VACCINIA VIRUS PROTEIN.....	POLYADENYLATE POLYMERASE.....	TP086
RNA METHYLTRANSFERASE.....	KSGA.....	SAH.....	TP112
RNA STRUCTURE .....	IRES.....	TRANSLATION .....	01.01.06
ROBOTIC CRYSTALLIZATION.....	ITERATIVE OPTIMIZATION.....	TAILORED SCREENING.....	TP180
ROBOTICS .....	MECHATRONICS.....	CRYSTAL HARVESTING .....	TP118
ROSETTA.....	PROTEIN DESIGN .....		SP157
ROSETTADOCK.....	STRUCTURE PREDICTION .....	PROTEIN COMPLEXES .....	01.07.05
ROTAMERS.....	RAMACHANDRAN DISTRIBUTIONS .....	STRUCTURAL BIOINFORMATICS .....	01.07.02
SACCHAROMYCES CEREVISIAE .....	THIAMIN BIOSYNTHESIS.....	THIAZOLE SYNTHASE .....	01.04.04
SAD .....	SHELX .....	MACROMOLECULAR PHASING .....	01.05.02
SAD PHASING.....	SAPOSIN D .....	CERAMIDE ACTIVATOR PROTEIN.....	SP084
SAH .....	RNA METHYLTRANSFERASE.....	KSGA.....	TP112
SAM.....	MICROCRYSTALLOGRAPHY.....	RIBOSWITCH .....	01.03.06
SANS.....	SOL-GEL.....	PROTEIN .....	09.01.06
SANS.....	NEUTRON REFLECTOMETRY .....	NEUTRON DIFFRACTION .....	13.09.11
SANS.....	MACROMOLECULAR COMPLEX .....	SAXS .....	13.11.08
SANS.....	HOMOPOLYMER.....	BLOCK COPOLYMER.....	MP131
SAPOSIN D.....	CERAMIDE ACTIVATOR PROTEIN .....	SAD PHASING.....	SP084
SARCOSINE DEHYDROGENASE.....	CRYSTAL STRUCTURE.....		SP126
SARS .....	RNA BINDING.....	MUTAGENESIS .....	SP071

# Keywords

SAXS.....	SELF-ASSEMBLY .....	SOFT MATTER .....	09.01.04
SAXS.....	SOLUTION PHASE.....	SELF-ASSEMBLY .....	13.08.06
SAXS.....	RNA.....	BIOPHYSICS.....	13.11.01
SAXS.....	UNFOLDED .....		13.11.03
SAXS.....	MOLECULAR DYNAMICS.....	PROTEIN FLEXIBILITY.....	13.11.06
SAXS.....	BIOMOLECULES.....	XFEL.....	13.11.07
SAXS.....	SANS.....	MACROMOLECULAR COMPLEX.....	13.11.08
SAXS.....	NANOSTRUCTURES.....	DRUG DELIVERY.....	MP140
SAXS.....	APOBEC.....	ACF.....	MP146
SAXS.....	SUPERCritical JET .....		MP153
SAXS.....	STATISTICS.....	LIKELIHOOD METHODS.....	SP091
SAXS.....	HUMAN FEZ1.....	UNFOLDED PROTEIN.....	TP012
SAXS.....	MEMBRANE PROTEIN.....	DETERGENT.....	TP024
SAXS.....	TIME-RESOLVED.....	CLOCK.....	TR.01.08
SAXS.....	ALTERNATIVE METHODS.....	APOBEC3G.....	TR.01.09
SAXS AND SANS.....	PENTABLOCK COPOLYMER GELS.....	CALCIUM PHOSPHATE NANOCRYSTALS.....	09.01.05
SAXS/SANS.....	AAA+ ATPASE.....	TRANSCRIPTION.....	TP092
SBEVSL.....	RASMOL.....	MAPS.....	MP039
SBEVSL.....	RASMOL.....	PYMOL.....	MP054
SCATTERING.....	OPPORTUNITIES.....	NEUTRON.....	13.09.09
SCIENTIFIC INQUIRY.....	TEACHING CRYSTALLOGRAPHY.....	INFERENCE.....	13.05.02
SCINTILLATORS.....	NEUTRON DETECTORS.....	METHANOL LNCL3 ADDUCTS.....	MP181
SCREENING.....	CRYSTALLIZATION.....	OPTIMIZATION.....	01.08.03
SCREENING.....	PHARMACEUTICAL COCRYSTAL.....	COCRYSTAL.....	13.10.07
SCREENING.....	IN-SITU.....	HIGH THROUGHPUT.....	TP170
SDS.....	PAGP.....	REFOLDING.....	AW.01.07
SEEDING.....	MATRIX.....	NUCLEATION.....	01.08.02
SELENIUM.....	NUCLEIC ACID.....	DERIVATIZATION.....	03.01.02
SELF ASSEMBLY.....	COORDINATION POLYMERS.....	PYRIDYL COMPOUND.....	SP048
SELF-ASSEMBLED MONOLAYERS.....	TEMPLATED GROWTH.....	POLYMORPHISM.....	AW.01.02
SELF-ASSEMBLY.....	SOFT MATTER.....	SAXS.....	09.01.04
SELF-ASSEMBLY.....	SAXS.....	SOLUTION PHASE.....	13.08.06
SEMET.....	FLUORESCENCE.....	DECAY.....	TR.01.03
SEMICONDUCTOR.....	NANOCCLUSERS.....	ZEOLITES.....	MP190
SENSE/ANTISENSE CODING.....	MULTIPLE STRUCTURE ALIGNMENT.....		01.06.03
SEQUENCE ALIGNMENT.....	REMOTE HOMOLOGS.....	DISTANT HOMOMOLOGY DETECTION.....	TP158
SERIAL CRYSTALLOGRAPHY.....	FREE ELECTRON LASER.....	PROTEINS.....	13.09.04
SERVICE.....	AUTOMATION.....		MP137
SERVICE CRYSTALLOGRAPHY.....	CHEMICAL CRYSTALLOGRAPHY.....	SYNCHROTRON RADIATION.....	TP019
SHELX.....	MACROMOLECULAR PHASING.....	SAD.....	01.05.02
SIGNALLING.....	REACTION MECHANISM.....	PHOTORECEPTOR.....	01.04.01
SILICATE MELT.....	LIQUID STRUCTURE.....	AERODYNAMIC LEVITATION.....	13.12.05
SIMULATION.....	LIPID DYNAMICS.....	DMPC & DOPC.....	09.02.06
SINGLE CRYSTAL.....	NEUTRON DIFFRACTION.....	HYDROGEN BONDING.....	06.01.07
SINGLE CRYSTAL.....	COORDINATION POLYMER COMPLEX.....	VAPOUR DIFFUSION.....	13.10.18
SINGLE CRYSTAL.....	SPALLATION NEUTRON SOURCE.....	NEUTRON DIFFRACTION.....	MP117
SINGLE CRYSTAL DIFFRACTION.....	X-RAY SOURCE.....	MULTILAYER OPTICS.....	03.02.03
SINGLE CRYSTAL MICROSPECTROPHO.....	DFT OPTIMIZATION.....	FLAVIN INTERMEDIATE.....	01.04.08
SINGLE CRYSTAL NEUTRON DIFFRACT.....	NEUTRON SCATTERING.....	NEW INSTRUMENTATION.....	MP121
SINGLE CRYSTAL SPECTROSCOPY.....	SYNCHROTRON FACILITY.....	MICO-DIFFRACTION.....	TP010
SIR DATA.....	DIRECT METHODS.....	NEUTRONS.....	TP083
SIR PHASING.....	DIRECT METHODS.....	NEUTRONS.....	AW.02.05
SIRNA BINDING DOMAIN.....	ARGONAUTE.....	PAZ.....	SP104
SIZE EFFECT.....	GISAXS.....	SIZE SELECTED NANOCATALYST.....	13.08.03
SIZE SELECTED NANOCATALYST.....	SIZE EFFECT.....	GISAXS.....	13.08.03
SMALL ANGLE NEUTRON SCATTERING.....	POLYELECTROLYTE-PROTEIN COMPLE.....	NANOPARTICLES IN POLYMER MATRIX.....	09.01.03
SMALL ANGLE NEUTRON SCATTERING.....	NEUTRON SPIN ECHO.....	QUASIE-ELASTIC.....	TP041
SMALL ANGLE NEUTRON SCATTERING.....	BIOFUELS.....	LIGNOCELLULOSE.....	TP122
SMALL ANGLE SCATTERING.....	NUCLEAR MAGNETIC RESONCANCE.....	SOLUTION.....	13.11.02
SMALL ANGLE SCATTERING.....	SOLUTION SCATTERING.....	LIPID DIFFRACTION.....	13.11.04
SMALL ANGLE X-RAY SCATTERING.....	PROTEIN FOLDING.....	RAPID MIXING.....	13.16.02
SMALL MOLECULE.....	NEUTRON.....	SYNCHROTRON.....	10.01.01
SMALL-ANGLE NEUTRON SCATTERING.....	MICROEMULSIONS.....	PROTEIN PURIFICATION.....	MP143
SMALL-ANGLE SCATTERING.....	CARBON BLACK.....	HIERARCHICAL STRUCTURES.....	09.01.02
SMALL-ANGLE SCATTERING.....	NEUTRON CONTRAST VARIATION.....	PROTEIN STRUCTURE AND FUNCTION.....	TR.01.07
SMALL-MOLECULAR.....	HYDROGEN BONDING.....	HIGH-PRESSURE.....	06.01.02
SODIMU NIOBATE.....	FERROELCTRIC.....	LOCAL ATOMIC STRUCTURE.....	13.15.06
SOFT MATTER.....	SAXS.....	SELF-ASSEMBLY.....	09.01.04
SOFTWARE.....	AUTOMATION.....	STRUCTURE BASED DRUG DESIGN.....	03.01.05
SOFTWARE.....	AREA DETECTORS.....	DETECTOR CALIBRATION.....	03.02.02
SOFTWARE.....	JANA2006.....	APERIODIC STRUCTURES.....	13.01.02
SOFTWARE.....	INCOMMENSURATE STRUCTURES.....		13.01.03
SOFTWARE.....	ANALYSIS TOOLS.....	2D ANALYSIS.....	MP006

## Keywords

SOL-GEL	PROTEIN	SANS	09.01.06
SOLID SOLUTION	PHARMACEUTICAL	COCRYSTAL	SP205
SOLID SOLUTION MODELING	NITROSOBENZENE DIMERIZATION	ORGANIC SOLID-STATE REACTION	SP193
SOLID STATE REACTIVITY	METAL CITRACONATES	THERMAL DECOMPOSITION	13.10.14
SOLID-STATE REACTION	CARBOXYLATE	TOPOTAXY	13.02.02
SOLID-STATE REACTIVITY	COCRYSTAL	MORPHOLOGY	SP005
SOLID-STATE REACTIVITY	POST-SYNTHETIC MODIFICATION	ORGANIC LIGANDS	SP008
SOLUBILITY SCREEN	CRYSTAL SCREEN IMPROVEMENT		01.08.05
SOLUBILIZATION	CRYSTALLIZATION	TECHNOLOGY	TP175
SOLUTION	SMALL ANGLE SCATTERING	NUCLEAR MAGNETIC RESONANCE	13.11.02
SOLUTION PHASE	SELF-ASSEMBLY	SAXS	13.08.06
SOLUTION SCATTERING	LIPID DIFFRACTION	SMALL ANGLE SCATTERING	13.11.04
SOLVENT FLATTENING	DUAL-SPACE ITERATION	DIRECT METHODS	AW.02.06
SOREL CEMENT	XRPD	RIETVELD ANALYSIS	04.01.04
SOURCES	OPTICS	ANOMALOUS	03.01.04
SPALLATION	NEUTRON DIFFRACTION	HIGH PRESSURE	MP128
SPALLATION NEUTRON SOURCE	NEUTRON DIFFRACTION	SINGLE CRYSTAL	MP117
SPALLATION NEUTRON SOURCE	POWDER DIFFRACTION		TP055
SPAR	DENDRITIC SPINES	PDZ DOMAIN	SP199
SPIN CROSSOVER	POWDER DIFFRACTION	PDF	SP195
SPLICING	FLUORESCENCE ANISOTROPY	RNA	MP025
SPLIT-COIL GEOMETRY	HIGH-FIELD PULSED MAGNET	X-RAY STUDIES IN HIGH MAGNETIC FIEL	TP067
SPONTANEOUS STRAIN	PHASE TRANSITIONS	LANDAU THEORY	13.02.04
STAPHYLOCOCCUS AUREUS	COMPLEMENT	EFB	MP212
STATISTICS	LIKELIHOOD METHODS	SAXS	SP091
STORAGE	NEUTRON	HYDROGEN	13.13.03
STRENGTH, SELECTIVITY	INTERACTIVE LECTURES	CRYSTALS GROWTH	13.05.05
STREPTOCOCCUS MUTANS	ANTIGEN I/II	ORAL	SP111
STRONGLY CORRELATED OXIDES	CHARGE AND SPIN ORDER	NEUTRON DIFFUSE SCATTERING	13.04.04
STRUCTURAL BIOINFORMATICS	ROTAMERS	RAMACHANDRAN DISTRIBUTIONS	01.07.02
STRUCTURAL DISTORTION	INCOMMENSURATE MODULATION	GROUP THEORY	13.01.04
STRUCTURAL GENOMICS	RESCUE STRATEGIES	CRYSTALLIZATION PREDICTION	01.08.01
STRUCTURAL GENOMICS	HIGH THROUGHPUT	PROTEIN CRYSTALLIZATION	03.01.01
STRUCTURAL GENOMICS	STRUCTURE DETERMINATION	TARGET SELECTION	MP001
STRUCTURAL GENOMICS	ACP REDUCATASE	THERMUS THERMOPHILUS	SP115
STRUCTURE	LAMELLAR PHASE	RHEO-SANS	09.01.07
STRUCTURE	BIPHENYL DIOXYGENASE	PCB	TP046
STRUCTURE ANALYSIS	MICROCRYSTALS	ELECTRON DIFFRACTION	04.01.02
STRUCTURE AND FUNCTION	PROTEIN-DNA INTERACTION		MP015
STRUCTURE AND PROPERTIES	THERMOELECTRIC	CA-SR-CO-O	13.13.06
STRUCTURE BASED DRUG DESIGN	SOFTWARE	AUTOMATION	03.01.05
STRUCTURE COMPARISONS	STRUCTURE-FUNCTION RELATIONSHI	ENZYME MECHANISM KINETICS	SP144
STRUCTURE DETERMINATION	AUTOMATION	MACROMOLECULAR CRYSTALLOGRAPHY	01.05.03
STRUCTURE DETERMINATION	TEACHING	DIFFRACTION	13.05.03
STRUCTURE DETERMINATION	TARGET SELECTION	STRUCTURAL GENOMICS	MP001
STRUCTURE DETERMINATION	PDF		TP196
STRUCTURE IMPROVEMENT	ALL-ATOM CONTACTS	MOLPROBITY VALIDATION	01.05.05
STRUCTURE PREDICTION	PROTEIN COMPLEXES	ROSETTADOCK	01.07.05
STRUCTURE PREDICTION	INCOMMENSURATE	RIGID UNIT MODES	13.01.06
STRUCTURE SYSTEMATICS	HIGH-PRESSURE	COORDINATION CHANGE	10.01.03
STRUCTURE-BASED DRUG DESIGN	INDUSTRIAL	CRYSTALLIZATION	04.01.07
STRUCTURE-BASED DRUG DESIGN	COCKTAIL CRYSTALLOGRAPHY	URACIL-DNA GLYCOSYLASE	MP042
STRUCTURE-BASED DRUG DESIGN	CANCER THERAPY	KINASE INHIBITOR	TP090
STRUCTURE-FUNCTION RELATIONSHI	ENZYME MECHANISM KINETICS	STRUCTURE COMPARISONS	SP144
STRUCTURE-GUIDED DRUG DESIGN	PARKINSON'S DISEASE	NEUROLOGY	13.03.01
STRUCTURE-GUIDED DRUG DESIGN	LIGAND RECOGNITION	ENZYME SPECIFICITY	TP124
STRUCTURE-PROPERTY RELATIONSHIPS	THERMOELECTRIC MATERIALS	THERMAL CONDUCTIVITY	13.13.02
SUBATOMIC RESOLUTION	PHENIX	MAXIMUM-LIKELIHOOD STRUCTURE	TP145
SUBSTRATE CHANNELING	PROLINE CATABOLISM	TWINNING	01.01.05
SUBSTRATE COMPLEXES	AMINOGLYCOSIDE	RESISTANCE	TP109
SUBSTRATE DETERMINATION	EVOLUTION	PHYLOGENY	01.06.02
SUBSTRATE IDENTIFICATION	BIOINFORMATICS		01.06.01
SUBSTRATE SPECIFICITY	GLYCOSIDASE	ENZYME INHIBITION	TP029
SUBSTRATE-TRAPPING MUTANT	HEPTP	PROTEIN TYROSINE PHOSPHATASE	SP135
SUBSTRUCTURE DETERMINATION	EXPERIMENTAL ERROR	DIRECT METHODS	01.05.06
SULFONATE	TRIENE	PINCER	MP165
SULFONATE	LAYERED	INORGANIC	MP184
SULFOTRANSFERASE	METHYLTRANSFERASE	GLYCOPEPTIDE ANTIBIOTICS BIOSYNTHET	TP038
SULFUR PHASING	MEDIUM-RESOLUTION	ARCHAEOGLOBUS FULGIDUS 1382	03.01.03
SULFUR RESPONSE (SURR)	TRANSCRIPTIONAL REGULATOR	PYROCOCCUS FURIOSUS	SP123
SULFUR SAD	CR RADIATION		AW.02.04
SUPERCRITICAL JET	SAXS		MP153
SUPERMIRROR TECHNOLOGY	NEUTRON POWDER DIFFRACTION	NEUTRON OPTICS	TP034

## Keywords

SUPEROXIDE DISMUTASE	METALLOENZYME	SP138
SUPRAMOLECULAR CHEMISTRY	MOLECULAR RECOGNITION	QUASIRACEMIC MATERIALS 13.10.11
SURFACE CHARACTERIZATION	CHEMICAL FORCE MICROSCOPY	URIC ACID SP023
SURFACE ENTROPY REDUCTION	KETOACYL ACYL CARRIER PROTEIN	FABF TP183
SURFACES AND MICROWAVE	POLYMORPHISM	PHARMACEUTICAL 13.10.03
SYNAPSE MATURATION	AUTISM	SYNAPTIC JUNCTION 13.03.05
SYNAPTIC JUNCTION	SYNAPSE MATURATION	AUTISM 13.03.05
SYNCHROTRON RADIATION	FIBER DIFFRACTION	POLYSACCHARIDES TP073
SYNCHROTRON	SMALL MOLECULE	NEUTRON 10.01.01
SYNCHROTRON	NANO	ESRF 13.09.06
SYNCHROTRON	BEAMLINE	MACROMOLECULAR CRYSTALLOGRAPHY 13.09.08
SYNCHROTRON	MICROCRYSTALLOGRAPHY	MICROBEAM 13.14.05
SYNCHROTRON	FULLERENES	WHOLE MOLECULE DISORDER AW01.04
SYNCHROTRON	POLYMER	CHARGE DENSITY MP162
SYNCHROTRON	BIOSAXS	FLOW-CELL TP186
SYNCHROTRON BEAMLINES	MEMBRANE PROTEINS	MICROCRYSTALS 13.14.04
SYNCHROTRON FACILITY	MICO-DIFFRACTION	SINGLE CRYSTAL SPECTROSCOPY TP010
SYNCHROTRON RADIATION	FREE-ELECTRON LASERS	13.09.02
SYNCHROTRON RADIATION	REMOTE ACCESS	MICROFOCUS BEAMLINE MP202
SYNCHROTRON RADIATION	SERVICE CRYSTALLOGRAPHY	CHEMICAL CRYSTALLOGRAPHY TP019
SYNCHROTRON RADITION	X-RAY SCATTERING	ENERGY RECOVERY LINAC 13.09.05
SYNCHROTRON SCIENCE	X-RAY FREE ELECTRON LASER	XFEL 13.09.01
T CELL RECEPTOR	MHC MOLECULE	SP163
TAILORED SCREENING	ROBOTIC CRYSTALLIZATION	ITERATIVE OPTIMIZATION TP180
TARGET SELECTION	STRUCTURAL GENOMICS	STRUCTURE DETERMINATION MP001
TEACHING	DIFFRACTION	STRUCTURE DETERMINATION 13.05.03
TEACHING	CYBERINFRASTRUCTURE	TUTORIAL 13.05.04
TEACHING CRYSTALLOGRAPHY	INFERENCE	SCIENTIFIC INQUIRY 13.05.02
TECHNOLOGY	SOLUBILIZATION	CRYSTALLIZATION TP175
TEMPERATURE DEPENDENCE	CRYOCRYSTALLOGRAPHY	RADIATION DAMAGE SP079
TEMPLATED GROWTH	POLYMORPHISM	SELF-ASSEMBLED MONOLAYERS AW01.02
TGO	BHLH-PAS	SP076
THERMAL CONDUCTIVITY	STRUCTURE-PROPERTY RELATIONSHIP	THERMOELECTRIC MATERIALS 13.13.02
THERMAL DECOMPOSITION	SOLID STATE REACTIVITY	METAL CITRACONATES 13.10.14
THERMAL STABILITY	PRION	YEAST SP211
THERMOELECTRIC	CA-SR-CO-O	STRUCTURE AND PROPERTIES 13.13.06
THERMOELECTRIC MATERIALS	THERMAL CONDUCTIVITY	STRUCTURE-PROPERTY RELATIONSHIPS 13.13.02
THERMOSTABILITY	LIGAND	CHEMICAL FINGERPRINTS 01.08.04
THERMOSTABILITY	ASPARTATE TRANSCARBAMOYLASE	CRYSTAL STRUCTURE TP120
THERMUS THERMOPHILUS	STRUCTURAL GENOMICS	ACP REDUCATASE SP115
THIAMIN BIOSYNTHESIS	RADICAL SAM SUPERFAMILY	HMP-P SYNTHASE 01.01.01
THIAMIN BIOSYNTHESIS	THIAZOLE SYNTHASE	SACCHAROMYCES CEREVISIAE 01.04.04
THIAZOLE SYNTHASE	SACCHAROMYCES CEREVISIAE	THIAMIN BIOSYNTHESIS 01.04.04
THREADLIKE	NEUTRON SPIN ECHO	MICELLES 09.02.03
TIME CORRELATION FUNCTIONS	QUANTUM-CLASSICAL DYNAMICS	AB INITIO MOLECULAR DYNAMICS 06.01.04
TIME RESOLVED	EXCITED STATE	LAUE DIFFRACTION 13.09.12
TIME RESOLVED	MUSCLE	FIBER DIFFRACTION 13.16.07
TIME RESOLVED SAXS	NANOFIBERS	TMV TP210
TIME-OF-FLIGHT	PROTON TRANSFER	NEUTRON MP113
TIME-RESOLVED	CATALYTIC NANOPARTICLES	PAIR DISTRIBUTION FUNCTION ANALYSIS 13.08.05
TIME-RESOLVED	LAUE	PICOSECOND MP204
TIME-RESOLVED	CRYSTALLOGRAPHY	HEMOGLOBIN TP206
TIME-RESOLVED	CLOCK	SAXS TR.01.08
TIME-RESOLVED LAUE CRYSTALLOGR	MYOGLOBIN	PROTEIN DYNAMICS 13.16.01
TIME-RESSOLVED X-RAY CRYSTALLOGR	X-RAY CRYSTALLOGRAPHY	REACTION INTERMEDIATE 13.16.06
TITRATION CURVES	PROTEIN IONIZATION	PK PREDICTION MP066
TMV	TIME RESOLVED SAXS	NANOFIBERS TP210
TOLL-LIKE RECEPTOR	HYBRID LRR	LEUCINE RICH REPEAT 01.03.04
TOPAQUINONE	ENZYME KINETICS	COPPER AMINE OXIDASE SP147
TOPOCHEMISTRY	MULTIVALENT TEMPLATE	PHOTOCYCLOADDITION 13.02.03
TOPOTAXY	SOLID-STATE REACTION	CARBOXYLATE 13.02.02
TOTAL SCATTERING	HIGH PRESSURE	PHASE TRANSITION 13.12.02
TR SAXS	HIGH PRESSURE	LIPIDS 13.16.03
TRANSCRIPTION	DCOH	HNF-1ALPHA SP166
TRANSCRIPTION	SAXS/SANS	AAA+ ATPASE TP092
TRANSCRIPTIONAL REGULATOR	PYROCOCCUS FURIOSUS	SULFUR RESPONSE (SURRE) SP123
TRANSFERED NOE	NUCLEAR MAGNETIC RESONANCE	HIV MEMBRAN FUSION & VIRAL ENTRY TR.01.12
TRANSITION	RELAXOR	FERROELECTRIC SP020
TRANSLATION	RNA STRUCTURE	IRES 01.01.06
TRANSLATOR	RASMOL	PYMOL TP161
TRIENE	PINCER	SULFONATE MP165
TRIOXACARCIN A	DNA INTERCALATION	EXPERIMENTAL PHASING SP097
TUNGSTEN	PLATINUM	GISAXS 13.08.02

## Keywords

TURBULENCE .....	COLD-STREAM .....	VIBRATION .....	MP200
TUTORIAL .....	TEACHING .....	CYBERINFRASTRUCTURE .....	13.05.04
TWINNING .....	SUBSTRATE CHANNELING .....	PROLINE CATABOLISM .....	01.01.05
TWINNING .....			01.02.06
TWINNING .....	VARIABLE TEMPERATURE EXPERIMENTS	PHASE TRANSITION .....	13.02.01
TWO PARTNER SECRETION .....	MEMBRANE TRANSPORT .....	VIRULENCE FACTORS .....	MP036
UBIQUITIN RECEPTOR .....	MERGER CRYSTALLOGRAPHY & NMR .....	PROTEASOME .....	TR.01.11
UNCHARACTERIZED PROTEIN .....	PYROCOCCLUS FURIOSUS .....	PF0899 .....	TP017
UNFOLDED .....	SAXS .....		13.11.03
UNFOLDED PROTEIN .....	SAXS .....	HUMAN FEZ1 .....	TP012
URACIL-DNA GLYCOSYLASE .....	STRUCTURE-BASED DRUG DESIGN .....	COCKTAIL CRYSTALLOGRAPHY .....	MP042
URANIUM .....	PHOSPHONOCARBOXYLATES .....	COORDINATION POLYMERS .....	10.01.04
URANIUM OXIDE .....	RIETVELD .....	DEFECT MODEL .....	TP192
URIC ACID .....	SURFACE CHARACTERIZATION .....	CHEMICAL FORCE MICROSCOPY .....	SP023
URIC ACID DIHYDRATE .....	KIDNEY STONES .....		SP209
UV .....	PROTEIN CRYSTAL .....	IMAGING .....	SP174
UV FLUORESENCE .....	PROTEIN RYSTALLIZATION .....	IDENTIFICATION .....	MP004
VACCINIA VIRUS PROTEIN .....	POLYADENYLATE POLYMERASE .....	RNA COMPLEX .....	TP086
VANADIUM OXIDE .....	DISORDERED STRUCTURE .....	MODULATED STRUCTURE .....	13.01.07
VAPOUR DIFFUSION .....	SINGLE CRYSTAL .....	COORDINATION POLYMER COMPLEX .....	13.10.18
VARIABLE TEMPERATURE EXPERIMENTS .....	PHASE TRANSITION .....	TWINNING .....	13.02.01
VIBRATION .....	TURBULENCE .....	COLD-STREAM .....	MP200
VIBRATIONAL SPECTROSCOPY .....	LOCAL STRUCTURE .....	MOLECULAR MAGNETS .....	13.06.06
VIBRIO CHOLERAEE .....	BACTERIAL TOXIN .....	MONO-ADP-RIBOSYLTRANSFERASE .....	AW.01.06
VIRULENCE .....	GTPASE .....	RIBOSOME .....	TP101
VIRULENCE FACTORS .....	TWO PARTNER SECRETION .....	MEMBRANE TRANSPORT .....	MP036
VIRUS .....	NON CRYSTALLOGRAPHIC SYMMETRY .....	EVOLUTION .....	01.03.03
VIRUS .....	FIBER DIFFRACTION .....	CRYO-ELECTRON MICROSCOPY .....	02.01.01
VISUALIZATION .....	DATABASES .....	CLUSTER ANALYSIS .....	03.02.04
WANG LIMIT .....	DIFFRACTION DATA .....	ANOMALOUS SIGNAL .....	AW.02.03
WATER NETWORK .....	CARBONIC ANHYDRASE .....	PROTON SHUTTLE .....	TP105
WHOLE MOLECULE DISORDER .....	SYNCHROTRON .....	FULLERENES .....	AW.01.04
X-RAY .....	DIFFUSE SCATTERING .....	METALLIC ALLOY .....	MP095
X-RAY .....	FLUX .....	OPTICS .....	SP177
X-RAY .....	MICROSTRUCTURE .....	MICROBEAM .....	TP088
X-RAY CRYSTALLOGRAPHY .....	REACTION INTERMEDIATE .....	TIME-RESSOLVED X-RAY CRYSTALLOGR .....	13.16.06
X-RAY CRYSTALLOGRAPHY .....	DNA-PROTEIN COMPLEX .....	NMR SPECTROSCOPY .....	TR.01.10
X-RAY DIFFRACTION .....	IMAGING .....	CCP4 .....	TP142
X-RAY DIFFUSE SCATTERING .....	CUPRATES .....	NANO-SCALE LATTICE MODULATION .....	13.15.05
X-RAY DOSE .....	MULTIPLE DATA SETS .....	DATA COLLECTION STRATEGY .....	SP043
X-RAY FREE ELECTRON LASER .....	XFEL .....	SYNCHROTRON SCIENCE .....	13.09.01
X-RAY OPTICS .....	LAUE .....	MICROCRYSTALLOGRAPHY .....	13.14.03
X-RAY SCATTERING .....	ENERGY RECOVERY LINAC .....	SYNCHROTRON RADITION .....	13.09.05
X-RAY SCATTERING .....	CRYSTALLOGRAPHY .....	CANADIAN LIGHT SOURCE .....	13.09.07
X-RAY SCATTERING .....	HIGH PRESSURE .....	CLATHRATE HYDRATE .....	13.12.04
X-RAY SCATTERING .....	ENZYMOMOLOGY .....	ALLOSTERIC TRANSITION .....	13.16.05
X-RAY SCATTERING .....	PROTEOMICS .....	NANOTECHNOLOGY .....	MP013
X-RAY SCATTERING .....	BIOLOGICAL MOLECULES .....	MACROMOLECULES .....	TP102
X-RAY SOURCE .....	MULTILAYER OPTICS .....	SINGLE CRYSTAL DIFFRACTION .....	03.02.03
X-RAY STUDIES IN HIGH MAGNETIC FIELDS .....	SPLIT-COIL GEOMETRY .....	HIGH-FIELD PULSED MAGNET .....	TP067
XAS .....	METAL ACTIVE SITE .....	RADIATION DAMAGE .....	TR.01.02
XFEL .....	SYNCHROTRON SCIENCE .....	X-RAY FREE ELECTRON LASER .....	13.09.01
XFEL .....	SAXS .....	BIOMOLECULES .....	13.11.07
XRPD .....	RIETVELD ANALYSIS .....	SOREL CEMENT .....	04.01.04
YEAST .....	THERMAL STABILITY .....	PRION .....	SP211
Z/E ISOMERIZATION .....	BILIPROTEIN .....		13.16.04
ZEOLITES .....	SEMICONDUCTOR .....	NANOCLUSTERS .....	MP190
ZINC FINGER TRANSCRIPTION FACTOR .....	BTB DOMAIN .....	PROTEIN-PROTEIN INTERACTIONS .....	SP089
ZINC TRANSPORTER .....	PROTEIN STRUCTURE .....	MEMBRANE PROTEIN .....	01.03.01
[3X3] METAL GRID .....	INTERMOLECULAR PI-PI INTERACTIONS .....	2D ARRAY .....	SP182
[4X4] METAL GRIDS .....	DESIGNED SELF-ASSEMBLY .....	MAGNETO-STRUCTURAL RELATIONSHIP .....	13.06.03

## Author Index

- Abad, Marta ..... 04.01.08  
 Abeykoon, A.M. Milinda ..... MP190  
 Abouimrane, Ali ..... TP189  
 Abrahams, J.P. .... 13.14.02  
 Abraini, Jacques ..... 01.04.06  
 Acharya, Priyamvada ..... TR.01.12  
 Adachi, Shin-Ichi ..... 13.09.12  
 Adachi, Hiroaki ..... SP172  
 Adams, Mike ..... MP013  
 Adams, Paul ..... MP001  
 Adams, Paul ..... TP145  
 Adams, Paul ..... TP150  
 Afonine, Pavel ..... TP145  
 Agbandje-McKenna, Mavis ..... TP065  
 Agbandje-McKenna, Mavis ..... TP105  
 Agniswamy, Johnson ..... TP124  
 Ahsbabs, Hans ..... 10.01.03  
 Aizawa, Kazuya ..... 09.01.02  
 Akiyama, Shuji ..... TR.01.08  
 Alexander, Richard ..... 04.01.08  
 Alexandre, Sebastien ..... 09.01.03  
 Alexis Rae, Del Castillo ..... 09.01.06  
 Alivisatos, Paul ..... MP013  
 Alkire, Randy ..... MP200  
 Allali-Hassani, Abdellah ..... 01.08.04  
 Allan, D.R. .... 06.01.02  
 Alvarado-Ramirez, Marina ..... SP028  
 Amino, Naoya ..... 09.01.02  
 Amodeo, Gabe ..... SP002  
 Amunts, Alexey ..... 01.03.05  
 Andersen, Ken ..... TP061  
 Anderson, David ..... 04.01.06  
 Andrey, Kovalevsky ..... SP179  
 Anfinrud, Phillip ..... MP204  
 Anfinrud, P. .... TP206  
 Angel, Ross ..... 13.02.04  
 Angel, Ross ..... MP106  
 Angel, Ross ..... SP197  
 Angst, M. .... 13.04.05  
 Ankner, John F. .... TP213  
 Anokhina, E.A. .... MP190  
 Antao, Sytle ..... 13.12.02  
 Antipin, Mikhail ..... SP188  
 Antipova, Olga ..... 02.01.05  
 Antipova, Olga ..... 02.01.06  
 Arac, Demet ..... 13.03.05  
 Arenas, Daniel ..... TP065  
 Arrowsmith, Cheryl ..... 01.08.04  
 Assmann, Eliana ..... TP012  
 Austin, Michael ..... MP117  
 Austin, Brian ..... SP016  
 Austin, Brian ..... TP112  
 Avvaru, Balendu ..... TP065  
 Awuah Asiamah, Isaac ..... MP039  
 Awuah Asiamah, Isaac ..... MP054  
 Axelrod, Herbert ..... MP202  
 Ayala, Alejandro ..... MP171  
 Baatz, John ..... MP015  
 Baba, Seiki ..... MP187  
 Back, A. Darren ..... SP185  
 Baden, Elizabeth M. .... SPO28  
 Baiz, Tamam ..... AW.01.03  
 Baker, Ted ..... TP109  
 Balas, Mark ..... TP118  
 Balasubramaniam, Deepa ..... SP132  
 Balch, Alan L. .... AW.01.04  
 Ball, L. Andrew ..... 01.03.03  
 Baltus, Doris ..... AW.01.05  
 Banchs, Christian ..... TP077  
 Barabash, Rozaliya ..... 13.15.02  
 Bard, Joel ..... 03.01.05  
 Barke, Ingo ..... 13.08.03  
 Barker, Megan ..... AW.01.08  
 Barnett, Bobby ..... MP018  
 Barr, Gordon ..... 03.02.04  
 Barriault, D. .... TP046  
 Bartlett, Douglas H. .... AW.01.06  
 Bartlett, Sue ..... TP094  
 Bauer, Eric ..... 13.01.08  
 Bauer, William ..... SP211  
 Baumgarten, Sarah ..... 02.01.01  
 Baur, Robin ..... MP030  
 Beale, Andrew ..... 13.08.04  
 Beauceage, Gregory ..... 13.11.05  
 Beavers, Christine M. .... AW.01.04  
 Beck, Tobias ..... SP056  
 Becker, Bruce ..... 04.01.05  
 Becker, Michael ..... 13.14.06  
 Becker, Michael ..... MP208  
 Becker, Jeffrey ..... TP024  
 Becker, Joseph ..... TP183  
 Begley, Tadhg ..... 01.01.01  
 Begley, Tadhg ..... 01.04.04  
 Begley, Tadhg ..... MP069  
 Behrouzi, R. .... 13.11.01  
 Bell, Jeffrey ..... TP148  
 Bellamy, Henry ..... SP108  
 Benmore, Chris ..... 13.12.05  
 Bennett, Ryan ..... MP146  
 Bennett, Ryan P. .... TR.01.09  
 Benning, Matthew ..... 03.02.01  
 Berk, Norman ..... 13.09.10  
 Berman, Helen M. .... MP001  
 Berman, L. .... TP010  
 Bernado, Pau ..... 13.11.03  
 Bernstein, Herbert J. .... MP039  
 Bernstein, Herbert J. .... MP054  
 Bernstein, Herbert J. .... SP161  
 Bernstein, Herbert J. .... TP169  
 Bewley, Carole ..... TR.01.12  
 Bhat, Sathesh ..... TP038  
 Bian, Wen ..... 02.01.01  
 Bigault, Thierry ..... TP061  
 Bilderback, Donald ..... 13.14.03  
 Billinge, Simon J.L. .... 13.15.03  
 Billinge, Simon J.L. .... MP049  
 Billinge, Simon J.L. .... TP196  
 Bing, Yonghong ..... 13.10.01  
 Bismayer, Ulrich ..... SP020  
 Blakeley, Matthew ..... TP022  
 Bleuel, Markus ..... TP041  
 Block, Helena ..... TP167  
 Boatner, Lynn ..... MP181  
 Boechat, Nubia ..... MP171  
 Boeckman, Robert ..... MP018  
 Boehm, M. .... SP201  
 Bohnsack, David ..... MP159  
 Bolin, J.T. .... TP046  
 Bolotovskiy, Robert ..... MP082  
 Boltan, Suzanne ..... 04.01.06  
 Borek, Dominika ..... 01.02.03  
 Borgstahl, Gloria E.O. .... 13.01.05  
 Bossev, Dobrin ..... 09.02.03  
 Boucard, Antony A. .... 13.03.05  
 Boue, Franaois ..... 09.01.03  
 Bourgeois, Dominique ..... 13.16.01  
 Bourgeois, Dominique ..... TR.01.01  
 Bourget, Gwanall ..... 09.01.03  
 Bourret, Gilles ..... 09.02.02  
 Bowles, Timothy ..... 02.01.01  
 Boycheva, Darina ..... MP054  
 Bozin, E. S. .... 13.15.03  
 Bozin, Emil ..... MP049  
 Brady, Jeannine ..... SP111  
 Brandl, Maria ..... TP139  
 Breidt, Jay ..... SPO91  
 Bressan, Gustavo ..... TP012  
 Briber, Robert ..... 13.11.01  
 Briceño, Alexander ..... 13.02.03  
 Briceño, Alexander ..... 13.10.14  
 Briceño, Alexander ..... SP048  
 Bricogne, Gerard ..... TP139  
 Bridgham, Jamie ..... 01.06.04  
 Briggs, Peter ..... TP136  
 Broadus, Richard ..... 04.01.06  
 Brock, Carolyn P. .... 13.10.09  
 Brock, Carolyn P. .... SP011  
 Brooker, Matthew D. .... MP165  
 Brown, William C. .... 04.01.07  
 Brown, Sonal ..... 13.06.05  
 Brown, Sonal ..... 13.06.06  
 Brown, Craig ..... 13.13.03  
 Brown, Craig ..... 13.13.04  
 Brown, Breann ..... SP135  
 Brown, C. Kent ..... SP144  
 Brown, Breann ..... SP199  
 Brown, Raymond S. .... TP101  
 Bruckman, Michael ..... TP210  
 Brugner, John W. .... 01.04.02  
 Brunger, Axel T. .... 13.03.05  
 Bryan, Courtney ..... SP108  
 Bucar, Dejan-Kresimir ..... SP005  
 Bucar, Dejan-Kresimir ..... SP008  
 Buckner, F.S. .... MP042  
 Bujnicki, Janusz M. .... MP044  
 Bundschuh, Ralf ..... TP158  
 Burgner II, John W. .... SP129  
 Butchard, James ..... 06.01.07  
 Butler, Paul ..... 09.01.07  
 Butler, Paul ..... 09.02.03  
 Butler, Paul ..... MP006  
 Byrne, Miranda L. .... 03.01.01  
 Byrne, Miranda L. .... MP052  
 Byrne, Miranda L. .... SP104  
 Byrnes, Laura ..... TP109  
 Cabelli, Diane ..... SP138  
 Cahill, Christopher L. .... 10.01.04  
 Cahill, Christopher L. .... 13.10.19  
 Caliskan, G. .... 13.11.01  
 Callow, Philip ..... 02.01.03  
 Campana, Charles ..... 04.01.05  
 Campbell, Branton J. .... 13.01.04

## Author Index

Cao, H.....	13.04.02	Chrzas, John.....	03.01.03	Dao, X. ....	MP018
Capacci, Christina.....	AW.01.02	Chrzas, John.....	SP043	Darakev, Georgi.....	MP054
Carlucci-Dayton, Mary.....	MP137	Chrzas, John.....	SP115	Darakev, Georgi.....	MP039
Carmen, Peter.....	TP117	Chu, Quanli.....	SP008	Darakev, Nikolay.....	MP039
Carmen, Peter.....	MP118	Chumanevich, Alexander.....	SP074	Darakev, Nikolay.....	MP054
Carpenter, Michael A.....	SP197	Chumanevich, Alexander.....	TP124	Daranciang, Dan.....	03.01.06
Carrasco, Nicolas.....	03.01.02	Chung, J. -H.....	SP201	Darnell, Greg.....	02.01.02
Carroll, Patrick.....	10.01.05	Chupas, Peter.....	13.08.05	Dassey, Adam.....	TP094
Carter, Campbell.....	MP153	Chupas, Peter.....	13.12.02	Dau, Phoung V.....	SP008
Carter, Charles.....	01.02.02	Chupas, Peter.....	SP195	Dauter, Zbigniew.....	01.02.01
Carter, Charles.....	01.06.05	Clantin, Bernard.....	MP036	Dauter, Zbyszek.....	AW.02.03
Carter, Charles.....	TP127	Claridge, Shelley.....	MP013	Davey, Roger.....	13.10.10
Carter, Charles.....	SP157	Clausen, H.F.....	MP162	Davidson, Amy.....	01.03.02
Caspers, Nicole.....	04.01.06	Clegg, William.....	10.01.01	Davidson, Isobel.....	TP189
Castro-Colin, M.....	MP190	Coates, Leighton.....	MP125	Davies, Chistopher.....	MP015
Ceder, Gerbrand.....	13.13.01	Coates, Leighton.....	SP151	Davis, Raymond E.....	13.10.08
Cedervall, Peder.....	TP130	Coates, Leighton.....	TR.01.05	Davis, L.É.....	MP121
Cerione, Rick.....	TP114	Coco, Cassandra.....	AW.01.05	Dawe, Louise.....	13.06.03
Chakoumakos, Bryan.....	13.12.03	Coetzee, Anita.....	03.02.01	Dawe, Louise.....	SP182
Chakoumakos, Bryan.....	13.12.04	Cohen, Aina.....	TP164	De Ponte, Daniel.....	13.09.04
Chakoumakos, Bryan.....	MP110	Coker, Nathan.....	SP185	Dealwis, Chris.....	MP009
Chakoumakos, Bryan.....	MP125	Colaneri, Michael.....	MP047	Deifel, Nicholas.....	13.10.19
Chakoumakos, Bryan.....	MP181	Colaneri, Michael.....	TP120	Deivanayagam, Champion.....	SP111
Chan, Michael.....	SP068	Collins, Edward.....	SP163	Delhommelle, Jerome.....	13.10.05
Chan, Michael.....	TP158	Colloc'h, Nathalie.....	01.04.06	deLivron, Megan A.....	TP101
Chancellor, Christopher J.....	AW.01.04	Connare, Sanjay.....	01.06.01	Delucas, Lawrence.....	SP111
Chandrasekaran, Rengaswami.....	02.01.04	Connare, Sanjay.....	01.06.02	DeLucas, Lawrence.....	TP175
Chandrasekaran, Rengaswami.....	TP073	Conner, M.M.....	13.06.06	Demarse, Neil.....	MP015
Chang, Mayland.....	10.01.08	Conrad, Brittany.....	MP057	Deng, Wei.....	MP042
Chang, Cindy.....	SP147	Cook, M.....	TP114	Denny, Richard.....	02.01.03
Chapman, Karena.....	13.08.05	Copley, J.R.D.....	13.15.04	Desgranges, Caroline.....	13.10.05
Chapman, Henry.....	13.09.04	Coppens, Philip.....	13.02.06	DeTitta, George.....	01.08.03
Chapman, Karena.....	SP195	Coppens, Philip.....	13.09.12	DeTitta, George.....	TP164
Chapon, L.C.....	TP034	Coppens, Philip.....	TP050	Detrie, Theresa.....	MP106
Chatake, Toshiyuki.....	SP179	Cooper, Ronald.....	MP072	Diaz de Delgado, Graciela.....	13.10.14
Chatterjee, Abhishek.....	01.01.01	Corbett, Mary C.....	TR.01.02	Diaz de Delgado, Graciela.....	SP048
Chatterjee, Abhishek.....	01.04.04	Cornaby, Sterling.....	13.14.03	Digre, Jeff.....	SP144
Chauhan, S.....	13.11.01	Costantino, David.....	01.01.06	Dillard, Bret.....	TP017
Chen, Weijun.....	01.01.03	Court, Donald.....	TP112	Dillard, Bret.....	TP178
Chen, Jue.....	01.03.02	Cousin, Fabrice.....	09.01.03	Ding, Fang.....	01.03.06
Chen, Lirong.....	03.01.03	Cox, Jason.....	SP203	Dinnebier, Robert.....	04.01.04
Chen, Wei-Ren.....	09.02.03	Craig, Paul.....	MP054	Dmowski, W.....	13.08.01
Chen, W.....	13.04.02	Craig, Paul.....	SP169	Dmowski, W.....	13.15.06
Chen, Ying.....	13.04.04	Craig, Paul.....	TP161	Doak, Bruce.....	13.09.04
Chen, Shuang.....	13.10.04	Criswell, Angela.....	03.01.04	Doebbler, Jennifer.....	13.09.13
Chen, Yu-Sheng.....	MP162	Criswell, Anglea.....	MP082	Domsic, John.....	SP138
Chen, Yu-Sheng.....	MP204	Critton, David.....	SP135	Domsic, John.....	TP105
Chen, Lu.....	SP043	Crow, Lowell.....	MP102	Donahue, Cornelius.....	MP072
Chen, Lu.....	SP089	Cuesta-Seijo, Jose Antonio.....	AW.01.07	Dong, Wei.....	03.02.04
Chen, Lu.....	SP115	Cuesta-Seijo, Jose Antonio.....	SP089	Dong, Aiping.....	AW.02.04
Chen, Xiaojiang.....	SP119	Cui, Qiang.....	TP198	Donner, W.....	MP190
Chen, Lirong.....	TP017	Cummings, Richard.....	TP183	Dorset, Douglas.....	04.01.02
Chen, Liqing.....	TP070	Curnow, Owen.....	06.01.07	dos Santos, Antonio.....	MP099
Chen, Baoyu.....	TP092	Curtis, Joseph E.....	09.02.06	dos Santos, Antonio.....	MP110
Chen, Lei.....	TP180	Custelcean, Radu.....	AW.01.01	Doucet, Mathieu.....	MP006
Chen, Y.-S.....	TP206	Custelcean, Radu.....	MP181	Dowell, Amber.....	MP082
Chevigny, Chloe.....	09.01.03	Cygler, Miroslaw.....	TP038	Downer, Spring.....	MP184
Chi, Young-In.....	01.01.02	Cymborowski, Marcin.....	01.02.03	Drory, Omri.....	01.03.05
Chiadmi, Mohamed.....	01.04.06	D'Arcy, Allan.....	01.08.02	Duax, William.....	01.06.01
Chinte, Unmesh.....	01.08.06	Dabros, Marta.....	SP205	Duax, William.....	01.06.02
Cho, Ki Joon.....	SP062	Dai, Sheng.....	13.08.01	DuBois, Jennifer.....	SP100
Chowdhury, Saikat.....	TP092	Dailly, Anne.....	13.13.04	Duke, Elizabeth.....	13.09.08
Christianson, A.D.....	13.04.05	Daniels, Lee.....	13.01.01	Duke, Norma.....	MP057
Christodoulou, John.....	13.03.03	Dann, Charles.....	01.01.04	Duke, Norma.....	MP200

## Author Index

Dunbrack, Roland.....	01.07.02	Franco, Jimmy .....	10.01.07	Gosavi, Rajendrakumar.....	01.08.06
Duncan, Chandra J. ....	01.04.02	Frankel, Kenneth A.....	13.11.06	Gospodinov, Martin.....	SP020
Duncan, Chandra J. ....	SP129	Frankel, Daniel.....	TP194	Goto, Yuji .....	13.16.02
Duncan, J.....	TP170	Frelinger, Jeffrey .....	SP163	Gourdon, Olivier.....	13.01.08
Dunford, James .....	MP018	French, Jarrod .....	SP141	Gout, Delphine.....	13.01.08
Dunwoody, John.....	TP192	Freudenthal, John.....	13.10.01	Gozo, Philip .....	MP054
Dusek, Michal.....	13.01.02	Frischknecht, Amalie.....	09.01.01	Graber, Timothy.....	MP204
Duxbury, Phillip M.....	09.01.01	Fromme, Petra.....	13.09.04	Graber, T. ....	TP206
Duxbury, Phillip M.....	TP196	Fronczek, Frank .....	MP060	Gradzielski, Michael .....	09.01.04
Ealick, Steven .....	01.01.01	Frost, Matthew .....	MP117	Graf, Jorgen.....	03.02.03
Ealick, Steven .....	01.04.04	Frost, M.J.....	MP121	Gray, Jeffrey .....	01.07.05
Ealick, Steven .....	TP003	Fu, Dax .....	01.03.01	Green, Michael .....	MP025
Ealick, Steven .....	SP058	Fu, Zheng-Qing .....	03.01.03	Grenier, B. ....	SP201
Ealick, Steven .....	MP069	Fu, Yigang .....	13.10.09	Grey, Clare .....	13.08.05
Ealick, Steven .....	SP141	Fu, Z.-Q. ....	SP043	Grishin, Nick.....	01.07.03
Earhart, Cathleen A. ....	SP144	Fu, Z. -Q. ....	SP115	Griswold-Prenner, Irene .....	13.03.02
Ebetino, Frank.....	MP018	Fuess, Hartmut.....	10.01.03	Grosse-Kunstleve, Ralf .....	TP145
Ebihara, A.S. ....	P115	Fujisawa, Tetsuro.....	13.16.02	Gruner, Sol .....	TP114
Ediger, Mark .....	13.10.04	Fung, Russell.....	13.11.07	Gu, Baohua .....	TP213
Edwards, Aled.....	01.08.04	Fung, Russell.....	TP103	Gu, Genda .....	13.04.04
Egami, Takeshi.....	13.08.01	Funk, Kylee.....	13.06.05	Gu, Minyi .....	MP057
Egami, Takeshi.....	13.15.06	Funk, Kylee.....	13.10.15	Gu, Zu-Yi .....	SP144
Egli, Martin .....	MP085	Gabel, Frank.....	13.11.02	Guettler, Bernd.....	SP020
Ehm, Lars .....	13.12.02	Gabison, Laure.....	01.04.06	Guise, William E.....	TP186
Ehm, Lars .....	13.12.03	Gadda, Giovanni.....	01.04.08	Gummel, Jeremie.....	09.01.03
Ehm, Lars.....	13.12.04	Gahler, Roland .....	TP041	Guo, Hongyu.....	09.02.02
Ehrenberg, Helmut .....	10.01.03	Galella, Michael.....	SP040	Guo, Wenyue.....	13.16.05
Elberry, Maria .....	MP027	Gallegos, Joey .....	03.01.06	Guo, Youzhong .....	SP160
Ellena, Javier.....	MP171	Galloway, Chad.....	MP146	Guo, Ling .....	TP092
Eltis, L.D. ....	TP046	Garavito, R. Michael .....	01.04.03	Gutmann, Matthias .....	10.01.01
Endo, Yaeta .....	MP044	Garavito, R. Michael .....	TP098	Guzei, Ilia .....	13.02.01
Engel, Jens Michael.....	10.01.03	Garcia-Sakai, Victoria .....	09.02.06	Habicht, K. ....	SP201
Englich, Ulrich.....	TP114	Gardberg, Anna S. ....	MP009	Hackert, Marvin.....	SP160
Enright, Gary.....	10.01.06	Gardberg, Anna S. ....	TP075	Haertlein, Isabelle .....	TP022
Erdogan, Ozgun.....	SP157	Gardner, Kenn.....	02.01.03	Haertlein, Michael .....	TP022
Esser, Lothar .....	MP027	Garlea, Ovidiu .....	SP201	Halasz, Ivan.....	SP193
Estroff, Lara .....	13.10.12	Garrett, David .....	06.01.07	Halder, Gregory .....	SP195
Etzkorn, Markus .....	MP165	Gaulin, Bruce.....	TP067	Hamelberg, Donald .....	01.07.04
Evans, Gwyndaf .....	13.14.04	Gehring, P.M. ....	13.04.02	Hamilton, William .....	09.01.07
Evans, Barbara.....	TP122	Geisbrecht, Brian V.....	MP212	Hammel, Michal .....	13.11.06
Evdokimov, Artem.....	MP018	Geiser, Urs.....	MP176	Hammel, Michal .....	MP013
Faehnle, Chris .....	TP116	Gembicky, Milan .....	13.02.06	Hammel, Michal .....	MP212
Fan, Hai-fu .....	AW.02.06	Gembicky, Milan .....	13.09.12	Hammons, Justin .....	10.01.07
Fang, Bin .....	TP124	Gembicky, Milan .....	TP050	Han, Ying .....	01.04.04
Ferguson-Miller, Shelagh.....	01.04.03	Genther, Dane .....	MP184	Hanson, Brett .....	TP161
Ferguson-Miller, Shelagh.....	TP098	Georgieva, D. ....	13.14.02	Hanson, Brian .....	10.01.02
Fernandez-Baca, Jaime .....	13.04.03	Gershon, Paul D.....	TP086	Hanson, Leif.....	01.08.06
Ferrara, Joseph.....	03.01.04	Gilbert, Nathan.....	TP094	Hanson, Leif.....	13.11.08
Fieldhouse, Robert J. ....	AW.01.06	Gillilan, Richard.....	MP146	Hao, Quan .....	13.14.03
Finerty, Patrick.....	01.08.04	Gillilan, Richard.....	TP114	Hao, Quan .....	TP114
Fink, Anthony .....	MP033	Gillilan, Richard .....	TR.01.09	Harbison, Gerard S. ....	06.01.03
Finnegan, Steffan.....	01.04.08	Gilmore, Chris .....	03.02.04	Harden, James.....	09.02.02
Finzel, Barry.....	04.01.07	Glatte, O. ....	MP140	Harris, Melissa .....	04.01.07
Fischetti, Robert F.....	13.14.06	Goblirsch, Brandon .....	SP100	Harrison, Robert .....	SP074
Fischetti, Robert F.....	MP208	Goblirsch, Brandon .....	TP130	Harrison, Robert .....	TP124
Fiser, Andras .....	MP001	Godzik, Adam.....	MP001	Hasegawa, Kazuya .....	MP187
Fisher, S. Zoe .....	MP113	Goldberg, Ilana .....	SP207	Hasegawa, Kazuya .....	TP133
Flensberg, Claus.....	TP139	Gomez del Rio, Javier .....	MP143	Hashimoto, Takeji.....	09.01.02
Florence, Quentin J.T. ....	TP178	Gomez-Gil, L. ....	TP046	Hattne, Johan.....	SP154
Fodje, Michel.....	13.09.07	Gonzalez, Teresa .....	13.10.14	Hauptman, Herbert .....	AW.02.05
Foltin, Susan.....	04.01.07	Gonzalez, Teresa .....	SP048	Hauptman, Herbert .....	TP083
Forsyth, V. Trevor.....	02.01.03	Good, David.....	13.10.07	Hayes, Douglas.....	MP143
Forsyth, V. Trevor.....	TP155	Goodwin, W. Brandon.....	MP099	Hazra, Amrita.....	01.04.04
Foxman, Bruce M.....	13.02.02	Gosavi, Raj.....	01.08.05	Hedman, Britt.....	TR.01.02

## Author Index

- |                                |          |                             |          |                              |          |
|--------------------------------|----------|-----------------------------|----------|------------------------------|----------|
| Heiniger, Ryan .....           | MP080    | Ice, Gene.....              | TP061    | Kamburov, Petko .....        | MP039    |
| Heller, William.....           | TP024    | Ice, Gene.....              | MP095    | Kaminsky, Werner .....       | 03.01.06 |
| Helquist, Paul.....            | SP132    | Ice, Gene.....              | MP128    | Kaminsky, Werner .....       | 13.10.01 |
| Hendrickson, Wayne A.....      | AW.02.02 | Ichimaida, Fumiko.....      | TP059    | Kamo, Masayuki .....         | MP044    |
| Henkin, Tina.....              | 01.03.06 | Ihee, Hyotcherl.....        | 13.16.06 | Kanapathipillai, Umair ..... | 09.01.05 |
| Henning, Robert.....           | MP204    | Ihringer, Joerg .....       | SP020    | Kanatzidis, M.G.....         | 13.15.03 |
| Henning, R. ....               | TP206    | Ilavsky, Jan .....          | MP153    | Kang, Hye Jung .....         | 13.04.04 |
| Henry, Charles .....           | TP175    | Inoue, Tsuyoshi.....        | SP172    | Kantardjieff, K.A. ....      | 13.05.04 |
| Her, Jae-Hyuk .....            | 13.13.04 | Irving, Tom.....            | 13.16.07 | Kantowitz, Evan.....         | 13.16.05 |
| Hernandez-Guzman, Francisco .. | MP066    | Ishikawa, Ken .....         | MP044    | Kasotakis, Manolis .....     | 02.01.03 |
| Heroux, A. ....                | TP010    | Ishikawa, Takuya .....      | SP179    | Kawamoto, Masahide.....      | MP187    |
| Herwig, Kenneth.....           | 13.09.09 | Islam, Zahirul.....         | 13.15.05 | Ke, Ailong.....              | 01.03.06 |
| Hesek, Dusan .....             | 10.01.08 | Islam, Zahirul.....         | TP067    | Keane, Denis T.....          | TP186    |
| Hikima, T.....                 | MP187    | Iversen, B.B.....           | MP162    | Keefer, Larry.....           | TP081    |
| Hilgart, Mark.....             | MP208    | Iyanaki, Takashi.....       | SP037    | Keegan, Ronan.....           | TP136    |
| Hinerman, Jennifer .....       | 01.08.06 | Iyengar, Srinivasan .....   | 06.01.04 | Keel, Amanda .....           | 01.01.06 |
| Hinerman, Jennifer .....       | 13.11.08 | Izaac, Aude.....            | 01.08.05 | Keller, Peter.....           | TP139    |
| Hirata, Kunio.....             | MP187    | Jacobson, A. ....           | MP190    | Kelley, L.L. Clancy.....     | TP017    |
| Hirata, Kunio.....             | TP133    | Jamilawon, John .....       | MP054    | Kendall, Amy .....           | 02.01.01 |
| Hiser, Carrie .....            | 01.04.03 | Janaswamy, Srinivas.....    | 02.01.04 | Kenzelmann, Michel .....     | 13.04.01 |
| Hiser, Carrie .....            | TP098    | Janaswamy, Srinivas.....    | TP073    | Khare, Dheeraj.....          | 01.03.02 |
| Hitchman, Michael .....        | 13.02.05 | Jayachandran, Sanjay .....  | SP068    | Kieft, Jeffrey .....         | 01.01.06 |
| Hodges, Jason.....             | TP055    | Jayasankar, Adivaraha ..... | 13.10.07 | Kiel, Jon .....              | 09.01.01 |
| Hodgson, Keith.....            | 13.09.01 | Jemilawon, John .....       | MP039    | Kielkopf, Clara.....         | MP025    |
| Hodgson, Keith O.....          | TR.01.02 | Jenkins, Jermaine.....      | MP025    | Kim, Rosalind.....           | 01.01.02 |
| Hoefl, Rebecca.....            | SP144    | Jenkins, Joby.....          | MP078    | Kim, Sung-Hou.....           | 01.01.02 |
| Hoffmann, C.M.....             | SP026    | Jenney Jr., Francis E. .... | TP017    | Kim, Hidong .....            | 13.03.02 |
| Hoffmann, C.M.....             | MP117    | Jennings, Guy.....          | 13.08.05 | Kim, HyunJeong.....          | 13.15.03 |
| Hoffmann, C.M.....             | MP121    | Jestin, Jacques .....       | 09.01.03 | Kim, HyunJeong.....          | MP049    |
| Hoffmann, C.M.....             | MP125    | Ji, Xinhua .....            | TP081    | Kim, Jung-Ja P. ....         | SP037    |
| Hoghoj, Peter .....            | SP177    | Ji, Xinhua .....            | TP112    | Kim, Kyung Hyun .....        | SP062    |
| Hol, Wim G.J. ....             | AW.02.07 | Jia, Nan.....               | MP039    | Kim, Jung-Ja .....           | SP126    |
| Hol, Wim G.J. ....             | MP042    | Jiang, Jiansheng .....      | 03.01.02 | Kim, Kun-Hae .....           | SP209    |
| Holden, Lauren .....           | SP119    | Jiang, Licai .....          | 03.01.04 | Kimber, Matthew S. ....      | AW.01.06 |
| Holman, K. Travis .....        | 13.10.19 | Jin, R.....                 | 13.04.05 | King, Daniel P.....          | 13.10.09 |
| Holton, James.....             | TR.01.03 | Jin, Rongying.....          | MP181    | Kireev, Artem.....           | SP188    |
| Homan, Kristoff T.....         | SP132    | Joachimiaz, Andrzej.....    | MP057    | Kirian, Richard.....         | 13.09.04 |
| Hong, Xinguo.....              | TP114    | Jobson, Andrew .....        | TP090    | Kirschbaum, Kristin .....    | MP184    |
| Hood, Chantelle.....           | TP180    | Johs, Alexander.....        | TP213    | Kitatani, Tomoya .....       | SP172    |
| Hope, Hakon .....              | 13.02.01 | Johnson, John E. ....       | 01.03.03 | Kleibert, Armin .....        | 13.08.03 |
| Horanyi, Peter .....           | TP077    | Johnson, Mark.....          | 03.01.05 | Klein, Michael .....         | SP119    |
| Horanyi, Peter .....           | TP178    | Johnson, Eleda .....        | 13.02.04 | Klema, Valerie.....          | SP147    |
| Howard, Judith.....            | 13.10.18 | Johnson, Michael.....       | MP080    | Klinman, Judith.....         | SP147    |
| Howard, Eduardo.....           | TP022    | Johnson, Carl H. ....       | MP085    | Klinman, Judith.....         | TP130    |
| Hu, Liangming.....             | 10.01.02 | Johnson, Bryan .....        | SP147    | Klug, D.D. ....              | 13.12.03 |
| Huang, Zhen.....               | 03.01.02 | Johnson, William .....      | SP160    | Klug, D.D. ....              | 13.12.04 |
| Huang, Jun .....               | 13.10.04 | Johnson, Bryan .....        | TP130    | Knafels, John.....           | 04.01.07 |
| Huang, Chih-Chin .....         | TR.01.12 | Johnson, David .....        | TP175    | Knapp, J.....                | TP206    |
| Hudson, Matthew .....          | 06.01.06 | Jones, Daniel S.....        | MP165    | Knight, K.S. ....            | TP034    |
| Hudson, Bruce S.....           | 06.01.06 | Jones, Chasity .....        | SP166    | Knope, Karah E. ....         | 10.01.04 |
| Huether, Robert.....           | 01.06.01 | Jordan, Michael.....        | 01.07.02 | Kobarg, Jorg.....            | TP012    |
| Huether, E.....                | 01.06.02 | Jorgensen, Rene .....       | AW.01.06 | Kobayashi, Ichizo .....      | MP044    |
| Hughes, Ronny C. ....          | 03.01.01 | Jouault, Nicolas.....       | 09.01.03 | Kodes, Petr .....            | 13.05.05 |
| Hughes, Ronny C. ....          | MP052    | Judaö, Nenad.....           | 13.10.17 | Kodess, Boris .....          | 13.05.05 |
| Hughes, Ronny C. ....          | SP104    | Juhas, Pavol.....           | MP049    | Kodess, Pavel.....           | 13.05.05 |
| Hunter, Mark.....              | 13.09.04 | Juhas, Pavol.....           | TP196    | Kodess, Polina .....         | 13.05.05 |
| Hupp, Joseph.....              | 13.08.06 | Jung, Yang Ouk.....         | 13.16.06 | Koetzle, Thomas .....        | 06.01.01 |
| Huq, Ashfia .....              | TP055    | Jurgenson, Christopher..... | 01.04.04 | Koetzle, Thomas .....        | MP173    |
| Hura, Gregory .....            | 13.11.06 | Kaduk, James .....          | 04.01.01 | Koga, Tadanori.....          | 09.01.02 |
| Hura, Gregory .....            | MP013    | Kaduk, James .....          | 13.13.06 | Kolopus, Jim .....           | MP181    |
| Hussan, Syed.....              | TR.01.12 | Kaercher, Joerg .....       | 03.02.02 | Konuma, Tsuyoshi.....        | 13.16.02 |
| Ibberson, Richard .....        | 13.09.11 | Kaercher, Joerg .....       | 04.01.05 | Kornienko, Alexander .....   | SP188    |
| Ibberson, Richard.....         | TP034    | Kahr, Bart.....             | 13.10.01 | Koshihara, Shin-Ya.....      | 13.09.12 |
| Ice, Gene.....                 | 13.15.02 | Kalathur, Ravi .....        | TP081    | Kosinski, Jan .....          | MP044    |

## Author Index

- Kotnik, P.....MP140  
 Kouranov, Andrei.....MP001  
 Kovalevsky, Andrey .....MP113  
 Kovalevsky, Andrey .....SP074  
 Kraabel, Brett.....SP177  
 Krause, Jeanette .....SP185  
 Krause, Jeanette .....TP019  
 Kriklsunov, I.....TP114  
 Krishnan, R.S.....09.01.01  
 Krucinska, Jolanta .....MP146  
 Krucinska, Jolanta .....TR.01.09  
 Krueger, Susan.....09.02.06  
 Kubicek, Jan.....TP167  
 Kuhlman, Brian .....SP157  
 Kumar, Pravin .....SP093  
 Kumar, Pravindra.....TP046  
 Kumasaka, Takashi.....MP187  
 Kumasaka, Takashi.....TP133  
 Kunitake, Miki.....13.10.12  
 Kuramitsu, S. ....SP115  
 Kurella, Vinodh.....SP108  
 Kurumbail, Ravi .....04.01.06  
 Kusunoki, Masami .....TP059  
 Kwong, Peter .....TP180  
 Kwong, Peter .....TR.01.12  
 Labahn, Jorg.....TP167  
 Lahti, Paul .....13.06.04  
 Lakshminarasimhan, M.....MP033  
 Lal, Jyotsana.....TP041  
 Lam, Suvana .....01.01.03  
 Lam, Son .....TR.01.12  
 Lamb, Sherry .....TP038  
 Lambris, John D. ....MP212  
 Lamzin, Victor .....SP154  
 Landee, C. P. ....13.06.06  
 Lang, Jonathan.....13.15.05  
 Lang, Ed .....TP041  
 Lang, Jonathan.....TP067  
 Langan, Paul .....MP113  
 Langan, Paul .....SP179  
 Langs, David.....AW.02.05  
 Langs, David.....TP083  
 Lanza, Daniel.....TP012  
 Larson, Eric.....MP042  
 Larson, Matt.....SP111  
 Larson, B.C.....TP088  
 Latimer, Matthew J.....TR.01.02  
 Lazzari, Remi .....13.08.02  
 Le Coq, Johanne .....MP021  
 Leal, Ricardo.....TP155  
 Lee, Byeongdu.....13.08.03  
 Lee, Byeongdu.....MP131  
 Lee, Byeongdu.....MP159  
 Lee, Byeongdu.....TP210  
 Lee, Byung-Kwon .....TP024  
 Lee, Doowon.....TP017  
 Lee, Han Seung.....TP017  
 Lee, Ji-Hye.....SP062  
 Lee, Jie-Oh.....01.03.04  
 Lee, L.....TP031  
 Lee, L.....TP210  
 Lee, Marianne .....TP158  
 Lee, Mijoon.....10.01.08  
 Lee, Peter.....13.08.05  
 Lee, Peter.....13.12.02  
 Lee, Suk Joong.....13.08.06  
 Lee, Sungsik.....13.08.03  
 Lee, Woo Cheol .....01.04.07  
 Leheny, Robert.....09.02.02  
 Lei, Yu .....13.08.03  
 Lennox, R. Bruce.....09.02.02  
 Leo, Stephen .....04.01.05  
 Leroy, Frederic.....13.08.02  
 Letoublon, Antoine.....13.08.02  
 Lewandowski, Frank.....04.01.08  
 Lewis, Rob .....MP078  
 Lewis, Steven.....SP157  
 Lewis, Tom.....TP175  
 Li, Yue .....01.01.01  
 Li, J.-F.....13.04.02  
 Li, Hanying .....13.10.12  
 Li, Tonglei .....SP011  
 Li, Xin .....SP068  
 Li, Changzheng.....TP086  
 Li, Huiying.....TP086  
 Li, Li .....TP127  
 Li, S. ....TP210  
 Liang, Liyuan.....TP213  
 Liang, Tong .....SP045  
 Lim, Seung Taik.....SP062  
 Lin, Kai.....01.01.03  
 Lin, J.S.....MP143  
 Lin, Kuo-Cheng.....MP153  
 Lind, Cora .....AW.01.03  
 Lipscomb, Gina .....SP123  
 Liu, Ping.....13.11.04  
 Liu, Yun.....13.13.03  
 Liu, Yun.....13.13.04  
 Liu, G.....13.13.06  
 Liu, Xuerong.....13.15.05  
 Liu, Yan .....AW.02.04  
 Liu, Z.-J .....SP043  
 Liu, Jian.....TP098  
 Liu, Qun .....TP114  
 Liu, Xuying.....TP116  
 Lo, Chieh-Tsung .....MP131  
 Londono, J. David .....TP186  
 Long, Sihui.....SP011  
 Longo, Antonella .....TP096  
 Lorrain, Sophie .....09.01.03  
 Louca, Despina .....13.15.01  
 Louis, John .....SP074  
 Lountos, George .....01.04.08  
 Lountos, George .....TP090  
 Lovelace, Jeffrey J. ....13.01.05  
 Lovell, Scott.....13.03.02  
 Lowhorn, N.....13.13.06  
 Lu, Min.....01.03.01  
 Lu, Changrui .....01.03.06  
 Luchetti, Giovanni .....SP188  
 Luft, Joseph.....01.08.03  
 Luft, Joseph.....TP164  
 Lumsden, M.D.....13.04.05  
 Lundy, Mark.....MP018  
 Luo, Guangming.....09.01.06  
 Luo, H.....13.04.02  
 Lupez de Castro, Jose A. ....SP093  
 Luther, Erik .....TP192  
 Lutz, Susanne.....AW.01.05  
 Lynch, Vincent M. ....13.10.08  
 Lystad, K.M. ....TP007  
 MacDonald, John.....TP031  
 MacGillivray, Leonard R. ....SP005  
 MacGillivray, Leonard R. ....SP008  
 Mackay, Michael .....09.01.01  
 Maclagan, Robert .....06.01.07  
 MacQueen, B.C.....TP007  
 Madey, Theodore .....13.08.02  
 Magedov, Igor.....SP188  
 Magid, Lee .....09.02.03  
 Magotti, Paola.....MP212  
 Maier, Bernd .....SP020  
 Majeed, Shahzad.....TP180  
 Majkrzak, Charles.....13.09.10  
 Major, J.....13.15.04  
 Makarov, Oleg .....MP208  
 Malcherek, Thomas.....SP020  
 Maldonado, Marien .....MP033  
 Malik, Radhika .....MP021  
 Malkowksi, Michael.....TP164  
 Mallapragada, Surya.....09.01.05  
 Malliakas, C.D. ....13.15.03  
 Mandros, D. ....13.04.05  
 Manpadi, Madhuri.....SP188  
 Manson, Jamie .....13.06.05  
 Manson, Jamie .....13.06.06  
 Manson, Jamie .....13.10.15  
 Mao, Zhiqiang.....TP067  
 Maranville, Brian B. ....13.09.10  
 Marassio, Guillaume .....01.04.06  
 Marmol, Brenda.....MP047  
 Marsic, D.....03.01.01  
 Martin, D. ....13.12.02  
 Martin, D. ....13.12.03  
 Martin, D. ....13.12.04  
 Marsic, D.....MP052  
 Masadeh, Ahmad .....MP049  
 Matrick, Monika .....01.01.02  
 Matsuda, Yasuhiro .....TP067  
 Matsumura, Hiroyoshi.....SP172  
 Matte, Allan.....TP038  
 Matuszna, Katarina.....TP050  
 Mayer, Lucia .....MP171  
 Mazzarino, Randall .....13.10.02  
 McCammon, J. Andrew .....01.07.04  
 McClellan, Kenneth.....TP192  
 McCombs, Debbie.....TP175  
 McConnell, A.C.....13.06.06  
 McCulloch, Kathryn.....MP069  
 McDonald, Michele.....02.01.01  
 McDowell, Laura.....04.01.07  
 McGarrity, Erin.....09.01.01  
 McGuire, Michael .....13.13.02  
 McKenna, Robert .....SP138  
 McKenna, Robert .....TP065  
 McKenna, Robert .....TP105  
 McQuillan, Greg.....MP039  
 Meckel, Marlene.....MP018  
 Meehan, Edward J. ....MP052  
 Meehan, Edward J. ....TP070  
 Mei, Qiang .....13.12.05  
 Meilleur, Flora .....MP125

## Author Index

Meissner, M. ....	SP201	Mosyak, Lydia .....	03.01.05	Niu, Zhongwei .....	TP210
Meiwes-Broer, Karl-Heinz.....	13.08.03	Mottarella, Scott.....	MP054	Nixon, B. Tracy.....	TP092
Mendonça, Jorge.....	MP171	Mottarella, Scott.....	TP161	Nojiri, Hiroyuki .....	TP067
Mennon, Angeli .....	MP013	Mourey, Robert .....	04.01.06	Noll, Bruce C. ....	10.01.08
Meredith, Stephen.....	02.01.02	Mueller, Natascha.....	MP042	O'Day, Elizabeth.....	13.16.05
Merino, Elena.....	SP093	Mueller-Dickmann, Christian .....	TP022	O'Neill, Hugh .....	09.01.06
Merrill, A. Rod.....	AW.01.06	Mueser, Timothy.....	01.08.05	O'Neill, Hugh .....	TP075
Merritt, Ethan.....	MP042	Mueser, Timothy.....	13.11.08	O'Neill, Hugh .....	TP122
Mertzenich, Claude L. ....	SP008	Mukherjee, Tathagata .....	MP069	Ofek, Gilad.....	TP180
Messerle, Louis.....	MP134	Mulfort, Karen .....	13.08.06	Ogata, Craig .....	MP208
Messerschmidt, Marc .....	13.09.12	Mulligan, Rory.....	MP057	Ogretmen, Besim.....	MP015
Messerschmidt, Marc .....	TP050	Murakami, Satoshi.....	SP172	Ohlendorf, Douglas H. ....	SP144
Mestrovic, Ernest.....	SP193	Mure, Minae.....	SP147	Ohren, Jeff.....	04.01.07
Meyers, Marvin.....	04.01.06	Murphy, Michael .....	01.04.07	Ojala, W.H.....	TP007
Michaelsen, Carsten .....	03.02.03	Musfeldt, Janice.....	13.06.05	Okazaki, Nobuo .....	MP187
Michalek, Suzanne .....	SP111	Musfeldt, Janice.....	13.06.06	Oldham, Michael.....	01.03.02
Michel, Marc.....	13.12.02	Mustyakimov, Marat .....	MP113	Oliveira, Mark.....	13.10.10
Mihailescu, Ella .....	TR.01.06	Mustyakimov, Marat .....	SP179	Oliver, Allen.....	TP019
Mihailova, Boriana .....	SP020	Muth, Joseph.....	MP099	Olivier, Pacaud.....	SP177
Miknis, Zachary.....	SP071	Myles, Dean .....	TP075	Olmstead, Marilyn.....	10.01.07
Milburn, Chloe.....	MP078	Myles, Dean .....	TP122	Olmstead, Marilyn.....	13.01.03
Miller, Echo.....	MP117	Myles, Dean .....	MP125	Olmstead, Marilyn .....	AW.01.04
Miller, Echo.....	TP118	Myles, Dean .....	TP213	Omary, Mohammad A.....	13.13.07
Miller, Gordon J.....	13.01.08	Mylonas, Efstratios .....	13.11.03	Omecinsky, Diana.....	04.01.07
Miller, Joel.....	13.06.01	Nabel, Gary.....	TP180	Orans, Jillian.....	MP080
Miller, Peter.....	SP163	Nagarajan, V.....	13.14.06	Orengo, Christine.....	MP001
Milligan, Cindy.....	04.01.08	Nagarajan, V.....	MP208	Orgel, Joseph.....	02.01.02
Mills, Denise A. ....	01.04.03	Nagata, K.....	MP044	Orgel, Joseph.....	02.01.05
Mills, Denise A. ....	TP098	Nagel, Raymond.....	01.08.03	Orgel, Joseph.....	02.01.06
Mills, Dennis M. ....	13.09.05	Nagel, Raymond.....	TP164	Ortlund, Eric.....	01.06.04
Minor, Wladek .....	01.02.03	Nagler, S.E. ....	13.04.05	Orville, Allen.....	01.04.08
Misra, Ila .....	SP037	Nagy, Lisa .....	TP175	Orville, A.M. ....	TP010
Misra, Ila .....	SP126	Nair, Rajesh.....	MP001	Osborn, Raymond.....	TP107
Misture, Scott.....	04.01.03	Nakamura, Masao.....	09.01.02	Otani, M. ....	13.13.06
Mitchell, Daniel .....	13.15.06	Nakayama, Toru.....	TP059	Otwinowski, Zbyszek.....	01.02.03
Mitchell, Edward .....	02.01.03	Nance, Mark R.....	AW.01.05	Ourmazd, Abbas .....	13.11.07
Mitchell, Edward .....	13.09.06	Nanda, Hirsh .....	09.02.06	Ourmazd, Abbas .....	TP103
Mitchell, Edward .....	TP155	Napuli, Alberto.....	MP042	Overbay, M.A. ....	MP121
Mitchell, John .....	MP049	Narayanan, Theyencheri .....	09.01.04	Overbury, Steve .....	13.08.01
Mitra, Amitabha.....	13.02.01	Narayanan, Suresh.....	MP153	Overgaard, J. ....	MP162
Mitraki, Anna .....	02.01.03	Neal, John.....	MP181	Ozkan, Engin .....	13.03.05
Mitschler, Andre .....	TP022	Neau, David .....	TP094	Paciorek, Wlodek.....	TP139
Miyazono, Kenichi .....	MP044	Neder, Reinhard .....	13.05.03	Page, Rebecca .....	SP135
Mo, Yiming .....	TP024	Neef, Tobias P. ....	TP101	Page, Rebecca .....	SP199
Mobashery, Shahriar.....	10.01.08	Nehm, Sarah.....	13.10.07	Pai, Emil F.....	AW.02.04
Moffat, Keith.....	MP204	Nelson, Nathan .....	01.03.05	Palatinus, Lukas .....	13.01.02
Moffat, Keith.....	TP206	Nestola, Fabrizio .....	13.02.04	Parise, J. B. ....	13.12.02
Moghaddam, S.....	13.11.01	Neubig, Richard R. ....	AW.01.05	Parise, J.B.....	13.12.03
Moitzi, Ch. ....	MP140	Neumann, Dan.....	13.13.03	Parise, J.B.....	13.12.04
Molaison, Jaime.....	13.12.04	Neumann, Dan.....	13.13.04	Park, Sam-Yong.....	SP179
Molaison, Jamie.....	TP061	Neumann, Dan.....	13.15.04	Parker, Melvin.....	01.08.03
Molaison, Jaime.....	MP110	Newcomer, Marcia .....	TP094	Parkin, Andy .....	03.02.04
Molaison, Jamie.....	MP128	Newell, Evan.....	13.03.05	Parkin, Sean .....	13.10.09
Morar, Mariya.....	TP003	Newton, M. Gary.....	TP017	Parkin, Sean .....	SP011
Moreira dos Santos, Antonio .....	MP128	Ng, Joseph D.....	03.01.01	Parris, Kevin.....	03.01.05
Mori, Tetsuya .....	MP085	Ng, Joseph D.....	MP052	Parthasarathy, Gopalakrishnan....	TP183
Mori, Yusuke.....	SP172	Ng, Joseph D.....	SP104	Pattanayek, Rekha .....	MP085
Moriarty, Nigel.....	TP145	Nguyen, Hiep-Hoa.....	SP068	Pattanayek, Sabuj.....	MP085
Morimoto, Yukio.....	SP179	Nichol, Gary.....	10.01.01	Patel, Anamika, .....	13.16.04
Mosier, Lisa.....	MP117	Nicolini, Claudio .....	13.14.01	Paulmann, Carsten.....	SP020
Moss, Simon C. ....	13.15.04	Nicolopoulos, S.....	13.14.02	Pavlovsky, Alexander .....	TP116
Moss, Simon C. ....	13.15.05	Niebuhr, Marc .....	13.11.04	Pawlitz, Jennifer.....	04.01.06
Moss, Simon C. ....	MP190	Nisawa, Atsushi .....	MP187	Pechkova, Eugenia .....	13.14.01
Mossou, Estelle.....	02.01.03	Nishino, Tokuzo.....	TP059	Pelikan, Martin.....	13.11.06

## Author Index

Perumal, Shiamalee .....	02.01.05	Quirit, Jeanne .....	TP105	Rose, John .....	TP178
Peterson, Matthew .....	13.10.10	Rae, Alan David.....	MP168	Rose, Robert.....	SP076
Peterson, Francis C. ....	SP028	Raghavan, Aravinda .....	MP156	Rose, Robert .....	SP166
Petoukhov, Maxim.....	13.11.03	Rajashankar, Kanagalaghatta.....	01.02.06	Rosenbaum, Gerold.....	13.14.06
Petricek, Vaclav.....	13.01.02	Rajashankar, Kanagalaghatta.....	01.03.06	Rosenbaum, Gerold.....	SP043
Petsko, Gregory A. ....	13.03.01	Rajashankar, Kanagalaghatta.....	SP111	Rosenkranz, Stephan .....	TP107
Pfingsten, Jennifer .....	01.01.06	Ramakrishnan, Kalpana .....	02.01.06	Ross, Nancy L.....	MP106
Pflugrath, James.....	01.05.01	Rambo, Robert P. ....	13.11.06	Ross, Nancy L.....	SP197
Pflugrath, James.....	MP082	Rambo, Robert P. ....	MP013	Rost, Burkhard.....	MP001
Pfoh, Roland .....	SP097	Ramesh, Arati.....	01.01.04	Rotella, Frank.....	MP200
Pham, Yen .....	01.06.05	Ramey, Joanne .....	MP181	Royer, William.....	01.01.03
Pham, Oanh.....	13.02.06	Rathbone, Daniel .....	MP173	Royer, William.....	TP206
Phillips, M.D.....	13.06.06	Ravich, G. ....	MP004	Ruan, S. ....	TP206
Phillips, George N., Jr.....	TP198	Rawn, Claudia.....	MP099	Rudolph, Michael .....	SP002
Piccoli, Paula M.B. ....	06.01.06	Reddy, L. Sreenivas.....	13.10.07	Ruf, Michael .....	03.02.02
Piccoli, Paula M.B. ....	06.01.07	Redinbo, Matthew .....	01.06.04	Ruf, Michael .....	04.01.05
Piccoli, Paula M.B. ....	13.02.05	Redinbo, Matthew .....	MP080	Ruf, Michael .....	13.01.03
Piccoli, Paula M.B. ....	MP134	Regnault, L.-P.....	SP201	Ruff, Jacob .....	TP067
Pingali, Sai Venkatesh .....	TP210	Reiter, George .....	06.01.05	Rupp, Bernhard.....	13.05.02
Pinkerton, Alan .....	MP184	Remacle, Francois .....	TP142	Rupp, Bernhard.....	TP118
Pitak, Mateusz.....	13.09.12	Ren, Zhong.....	MP204	Ryan, Michael .....	MP153
Pitak, Mateusz.....	TP050	Ren, Zhong.....	TP206	Saenger, Wolfram .....	SP093
Pletnev, Vladimir .....	01.06.01	Renaud, Gilles.....	13.08.02	Sagineedu, Sreenivasa.....	MP173
Pletnev, Vladimir .....	01.06.02	Reniere, Michelle.....	01.04.07	Said, Meriem.....	01.08.03
Poda, Gennadiy .....	04.01.06	Responde, Donald .....	03.01.06	Said, Meriem.....	TP164
Podjarny, Alberto .....	TP022	Ressouche, E. ....	SP201	Saigo, Kaoru .....	TP053
Pol, Vilas .....	MP131	Reuter, Monika .....	TP070	Saito, Atsushi .....	TP059
Pol, Vilas .....	MP159	Reuter, Wolfgang.....	13.16.04	Sakiyama, Naoki.....	13.04.04
Pommier, Yves.....	TP090	Revenant, Christine .....	13.08.02	Saldin, Dilano .....	13.11.07
Pomroy, Neil C. ....	SP089	Revis, Dawn A. ....	MP165	Sales, B.C. ....	13.04.05
Poon, Billy.....	TP150	Rey-Bakaikoa, Vicente.....	TP155	Salter, Jason.....	MP146
Popov, Alexander.....	TP022	Rheinstadter, Maikel.....	09.02.01	Salter, Jason.....	TR.01.09
Popovic, Konstantin .....	SP084	Rho, Helen .....	SP166	San Antonio, James .....	02.01.05
Porcar, Lionel.....	09.01.07	Riccardi, Demian.....	TP198	Sandy, Alec.....	MP153
Porta, Jason C.....	13.01.05	Richards, John .....	MP072	Sandy, Alec.....	MP156
Portillio, J. ....	13.14.02	Richardson, David .....	01.05.05	Sandy, Alec.....	MP159
Pothineni, Sudhir Babu .....	MP208	Richardson, David .....	01.07.01	Sanghera, Jas.....	MP078
Poulos, Thomas.....	TP086	Richardson, Jane .....	01.05.05	Sanishvili, Ruslan .....	13.14.06
Poulos, Thomas.....	TR.01.02	Richardson, Jane .....	01.07.01	Sanishvilli, Ruslan .....	MP208
Powell, Kyle.....	13.03.02	Ricklin, David.....	MP212	Sarver, Ronald.....	04.01.07
Prabhakar, Rajeev .....	01.04.08	Ricks, Jessica .....	SP108	Sauter, Nicholas .....	TP150
Prange, Thierry .....	01.04.06	Riddle, David.....	SP163	Sauve, Anthony.....	SP141
Presores, Janeth.....	SP023	Ridilla, Marc .....	AW.01.05	Saveedra, Joseph.....	TP081
Pressprich, Mark.....	TP152	Ringe, Dagmar.....	13.03.01	Savici, Andrei.....	13.04.04
Pringle, Fiona M. ....	01.03.03	Ripmeester, John.....	10.01.06	Savoy, A. ....	TP105
Prive, Gilbert.....	AW.01.07	Robert, Rose.....	TP096	Sawasaki, Tatsuya.....	MP044
Prive, Gilbert .....	SP084	Robertson, Michael P.....	01.06.06	Saxena, A.M.....	TP010
Prive, Gilbert.....	SP089	Robertson, J.L.....	13.15.04	Schaefer, Frank .....	TP167
Proffen, Thomas .....	13.01.08	Robinson, Howard.....	MP137	Schall, Constance.....	01.08.05
Proffen, Thomas .....	13.15.03	Robinson, H.H. ....	TP010	Schall, Constance.....	01.08.06
Proffen, Thomas .....	13.15.06	Robinson, Victoria L. ....	TP101	Schertler, Gebhard .....	01.03.07
Proteau, Ariane.....	TP038	Rodaelli, P.G. ....	TP034	Schertler, Gebhard .....	13.14.05
Purdy, Alexandra E. ....	AW.01.06	Rodriguez, J.A. ....	13.15.04	Schierbeek, Bram .....	03.02.01
Purdy, Michael.....	TP077	Rodriguez-Hornedo, Nair .....	13.10.07	Schiffer, Celia.....	01.01.03
Puzyrev, Yevgeniy .....	MP095	Rodwell, Victor W. ....	01.04.02	Schlecht, Thomas.....	04.01.04
Qin, Ling .....	01.04.03	Rodwell, Victor W. ....	SP129	Schlichting, Ilme.....	01.04.01
Qin, Ling .....	TP098	Roger, Vincent .....	SP177	Schlueter, John.....	13.06.05
Qiu, Dengli.....	02.01.06	Roh, J.-H. ....	13.11.01	Schlueter, John .....	13.06.06
Qiu, Y.....	SP201	Rose, David.....	AW.01.08	Schlueter, John.....	13.10.15
Qiu, Li .....	TP070	Rose, David R. ....	TP029	Schlueter, John.....	MP176
Qu, Zhe.....	TP067	Rose, John .....	03.01.03	Schmidt, Tim.....	01.04.02
Quaresma, Alexandre .....	TP012	Rose, John .....	AW.02.08	Schmidt, Kevin .....	13.09.04
Quint, Patrick .....	SP138	Rose, John .....	SP043	Schmidt, Marius.....	13.16.04
Quiocho, Florante .....	01.03.02	Rose, John .....	SP115	Schmidt, Tim.....	SP129

## Author Index

Schnablegger, H.....	MP140	Siegler, Maxime.....	SP011	Stepanov, Sergey.....	MP208
Schneider, Jochen.....	13.09.02	Sillau, Stefan.....	SP091	Sterling, Craig.....	SP174
Schneider, Dieter.....	MP137	Silva, Cecilia.....	MP171	Sternstein, Sanford.....	MP156
Schneider, D.K.....	TP010	Silva, Julio Cesar.....	TP012	Steussy, C. Nicklaus.....	01.04.02
Schoenborn, Benno.....	MP113	Silverman, David.....	SP138	Steussy, C. Nicklaus.....	SP129
Schotte, Friedrich.....	MP204	Silverman, David.....	TP065	Stevens, Raymond.....	13.03.06
Schotte, F.....	TP206	Silverman, David.....	TP105	Stewart, Phoebe.....	02.01.01
Schroeder, Frank.....	01.04.04	Sim, Lyann.....	TP029	Stewart, Phoebe.....	MP085
Schroll, Cynthia.....	SP185	Simmons, Charles.....	13.02.05	Stillwell, Benjamin.....	TP186
Schubert, Carsten.....	04.01.08	Simpson, Bret.....	03.01.04	Stivers, James.....	TR.01.10
Schubot, Florian.....	SP016	Simpson, Greg H.....	13.10.09	Stock, C.....	13.04.02
Schuller, David.....	13.14.03	Sinha, Sunil.....	13.15.05	Stogios, Peter J.....	SP089
Schuller, Dave.....	TP114	Sippel, Katherine.....	TP105	Stokes, Harold T.....	13.01.04
Schultz, Arthur.....	06.01.06	Skaar, Eric.....	01.04.07	Stoppelkamp, Vera.....	09.01.07
Schultz, Arthur.....	06.01.07	Slambrouck, Severine.....	SP188	Storm, Arjen.....	03.02.01
Schultz, Arthur.....	13.02.05	Slebodnick, Carla.....	03.02.05	Stosch, Rainer.....	SP020
Schultz, Arthur.....	MP134	Slebodnick, Carla.....	10.01.02	Streit, Bennett.....	SP100
Schultz, Arthur.....	MP173	Smart, Oliver.....	TP139	Strop, Pavel.....	13.03.05
Schultz, L. Wayne.....	SP071	Smilgies, Detlef.....	13.14.03	Stroud, Tonia.....	SP185
Schulz, Thomas.....	03.02.03	Smith, Clyde.....	MP202	Stubbs, Gerald.....	02.01.01
Schwalbe, Carl.....	MP173	Smith, Clyde.....	TP109	Stults, Teena.....	04.01.06
Schwede, Torsten.....	MP001	Smith, Jeremy C.....	09.02.04	Sudhof, Thomas C.....	13.03.05
Schönleber, Andreas.....	13.01.03	Smith, J.L.....	13.14.06	Sugar, Frank J.....	TP017
Scott, William G.....	01.01.02	Smith, Harold C.....	TR.01.09	Sugimoto, Kunihisa.....	04.01.04
Scott, William G.....	01.06.06	Smith, Harold.....	MP146	Sugiyama, Shigeru.....	SP172
Scott, Robert.....	SP123	Smith, S.....	TP114	Sulea, Traian.....	TP038
Sell, Kristian.....	13.08.03	Snell, Edward.....	01.08.03	Sun, Ping.....	SP016
Senisterra, Guillermo.....	01.08.04	Snell, Edward.....	TP075	Sung, Herman H-Y.....	03.02.06
Sentman, Judith.....	04.01.01	Snell, Edward.....	TP164	Sutton, Mark.....	09.02.02
Seppala, Jon.....	09.01.01	Snell, Edward.....	SP191	Suzuki, Hirokazu.....	TP059
Serrano, Hector.....	SP160	Snell, M. Elizabeth.....	01.08.03	Svenson, Kristine.....	03.01.05
Sevrioukova, Irina F.....	TR.01.02	Snell, M. Elizabeth.....	TP164	Svensson, Christer.....	13.01.01
Shah, Binal.....	01.08.06	Soares, Alexei.....	MP137	Svergun, Dmitri I.....	13.11.03
Shakir, Khalid.....	TP180	Soares, A.....	TP010	Swainson, Ian.....	13.01.06
Sham, Hing.....	13.03.02	Soisson, Stephen.....	TP183	Sweeney, Shawn.....	02.01.05
Shankaranarayanan, Aruna.....	AW.01.05	Soltis, S. Michael.....	TP164	Sweet, Robert.....	TP010
Shapiro, David.....	13.09.04	Somers, Will.....	03.01.05	Sweet, Robert.....	MP137
Shapovalov, Maxim.....	01.07.02	Sommerfeld, Stacy C.....	SP008	Swenson, Dale C.....	MP134
Sharpe, Martyn A.....	TP098	Song, X.....	MP018	Swift, Jennifer A.....	13.10.06
Shastri, Sarvjit.....	13.12.02	Sours, Ryan.....	13.10.02	Swift, Jennifer A.....	AW.01.02
Shaw, Neil.....	TP017	Sours, Ryan.....	SP209	Swift, Jennifer A.....	SP023
Sheldrick, George.....	01.05.02	Southerland, Heather.....	13.06.06	Swindell, James T.....	TP178
Sheldrick, George.....	SP056	Southerland, Heather.....	13.10.15	Swift, Jennifer A.....	SP207
Sheldrick, George.....	SP097	Spassov, Velin.....	MP066	Swift, Jennifer A.....	SP209
Shen, Haihong.....	MP025	Speir, Jeffrey A.....	01.03.03	Swindell, James Tucker,II.....	SP115
Shen, Chen-Hsiang.....	SP074	Spence, John.....	13.09.04	Syfroera, Georgia.....	MP212
Sheng, Jia.....	03.01.02	Spencer, Elinor.....	10.01.02	Sylvestre, M.....	TP046
Shi, Jian.....	02.01.01	Spencer, Elinor.....	13.10.18	Sysoeva, Tatyana.....	TP092
Shi, Ke.....	SP144	Spicer, Eleanor.....	MP015	Szczepek, Michal.....	TP070
Shi, Rong.....	TP038	Spitale, Robert.....	SP149	Szebenyi, Doletha M.E.....	13.14.03
Shibata, Sayaka.....	MP042	Spude, J.M.....	TP007	Szebenyi, Doletha M.E.....	TP114
Shibayama, Naoya.....	SP179	Spurlino, John.....	04.01.08	Tainer, John A.....	13.11.06
Shieh, Huey Sheng.....	04.01.06	Squatrito, Philip.....	MP184	Takacs, Peter.....	TP061
Shimizu, Nobutaka.....	MP187	Srajer, Vukica.....	MP204	Takahashi, Satoshi.....	13.16.02
Shimizu, Tetsuya.....	TP133	Srajer, V.....	TP206	Takahashi, Seiji.....	TP059
Shimizu, Tetsuya.....	MP187	Srinath, Hema.....	01.01.03	Takano, Kazufumi.....	SP172
Shin, Hye Jeong.....	SP062	Stalke, Dietmar.....	03.02.03	Takenaka, Mikihiro.....	09.01.02
Shinkai, A.....	SP115	Stallings, William.....	04.01.06	Takeshita, Daijiro.....	TP053
Shneerson, Valentin.....	13.11.07	Stanek, Christopher.....	TP192	Tanaka, Yoshikazu.....	TP059
Shneerson, Valentin.....	TP103	Stanslas, Johnson.....	MP173	Tanner, Jack.....	01.01.05
Shoemaker, Robert.....	TP090	Stauffacher, Cynthia V.....	01.04.02	Tanner, David.....	TP065
Shukla, Anuj.....	09.01.04	Stauffacher, Cynthia V.....	SP129	Tanokura, Masaru.....	MP044
Sidoreko, Felix.....	13.05.05	Stauffacher, Cynthia V.....	SP132	Tanokura, Masaru.....	TP053
Siegler, Maxime.....	13.10.09	Steelant, Wim.....	SP188	Tao, Jing.....	13.10.04

## Author Index

- Tao, Wendy ..... MP001  
 Tarantino, Serena C. .... SP197  
 Taylor, Derek J. .... 01.03.03  
 Teh, A.-H. .... MP187  
 Teixeira, Susana ..... TP155  
 Tempel, Wolfram ..... TP017  
 Terwilliger, Thomas ..... 01.05.03  
 Tesh, Kris ..... 03.01.04  
 Tesmer, John J. G. .... AW.01.05  
 Thalladi, Venkat ..... 13.10.03  
 Thalladi, Venkat ..... SP203  
 Thalladi, Venkat ..... SP205  
 Thirumalai, D. .... 13.11.01  
 Thiyagarajan, Pappannan ..... 09.01.05  
 Thiyagarajan, Pappannan ..... MP131  
 Thiyagarajan, Pappannan ..... MP156  
 Thiyagarajan, Pappannan ..... MP159  
 Thiyagarajan, Pappannan ..... TP210  
 Thomas, Tissa ..... 13.10.02  
 Thomas, E. .... 13.13.06  
 Thomison, J.B. .... MP121  
 Thompson, Joe D. .... 13.01.08  
 Thompson, Laurence ..... 13.06.03  
 Thompson, James R. .... SP028  
 Thompson, L.K. .... SP182  
 Thorne, Robert ..... MP030  
 Thorne, Robert ..... SP079  
 Thornton, Joseph ..... 01.06.04  
 Tian, W. .... 13.04.05  
 Tie, Yunfeng ..... SP074  
 Tiede, David ..... 13.08.06  
 Tiggelaar, Sarah ..... 02.01.03  
 Timofeevac, Tatiana ..... SP188  
 Ting, Daniel ..... 01.07.02  
 Tobias, Douglas ..... 09.02.05  
 Tobias, Douglas ..... TR.01.04  
 Toby, Brian ..... 13.05.01  
 Todorov, Georgi ..... MP039  
 Tokonzaba, Etienne ..... SP119  
 Tong, Liang ..... SP002  
 Tongwa, Paul ..... SP188  
 Tooke, Duncan ..... 10.01.01  
 Torriani, Iris ..... TP012  
 Tortajada, Antoni ..... SP135  
 Toth, Gergely ..... 13.03.02  
 Tran, Vu ..... MP004  
 Trehwella, Jill ..... TR.01.07  
 Tripathi, Sailish ..... 13.14.01  
 Tronrud, Dale ..... 01.05.07  
 Tropea, Joseph ..... TP090  
 Tropea, Joseph ..... TP112  
 Tse, John ..... 13.12.01  
 Tseng, Erica ..... 09.01.01  
 Tsuruta, Hiro ..... 13.11.04  
 Tsuruta, Hiro ..... 13.16.05  
 Tu, Chingkuang ..... TP065  
 Tu, Chingkuang ..... TP105  
 Tu, Chao ..... TP112  
 Tuan, Han-Fang ..... SP151  
 Tulk, Christopher ..... 13.12.03  
 Tulk, Christopher ..... 13.12.04  
 Tulk, Christopher ..... TP061  
 Tulk, Christopher ..... MP110  
 Tulk, Christopher ..... MP125  
 Tulk, Christopher ..... MP128  
 Turnbull, M.M. .... 13.06.06  
 Tuteja, Anish ..... 09.01.01  
 Twamley, Brendan ..... 13.10.15  
 Uchanska-Ziegler, Barbara ..... SP093  
 Udachin, Konstantin ..... 10.01.06  
 Udovic, Boris ..... MP087  
 Ueno, Go ..... MP187  
 Ueno, Go ..... TP133  
 Ukpabi, Georgi ..... 01.04.07  
 Umland, Timothy ..... 01.06.01  
 Umland, Timothy ..... SP071  
 Umland, Timothy ..... SP211  
 Unno, Hideaki ..... TP059  
 Urban, Volker ..... 09.01.06  
 Urban, Volker ..... MP143  
 Urban, Volker ..... TP122  
 Vahedi-Faridi, Ardeschir ..... SP093  
 Vajda, Stefan ..... 13.08.03  
 van der Woerd, Mark ..... SP091  
 van der Woerd, Mark ..... SP191  
 Van Voorhis, W.C.E. .... MP042  
 Vancik, Hrvoj ..... SP193  
 Vande Velde, Cris ..... 13.02.06  
 Variankaval, Narayan ..... 13.10.13  
 Veatch, Christina ..... TP164  
 Vedadi, Masoud ..... 01.08.04  
 Vergis, James ..... TP077  
 Verlinde, Christophe ..... MP042  
 Verman, Boris ..... 03.01.04  
 Vettel, Christiane ..... AW.01.05  
 Viehland, D. .... 13.04.02  
 Villard, Frederic ..... 01.08.02  
 Villeret, Vincent ..... MP036  
 Viola, Robert ..... MP117  
 Viola, Robert ..... TP118  
 Viola, Ronald ..... MP021  
 Viola, Ronald ..... TP116  
 Visscher, Theodore ..... MP072  
 Vitali, Jacqueline ..... MP047  
 Vitali, Jacqueline ..... TP120  
 Viterbo, Davide ..... 13.10.01  
 Vogan, Erik ..... 03.01.05  
 Vogt, Stefan ..... 13.14.06  
 Voit, Stewart ..... TP192  
 Volker, Urban ..... TP096  
 Volkman, Brian F. .... SP028  
 Volz, Armin ..... SP093  
 Volz, Heather ..... TP192  
 von Delft, Frank ..... TP194  
 Von Dreele, Robert ..... 13.09.13  
 von Oyenhausen, Viola ..... 13.08.03  
 Vonrhein, Clemens ..... TP139  
 Wachter, Greg ..... 04.01.05  
 Wagner, Trixie ..... 13.01.03  
 Wagner, Armin ..... 13.14.04  
 Wakeman, Catherine ..... 01.01.04  
 Walsh, Jace ..... TP118  
 Walter, Richard ..... MP018  
 Walters, Kylie ..... TR.01.11  
 Waltman, Mary Jo ..... MP113  
 Wang, Bi-Cheng ..... 03.01.03  
 Wang, Bi-Cheng ..... AW.02.01  
 Wang, Bi-Cheng ..... SP043  
 Wang, Bi-Cheng ..... SP115  
 Wang, Bi-Cheng ..... SP123  
 Wang, Bi-Cheng ..... TP178  
 Wang, Dongli ..... SP076  
 Wang, Ganggang ..... SP119  
 Wang, Jin ..... MP153  
 Wang, Rong ..... 02.01.05  
 Wang, Rong ..... 02.01.06  
 Wang, Xiaoping ..... 13.13.07  
 Wang, Yu ..... TP031  
 Wang, Qian ..... TP210  
 Ward, Michael ..... 13.10.16  
 Warkentin, Matthew ..... SP079  
 Wasney, Gregory ..... 01.08.04  
 Watanabe, Miki ..... MP044  
 Waugh, David ..... SP016  
 Waugh, David ..... TP090  
 Waugh, David ..... TP112  
 Weber, Richard ..... 13.12.05  
 Weber, Irene ..... SP074  
 Weber, Irene ..... TP124  
 Weckhuysen, Bert ..... 13.08.04  
 Wedekind, Joseph ..... MP146  
 Wedekind, Joseph ..... SP149  
 Wedekind, Joseph ..... TR.01.09  
 Weeks, Charles M. .... 01.05.06  
 Weeks, Charles M. .... 01.06.01  
 Wei, Wang ..... TP213  
 Weierstall, Uwe ..... 13.09.04  
 Weigand, Steven ..... TP186  
 Weik, Martin ..... 09.02.05  
 Weinberg, Robin ..... 04.01.06  
 Weinreb, Violetta ..... TP127  
 Weiss, Thomas M. .... 09.01.04  
 Weiss, Thomas M. .... 13.11.04  
 Welch, Mark ..... MP106  
 Welp, Ulrich ..... 13.15.05  
 Westin, Charles ..... TP161  
 Wheeler, Kraig ..... 13.10.11  
 White, Robert H. .... SP058  
 White, Stephen ..... TR.01.06  
 Whitfield, Pamela ..... TP189  
 Whitman, Christian ..... SP160  
 Wieland, Thomas ..... AW.01.05  
 Wiener, Michael ..... TP077  
 Wiesmann, Jorg ..... 03.02.03  
 Wiest, Olaf ..... SP132  
 Wilding, Martin ..... 13.12.05  
 Willett, Roger ..... 13.06.02  
 Williams, Ian D. .... 03.02.06  
 Williams, Dewight ..... MP085  
 Willis, Michael ..... SP174  
 Wilmot, Carrie ..... SP100  
 Wilmot, Carrie ..... SP147  
 Wilmot, Carrie ..... TP130  
 Wilson, Ian A. .... 01.08.01  
 Wilson, Chick ..... 03.02.04  
 Wilson, Mark ..... MP033  
 Wilson, William ..... TP175  
 Winans, Randall ..... 13.08.03  
 Winans, Randall ..... MP131  
 Winans, Randall ..... MP159  
 Winkler, Wade ..... 01.01.04  
 Winn, Martyn ..... TP136

## Author Index

---

- |                           |          |                         |          |
|---------------------------|----------|-------------------------|----------|
| Winter, Roland .....      | 13.16.03 | Zaccai, Giuseppe .....  | 09.02.05 |
| Winter, Graeme.....       | TP142    | Zaliznyak, Igor.....    | 13.04.04 |
| Wischmeyer, Corey .....   | MP054    | Zanchi, Drazen.....     | 09.01.04 |
| Wischmeyer, Corey .....   | SP169    | Zandbergen, H.W.....    | 13.14.02 |
| Wisniewski, Dariusz.....  | MP181    | Zavalij, Peter .....    | 13.01.07 |
| Wojtaszczyk, Ann .....    | 01.08.03 | Zellelow, Amanuel.....  | SP209    |
| Wolfgang, Matthew .....   | MP080    | Zenno, Shuhei .....     | TP053    |
| Wolfley, Jennifer .....   | 01.08.03 | Zhang, Qiu .....        | 09.01.06 |
| Wolfley, Jennifer .....   | TP164    | Zhang, Zhongsheng.....  | MP042    |
| Womack, T.O. ....         | TP114    | Zhang, Yang .....       | SP058    |
| Wong-Ng, W. ....          | 13.13.06 | Zhang, Di.....          | TP090    |
| Wood, Kathleen .....      | 09.02.05 | Zhang, Yi .....         | SP119    |
| Woodson, S. ....          | 13.11.01 | Zhao, Jing .....        | 13.02.04 |
| Worcester, David.....     | TR.01.06 | Zhao, Jing .....        | SP197    |
| Worthylake, David.....    | SP108    | Zhao, Xingang .....     | 06.01.03 |
| Wrensford, Louise V.....  | 01.04.02 | Zheludev, A. ....       | SP201    |
| Wrensford, Louise V.....  | SP129    | Zheng, Jiayin.....      | SP138    |
| Wright, Gerard .....      | TP038    | Zheng, Shao-Liang ..... | 13.02.06 |
| Wright, Cameron .....     | TP118    | Zheng, Shao-Liang ..... | 13.09.12 |
| Wu, Jing.....             | 13.03.02 | Zhou, Jun.....          | 06.01.03 |
| Wu, Hui .....             | 13.13.05 | Zhou, Sufeng.....       | TP086    |
| Wunsch, Kristin .....     | SP191    | Zhou, Tongqing.....     | TP180    |
| Xhu, Yaqi.....            | 04.01.07 | Zhou, Wenbo.....        | MP033    |
| Xi, Hanmi.....            | 13.10.04 | Zhu, Jin-Yi.....        | 03.01.03 |
| Xia, Jiarong .....        | 13.16.05 | Ziegler, Andreas.....   | SP093    |
| Xia, Di .....             | MP027    | Zschack, Paul .....     | MP095    |
| Xia, Chuanwu .....        | SP037    | Zucker, F.....          | MP042    |
| Xiang, Song.....          | SP045    | Zwart, Peter .....      | TP145    |
| Xiao, Liren .....         | MP042    | Zwart, Peter .....      | TP150    |
| Xu, Hongliang.....        | 01.05.06 |                         |          |
| Xu, Qifang.....           | 01.07.02 |                         |          |
| Xu, G. ....               | 13.04.02 |                         |          |
| Xu, Hao .....             | TP178    |                         |          |
| Xu, Hongliang.....        | TP083    |                         |          |
| Xu, Hao .....             | 03.01.03 |                         |          |
| Xu, Jian.....             | SP174    |                         |          |
| Xu, S. ....               | 13.14.06 |                         |          |
| Xu, Shenglan.....         | MP208    |                         |          |
| Xu, Yao.....              | MP085    |                         |          |
| Yamamoto, Masaki.....     | TP133    |                         |          |
| Yamamoto, Masaki.....     | MP187    |                         |          |
| Yamani, Z. ....           | 13.04.05 |                         |          |
| Yang, Chang .....         | 03.01.04 |                         |          |
| Yang, Ling .....          | 13.12.03 |                         |          |
| Yang, Ling.....           | 13.12.04 |                         |          |
| Yang, Cheng.....          | MP082    |                         |          |
| Yang, Chi.....            | 13.13.07 |                         |          |
| Yang, Hua.....            | SP123    |                         |          |
| Yang, In Seok.....        | SP062    |                         |          |
| Yang, Wanjuan .....       | TP136    |                         |          |
| Yannette, Clare.....      | 13.10.06 |                         |          |
| Yardimci, G. Gurkan ..... | 01.06.03 |                         |          |
| Ye, Z.-G. ....            | 13.04.02 |                         |          |
| Ye, Sun .....             | 13.10.04 |                         |          |
| Yearley, Eric .....       | MP184    |                         |          |
| Yoder, Derek .....        | 13.14.06 |                         |          |
| Yokoyama, S. ....         | SP115    |                         |          |
| Yong, Wei.....            | SP126    |                         |          |
| Yoshii, Shunsuke .....    | TP067    |                         |          |
| Yoshizawa, Hideki.....    | 13.04.04 |                         |          |
| Young, Paul .....         | TP109    |                         |          |
| Yu, Lian .....            | 13.10.04 |                         |          |
| Yu, Chang-An .....        | MP027    |                         |          |
| Yu, Linda.....            | MP027    |                         |          |

## Notes

---